

NI

NASA CONTRACTOR REPORT

NASA CR-161889

FEASIBILITY STUDY -- ATMOSPHERIC GENERAL CIRCULATION EXPERIMENT, VOLUME II

Edited by R. J. Homsey
General Electric Company
Space Systems Division
Post Office Box 8555
Philadelphia, Pennsylvania 19101

Final Report - Volume II

September 1, 1981



(NASA-CR-161889-Vol-2) FEASIBILITY STUDY:
ATMOSPHERIC GENERAL CIRCULATION EXPERIMENT,
VOLUME 2 Final Report (General Electric
Co.) 604 p HC A99/MF A01

N82-15085

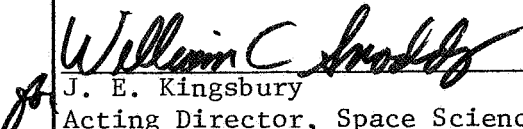
CSSL 20D

Unclas
06427

G3/12

Prepared for

NASA - George C. Marshall Space Flight Center
Marshall Space Flight Center, Alabama 35812

1. REPORT NO. NASA CR-161889	2. GOVERNMENT ACCESSION NO.	3. RECIPIENT'S CATALOG NO.	
4. TITLE AND SUBTITLE Feasibility Study - Atmospheric General Circulation Experiment, Volume II		5. REPORT DATE September 1, 1981	6. PERFORMING ORGANIZATION CODE
7. AUTHOR(S) Edited by R. J. Homsey		8. PERFORMING ORGANIZATION REPORT #	
9. PERFORMING ORGANIZATION NAME AND ADDRESS General Electric Company Space Systems Division P.O. Box 8555 Philadelphia, Pennsylvania 19101		10. WORK UNIT NO.	11. CONTRACT OR GRANT NO. NASA8-34049
12. SPONSORING AGENCY NAME AND ADDRESS National Aeronautics and Space Administration Washington, D.C. 20546		13. TYPE OF REPORT & PERIOD COVERED Contractor Final Report - Volume II	
15. SUPPLEMENTARY NOTES Prepared under the technical monitorship of the Atmospheric Sciences Division, Space Sciences Laboratory, Science and Engineering Directorate, NASA/MSFC		14. SPONSORING AGENCY CODE	
16. ABSTRACT Volume II, Feasibility Study - Atmospheric General Circulation Experiment, contains all of the documentation that contributes to the results given in Volume I. The documentation, generated during the course of the program, includes the analysis performed in each technical area, the rationale and substantiation for the design approaches selected for the hardware, and the design details for the baseline AGCE.			
17. KEY WORDS Spacelab zero-gravity experiment Photochromic flow visualization Electro-convection Spherical baroclinic instability		18. DISTRIBUTION STATEMENT Unclassified - Unlimited  J. E. Kingsbury Acting Director, Space Sciences Laboratory	
19. SECURITY CLASSIF. (of this report) Unclassified	20. SECURITY CLASSIF. (of this page) Unclassified	21. NO. OF PAGES	22. PRICE NTIS

SECTION 3.0
DETAILED FEASIBILITY STUDY

- 3.1 MATERIALS FOR DIELECTRIC FLUID AND EXPERIMENT SPHERE
- 3.2 OPTICS FOR DATA RETRIEVAL
- 3.3 THERMAL ANALYSIS AND DESIGN
- 3.4 HIGH VOLTAGE POWER SUPPLY
- 3.5 EXPERIMENT CONTROL AND DATA HANDLING
- 3.6 APPARATUS CONFIGURATION
- 3.7 EXPERIMENT DESIGN

OVERVIEW

Volume II of the Final Report for the Feasibility Study of the Atmospheric General Circulation Experiment contains all of the documentation that contributes to the results given in Volume I. This documentation, generated during the course of the program, includes the analysis performed in each technical area, the rationale and substantiation for the design approaches selected for the hardware and the design details for the baseline AGCE.

The documentation produced in the form of Program Information Releases (PIR) dockets has been arranged by technical area to provide a cohesive flow of information. Each major technical area has been separated by blue dividers for ease in locating specific categories such as Materials for the AGCE, high voltage power supply, apparatus configuration, etc. The order in which the technical areas are arranged coincides with that given in Section 2.0 of Volume I.

3.1 MATERIALS FOR DIELECTRIC FLUID AND EXPERIMENT SPHERE

	<u>PIR NO.</u>
Task 1 - Dielectric Fluid Requirements	-006
Parametric Presentation of AGCE Variables	-028
Task 1 - Dielectric Heating Due to Electrical Power Dissipation	-014
Task 1 - Calculation of g_E for Nominal GFFC and AGCE Parameters	-015
Task 1 - Fluid Viscosity Assessment	-017
Photochromic Dyes for Flow Visualization in High Dielectric Solvents	-025
Dielectric Solvent/Photochromic Dye Solutions	-032
Photochromic Dyes for Flow Visualization in High Dielectric Solvents - III	-037
Photochromic Dyes for Flow Visualization in High Dielectric Solvents - II	-036
Fluid Filtration Theory	-002
Task 2 - Purification, Characterization and Handling of High Dielectric Constant Fluids	-021
Task 3 - Dust Removal Feasibility Report	-016
Task 3 - Dust Removal Design Requirements	-005
Dielectric Material for the AGCE Baffle	-019
Cost of Material for the AGCE Baffle	-026
Task 8 - Requirements for Outer Sphere Material	-009
Task 8 - Material for the Outer Sphere	-020

PROGRAM INFORMATION REQUEST / RELEASE

FROM DR. S. L. NESTE	TO DISTRIBUTION
-------------------------	--------------------

DATE SENT 1-28-81	DATE INFO. REQUIRED	PROJECT AND REQ NO	REFERENCE DIR. NO.
----------------------	---------------------	--------------------	--------------------

SUBJECT
TASK 1 - DIELECTRIC FLUID REQUIREMENTS

INFORMATION REQUESTED/RELEASED

The attached AGCE dielectric fluid requirements have been generated for use in making a survey of dielectric fluids and selecting candidates for use in the Atmospheric General Circulation Experiment (AGCE).

TASK 1 - SURVEY OF DIELECTRIC FLUIDS

1.0 SCOPE

The dielectric fluid survey and photochromic compatibility assessment will be conducted so that a fluid/photochromic system can be selected for use in the AGCE. The dielectric performance requirements to be used as guidelines in this effort are provided below.

2.0 GENERAL

The dielectric fluid requirements are based on the AGCE RFP, the GE AGCE proposal and personal communication with Dr. Fowlis of NASA/MSFC. Since the required information is not readily available in the open literature, the expertise of Dr. Ronald Francis (Rochester Institute of Technology), Dr. David Shaw (GE Capacitor Department), the GE Dielectric Materials Laboratory and other technical information sources will be utilized in assessing the fluids and photochromics.

3.0 PERFORMANCE REQUIREMENTS

3.1 General

The goals of the dielectric fluid survey are to identify a dielectric fluid which will:

- 1) permit an increase (~5-10 x) in the value of the dielectric body force, g_E , over that currently achievable in the GFFC.

L. R. Eaton G. Fogal S. Neste W. Yager	PAGE NO.	RETENTION REQUIREMENTS	
	1 OF 3	COPIES FOR	MASTERS FOR
		<input type="checkbox"/> 1 MO.	<input type="checkbox"/> 3 MOS.
		<input type="checkbox"/> 3 MOS.	<input type="checkbox"/> 6 MOS.
		<input type="checkbox"/> 6 MOS.	<input type="checkbox"/> 12 MOS.
		<input type="checkbox"/> MOS.	<input type="checkbox"/> MOS.
		<input type="checkbox"/>	<input type="checkbox"/> DO NOT DESTROY

- 2) be compatible with a photochromic material and permit the flow visualization principle used in the GFFC to be used for the AGCE.

3.2 Dielectric Constant

A dielectric constant greater than 2.2 is required with a value greater than 40 desired. The upper value acceptable may be limited by other parameter requirements such as dissipation factor.

3.3 Dissipation Factor

The fluid dissipation factor must be minimized so that the fluid heating rate does not exceed $0.001^{\circ}\text{C}/\text{sec}$. Values of fluid dissipation factor are not readily available in the literature due to their dependence on fluid purity. The values of dissipation factor for candidate fluids may have to be measured (GE Dielect. Materials Laboratory), and therefore will be limited to two or three fluids.

3.4 Electrical Volume Resistance

This parameter is also highly dependent on fluid purity and will be measured for 2 or 3 fluids (GE Dielectric Materials Laboratory). The objective is to minimize fluid heating as given in Paragraph 3.3.

3.5 Dielectric Strength

Comments of 3.3 and 3.4 apply here also. The goal is a dielectric strength factor of 2 above that required to sustain the impressed voltage, a maximum of 30 kv.

3.6 Viscosity

Values of viscosity less than 1 cp are desired with a maximum of 3 cp acceptable.

3.7 Coefficient of Volume Expansion

A value of the coefficient of volume expansion will be sought which is compatible with the optical detection concept and a minimum temperature gradient of $0.1^{\circ}\text{C}/\text{cm}$ with a 10% uncertainty.

3.8 Photochromic Fade Time

Photochromic fade times of 1 to 2 minutes will be sought.

4.0 INPUTS REQUIRED

Priority of Parameters - A prioritization of the above parameters will be provided by NASA so that the relative importance of each parameter can be considered in selecting candidate fluids (c.f. PIR No. 1254-AGCE-08).

SAFETY

The fluid will be enclosed within the concentric hemisphere assembly which, in turn, is located within the confines of the gaseous nitrogen filled outer sealed enclosure.

Approved by: 
ACGE Program Manager

/c

*CLASS. LTR.	OPERATION	PROGRAM	SEQUENCE NO.	REV. LTR.
U	1254	AGCE	028	
*USE "C" FOR CLASSIFIED AND "U" FOR UNCLASSIFIED				

PROGRAM INFORMATION REQUEST / RELEASE

FROM	TO		
S.L. Neste	Distribution		
DATE SENT	DATE INFO. REQUIRED	PROJECT AND REQ. NO.	REFERENCE DIR. NO.
6/5/81			

SUBJECT
 PARAMETRIC REPRESENTATION OF AGCE VARIABLES

INFORMATION REQUESTED/RELEASED

1.0 SUMMARY

Two important considerations for the AGCE include the fluid heating rate and the dielectric body force as discussed in PIR No. 1254-AGCE-014A and -015, respectively. The equations describing these quantities contain common variables which allow several parametric analyses to be performed and used as a guide in assessing the AGCE performance. Definitions of the relevant parameters, the equations relating these parameters, the resulting parametric plots and examples of their use are provided. The families of curves presented herein are intended to be used as tools in selecting a feasible set of operating conditions for the AGCE.

2.0 VARIABLE DEFINITIONS AND RELEVANT EQUATIONS

Definitions of variables required for a partial theoretical evaluation and assessment of the AGCE are given below. The variables are listed in the approximate order of usage in the equations which follow.

- P_d = power dissipated in the fluid per unit volume (watts/m³)
- σ = fluid conductivity ($\Omega^{-1} m^{-1}$)
- E = applied electric field (volts/m)
- ω = electric field frequency (rad/sec) = $2\pi f$
- f = frequency (Hz)
- ϵ_0 = dielectric constant of free space (8.85×10^{-12} farad/m)
- K = relative dielectric constant

G. Foga1 R. Homsey S. Neste	PAGE NO. 1 OF 9	RETENTION REQUIREMENTS	
		COPIES FOR	MASTERS FC
		<input type="checkbox"/> 1 MO.	<input type="checkbox"/> 3 MOS.
		<input type="checkbox"/> 3 MOS.	<input type="checkbox"/> 6 MOS.
		<input type="checkbox"/> 6 MOS.	<input type="checkbox"/> 12 MOS.
		<input type="checkbox"/> MOS.	<input type="checkbox"/> MOS.
		<input type="checkbox"/>	<input type="checkbox"/> DONOT DESTROY

$\tan \delta$ = fluid dissipation factor

r_i = outer radius of inner sphere (m)

r_o = inner radius of outer sphere (m)

V = applied voltage (volts), $E = V/(r_o - r_i)$

\dot{T} = fluid heating rate ($^{\circ}\text{C}/\text{sec}$)

C_p = fluid heat capacity (joules/ $\text{Kg}^{\circ}\text{C}$)

ρ_o = fluid density (Kg/m^3)

P_d^T = total power dissipated in the fluid (watts)

γ = thermal coefficient of dielectric constant ($^{\circ}\text{C}^{-1}$)

α = thermal coefficient of volume expansion ($^{\circ}\text{C}^{-1}$)

g_E = dielectric body force (g's or m/sec^2)

POWER DISSIPATED PER UNIT VOLUME

$$P_d = \sigma E^2 (\text{watts}/\text{m}^3)$$

$$= \omega K \epsilon_o \tan \delta E^2$$

$$= 2\pi f K \epsilon_o \tan \delta \frac{V^2}{(r_o - r_i)^2}; f = 300 \text{ Hz}, r_o = .06\text{m}, r_i = .05\text{m}$$

$$P_d = 1.67 \times 10^{-4} K \tan \delta V^2 (\text{watts}/\text{m}^3) \quad (1)$$

HEATING RATE

$$\dot{T} = \frac{P_d}{C_p \rho_o}$$

$$= \frac{1.67 \times 10^{-4} K \tan \delta V^2}{C_p \rho_o}; C_p \approx 2 \times 10^3 \text{ joules}/\text{Kg}^{\circ}\text{C}$$

$$\rho_o \approx 10^3 \text{ Kg}/\text{m}^3$$

$$\dot{T} = 8.4 \times 10^{-11} K \tan \delta V^2 \quad (2)$$

VOLUME OF FLUID CELL

$$\begin{aligned} \text{Vol.} &= \frac{4/3\pi}{2} (r_o^3 - r_i^3); r_o = .06\text{m}, r_i = .05\text{m} \\ &= 1.9 \times 10^{-4} (\text{m}^3) \end{aligned}$$

TOTAL POWER DISSIPATED

$$\begin{aligned} P_d^T &= P_d \times \text{Vol.} \\ &= 1.67 \times 10^{-4} K \tan \delta V^2 (1.9 \times 10^{-4}) \\ &= 3.17 \times 10^{-8} K \tan \delta V^2 \text{ (watts)} \end{aligned} \quad (3)$$

DIELECTRIC BODY FORCE

$$\begin{aligned} g_E &= \frac{2\epsilon_o K \gamma}{\alpha \rho_o} \left(\frac{r_i r_o}{r_o - r_i} \right)^2 \cdot \frac{V^2}{r^5}; \left. \begin{array}{l} \gamma = 0.0035 \text{ } ^\circ\text{C}^{-1} \\ \alpha = 0.00088 \text{ } ^\circ\text{C}^{-1} \\ \rho_o = 10^3 \text{ Kg/m}^3 \\ r = 0.055 \text{ m} \end{array} \right\} \text{DMSO} \\ &= 1.27 \times 10^{-8} K V^2 (\text{m/s}^2) \\ &= 1.29 \times 10^{-9} K V^2 (\text{g's}) \\ K &= 7.7 \times 10^8 g_e V^{-2} \end{aligned} \quad (4)$$

$$\begin{aligned} \frac{g_E}{P_d^T} &= \frac{4.1 \times 10^{-2}}{\tan \delta} \\ g_E &= 4.1 \times 10^{-2} \frac{P_d^T}{\tan \delta} \end{aligned} \quad (5)$$

Two assumptions in the above equations limit their unconditional application to the assessment of the AGCE performance. The total fluid volume is determined by hemispheres with radii of 0.05 and 0.06 meters and thus the total power dissipated (Equation 3) will change for other configurations. Also, note that Equation 6 assumes values of α and γ for DMSO. Although, as indicated in PIR 1254-AGCE-015 (page 5), the values of α and γ do not change greatly for high dielectric constant fluids, caution should be used in applying this equation to other fluids.

3.0 PARAMETRIC PLOTS

Figures 1 through 5 are parametric plots of Equations (2) through (6) and provide a quick means of assessing the effect of changing the experiment requirements. For example, suppose a value of $g_E = 5g$ is required without exceeding either a fluid heating rate of $0.001^\circ\text{C}/\text{sec}$ or a voltage of 15 Kv. For these conditions, Figures 1, 2 and 3 give values of $P_d^T \approx 0.38$ watts, $\tan\delta = 0.003$ and $K \approx 17.5$, respectively. In other words, a fluid with a dielectric constant of ~ 17.5 which has been purified to give a dissipation factor of 0.003 will meet the required conditions. If the maximum allowable voltage is reduced to 10 Kv then a higher fluid dielectric constant of ~ 38 is required (Figure 3).

As a second example, suppose a fluid with a dielectric constant of 40 can be purified to give a dissipation factor of 0.001. Figures 4 and 5 then give heating rates and total power dissipations of $\sim 0.0007^\circ\text{C}/\text{sec}$ and 0.29 watts, respectively ($V = 15$ Kv) and Figure 2 indicates that a value of $g_E \approx 10.5$ g can then be achieved.

Thus, given the operating requirements of the AGCE, the required fluid characteristics can be determined, or alternatively, if the fluid characteristics are known, the AGCE performance can be evaluated as a function of applied voltage.

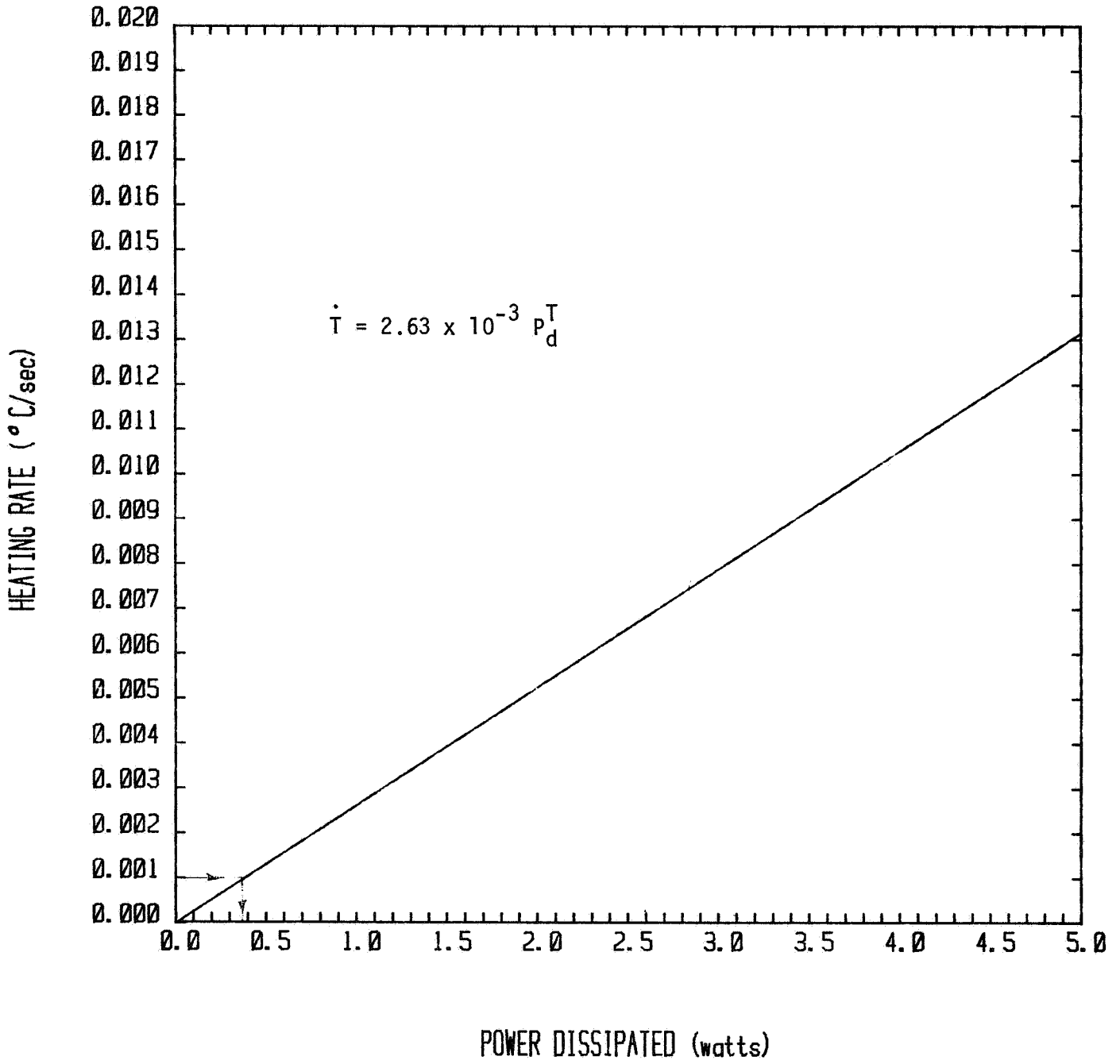


Figure 1. Fluid Heating Rate as a Function of Total Power Dissipated.

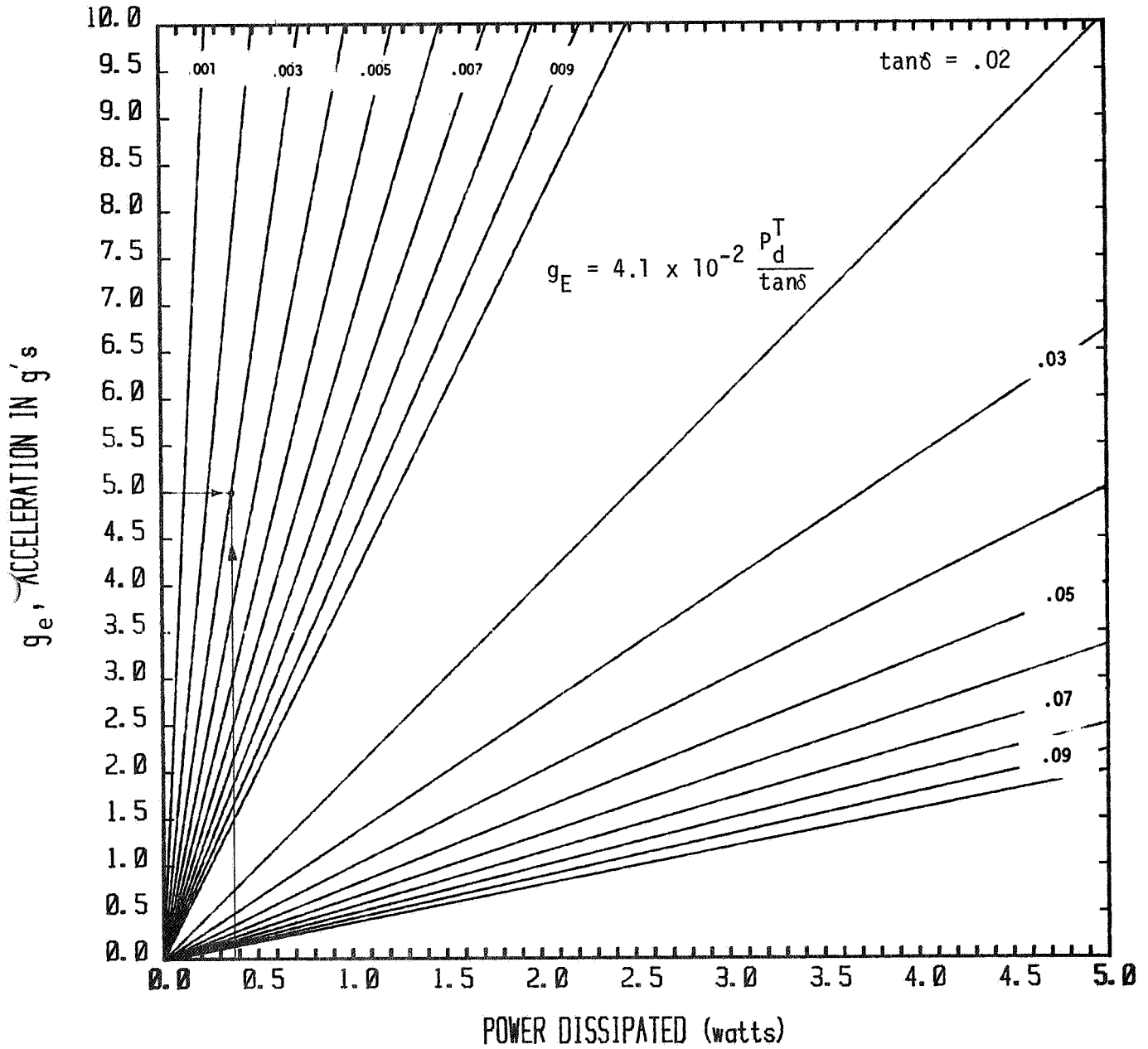


Figure 2. Attainable values of g_e as a function of total power dissipated and fluid dissipation factor.

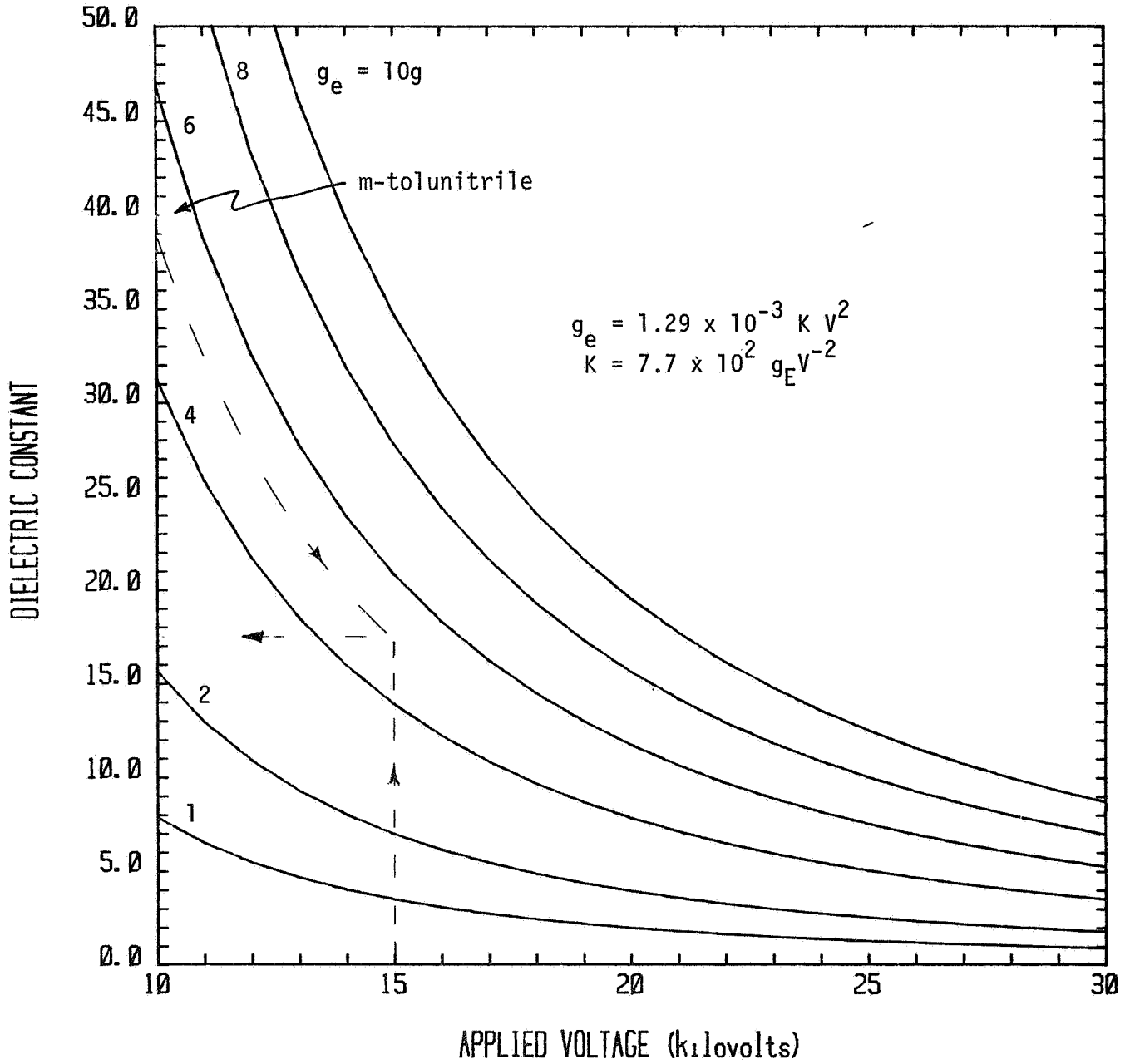


Figure 3. Values of applied voltage and dielectric constant required to achieve specified values of g_e .

ORIGINAL PAGE IS
OF POOR QUALITY

————— $\tan \delta = 0.01$
- - - - - $\tan \delta = 0.001$

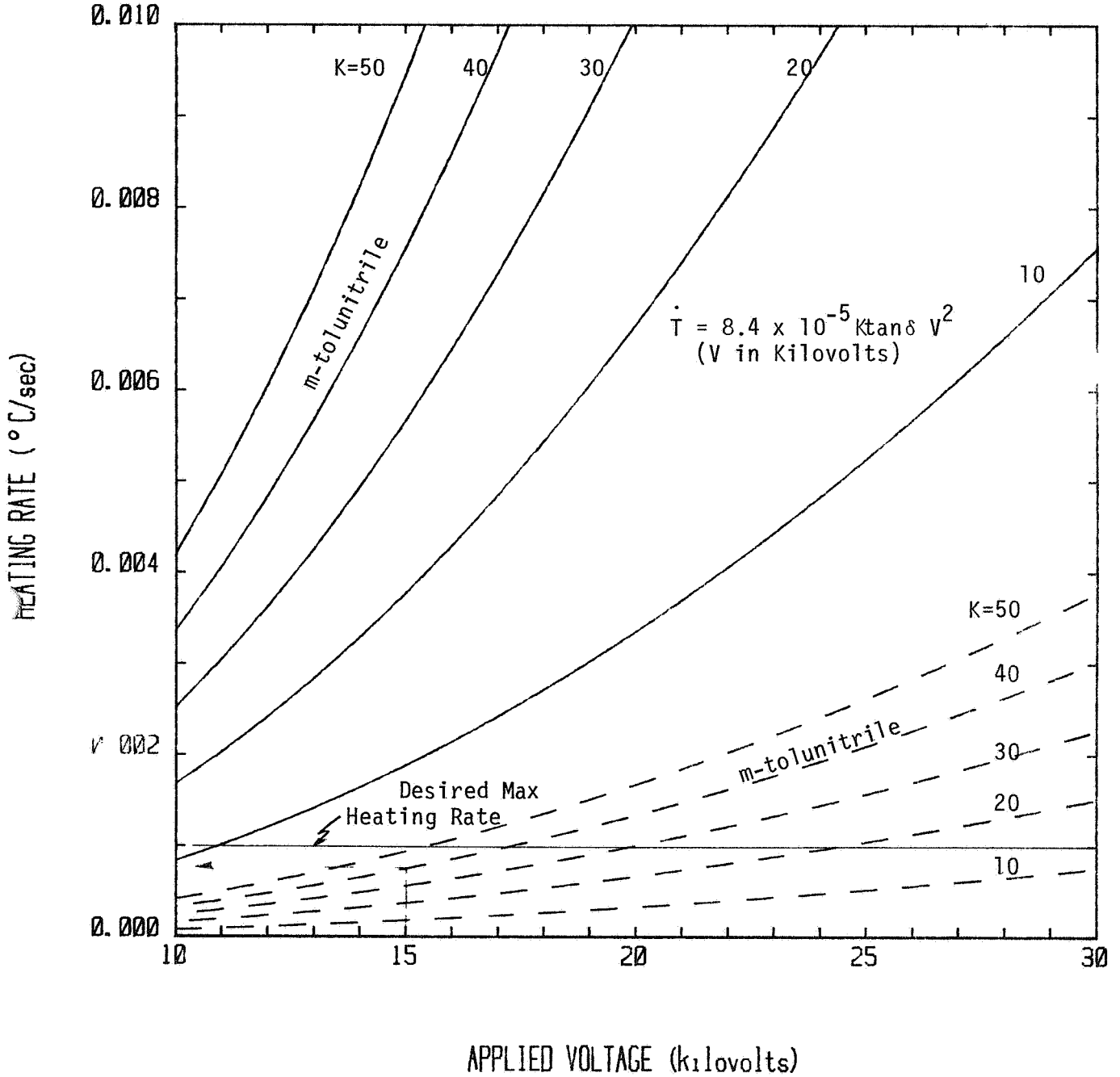


Figure 4. Fluid heating rate as a function of applied voltage for specified values of dielectric constant (K) and dissipation factor ($\tan \delta$).

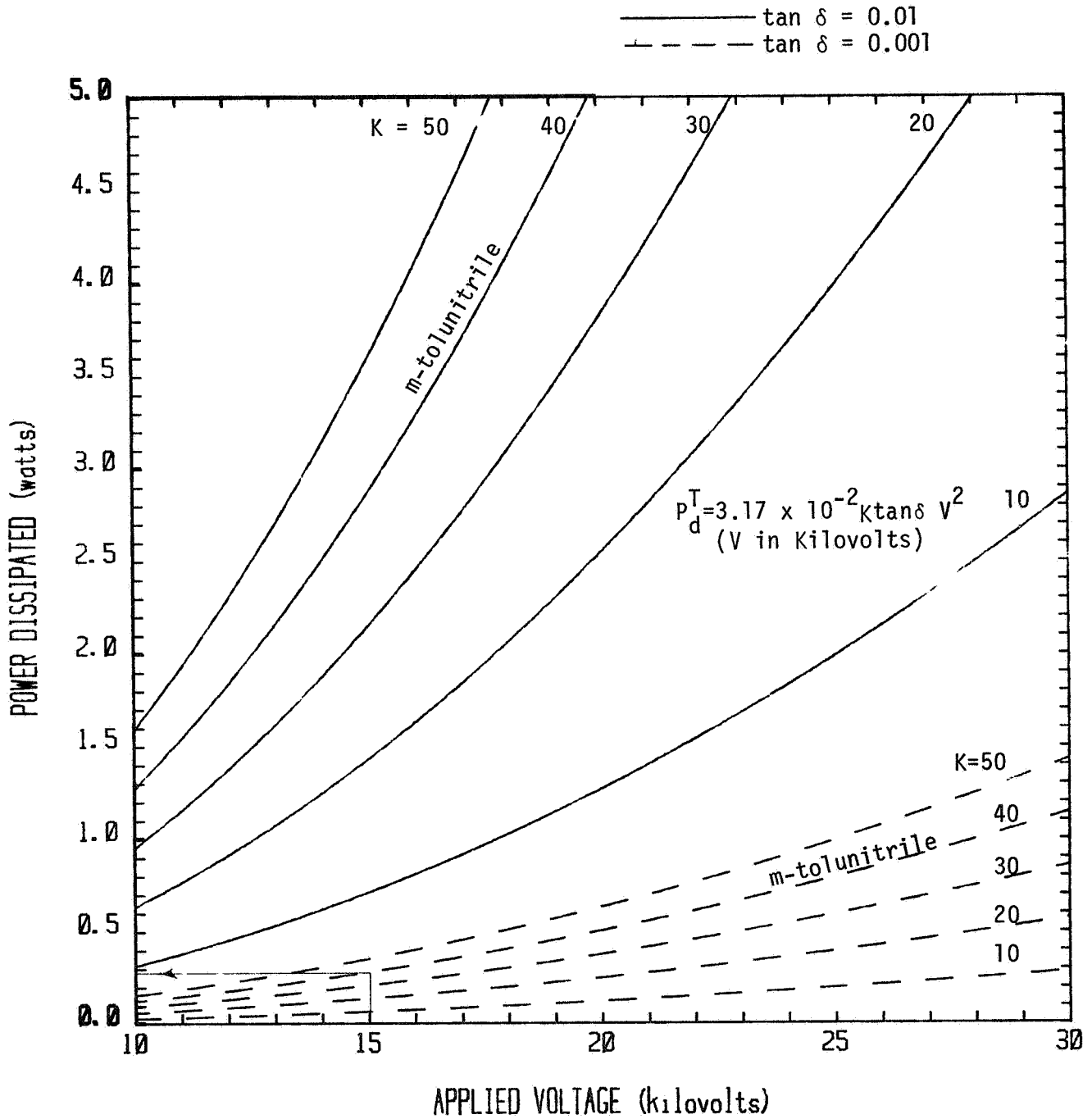


Figure 5. Total power dissipated as a function of applied voltage for specified values of dielectric constant (K) and dissipation factor ($\tan \delta$).

PROGRAM INFORMATION REQUEST / RELEASE

*USE "C" FOR CLASSIFIED AND "U" FOR UNCLASSIFIED

FROM S.L. Neste	TO
--------------------	----

DATE SENT 5/7/81	DATE INFO. REQUIRED	PROJECT AND REQ. NO.	REFERENCE DIR. NO.
---------------------	---------------------	----------------------	--------------------

SUBJECT
Task 1 - Dielectric Heating Due to Electrical Power Dissipation

INFORMATION REQUESTED/RELEASED

1.0 SUMMARY

The dielectric heating caused by an applied AC voltage was calculated for ranges of dielectric constant and dissipation factor assuming the nominally agreed upon values (PIR No. 1254-AGCE-008) for AGCE electrical and geometrical parameters. The values assumed are as follows:

- Outer radius inner sphere - 5.0 cm
- Inner radius outer sphere - 6.0 cm
- Applied AC voltage - 20 kV RMS
- AC frequency - 300 Hz

The analytical results indicate that the major parameters controlling the fluid heating rate (T) are the applied voltage and the fluid dissipation factor. Using the parameter values listed above, and assuming a dielectric constant of 40, a dissipation factor of ~0.003 will be necessary to maintain fluid heating below 0.001°C/sec. The difficulties of obtaining a high dielectric constant fluid (i.e., polar liquid) of sufficient purity to achieve and maintain this low dissipation are very difficult, although perhaps not impossible. Applicable purification and measurement procedures are discussed in PIR No. 1254-AGCE-021.

2.0 BACKGROUND

The AGCE Statement of Work (SOW) listed several characteristics which the "ideal" dielectric fluid should possess. Most of the values listed were for the Dow Corning 200 oil used in the GFFC with the exception of the dielectric constant for which a factor of 20 increase is desired. The key parameters identified in the SOW and the desired values are given on the following page.

G. Fogal R. Homsey S. Neste	PAGE NO.	<input checked="" type="checkbox"/> RETENTION REQUIREMENTS	
	OF	COPIES FOR	MASTERS FOR
		<input type="checkbox"/> 1 MO.	<input type="checkbox"/> 3 MOS
		<input type="checkbox"/> 3 MOS.	<input type="checkbox"/> 6 MOS.
		<input type="checkbox"/> 6 MOS.	<input type="checkbox"/> 12 MOS.
		<input type="checkbox"/> MOS.	<input type="checkbox"/> MOS.
		<input type="checkbox"/>	<input type="checkbox"/> DO NOT DESTROY

- 1) Dielectric Constant: $>40\epsilon_0$. However, any value greater than $2.2 \epsilon_0$ will be helpful (ϵ_0 = dielectric constant of free space = 8.85×10^{-12} farad/meter).
- 2) Dissipation Factor: 4×10^{-5} in the frequency range around 500 Hz. The heating rate should not exceed $0.001^\circ\text{C}/\text{sec}$.
- 3) Electrical Volume Resistance: 1×10^{14} ohm cm. A lower value might be satisfactory to maintain the heating rate below $0.001^\circ\text{C}/\text{sec}$.
- 4) Dielectric Strength: >50 volts/mil. The required value will depend on the sphere separation and voltage level. For the nominal values of 20 kV and 1 cm separation, a rating of ~ 51 volts/mil would be required at 1 cm. Translating this requirement to the standard rating, usually measured for a separation of 0.1 inch, yields a value of ~ 102 volts/mil (dielectric strength is inversely proportional to square root of dielectric thickness).
- 5) Viscosity: <5 centipoise. Preferably <1 centipoise. More recently (PIR No. 1254-AGCE-09) the upper limit has been fixed at 3 cp.
- 6) Coefficient of Volume Expansion: $>1 \times 10^{-4}^\circ\text{C}^{-1}$.
- 7) Transparency: Clear or almost clear. In addition, the fluid must be compatible with a photochromic dye to permit implementation of the flow visualization technique.

Realistically, the above parameter values probably cannot be achieved in any fluid and hence relaxation trade-offs will be required. For example, the high dielectric constant and the high resistivity values desired are physically incompatible in a single fluid. However, a parameter more relevant than the resistivity alone is the fluid heating or power dissipation which results. Section 3.0 discusses the expected power dissipation and fluid heating as a function of fluid dissipation factor and resistivity (items 2 and 3 above) and provides a guide for determining realistic values of dissipation factor to impose on the fluid.

3.0 TASK IMPLEMENTATION

Two derivations for an expression relating the fluid heating rate to the applied electric field, and the fluid dissipation factor are given below. Both approaches yield the same final expression and provide a relationship between the fluid dissipation factor and the fluid conductivity.

Fluid Heating Rate - First Approach

One of the key parameters required to assess the dielectric fluid heating produced by an applied AC voltage is the power factor (δ), which is defined as: the ratio of the total power (in watts) flowing in an electrical circuit to the total equivalent volt-amperes flowing in that circuit. In normal dielectrics it is exactly equal to (Tweney and Hughes, 1967):

$$\delta = \frac{G}{\sqrt{G^2 + \omega^2 C^2}} \quad (1)$$

where: G = conductance of the dielectric (ohm^{-1})
 $= 1/R$ where R is the dielectric resistance in ohm
 ω = frequency of the impressed AC voltage (rad-sec^{-1})
 $= 2\pi f$ where f is the voltage frequency in Hz
and C = capacitance (farads)

The resistance (R) and capacitance (C) of a concentric sphere assembly as proposed for AGCE are given by:

$$R = \rho \frac{(r_1 - r_2)}{4\pi r_1 r_2} \quad (2)$$

$$\approx \pi d/A$$

and
$$C = \frac{4\pi K \epsilon_0 r_1 r_2}{r_1 - r_2} \quad (3)$$

$$\approx K \epsilon_0 A/d$$

where: r_1 = radius of the outer sphere
 r_2 = radius of the inner sphere

Page four

- ρ = resistivity of dielectric (ohm-m)
 A = $4\pi r_1 r_2$
 d = $r_1 - r_2$
 ϵ_0 = dielectric constant of free space (8.85×10^{-12} farads/m)
 K = dielectric constant of material relative to ϵ_0

Writing Equation (2) in terms of the conductivity $\sigma (=1/\rho)$ gives:

$$G = \frac{4\pi r_1 r_2}{r_1 - r_2} \sigma. \quad (4)$$
$$\approx A\sigma/d$$

Equations (3) and (4) can be substituted in Equation (1) and reduced by cancellation of like terms to give the simplified expression for the power factor as:

$$\delta = \frac{\sigma}{\sqrt{\sigma^2 + \omega^2 K^2 \epsilon_0^2}} \quad (5)$$

For values of $\delta < 0.1$ (the region of interest for AGCE) the power factor may be considered equal to the dissipation factor (Reference Data for Radio Eng., 1967).

The rate of energy dissipation per unit volume due to the sinusoidal electric stress within the dielectric is given by Tweney and Hughes (1967) as:

$$P = \omega C V^2 \delta \quad (6)$$

The dissipated energy will raise the temperature of the total fluid by:

$$mC_p(\text{joules}/^\circ\text{C}) \quad (7)$$

where C_p is the heat capacity of the fluid (joules/Kg $^\circ$ C) and m is the total mass of the fluid.

Substituting $K\epsilon_0 A/d$ for C , and Ed for V , respectively, in Equation 6 and dividing the resulting equation by mC_p gives the rate of rise of the fluid temperature \dot{T} :

$$\begin{aligned}
 \dot{T} &= \frac{\omega K \epsilon_0 E_0^2 \delta (Ad)}{m C_p} \\
 &= \frac{\omega K \epsilon_0 E_0^2 \delta}{\rho_0 C_p} \\
 &= \frac{(\omega K \epsilon_0 \delta) E_0^2}{\rho_0 C_p} \quad (^\circ\text{C}/\text{sec}) \quad (8)
 \end{aligned}$$

Fluid Heating Rate - Alternate Approach

The dielectric heating associated with an electric field of amplitude E_0 can also be derived from the expression for the power absorbed per unit volume (von Hippel, 1966) as:

$$P = \frac{\sigma E_0^2}{2} \quad [\text{watt}/\text{m}^3] \quad (9)$$

The parameter σ is an equivalent dielectric conductivity which sums over all dissipative effects and represents any ohmic conductivity caused by migrating charge carriers as well as any energy loss associated with a frequency dependence of the dielectric constant, ϵ' , such as the friction accompanying the orientation of dipoles. Replacing E_0 by its RMS equivalent ($E = E_0/\sqrt{2}$) gives:

$$P = \sigma E^2 \quad (10)$$

Derivations of loss tangent (dissipation factor), and equivalent dielectric conductivity are given by von Hippel (see Appendix) and only the results will be given below.

$$\text{Loss Tangent: } \tan \delta = \frac{\text{loss factor}}{\text{dielectric constant}} \frac{\epsilon''}{\epsilon'} \quad (11)$$

$$\text{Effective Conductivity: } \sigma = \omega \epsilon'', \text{ angular frequency} \times \text{loss factor} \quad (12)$$

$$\text{Relative Dielectric Constant: } K = \frac{\epsilon'}{\epsilon_0} \quad (13)$$

where ϵ_0 = dielectric constant of a vacuum (8.85×10^{-12} Farad/meter).

Combining Equations (11), (12) and (13) gives an expression for the effective conductivity as:

$$\sigma = \omega K \epsilon_0 \tan \delta \quad (14)$$

and the power dissipation per unit volume (Equation 10) becomes:

$$P = \omega K \epsilon_0 \tan \delta E^2 \text{ [watts/m}^3\text{]} \quad (15)$$

Dividing Equation (15) by the product of the fluid heat capacity and density (i.e., $C_p \rho_0$ [joules/m³ °C]) gives the heating rate of the dielectric fluid as:

$$\dot{T} = \frac{(\omega K \epsilon_0 \tan \delta) E^2}{C_p \rho_0} \text{ (}^\circ\text{C/sec)} \quad (16)$$

which is identical to Equation (8), for $\delta < 0.1$.

The parameter usually measured to determine the quality of dielectric fluids is the dissipation factor ($\tan \delta$), rather than the DC resistivity (conductivity), since the latter changes with time due to "plating out" of charge carrying impurities. Thus, the dissipation factor will also be used as the indicator of fluid quality for AGCE applications.

Equation (16) and the parameter values below give the fluid heating rate as a function of applied voltage as shown in Figure 1. The ranges of dielectric constant and dissipation factor are intended to bracket values attainable for the AGCE. The resulting curves can be used to aid in the selection of the operating voltage given the dielectric constant and the achievable dissipation factor for a fluid. For example, assuming that m-tolunitrile which has a value of $K \approx 40$ can be purified to attain a $\tan \delta$ of 0.001, then operating voltages up to ~ 17 Kv could be used without exceeding the desired maximum heating rate of 0.001°C/sec . However, using a voltage of 10 Kv would permit a dissipation factor of ~ 0.003 without exceeding the 0.001°C/sec fluid heating rate. A similar easing of requirements on the dissipation factor and the fluid purification process can be achieved by operating at a lower frequency (see Equation 16).

$$\begin{aligned} E &= 100V \text{ (volts/m), for } r_1 = 0.06, r_2 = 0.05 \\ &= 10^5 V, V \text{ in kilovolts} \end{aligned}$$

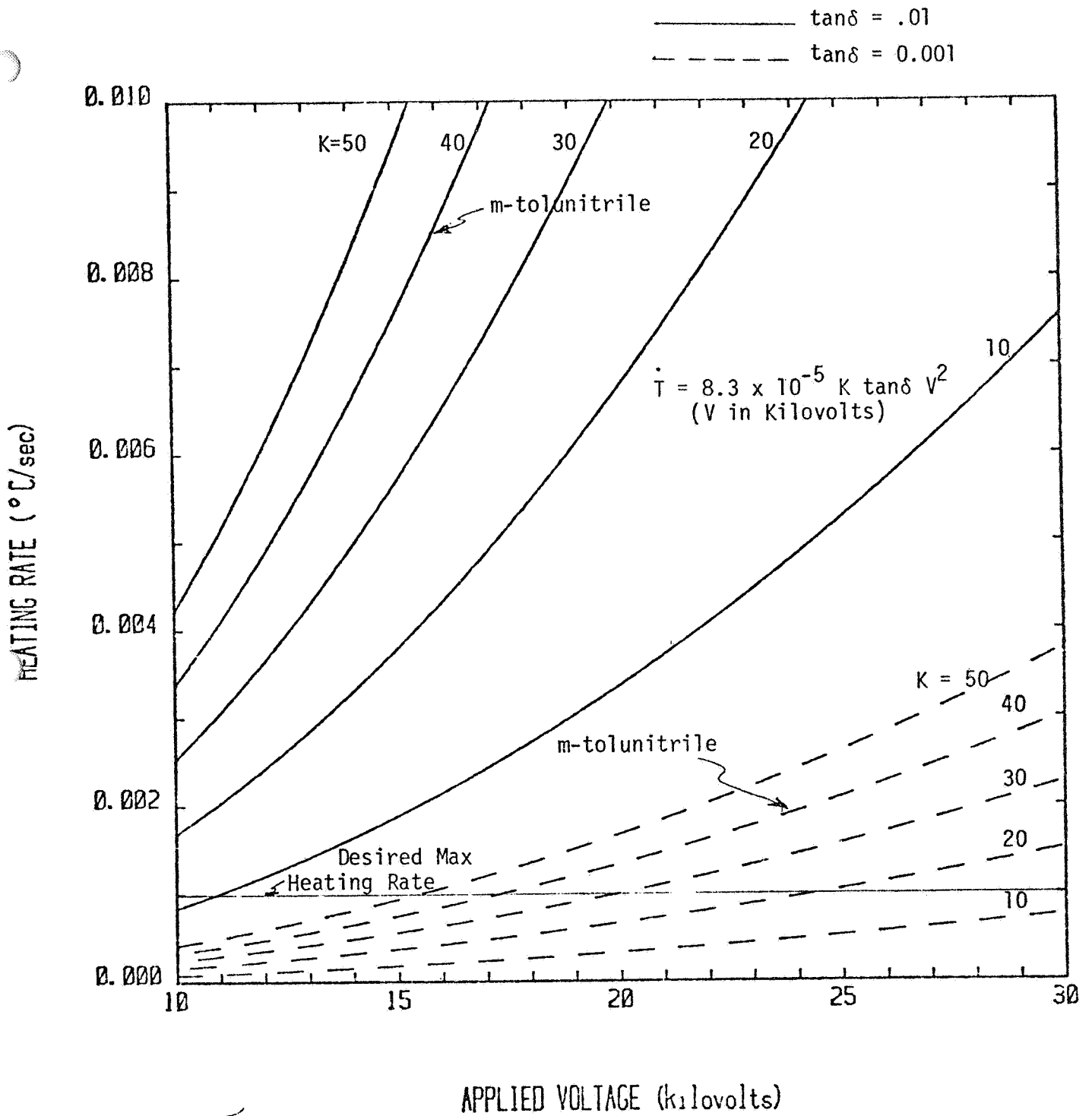


Figure 1. Fluid Heating Rate as a Function of Applied Voltage for Selected Values of Dielectric Constant (K) and Dissipation Factor ($\tan\delta$).

$$\begin{aligned}\omega &= 1885 \text{ rad/sec (for } f = 300 \text{ Hz)} \\ \epsilon_0 &= 8.85 \times 10^{-12} \text{ farad/meter} \\ \rho_0 &\approx 10^3 \text{ Kg/m}^3 \\ C_p &\approx 2 \times 10^3 \text{ joule/Kg } ^\circ\text{C}\end{aligned}$$

As indicated in the above discussion, it is a rather straightforward procedure to determine the anticipated fluid heating if the fluid characteristics and operating conditions are well defined. However, the process of achieving, measuring and maintaining the fluid purity levels, i.e., low dissipation, needed for the AGCE, requires further investigation. This area is discussed in PIR No. 1254-AGCE-021.

4.0 RECOMMENDATIONS

The following steps will be taken to aid in the assessment and selection of fluids for the AGCE application:

- 1) Determine reasonable dissipation factors to be expected for highly polar fluids, in particular, DMSO and m-tolunitrile. Consideration must be given to purification requirements (are they feasible for AGCE) and long term (several months) degradation of the fluid.
- 2) Identify other fluids for which required dissipation factors can be achieved with some sacrifice in dielectric constant and assess the compatibility of these fluids with a photochromic dye.
- 3) Calculate the expected value of g_E for a typical high dielectric constant fluid (e.g., DMSO) so that a parameter trade-off can be performed to determine if any requirements can be relaxed.

The first two steps above will utilize extensive interaction with experts in the dielectric fluid and photochromic dye areas while the third step can be performed independently.

References

Tweney, C.F. and L.E.C. Hughes, ed., Chamber's Technical Dictionary, The MacMillan Company, New York, 1967.

Reference Data for Radio Engineers, 4th edition, International Telephone and Telegraph Corp., 1967.

von Hippel, A.R., Dielectrics and Waves, The M.I.T. Press, Cambridge, MA, 1966.

APPENDIX

PERTINENT INFORMATION ON DIELECTRIC DISSIPATION AND HEATING FROM:

von HIPPEL, A.R., DIELECTRICS AND WAVES, THE MIT PRESS,
CAMBRIDGE, MA, 1966.

pearance of one pair of field components when the wave is reflected at Brewster's angle, and the occurrence of total reflection accompanied by the formation of a guided surface wave with longitudinal components (Sec. 16). At normal incidence, standing waves (Sec. 17) and useful methods of measuring dielectric properties by interference (Sec. 18) result.

When electromagnetic waves strike a metal, nearly total reflection ensues, and the weak transmitted beam is rapidly attenuated (Sec. 19). The general case of oblique incidence on media with loss is of great complexity. The index of refraction becomes a function of the angle of incidence, and complicated phase shifts arise because of the appearance of longitudinal field components (Sec. 20).

Viewed from an alternative standpoint, the incident wave, striking a boundary obliquely, forms, with the reflected wave, an interference pattern which glides along the interface with a phase velocity greater than that of the incident wave; the boundary acts as a wave guide. To make such a guide more effective, a second boundary may be placed parallel to the first one in one of the dark interference fringes, and a parallel-plane wave guide with cut-off properties results (Sec. 21). By completing the enclosure we obtain hollow wave guides which behave like highly dispersive dielectrics and propagate characteristic wave types (Sec. 22). Dielectrics

can be measured in such wave guides with great precision, whether by mapping with a traveling detector the standing-wave pattern formed in front of the sample (Sec. 23) or by evaluating the effect of the material on the impedance of a cavity resonator (Sec. 24).

Frequently it proves convenient to handle field phenomena by an equivalence approach, in which the role of the electric and the magnetic fields is assumed by voltages and currents in electric circuits. By introducing this complementarity we return to distributed and lumped-circuit concepts (Sec. 25) and close the macroscopic discussion with a formalistic representation of dielectrics by lumped equivalent circuits (Sec. 26).

Summarizing: Part I of this book introduces the complex permittivity and permeability as the fundamental parameters, develops in rapid succession the essential field concepts, considers the propagation of electromagnetic waves in unbounded space and under successively more stringent boundary conditions. In the course of this treatment we are logically led to alternative ways of describing the interaction between fields and matter and to conversion formulas interlinking the various parameters. In addition to this quantitative description of fields and dielectrics, the macroscopic theory provides a quantitative basis for measuring ϵ^* and μ^* .

1 Complex Permittivity and Permeability

A capacitor, connected to a sinusoidal voltage source

$$V = V_0 e^{j\omega t} \quad (1.1)$$

of the angular frequency

$$\omega = 2\pi\nu \quad (1.2)$$

stores, when vacuum is its dielectric, a charge

$$Q = C_0 V, \quad (1.3)$$

† Throughout this book we will use complex quantities in treating periodic phenomena and represent them in the complex plane. Here the x -axis corresponds to the axis of reals and the y -axis to the axis of imaginaries. The factor $j = \sqrt{-1}$ in front of a real quantity signifies an imaginary component oriented in the $+y$ -axis or $+j$ -axis direction. A complex quantity $z = x + jy$ plotted in the complex plane corresponds in polar co-ordinates to a radius vector $\rho = \sqrt{x^2 + y^2}$ inclined by an angle $\theta = \tan^{-1}(y/x)$ towards the real axis: $z = \rho e^{j\theta}$.

The complex function $V = V_0 e^{j\omega t} = V_0(\cos \omega t + j \sin \omega t)$ consequently can be plotted in the complex plane as a radius vector of length V_0 , the voltage amplitude, making an angle of ωt radians with the axis of reals. As long as the voltage and current vectors rotate at the same angular velocity of ω radians per second, we

and draws a charging current

$$I_c = \frac{dQ}{dt} = j\omega C_0 V = I_0 e^{j(\omega t + \frac{\pi}{2})}, \quad (1.4)$$

leading the voltage by a temporal phase angle of 90°

can forget this rotation in discussing their relative positions in the complex plane.

We return from the complex functions to actual currents and voltages by taking the real or the imaginary part: $\text{Re}(V) = V_0 \cos \omega t$, $\text{Im}(V) = V_0 \sin \omega t$. In dealing with products of complex functions it has to be kept in mind that the product of the real parts of two complex quantities A_1 and A_2 is not equal to the real part of their product, but

$$\text{Re}(A_1) \text{Re}(A_2) = \frac{1}{2}(A_1 + \bar{A}_1)(A_2 + \bar{A}_2).$$

The symbol \bar{A}_1 signifies the conjugate of A_1 ; for example, if $A_1 = (x + jy)e^{j\omega t}$, then $\bar{A}_1 = (x - jy)e^{-j\omega t}$.

The time average of a periodic function A is $\bar{A} = \frac{1}{T} \int_0^T A dt$, where T is the period of the function. If A_1 and A_2 are such functions, the product of the averages of their real parts is $\text{Re}(A_1) \text{Re}(A_2) = \frac{1}{2} \text{Re}(A_1 \bar{A}_2)$.

(Fig. 1.1). C_0 is the vacuum (or geometrical) capacitance of the condenser.

When filled with some substance, the condenser increases its capacitance to

$$C = C_0 \frac{\epsilon'}{\epsilon_0} = C_0 \kappa', \quad (1.5)$$

where ϵ' and ϵ_0 designate the real permittivities or dielectric constants of the dielectric and of vacuum, respectively, and their ratio κ' the relative dielectric constant of

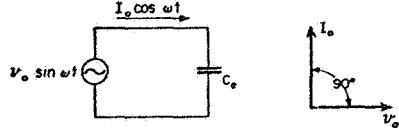


Fig. 1.1. Current-voltage relation in ideal capacitor.

the material. Simultaneously, there may appear, in addition to the charging current component I_c , a loss current component

$$I_l = GV \quad (1.6)$$

in phase with the voltage: G represents the conductance of the dielectric. The total current traversing the condenser,

$$I = I_c + I_l = (j\omega C + G)V, \quad (1.7)$$

is inclined by a power factor angle $\theta < 90^\circ$ against the applied voltage V , that is by a loss angle δ against the $+j$ -axis (Fig. 1.2).

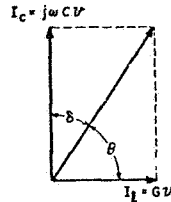


Fig. 1.2. Capacitor containing dielectric with loss.

It would be premature to conclude that the dielectric material corresponds in its electrical behavior to a capacitor paralleled by a resistor (RC circuit) (Fig. 1.3). The frequency response of this circuit, which can be expressed by the ratio of loss current to charging current, that is, the dissipation factor D or loss tangent $\tan \delta$, as

$$D \equiv \tan \delta = \frac{I_l}{I_c} = \frac{1}{\omega RC}, \quad (1.8)$$

may not at all agree with that actually observed because

the conductance term need not stem from a migration of charge carriers, but can represent any other energy-consuming process. It has therefore become customary to refer to the existence of a loss current in addition to a charging current noncommittally by the introduction of a complex permittivity

$$\epsilon^* = \epsilon' - j\epsilon'' \quad (1.9)$$

The total current I of Eq. 1.7 may thus be rewritten

$$I = (j\omega\epsilon' + \omega\epsilon'') \frac{C_0}{\epsilon_0} V = j\omega C_0 \kappa^* V, \quad (1.10)$$

where

$$\kappa^* \equiv \frac{\epsilon^*}{\epsilon_0} = \kappa' - j\kappa'' \quad (1.11)$$

is the complex relative permittivity of the material and

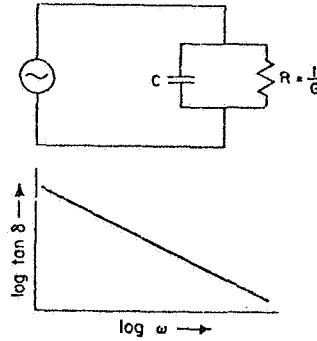


Fig. 1.3. RC circuit and its frequency response.

ϵ'' and κ'' the loss factor and relative loss factor, respectively. The loss tangent becomes

$$\tan \delta = \frac{\epsilon''}{\epsilon'} = \frac{\kappa''}{\kappa'} \quad (1.12)$$

Since a parallel-plate condenser of the area A and the plate separation d , fringing effects neglected, has the vacuum capacitance

$$C_0 = \frac{A}{d} \epsilon_0, \quad (1.13)$$

the current density J traversing a condenser under the applied field strength

$$E = V/d \quad (1.14)$$

becomes, according to Eq. 1.10,

$$J = (j\omega\epsilon' + \omega\epsilon'')E = \epsilon^* \frac{dE}{dt} \quad (1.15)$$

(Fig. 1.4). The product of angular frequency and loss factor is equivalent to a dielectric conductivity

$$\sigma = \omega \epsilon'' \quad (1.16)$$

This dielectric conductivity sums over all dissipative effects and may represent as well an actual ohmic conductivity caused by migrating charge carriers as refer

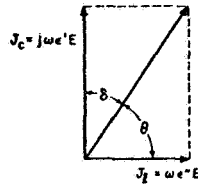


Fig. 1.4. Charging and loss current density.

to an energy loss associated with a frequency dependence (dispersion) of ϵ' , for example, to the friction accompanying the orientation of dipoles.

If the dielectric material is transferred from the electric field of the capacitor into the magnetic field of a coil, the voltage \mathcal{U} drives through the coil a magnetization current I_m according to Faraday's inductance law ($\mathcal{U} = L \frac{dI}{dt}$) as

$$I_m = \frac{\mathcal{U}}{j\omega L_0 \frac{\mu'}{\mu_0}} = -j \frac{\mathcal{U}}{\omega L_0 \kappa_m'} \quad (1.17)$$

L represents the inductance and L_0 the vacuum (or geometrical) inductance of the coil. This magnetization current lags behind the applied voltage by 90° (Fig. 1.5). The permeabilities μ' and μ_0 designate the mag-

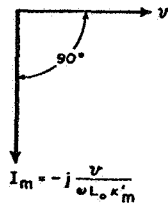


Fig. 1.5. Current-voltage relation in ideal inductor.

netization of the material and of vacuum, respectively, and their ratio

$$\kappa_m' \equiv \mu' / \mu_0 \quad (1.18)$$

the relative permeability of the material in which the magnetic field of the coil resides.

Because of the resistance R of the coil windings, an ohmic current component \mathcal{U}/R exists. In addition, there may appear, in phase with \mathcal{U} , a magnetic loss current I_l caused by energy dissipation during the magnetization cycle. We shall allow for this magnetic loss by introducing a complex permeability

$$\mu^* = \mu' - j\mu'' \quad (1.19)$$

and a complex relative permeability

$$\kappa_m^* = \frac{\mu^*}{\mu_0} = \kappa_m' - j\kappa_m'' \quad (1.20)$$

in complete analogy to the electric case. Thus we obtain the total magnetization current

$$\begin{aligned} I = I_m + I_l &= \frac{\mathcal{U}}{j\omega L_0 \kappa_m^*} \\ &= - \frac{j\mathcal{U}(\mu' + j\mu'')}{\omega \frac{L_0}{\mu_0} (\mu'^2 + \mu''^2)} \end{aligned} \quad (1.21)$$

According to these lumped-circuit considerations the macroscopic electric and magnetic behavior of a dielectric material in sinusoidal fields is determined by the two complex parameters ϵ^* and μ^*

The real and imaginary parts of these complex variables (ϵ' and ϵ'' or μ' and μ'') are even and odd functions, respectively, of the variable ω , that is, conjugate functions, and therefore not entirely independent of each other. Physically speaking, the mechanisms of energy storage and energy dissipation are two aspects of the same phenomenon, hence if one of them is given over the whole frequency spectrum, the other one is prescribed (see II, Fig. 19.1). Mathematically expressed, the calculation of an imaginary part (conjugate function) from a given real part [an arbitrary function $f(\omega)$] and, vice versa, is prescribed by the *Hilbert transforms*, known to physicists as *Kramers' theorem*.¹ This interrelation between the frequency response characteristics of dielectric constant and loss can sometimes prove helpful in checking the reliability of measurements but, in general, various polarization and conduction phenomena superpose and the available frequency range is insufficient for this type of unscrambling (see also Appendix A, I, 1).

¹ See, for example, E. A. Guillemin, *The Mathematics of Circuit Analysis*, John Wiley and Sons, New York, 1949, p. 339; H. Fröhlich, *Theory of Dielectrics*, Clarendon Press, Oxford, 1949, pp. 6 ff.

9 · Description of Dielectrics by Various Sets of Parameters

In Sec. 1 the response of a dielectric material to sinusoidal electric and magnetic fields was expressed by the two complex parameters ϵ^* and μ^* which determine the storage and dissipation of electric and magnetic energy in the medium. These parameters were derived from the amplitude and temporal-phase relations between voltage and current in capacitors and coils. It is now obvious that we are not restricted to using ϵ^* and μ^* , but may refer to alternate parameters that convey the same information.

The power engineer replaces the dielectric constant ϵ' and the loss factor ϵ'' by the combination of ϵ' and power factor $\cos \theta$; the radio engineer may choose ϵ' and the loss tangent $\tan \delta$, where

$$\tan \delta = \frac{\epsilon''}{\epsilon'} = \frac{\text{loss current}}{\text{charging current}} \quad \dagger \quad (9.1)$$

Frequently the inverse of the loss tangent, the quality factor Q of the dielectric,

$$\begin{aligned} Q &= \frac{1}{\tan \delta} = \frac{\omega \epsilon' E_0^2}{\omega \epsilon'' E_0^2} \\ &= 2\pi \nu \frac{\frac{1}{2} \epsilon' E_0^2}{\frac{1}{2} \sigma E_0^2} = 2\pi \frac{\text{av energy stored per half cycle}}{\text{energy dissipated per half cycle}} \\ &= \left[\frac{\text{reactive v-amp}}{\text{watts}} \right] \end{aligned} \quad (9.2)$$

serves as the *figure of merit*, especially in wave-guide problems. An engineer interested in dielectric heating will probably refer to ϵ' and the *dielectric conductivity*

$$\sigma = \omega \epsilon'' \quad [\text{ohm}^{-1} \text{ m}^{-1}], \quad (9.3)$$

because the power absorbed per unit volume is

$$P = \sigma \frac{E_0^2}{2} \quad [\text{watt m}^{-3}]. \quad (9.4)$$

If, instead of the time relation between current and voltage, the electromagnetic field in space is considered, new substitutes for ϵ^* and μ^* offer themselves. To de-

† It should be noted that, since $\cos \theta = \sin \delta$, the power factor and loss tangent (dissipation factor) may be considered equal only for sufficiently small loss angles δ , where $\sin \delta \approx \tan \delta$ because $\cos \delta \approx 1$.

rive them conveniently, we visualize the spatial electric wave train at some moment t_1 ,

$$E_y = E_1 e^{-\gamma x} = E_1 e^{-\alpha x} e^{-j2\pi x/\lambda} \quad (9.5)$$

(cf Eq. 7.13). The wave amplitude oscillates in space with a periodicity λ , it is enclosed between exponential envelopes determined by the attenuation constant α (Fig. 9.1a). Alternatively in polar co-ordinates, the wave amplitude may be depicted as a radius vector which, rotating clockwise as the distance increases, describes a logarithmic spiral (Fig. 9.1b). The parameter x is replaced in the latter representation by the phase angle ϕ according to the relation

$$\frac{x}{\lambda} = \frac{\phi}{2\pi}, \quad (9.6)$$

and the electric field strength is rewritten as

$$E_y = E_1 e^{-\alpha \left(\frac{\lambda}{2\pi} \phi \right)} \quad (9.7)$$

In vacuum the wavelength is λ_0 , and the wave travels with the velocity of light (cf Eq. 7.19),

$$c = \lambda_0 \nu = \frac{1}{\sqrt{\epsilon_0 \mu_0}} \quad (9.8)$$

In other media the wavelength normally shortens and the phase velocity slows down. The ratio of the wavelength or phase velocity in vacuum to that in the dielectric designates the *index of refraction* of the dielectric medium,

$$n \equiv \frac{\lambda_0}{\lambda} = \frac{c}{v} = \frac{\lambda_0}{2\pi} \beta. \quad (9.9)$$

For a loss-free medium this equation simplifies to

$$n = \sqrt{\epsilon' \mu' / \epsilon_0 \mu_0} \equiv \sqrt{\kappa' \kappa_m'} \quad (9.10)$$

If, in addition, the magnetization can be neglected ($\mu' = \mu_0$), the well-known *Maxwell relation* † results,

$$n^2 = \frac{\epsilon'}{\epsilon_0} = \kappa' \quad (9.11)$$

† This relation has been abused frequently in predicting static dielectric constants from optical refraction data. Actually, it states only that the square of the index of refraction of a non-absorbing, nonmagnetic material is equal to the relative permittivity at that frequency.

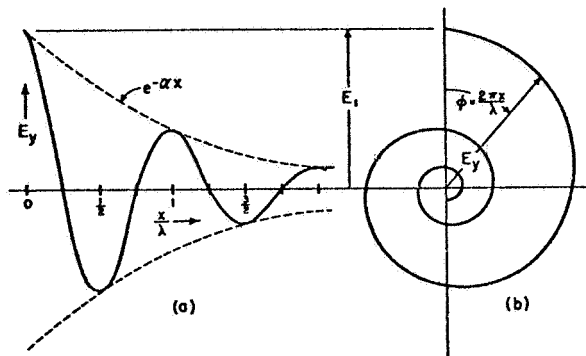


Fig. 9.1. Electric wave train in space.

The physicist normally uses the index of refraction as one of his parameters and pairs with it, by making use of the polar representation of the wave, the attenuation per radian called *index of absorption*,

$$k = \frac{\alpha\lambda}{2\pi} = \frac{\alpha}{\beta} \quad (9.12)$$

By substituting these indices of refraction and absorption for the attenuation factor α and the phase factor β of the propagation factor in Eq. 7.12 we obtain

$$\gamma = j \frac{2\pi}{\lambda_0} n(1 - jk) = j \frac{2\pi}{\lambda_0} n^* \quad (9.13)$$

The propagation factor γ used by the communication engineer may thus be replaced by the *complex index of refraction*

$$n^* = n(1 - jk) \quad (9.14)$$

employed in the calculations of physical optics.

The propagation factor γ is proportional to the product $\sqrt{\epsilon^* \mu^*}$, whereas the intrinsic impedance Z is equal to the ratio $\sqrt{\mu^* / \epsilon^*}$. Both complex quantities have to be determined to obtain ϵ^* and μ^* individually.

From the intrinsic impedance

$$Z = \frac{E}{H} = \sqrt{\frac{\mu^*}{\epsilon^*}} \quad (9.15)$$

in polar form,

$$Z = |Z| e^{j\zeta} = \left[\frac{(\epsilon''\mu' + \epsilon'\mu'')^2 + (\epsilon'\mu' - \epsilon''\mu'')^2}{(\epsilon'^2 + \epsilon''^2)^2} \right]^{1/2} e^{j\zeta} \quad (9.16)$$

with

$$\tan 2\zeta = \frac{\epsilon''\mu' - \epsilon'\mu''}{\epsilon'\mu' + \epsilon''\mu''} \quad (9.17)$$

we can derive the phase relation between the electric and the magnetic wave. It is evident that the electric field vector is advanced or retarded with respect to the magnetic vector in temporal phase, depending on the preponderance of the term pertaining to the electric or the magnetic loss. For negligible magnetic loss ($\mu'' = 0$),

$$\tan 2\zeta = \tan \delta = \frac{2k}{1 - k^2} \quad (9.18)$$

or

$$\tan \zeta = k; \quad (9.19)$$

the phase advance of the electric wave is equal to the arc tangent of the index of absorption. In a loss-free medium in unbounded space the electric and magnetic field vectors of an electromagnetic wave are exactly in phase (Fig. 9.2).

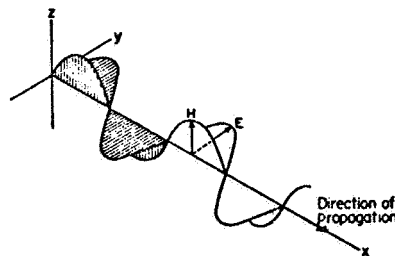


Fig. 9.2. Traveling TEM wave in loss-free dielectric.

The general characterization of a dielectric as the carrier of an electromagnetic field requires two independent complex parameters which have to be determined by four independent measurements; however, the situation fortunately simplifies in practice. Ferro-magnetics excepted, the magnetic polarization is, in

general, so weak that μ^* may be replaced by the permeability μ_0 of free space for all practical purposes. Thus, two measurements normally suffice to determine the dielectric response of homogeneous isotropic materials at a given frequency. Consequently, in most cases, our dielectric characteristics show only the specific dielectric constant,

$$\kappa' = \epsilon'/\epsilon_0, \quad (9.20)$$

and the loss tangent $\tan \delta$.

To allow a convenient change-over from these to other parameters, we equate the real and imaginary parts of Eq. 7.12. It follows for the attenuation factor of a transversal electromagnetic wave (TEM wave)

$$\alpha = \frac{\lambda\omega^2}{4\pi} (\epsilon'\mu'' + \epsilon''\mu'), \quad (9.21)$$

and for the phase factor

$$\beta = \frac{2\pi}{\lambda} = \omega \left[\frac{(\epsilon'\mu' - \epsilon''\mu'')}{2} \right. \\ \left. \times \left\{ 1 + \sqrt{1 + \left(\frac{\epsilon'\mu'' + \epsilon''\mu'}{\epsilon'\mu' - \epsilon''\mu''} \right)^2} \right\} \right]^{1/2} \quad (9.22)$$

Thus we arrive at the conversion formulas:

For materials with negligible magnetic loss ($\mu'' = 0$) we obtain from Eq. 9.22 for the wavelength the simplified expression

$$\lambda = \frac{1}{\sqrt{\frac{1}{2}\epsilon'\mu' \{1 + \sqrt{1 + \tan^2 \delta}\}}} \quad (9.23)$$

If, in addition, the permeability is that of vacuum ($\mu' = \mu_0$), we may write for the index of refraction

$$n = \frac{\lambda_0}{\lambda} = \left[\frac{1}{2} \kappa' \{ \sqrt{1 + \tan^2 \delta} + 1 \} \right]^{1/2} \quad (9.24)$$

Similarly the attenuation factor becomes

$$\alpha = \frac{2\pi}{\lambda_0} \left[\frac{1}{2} \kappa' \{ \sqrt{1 + \tan^2 \delta} - 1 \} \right]^{1/2}, \quad (9.25)$$

and the index of absorption

$$k = \frac{\alpha}{\beta} = \left[\frac{\sqrt{1 + \tan^2 \delta} - 1}{\sqrt{1 + \tan^2 \delta} + 1} \right]^{1/2} \quad (9.26)$$

These equations show that it is convenient to discuss the effect of the dielectric loss on other parameters by studying the three boundary cases: $\tan^2 \delta \ll 1$, $\tan^2 \delta \simeq 1$, and $\tan^2 \delta \gg 1$.

The attenuation produced by a dielectric is frequently expressed as the *attenuation distance* $1/\alpha$ through which the field strength decays to $1/e = 0.368$ of its original value,

$$\frac{1}{\alpha} = \frac{\lambda_0}{2\pi} \left[\frac{2}{\kappa'(\sqrt{1 + \tan^2 \delta} - 1)} \right]^{1/2} \text{ [m]}, \quad (9.27)$$

or as the attenuation in *decibels per meter* produced by the material. If the field strength falls from $E(0)$ to $E(x)$, or the power from $P(0)$ to $P(x)$, over a length x of the dielectric, this decibel loss is defined as

$$20 \log \frac{E(0)}{E(x)} = 10 \log \frac{P(0)}{P(x)} = 8.686\alpha x \text{ [db]}; \quad (9.28)$$

that is, the decibel loss per meter is given as

$$8.686\alpha = 8.686 \frac{2\pi}{\lambda_0} \left[\frac{1}{2} \kappa' \{ \sqrt{1 + \tan^2 \delta} - 1 \} \right]^{1/2} \\ \left[\frac{\text{db}}{\text{m}} \right] \quad (9.29)$$

For low-loss materials ($\tan \delta \ll 1$) this loss becomes simply

$$8.686 \frac{\pi}{\lambda_0} \sqrt{\kappa'} \tan \delta = 1637 \frac{\sigma}{\sqrt{\kappa'}} \left[\frac{\text{db}}{\text{m}} \right]. \quad (9.30)$$

For the convenience of the reader *nomographic charts* have been provided which allow a quick evaluation of $1/\alpha$ (Charts 9.1-9.3), of the decibel loss per meter (Charts 9.4-9.6), of β (Chart 9.7), and of n and k (Chart 9.8), when the specific dielectric constant and the loss tangent are given. Chart 9.9, in addition, gives the dielectric conductivity in terms of the same parameters calculated from the equation

$$\sigma = \omega\epsilon'' = 5.56 \times 10^{-11} \nu \kappa' \tan \delta \text{ [ohm}^{-1} \text{ m}^{-1} \text{]}. \quad (9.31)$$

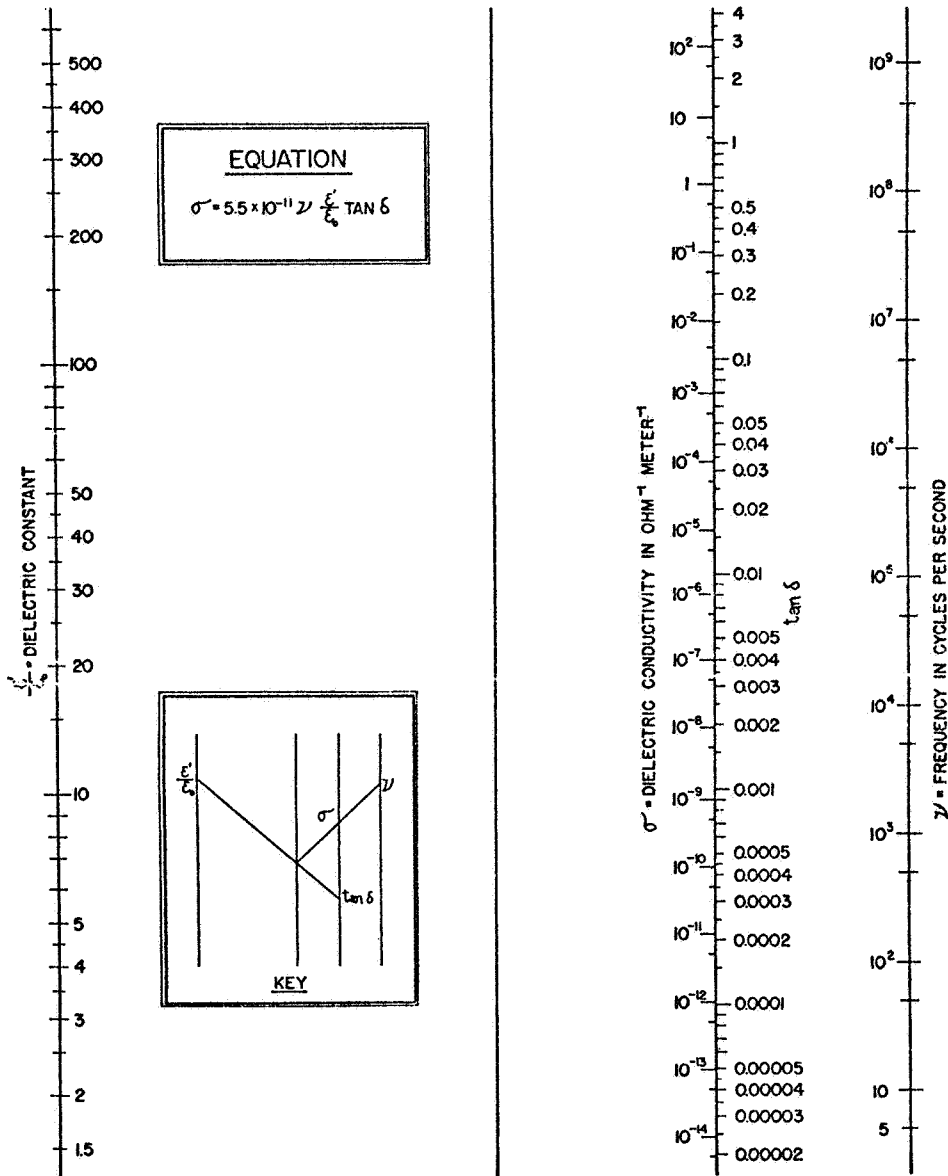


Chart 9.9. Dielectric conductivity as function of frequency, dielectric constant, and loss.

PROGRAM INFORMATION REQUEST / RELEASE

PIR NO. U — 1254 — AGCE — 015
 *USE "C" FOR CLASSIFIED AND "U" FOR UNCLASSIFIED

FROM S.L. Neste	TO L.R. Eaton
--------------------	------------------

DATE SENT 3/5/81	DATE INFO. REQUIRED	PROJECT AND REQ NO.	REFERENCE DIR. NO.
---------------------	---------------------	---------------------	--------------------

SUBJECT
 Task 1 - Calculation of g_E for Nominal GFFC and AGCE Parameters

INFORMATION REQUESTED/RELEASED

1.0 SUMMARY

The impact of utilizing a high dielectric fluid for AGCE is assessed in terms of its effect on the dielectric body force, g_E . Using the nominal AGCE design values for sphere sizes (5.0 and 6.0 cm radii) and applied voltage (20 kV) and assuming the fluid parameters of dimethylsulfoxide (DMSO) a value of $g_E \approx 22g$ is obtained, where g is the earth's acceleration. This large increase over typical GFFC values for g_E ($\approx 0.2g$) is almost entirely due to the high polarity of DMSO relative to that of the Dow Corning Silicone oil used in GFFC. Fluids of increasing polarity are characterized by higher values of both dielectric constant and thermal coefficient of dielectric constant. Since the value of g_E varies as the product of these parameters, a sufficiently higher value of g_E can probably be achieved even if the highest dielectric fluids are not acceptable (e.g., due to excessive fluid heating, PIR No. 1254-AGCE-014). Furthermore, it may also be feasible to work at lower voltage levels (i.e., less than 20 kV) and thereby avoid increased fluid heating.

2.0 BACKGROUND

The scientific theoretical design studies for the AGCE indicate that in order to achieve strong baroclinic instability a large value of the dielectric body force, g_E , is required. This body force is given by:

$$g_E = \frac{2K\epsilon_0\gamma}{\alpha\rho_0} \left(\frac{R_o R_i}{R_o - R_i} \right)^2 \frac{V^2}{r^5}$$

L.R. Eaton G. Fogal R. Homsey S.L. Neste	PAGE NO. 1 OF 6	<input checked="" type="checkbox"/> RETENTION REQUIREMENTS	
		COPIES FOR	MASTERS FOR
		<input type="checkbox"/> 1 MO.	<input type="checkbox"/> 3 MOS.
		<input type="checkbox"/> 3 MOS.	<input type="checkbox"/> 6 MOS.
		<input type="checkbox"/> 6 MOS.	<input type="checkbox"/> 12 MOS.
		<input type="checkbox"/> MOS.	<input type="checkbox"/> MOS.
		<input type="checkbox"/>	<input type="checkbox"/> DO NOT DESTROY

where: ϵ_0 = dielectric constant of free space (8.85×10^{-12} farad/meter)
 K = dielectric constant of the fluid relative to free space
 ρ_0 = density (Kg/m^3)
 α = thermal coefficient of density ($\text{T}/^\circ\text{C}$)
 $= 1/\rho_0 \frac{d\rho_0}{dT}$, ($\%/^\circ\text{C}$)
 γ = thermal coefficient of dielectric constant
 $= 1/K \frac{dK}{dT}$, ($\%/^\circ\text{C}$)
 R_i = radius of inner sphere (m)
 R_o = radius of outer sphere (m)
 V = voltage difference (volts)
 r = radius, $R_i < r < R_o$

Although the Dow Corning 200 Series silicone fluid, used in the GFFC, provided many desirable properties (e.g., low power dissipation, high electrical resistance and high dielectric strength), it has a relatively low dielectric constant ($K \approx 2.18$) and the value of g_E achieved was much lower than is desired for the AGCE. An obvious way of increasing g_E is to use a fluid with a higher dielectric constant and/or use a higher voltage. The impact of choosing fluids with higher dielectric constant is addressed in Section 3.0.

3.0 TASK IMPLEMENTATION - IMPACT OF HIGH DIELECTRIC FLUID ON g_E

Typical values for the experimental dimensions and the properties of the silicone oil used for the GFFC experiment (Fichtl and Fowles, 1977) are given in Table 1 together with nominal values for the AGCE. Dimethylsulfoxide was used as a representative dielectric fluid for the AGCE.

The calculated values of g_E are:

$$\begin{aligned} \text{GFFC: } g_E &= 1.6 \text{ meter/sec}^2 \\ &= .18 \text{ g} \end{aligned}$$

$$\begin{aligned} \text{AGCE: } g_E &= 2.2 \times 10^2 \text{ meter/sec}^2 \\ &\approx 22 \text{ g} \end{aligned}$$

TABLE 1

Parameter	GFFC	AGCE	Parameter Ratio (AGCE/GFFC)	Units
ϵ	$2.2*(8.85 \times 10^{-12})$	$48.9*(8.85 \times 10^{-12})$	22	Farad/meter
ρ_0	0.82×10^3	1.101×10^3	1.3	Kg/meter ³
α	1.34×10^{-3}	8.8×10^{-4}	0.66	$^{\circ}\text{C}^{-1}$
γ	1.34×10^{-3}	.0035	2.6	$^{\circ}\text{C}^{-1}$
R_i	0.02	0.05	2.5	meter
R_o	0.03	0.06	2.0	meter
V	10^4	2×10^4	2.0	volts
r	0.025	0.055	2.2	meter

The increase in g_E is achieved primarily through two characteristics of the dielectric fluid, the dielectric constant and the temperature dependence of the dielectric constant. They are larger by factors of 22x and 2.6x, respectively than the values for the Dow Corning 200 fluid used in the GFFC.

A characteristic of polar (high dielectric) fluids is that the variation of ϵ with temperature (i.e., γ) is greater than for non-polar fluids (see Table 2). This variation of γ as a function of K is shown in Figure 1. The thermal coefficient of volume (or density) is shown to be relatively independent of K for values less than ~ 40 .

TABLE 2. VALUES OF DIELECTRIC CONSTANT* AND THERMAL COEFFICIENTS OF DIELECTRIC CONSTANT AND VOLUME.

Liquid	*Dielectric Constant		Thermal Coeff of K		Thermal Coeff of Vol. $\alpha(T)$
	K(20°C)	K(25°C)	dK/dT	$\gamma(T)$	
Cyclohexane	2.023	2.015	.0016	.0008	
Carbon Tetrachloride	2.238	2.228	.002	.0009	.001236
Benzene	2.284	2.274	.002	.0009	.00124
DC 200	2.2		.00286	.0013	
Chlorobenzene	5.708	5.621	.0174	.0030	
1,2 Dichloroethane	10.65	10.36	.058	.0054	
Methanol	33.62	32.63	.198	.0059	.00120
Nitrobenzene	35.74	34.82	.184	.0051	
DMSO	48.9		.17	.0035	.00088
Water	80.37		.366	.0045	.0002
Formamide	109		.72	.0066	

*Values given for the dielectric constant, K, are relative to the free space value of $\epsilon_0 = 8.85 \times 10^{-12}$ Farad/meter.

Note: Values of K and γ were obtained from the 43rd edition of the Handbook of Chemistry and Physics. Values for α were obtained from the 4th edition of Reference Data for Radio Engineers.

These characteristics of polar fluids are all advantageous for the AGCE application and may allow greater latitude in fluid selection and/or permit relaxation of other requirements.

4.0 RECOMMENDATIONS

Since the desired value of g_E is 5-10g, trade-offs can be made among the parameters to alleviate potential problem areas. The most obvious parameter value to relax is the applied voltage since this will, in turn, reduce the fluid heating. For example, reducing V by 2x to a value of 10,000 volts will reduce fluid heating by a factor of 4x (and/or relax requirements on fluid purity - refer to PIR No. 1254-014). The reduced value of g_E will then be ~5.5g.

ORIGINAL PAGE IS
OF POOR QUALITY

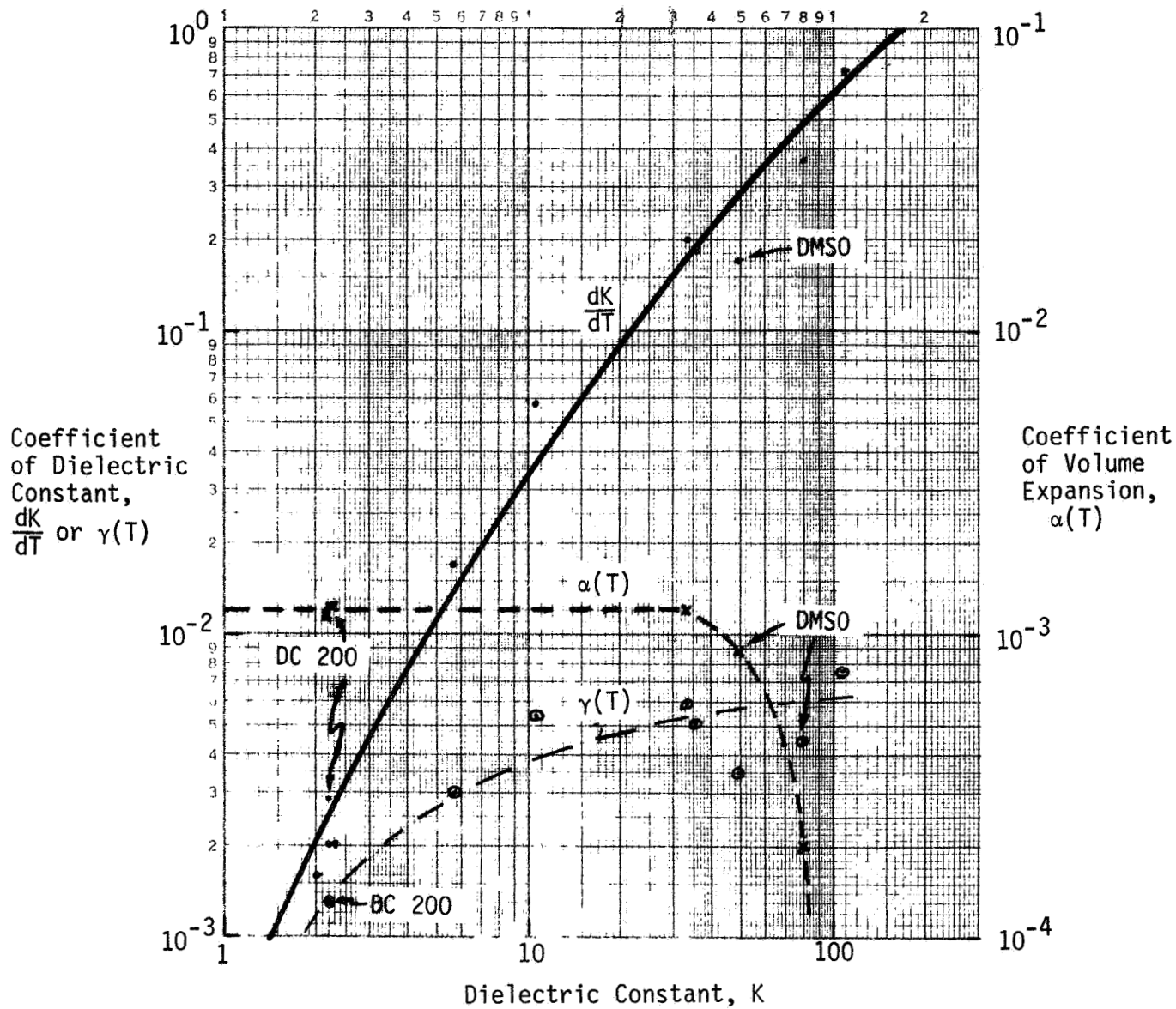


Figure 1. Thermal coefficients of dielectric constant and volume as a function of dielectric constant.

PIR 1254-015
Page six

References

W.W. Fowles and G.H. Fichtl, "Geophysical Fluid Flow Model Experiments in Spherical Geometry", Proceedings of the Third NASA Weather and Climate Program Science Review, NASA Conference Publication 2029, Paper No. 32, p. 177, 1977.

Handbook of Chemistry and Physics, 43rd edition, Chemical Rubber Publishing Co., Cleveland, OH, 1961-1962.

Reference Data for Radio Engineers, 4th edition, International Telephone and Telegraph Corp., New York, NY, 1967.

PROGRAM INFORMATION REQUEST / RELEASE

*CLASS. LTR.	OPERATION	PROGRAM	SEQUENCE NO.	REV. LTR.
U	1254	AGCE	017	

PIR NO. U - 1254 - AGCE - 017
*USE "C" FOR CLASSIFIED AND "U" FOR UNCLASSIFIED

FROM S.L. Neste	TO Distribution
--------------------	--------------------

DATE SENT 3/11/81	DATE INFO. REQUIRED	PROJECT AND REQ. NO.	REFERENCE DIR. NO.
----------------------	---------------------	----------------------	--------------------

SUBJECT
TASK 1 - FLUID VISCOSITY ASSESSMENT

INFORMATION REQUESTED/RELEASED

1.0 SUMMARY

Assessment of a representative list of 42 solvents having dielectric constants ranging from 1.8 to 109.5 indicates an essentially random variation of viscosity with dielectric constant. More than 80% of the fluids considered had viscosities less than the required upper limit of 3 cp while over 50% had viscosities below 1 cp, the preferred upper value (PIR 1254-AGCE-009). Thus, selection of a dielectric fluid with an acceptable viscosity for the AGCE should not present a significant problem. However, as stated in the GE Proposal for the AGCE, fading rates of photochromic solutions generally increase as viscosity of the solvent increases and may impact the final selection. The magnitude of this fading effect is unquantified and laboratory testing (not in the scope of this study) will be required to determine the significance of this characteristic.

2.0 BACKGROUND

The convective motion which will be observed in the AGCE is a function of the $\alpha g_E T$ where α is the coefficient of volume expansion, g_E is the dielectric body force as defined in the Statement of Work (Task 1) and T is the fluid temperature. Larger values of g_E are desired to increase the driving force. The fluid instability threshold is proportional to the quantity μ/d^2 where μ is the viscosity and d is the fluid thickness. For lower thresholds, smaller μ and larger d are important. Thus, large values of g_E and/or small values of μ are required characteristics of the dielectric fluid.

G. Foga1 R. Homsey S. Neste	PAGE NO. 1 OF 5	RETENTION REQUIREMENTS	
		COPIES FOR	MASTERS FOR
		<input type="checkbox"/> 1 MO.	<input type="checkbox"/> 3 MOS.
		<input type="checkbox"/> 3 MOS.	<input type="checkbox"/> 6 MOS.
		<input type="checkbox"/> 6 MOS.	<input type="checkbox"/> 12 MOS.
		<input type="checkbox"/> MOS.	<input type="checkbox"/> MOS.
		<input type="checkbox"/>	<input type="checkbox"/> DO NOT DESTROY

Since g_E is proportional to K , the fluid dielectric constant, an assessment of μ as a function of K was performed to determine if small μ and large K (hence large g_E) were compatible characteristics of a dielectric fluid. The results are given in Section 3.0.

3.0 TASK IMPLEMENTATION - FLUID VISCOSITY ASSESSMENT

A table of solvents used for chromatography (Kodak Publication No. JJ-3) was used as the basis for this assessment. A representative selection of fluids from that listing is given in Table 1 with values for the dielectric constant (K), and the viscosity (μ). The essentially random variation of viscosity as a function of dielectric constant is clearly indicated in Figure 1.

Selecting a fluid with viscosity acceptable to the AGCE should not be a problem. More than 80% of the fluids in Table 1 have viscosities less than the required upper limit of 3 cp and over 50% have values below the desired upper limit of 1 cp.

4.0 RECOMMENDATION

As stated in Section 3.0, selection of a dielectric fluid with acceptable viscosity does not appear difficult due to the large number of fluids with low viscosity and their apparent independence of dielectric constants. Primary consideration should continue to be given parameters such as dielectric constant, power dissipation (fluid heating) and resistivity.

In the final selection of a photochromic solution, the viscosity may have second order effects which should be considered. As stated in the GE proposal for the AGCE, fade rates of photochromic solutions generally increase as the viscosity of the solvent increases. However, the magnitude of this effect is unquantified and must be assessed in the laboratory for specific fluid/photochromic systems. Since such an assessment is not within the scope of this study, it is recommended that future efforts be directed toward laboratory assessment of this characteristic using the solvent(s) and photochromic dye(s) recommended by the final report for the present study.

TABLE 1

REPRESENTATIVE LIST OF SOLVENTS COMMONLY USED IN
CHROMATOGRAPHY WITH VALUES OF DIELECTRIC CONSTANT AND VISCOSITY

Chemical	Dielectric Constant K	Viscosity μ
Pentane	1.80	0.240
Hexanes, Reagent ACS	1.89	0.326
Cyclohexane, Reagent ACS	2.02	1.020
Cyclohexene	2.22	0.660
Carbon Tetrachloride, Reagent ACS	2.24	0.969
Benzene, Reagent ACS	2.30	0.652
m-Xylene	2.37	0.620
Toluene, Reagent ACS	2.38	0.590
Ethylbenzene	2.41	0.691
x-Xylene	2.57	0.810
Propyl Ether	3.40	0.448
Bromoform	4.39	2.152
Chloroform, Reagent ACS	4.81	0.580
Butyl Acetate	5.01	0.732
Bromobenzene	5.40	1.196
Chlorobenzene	5.90	0.799
Ethyl Acetate, Reagent ACS	6.02	0.455
Acetic Acid, Glacial, Reagent ACS	6.15	1.300
Methyl Acetate	6.68	0.381
Aniline, Reagent ACS	6.89	4.400
Ethyl Formate ACS (Pract.)	7.10	0.402
1,1,1-Trichloroethane (Techn.)	7.52	1.200
Octyl Alcohol	10.34	10.600
m-Cresol (Pract.)	11.80	20.800
Pyridine, Reagent ACS	12.30	0.974
Benzyl Alcohol	13.10	5.800
Butyl Alcohol, Reagent ACS	17.10	2.948
Isobutyl Alcohol, Reagent ACS	17.70	4.703
Isopropyl Alcohol, Reagent ACS	18.30	2.320
Prphyl Alcohol	20.10	2.256
Acetone, Reagent ACS	20.70	0.316
Acetaldehyde	21.10	0.220
m-Nitrotoluene	23.00	2.330
Benzonitrile, Spectro Grade	25.20	1.240
o-Nitrotoluene	27.40	2.370
Methanol, Reagent ACS	32.80	0.597
Nitrobenzene, Reagent ACS	36.10	2.030
Acetonitrile, Reagent ACS	37.50	0.345
Ethylene Glycol	37.70	19.900
Nitromethane, Spectro Grade	39.40	0.620
Formic Acid, Reagent ACS	47.90	1.804
Formamide, Reagent ACS	109.50	3.300

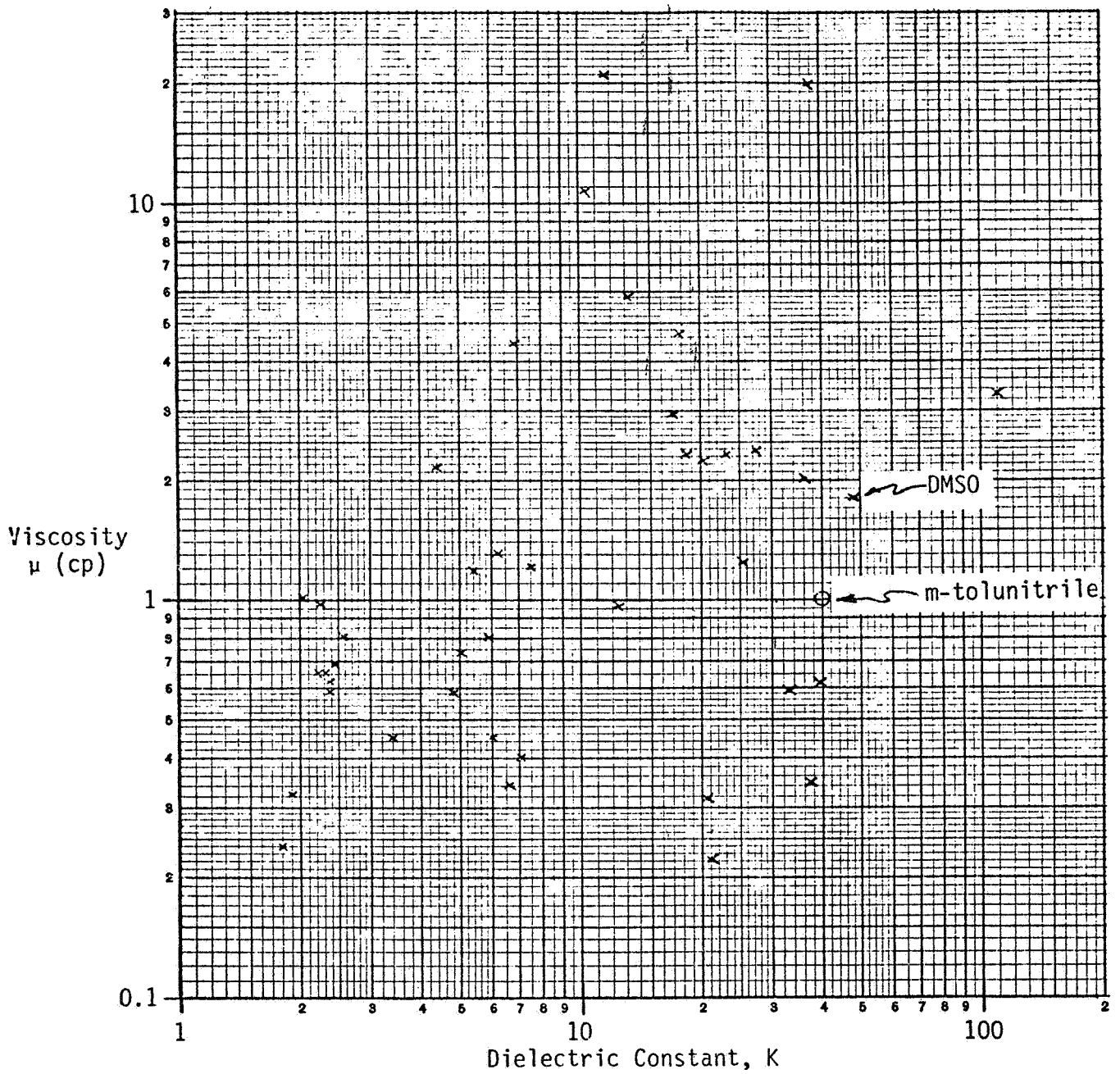


Figure 1. Illustration of variation in fluid viscosity for fluids of increasing dielectric constant.

References

"Feasibility Study for an Apparatus for Atmospheric General Circulation Experiments for Spacelab Flights," GE Proposal No. C-80163, GE Space Division, Philadelphia, PA, 9 June 1980.

"Eastman Products for Chromatography," Kodak Publication No. JJ-3, Eastman Kodak Company, Rochester, NY, 1979.



*CLASS. LTR.	OPERATION	PROGRAM	SEQUENCE NO.	REV. LTR.
PIR NO. U	- 1254	- AGCE	- 025	
*USE "C" FOR CLASSIFIED AND "U" FOR UNCLASSIFIED				

PROGRAM INFORMATION REQUEST / RELEASE

FROM S. L. Neste	TO Distribution
---------------------	--------------------

DATE SENT 5/12/81	DATE INFO. REQUIRED	PROJECT AND REQ. NO.	REFERENCE DIR. NO.
----------------------	---------------------	----------------------	--------------------

SUBJECT
 PHOTOCROMIC DYES FOR FLOW VISUALIZATION IN HIGH DIELECTRIC SOLVENTS

INFORMATION REQUESTED/RELEASED

The attached document represents interim results from Dr. Ronald Francis of the Rochester Institute of Technology regarding the above subject. This report will constitute a portion of the final report for Task 1 (Survey of Dielectric Liquids) of the AGCE feasibility study.

G. Fogal R. Homsey S. Neste	PAGE NO. OF	RETENTION REQUIREMENTS	
		COPIES FOR	MASTERS FOR
		<input type="checkbox"/> 1 MO.	<input type="checkbox"/> 3 MOS.
		<input type="checkbox"/> 3 MOS.	<input type="checkbox"/> 6 MOS.
		<input type="checkbox"/> 6 MOS.	<input type="checkbox"/> 12 MOS.
		<input type="checkbox"/> MOS.	<input type="checkbox"/> MOS.
		<input type="checkbox"/>	<input type="checkbox"/> DO NOT DESTROY

PHOTOCHROMIC DYES FOR FLOW VISUALIZATION IN HIGH DIELECTRIC SOLVENTS

1. Literature Survey

A survey was carried out to determine what literature in the field of photochromic marking of fluids in fluid flow studies might exist. The following are citations to three of the papers found, copies of which are attached:

J. W. Smith and R. L. Hummel, "Studies of Fluid Flow by Photography Using a Non-Disturbing Light-Sensitive Indicator," J. SMPTE 82, 278 (1973).

H. Sovova, J. Prochazka and R. L. Hummel, "Flow Near the Surface of a Mixing Vessel: An Example of the Photochromic Technique Using Inexpensive Equipment," J. SMPTE 82, 282 (1973).

W. W. Fowles, "Remote Optical Techniques for Liquid Flow and Temperature Measurement for Spacelab Experiments, Optical Engineering 18, 281 (1979).

The solvents reported in these papers as having been successfully used, from the view of solubility, fatigue, degree of coloration and fade time, in the photochromic marking technique are:

2-(2',2'-dinitrobenzyl) pyridine (DNBP) in 95% "alcohol".

1,3,3-trimethyl-6-nitro-indoline-2-spiro-2,2-benzopyrane (TNSB) in "polar solvents such as alcohol" and in Dow Corning 200 series silicone oil.

2. Commercial Availability of Photochromic Compounds

A catalog and phone call search was initiated to determine the commercial availability of compounds known to be photochromic. Although photochromism is a phenomenon occurring in many classes of chemical compounds, the number of compounds which yield useful optical densities upon exposure is very limited. These compounds are principally compounds in the spiropyran and triarylmethane class and a few other individual materials such as 2-(2,4-dinitrobenzyl) pyridine.

Only four compounds thus far have been found to be commercially available. They are:

2-(2,4-dinitrobenzyl) pyridine

(diphenylthiocarbazono) phenyl mercury

ethyl bis (2,4-dinitrophenyl) acetate

1',3',3'-trimethyl-6-hydroxyspiro[2H-1-benzopyran-2,2'-indoline]

Eastman Kodak, approximately ten years ago, was a commercial source of nineteen photochromic compounds (see next page). This is no longer the case,

EASTMAN Organic Chemicals

ORIGINAL PAGE IS
OF POOR QUALITY

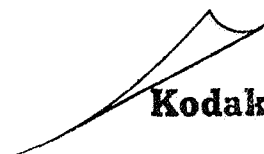
PHOTOCHROMIC COMPOUNDS

The nineteen photochromic compounds listed below are available from Eastman Organic Chemicals. Those having a 6 digit "92" number have been made in experimental quantities only, and are offered on a first-come, first-served basis. However, when sufficient interest is shown in any of these, they are made for catalog listing, and a new number is assigned.

<u>NUMBER</u>	<u>CHEMICAL</u>	<u>STANDARD PACKAGES</u>			
921060	Bis(diphenylthiocarbazono)nickel	5 g.	\$7.00	25 g.	\$25.00
920916	Bis(diphenylthiocarbazono)zinc	5 g.	7.00	25 g.	25.00
923476	N-(5-Bromosalicylidene)amiline	5 g.	7.00	25 g.	25.00
922643	3,3'-Dimethyl-6-nitro-1'-phenylspiro[2H-1-benzopyran-2,2'-indoline]			1 g.	15.00
921988	Di-β-naphthospiran			1 g.	15.00
7732	2-(2,4-Dinitrobenzyl)pyridine	5 g.	4.50	25 g.	16.30
8533	(Diphenylthiocarbazono)phenylmercury	5 g.	5.25	25 g.	20.10
921243	Diphenylthiocarbazono Silver	5 g.	7.00	25 g.	25.00
5488	Ethyl Bis(2,4-dinitrophenyl)acetate	5 g.	3.75	25 g.	12.60
8530	Mercury Bis(dithizonate)	25 g.	4.55	100 g.	13.90
920666	6'-Nitro-3-methylspiro[2H-1β-naphthopyran-2,2'-(2'H-1'-benzopyran)]			1 g.	15.00
923469	4'-(Salicylideneamino)acetophenone	5 g.	7.00	25 g.	25.00
923467	2-(Salicylideneamino)pyridine	5 g.	7.00	25 g.	25.00
923474	N-Salicylideneaniline	5 g.	7.00	25 g.	25.00
923475	N-Salicylidene-p-bromoaniline	5 g.	7.00	25 g.	25.00
923477	1',3',3'-Trimethyl-6-hydroxyspiro[2H-1-benzopyran-2,2'-indoline]			1 g.	15.00
920652	1',3',3'-Trimethyl-6-nitrospiro[2H-1-benzopyran-2,2'-indoline]			1 g.	15.00
10060	1',3',3'-Trimethylspiro[2H-1-benzopyran-2,2'-indoline]	1 g.	4.50	5 g.	16.35
10062	1',3',3'-Trimethyl-4'-(1,3,3,-trimethyl-2-indolinylmethyl)indoline-2-spiro-2-benzopyran				Price available on request

Prices shown are list prices only, and are subject to change without notice.

EASTMAN KODAK COMPANY
EASTMAN ORGANIC CHEMICALS
ROCHESTER, NEW YORK 14650



and through personal contacts, it was learned that unsold supplies were burned several years ago. Hopefully, less than advertizable amounts might have still been available.

Thus, only one spiropyran and no triarylmethanes are available. Samples of each of the above compounds have been ordered, except for the phenyl mercury compound. Only 1,3',3'-trimethyl-6-hydroxyspiro[2H-1-benzopyron-2,2'-indoline] has thus far been received. Tests of the photochromism of this compound has shown it to be useless compared to other compounds available showing no photochromism, to the sources used, in high dielectric solvents and very slight photochromism in toluene, having a low dielectric constant. Further, the compound shows negative photochromism forming colored solutions which become lighter upon exposure. I don't believe this is preferable in the photography of a small dot pattern in solution.

The spiropyran referred to in the three attached journal articles, referred to on page 2 as TNSB, is not commercially available. The compound referred to as 2-(2',2'-dinitrobenzyl) pyridine appears to be incorrectly named in the Smith and Hummel paper, since "2',2'-dinitrobenzyl" is impossible, and the compound is probably 2-(2,4-dinitrobenzyl) pyridine which has been listed as commercially available from several sources for some time but to the present has not been delivered from recent orders.

The author has considerable experience in the preparation of spiropyran and triarylmethane compounds. While one cannot be certain in the case of any specific compound, procedures are known for the preparation of a wide variety of these two classes of compounds and it should be possible to prepare a variety of them, in quantity, without any experimental difficulty. The synthesis of the spiropyrans generally require a number of procedural steps, and the preparation of specific compounds can be time consuming. One such compound for example required 80 hours to prepare. The triarylmethanes are generally simpler to obtain.

One spiropyran compound is presently on-board in quantity, namely 5'-bromo-8'-methoxy-6'-nitro-1-phenyl-3,3-dimethyl indolinobenzopyrylospiran (BMS), and six triarylmethane leucocyanides. After a precautionary step of recrystallization of the indolinobenzopyrylospiran and malachite green leucocyanide, screening experiments proceeded with these two compounds, as compounds whose properties would represent a reference point, in solvents of high dielectric constant.

3. Choice of Solvent System

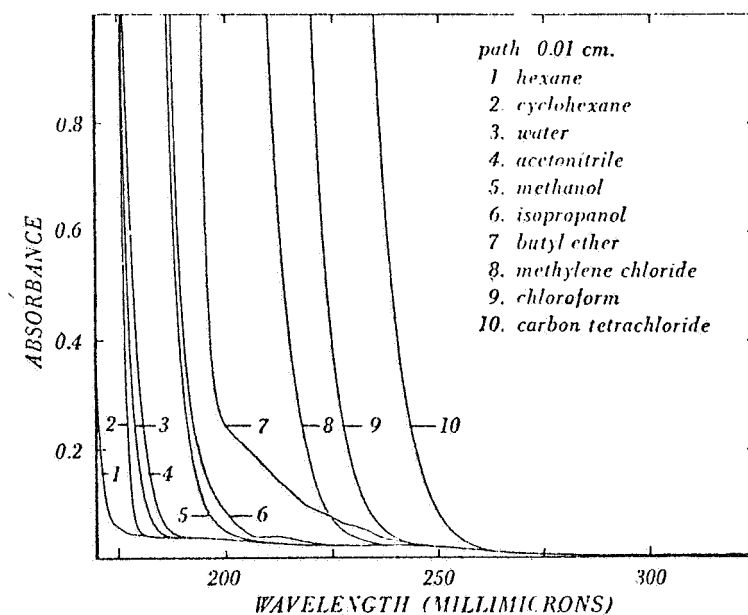
For the initial investigation, solvents have been selected on the basis of dielectric constant only.

Methanol	32.8
Acetonitrile	37.5
Dimethylformamide	37.6
Ethylene glycol	37.7
Nitromethane	39.4
m-Tolunitrile	40.0
Glycerol	42.5
Dimethylsulfoxide	46.7
Formamide	109.5
2-(2-ethoxyethoxy) ethanol	?

Not all of these solvents are immediately available as is also the case with the Dow Corning 200 series silicone oils referred to in the section above.

Subsequent attention will be paid to the purity in which these solvents can be obtained, the purity that can be maintained in contact with the surfaces of the system in which they are to be used, and their stability to exposure to the photochromic dye activation radiant source.

The absorbance vs. wavelength of several solvents is diagramed below.



Of consequence here is an awareness of the transmittance of the solvents at wavelengths of radiation which activate the dye. Most of the sensitivity (possibly 95%) of most photochromic dyes lies at wavelengths shorter than 275 nm. Toluene, which shows absorbance out to 350 nm, would be a particularly poor choice. Nitrobenzene, with a dielectric constant of 36.1, is nonetheless eliminated from further consideration because it is yellow in color and therefore a strong ultraviolet and blue filter.

4. Test Results

The breath of relevant photochromic dye-solvent system response properties is shown in the representative results obtained thus far tabulated on the next page.

Exposures were made using two Speedotron strobe lamps positioned one inch away, on either side, from the solution sample cell. The lamps are xenon-filled and driven by a 600 watt-second transformer.

The path length through which the solution is exposed is 3 mm. The density of the solution is read, using a Macbeth densitometer, through a one centimeter section of solution.

The density of the solutions were measured at 625 nm (as the dyes tested yield solutions which are cyan and green in color). The density values given are to be considered to be only relative numbers, for intercomparing the solutions only. However, in this density specification system, a cyan-colored solution with a density rating of 0.50 approximates the color and density of an Eastman Kodak CC50C color-correction cyan filter.

With regard to obtaining density, there is no difficulty in dissolving either dye in any solvent tested thus far. (Mild heating to 80°C for a few minutes was required in the case of ethylene glycol.) The dye concentrations used were 1 mg/cc of solvent. The saturation point of dye in solvent does not appear to have been even closely approached in these solutions. More dye dissolved in the solutions will result in more density, but linear increases with concentration are not expected, since dye solutions show departures from Beer's law behavior. The colored form of the dye will also absorb actinic radiation that could otherwise be used to activate as yet uncolored dye molecules in the solution. This phenomenon is known as "internal filtering."

<u>Dye</u>	<u>Solvent</u>	<u>Dielectric Constant</u>	<u>Color of Solu. Before Exposure</u>	<u>D₆₂₅</u>	<u>Fade_{total} (seconds)</u>	<u>Fade_{1/2} (sec)</u>	<u>Color of Solu. After Exposure</u>
BMS	DMSO	47	pale yellow	0.12	48	27	pale yellow
BMS	Eth. glycol	38	colorless	0.02	~500	78	colorless
BMS	2(2-ethoxy)	?	v. pale yellow	0.31	40	9	v. pale yellow
BMS	MEOH	33	colorless	0.05	74	19	colorless
MGCN	DMSO	47	colorless	0.89	540	110	colorless
MGCN	2(2-ethoxy)	?	colorless	1.30	~10,000	~3600	colorless

BMS = 5'-bromo-8'-methoxy-6'-nitro-1-phenyl-3,3-dimethyl-indolinobenzopyrylospiran

MGCN = malachite green leuco cyanide

DMSO = dimethylsulfoxide

Eth. glycol = ethylene glycol

2(2-ethoxy) = 2(2-ethoxyethoxy) ethanol

MEOH = methylalcohol

D₆₂₅ = density of the exposed solution at 625 nm

Fade_{total} = time for exposed solution to lose its color and return to original, unexposed color

Fade_{1/2} = time for exposed solution to lose one-half the maximum density obtained upon exposure

Increased densities are also expected with radiant sources of greater output at actinic wavelengths.

Relative densities up to 1.30 have been produced with fade times up to 10,000 seconds. In the case of the MGCN, the fade times can be adjusted to shorter times by small concentrations of sodium cyanide added to the solutions, a control not available in most photochromic dye systems. Sodium cyanide is freely soluble in dimethylsulfoxide and 2(2-ethoxyethoxy) ethanol. It is to be anticipated that this will be accompanied by some loss of density.

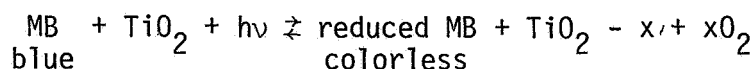
Relative densities from 0.02 to 0.89 have been realized for single fade times, in this case approximately 500 seconds.

The solvent 2(2-ethoxyethoxy) ethanol has been found to give the highest densities thus far for both BMS and MGCN dye. The dielectric constant for this solvent has not been found, but the results are included as it is conceivable that it is in the range of interest since this solvent is in the alcohol class of compounds.

Limited fatigue studies have been performed by cycling solutions through expose and fade for as many as twenty times. Fatigue is the property of photochromic solutions whereby their optical properties change upon repeated cycling. The photochromic solution may show less density with repeated exposure; it may fade more slowly; or it may take on permanent color. Examples in the literature show that some photochromic spiropyrans may be cycled 10,000 times without fatigue effects. The solutions under study in this current effort show no sign of fatigue after twenty cycles. Further, the density, color and fade rates are reproduced apparently exactly over a period of days.

5. The Titanium Dioxide-Methylene Blue System

A different approach has been previously discussed. The dye methylene blue is bleached to colorless when exposed to ultraviolet radiation in the presence of some photoconductors such as zinc oxide and titanium dioxide. The reaction is reversible:



These two oxides are available perhaps from 25 manufacturers in the world. Samples vary considerably in mean particle size, photoconductivity, and ability to reduce methylene blue.

Degussa, Inc. (Teterboro, NJ) P-25 is known to be one of the more photo-sensitive titanium dioxide products. Its mean particle size diameter is 0.03μ . These very small particles of colloidal dimensions will stay suspended in water for days.

This approach was investigated by slurring P-25 in water in which methylene blue dye had been previously dissolved. Thus far, however, this system has been found to be considerably less sensitive, photographically, than the dye systems described earlier in this report.

6. Questions

For continued investigation, I have the following questions about the photochromically-marked solutions sought:

- a) What optical densities and fade times are desired?
- b) What source will be used to expose the solutions?
- c) How many cycles of expose and fade are required, and what fatigue problems can be tolerated?
- d) What are the photographic conditions under which the photochromic dot pattern is to be recorded?

will know that a complete new science of reliability has been evolved.

In an ICBM early warning system, or a moonshot, there is no second chance. The complete system must work the first (and only) time for, if it fails, some 25 million lives may be at stake. On a lesser scale, but still catastrophic, the loss of an aircraft due to the failure of some small, but vital mechanism, is equally unthinkable. Such parts must not only work first time; they must go on working. This is achieved by establishing the wear-out life of every subassembly (this being the time it takes to arrive at the point at which performance deteriorates below acceptance limits). At half this time the subassembly is replaced by a new one,

and the old one is returned for overhaul. Some assemblies may have longer wear-out lives than others and do not need to be replaced so frequently; but, evidently, with this system, the whole equipment is maintained perpetually in a fully operable condition; its total wear-out life is infinite. Naturally, the equipment has to be designed with this in mind, so that the subassemblies can be replaced easily and quickly and without elaborate tools and skills. Some form of elapsed time indicator is also helpful so that the user does not have to keep complete records.

Human Engineering

Although we are dealing with it last, almost the first plea that every camera-

man put to us was to just try to remember that neither he nor any of his colleagues has four arms, retractable eyeballs, rubber necks, is a professional weight lifter or contortionist, or has any particular yen for being trussed up in belts and straps and struts, or any other form of surgical appliance.

In the past when a camera that was designed for studio work was taken out in the open air and the cameraman held it on his shoulder, he had no one but himself to blame for his discomfort. But when he openly declares that this is what he wants to do, the designer is to blame if he continues to design "unable" equipment, merely because this was the way cameras were always made.

Studies of Fluid Flow by Photography Using a Non-Disturbing Light-Sensitive Indicator

ORIGINAL PAGE IS
OF POOR QUALITY

By J. W. SMITH
and R. L. HUMMEL

A powerful flow-visualization technique is described which overcomes the disadvantages of primitive flow-visualization methods (lack of precision, clarity and/or convenience relative to the commonly used probe techniques). The new technique uses a tracer fluid which is continuously present in latent form in the test fluid (eliminating injection problems) and which undergoes a dramatic color change (a reversible photochromic reaction) in a pattern generated instantly by irradiation with a pattern of ultraviolet light. A typical setup employs this fluid in some transparent flow channel, with an ultraviolet light source (such as a frequency-doubled ruby laser), a suitable background light source and a high speed motion-picture camera. Many previously intractable fluid dynamics problems have yielded to this technique, and improved resolution and the use of computer logging should greatly increase its utility.

Introduction

The details of fluid flow are important to a broad range of problems relating to transportation systems (boats and airplanes), air and water pollution, weather prediction, fusion power devices, petrochemical production, etc. Velocity fields and flow systems can be studied by the use of probes (such as the hot-wire probe where wire temperature is related to flow velocity) or by flow visualization. Probe techniques have the advantage of being quantitative and easily analyzed and recorded, but they can "sample" the flow at only one or two points at a time. Because flow visualization makes it possible to record a phenomenon completely, it can, in principle, lead to easy and rapid analysis and interpretation. Sometimes it is the only way an event or occurrence can be identified and thus measured.

Flow visualization studies generally involve either (1) observation of physical changes that occur in the field, or (2) addition of substances (tracers) to the stream of fluid which follow the streamlines and make them visible to the eye or camera. In the first approach, shadowgraph, schlieren, and interferometric interference techniques are among the methods used to detect refractive index variations resulting from changes in pressure, temperature or density. Unfortunately, because the patterns recorded show the cumulative effects of refractive index variations along the entire light path, individual points along this path cannot be clearly distinguished and spatial resolution is not sharply defined.

Numerous kinds of tracers have been used in the second approach to show how velocity fields may be represented.¹ Smoke, dust and titanium chloride are commonly used to make the flow of gases visible, and malachite green, Durazol and brilliant red (simple biological stains) are often used, along with an effective illumination source, in liquid flow studies. Alternatively, aqueous solutions of fluorescein-sodium, which

are strongly fluorescent under UV light, may be injected into a flow stream upstream from the points of interest. Water flows have been made visible very effectively by injecting streams of air or oxygen bubbles through probes; in a refinement of this method, hydrogen bubbles are electrolytically generated at electrodes.² Another tracer technique uses solid objects such as spherical polystyrene beads or paraffin wax particles to make fluid flows visible.³

Each of these tracer flow-visualization techniques is unfortunately subject to one or more of the following four serious disadvantages.

(1) The tracer materials must be injected into the flow stream and thus cannot have the same physical properties as the fluid.

(2) The flow stream must be disturbed by the injection tube or other probe.

(3) Solid particles, no matter how small, inevitably create disturbances in the flow stream — disturbances that are very important at phase boundaries, such as at the wall of the pipe or a submerged object.

(4) Injected dyes stream along from the injection point in a manner which makes it difficult to "read" velocities at all and certainly impossible to do it accurately.

For these reasons, conventional direct visualization of the velocity field and other fluid flow properties in the region very close to the wall cannot be reliable; these disadvantages make exact quantitative measurements of the velocity field impossible.

There are three modern techniques for studying fluid flows that do not disturb the flows: a Doppler laser probe tech-

Presented on 6 October 1971 at the Society's Technical Conference in Montreal by J. W. Smith and R. L. Hummel (who read the paper), Dept. of Chemical Engineering, University of Toronto, Toronto 5, Ont., Canada.

(This paper was received on 13 September 1971; its publication has been delayed by editorial operations and through no fault of the authors.)

nique, a holographic flow-visualization technique and the photochromic-dye-tracer flow-visualization technique. The first and last are not only precise but also easy to use and interpret. The photochromic dye method has been particularly successful compared with conventional tracer methods, and it is the subject of this paper.

History and Principle of the Method

In 1960, one of the authors (Hummel) suggested the principle of the photochromic dye tracer technique,⁴ but work using it was not begun until late in 1963 by Popovich. In 1965, Goldish et al.⁵ published results of a measurement of dilution time-constant for a chamber which was instantaneously filled with a colored solution generated by a flash of light. The flowing solution contained the ingredients for the blueprint reaction to react with the light and form the color only during the time of the intense light flash. They also suggested that in some undisclosed way this technique could be used for measuring velocities. The following year Popovich described in his Ph.D. thesis⁶ his use of a focused beam of light rather than a diffused light source to form a sharply defined blue line in the solution which could be followed to give precise velocity data. This thesis and two papers by Popovich and Hummel^{7,8} described for the first time the technique now used and noted that the relatively insensitive blueprint reaction previously used had been replaced by the reaction of a photochromic indicator, 2-(2',2'-dinitrobenzyl) pyridine (DNBP). This work also established for the first time the existence of the viscous sublayer for turbulent pipe flow — a very important concept in fluid mechanics, proposed in 1905 but always previously beyond the capacity of conventional techniques to detect and measure.

DNBP has been known since 1925 to respond to irradiation with ultraviolet by undergoing an irreversible photochromic reaction in which the initial pale yellow color darkens to a deep blue in the 95% alcohol solution used.⁹ The color change is believed to be due to the formation of the tautomeric aci-nitro structure and is known to take place in less than $1 \mu\text{s}$.^{10,11,12}

Our research group presently prefers to use deodorized kerosene solutions of 1,3,3-trimethyl-6-nitro-indoline-2-spiro-2-2-benzopyrane (TNSB). Much more dilute solutions can be used (i.e. 0.01% by weight) and the color generation is more efficient. The color-producing reaction occurs when the carbon-oxygen bond in the spiroopyrane ring is broken, producing a merocyanine structure; it is reversible. TNSB can be used also in polar solvents such as alcohol, in which case it forms a red color rather than a blue and is no more effective than the DNBP. The half life of the fading of

both indicators due to the reverse reaction depends on the solvent but is typically between 5 s and 5 min. This fading is desirable so that solutions can be used under ambient light conditions rather than only under darkened conditions.

The light sources currently used are generally lasers because they provide well-collimated light beams of high intensity in very short periods of time (10 ns). One laser used has been the TRG-104A ruby laser.* Its red light in the giant pulse mode can be frequency-doubled by means of a second-harmonic generator into the ultraviolet region. The overall energy output has been estimated to be roughly 0.01 J. For multiple pulses (100 pulses/s), an Avco C950 nitrogen laser is used. It gives a more divergent beam with an energy of only 0.001 J per pulse, but the pulse duration is still 10 ns. Because of the short duration, the instantaneous power level is 10–100 MW which can cause damage to conventional cemented lenses and the focused beam can damage quartz plates or lenses.

The dye trace is best photographed against a background of uniform illumination. The contrast between the dye and the background is improved if a yellow light which is absorbed strongly by the dye is used in black-and-white photography. A 400-W sodium street lamp (GE Lucalox 400) was found to combine high intensity with a suitable color. This lamp is designed for ac operation, but to avoid flicker in high-speed motion pictures it must be operated from a dc power supply (even though this reduces the life of the lamp). The center contact of the bulb's base must be positive or the bulb will fail in very short order.

The photographic equipment used to take cine photographs at up to 8,000 frames/s is usually either a Hycam 400-ft (121.9-m) model or a Locam. When the flow rates are low a Bolex has been substituted. When very high resolution has been required 35mm stills have been taken using a yellow filtered electronic flash for the background light.

In addition to the major items of equipment various other obvious items such as tripods, lenses, ground glass for diffusing the light, etc. have been used to obtain suitable photographs.

Flow Systems

The flow systems are generally quite simple as the only special requirement of the technique is that the test region be visible without serious distortion to the eye and to the camera. There is no need for holes, for probes, or micrometer positioners, and the extremely precise

* Manufactured by the Melville, N.Y., Space & Defense Systems Division of Control Data Corp.

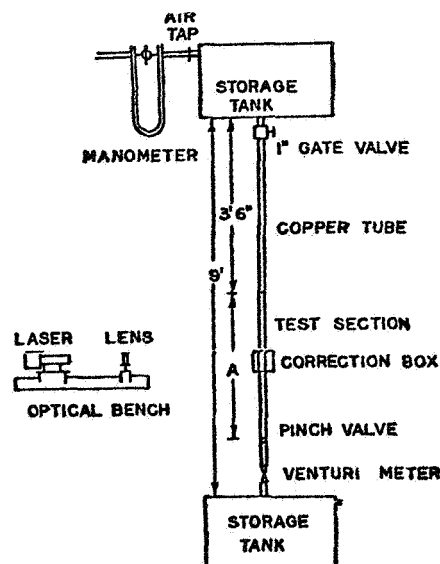


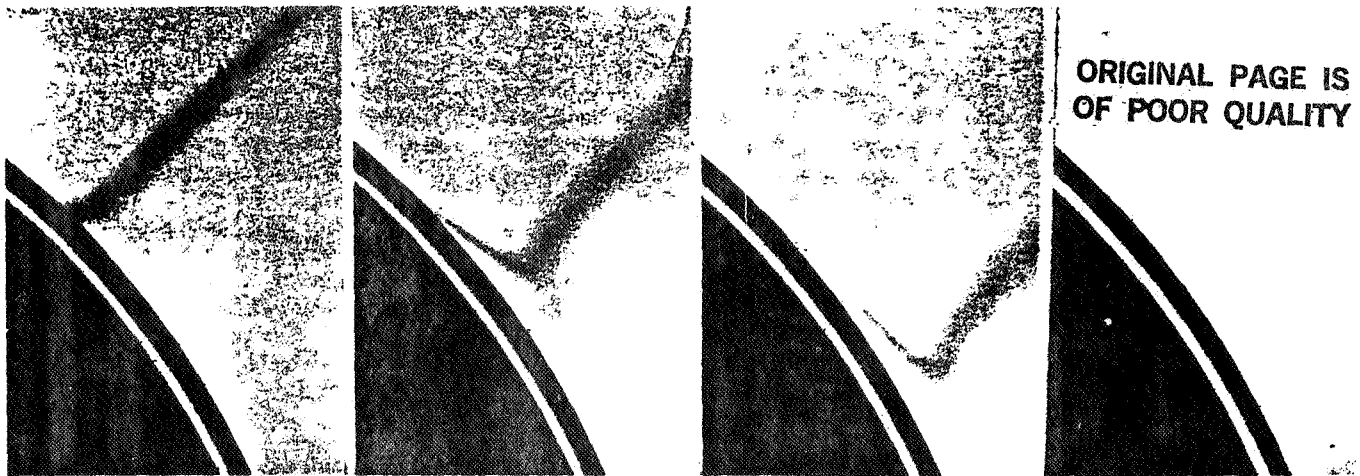
Fig. 1. Schematic front view of the flow system.

optical requirements of schlieren or interferometric set-ups are not required. To set up a run without a test body or model in the flow, reservoirs (typically 5-gal (18.9-l) alcohol jugs with a side opening at the bottom) are mounted at floor and ceiling and connected by Tygon tubing to a glass flow chamber of appropriate geometry. The test fluid is pumped to the upper reservoir before the run and is allowed to flow downward during the run under the force of gravity (possibly aided by additional air pressure) through the flow chamber to the lower reservoir at a controlled rate. In tests on a larger scale the liquid is pumped through a blow-down wind tunnel 14 in (356 mm) in diameter in which models can be installed.

The general arrangement of components is usually that shown in Fig. 1, and can be best described in terms of rectangular coordinates. The flow direction is typically along one axis (from positive to negative z) with the camera and background light along another axis, (positive and negative x). The light beam from the laser passes along the y axis to draw a tracer line perpendicular to both the flow and the camera view.

Typical Results

Figure 2 shows the flow around a transparent glass sphere mounted in the 14-in flow channel on a 1/8-in (3-mm) diameter thin-walled supporting tube positioned to give minimum disturbance to the flow. Measurement of flow symmetry showed the support to have a negligible effect. The UV light was introduced through this support to the center of the sphere where a small prism reflected it at an angle of 90° through the sphere's surface to form the dye trace. The alternative of bringing the light beam in through a viewing port in the flow chamber would have severely reduced the sharpness and intensity of the beam. The first frame shows the



ORIGINAL PAGE IS
OF POOR QUALITY

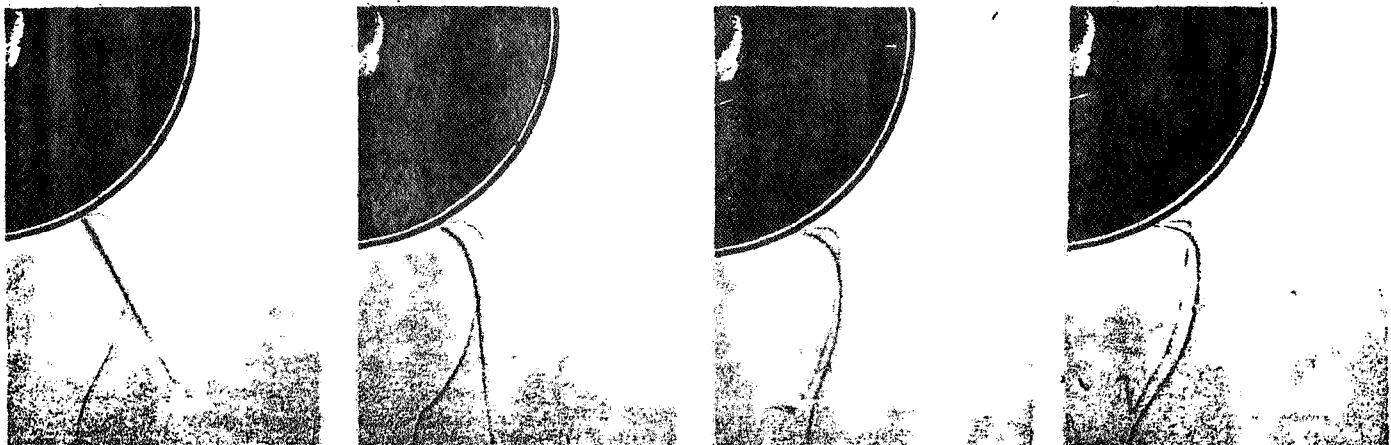
Frame 1

Frame 2

Frame 3

Frame 4

Fig. 2. Flow past a 6-cm glass sphere (flow vertically downward). Laser beam was flashed through the sphere's surface upward and to the right just before frame 1 was taken. Frames 2, 3, 4 were taken subsequently.



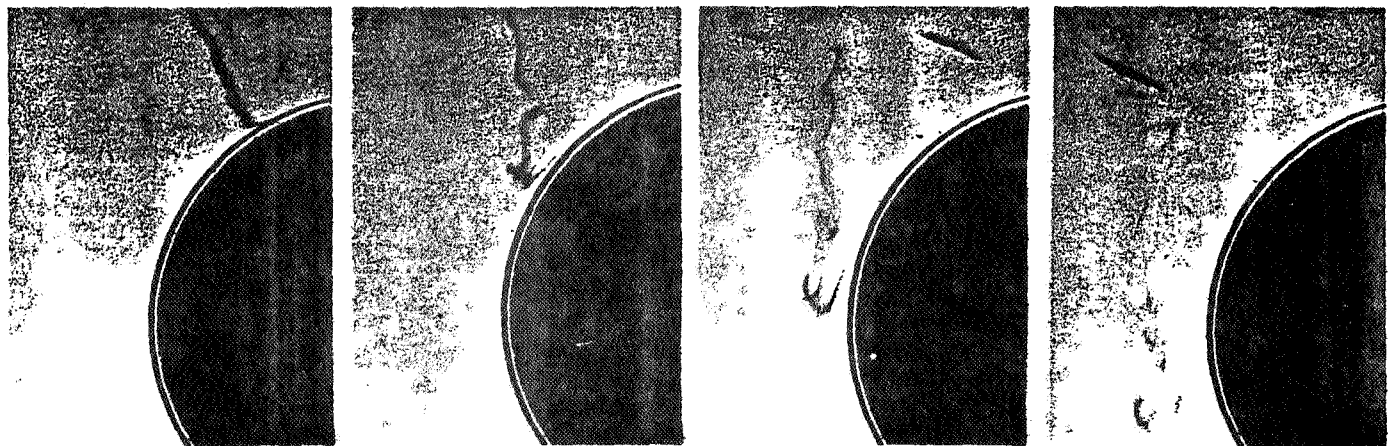
Frame 1

Frame 2

Frame 3

Frame 4

Fig. 3. Wake region below a 6-cm glass sphere. Laser was flashed twice. Frame 1 was taken at virtually the time of the second flash; frames 2, 3 and 4 were taken respectively 1.908, 4.73 and 7.56 s later.



Frame 1

Frame 2

Frame 3

Frame 4

Fig. 4. Flow past a 6-cm sphere with a Reynolds Number of 3190. Flow was downward and laser flash upward (30° from the vertical). Frame 1 was almost simultaneous with the laser flash; Frames 2, 3 and 4 were later by 0.127, 0.254 and 0.381 s respectively.

shape of the trace shortly after the UV beam emerged from the sphere and frames 2, 3 and 4 are at later times. Notice how clearly the region of sphere influence and the maximum velocity for the flow are defined. These had not been possible to measure using probes and had been inferred incorrectly from theory.

Actual three-dimensional velocities

cannot be determined directly from observation, but must include a calculation of material balanced to split the raw velocity data into radial and tangential velocity components. Figure 3, at a greater reduction ratio, shows the flow reversal near the sphere and the turbulence in the wake of the sphere. In the turbulent wake, it is no longer convenient

to obtain flow components by material balance, but rather features generated by the turbulence may be followed to give the 3-dimensional motion. In this study reported by Seeley,¹² where measurement was done manually, turbulent motions were not digitized, but in the future it is planned to use a computer system to read the film. Figure 4 shows the sphere in a

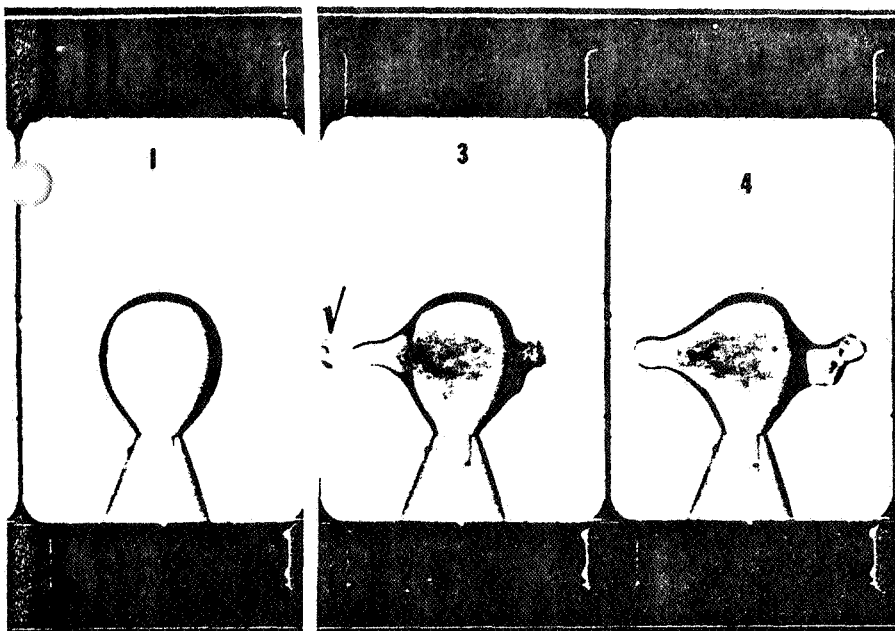


Fig. 5. Eruption of a stationary liquid drop containing a photochromic dye. Mechanism is probably the same as the one where lenses are sometimes shattered by laser light, namely the generation of strong nonlinear effects at the interfaces.

turbulent flow regime. This condition was not studied quantitatively, but one can easily see that near the surface there is a region where the flow has been smoothed. This effect is contrary to what was previously believed to occur under these particular conditions. Because this nearly laminar flow near the surface is not strictly steady, the effect could not have been detected easily with probe techniques — even the non-disturbing Doppler laser technique. Obviously, actually seeing a phenomenon or viewing its record on film is superior to making suppositions or speculations about its existence.

Other systems which have been studied include falling liquid films, rough-pipe momentum transfer, pipe jets and growing liquid drops. Figure 5, from Humphrey's study of growing liquid drops,¹⁴ illustrates that the question of the technique being non-disturbing must always be examined and tested. In this particular case, a very substantial effect on the drop can be seen. When the laser beam strikes the drop and the dye trace is formed, the drop erupts. Two possible explanations for this phenomena have been considered. One explanation is the surface tension of the closed form of the photochromic compound changes and this produces the disturbance. A more likely explanation, however, con-

sidering the magnitude of the energy shown is that a phenomenon similar to the breaking of lenses mentioned earlier is responsible. Lenses are broken not because they are not completely transparent to the light, but because the very high power level reached in the laser beam produces nonlinear effects or even ionization at the interface between two materials. A substantial fraction of the energy can be discharged in the interface during a period of a few nanoseconds, and this could result in the large acceleration that is observed. Again, because this technique makes it possible to view a phenomenon, unexpected disturbances that spoil a run can be easily detected so that invalid results may be discarded. When the energy of the beam is reduced by 50% the disturbance disappears. The generation of this disturbance is very dependent on the type of liquids used and does not occur for most liquid-liquid combinations.

Conclusions

Many previously intractable fluid dynamics problems have yielded to the optical flow visualization technique described above. Future development of computer logging methods will greatly increase its utility.

Acknowledgments: The authors are greatly indebted to the National Research Council of Canada for financial support, and to L. E. Seeley, S. G. Dunn, A. Iribarne, F. Frantisak, B. D. Allen, V. R. Arunachalam, B. Davey and J. A. C. Humphrey for permission to use parts of their work in this paper.

References

1. E. W. G. Dancy, ASME Symposium of Flow Visualization, Nov. 1960; *Inst. Gas Engineers J.* 4: 282, 1967.
2. S. J. Kline and R. A. Schraub, Stanford Univ. Mech. Engrg. Dept. Rept. MD-72, 1965.
3. J. P. Hettler, P. Muntzer and O. Scrivener, *Compt. Rend.* 258: 4201-4207, 1964.
4. R. L. Hummel, UMRI-60-250-LL, "Precise Measurement of Velocity Distribution of a Flowing Stream at and Very Near the Wall," to NSF, Jan. 8, 1960.
5. L. H. Goldish, J. A. Koutsky and R. J. Adler, *Chem. Eng. Sci.*, 20: 1011-1014, 1965.
6. A. T. Popovich, Ph.D. Thesis, Dept. of Chemical Engineering, Univ. of Toronto, 1966.
7. A. T. Popovich and R. L. Hummel, *Chem. Eng. Sci.*, 22: 21-25, 1967.
8. A. T. Popovich and P. L. Hummel, *AIChE J.*, 14: 854-860, 1967.
9. A. E. Tschitschibabin, B. M. Kuindshsi and S. W. Benewolens Kaya, *Ber. Deut. Chem. Ges.*, 59: 1580-1587, 1925.
10. H. S. Mosher, C. Souer and E. R. Hardwick, *J. Chem. Phys.*, 33: 1888-1892, 1960.
11. J. A. Sousa and J. Weinstein, *J. Org. Chem.*, 27: 3155-3159, 1962.
12. H. S. Mosher, E. R. Hardwick and D. BenHur, *J. Chem. Phys.*, 37: 904-909, 1962.
13. L. E. Seeley, Ph.D. Thesis, Dept. Chemical Engineering, University of Toronto, 1972.
14. J. A. C. Humphrey, Dept. of Chem. Eng., Univ. of Toronto, Private Communication.

Discussion

Dahya Bhaga (McGill University, Montreal, Quebec, Canada): What technique would you use to make a grid of the tracer fluid?

Dr. Hummel: I would use a dichroic-mirror type of beam splitter to split the laser beam. Beam splitting will be discussed in the following paper (by Sovova, Prochazka and Hummel).

Mr. Bhaga: What are the limitations on the type of liquid that can be used with your photochromic visualization technique, and can aqueous glycerol and sugar solutions be used to take advantage of the ease with which one can vary their viscosities?

Dr. Hummel: At present the materials we've used dissolve only in organic solvents. Glycerin can be used quite easily, and we have done studies where we have varied the viscosity.

I. Feuerstein (McMaster University, Hamilton, Ont., Canada): How do you obtain quantitative information?

Dr. Hummel: We measure the x and y components of a point in the trace in subsequent frames. The motion on the surface is easy to follow to get an indication of compressions and extensions. You can use the continuity equation to calculate the motions that these imply.

ORIGINAL PAGE IS
OF POOR QUALITY

Flow Near the Surface of a Mixing Vessel: An Example of the Photochromic Technique Using Inexpensive Equipment

By H. SOVOVA, J. PROCHAZKA and R. L. HUMMEL

Most applications of the photochromic technique of flow visualization have involved elaborate or expensive equipment. A simple, inexpensive application of the technique is described applied to a study of the fluid dynamics phenomena involved in mass transfer across a liquid gas interface. Essentially the set-up requires only a stirred beaker with photochromic dye solution, several relatively inexpensive sources of illumination (no laser) and a 35mm still camera or, alternatively, a movie camera. The analysis of the trace patterns photographed as described and the association between the flow pattern observed and the expected heat and mass transfer mechanisms is discussed.

IN MANY types of chemical equipment, gas and liquid streams are contacted to bring about heat and mass exchange between them. Usually the phases are kept in intensive motion so that the bulk transport is very rapid. Under such conditions the main impediment to the transfer is found in the space close to the interface because this interface provides an obstacle to free convective motion of the fluid phases. Consequently, a detailed understanding of this phenomenon is of major importance.

Numerous theoretical and experimental investigations of heat and mass transfer¹⁻⁵ across liquid-liquid and gas-liquid boundaries have been performed, and several models of the process have been proposed. Most experimental work has been done in a cell with stirrers and a plane interface of known area.^{3,4} However, detailed understanding is still elusive, primarily because the measurements of the overall rate of heat or mass transfer can provide only limited evidence of the local flow pattern near the interface.

The photochromic flow visualization technique introduced by one of the authors (Hummel) and co-workers⁶⁻⁸ represents a promising means for such study. In this technique, a photochromic indicator is added to a clear liquid to make up a test solution which is virtually clear. When selected areas of this test solution are subsequently irradiated with ultraviolet light these areas instantly become deeply colored, and remain so for some tens of seconds before the color fades. This permits the traces to be unambiguously observed or photographed. How this principle can be used to study fluid flows will become clear in

the following discussion. It has been successfully applied to the investigations of flow along rigid walls and in a forming liquid drop. Its main advantage is that it allows the observer to follow the motion in the narrow space near an interface without distorting the flow pattern. The present work is the first step in the application of this technique to the investigation of convective transport across the fluid interface, particularly the gas-liquid interface in a stirred vessel.

In its most elaborate form,⁸ the photochromic technique implies the use of rather expensive equipment, e.g., an N₂ laser or a giant-pulse ruby laser with a frequency doubler, and a high-speed camera. The purpose here is to show that a good deal of information, at least in the preliminary stages of investigation, can be obtained with relatively simple and inexpensive means.

Apparatus and Equipment

Experiments were carried out in a glass beaker with a mixer (Fig. 1). The mixer, a four-blade turbine with inclined blades (a), was driven by a variable-speed motor and was surrounded by a

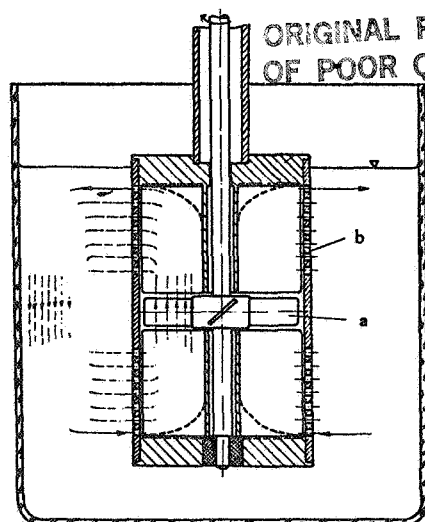


Fig. 1. Schematic representation of the mixer, showing (a) the inclined blades and (b) the special stator designed to eliminate tangential flows and excessive rippling of the gas-liquid interface.

special stator cage (b). The purpose of the stator was to eliminate tangential flows and excessive rippling of the gas-liquid interface. The beaker was filled with toluene, in which a photochromic indicator (1,3,3 trimethyl-6-nitro-indoline-2-spiro-2-2 benzopyrane) was dissolved. This chemical compound changes from clear to blue in color after irradiation with ultraviolet (UV) light. The optical arrangement is shown in Fig. 2. The cylindrical beaker was immersed in a rectangular Lucite tank filled with water to minimize the distortions and reflections caused by the cylindrical walls. The camera used was a 35mm Exacta Varex 2 still camera with an Orestor 2.8/100 lens and extension rings or, alternatively, an AK 16 motion-picture camera operating at a rate of 32 frames/s and 50mm, f/1.4 lens.

With the still camera, a second xenon lamp was used as a background light source; the lamp was triggered by a delay circuit. Although the background light had a greater light output at all wavelengths, including the UV, the intensity was far lower (being unfocused) and created no perceptible color. The yellow filter placed on the camera to improve contrast could have been applied to the flash to remove the UV as well as the blue light.

With the motion-picture camera, a 400-W sodium lamp (the General Electric LU-400/BD), which has the desired yellow hue, was used.

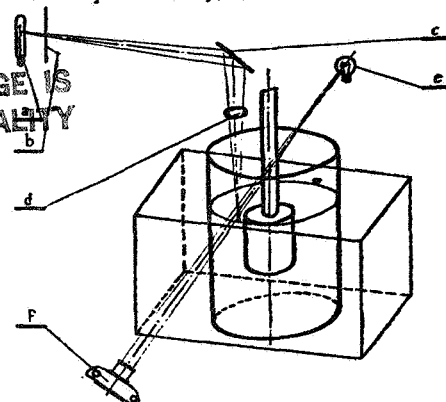


Fig. 2. Optical arrangement for the study: (a) 200-joule xenon flashlamp for UV light source; (b) mask with six parallel slots to create six light sources; (c) plane mirror inclined so as to direct the light sources downward toward the gas-liquid interface; (d) quartz lens of 40-mm diam and 45-mm focal length to form six images on the interface; (e) auxiliary light source to illuminate the traces; and (f) still or motion-picture camera to record the traces.

Presented at the Society's Technical Conference in Montreal on 6 October 1971 by H. Sovová and J. Procházka of the Institute of Chemical Process Fundamentals, Czechoslovak Academy of Sciences, Prague 6, Suchbát 2, Czechoslovakia; and by R. L. Hummel (who read the paper), Dept. of Chemical Engineering and Applied Chemistry, University of Toronto, Toronto 5, Canada.

(This paper was first received on 13 September 1971; its publication has been delayed by editorial operations and through no fault of the authors.)

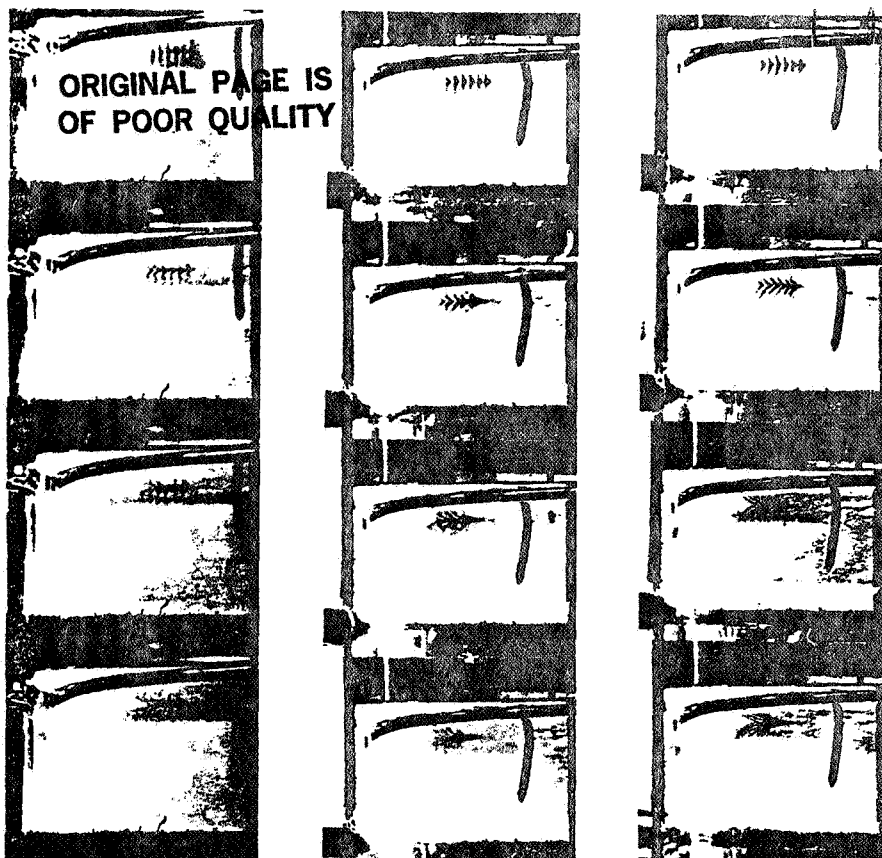


Fig. 3. Motion of traces during stirring at (a) 200 r/min, (b) 150 r/min, and (c) 100 r/min.

optical axis inclined to it, so that both the traces and their mirror images (due to total reflection from the underside of the interface) could be photographed. By this means it was possible to follow traces to the very interface. Comparing the inclination of the traces and their mirror images it is also possible to assess the direction of the traces in space. This is, of course, limited to the case of a plane interface free of ripples. It is easy, however, to study the traces in three dimensions by using a system of four mirrors: in this way, two views of the traces can be obtained in a single picture, with the views at right angles to one another.

Results and Analysis

In Fig. 3, motion-picture sequences show the motion and deformation of the traces in the radially-moving liquid near the interface and stirred at rates of 200, 150 and 100 r/min, respectively. The first striking feature of these pictures is that the radial velocity of the surface is much less than that of the liquid just below it. One would not expect this to be the case for a large surface in contact with gas. The flow under the surface is almost laminar for the lowest rate of revolution, as is seen from the parabolic shape of the lines. The velocity profile can be easily determined from the measurements of the position of the corresponding

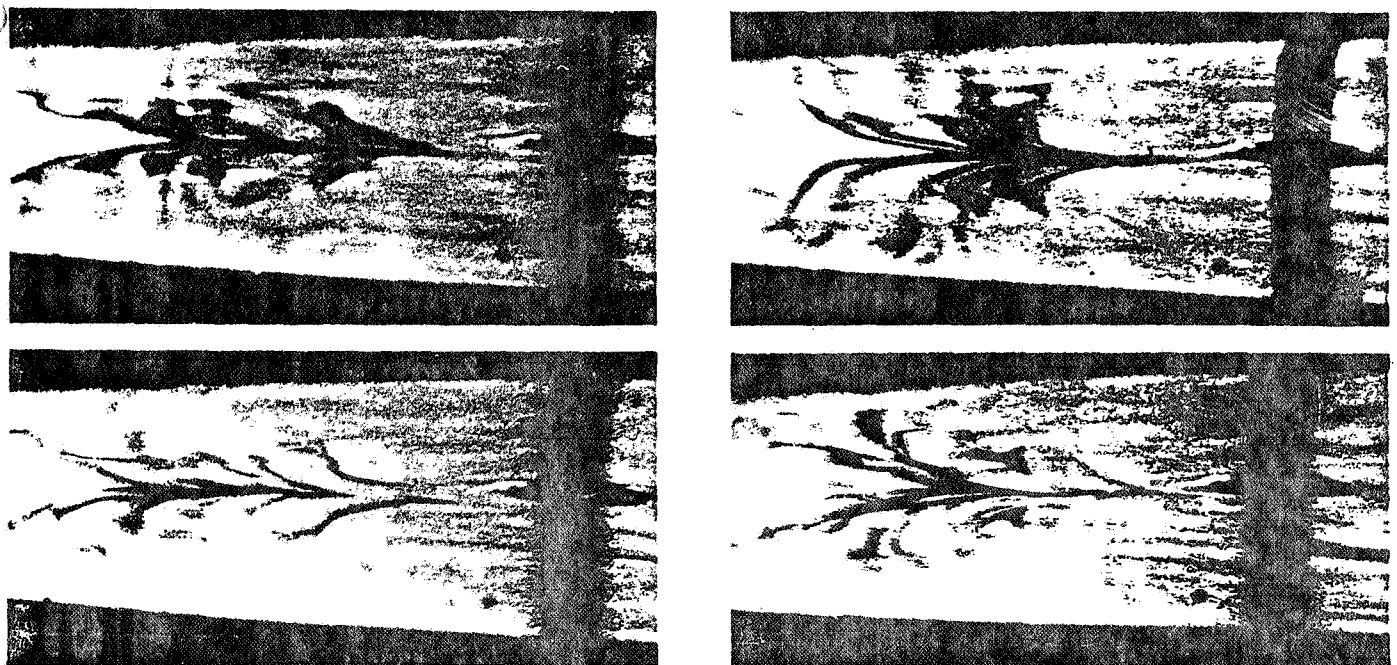


Fig. 4. Still camera pictures of traces, with stirring at 250 r/min and 100-ms delay.

The film material was Agfa 35mm Copex pan, type A.H.I and Foma 16mm Mikropan, 17 DIN.

For the xenon lamp power supply, which was constructed in the workshop of the Institute, had a total capacitance of 180 μF and an operating voltage of 1.25 kV. The discharge duration was approximately 100 μs .

The formation of several parallel

traces is particularly advantageous as it provides more information than a single line. For example, it is possible to follow the deformation of the plane in which the traces are lying. It is also much easier to estimate the shape and direction of motion of a fluid element.

In the arrangement described above the camera was positioned slightly below the interface of the liquid with the

points of the traces in subsequent frames. It can be concluded that the prevailing mechanism of heat and mass transfer in this case will be the unsteady diffusion into the surface during its exposure to the gas.

The other two sequences show a less regular motion near the interface. Local stretching and compression of the liquid near the surface can be observed, which

is the result of impact of large eddies. Small eddies of wavy or circular form are also present. The dimensions of these eddies and their time of decay could be determined from the film. More details can be recognized in the still photographs shown in Fig. 4, which were taken for a stirring rate of 250 r/min. The time delay between flash 1 (formation) and flash 2 (observation) was 100 ms. In Fig. 4 it can be clearly seen that sometimes a trace is detached from its mirror image and a gap appears at the surface. We conclude that a surface renewal by a small eddy has occurred and the old colored liquid element was replaced by a new one from the bulk of the liquid phase. Also very

interesting is the splitting and widening of some lines. This phenomenon can be ascribed to the action of disturbances of a lower order of magnitude than the original width of the traces.

The above description gives an impression that there are several mechanisms of heat and mass transfer at the interface during a forced turbulent flow in the bulk of the liquid. The first of those mechanisms is surface renewal by sweeping, stretching and compression due to large disturbances and similar small-scale phenomena due to small eddies, and the second is turbulent transport from the surface to the bulk by microscopic disturbances. Which of these mecha-

nisms is dominant can be decided only after quantitative evaluation of the pictures and is beyond the scope of the present paper.

References

1. R. Higbie, *Trans. AICHE.*, 31: 365, 1935.
2. P. V. Danckwerts, *Ind. Eng. Chem.*, 43: 1460, 1951.
3. J. B. Lewis, *Chem. Eng. Sci.*, 3: 248, 1954.
4. J. K. Sherwood, *Chem. Eng. Sci.*, 4: 290, 1955.
5. C. J. King, *Ind. Eng. Chem. Fund.*, 5: 1, 1966.
6. A. T. Popovich and R. L. Hummel, *Chem. Eng. Sci.*, 22: 21, 1967.
7. F. C-K. Ho and R. L. Hummel, *Chem. Eng. Sci.*, 25: 1967.
8. J. W. Smith and R. L. Hummel, *Jour. SMPTE*, 82: Apr. 1973.

ORIGINAL PAGE IS
OF POOR QUALITY

Television Receiver White Color: A Comparison of Picture Quality With White References of 9300 K and D6500

By DAAN M. ZWICK

Color television receivers in the U.S.A. generally have a white color approximately equivalent to the appearance of a black-body at 9300 K, or higher. The white reference of a studio monitor is specified at D6500. In connection with the study of color television variability being conducted by an Ad Hoc Committee (AHCCTS) of JCIC, the question was asked, "Is a viewer's tolerance to color variation different for the two display situations?" To answer this question observers were asked to rate for quality pictures having a wide gamut of color variation originating from photographic slides, presented through telecine separately on two receivers adjusted to the two display conditions. Observers ranked the pictures displayed on the D6500 receiver consistently higher in quality than the pictures displayed on the 9300-K receiver.

The conclusion that viewers prefer pictures displayed at a white reference of D6500 to those referenced to 9300 K prevented obtaining an answer to the original question on tolerance to color variability, but in itself is a more important fact bearing on the choice of a white reference for television receivers.

Introduction

Although there are no industry standards, the white reference for television receivers in the U.S.A. is generally intended to be in the vicinity of a black-body radiator at 9300 K. This relatively high color temperature (compared with other "white" colors in our environment) is partly a legacy from monochrome television (the color of "bright" phosphors), but even more it is a result of the compromise between brightness and color required in the past by the available phosphors in color receivers. For example, for a particular phosphor combination in shadow-mask receivers, the electrically desirable condition of equal drives to the three electron beams resulted in the 9300-K color. It appears that colorimetric fidelity has not been a primary factor in the choice of receiver white color. The dominating factor has been a desire for high brightness.

The original NTSC specification¹ was based on a white reference of Illuminant C, or 6774 K, which is related to a white color of our environment (skylight plus sunlight). The white reference of the studio color monitor is defined in an SMPTE Recommended Practice as that having the appearance of D6500; this white color is a part of television colorimetry specifications, internationally. The reasons for the NTSC choice of white are documented²; they include some arguments based on picture quality.

Although Townsend³ has described further experiments which might lead to a different white reference, and Lisk⁴ has shown that the specified white color may not always be the actual white color, the fact remains that there are two different white references, one for monitors and one for receivers, the former being significantly "warmer" or lower in correlated color temperature than the other. The need for, and the effect of, this difference have been questioned periodically; no compelling arguments for change have arisen.

In a thorough discussion of this ques-

tion⁵ C. J. Hirsch pointed out that there are several complications resulting from having the white reference of studio monitors different from that of the home receiver. He recommended that a survey be made by a professional committee or industry group to determine what value of reference white the public prefers for color reception.

In the course of their broad investigation into the causes of color variability in the entire television system, members of the Ad Hoc Committee on Color Television Study (AHCCTS) of the Joint Committee for Intersociety Coordination (JCIC)⁶ raised the question of the contribution of the white reference to the problem. A statement was made,⁷ that the variation in color was more noticeable on a receiver having a white referenced to 9300 K, than on one referenced to Illuminant C or D6500. To provide data on this question two experiments were performed; they are described here.

Preliminary Experiment

In connection with experiments designed to study the preferred color balance and the neutral gray point for television films,^{8,9} we had available a set of color transparencies that included a wide gamut of color variation on each of nine different scenes. We presented these transparencies by optical projection to a panel of observers, using four different illuminant white colors, which were the unfiltered tungsten projector and three levels of increased color temperature obtained by placing specific thicknesses of Corning filter No. 5900 over the projection lens. Measurement of the light reflected from the screen gave correlated color-temperature values of 3600 K, 6500 K, 9003

Presented on 24 October 1972 at the Society's Technical Conference in Los Angeles by Daan M. Zwick, Physics Div., Research Laboratories, Eastman Kodak Co., Rochester, NY 14650. (This paper, first received on 5 October 1972, received in final form on 6 March 1973.)

Remote optical techniques for liquid flow and temperature measurement for Spacelab experiments

William W Fowles

Fluid Dynamics Laboratory
Space Sciences Laboratory
NASA, Mail Code: ES82
Marshall Space Flight Center, Alabama 35812

ORIGINAL PAGE IS
OF POOR QUALITY

Abstract

The near-zero gravity environment of Spacelab presents the opportunity to perform many new fluids experiments which cannot be done in earth-bound laboratories. A large number of these investigations involve relatively small and confined volumes of fluid. Hence fluid measurement techniques are required which do not disturb the flow. Several nonintrusive measurement techniques are being investigated. A photochromic dye method is being developed for flow measurement. Photochromic dyes are substances which darken upon exposure to ultraviolet (UV) radiation and then clear up again spontaneously. A small amount of dye ($\sim .025\%$ by weight) has been successfully dissolved in a low viscosity silicone oil and dye streaks created upon exposure to an UV source. The movement of the streaks reveals the flow. The streaks then clear up so that the procedure can be continued without the liquid becoming opaque. A laser Doppler dual-scatter system is also being developed for low flow speed measurement. An accuracy of a few percent has been demonstrated for flows of a few millimeters per sec. A double grid schlieren system is being developed for temperature measurement. The optical arrangement is such that an image of a Ronchi ruling is superposed on the original ruling giving a uniform grey field of view. Departures from the background are caused by light being refracted as it passes through the experimental volume.

I. Introduction

When the Space Shuttle becomes operational in the 1980s, some of the flights will take into orbit a laboratory known as Spacelab. Spacelab will have the environment of a laboratory on the earth's surface except that when in orbit the value of gravity will be very small. The fact that Spacelab gravity will not be exactly zero is due to astronaut movements, the vibration of Spacelab and Shuttle equipment, orientation rocket firings, etc. However these sources will give a value of about 0.1 cm/s^2 which is about 10^{-4} of the value of gravity at the earth's surface.

A principal use of Spacelab will be to exploit this low-gravity environment for science and technology. Experiments which cannot be undertaken in laboratories on the earth's surface will be performed. One of the most striking phenomena of a low gravity environment is the suppression of buoyancy forces and hence of free convection in fluids. This absence of convection has great

potential for improved and unique studies of crystal growing, fluid mixing, electrophoretic separation, geophysical fluid flow modeling and other research areas.

A large number of these fluids investigations involve relatively small and confined volumes of fluid. Hence measurement techniques are required which do not disturb the flow. Further, if the Spacelab fluids experiments are to be well defined, critical investigations, rather than simple qualitative demonstrations, quantitative, sensitive and accurate measurement techniques are required.

The Fluid Dynamics Laboratory at NASA MSFC is concerned with developing techniques for nonintrusive flow and temperature measurements in liquids for Spacelab experiments and for the development of Spacelab experiments in ground-based laboratories. Three techniques have been selected for systematic study and development. A photochromic dye technique is being investigated for flow field measurement and a laser Doppler velocimeter for point velocity measurements and particularly for low velocity measurements. A double grid schlieren system is being examined for temperature field measurement. The following three sections are devoted to discussions of these techniques. In each case the section begins with an outline of the essential physics of the technique and with references to further discussions in the open literature. The sections then proceed to discuss the specifics of interest to the Fluid Dynamics Laboratory and the progress that has been made.

II The Photochromic Dye Technique

The use of dyes to show the flow of gases and liquids is a well known technique which has a long history and a very great number of different manifestations. An outstanding early application was that of Reynolds¹ and recent comprehensive reviews have been given by Werlé² and Merzkirch.³ In general dye is inserted or somehow produced in the flow and measurements made by following the movement of the dye by direct observation or by photography. The principal disadvantage for confined fluids is that the dye already inserted will disperse through all the fluid and additional dye will be obscured. Further drawbacks are that the dye insertion probe or the insertion of the dye itself may disturb the flow. If the density of the dye is different from the host fluid, significant rising or sinking motions may occur. A technique introduced by Baker⁴ known as the thymol blue technique,

produces neutrally buoyant dye at a wire in a liquid when a low voltage is applied to the wire. However, a drawback can be the drag produced by the wire. For low Reynolds number flow the drag on a sphere decreases linearly with the diameter of the sphere but for a cylinder the drag depends logarithmically on the diameter.⁵ Thus, not much is gained in decreasing the diameters of probe wires or struts in attempting to reduce disturbance of the flow.

A dye technique which does not suffer from the above disadvantages is the photochromic dye technique. Chemical substances exist which change their radiation absorption characteristics when exposed to ultraviolet radiation. These substances are known as photochromics and they are used commercially in sunglasses. They darken upon exposure to UV radiation and then clear again spontaneously when the UV is removed. These dyes have been used by Popovich and Hummel⁶ and Smith and Hummel⁷ and others for liquid flow measurement.

The photochromic dye 1, 3, 3, Trimethyl, 6, Nitro Indoline, 2, Spiro 2, 2 Benzo Pyrane (TNSBP) was found to be soluble in silicone oil (Dow Corning 200 Series). After stirring, some simple filtering was required to make the oil clear again. Three different types of UV sources, (1) xenon flash lamps, (2) continuous discharge mercury lamps and (3) UV lasers were tried and all produced a dark blue coloring in the oil.

Figure 1 is a photograph showing a sheet of dye produced in a volume of oil contained between two concentric spheres. The oil

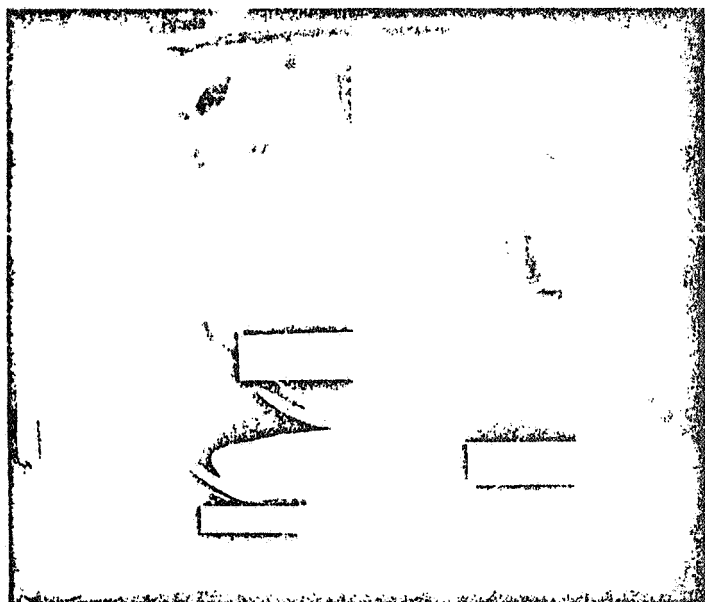


Figure 1. Photochromic dye sheet created in silicone oil contained between two spheres by exposure to an UV source. The spheres were differentially heated. This photograph was taken about one minute after the exposure. Note the effect of the sinking fluid at the cooler outer sphere.

was Dow Corning 200 Series 1 centistoke silicone oil which contained about 0.025% of TNSBP by weight. The tube of a continuous mercury discharge lamp (Phillips 93136F) was focused into the volume. The oil was exposed to this UV source for about 3 seconds. The dye was illuminated by an expanded laser beam (Spectra Physics, Model 120) projected at 90° to the line of sight. The spheres were part of an apparatus constructed for the development of geophysical fluid flow models for Spacelab.⁸ The inner sphere had a diameter of 4.0 cm and the outer sphere an inner diameter of 6.0 cm. For this work the inner sphere was heated and the outer sphere cooled, a temperature difference of about 10 C having been maintained. Figure 1 was taken about 1 minute after the exposure to the UV lamp. Sinking of the cool oil at the outer sphere is shown. Figure 2 shows the dye about 8 minutes

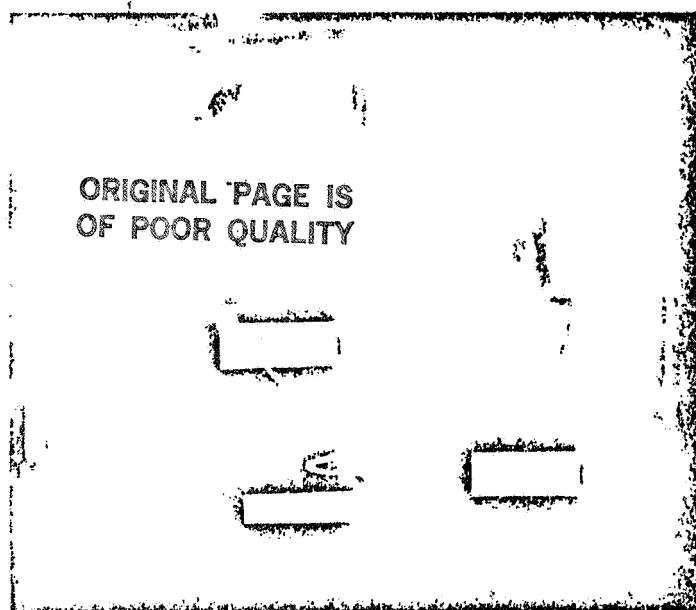


Figure 2. The same dye sheet as shown in Figure 1 eight minutes after the exposure to UV. The dye is still visible as a narrow line which corresponds to a streamline of the convergent flow in the lower part of the spheres.

after the exposure. The convergent flow in the lower part of the spheres has concentrated the dye into a narrow line which is still visible. This line actually corresponds to a streamline of the flow with the liquid moving upwards close to the inner sphere. Note that the dye is much less intense in Figure 2 than in Figure 1. The fact that it is still observed at all is due to the particular sensitivity of the 90° laser illumination.

Dye was also produced using xenon flash lamps. However, because of the short duration of the flashes, substantial UV intensity and efficient collecting and projecting optics are required to make the dye visible. A UV laser (Spectra Physics, Model 170) was used to produce dye in the oil. With this laser operating in its integrating mode with a UV power of about 50 milliwatts, sharp dye lines were produced by focusing the beam into the oil and exposing for about 3 seconds.

To optimize the use of this technique, systematic surveys of the effects of dye concentration, UV exposure levels and dye relaxation times were carried out. This work was done by Aerojet ElectroSystems Co. under contract from NASA/MSFC. The following results were obtained using samples of Dow Corning 200 Series 0.65 centistoke silicone oil in a Beckman Mark IV spectrophotometer. The samples were contained in fused silica flasks and the temperatures of the samples were maintained and measured. The dye concentration is given as the percentage of TNSBP by weight and the UV exposure levels in joules/cm². The transmittance of the unexposed solution for various dye concentrations at 30 C was measured first. The results are shown in Figure 3. Note that even when a very small amount of TNSBP has been added the short wavelength cutoff moves from about 0.3 micron to about 0.4 micron. This tells us that the wavelengths activating the TNSBP are in this range. The measurements were made for very low UV exposure levels so that no detectable darkening of the solution occurred.

Next, the transmittance at various exposure levels for a fixed concentration of 0.025% was measured. The results are shown in Figure 4. Note the large absorption of the exposed solution in the yellow region of the spectrum around 0.6 micron. This is why the dye appears blue in white light. Figure 5 shows the results for various concentrations for a fixed exposure of 0.035 joule/cm². Figures 6 and 7 show the time relaxation curves for various concentrations and exposures at 30 C and 45 C, respectively. The

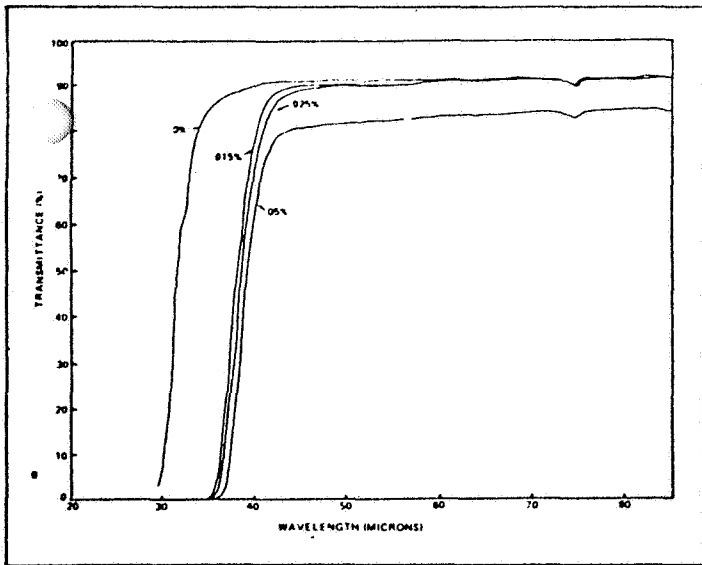


Figure 3. The transmittance of unexposed solutions of TNSBP in Dow Corning 200 Series 0.65 centistoke silicone oil as a function of wavelength for various dye concentrations at 30 C.

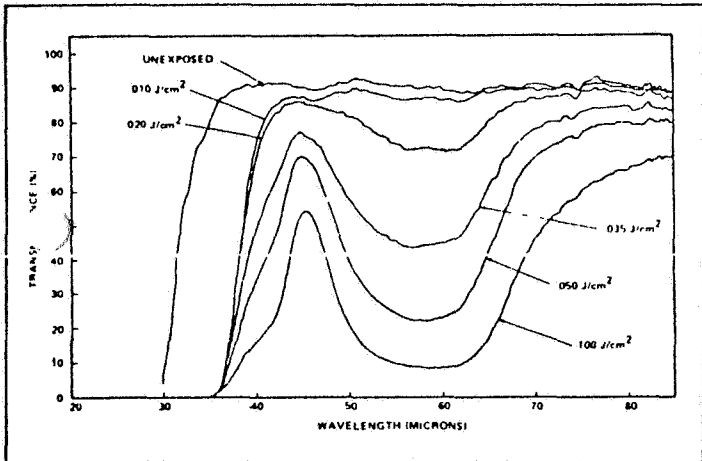


Figure 4. The transmittance of an exposed 0.025% solution as a function of wavelength for various exposure levels.

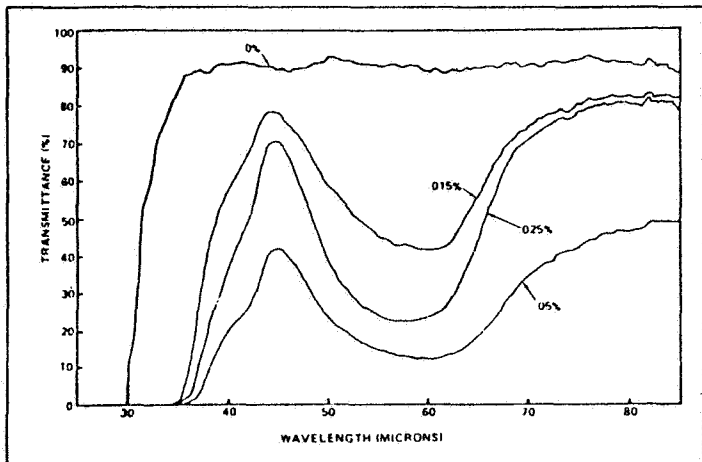


Figure 5. The transmittance of solutions exposed to 0.035 joule/cm² as a function of wavelength for various dye concentrations.

transmittance was measured for 0.6 micron. Note that the time relaxation is a strong function of temperature: the dye disappears

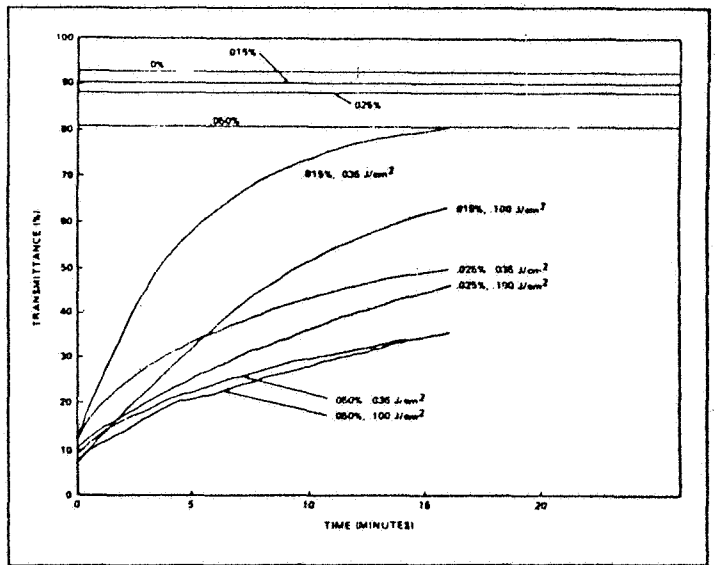


Figure 6. Time relaxation curves for various concentrations and exposures at 30 C. The transmittance was measured at 0.6 micron. The reference transmittance data for the unexposed solutions are also shown.

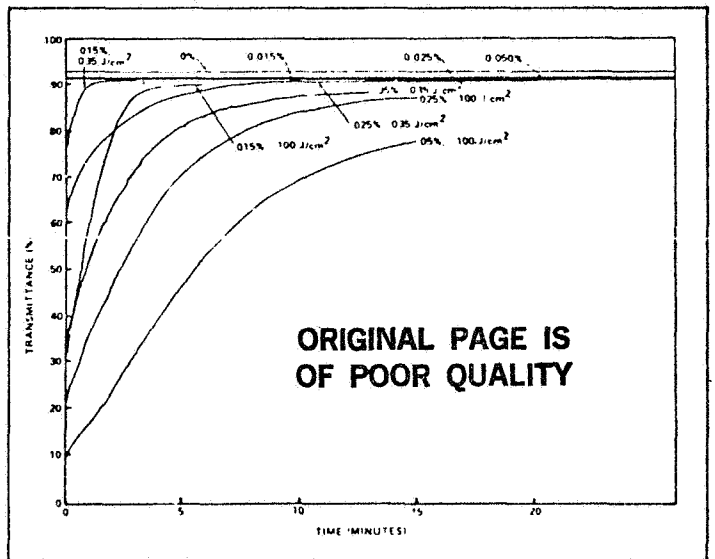


Figure 7. Time relaxation curves for various concentrations and exposures at 45 C. The transmittance was measured at 0.6 micron. The reference transmittance data for the unexposed solutions are also shown.

much more quickly in the warmer oil.

The fact that the dye is strongly visible when illuminated at 90° to the line-of-sight means that in its activated form it is not truly in solution. In this form, it must be less soluble and in a colloidal state. Under the range of conditions presented above, no sedimentation of the dye was ever noticed. If, however, the solution is exposed to UV radiation orders of magnitude greater than the above, the dye forms coarse grains and settles out and it will only redissolve after several hours.

III. A Laser Doppler Velocimeter

The laser Doppler velocimeter (LDV) technique for fluid flow measurement was first demonstrated by Yeh and Cummins. These authors showed that the Doppler shift of laser light scattered by particles immersed in moving water could be detected by beating (heterodyning) the scattered light with some of the original laser radiation. The amount of literature on various

aspects of LDV techniques and applications is substantial; bibliographies and reviews are available.^{3,10,11} The development of electrophoretic separation chambers and the direct measurement of cell mobilities requires accurate measurement at low flow speeds with fine spatial resolutions. The Fluid Dynamics Laboratory is examining the low flow speed limitations of the laser Doppler technique.

In this paper, the LDV system chosen to measure low speed flows (<0.1 cm/sec) is briefly described. A detailed description of the system has already been presented by Fowllis and Martin.¹² Figure 8 is a drawing showing the essential geometry of the dual-scatter or fringe system. The original laser beam (Spectra Physics,

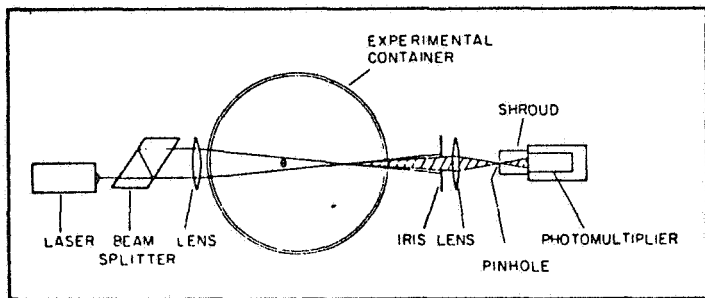


Figure 8. A schematic drawing showing the essential geometry of the dual-scatter LDV system.

Model 120) is first split into two parallel beams of equal intensity. A lens then focuses these beams to a point within the fluid. The crossover point of the beams defines the location of the measurement and the volume of intersection of the beams defines the spatial resolution. Clearly, because of the focusing down, excellent resolution can be obtained. On emerging from the test volume the beams are terminated on an iris. Light scattered by particles or cells in the beams passes through the iris to a second lens which focuses the scattered light into a pinhole. By adjusting the distance between this lens and the pinhole and the pinhole diameter, only scattered light from the crossover volume passes through the pinhole and reaches the photomultiplier (Centronic, Type P4283B).

A particle passing through the scattering volume scatters light from both incident beams. Because of the angle between these beams (θ), the scattered light from each beam is Doppler shifted by a different amount. Heterodyning of these two frequencies by the photomultiplier produces the difference frequency.

$$v_D = \frac{2n \sin \frac{\theta}{2}}{\lambda} V \quad (1)$$

where n is the refractive index of the fluid, λ is the wavelength of the laser and V is the component of the flow velocity perpendicular to the optic axis of the system and in the plane of the laser beams.

The component V was determined from a measurement of the frequency v_D . The photomultiplier output was amplified and then passed through a bandpass filter to remove unwanted dc, high frequency signals and noise. It was then amplified again and clipped and finally sampled by a counter (Hewlett Packard, Model 5246L).

The capability of this LDV is demonstrated by the results presented in Figure 9. These results show the decay of a spin-up flow in a rotating cylinder of water.^{12,13} The LDV and a cylinder of water were attached to a turntable. After allowing sufficient time for the water to have achieved solid body rotation, the rotation rate of the table was changed impulsively by a small amount. Figure 9 shows the adjustment of the azimuthal flow to the rotation rate. Quantitative information on this experiment is given in

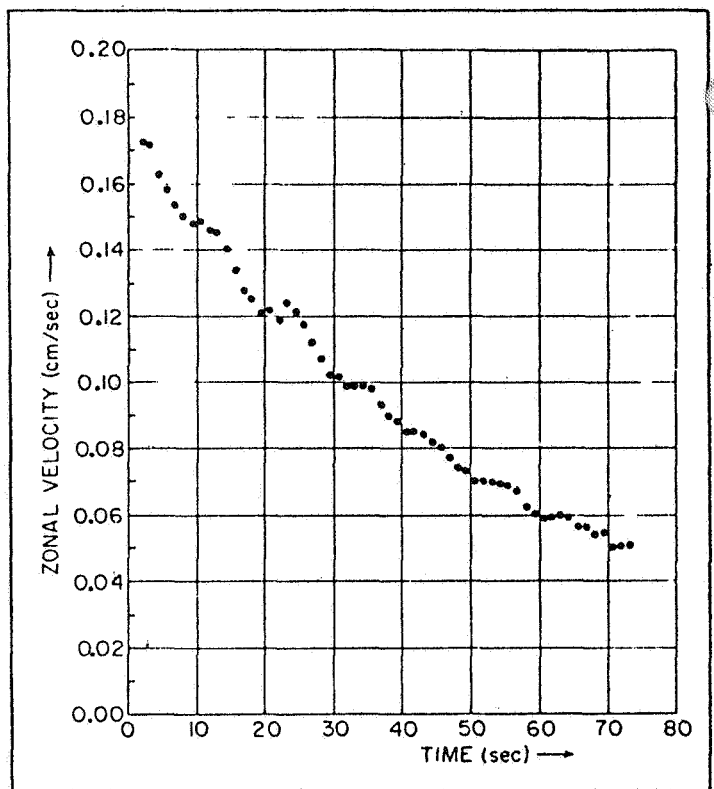


Figure 9. Measurements of the azimuthal velocity during the spin-up of a homogeneous cylinder of water. Rotation rate change, from 18°/sec to 20°/sec; cylinder dimensions, diameter 18.970 cm, depth 5.987 cm; position of scattering volume, radius 4.74 cm, height above base 3.00 cm.

the caption for Figure 9. The significant aspects are that a flow of less than 0.1 cm/s can be accurately measured. The "bumps" on the decay curve are real; they are inertial standing waves excited in the liquid by the impulsive change. Clearly, the flow speed resolution is close to 0.001 cm/sec.

In attempting to calculate the low speed limit of the LDV, the sources of frequency broadening must be taken into account. These sources are: (1) Brownian motion of the scatterers, (2) Flow gradients across the scatterer volume, (3) Turbulent flow fluctuations within the scattering volume, (4) The finite record in time from each scatterer as it passes through the scattering volume. Because of the heterodyning, the laser line width is not significant if the optical path differences are less than the laser coherence length. For further discussion of these sources of broadening see Fowllis and Martin¹² and the references therein.

For steady flows, Source 3 does not make any contribution. Sources 2 and 4 give constant relative broadening which is independent of the magnitude of the flow. The low flow speed limit is determined by Brownian motion broadening. The spectrum of the scattered radiation for a laser Doppler system has been derived by Edwards et al.¹⁴ In that paper, the special case of an infinite sample volume with no spatial or temporal gradients of the flow is discussed. The only remaining source of frequency broadening is Brownian motion of the scatterers. The scatterers are assumed to be small spheres in low concentrations and the Stokes-Einstein relation was used.¹⁵ The result is a Lorentzian shaped spectrum for which the center frequency is the Doppler frequency. The derivation by Edwards et al.¹⁴ is for a reference-scatter system. The author modified this derivation for a dual-scatter system. The modified result is again a Lorentzian and the half-width of the voltage spectrum is given by,

$$\Delta v_{1/2} = \frac{16n^2 kT \sin^2 \frac{\theta}{4}}{\sqrt{3} \lambda^2 \eta d} \quad (2)$$

ORIGINAL PAGE IS OF POOR QUALITY

where k is Boltzmann's constant, T is the absolute temperature, η is the viscosity of the liquid and d is the diameter of the scatterers.

To resolve the Doppler signal, the following criterion must be met

$$v_D > \Delta v_{1/2} \tag{3}$$

that is,

$$V > \frac{4nkT \tan \frac{\theta}{4}}{\sqrt{3} \lambda \eta d} \tag{4}$$

For typical values, namely $n = 1.33$, $T = 300^\circ$, $\lambda = 0.6328$ microns, $\eta = 10^{-2} \text{cm}^2/\text{sec}$, $d = 1$ micron and $\theta = 30^\circ$ we find the condition met for values of $V > 2.6$ microns/sec. This criterion corresponds to a very low flow speed and means that the LDV system could be used for the proposed studies. The limit can be reduced by working with larger values of viscosity and with larger scatterers.

IV. A Double Grid Schlieren

Optical techniques for measuring the temperature variation, or more accurately the refractive index variation of transparent fluids are well known. A recent review containing many excellent references has been given by Eckert and Goldstein.¹⁰ These techniques fall into three general classifications: (1) interferometers, (2) schlieren systems, and (3) shadowgraphs. All are essentially integrating measurement techniques. Interferometers measure refractive index variations directly; schlieren systems detect refractive index gradients and shadowgraphs sense the second derivative of the refractive index. In general the techniques give good qualitative information; they can be made quantitative, but calibration is difficult.

Our specific application is to visualize the convection cells occurring between the two spheres in the spherical convection apparatus (see Section II). It was determined that an interferometer would be too sensitive both from the point of view of construction and for the data required and that a shadowgraph would not be sensitive enough. A schlieren system was chosen, and the concept is shown in Figure 10. The optics are symmetrically arranged

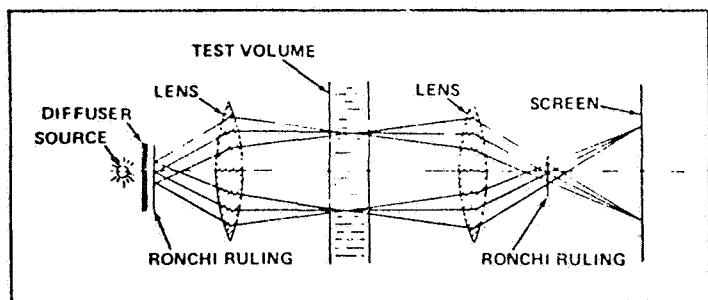


Figure 10. Single pass, double grid schlieren system.

about the test volume so that in the absence of refractive index disturbances in the test volume, an image of the first grating or Ronchi ruling falls exactly on top of an identical second Ronchi ruling. In this case, a uniform light field is obtained at the screen or film. Note that although the technique is an integrating one, the focusing at a plane in the test volume and again at the screen gives the technique a weighted local sensitivity. If temperature and hence refractive index variations now occur in the test volume, patterns of light and shade corresponding to gradients in the test volume will appear on the screen.

This apparatus can also be used in another mode. If the optics are arranged asymmetrically so that the image of the first ruling does not fall exactly on the second ruling, a moire fringe pattern is observed on the screen. This pattern is also sensitive to refractive

index variations in the test volume. Good quality lenses are required to superpose accurately the Ronchi rulings.

For test volumes which cannot have two transparent boundaries, a simple modification to the configuration shown in Figure 10 can be made. This modification is shown in Figure 11. The sec-

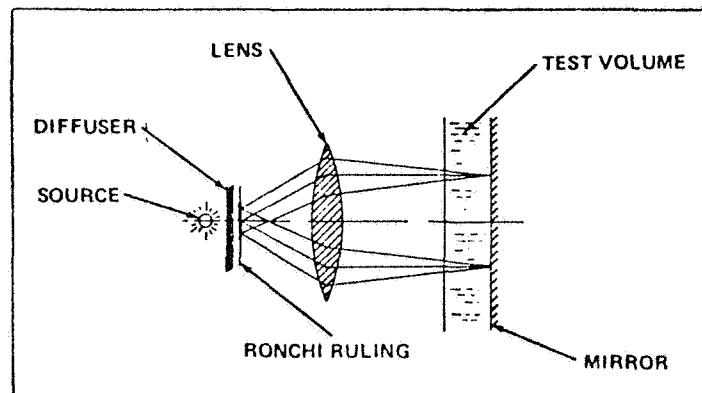


Figure 11. Double pass, reflecting, double grid schlieren system.

ond boundary of the test volume is a mirror which reflects back so that the image of the original Ronchi ruling is superposed on the original ruling. For this arrangement only one Ronchi ruling and one lens are required. The final superposed image may be viewed directly through the original ruling, if a split ruling with appropriate light source is available, or from the side with a beamsplitter inserted into the axis of the system.

Figures 12 and 13 show results obtained using the reflecting system in the moire fringe mode to observe convection cells. The



Figure 12. Undisturbed moire fringe pattern observed using the configuration shown in Figure 11.

apparatus shown in Figure 11 was arranged vertically so that one was looking down into the test volume. Figure 12 shows the undisturbed fringes present for a uniform fluid and Figure 13 shows the fringes disturbed by convection cells in the fluid due to heating at the lower boundary.

One further optical design problem remained before we could use the arrangement of Figure 11 for our spherical apparatus. For this apparatus, the inner sphere must become the back reflecting surface, thus optical compensation for the spherical curvature is required. In order for the rays to be reflected back along their paths, they must strike the inner sphere normally and hence must be focused by the focusing lens to the center of the sphere. In order



Figure 13. Moiré fringes disturbed by convection. These fringes were observed using the configuration shown in Figure 11.

for this to be achieved with small distortions for the sphere (radius 4.0 cm) and for the angular field required (90°), four aplanatic lenses had to be added between the sphere and the focusing lens.

Acknowledgments

The author wishes to acknowledge the advice and assistance of Peter D. Poulsen and Charles L. Densmore of Science Applications, Incorporated of Huntsville, Alabama. Mr. Poulsen's con-

tributions to the photochromic dye technique and the schlieren technique were particularly valuable. The author also wishes to acknowledge the help of Barry Browne of Aerojet ElectroSystems Company of Azusa, California, who contributed to the design of the reflecting spherical schlieren system. Acknowledgment of assistance is also due to Glynda Meeks who did the typing.

References

1. O. Reynolds. *Phil. Trans. Roy. Soc. London* II, 51 (1883)
2. H. Werlé. *Annual Review of Fluid Mechanics*, 5, 361 (1973)
3. W. Merzkirch. *Flow Visualization*. Academic Press, New York, New York (1974)
4. D. James Baker. *J. Fluid Mech.* 26, 573 (1966)
5. C. K. Batchelor. *An Introduction to Fluid Dynamics*. Cambridge University Press, Cambridge, England (1967)
6. A. T. Popovich and R. L. Hummel. *Chem. Eng. Science*, 22, 21 (1967)
7. J. W. Smith and R. L. Hummel. *J. Soc. Mot. Pict. Tel. Eng.* 82, 278 (1973)
8. W. W. Fowles and C. H. Fichtl. *Proceedings of the Third NASA Weather and Climate Program Science Review*. NASA Conference Publication 2029, Paper No. 32 (1977)
9. Y. Yeh and H. Z. Cummins. *Applied Physics Letters*, 4, 176 (1964)
10. F. Durst, A. Melling and J. H. Whitelaw. *J. Fluid Mech.* 56, 143 (1972)
11. S. S. Penner and T. Jersky. *Annual Review of Fluid Mechanics*, 5, 9 (1973)
12. W. W. Fowles and P. J. Martin. *Geophys. Fluid Dynamics*, 7, 67 (1975)
13. H. P. Greenspan. *The Theory of Rotating Fluids*. Cambridge University Press, Cambridge, England (1969)
14. R. V. Edwards, J. C. Angus, M. J. French and J. W. Dunning, Jr. *J. Applied Phys.* 42, 837 (1971)
15. L. D. Landau and E. M. Lifshitz. *Fluid Mechanics*. Pergamon Press Ltd., London, England (1959)
16. E. R. G. Eckert and R. J. Goldstein. *Measurements in Heat Transfer*. Hemisphere Publishing Corp., Washington, D. C. (1976)

ORIGINAL PAGE IS
OF POOR QUALITY

PROGRAM INFORMATION REQUEST / RELEASE

*CLASS. LTR.	OPERATION	PROGRAM	SEQUENCE NO.	REV. LTR.
U	-1254	- AGCE	- 032	
*USE "C" FOR CLASSIFIED AND "U" FOR UNCLASSIFIED				

FROM S. L. Neste	TO Distribution
---------------------	--------------------

DATE SENT 6/19/81	DATE INFO. REQUIRED	PROJECT AND REQ. NO.	REFERENCE DIR. NO.
----------------------	---------------------	----------------------	--------------------

SUBJECT
LABORATORY ASSESSMENT OF CANDIDATE DIELECTRIC SOLVENT/PHOTOCHROMIC DYE SOLUTIONS

INFORMATION REQUESTED/RELEASED

1.0 SUMMARY

Qualitative laboratory tests were performed to assess several photochromic dye/fluid combinations in terms of (1) the solubility of the dye, (2) the response of the solution to exposure with UV light and (3) the fade time of the solution. Two combinations which exhibited behavior consistent with the requirements of the AGCE were a spiropyran photochromic dissolved in m-tolunitrile and a triarylmethane photochromic dissolved in dimethylsulfoxide (DMSO). Both solutions darkened when exposed to UV light and returned to their original, nearly transparent states within a few minutes. The compatibility of the triarylmethane/DMSO combination was also verified by Dr. Francis of the Rochester Institute of Technology (PIR No. 1254-AGCE-025).

2.0 TEST PROCEDURES AND RESULTS

The laboratory tests were qualitative in nature and consisted of exposing a solvent/photochromic dye solution to UV light and then measuring the transmission as a function of wavelength. The concentration of photochromic dye was 0.5-1.0 mg per cc of solvent or 0.05-0.1% by weight.

For each solution which demonstrated photochromism upon exposure to UV light the following sets of data were taken:

- 1) Transmittance vs. wavelength of the unattenuated light source to characterize the detector/source combination and provide a baseline value.
- 2) Transmittance of an empty test tube to quantify the decrease in transmittance due to the glass tube.

Distribution: File (5) G. Fogal R. Homsey S. Neste	PAGE NO. 1 OF 10	RETENTION REQUIREMENTS	
		COPIES FOR	MASTERS FOR
<input type="checkbox"/> 1 MO.	<input type="checkbox"/> 3 MOS.	<input type="checkbox"/> 6 MOS.	<input type="checkbox"/> 12 MOS.
<input type="checkbox"/> 3 MOS.	<input type="checkbox"/> 6 MOS.	<input type="checkbox"/> MOS.	<input type="checkbox"/> MOS.
<input type="checkbox"/> 6 MOS.	<input type="checkbox"/> MOS.	<input type="checkbox"/> DONOT DESTROY	

- 3) Transmittance of the test tube and the unactivated solution to assess the transmittance of the clear solution.
- 4) Transmittance of the solution immediately after activation to record the decrease in transmittance due to fluid darkening as a function of wavelength.
- 5) A second transmittance run 3-4 minutes after activation to assess fade time as a function of wavelength.
- 6) Transmittance at a single wavelength as a function of time from activation to more quantitatively assess the fade time.

Transmittance measurements were made using an EG&G Model 585-22 Monochromator with a motor drive attachment. A Hewlett-Packard 3052A data acquisition system was used to sample the EG&G analog output, store the data and generate the plots at the end of each scan.

Transmission curves of the above data sets are given in Figures 1 to 4 for two solvent/photochromic dye solutions: m-tolunitrile/spiropyran (TNSB) and dimethylsulfoxide (DMSO)/triarylmethane (malachite green leucocyanide, MGCN).

As shown, although the maximum absorption regions of the two solutions differ slightly (see Figure 5 also), both combinations are capable of reducing the transmittance by up to 75%. If the fade time (τ) is defined as a function of transmittance by Equation (1)

$$\tau = t \left[T_0 + \frac{(T_F - T_0)}{2} \right], \quad (1)$$

where T_0 and T_F are the initial ($t = 0$) and final transmittances, then from Figures 2 and 4 fade times of ~ 110 sec and 70 sec are calculated for the m-tolunitrile and DMSO solutions respectively. Therefore, both solutions appear acceptable from the standpoint of transmittance change when activated and fade time.

The effects of aging are shown in Figure 6 for a DMSO/MGCN solution where an old and a fresh mixture are compared. Although the transmittance of the old solution is markedly lower, a significant decrease in transmittance was observed when the solution was activated. Four additional solvent/photochromic dye combinations were investigated with negative results and are summarized below:

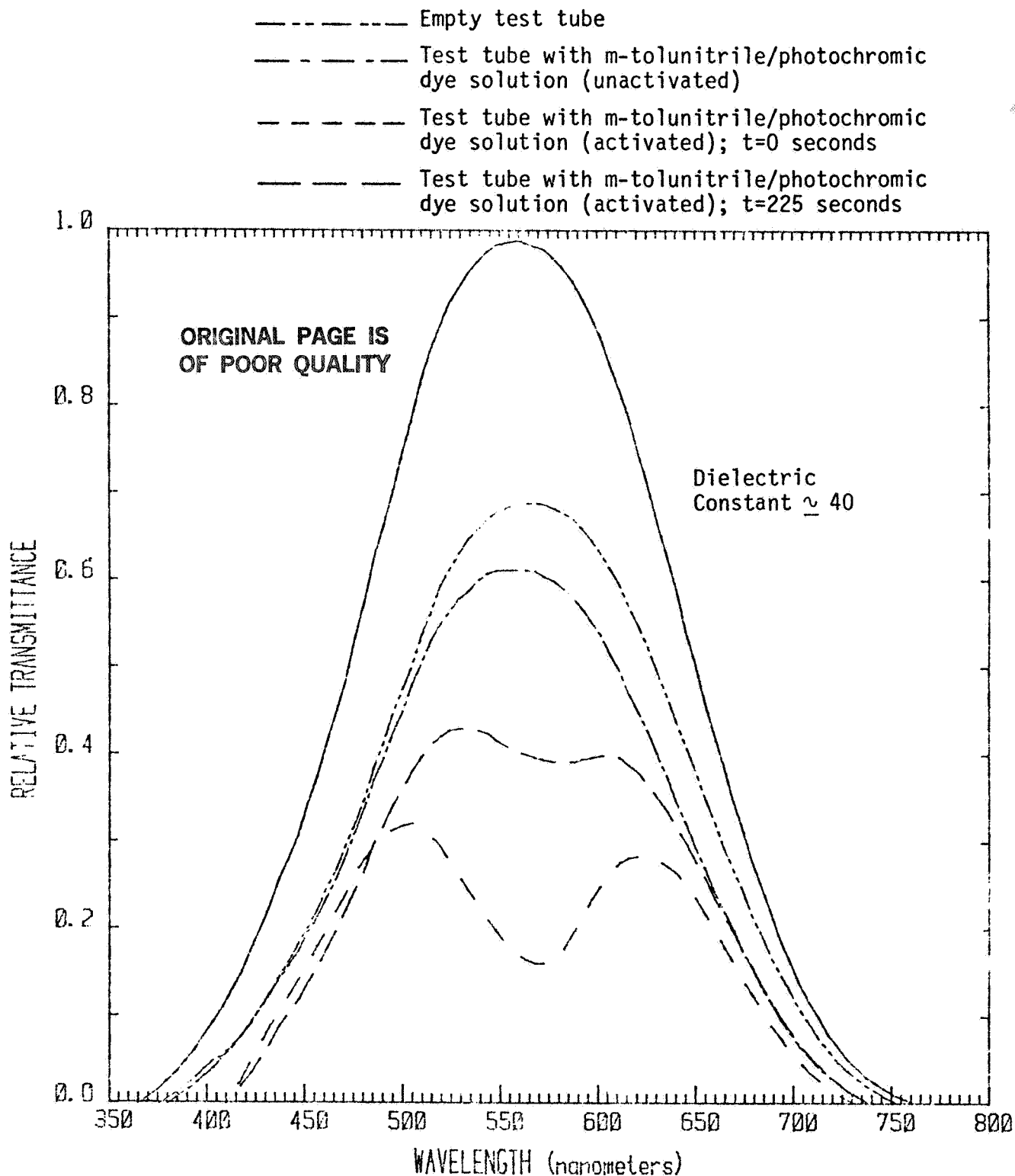
<u>Solvent</u>	<u>Dye</u>	<u>Result</u>
DMSO	Spiropyran (TNSB)	Spontaneous activation (see Figure 7).
m-tolunitrile	MGCN	Did not exhibit photochromism.
dimethylformamide	Spiropyran (TNSB)	Spontaneous activation.
dimethylformamide	MGCN	Did not exhibit photochromism.

3.0 CONCLUSIONS AND RECOMMENDATIONS

The above results, and the preliminary results of Dr. Francis at the Rochester Institute of Technology (PIR No. U-1254-AGCE-025), indicate that suitable combinations of high dielectric constant solvents and photochromic dyes can be found to satisfy the optical requirements of the flow visualization concept used for the AGCE. As pointed out in previous PIR's (e.g. 1254-AGCE-014A), the electrical properties of the high dielectric constant fluids may be more difficult to achieve. Consequently, the following recommendations are given:

- 1) Perform a fluid purification and electrical properties assessment of the most promising solvents identified (e.g. DMSO and m-tolunitrile).
- 2) Identify fluids with lower dielectric constants (5-10) which are compatible with photochromic dyes and can be easily purified and hence provide the required electrical properties.

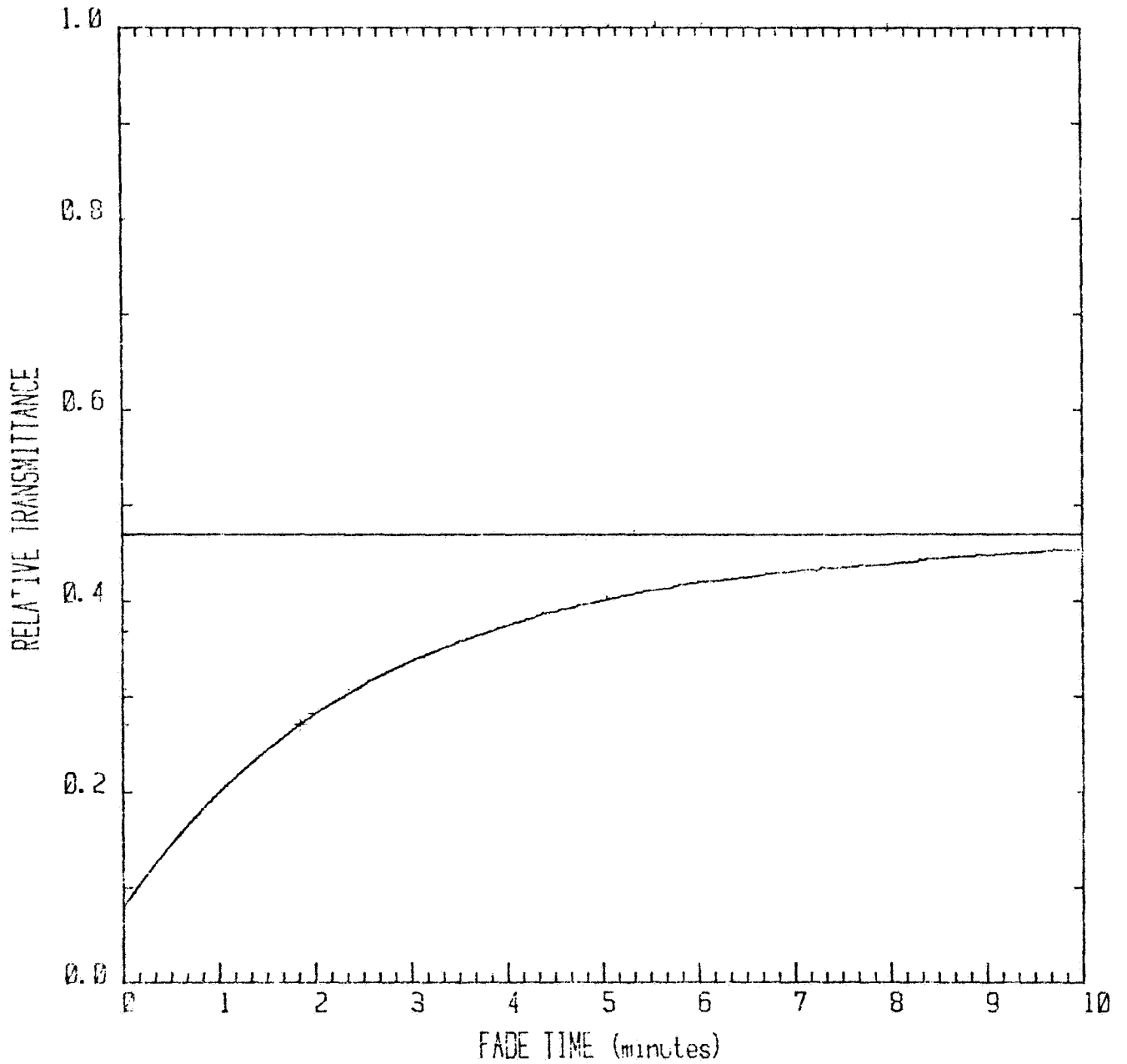
Although implementation of the first item above is beyond the scope of the present study, a general procedure for conducting a fluid purification and electrical properties assessment has been defined (PIR No. 1254-AGCE-021). The second item above is being investigated by Dr. Francis of the Rochester Institute of Technology.



Relative transmittance of m-tolunitrile with a photochromic dye (spiropyran, TNSB) in solution. Transmittance curves in the activated state were obtained immediately after and ~ 225 seconds after activation.

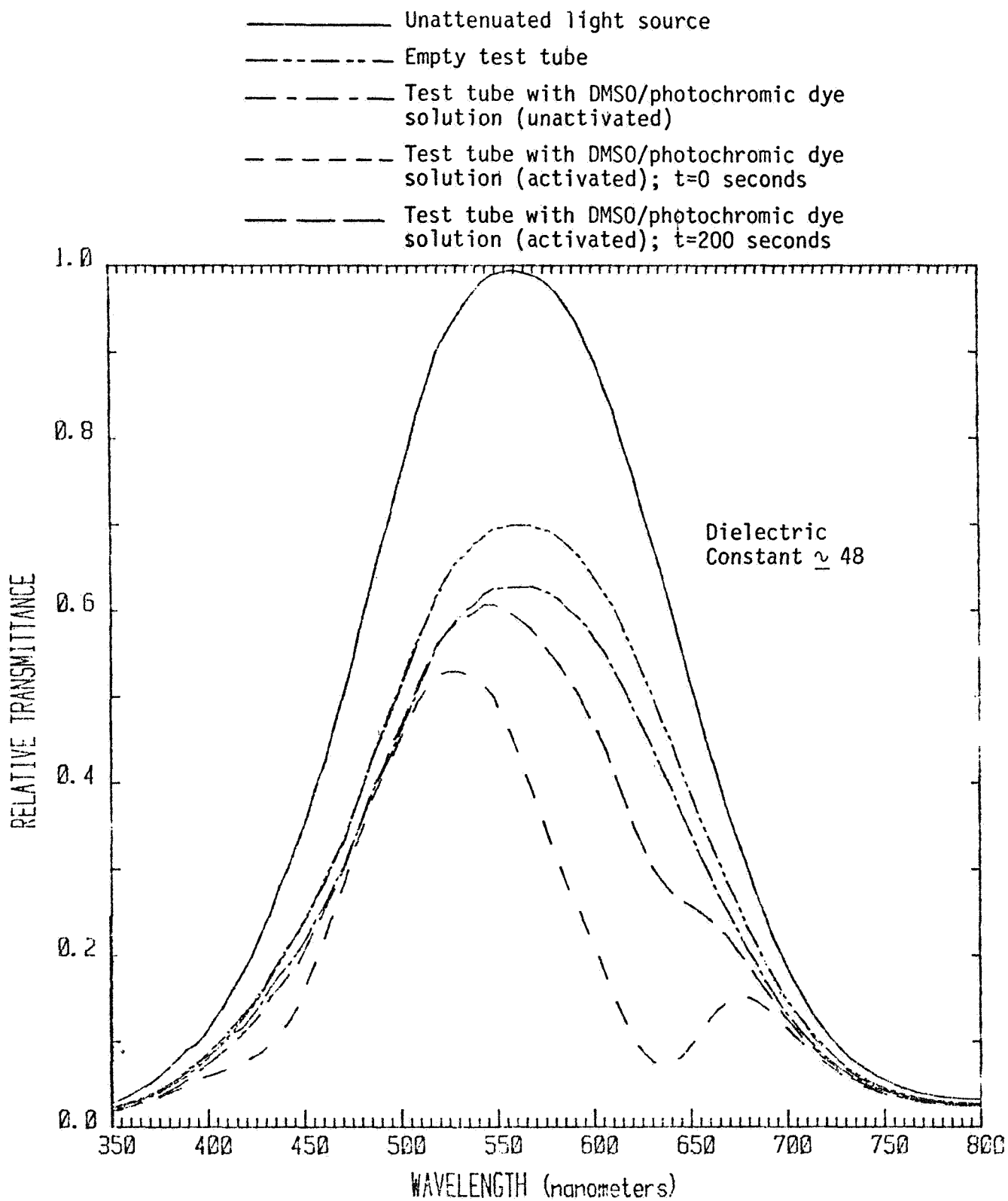
Figure 1

ORIGINAL PAGE IS
OF POOR QUALITY



Fade time for a solution of m-tolunitrile and a
spiropyran class of photochromic dye (TNSB).
Transmittance measured at ~ 560 nm.

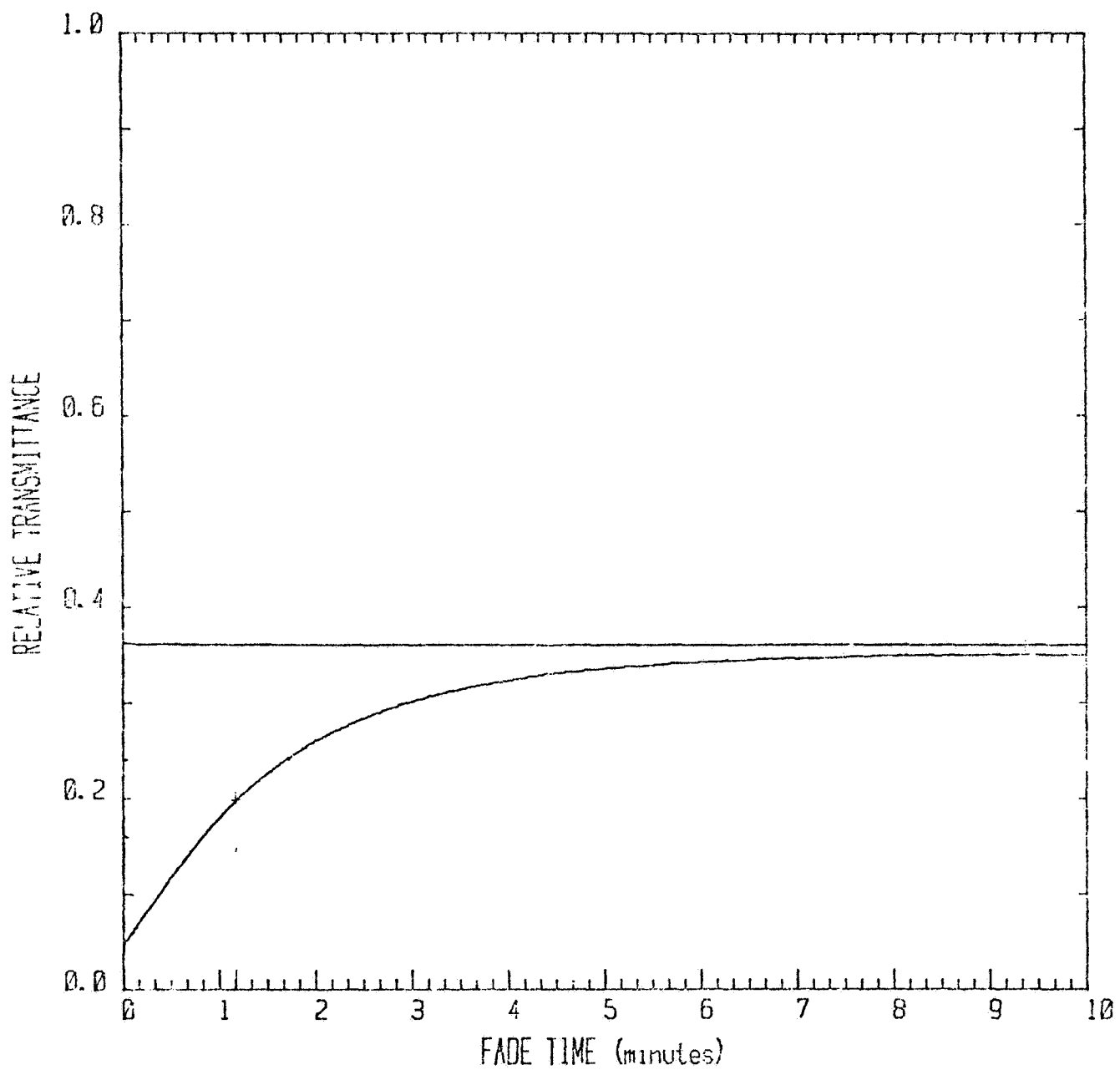
Figure 2



Relative transmittance of DMSO with a photochromic dye (triarylmethane, malachite green leucocyanide) in solution. Transmittance curves in the activated state were obtained immediately after and ~ 200 seconds after activation.

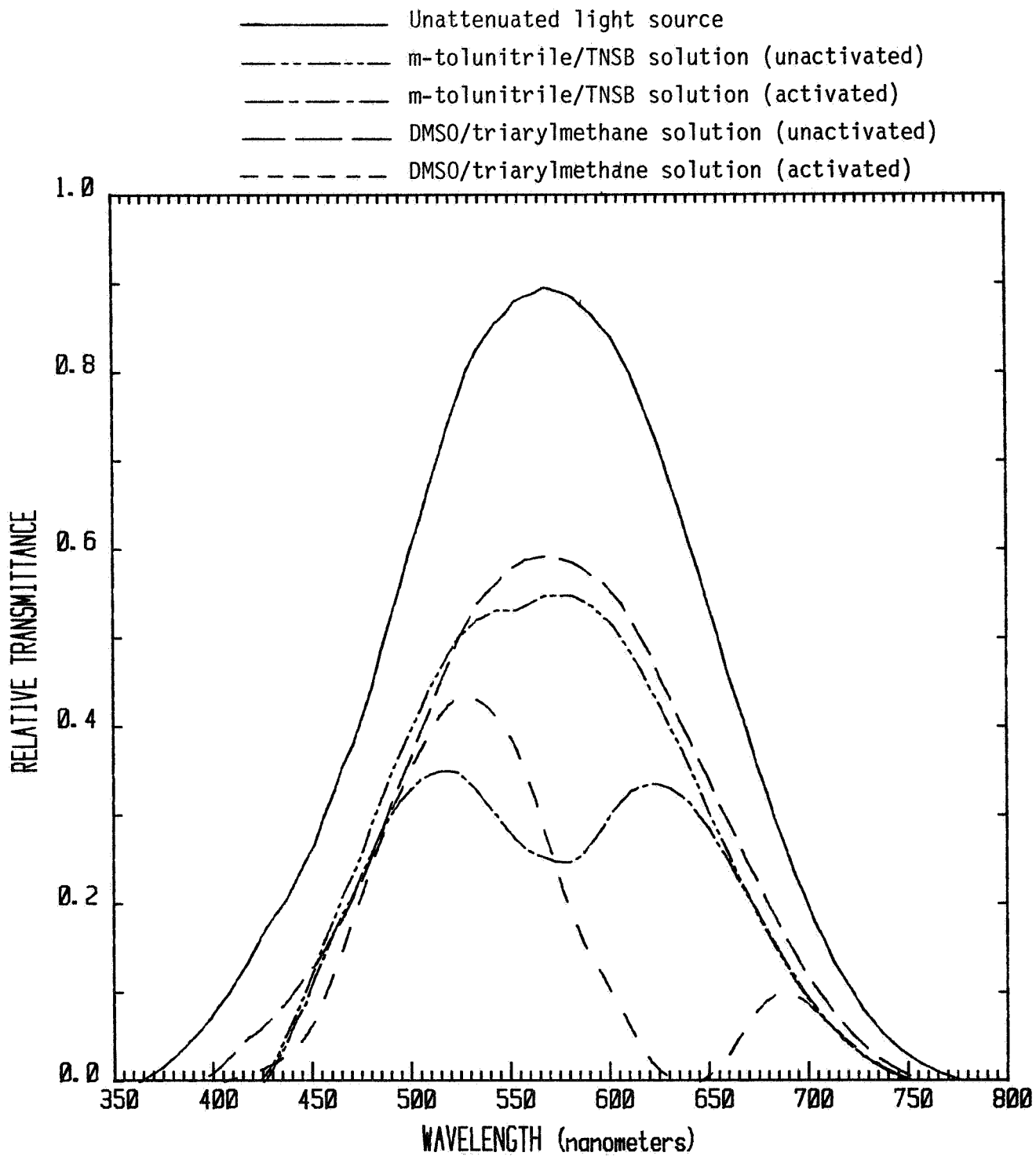
Figure 3

ORIGINAL PAGE IS
OF POOR QUALITY



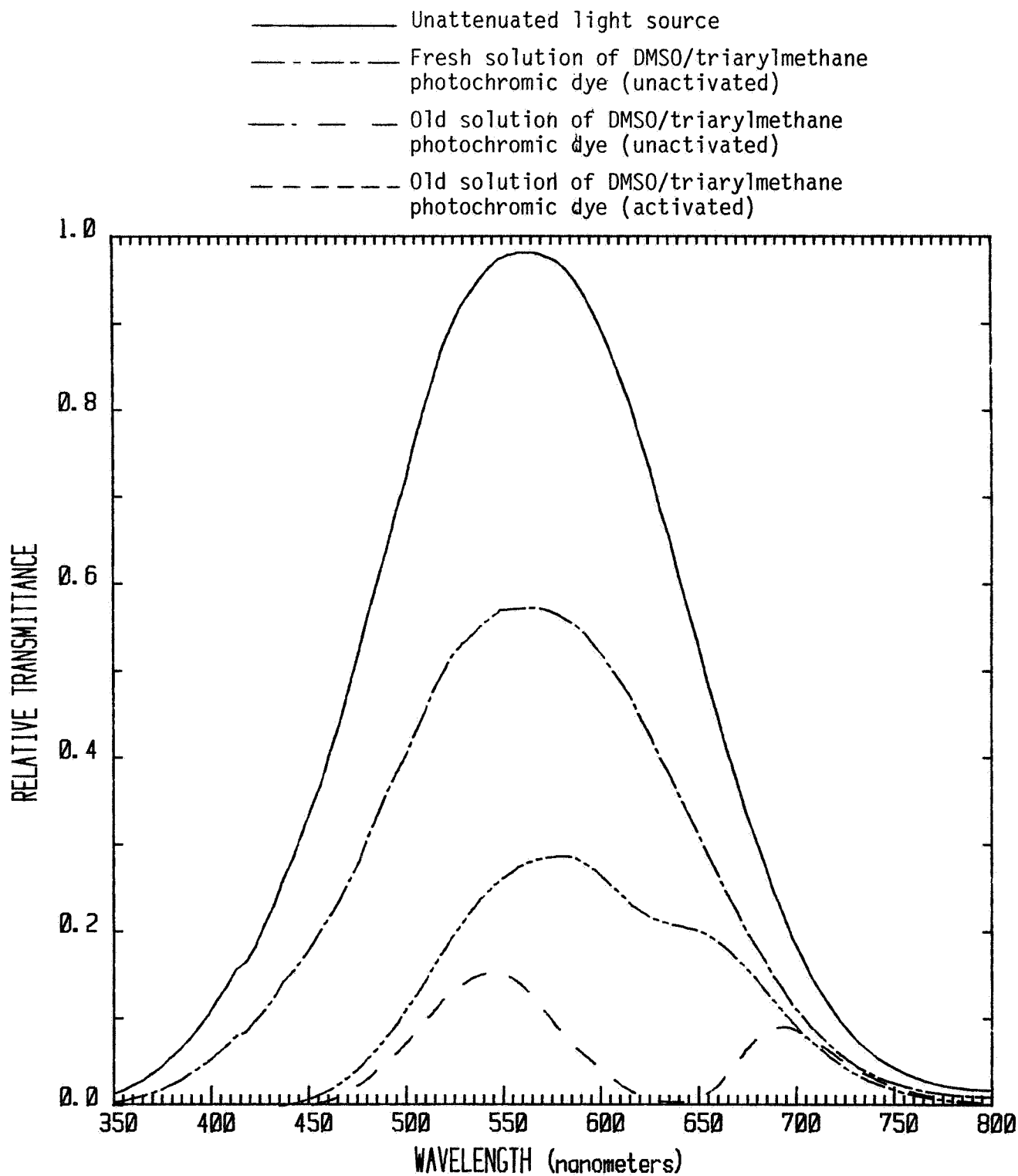
Fade time for a solution of DMSO and a triarylmethane class of photochromic dye (malachite green leucocyanide). Transmittance measured at ~ 640 nm.

Figure 4



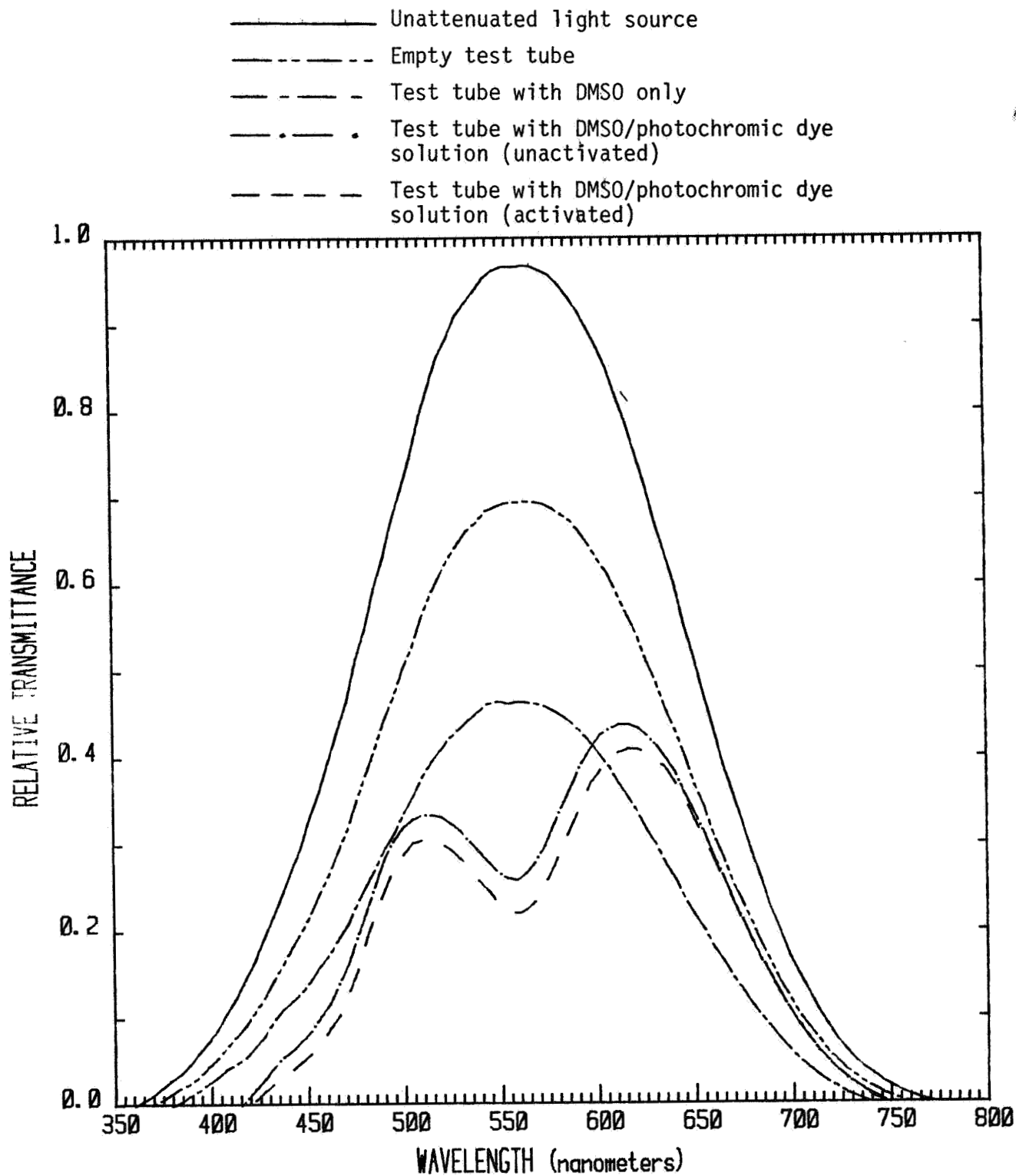
Absorption regions of two dielectric fluid/photochromic dye solutions.

Figure 5



Relative transmittance of a fresh mixture of DMSO/ photochromic dye compared to a mixture ~1 year old. The old mixture was stored in a closed container in the laboratory (not in darkness) and has been activated ~50 times during that period of time.

Figure 6



Relative transmittance of DMSO with and without a spiropyran photochromic dye (TNSB) in solution. This combination demonstrated spontaneous activation and additional exposure to UV light did not appreciably reduce the transmittance.

Figure 7

PIR NO.	*CLASS. LTR.	OPERATION	PROGRAM	SEQUENCE NO.	REV. LTR.
	U	- 1254	- AGCE	- 037	
*USE "C" FOR CLASSIFIED AND "U" FOR UNCLASSIFIED					

PROGRAM INFORMATION REQUEST / RELEASE

FROM S. L. Neste	TO Distribution
---------------------	--------------------

DATE SENT 7/13/81	DATE INFO. REQUIRED	PROJECT AND REQ. NO.	REFERENCE DIR. NO.
----------------------	---------------------	----------------------	--------------------

SUBJECT
 PHOTOCHROMIC DYES FOR FLOW VISUALIZATION IN HIGH DIELECTRIC SOLVENTS - III

INFORMATION REQUESTED/RELEASED

The attached document is the third report from Dr. Ronald Francis of the Rochester Institute of Technology on the above subject.

PIR No. _____

G. Fogal R. Homsey S. Neste	PAGE NO. 1 OF 3	RETENTION REQUIREMENTS	
		COPIES FOR	MASTERS FOR
		<input type="checkbox"/> 1 MO.	<input type="checkbox"/> 3 MOS.
		<input type="checkbox"/> 3 MOS.	<input type="checkbox"/> 6 MOS.
		<input type="checkbox"/> 6 MOS.	<input type="checkbox"/> 12 MOS.
		<input type="checkbox"/> MOS.	<input type="checkbox"/> MOS.
		<input type="checkbox"/>	<input type="checkbox"/> DONOT DESTROY

SUBJECT: PHOTOCROMIC DYES FOR FLOW VISUALIZATION IN
HIGH DIELECTRIC SOLVENTS

Attached please find a plot of relative maximum density achieved upon exposure vs. relative time to fade to one-half maximum density for BMS spiro-pyran dissolved in 32 solvents. High optical densities and long dye fade times would plot in the upper right hand corner of the page.

Best compromise between high densities and long fade times appear to be:

	<u>Dielectric Constant</u>
m-tolunitrile	40 ⁺
cyclohexanone	18.3
chloroform	4.8

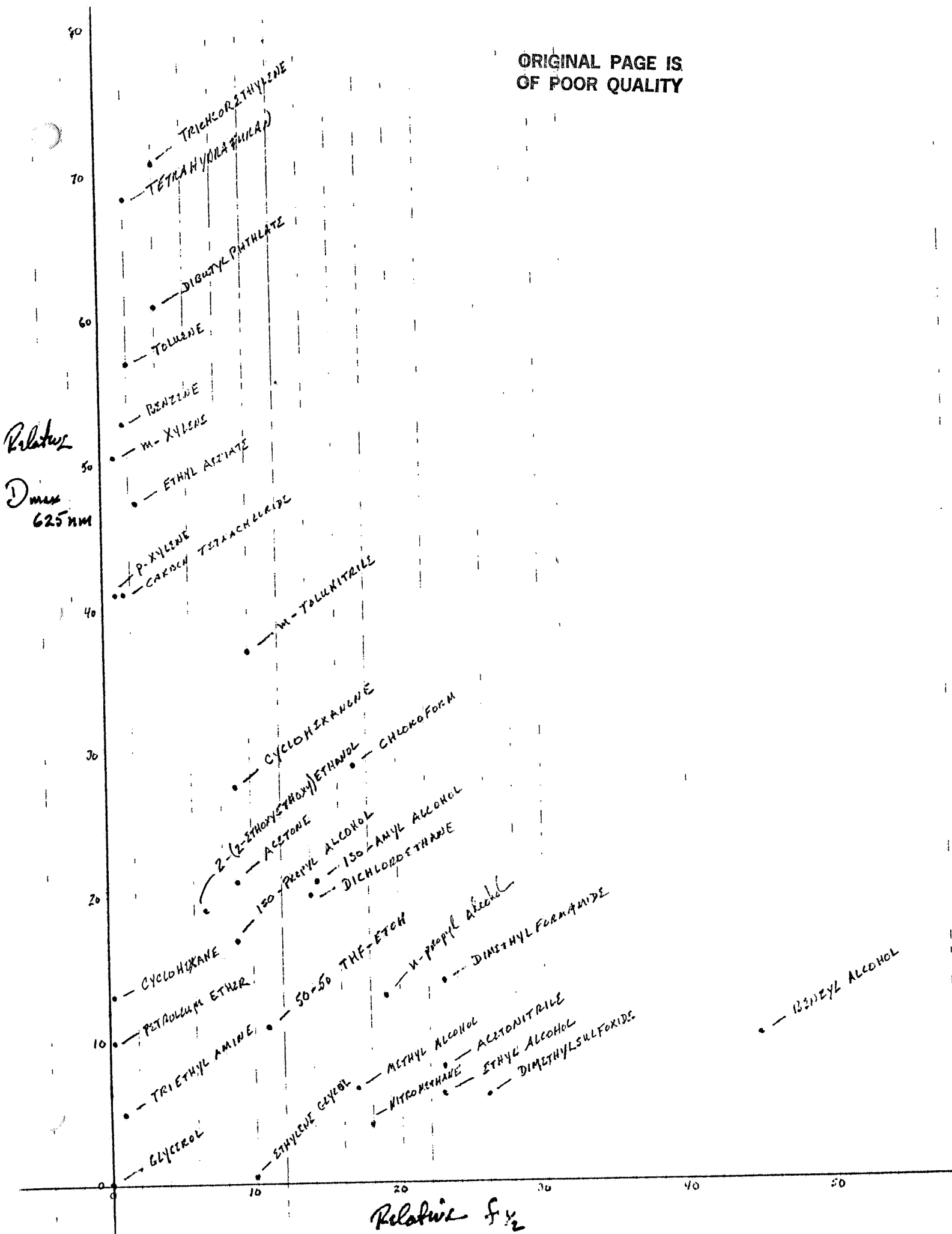
D_{\max} values are relative densities and should not be construed as absolute densities, a difficult measurement at a single wavelength. They are, however, indications of the high performance spiroyrans can give.

To convert the $f_{1/2}$ values to seconds, the numbers on the $f_{1/2}$ axis should be multiplied by 0.532. Thus, the particular spiroyan fades rapidly compared to others. It was designed and synthesized to do so, specifically, for a totally different application, where it was required that the BMS solution fade from maximum density upon exposure back to a transparent solution in 3 seconds. It is, therefore, the wrong spiroyan for the General Electric application, but it has been found to be the only one, in checking many, what now prove to be out-of-date sources, that was available to this study.

It has, however, served well as a model system to demonstrate:

1. The broad range of photochromic response available.
2. The compromise between D_{\max} and $f_{1/2}$ given by solvent classes.
3. Exceptions to this compromise.
4. The control parameters of:
 - a) solvent and solvent mixtures
 - b) photochromic compound concentration in solvent
 - c) photochromic structure as dictated by Hammett sigma functions
5. Direction in the selection of photochromic compound - solvent pair.

ORIGINAL PAGE IS
OF POOR QUALITY





GENERAL ELECTRIC

SPACE DIVISION
PHILADELPHIA

PROGRAM INFORMATION REQUEST / RELEASE

*CLASS. LTR.	OPERATION	PROGRAM	SEQUENCE NO.	REV. LTR.
PIR NO. U	- 1254 -	AGCE	- 036	
*USE "C" FOR CLASSIFIED AND "U" FOR UNCLASSIFIED				

FROM S.L. Neste	TO Distribution
--------------------	--------------------

DATE SENT 7/7/81	DATE INFO. REQUIRED	PROJECT AND REQ. NO.	REFERENCE DIR. NO.
---------------------	---------------------	----------------------	--------------------

SUBJECT
PHOTOCHROMIC DYES FOR FLOW VISUALIZATION IN HIGH DIELECTRIC SOLVENTS-II

INFORMATION REQUESTED/RELEASED

The attached document is the second report from Dr. Ronald Francis of the Rochester Institute of Technology on the above subject.

G. Fogal R. Homsey S. Neste	PAGE NO. 1 of 10	RETENTION REQUIREMENTS	
		COPIES FOR	MASTERS FOR
		<input type="checkbox"/> 1 MO.	<input type="checkbox"/> 3 MOS.
		<input type="checkbox"/> 3 MOS.	<input type="checkbox"/> 6 MOS.
		<input type="checkbox"/> 6 MOS.	<input type="checkbox"/> 12 MOS.
		<input type="checkbox"/> MOS.	<input type="checkbox"/> MOS.
		<input type="checkbox"/>	<input type="checkbox"/> DO NOT DESTROY

Further Search for Commercially Available Photochromic Compounds

Search for commercially available photochromic has consisted of contacting companies, having previously searched what is probably all the chemical catalogs available in the U.S., known to have been in photochromic research. It is possible that some spiropyrans may be available from the National Cash Register Co., but no other companies had anything to offer, with the exception of Eastman Kodak previously mentioned, it being approximately 10 years since photochromism was being commercially researched to any degree. Contact will be maintained with National Cash Register.

During the reporting period, two compounds listed in Kodak's general organic chemical catalog, and in previous separate listings being cited as photochromic materials, have been received and evaluated.

The compounds are:

2-(2,4 - dinitrobenzyl) pyridine
Ethyl bit (2,4 - dinitrophenyl) acetate

These compounds are manufactured by Eastman Kodak Co. and sold through Fisher Scientific.

These compounds have been tested in eight different solvents of interest and found not to be photochromic in any solvent tested. In most cases, when dissolved they produced highly colored solutions in which no change could be detected upon exposure.

Solvent-Photochromic Dye Evaluation

Some three hundred evaluations have been performed in the following with a spiropyran (the only apparently currently available) and five triarylmethane leucocyanide and one leucohydroxide compound.

The solvents, with approximate dielectric constants, and the photochromic materials are listed below:

Solvents:	ϵ (approx.)
Formamide	110
Water	80
m-Tolunitrile	40
Dimethyl sulfoxide	47
Glycerin	43
Nitromethane	40
Ethylene glycol	38
Dimethyl formamide	38
Acetronitrile	38
Ethyl alcohol	24
methyl alcohol	33
MDW (70% M_2OH -28% H_2O -2% DMSO)	
Acetone	21
Isopropyl alcohol	18
Trichloroethane	7.5
Chloroform	4.8
Benzene	2.8
Toluene	2.4

Photochromic Compounds: BMS
Malachite green leucocyanide
Malachite green leucohydroxide
New Fuchsine leucocyanide
Fuchsine leucocyanide
Crystal violet leucocyanide
Brilliant blue leucocyanide

Of the literally thousands of compounds which show photochromic behavior, the past hundred years of research has revealed the spiropyrans to be the most responsive in terms of optical densities obtainable and the rate, upon exposure, with which it is achieved.

It was also recognized some years ago, on the basis of Beer's law predictions, that the triarylmethanes were capable in theory of producing even greater densities. In accord with Beer's law,

$$D = \epsilon c \ell$$

D = optical density (or absorbance)

ϵ = extinction coefficient

c = concentration of absorber

ℓ = path length through which the density is measured.

The triarylmethanes are believed to produce their colored form upon exposure with a quantum yield of 1.00. The spiropyrans show quantum yields more in the 0.5 range. Thus, the "c" term in the Beer's law expression would be two times as large for a triarylmethane, on the average, than a spiropyran. Further, representative extinction coefficients for the triarylmethanes are twice as large as for the spiropyrans. Thus, for a given path length, the triarylmethane should produce four times as much density as the spiropyrans.

It is one of the more prominent questions of photochromism as to why this has never been achieved in practice and the best triarylmethanes have not been found to outperform the better spiropyrans. These two classes of compounds remain, by far, the major focus of interest in photochromic research for their general properties.

The wide variety of solvents and photochromic compounds have been chosen to provide both a broad data base and to be assured more than adequate experience to search for Hammett substituent coefficients and Brownstein solvent constant correlations in the prediction of the behavior of the photochromic systems in this design work.

It is understood that the present objectives are:

- a) a high dielectric solvent system
- b) a low dielectric solvent recommendation as back-up
- c) density which decreases transmittance by 10%
- d) fade times of one-two minutes
- e) as low a viscosity solvent as possible
- f) a solvent which may be easily purified and will retain its purity in the system
- g) a solvent which is readily available in 200 cc lots

Of particular interest in this study are the properties of *m*-tolunitriles. The three commercially available "so-called" photochromic compounds, the triaryl-methanes available, and the BMS spiropyran were each tested. Only the BMS compound was found to give any significant response in the *m*-tolunitrile solvent, and this proved to be one of the most responsive combinations thus far achieved. For example, malachite green and new fuchsine leucocyanide gave no photochromic response in *m*-tolunitrile; crystal violet leucocyanide immediately turned deep purple (which possibly could be controlled by radium cyanide additives and then found to be photochromic); and brilliant blue leucocyanide showed slight negative photochromism. *m*-tolunitrile is thus found to not support triarylmethane photochromism generally and is concluded to be a high risk direction for the program.

BMS in tolunitrile is very responsive, giving a relative density (defined in previous communications) of 1.2 which ranks it very high among the dye-solvent systems tested. The fade time of this particular spiropyran is however rapid. It fades to half its original density in 10 seconds and to zero density in forty seconds. There are three comments on this however.

First, this particular spiropyran was designed to fade rapidly, and recall it is being used in this project only as a benchmark and because it is the only photochromic spiropyran presently available. Secondly, attached to this report is the journal article by Berman, Fox and Thomson appearing in the Journal of the American Chemical Society 81, 5605 (1959) in which the density and fading

characteristics of the spiropyran were correlated to the spiropyran's molecular structure by Hammett sigma functions of substitutions of halogen, methoxy and nitro groups into the spiropyran ring system. Although the $\Sigma\sigma$ value of BMS has not been calculated as yet, Berman, et al were able to change the fade rates by four orders of magnitude by appropriate substitutions. It, therefore, seems likely that a spiropyran is available that will satisfy the fade time requirements of this task, and that the synthesis procedure, once the correct spiropyran is predicted from the approach represented in Figure 2 of the Berman et al, is available or could be prescribed.

And, thirdly, in order to conserve limited BMS spiropyran, dilute solutions have been used in the testing. Undoubtedly, saturation in solubility and in density which may be achieved has not been approached and more concentrated dye solution probably will produce more density and longer fade times.

The preferred systems at this time are:

1. BMS in m-tolunitrile (TN)
2. BMS in 2-(2-Ethoxyethoxy) ethanol (2-2)
3. Malachite green leucocyanide in DMSO
4. Malachite green leucocyanide in dimethylformamide (DMF)
5. Malachite green leucocyanide in acetonitrile (AN)
6. Malachite green leucocyanide in 2-(2-ethoxyethoxy) ethanol

<u>Dye</u>	<u>Solvent</u>	<u>Dielectric Constant</u>	<u>Viscosity</u>	<u>Dil. Conc. Half-Fade Time</u>	<u>(1mg/10ml) Max. Rel. Density</u>	<u>Probable Ease of Purification</u>
BMS	TN			5 sec	1.2	High
BMS	2-2			9 sec	.3	Moderate
MGCN	DMSO	47		110 sec	.9	Low
MGCN	DMF	38		25 sec	.6	High
MGCN	AN	38		See below	.6	High
MGCN	2-2			~3600 sec	1.3	Moderate

Of the systems listed, perhaps the most attractive is malachite green leucocyanide-dimethylsulfoxide with a high relative density, a 110 second half-fade time, and a dielectric constant of 47 is the most attractive. However, dimethylsulfoxide is not an easy solvent to purify. It holds water tenaciously, and it boils at a very high temperature (189°C) with considerable decomposition into a complex mixture of by-products. Distillation at lower temperatures under

vacuum alleviates this problem somewhat, and chemical methods have been proposed to remove the water. Dimethylsulfoxide's extraordinary solvent properties also put limitations on materials which are to be used in the apparatus in which it will be used. DMSO's viscosity is also somewhat high.

Malachite green leucocyanide and 2-(2-ethoxyethoxy) ethanol also suggest another favored combination although a value for its dielectric constant has not been found. Other alcohols show values in the 20 to 35 range. Their viscosities are low. The ease with which alcohols may be purified vary considerably. The density achieved with malachite green leucocyanide is quite attractive and, although the fade time is quite long, presumably this can be shortened by the addition of sodium cyanide, and the mixing of the solution where only a small fraction of it is exposed also lessens this problem.

Malachite green leucocyanide in acetonitrile requires a special note. In previously unpublished work by the author, it has been noted that, in the case of some triarylmethane photochromic - solvent pairs, carbon dioxide, oxygen or water from the air influence response. One result is the continued increase in density after exposure is terminated and very long fade times. Precipitations have been noted. A spontaneous switching of the solution from the colored to colorless state, repeating many times can also be observed. The nature of these complex solutions has not been completely elucidated.

Malachite green leucocyanide in acetonitrile represents one such case, and while exposure produces significant density, the complex behavior described above lessens the attractiveness of this system. The solution eventually fades, and stirring of the solution diminishes the effect of any long-fade time density. The malachite green leucocyanide-acetonitrile system can be returned to normal fading behavior immediately upon termination of exposure if the acetonitrile is purged with nitrogen (approx, 4 minutes for 10 ml of acetonitrile). Air must be scrupulously excluded subsequently.

This behavior is not observed with all triarylmethane-solvent pairs and it has not been observed in any case with the spiropyrans.

Fatigue Study

It is anticipated that fatigue behavior encountered with photochromism will not be a major factor in the design of high dielectric constant photochromic marking systems since only a small percent of the solution will be exposed in each use of the solution. However, the literature reports that some fatigue mechanisms, resulting in longer fade times, lower maximum densities, and/or coloration of the

ORIGINAL PAGE IS
OF POOR QUALITY

solution are not the simple result of the destruction of the photochromic molecule, but also result in the formation of inhibitors to photochromism in the solution. In one citation, it is reported, for example, that a solution was no longer capable of producing density upon exposure, even though 98% of the photochromic molecule was still present in the solution undestroyed.

Fatigue tests are being performed and are proving not to be of concern. The worst case thus far encountered is with malachite green leucohydroxide in the methanol-water-dimethylsulfoxide solvent system where full solution exposure (not a small dot pattern) cut the solution density in half in twenty-eight exposures, with an equal decrease in fade time, although density was still achieved with one-hundred exposures.

Influence of Anion Concentration on Triarylmethane Photochromic Behavior

If the densities produced in triarylmethane solutions do not significantly exceed that produced in spiropyran solutions, and, as stated above the prediction in this regard made originally some sixty years ago, in other solvent systems has not been realized, then the remaining advantage of the triarylmethane is the ability to adjust fading characteristics, principally time, by adjustment of the concentration of the triarylmethane-dye anion in the solution. This does, however, raise the concern as to the effect of the salt concentration, required to obtain the anion, on the electrical properties of the solvent.

Several investigations have been performed to gauge the general level of anion required to influence fading rates. These tests have been on triarylmethane hydroxide photochromic compounds in order to avoid using sodium cyanide in the work, at least at this time. The following is representative:

	<u>Rel. Density</u>	<u>Fade Time to D = 0</u>
MGOH in 10 ml MDW solvent	off-scale (1.0)	Possibly 1 hour
MGOH in 10 ml MDW solvent + .03 ml 1M NaOH	.35	10.6 sec
MGOH in 10 ml MDW solvent + .06 ml 1M NaOH	.29	5.3 sec
MGOH in 10 ml MDW solvent + .15 ml 1M NaOH	.16	3.2 sec
MGOH in 10 ml MDW solvent + .90 ml 1M NaOH	.00	-

Current Conclusions

- a) Significant photochromic response is achieved in some triarylmethane leucocyanide - high dielectric constant solvents. The triarylmethanes offer the advantage that structural changes in the cationic portion of the molecule and, more easily, in anionic concentration in the solvent both may be utilized to modify the optical density achieved upon ultraviolet exposure and to modify fade times. There is, however, a concern about the amount of anion that is needed to regulate a given property, and the effect that concentrations of this ion would have on the electrical, particularly the dielectric properties of the solvent. Further, some triarylmethane-solvent pairs are found to form complex solutions upon simultaneous exposure to ultraviolet and to atmosphere gases. One result is continued increase in density after exposure and very long fade times. Precipitations and spontaneous switching of the solution from the colorless to the colored form through many cycles. None of this is attractive from the view of the proposed use of triarylmethane photochromism for flow visualization. The problem has been resolved in many cases by excluding atmospheric gases by a nitrogen purge.
- b) At this writing, as the triarylmethanes have not offered a particular advantage in density and fade characteristics, with the exception of the malachite green leucocyanide-dimethylsulfoxide pair, and are revealing some complicating factors, it is favored that photochromic marking solutions be based on the spiropyrans. BMS spiropyran has shown strong photochromic response in a number of solvents including m-tolunitrile, although the fade time in this solvent, predictably, is much too short. This demonstrates feasibility, however, using the only available spiropyran, and Hammett sigma coefficients and Brownstein solvent values would assist in predicting spiropyrans and solvent pairs of longer fade times.

The spiropyrans are predicted to offer less complex photochromic behavior in high dielectric solvents, more optical density upon exposure and less fatigue. Such compounds are not commercially available, however, but a substantial literature on their synthesis exists and would assist in the preparation of the compounds.

c) Specific photochromic behavior as to optical density achieved and fade times in a low viscosity, high dielectric solvent which may be easily purified represent a demanding set of conditions. The evaluations will continue.

graphed over 25 g. of alumina. The petroleum ether eluates yielded 1.43 mg. of a colorless oil whose infrared spectrum was identical with that of liquid *cis*-ketone III.²⁴ None of the further eluates revealed the presence of any *trans*-ketone IIa.

A mixture of 100 mg. of the crude product from the hydrogenation of Ic, 10 ml. of concentrated hydrochloric acid and 10 ml. of methanol was refluxed for 12 hr. The cooled mixture was poured into 25 ml. of water and extracted with chloroform. The extract was washed with 10% sodium bicarbonate solution, dried over magnesium sulfate and the solvent evaporated. The remaining gum, 56 mg., was chromatographed on alumina. The early petroleum ether eluate yielded a colorless oil whose infrared spectrum proved it to be *cis*-ketone III, while the later petroleum ether fraction gave a solid, m.p. 104° whose infrared spectrum was identical with that of *trans*-ketone IIa.

A mixture of 75 mg. of pure ketoester Ic, 5 ml. of concentrated hydrochloric acid and 7 ml. of ethanol was refluxed for 18 hr. After dilution of the cooled reaction mixture with 50 ml. of water, saturation with sodium chloride and extraction with chloroform, the combined extracts were dried over magnesium sulfate and evaporated to dryness. Crystallization of the slowly crystallizing residue from petroleum ether gave 0.1 mg. (0.3%) of a solid, m.p. 98–103° which on recrystallization from the same solvent proved to be *trans*-ketone IIc, m.p. 107–108°, identical infrared spectrum with that of an authentic sample.²⁵

Methylation of Ib — A solution of 200 mg. of Ib in 100 ml. of butyl alcohol was added to a stirred, nitrogen-blandeted solution of 100 mg. of potassium in 100 ml. of butyl alcohol. From a stirring 50 ml. of methyl alcohol was added. The cuprous solution was refluxed for three hours, cooled, filtered and the filtrate evaporated to dryness. The residue was taken up in chloroform and water, the chloroform layer separated and the aqueous phase extracted twice with chloroform. The combined extracts were dried over anhydrous magnesium sulfate and evaporated to dryness. Titration of the crystalline residue with petroleum ether yielded 110 mg. of a solid, m.p. 153–156° which on four recrystallizations from methanol gave colorless prisms of VII, m.p. 158°, spectra: ultraviolet, λ_{max} 233 m μ (ϵ 15,000); infrared (CCl₄), C=O 5.79(s), 5.98(s) μ , C=C 6.12(m) μ .

Anal. Calcd. for C₁₈H₂₀O₂: C, 76.03, H, 7.09. Found: C, 75.89, H, 7.44.

Dehydration of the Ketoesters Ic and IIc — A mixture of 50 mg. of Ic and 50 mg. of ethanedithiol, 510 mg. of freshly fused zinc chloride, 1.02 g. of anhydrous sodium sulfate and 2 ml. of anhydrous benzene was stirred at room temperature for 24 hr. The mixture then was taken up in ether and water. The organic layer separated and washed twice with 5% sodium hydroxide solution and once with water. The organic extracts were dried over magnesium sulfate, the solvent evaporated and the resulting yellow gum chromatographed over alumina. Elution with benzene gave 490 mg. (74%)

of a solid, m.p. 120–122°, which yielded colorless prisms of thioketal XVIII, m.p. 124.5–125.5°, after three crystallizations from aqueous methanol. Spectra: ultraviolet, λ_{max} 272 m μ (ϵ 990), strong end absorption in the 220 m μ region, infrared (CCl₄), C=O 5.82(s) μ .

Anal. Calcd. for C₁₉H₂₂O₂S₂: C, 65.88, H, 6.40. Found: C 66.09, H 6.26.

A mixture of 490 mg. of XVIII, 1 g. of Raney nickel and 25 ml. of ethanol was refluxed for 12 hr. After filtration of the nickel the solution was evaporated to dryness and the remaining 306 mg. of colorless oil chromatographed on 5 g. of alumina. Petroleum ether elution yielded 211 mg. (68%) of liquid olefinic ester XIX, spectra: ultraviolet, λ_{max} 260 m μ (ϵ 720) and 272 m μ (ϵ 535), strong end absorption in the 220 m μ region, infrared (CCl₄), C=C 5.82(s) μ .

A mixture of 100 mg. of IIc, 0.1 ml. of ethanedithiol, 100 mg. of freshly fused zinc chloride, 200 mg. of anhydrous sodium sulfate and 10 ml. of benzene was stirred at room temperature for 48 hr. The reaction mixture then was filtered, the filtrate washed with 5% sodium hydroxide solution, dried over magnesium sulfate and evaporated. The residue was crystallized from petroleum ether to give 94 mg. of a solid, m.p. 163–166°. Evaporation of the mother liquors, chromatography of the residue over 5 g. of alumina and elution with 10:1 petroleum ether-ether led to an additional 10 mg. of the same solid, m.p. 165–167°. Four crystallizations from petroleum ether yielded colorless prisms of thioketal XVI, m.p. 165.5–166.5°, infrared spectrum (CCl₄), C=O 5.78(s) μ .

Anal. Calcd. for C₁₉H₂₂O₂S₂: C, 65.50, H, 6.91. Found: C, 65.18, H, 7.06.

A mixture of 160 mg. of XVI, 2 g. of Raney nickel and 15 ml. of ethanol was refluxed for 10 hr. After filtration of the nickel and evaporation of the solvent under vacuum a petroleum ether solution of the crude product was passed through a short alumina column. Elution with the same solvent yielded 105 mg. (88%) of liquid ester XVIIa, infrared spectrum (CCl₄), C=O 5.78(s) μ .

A mixture of 75 mg. of XVIIa, 10 ml. of 10% sodium hydroxide solution and 10 ml. of ethanol was refluxed for 8 hr. The reaction mixture then was diluted with 100 ml. of water and extracted with chloroform. The aqueous solution was acidified with hydrochloric acid and extracted with chloroform. The latter extract was dried over magnesium sulfate, the solvent evaporated and the crude product crystallized from methanol-water, giving 43 mg. (61%) of solid. Three recrystallizations from aqueous methanol led to colorless needles of the acid XVIIb, m.p. 153–154°, infrared spectrum (CCl₄), OH 2.83(w), 3.30(m) μ and shoulders at 3.07(w) and 3.14(m) μ , C=O 5.75(w), 5.89(s) μ .

Anal. Calcd. for C₁₈H₂₀O₂: C, 78.65, H, 8.25. Found: C, 78.71, H, 8.42.

AMES, IOWA

[CONTRIBUTION FROM THE FUNDAMENTAL RESEARCH DEPARTMENT, THE NATIONAL CASH REGISTER CO.]

Photochromic Spiropyrans. I. The Effect of Substituents on the Rate of Ring Closure

BY ELLIOT BERMAN * RICHARD E. FOX AND FRANCIS D. THOMSON

RECEIVED MAY 16, 1959

The thermal formation of a number of 1,3,3-trimethylindolinobenzopyrrolospirans, spiro-(2'H-1'-benzopyran-2,2'-(1,3,3-trimethylindoline)), from their "open form" precursors has been studied spectrophotometrically in ethanol at 6°. The dependence of the rate of ring closure on substituent shows good agreement with the Hammett equation.

Phototropic spiroyrans have been previously investigated notably by Bloch-Chaudé¹ and Hirschberg.² These authors have studied both the ther-

mochromic and photochromic phenomena associated with this class of compounds. Our interest in these materials stems from their potential application to chemical systems for data storage.³

* Special Processes Section, Ittek Corporation, 700 Commonwealth Avenue, Boston 15, Massachusetts.

(1) O. Bloch-Chaudé, in J. L. Macle, Ed., *Chem. Rev.* 35 (1955), 109; O. Bloch-Chaudé, P. Furr, and J. S. Let, *Compt. rend.* 240 (1955), 1005; O. Chaudé, *Cahiers phys.* 60, 1 (1951), 11, 6 (1951), 62, 3 (1951).

(2) Y. Hirschberg, *This Journal*, 70, 2301 (1955); *J. Chem. Phys.*, 27, 768 (1957).

(3) B. K. Green, E. Berman, B. Katchen, L. Schleicher and J. J. Stansbury, "Chemical Switches," paper presented at Harvard University International Symposium on the Theory of Switching, April 5, 1957.

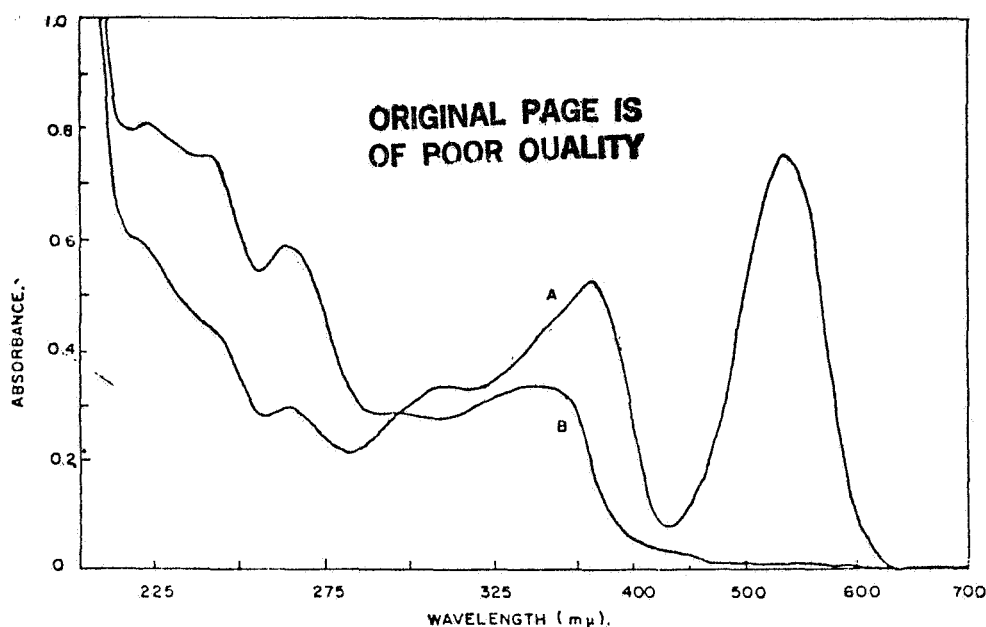
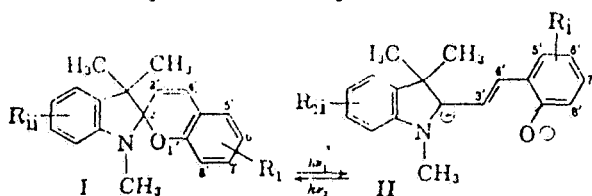


Fig 1.—Spectra of $3.1 \times 10^{-5} M$ solution of 1,3,3-trimethylindolino-6'-nitrobenzopyrpylospiran in ethanol at 6° : curve A, after exposure to ultraviolet; curve B, before exposure

Use of the photochemical system



in data storage requires that states I and II should be reasonably stable at ordinary temperatures in the absence of provoking illumination and that photochemical interconversion of states I and II should also be possible at ordinary temperatures. Through work in these laboratories, spiropyrans which are photochemically active at room temperature and above have been developed, but until recently the thermal instability of state II excluded their use in practical data storage devices. We have found that the thermal stability of state II can be increased by discrete choice of substituents without apparent adverse effect on the photochemical process. As a quantitative measure of the thermal stability of II the rate constant for the dark reaction $II \rightarrow I$ has been determined. The rates are found to differ by more than one thousand fold with different substituents. The rates can be correlated with substituents by applying the Hammett equation

Results

The rate of ring closure ($II \rightarrow I$) was measured at 6° in absolute ethanol for twelve substituted 1,3,3-trimethylindolino-6-nitrobenzopyrpylospirans by following the disappearance of the absorption band in the 500-600 m μ region. Figure 1 gives the ultraviolet and visible absorption spectra for 1,3,3-trimethylindolino-6-nitrobenzopyrpylospiran in the colorless state (I), curve B, and in the colored state (II), curve A. The absorption curve for state II represents a mixture of ring-closed and ring-opened materials at the photochemical steady state. Table

I summarizes the rate data obtained by exposing a solution of the colorless photochromic spiropyran to ultraviolet light and following the rate of disappearance of the resultant visible absorption band. In all cases, the rates appear to follow good first-order kinetics. The rate constants in Table I are based on at least two runs at different concentrations. When necessary, the constants were obtained by a least square treatment of the data. The collection of rate constants in Table I shows clearly that the

TABLE I
RATE CONSTANTS FOR THERMAL STABILITY AND SIGMA VALUES OF SUBSTITUTED 1,3,3-TRIMETHYLINDOLINO-6-NITROBENZOPYRPYLOSPIRANS

Substituent	$\Sigma\sigma^o$	k sec. ⁻¹ (ethanol 6°) ^a
6'-Nitro	0.79	4.28×10^{-5}
7'-Nitro	0.67	7.11×10^{-5}
7'-Chloro	0.40	1.26×10^{-4}
6',8'-Dibromo	0.36	3.97×10^{-4}
6'-Nitro-8'-allyl	0.22 ^b	2.10×10^{-4}
6'-Nitro-8'-fluoro	1.03	6.33×10^{-4}
6'-Chloro-8'-nitro	0.91	2.27×10^{-3}
6'-Bromo-8'-nitro	0.95	1.70×10^{-3}
6'-Nitro-8'-methoxy	0.37	5.53×10^{-4}
6'-Methoxy-8'-nitro	0.01	1.32×10^{-3}
7'-Nitro-8'-methoxy	0.28	2.52×10^{-3}
6'-Nitro-8'-bromo	1.00	3.67×10^{-4}

^a It is assumed that the unsaturated side chain *ortho* to the phenoxide group makes an equal sigma contribution in all compounds; this contribution is not included in $\Sigma\sigma^o$. ^b The rate constant for the dark reaction $I \rightarrow II$ is neglected.¹

stability of the open form depends markedly on the substituents present. In the compounds studied, the rate constant for closure ranged from 1.3×10^{-5} for the 6'-methoxy-8'-nitro compound to 6.3×10^{-4} for the 6'-nitro-8'-fluoro compound.

An attempt was made to correlate rate of thermal reversal with substituent. It was found that using

TABLE II
SUBSTITUTED 1,3,3-TRIMETHYLINDOLINOBENZOPYRROLOSPIRANS

Substituent	M.p. °C	Color of melt	Yield, %	Formula	Analyses, %			
					Calcd.		Found	
					C	H	C	H
Nitro	176-177	Purple	89	C ₁₉ H ₁₅ N ₂ O ₃	70.8	5.6	70.5	5.6
Nitro	107-108	Orange	92	C ₁₉ H ₁₅ N ₂ O ₃	70.8	5.6	70.6	5.8
Chloro	116-117	Purple	74	C ₁₉ H ₁₅ NOCl	73.2	5.8	73.2	5.5
6,8-Dibromo	115-116	Blue	84	C ₁₉ H ₁₇ NOBr ₂	52.4	3.9	52.3	3.9
6-Nitro-8-allyl	108-109	Purple	87	C ₂₂ H ₂₁ N ₂ O ₃	73.1	5.9	73.3	6.0
6-Nitro-8-bromo	105-106	Purple	88	C ₁₉ H ₁₇ N ₂ O ₃	56.9	4.3	56.9	4.5
6-Nitro-8-fluoro	301-301	Purple	90	C ₁₉ H ₁₇ N ₂ O ₃ F	67.1	5.0	67.4	5.0
6-Chloro-8-nitro	134-135	Purple	86	C ₁₉ H ₁₇ N ₂ O ₃ Cl	61.0	4.8	61.3	4.8
6-Bromo-8-nitro	122-123	Purple	80	C ₁₉ H ₁₇ N ₂ O ₃ Br	56.9	4.3	56.9	4.3
6-Nitro-8-methoxy	152.5-153.5	DK blue	90	C ₂₀ H ₂₀ N ₂ O ₄	68.2	5.7	68.2	6.0
6-Methoxy-nitro	116-117	Green	84	C ₂₀ H ₂₀ N ₂ O ₄	68.2	5.7	67.8	5.9
6-Nitro-8-methoxy	166-167	Dk green	91	C ₂₀ H ₂₀ N ₂ O ₄	68.2	5.7	68.1	5.8

Br and σ^+ relationship for *meta* and *para* positions and σ^+ values for the *ortho* positions gave reasonable correlation as indicated in Fig. 2

89-91^o were prepared by Thomason Chemicals, Inc. 25 Brvant St. Woburn, Mass. 5-Nitrosalicylaldehyde was commercial material used directly (m.p. 126-127). 4-Chlorosalicylaldehyde⁸ was prepared in 34% yield by a Reimer-

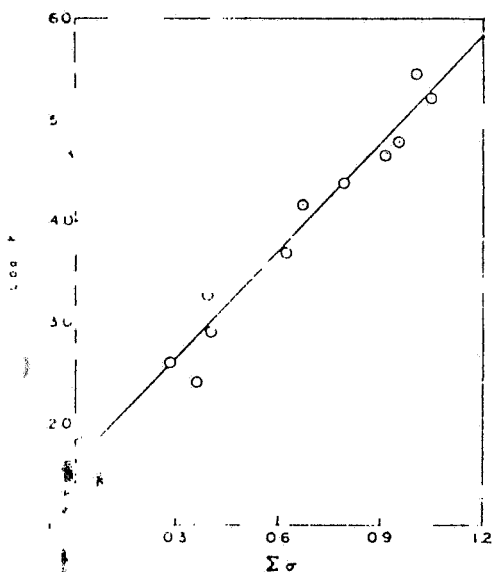


Fig. 2. $\log k$ versus sigma value for substituted 1,3,3-trimethylindolinobenzopyrrolospirans.

Solution of the Hammett equation⁶

$$\log k = \rho \sigma$$

for the data in Fig. 2 gives a value of -3.47 for the reaction constant, ρ . The correlation between rates and substituent constants suggests that *ortho* values may be used in electrophilic reactions at least in this specific case.

Further papers will deal with the effect of other substituents on thermal stability of the spirocyan, and a more detailed investigation of the photochemical behavior of the 1,3-dibromo spirocyan.

Experimental

Salicylaldehyd,⁸ 3-bromo-5-methoxysalicylaldehyde, m.p. 16-17^o, and 5-fluoro-5-nitrosalicylaldehyde, m.p. 107-108^o, were prepared by Newman.⁹ 3,5-Dibromosalicylaldehyde⁹ was obtained by bromination of salicylaldehyde, m.p. 83-84^o. 3-Allyl-5-nitrosalicylaldehyde was synthesized by a Claisen rearrangement of the allyl ether of salicylaldehyde followed by nitration, m.p. 157-158^o. Anal. Calcd. for C₁₁H₉NO₃: C, 58.0; H, 4.4. Found: C, 57.9; H, 4.2. 3-Nitro-5-chlorosalicylaldehyde¹⁰ was prepared by nitration of 5-chlorosalicylaldehyde (m.p. 105-107^o). 3-Nitro-5-bromosalicylaldehyde¹¹ was obtained by nitration of 5-bromosalicylaldehyde, m.p. 117-118^o. 3-Methoxy-5-nitrosalicylaldehyde¹² was obtained by nitration

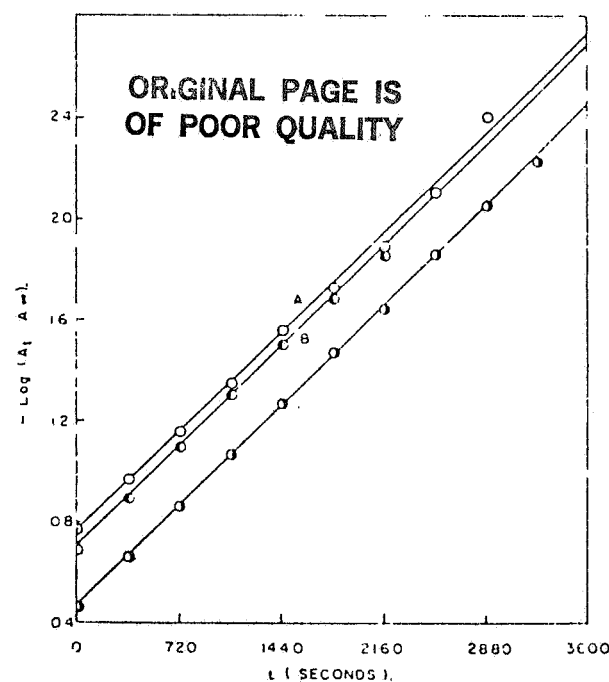


Fig. 3.—First-order rate plots for the disappearance of the colored form of 1,3,3-trimethylindolinobenzopyrrolospirans at 6^o in ethanol.

Curve	A	B	C
k , sec ⁻¹	1.26×10^{-3}	1.27×10^{-3}	1.26×10^{-3}
concn. of color less form before exposure, moles/l.	3.07×10^{-4}	7.67×10^{-4}	1.33×10^{-3}

Tiemann reaction with *m*-chlorophenol, m.p. 50-51^o. 3,5-Dibromosalicylaldehyde⁹ was obtained by bromination of salicylaldehyde, m.p. 83-84^o. 3-Allyl-5-nitrosalicylaldehyde was synthesized by a Claisen rearrangement of the allyl ether of salicylaldehyde followed by nitration, m.p. 157-158^o. Anal. Calcd. for C₁₁H₉NO₃: C, 58.0; H, 4.4. Found: C, 57.9; H, 4.2. 3-Nitro-5-chlorosalicylaldehyde¹⁰ was prepared by nitration of 5-chlorosalicylaldehyde (m.p. 105-107^o). 3-Nitro-5-bromosalicylaldehyde¹¹ was obtained by nitration of 5-bromosalicylaldehyde, m.p. 117-118^o. 3-Methoxy-5-nitrosalicylaldehyde¹² was obtained by nitration

(8) H. H. Hodgson and T. A. Jenkinson, *J. Chem. Soc.* 1710 (1927).
 (9) V. Wentworth and O. L. Brady *ibid.* 117, 1010 (1920).
 (10) A. B. Lunett and E. Roberts, *ibid.* 1975 (1928).
 (11) A. Auwers and O. Barger, *Ber.* 37, 3915 (1904).
 (12) W. Davies, *J. Chem. Soc.*, 123, 1663 (1911).

of *o*-vanillin, m.p. 141-142°. 3-Methoxy-6-nitrosalicylaldehyde¹³ was synthesized by nitration of the benzenesulfonate of *o*-vanillin and then basic hydrolysis of the ester, m.p. 103-104°. 4-Nitrosalicylaldehyde, m.p. 133-134°, and 3-bromo-5-nitrosalicylaldehyde, m.p. 149-150°, were prepared at Boston University under the direction of Professors J. P. Mason and W. J. Gensler.

1,3,3-Trimethylindolinobenzopyrylospirans. General Directions.¹⁴ A mixture of equimolar amounts of the salicylaldehyde and commercially available 2-methylene-1,3,3-trimethylindoline in absolute ethanol (25 ml/0.01 mole of aldehyde) was refluxed on a steam-bath for two to five hours. The resultant highly colored mixture was cooled in an ice-water bath, filtered, washed with cold ethanol, and recrystallized from ethanol or an ethanol-water mixture. The yields, melting points and elemental analyses for the compounds prepared are given in Table II.

Rate Measurements. Procedure.—The photochromic spiran was dissolved in absolute ethanol (C. S. I. Reagent Grade) and placed in a quartz, glass-stoppered spectrophotometer cell. The cell was placed in a cell holder equipped with a thermostat and allowed to come to thermal

(13) W. Reid and H. Schaller, *Rev.* **85**, 216 (1952).

(14) C. P. Koelsch and W. R. Workman, *THIS JOURNAL*, **74**, 6288 (1952).

equilibrium. After 30 minutes, the temperature was measured by placing a thermocouple junction in the cell. The cell was then exposed to ultraviolet light from a four watt "Blak-Ray" (Ultra-violet Products Inc., San Gabriel, Calif.) or a 100 watt source (George W. Coates and Co., Long Island, N. Y.) for one to five minutes and immediately placed in either a Beckman DK-1 recording spectrophotometer or a Beckman DU spectrophotometer. The disappearance of the colored form of the photochromic spiran was followed automatically or manually by recording the absorbance at the maximum visible peak. The reaction was followed to 95-100% of completion. Absorbance at infinite time (A_{∞}) was zero or was taken as the absorbance after several days. Figure 3 gives results typical of those obtained.

Acknowledgment.—We wish to acknowledge, with thanks, the partial financial support of this work by The School of Aviation Medicine, USAF, Randolph Air Force Base, Texas, through contract AF 41(657) 215 and by the Wright Air Development Center, Aerial Reconnaissance Laboratory, Dayton, Ohio, through contract AF 33(616) 5510.

DAYTON 9, OHIO

**ORIGINAL PAGE IS
OF POOR QUALITY**

[CONTRIBUTION FROM THE RICHARD B. WETHERILL LABORATORY OF PURDUE UNIVERSITY]

Rate Data and Isomer Distributions in the Reaction of *t*-Butylbenzene with Mercuric Acetate in Acetic Acid Solution. Partial Rate Factors for the Mercuriation Reaction¹⁻³

By HERBERT C. BROWN AND M. DUBECK⁴

RECEIVED MARCH 21, 1959

The rate constants for the mercuriation of *t*-butylbenzene with mercuric acetate in glacial acetic acid are (l mole⁻¹ sec.⁻¹) 8.0×10^{-4} at 9.0°, 1.52×10^{-3} at 70.0° and 0.245×10^{-3} at 50.0°. Substitution occurs predominantly in the *meta* and *para* positions, with substitution in the *ortho* position amounting to less than 1% of the total. The isomer distribution data are 34.9% *m*-, 65.1% *p*- at 90.0°, 32.9% *m*-, 67.1% *p*- at 70.0°, 31.0% *m*-, 69.0% *p*- at 50.0°. Utilizing previously available data on the mercuriation of benzene under these conditions, the following partial rate factors at 25.0° are calculated: m , 3.41; p , 17.2. Consequently, in this reaction substitution *meta* to a *t*-butyl group occurs more readily than *meta* to a methyl group (m , 2.23), whereas substitution *para* to a *t*-butyl group occurs less readily than *para* to a methyl group (p , 23.0).

Different electrophilic substitution reactions result in major changes in the relative rates of reaction of the *meta* and *para* positions of toluene. The Selectivity Relationship (1) was proposed as a quantitative correlation of these data.⁵

$$\log p_i^{rel} = L \log (p_i^{rel}/m_i^{rel}) \quad (1)$$

Data for some forty-seven electrophilic substitution reactions are now available. These data are correlated by the Selectivity Relationship with quite satisfactory precision.⁶

It was suggested that the Selectivity Relationship might be applicable to benzene derivatives other than toluene.⁷ Unfortunately, with the exception of the detailed nitration data of Ingold and his co-workers,⁸ the available data were far

too sparse to permit a satisfactory test of this possibility.⁹

Accordingly it appeared desirable to undertake a determination of the relative rates and isomer distributions in the substitution of several typical aromatic derivatives. As representative substitution reactions, we selected uncatalyzed mercuriation,¹⁰ acylation¹¹ and halogenation,¹² and applied them to *t*-butylbenzene and other selected aromatic compounds.

The results of the mercuriation study with *t*-butylbenzene are presented in the present publication. The acylation¹³ and halogenation¹⁴ studies are reported in the following papers. In the final paper of this group,¹⁵ the utility of the Selectivity Relationship in correlating all of the available substitution data for *t*-butylbenzene is examined.

(1) Directive Effects in Aromatic Substitution. XXXVIII.
(2) This research supported in part by a grant from the Petroleum Research Fund administered by the American Chemical Society. Grateful acknowledgment is hereby made to the donors of the Petroleum Research Fund.

(3) Based upon a thesis submitted by M. Dubeck in partial fulfillment of the requirements for the degree of Doctor of Philosophy.

(4) Monsanto Chemical Co. Flow 1959 P-10.

(5) H. C. Brown and K. L. Nelson, *THIS JOURNAL*, **76**, 6292 (1953).

(6) L. M. Stock and H. C. Brown, *ibid.*, **81**, 3323 (1959).

(7) H. C. Brown and C. W. McGary, Jr., *ibid.*, **77**, 2300 (1955).

(8) For a summary of the data and pertinent references, see C. K. Ingold, "Structure and Mechanism in Organic Chemistry," Cornell University Press, Ithaca, N. Y., 1953, Chapter VI.

(9) C. W. McGary, Jr., Y. Okamoto and H. C. Brown, *THIS JOURNAL*, **77**, 3037 (1955).

(10) H. C. Brown and C. W. McGary, Jr., *ibid.*, **77**, 2306-2410 (1955).

(11) F. R. Jensen, G. Marino and H. C. Brown, *ibid.*, **81**, 3321 (1959).

(12) H. C. Brown and G. Marino, *ibid.*, **81**, 3308 (1959); H. C. Brown, G. Marino and L. M. Stock, *ibid.*, **81**, 3310 (1959).

(13) P. W. Robertson, P. B. D. de la Mare and W. T. G. Johnson, *J. Chem. Soc.* 276 (1943).

(14) P. B. D. de la Mare and P. W. Robertson, *ibid.*, 279 (1943).

(15) H. C. Brown and L. M. Stock, *THIS JOURNAL*, **79**, 1421-1575 (1957).

(16) H. C. Brown and G. Marino, *ibid.*, **81**, 3311 (1959).

(17) L. M. Stock and H. C. Brown, *ibid.*, **81**, 3322 (1959).

(18) L. M. Stock and H. C. Brown, *ibid.*, **81**, 3324 (1959).

	*CLASS. LTR.	OPERATION	PROGRAM	SEQUENCE NO.	REV. LTR.
PIR NO.	U	— 1254 —	AGCE	— 002	
*USE "C" FOR CLASSIFIED AND "U" FOR UNCLASSIFIED					

PROGRAM INFORMATION REQUEST / RELEASE

FROM DR. S. NESTE	TO FILE
----------------------	------------

DATE SENT 1-13-61	DATE INFO. REQUIRED	PROJECT AND REQ. NO.	REFERENCE DIR. NO.
----------------------	---------------------	----------------------	--------------------

SUBJECT
 FLUID FILTRATION THEORY

INFORMATION REQUESTED/RELEASED

The attached articles are applicable to fluid filtration requirements for the AGCE.

	PAGE NO. 1 OF	RETENTION REQUIREMENTS	
		COPIES FOR	MASTERS FOR
		<input type="checkbox"/> 1 MO.	<input type="checkbox"/> 3 MOS.
		<input type="checkbox"/> 3 MOS.	<input type="checkbox"/> 6 MOS.
		<input type="checkbox"/> 6 MOS.	<input type="checkbox"/> 12 MOS.
		<input type="checkbox"/> MOS.	<input type="checkbox"/> MOS.
		<input type="checkbox"/>	<input type="checkbox"/> DO NOT DESTROY

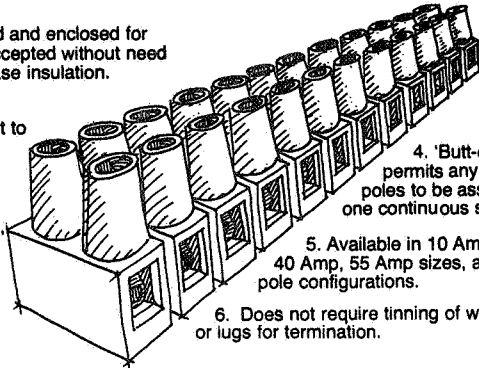
6 important features to look for in a terminal strip

Wiba® Europa Series

1. All metal parts recessed and enclosed for dead-front safety; U.L. accepted without need for covers or additional base insulation.

2. Flexible Polyamid 6 insulating body can be cut to any pole configuration.

3. Screw clamp type pressure connector. Non-ferrous, nickel-plated, stress relieved brass to resist corrosion. Supplied with clamp in open position for solid or stranded wire.



4. 'Butt-end' design permits any number of poles to be assembled as one continuous strip.

5. Available in 10 Amp, 20 Amp, 40 Amp, 55 Amp sizes, and in 2-12 pole configurations.

6. Does not require tinning of wire leads or lugs for termination.



Available at Authorized Distributors

and only **ELECTROVERT** has it all.

399 Executive Blvd., Elmsford, N.Y. 10523
Atlanta (404) 451-9366 Dallas (214) 241-5696
Chicago (312) 678-5557 Elmsford (914) 592-7322 / Santa Ana (714) 835-2033

Circle 24

FLUID POWER *continued*

New filtration theory

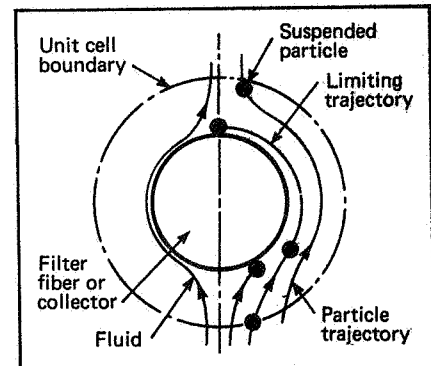
Up until now, the only published material dealing with fluid filtration on any sort of a scientific basis was the work of Dr. E.C. Fitch and his co-workers at Oklahoma State Univ. (Stillwater).

A sequel to this research was announced by J.A. Tichy, a professor at Rensselaer Polytechnic Institute (Troy, NY) during the recent ASME Century II conference. Tichy points out that Fitch's beta ratio concept (explained following) is based on only one type particle: AC test dust.

Not included are variables such as different shaped particles, different kinds of contamination, varying flow rates, wide ranges of temperature, various particle trajectories, adhesion and geometrical parameters.

The beta ratio (DE—Mar'80p47) is the number of particles greater than $x\mu\text{m}$ upstream divided by the number of particles greater than $x\mu\text{m}$ downstream where $x\mu\text{m}$ is contaminant particle size in micrometers.

Tichy proposes and has worked out preliminary math for an improved theory that considers effects of viscosity, van der Waals forces, Stokes number, fluid flow patterns (velocity fields), force and torque balance on



The unit cell for filter theory

each particle, particle trajectories, filter length, porosity, temperature and particle shapes.

The research, supported by the Office of Naval Research (ONR), has progressed to the point now where lubrication engineers can predict trends and perform sealing experiments. Tichy's paper is available from ASME, 345 E. 47 St., New York, NY 10017. Ask for ASME/ASLE 80-C2/Lub-20.□

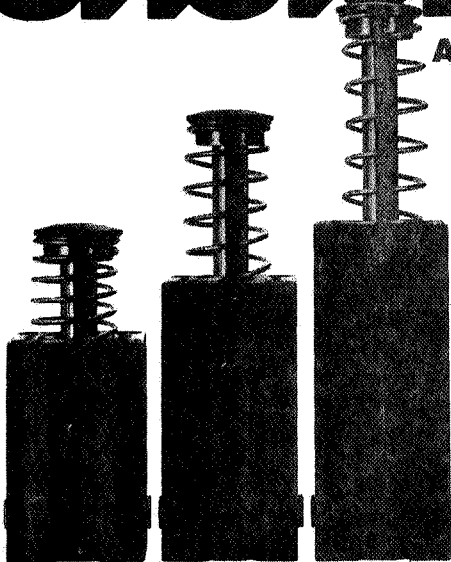
CONTROL DECELERATION WITH SHOK-BLOC®

ADJUSTABLE SHOCK ABSORBERS

The rugged Shok-Bloc from Efdyn has up to three times the working capacity per bore size of conventional units! You gain high capacity energy absorption at lower cost. Fewer parts increase life. Capacities to 188,000 inch lbs. Adjustment range is 180° Bore sizes: 7/8", 1 1/8", 2" Strokes: 1" to 8" Spring or air return. Efdyn, Box 1058, Guthrie, OK 73044, (405) 282-0600, Telex: Autoquip GTRE 74-8566

EFDYN®

DIVISION OF
AUTOQUIP CORPORATION



Hydraulic and pneumatic

Filter users and suppliers speak

For over a decade, researchers have been gathering proof that contaminants cause most of the downtime in fluid power systems. Now the OEM users seem to be listening

A filtration manual recently issued by Purolator (Newbury Park, CA) sums up the problem well for hydraulics: "Particles greater than 25 μm can jam pumps, valves and motors. Particles less than 25 μm , and more specifically between 0.5 μm and 5 μm , cause degradation failure. These fine abrasive particles, called 'silt,' can enter the clearances between moving parts, where they score and abrade the surfaces. Such wear generates more contaminants, increases the leakage clearances, lowers efficiency, and generates a considerable amount of excess heat."

That sounds like a clarion call for super-filtration, and more and more OEMs are sounding it. But the cry has been generally ignored because of the difficulty and expense of accomplishing it.

Who wants to assemble a system under clean-room conditions? Pre-filter all oil? Demand pure, dry air in shop systems? Never add new oil to a sensitive hydraulic system directly? Specify system flushing at high Reynolds Number? Monitor and maintain the system frequently? Yet that's what is required if you want to get rid of

wear and failure. You might as well write it into the specifications.

Advice from SAE. Nothing can happen until users demand clean air and oil. Fortunately, that seems to be the trend. The SAE (Society of Automotive Engineers) recently approved Recommended Practice SAE-J1227 for hydraulic systems, which concurs with the above and adds a lot of specifics:

"There is strong evidence that start-up failures of both new and overhauled systems often are contaminant-caused catastrophic failures. Contaminants built into each component making up an hydraulic system, and contaminants generated in assembling the components and systems, are significant contributors to these failures."

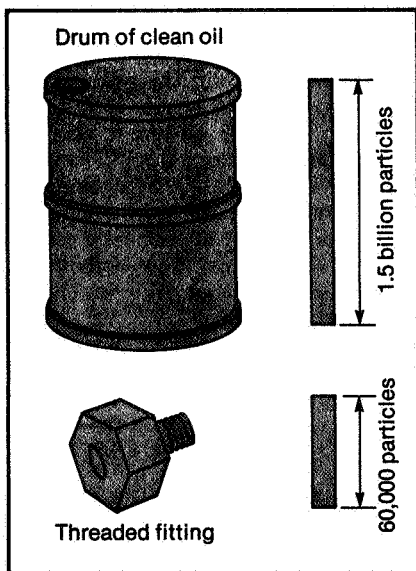
Reynolds number has been rediscovered as an important key to flushing dirty systems after they're assembled. Extensive tests prove that it is not just velocity, or just temperature or just low viscosity that insures good flushing; but it's Reynolds number: $(\text{velocity}) \times (\text{pipe I.D.}) / (\text{absolute viscosity})$. If Reynolds number during

flushing is over 4000, and higher than the maximum expected in the delivered system, most of contaminants will be flushed out. If not, danger lurks.

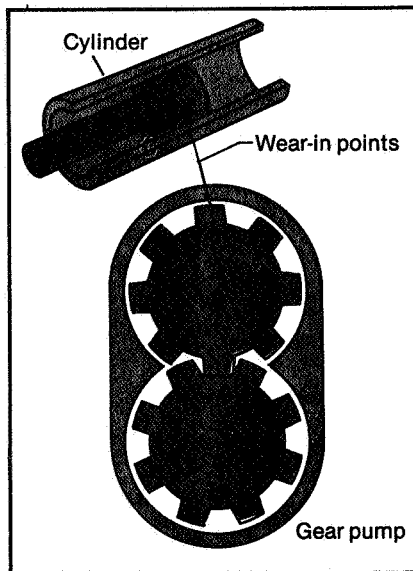
John Farris, corporate director, aerospace and fluid power, Pall Corp., (Glen Cove, NY) offers this typical example: SAE 10 engine oil; normal operating temperature, 180 F; normal flushing temperature, 75 F; max pump flow, 100 gpm; pipe I.D., 1.5 in., system fluid volume, 200 gal; viscosity at 75 F, 420 SUS; and viscosity at 180, 54 SUS.

With these figures, Reynolds number is 2325 at 75 F and 18,081 at 180 F. And there lies the problem. Even with ten turnovers of the tank volume at 75 F (contaminant level by then will be very stable), enormous additional amounts of contamination will be dislodged when the system runs at 180 F, because the Reynolds number is 7.8 times higher!

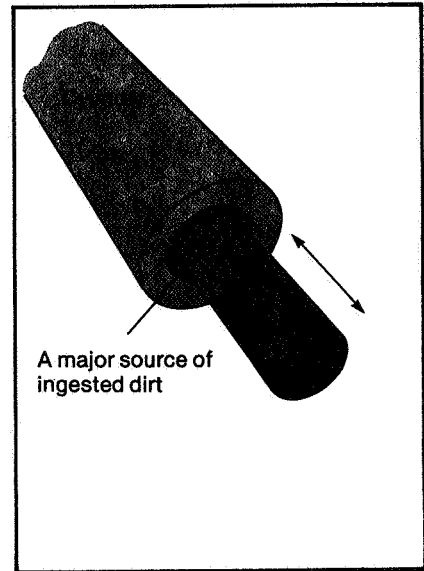
One answer, exploited by the military for critical components and systems, is to substitute a low viscosity fluid for flushing, then drain and refill with the correct fluid before shipping. Great care must be taken



1. A drum of clean oil can contain 1.5 billion particles; a fitting 60,000



2. Contaminants are generated by piston rings and gears wearing in



3. Ingested dirt is a major source of contamination, such as at rod seals

in choice of flushing fluid, because adverse chemical reactions could occur

The SAE recommended practice points out another danger area: vibration and shock. If the system or vehicle is shipped after final flush, contaminants can be dislodged by mechanical abuse in the shipping process itself. Field operation can have the same effect, and for a safe flushing procedure, you should vibrate the system at least as vigorously as you expect it to shake in operation.

Construction equipment. Pall Corporation has singled this industry out for a special newsletter, and sent us a copy of

the first one. Off-highway equipment takes a brutal beating, so we figure if a filter works there, it should work almost anywhere.

"Don't try to clean components or systems after they are fully assembled," they warn. "That's like trying to wash your underwear by taking a shower with all your clothes on." They further note that "there are five sources of dirt in hydraulic systems: built-in dirt, generated dirt, drawn in (ingested) dirt, repair or rework dirt and escaped dirt." Here are design tips for all of them:

- Avoid components with built-in dirt

traps—you'll never win.

- Clean the components beforehand in one or several of these ways: soap and water, acid cleaner, alkaline cleaner, solvent, ultrasonics, and mechanical cleaning

- Use rust preventative for steel or iron parts, but make sure it's clean

- Flex the hoses to release dirt that might be trapped. One manufacturer uses 50 flex cycles

- Don't trust that a new barrel has clean oil (Fig 1). Even a clean 55 gal barrel of oil can add 1-1/2 billion particles 10 μ M or larger to your system. Filter the oil before using it

- Do you think straight-thread O-ring fittings are clean? Not so. Tests at Pall show that it is not unusual to add 60,000 particles greater than 5 μ m each time you assemble one. Pipethreads are worse, and sometimes they add a little Teflon tape as well.

There is a way to get all that dirt out: hook up a filter cart ("kidney machine") with high performance fine filters. In fifteen minutes or less, a good flush is possible. Also, it's a good way to fill the reservoir. See drawing at left.

Another warning: remember that some gear pump manufacturers achieve close clearances by machining the pump housing undersize, and letting the gears cut the housing during startup! It's a neat trick, but generates metal particles. Piston rings also generate particles as they wear in (Fig 2).

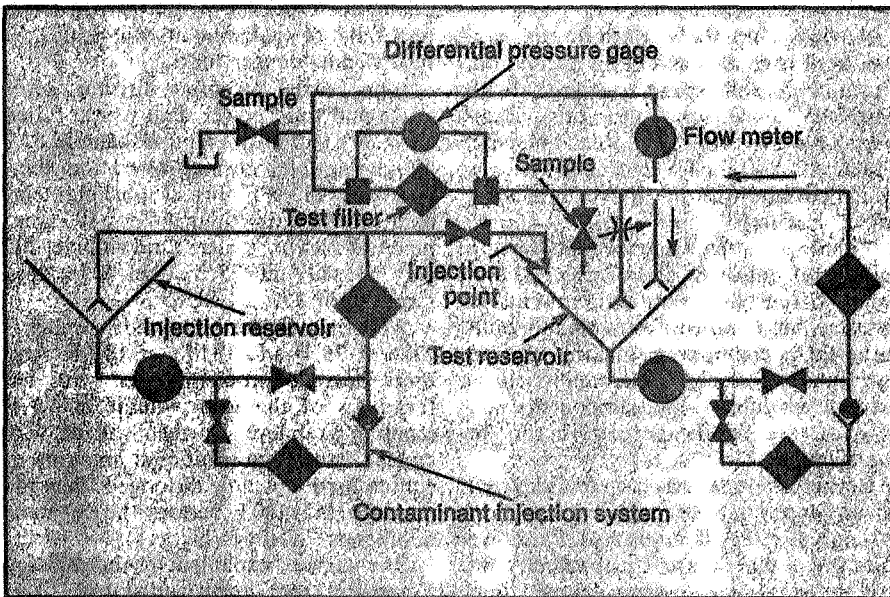
If a repair mechanic replaces a component, make sure he or she has been given detailed instructions on all of the preceding dangers. If a rod seal is worn, it can ingest dirt (Fig 3). Even new seals have greatly varying ingestion characteristics, and tests at OSU (Oklahoma State University) show 10 to 1 spread.

Escaped dirt is dirt that was caught at one time by the filter, but gets knocked off by a flow surge. Be sure to choose the right filter to prevent this.

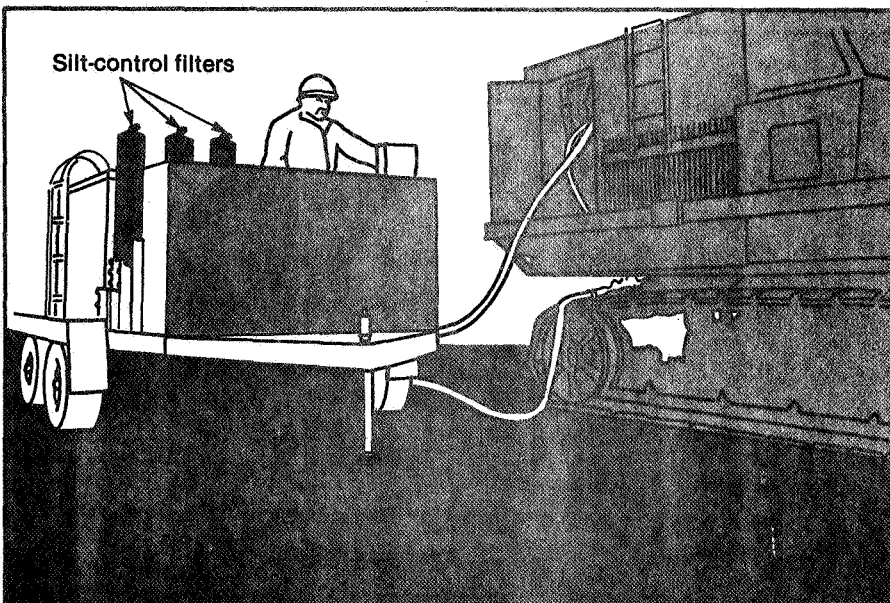
Every kind of test. There are national and international standards for classifying and measuring contaminants (size or weight), acid content, flow, collapse pressure, structural integrity, filtering capacity, and pressure drop.

Wayne Conner, project engineer for Facet Enterprises, Filter Products Div. (Madison Heights, MI) just completed Engineering Report #745, in which he summarizes the latest tests and standards. Here are the highlights:

Particles can be either counted or weighed, but counting is preferred because of the availability of accurate automatic particle counters. The counted sizes can be classified per existing standards, such as: National Fluid Power Association



4. Multi-pass filter test developed at OSU is one test that every company and country seems to accept as worthwhile, even though not all have rigs



5. Filter cart solves problems of massive flushing of system or replacement of oil cleanly for large machines. Viable alternatives are few (Pall)

(NFPA) recommended standard T2.9.3 R1 1979; American National Standards Institute (ANSI) B93.30-1973; National Aerospace Standard (NAS) 1638; Military Standard (MIL-STD) 1246A; and International Standards Organization (ISO) 4402.

Measurement and test of liquid contamination is more difficult. Water content may be found by a distillation technique issued by American Society for Testing and Materials: ASTM D-95-62. Acid content is measured in terms of neutralization number using ASTM D974.

Then there are a whole series of older tests that Conner does not recommend: permeability of AC test dust measured in seconds/1000 cc of reference fluid; bubble point to measure max pore size; mean flow pore size; DOP (dioctylphthalate) efficiency; filter capacity; and air flow resistance. These tests have never correlated well with actual filter performance.

Instead, he recommends the *Multi-pass method for evaluating the filtration performance of a fine hydraulic fluid power filter element* (Fig 4). It was developed a decade ago under the direction of Dr. E. C. Fitch at the Fluid Power Research Center, Oklahoma State University (OSU), and now is an accepted national and international standard NFPA T3.10.8.8-1973; ANSI B93.31-1973; and ISO 4572. Pall Corporation was the first filter manufacturer to build a multi-pass rig.

Now this multi-pass test method is the only industrially accepted means for filter element evaluation. It measures contaminant separation, retention and pressure loss. In essence, the same contaminated fluid is circulated continuously through the test filter, and additional contaminant is added continuously to the stream to maintain the original concentration.

Pressure drop across the filter vs time is recorded. At a predetermined drop, fluid samples are taken upstream and downstream of the filter. Using an automatic particle counter calibrated per ANSI B93-28-1973, the samples are analyzed for the number of particles per milliliter greater than selected sizes. These counts are used to calculate the "filtration ratios" (called Beta ratios):

$$\beta_{x\mu\text{m}} = \frac{\text{number of particles} > x\mu\text{m upstream}}{\text{number of particles} > x\mu\text{m downstream}}$$

where $x\mu\text{m}$ is particle size in micrometres.

The Beta ratios are plotted and manipulated in many ways to show separation efficiency, apparent capacity, actual capacity, and filter life profile—all for any chosen particle sizes within the capability of the instruments.

All the experts we contacted agree that Beta ratios are practical, and are using them or plan to. One warning: the values

measured with a clean filter are not always the same as those measured with a dirty filter. Be sure to ask for Beta values taken at flows and pressure losses expected in actual service. Don't accept data taken at 10 psid if your system will experience surges to 150 psid—or 1500 psid.

The latest interest is in plotting Beta ratios for numerous particle sizes. You then can write specs like these: minimum Beta ratio is 1.8 at β_{10} , 28 at β_{20} and 80 at β_{30} .

Radioactive wear tracer. Spot measurement of wear during operation is a great way to measure how your filters are doing, but how do you sense wear? Gordon Jones, Fram Corp (Providence, RI) has adapted an aerospace technique to industrial hydraulics. Called the SPI-wear method, developed by Spire Corp (Bedford, MA), it irradiates the surface of interest—say a spool valve land—and monitors that spot with an external radiation detector (Fig 6). As the irradiated spot wears, the intensity of radiation is measurably less.

Alternate methods involve measuring the contaminants generated by the wear, but not the wear point itself. Ultracentrifuging techniques developed by Mobil Corp. (New York, NY) are able to isolate wear particles too small to be sensed.

Materials and structure. With the advent of synthetic fluids, water-based fluids, and other chemical combinations, filter materials become touchy. Cellulose, for example, swells in water and closes off pores. Here are some other observations important today:

Micro fiber glass media are state-of-the-art and doing very well in regular and fine

filtration. They include fine enough fibers for silt control ($5\mu\text{m}$ and smaller particles), are not too expensive, and are made to be disposable. The disadvantage is low strength, but with epoxy bonding the problem is eliminated. The epoxy withstands synthetic fluids well.

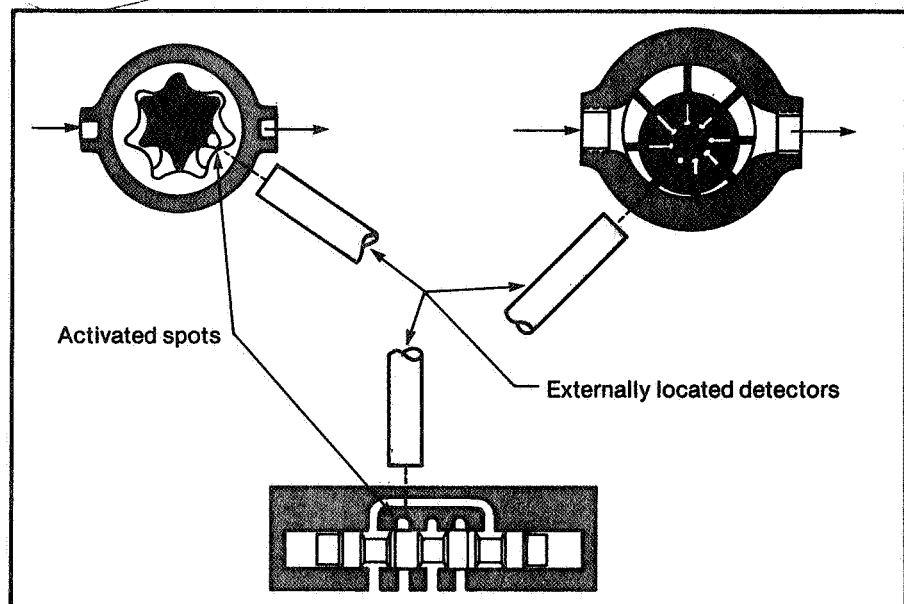
Gaskets are not as good as O-rings in filter assemblies that experience flow surges and other abuse. An O-ring seals better as pressure is increased. A gasket is more likely to leak or bypass.

Five international test standards, developed at OSU, evaluate structural integrity of the filter itself: fabrication integrity ISO 2942; collapse-burst ISO 2941; material compatibility ISO 2943; end load ISO 3723; and flow fatigue ISO 3724.

Fabrication integrity is a bubble point test that searches for defects, not for pore size. Collapse-burst applies high differential pressures such as those caused by contaminant loading, cold startups and flow surges. The test is run by adding contaminant upstream of the elements at rated flow until the required pressure drop is exceeded, or rupture occurs.

To test for material compatibility, the element is immersed for 72 hours in system fluid 15 C higher than rated max temperature. This test is followed by an end load test and a collapse-burst test. Flow fatigue is performed on an element that is loaded with contaminant to yield a specified pressure drop. Flow is cycled between zero and rated flow.

Another fatigue test, though not an international standard, is NFPA recommended standard T2.6.1 1974. It's a statistical method for estimating probabili-



6. Irradiated spot on any component can be monitored externally, and the amount of wear detected continuously. Method is based on missile research (Fram)

ORIGINAL PAGE IS OF POOR QUALITY

ty of failure caused by pressure cycling, based on actual data for the materials of construction, but not based on finished components. It's controversial (PE—June '73p26), but probably is the best way to predict fatigue failure without testing to destruction.

Failsafe filters. Many filter manufacturers offer built-in valves and special safety features that protect the system in the event of careless maintenance or some unusual failure upstream of the filter.

The "dirt fuse" offered by Pall is one example. It is designed to continue functioning until the entire system pressure—up to 6000 psi—appears as pressure loss across the filter element. The filter will not fail, but merely stops the flow.

Internal check valves, reliefs, bypasses, reverse-flow valves and shutoffs are available in many filter models from various manufacturers. Some are designed to prevent backflushing filter dirt into the main-stream when flow reversal or bypass occurs. Others automatically close off flow ports when the filter element is removed, to prevent loss of fluid or ingestion of dirt during routine maintenance. Still others offer differential pressure indication—even remotely—to warn that filter life is nearing its end.

One warning: the built-in valves are not precision instruments and have reasonable tolerances on operating points. If you rely on them, incorporate a safety margin.

Another warning: don't overdo the operating differential pressure loss. A differential of 85 psid at 20 gpm wastes 1 hp at the pump.

Pneumatic filtration. There is intense concentration on shop air systems, to keep out oil, water, debris, vapors and aerosols. Fargo Air (Buffalo, NY) just introduced a "package deal"—a total air system starting with a compressor of your choice, plus dryers, aftercoolers, filters, by-passes, electric wiring and piping. The company says it is first to offer the total package, pre-engineered, ready to run (Fig 7).

There should be a ready market, judging from the constant pressure on plant engineers to purify the exhaust air, keep oil out of close-clearance air logic spool valves, and get rid of water in airlines—all a source of trouble.

Pneumatics is becoming favored over hydraulics in instances where oil leaks (or fear of leaks) will compromise the application. Improved filtering practices—particularly the more universal acceptance of coalescing type media that take out aerosols as small as bacteria—are cleaning up pneumatic systems better than ever before.

What some users say. Ed Fletcher, manager of advanced hydraulic engineering, John Deere (Waterloo, IA), readily admits that much more must be done: "We have just scratched the surface of contamination technology." He suggests increased research at university and govern-

For more information

All NFPA, ANSI and ISO standards are available from National Fluid Power Assoc., 3333 N. Mayfair Rd., Milwaukee, WI 53222. SAE recommended practices may be obtained from Society of Automotive Engineers, Inc., 400 Commonwealth Dr., Warrendale, PA 15096.

ment levels to provide the design tools for making right filter decisions. He says:

"Contamination itself must be even better defined. Repeatable tests must be perfected. We need to identify contaminant sensitivities of basic parts and components such as a spool-and-bore, poppet-and-seat, shaft-in-bushing, sliding valve plates, and even orifices. It is impractical to run contaminant tolerance tests in sufficient numbers on every design of hydraulic component so that meaningful predictions can be made. More basic research is the answer."

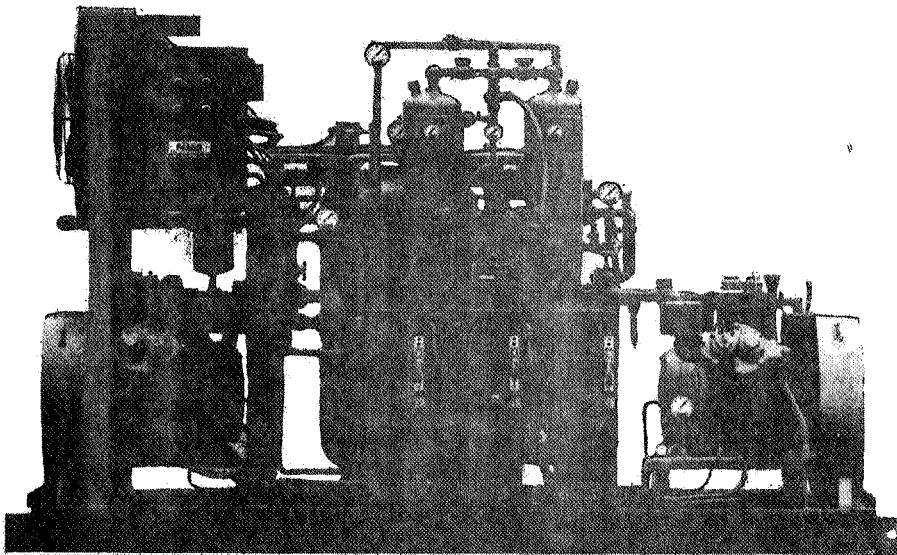
Furthermore, he points out that the greatest source of contamination is "built in" during manufacture. Better cleaning methods are needed. Don't overlook degaussing as a way of reducing accumulation of metal particles.

Finally, filter manufacturers should label their product with complete performance specifications. Statements such as "interchangeable with original equipment specifications" or "will interchange with XY1234 filter element" doesn't tell customer what he is buying.

Ed Askey, vp, Snap-Tite (Union City, PA) suggests some good ways to reduce installation-injected contaminants. For one, improve deburring and cleaning of parts before final assembly. Eliminate sealing compounds. Initiate the new "thermal deburring" techniques on critical parts such as seats, small pilot orifices, and pipe threads. Avoid getting lapping compounds into reservoir fluids. Remember that high humidity from the air can condense in bench fluids, and sweaty palms can start corrosion spots on parts. He also suggests:

Don't neglect filtering of case drains on pumps, motors and valves. There are too many instances where all proper filtering steps elsewhere are taken, but dirty oil from case drains goes right back to the reservoir.

When sizing filters, be sure to include surge flows from accumulators, differential cylinder areas, pump full stroking. Remember the nature and quantity of the contaminants. For example, when testing sand cast products, filters load up fast.
Frank Yeaple



7. This packaged compressed air system is designed to plug in and operate in any plant. It contains compressors, filters, dryers, and controls (Fargo Air)

	*CLASS LTR.	OPERATION	PROGRAM	SEQUENCE NO.	REV. LTR.
PIR NO.	U	1254	AGCE	021	
*USE "C" FOR CLASSIFIED AND "U" FOR UNCLASSIFIED					

PROGRAM INFORMATION REQUEST / RELEASE

FR	TO
S.L. Neste	Distribution

DATE SENT	DATE INFO. REQUIRED	PROJECT AND REQ. NO.	REFERENCE DIR. NO.
4/24/81			

SUBJECT
 Task 2 - Purification, Characterization and Handling of High Dielectric Constant Fluids

INFORMATION REQUESTED/RELEASED

1.0 SUMMARY

A procedure for evaluating fluids for use in the AGCE is outlined based on personal communication with experts in the area of fluid purification and evaluation, together with a review of pertinent published papers. These sources all indicated that special facilities were required to accurately measure electrical properties such as dielectric constant and dissipation factor of high dielectric fluids. When highly purified fluids are required it is almost essential that the purification and characterization be performed in the same laboratory. At present only the GE Capacitor Products Department appears to have this combined capability. Unfortunately, the time and funding available for the present AGCE feasibility study do not permit laboratory evaluation of candidate fluids to be conducted at this time.

In lieu of such test data, methods for purifying and measuring the electrical properties of dielectric fluids were investigated and a general approach recommended. The procedures outlined herein have been informally approved by the GE Capacitor Products Department and will form the basis for evaluating candidate AGCE fluids during a subsequent study phase and for determining specific handling procedures which must be observed.

A tabulation of available data for candidate fluids is presented to give an indication of achievable values.

G. Fogal R. Homsey S. Neste	PAGE NO.	RETENTION REQUIREMENTS	
	1 OF 11	COPIES FOR	MASTERS FOR
		<input type="checkbox"/> 1 MO.	<input type="checkbox"/> 3 MOS.
		<input type="checkbox"/> 3 MOS.	<input type="checkbox"/> 6 MOS.
		<input type="checkbox"/> 6 MOS.	<input type="checkbox"/> 12 MOS.
		<input type="checkbox"/> MOS.	<input type="checkbox"/> MOS.
		<input type="checkbox"/>	<input type="checkbox"/> DO NOT DESTROY

2.0 BACKGROUND

As identified in PIR 1254-AGCE-014A a critical element in obtaining fluids which have both high dielectric constant and low dissipation factor (high resistivity) lies in the purification of the fluid. The ability of high dielectric constant fluids to efficiently dissolve and dissociate impurities not only makes it difficult to achieve a high state of purity for these fluids, but it greatly complicates the process of measuring their electrical properties and requires special facilities to make these measurements accurately.

The problem of measuring electrical properties associated with dielectric fluids has long been recognized by the ASTM and attempts to establish reliable methods for their measurement has been outlined in Methods D924 and D1169. In spite of these procedures, highly erratic results are often obtained for measurement of the dissipation factor and resistivity. In addition, the difficulties are greatly increased when working with highly purified fluids and fluids of high dielectric constant. Since the AGCE will most likely require use of these more difficult fluids, a program for purifying, characterizing and handling these fluids must be established.

3.0 FLUID PURIFICATION

There are three objectives which must be achieved by the fluid purification process. First, the concentration of particulates of size 0.5 to 1.0 micron must be reduced to levels which do not disturb the photochromic dye patterns used to assess the fluid motions, e.g., fluid perturbation due to the oscillation of the dust particles in the applied AC field. Second, the fluid must have a dielectric strength sufficient to withstand an electric field of 20 Kv over a distance of ~ 1 cm. Third, the dissipation (i.e., fluid heating due to the applied voltage)

must be minimized so that observation of other thermally generated flow patterns are not obscured. The latter two properties will be determined primarily by the concentration of gaseous and colloidal impurities.

A summary of various purification techniques and their efficiency for removing various classes of contaminants is given in Figure 1. Note that in some cases the type of contaminant is harmful to the efficiency of a treatment method. For example, water and solids affect the Fuller's earth efficiency. Figure 1 also illustrates that a definite sequence of treatments is required to achieve the greatest fluid purity. Based on discussions with experts in the field of fluid purification and a survey of recent pertinent literature, the following general steps were identified as the best AGCE fluid purification procedure.

- 1) Fluid filtration to remove non-colloidal solid particulates (>0.1 micron)
- 2) Dehydration and deaeration to remove dissolved water and gases
- 3) Final purification to remove colloidal solids (<0.1 micron) molecules and ions.

The specifics of implementing each of these steps can vary depending on fluid characteristics such as viscosity, density and dielectric constant, and in some cases the procedures are proprietary. For example, although the Monsanto Chemical Company and Crown-Zellerbach have what they consider to be good purification procedures, neither would divulge any details of their processes.

An additional difficulty associated with the AGCE application for these fluids is that the dissolved photochromic material must be a component of the

TYPE OF CONTAMINATION	TREATMENT METHOD AND EFFICIENCY							
	FILTRATION SURFACE	FILTRATION DEPTH	COALESCENCE	FILTER PRESS	CENTRIFUGE	FULLER'S EARTH	THERMO-VACUUM PROCESS	MOBILE PROC. PLANT
WATER EMULSIFIED	N	N	E	P*	E	P*	P*	E
WATER DISOLVED	N	N	N	P	N	P*	E	E
AIR & GAS	N	N	N	N	N	N	E	E
SOLIDS - Non Colloidal	E	E	P	E	P	P*	N	E
COLLOIDAL - Particals & Sludge	N	N	N	P	P	E	N	E
ACIDITY	N	N	N	N	N	E	N	E
WATER & GAS - For EHV Application	N	N	N	N	N	N	E	E
TRANSFORMER DRY OUT	N	N	N	N	N	N	P	E
TEMPERATURE OF TREATMENT								
TEMP. LIMITS °C FOR PROCESSING	0-95	0-95	0-60	20-70	40-80	20-80	0-95	Var.
OPT. RECOMMENDED TEMPERATURE °C	Over 25	Over 25	20-40	60	60	60	25-50	Var.

* Substantial contamination is harmful to the efficiency of treatment

FIGURE 1. SUMMARY OF TRANSFORMER OIL TREATMENT METHODS

fluid. This requirement raises at least two additional questions:

- 1) Will the purification process remove the photochromic dye?
- 2) How much will the photochromic dye contaminate the purified fluid (i.e., increase dissipation) if it survives the purification process or if it must be added later?

In order to answer the first question, the candidate fluids should have the proper concentration of photochromic dye dissolved in them prior to beginning the purification process. This will permit periodic activation of the dye throughout the cleaning sequence to determine if the dye survives the purification process or at what point the dye is removed along with other contaminants. This information is essential for determining when the fluid and dye can be mixed, and what type of on-line fluid processing can be implemented. The second question requires purifying and characterizing the fluid prior to adding the photochromic dye. Subsequent addition of the dye and a recharacterization of the fluid will provide data on the effect of the dye.

3.1 Fluid Filtration

Solids in the size range from ~ 0.1 micron and larger are commonly removed from fluids using membrane or depth type filters. These filters are available in a range of pore sizes or porosities as discussed in PIR No. 1254-AGCE-016. Selection of the proper filter media should be relatively straightforward.

3.2 Dehydration and Deaeration

Removal of dissolved water and gases from the dielectric fluid can be performed as a two-step process using a molecular sieve to adsorb the water followed by a vacuum treatment, i.e., exposing the fluid surface to a vacuum to allow the escape of trapped gases. A single step approach, called the thermo-vacuum treatment, involves exposing the heated fluid to a vacuum which allows

release of both gases and dissolved water from the liquid. Both vacuum procedures require maximizing the exposed surface area to permit effective removal of dissolved water/gas. However, based on the experience of the GE Capacitor Department, it is recommended that the two-step procedure be implemented. The GE group and Crown-Zellerbach have both used the Linde Molecular Sieve Type 4A to dry toluenitrile and DMSO respectively with good results.

3.3 Final Purification

The last step in the fluid purification must remove any remaining submicron particles, as well as molecules and ions which will contribute to dissipation. The most efficient method for performing this final purification utilizes an adsorbent such as Fuller's earth which involves the following processes:

- 1) filtration - physical entanglement of small solid particles,
- 2) adsorbtion - adherence of molecules or ions to the surface of the adsorbent,
- 3) catalytic activity - causing reactions whose products are more readily adsorbed.

There are two potential methods of implementing the Fuller's earth purification process:

Contact Method - A batch type process in which a slurry of colloidal Fuller's earth and the liquid are agitated at elevated temperatures to achieve good contact and adsorbtion. After equilibrium has been reached (1-2 hours) the slurry is filtered and the Fuller's earth is removed from the purified fluid. The process is repeated until the desired purity is achieved.

Fixed Bed Method - The liquid is passed through a packed layer of Fuller's earth via a gravity feed or a pressurized system. The final purity will be determined by contact time, velocity of fluid flow and the size and type of Fuller's earth. This basic method can also be implemented by using disposable cartridges or re-fillable canisters as applicable.

For laboratory purification of fluids the contact method is recommended by the GE group while an on-line process (filtering in orbit) will require a variation of the fixed bed method.

4.0 FLUID CHARACTERIZATION

Candidate fluids chosen for the AGCE application must be characterized to establish their electrical parameters and to assess their contamination potential. Electrical property measurements should be made at several points in the purification process to establish the effectiveness of each step and to determine the optimum purity achievable, i.e., the point at which further processing is of no value.

Assessment of contamination potential requires that the same set of fluid property measurements be made periodically after the purification is completed. During this post purification time, the fluid will be placed in contact with candidate materials to be used in the AGCE fluid system and exposed to various light sources. Typical materials include stainless steel (tubing, fittings and valves), SnO (outer sphere coating), fluorocarbon (gaskets and seals), glass fibers (filter material) and gases (air, dry nitrogen, etc.). If the photochromic response of the fluid was lost or greatly diminished during the refining process, the photochromic dye must also be mixed with the purified

fluid at this time and its effects on the fluid properties assessed. Periodic measurements will also be made on a control sample of the purified fluid which is maintained in a dark place in a non-reactive container. These measurements will allow the effects of various materials to be compared with fluid degradation due to the normal aging process.

The care to be exercised during the measurement process cannot be over emphasized. The measuring electrodes and the glass vessel for the cell must be cleaned with special care to insure that the measurement process itself does not degrade the fluid. A cleaning procedure which has been used by the Monsanto Chemical Co. (Much, 1970) is outlined below:

- 1) Xylene vapor clean for 15 minutes.
- 2) Clean in boiling 29% NH_4OH for 10 minutes.
- 3) Steam clean for 30 minutes.
- 4) Acetone vapor clean for 15 minutes.
- 5) Dry in 100°C oven for 30 minutes.

Even with this type of facility preparation, several measurements per sample may be required to establish confidence in the results.

5.0 FLUID HANDLING

A logical conclusion of the preceding two sections is that all fluid handling procedures must be minimized. For example, purification and characterization of the fluids should be done in a single laboratory. The recommended handling procedure for storage and/or transfer of the fluid from the purification apparatus to the AGCE assembly will be based on the results of the fluid characterization (i.e., contamination susceptibility). The major environmental parameters which are likely to require special consideration during the transfer process are: (1) exposure to air, (2) contact materials, and (3) exposure to light.

6.0 FLUID PROPERTIES SURVEY

The aforementioned difficulties associated with the purification and characterization of high dielectric fluids has resulted in a paucity of data for fluids of interest to the AGCE application. Although, scattered data are available for a few fluids, the values depend strongly on the fluid purity and the measurement techniques, making it difficult to establish trends. The results presented in Table 1 should be interpreted as indicative of what may be feasible in terms of dissipation factor and/or resistivity.

Table 1. Data for a Range of Dielectric Fluids

FLUID (DIELECTRIC CONSTANT)	PURIFICATION PROCESS	LABORATORY	DISSIPATION FACTOR (RESISTIVITY)	COMMENTS
*m-tolunitrile (40)	Molecular Sieve & Fuller's Earth	GE Capacitor Products Department	<0.01	A tan δ of ≈0.001 may be achievable.
*DMSO (∞48)	Proprietary	Crown Zellerbach	(∞10 ⁸ Ω cm)	
Aroclor 1242 (5)	Proprietary	Monsanto Company	∞0.0015	Very viscous
MCS 1489 (6.5)	Proprietary	Monsanto Company	0.05	Developed as a substitute for Aroclor fluids
Nitrobenzene (∞35)	Not specified	NBS	(6.67x10 ⁸ Ωcm)	This sample probably was not highly purified
Nitrobenzene (∞35)	Fractional Distillation & Freezing followed by Electrolysis	-----	(7.5x10 ¹³ Ωcm)	This value was reported in a paper by Pearmain, et al.

*These fluids are known to be compatible with photochromic dye material.

7.0 CONCLUSIONS & RECOMMENDATIONS

The difficulties associated with the purification, characterization and handling of the high dielectric constant fluids which may be required for the AGCE point out the need for a specific effort directed to this area. The work should be confined to a study of only those fluids shown to be compatible with photochromic material and which exhibit other desirable qualities for the AGCE such as low viscosity, high thermal coefficient of dielectric constant (i.e., $1/k \text{ dK/dT}$) and good optical transmission. The two or three fluids with highest potential should then be purified and characterized using the basic procedures outlined in Sections 3 and 4. The specific objectives of this effort would include:

- 1) Define a specific purification procedure to be used for refining dielectric fluids for the AGCE.
- 2) Determine the lifetime (or degradation as a function of time) of the purified fluids as a function of storage environment (e.g., contact materials, lighting, temperature, etc.).
- 3) Determine what level of in orbit fluid purification is required.
- 4) Determine if in orbit monitoring of fluid dissipation factor should be considered. This assessment will depend on the results of item 2.
- 5) Define fluid handling procedure which includes fluid purification, photochromic/fluid mixing, storage and transfer to the AGCE fluid flow cell.

Since the results of this effort may impact the selection of materials for the AGCE (e.g., sphere coating, plumbing, filter material, etc.), the work should be completed as a precursor to the hardware development program.

8.0 REFERENCES & BIBLIOGRAPHY

1. Daniels, B., Personal Communication, Monsanto (1981).
2. Gallagher, T.J., Simple Dielectric Liquids, The M.I.T. Press, Cambridge, Mass. (1966).
3. Levy, L.C., "Power Factor and Specific Resistance (Resistivity) Measurements on Electrical Insulating Liquids", Insulation 16(6), 41-44 (1970).
4. Lukchis, G.M., "Adsorption Systems Part I: Design by Mass Transfer-Zone Concept", Chemical Engineering, June 11, 1973.
5. Lukchis, G.M., "Adsorption Systems Part II: Equipment Design", Chemical Engineering, July 9, 1973.
6. Lukchis, G.M., "Adsorption Systems Part III: Adsorbent Regeneration", Chemical Engineering, August 6, 1973.
7. Munch, R.H., "Measuring the Dissipation, Dielectric Constant and Resistivity of Liquids", Insulation 16 (3), 46-49 (1970).
8. Orle, J., Personal Communication, Crown Zellerbach (1981).
9. Povazan, E., "Modern Techniques in Processing Transformer Oils", CEA Engineering & Operating Division Transactions, March 1975.
10. Shaw, D., Personal Communication, GE Capacitor Products Department (1981).
11. Smyth, C.P., Dielectric Behavior and Structure, McGraw-Hill Book Company, Inc., New York (1955).
12. vonHippel, A.R., Dielectrics and Waves, The M.I.T. Press, Cambridge, Mass. (1966).

*CLASS. LTR.	OPERATION	PROGRAM	SEQUENCE NO.	REV LTR
U	1254	AGCE	016	

PIR NO. U 1254 AGCE 016
*USE "C" FOR CLASSIFIED AND "U" FOR UNCLASSIFIED

PROGRAM INFORMATION REQUEST / RELEASE

FROM S. L. Fogal <i>[Signature]</i>	TO Distribution
--	--------------------

DATE SENT 3/10/81	DATE INFO. REQUIRED	PROJECT AND REQ. NO.	REFERENCE DIR. NO.
----------------------	---------------------	----------------------	--------------------

SUBJECT
TASK 3 - DUST REMOVAL FEASIBILITY REPORT

INFORMATION REQUESTED/RELEASED

1.0 SUMMARY

The objective of TASK 3 is to determine the feasibility of incorporating a hardware capability for programmed circulation and filtration of the dielectric fluid after assembly of the AGCE system. Results of the TASK 3 effort indicate that a dust removal capability can be readily accommodated; the corresponding weight and peak power penalty are 1.7 kg and 35 watts respectively. Suitable hardware elements are available for incorporating the capability into the AGCE. Preflight and periodic in-flight operation of this AGCE capability is recommended.

2.0 BACKGROUND

During laboratory development studies conducted by Dr. W. Fowles, it was found that dust particles in the dielectric fluid oscillate due to the implied electric field. This oscillation can disturb the activated photochromic dye markers used to assess dielectric fluid flow (within the spherical capacitor test cell) during an experiment. The amplitude excursion of the dust and consequently the disturbing effect is reduced by increasing the frequency of the electric field. Amplitude decreases inversely as the square of the frequency, the disturbing effect being much reduced for frequencies

S. Neste G. Fogal R. Homsey C. Mosley T. Scollon	PAGE NO.	<input checked="" type="checkbox"/> RETENTION REQUIREMENTS	
	OF	COPIES FOR	MASTERS FOR
		<input type="checkbox"/> 1 MO.	<input type="checkbox"/> 3 MOS.
		<input type="checkbox"/> 3 MOS.	<input type="checkbox"/> 6 MOS.
		<input type="checkbox"/> 6 MOS.	<input type="checkbox"/> 12 MOS.
		<input type="checkbox"/> MOS.	<input type="checkbox"/> MOS.
		<input type="checkbox"/>	<input type="checkbox"/> DO NOT DESTROY

over about 300 Hz. Thus a combination of a high frequency voltage source (see TASK 2) and filtration of the dielectric fluid should eliminate the problem.

The source of the offending particulates is twofold based on the experience of Dr. Fowlis. First, the particulates may be in the dielectric fluid either in the as received state or inadvertently introduced during the assembly of the AGCE system. Second, the particulates may be attached to internal surfaces due to inadequate cleaning during the manufacturing and assembly process and are subsequently detached by the action of the electric field or by mechanical vibration/shock during ground handling and during launch. Laboratory development tests by Dr. Fowlis have demonstrated that one equatorial entrance port can provide an effective flush of the spherical capacitor dielectric volume, provided sufficient time is allowed. In his tests, Dr. Fowlis used a flow rate of $200 \text{ cm}^3/\text{min}$; about 15 minutes were required to purge the dielectric fluid volume of most particles over about 1.0 micron diameter. When filtering without the electric field was followed by filtering with the electric field applied (20KV at 60Hz), additional particles were immediately detected in the dielectric fluid (and filtered out). Subsequent applications of the electric field did not generate more particles.

The dust removal capability discussed below is based on this background experience of Dr. Fowlis.

3.0 TASK IMPLEMENTATION

Key design requirements related to the dust removal capability were generated and are included in section 5.1. These design requirements, based on previous development experience, the Spacelab Payloads Accommodation Handbook SLP/2104 and an estimate of the AGCE flight design, are intended as guidelines for the feasibility study only.

3.1 Spherical Capacitor Assembly

**ORIGINAL PAGE IS
OF POOR QUALITY**

Based on the laboratory development experience of Dr. Fowles, purging the internal volume of the spherical capacitor assembly can be readily accomplished. Mechanically, the preferred approach is that shown in figure 1. If an equatorial baffle is required, the configuration shown in Figure 2 can be used. In either case, multiple entrance/exit ports are provided to improve the efficiency of the purge flow over that for a single entrance/exit port arrangement. A more efficient purge flow can reduce purge time requirements, an important consideration for on-orbit operations. The three in/out ports shown can be sized such that the center pair flow is somewhat larger than either of the two side flows (to compensate for the larger swept volume of the center pair flow). In the figure 1 arrangement, leaving out the entrance/exit ports labeled "A" can provide a clockwise rotation of the dielectric fluid during the purge cycle, further improving purging efficiency and thus minimizing the purge time required.

The arrangement shown in Figure 2(a) features a baffle which, in addition to the equatorial portion also includes two meridian segments. These segments divide the fluid volume below the equator into entrance and exit plenums. Two problems are apparent. First the baffle must make a good fit with mating elements to prevent excessive leakage between the two plenums and second the baffle material dielectric constant should match that of the dielectric fluid to minimize distortion of the electric field. Such a match may not be possible considering the high dielectric constant desired for the fluid (see TASK 1). One possible solution to this potential mismatch is to construct the baffle of a porous material such as sintered teflon. This type material is available with pore volumes up to 90% (see section 5.2, Porex catalog). A custom molding may be necessary if this material is used. An alternate baffle arrangement is shown in Figure 2 (b).

ORIGINAL PAGE IS
OF POOR QUALITY

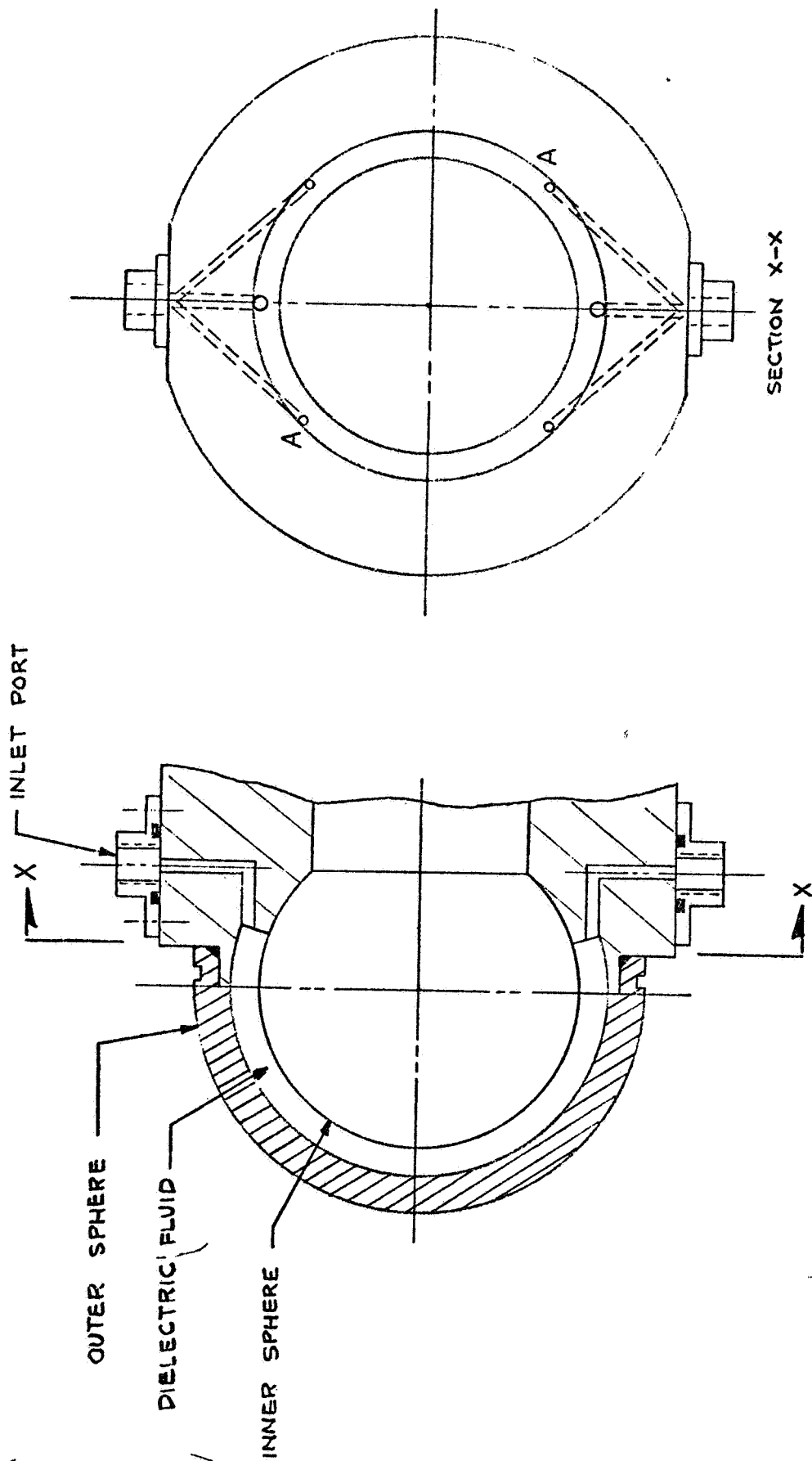


FIGURE 1 INLET/EXIT PORT ARRANGEMENT WITHOUT EQUATORIAL BAFFLE (NOT TO SCALE)

ORIGINAL PAGE IS
OF POOR QUALITY

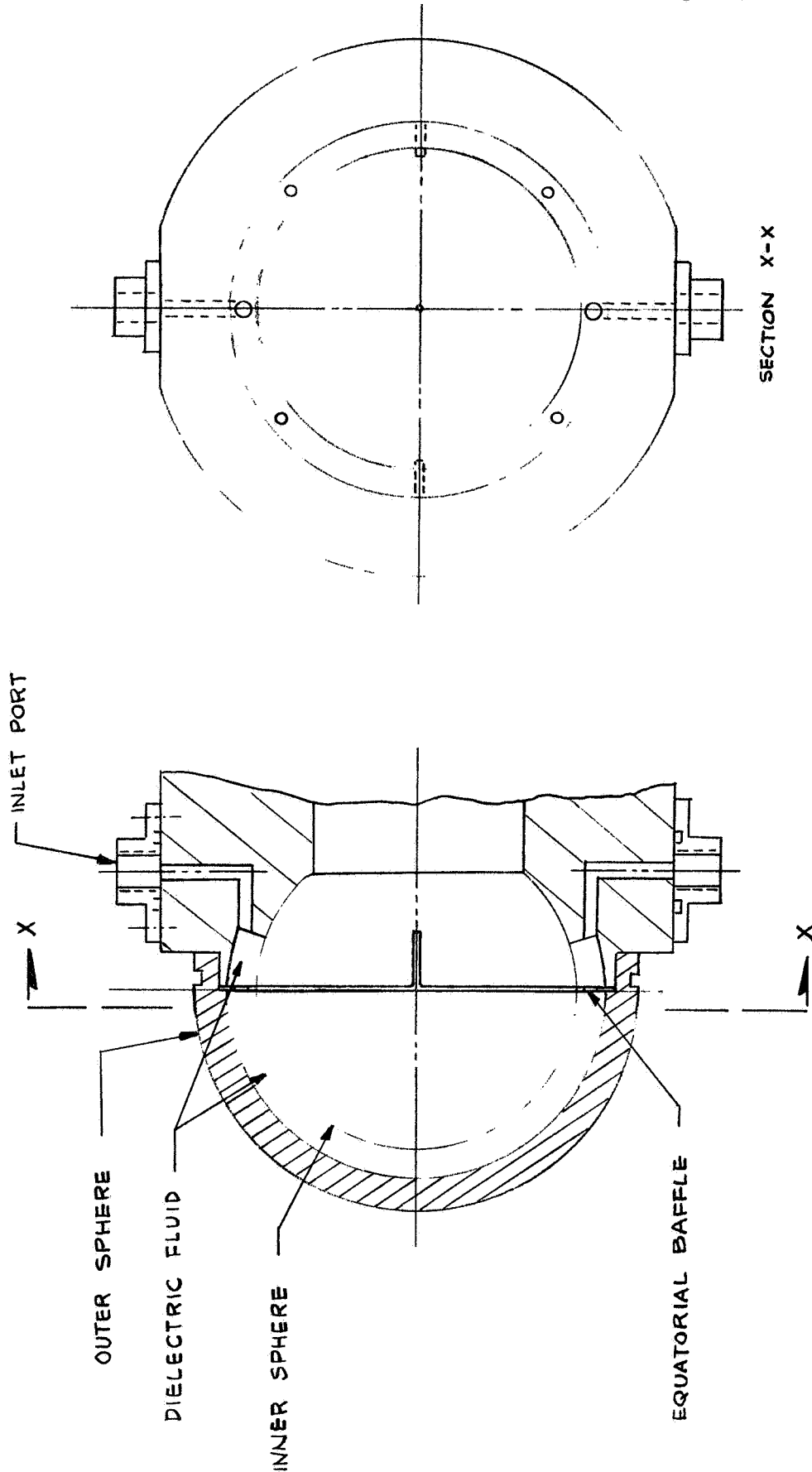


FIGURE 2 (a) ENTRANCE/EXIT PORT ARRANGEMENT WITH EQUATORIAL BAFFLE (NOT TO SCALE)

ORIGINAL PAGE IS
OF POOR QUALITY

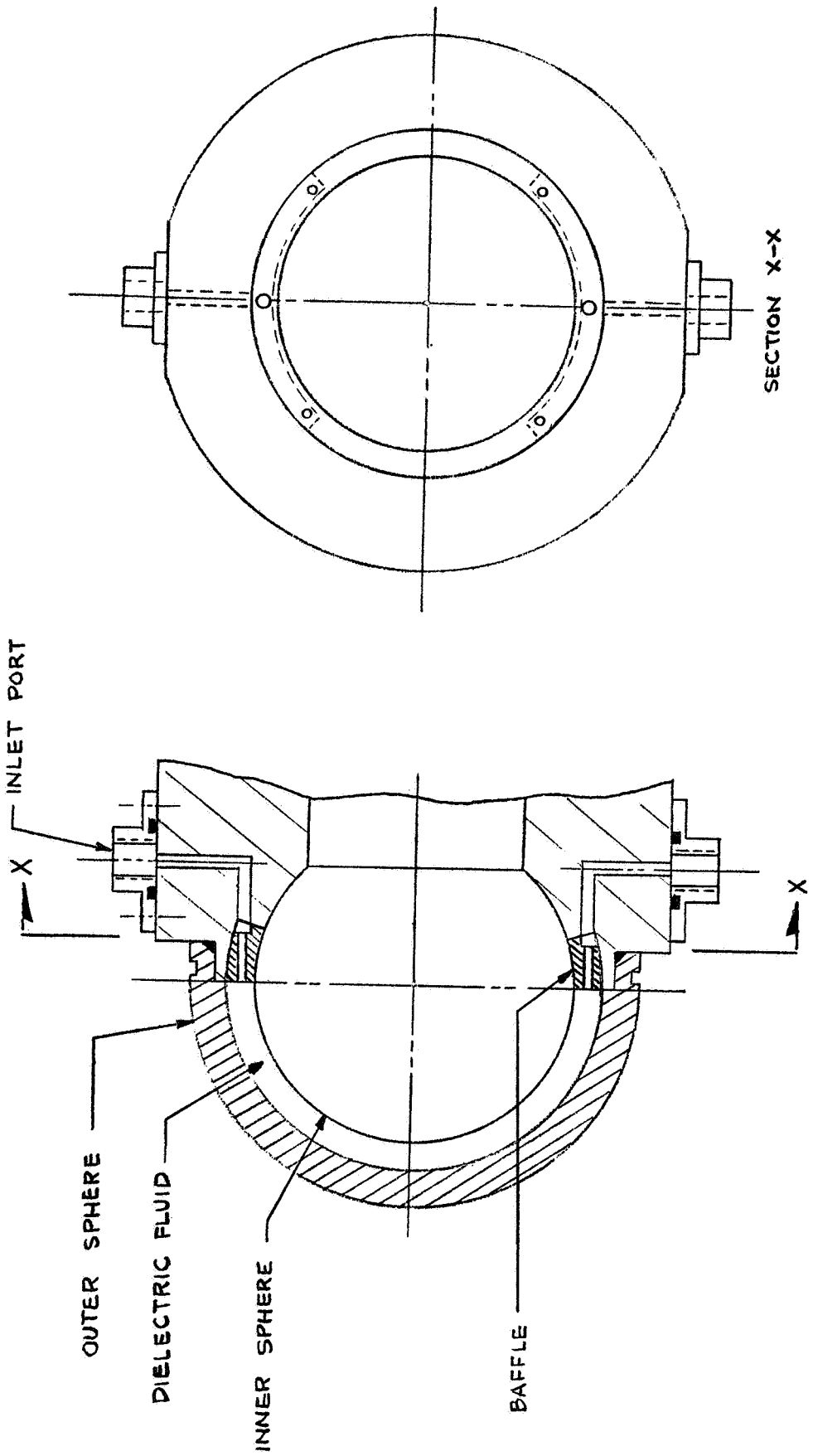


FIGURE 2 (b) ALTERNATE ENTRANCE/EXIT PORT ARRANGEMENT
WITH EQUATORIAL BAFFLE (NOT TO SCALE)

3.2 Circulation Pump

Figure 3 shows the circulation loop block diagram. As shown in Table 1, dielectric fluid volume is estimated at 275 cm^3 . This assumes that the fluid volume does not extend below 10°S latitude. Table 2 shows an estimated pressure budget for three flow rate conditions. As would be anticipated, the filter is the major contributor to the pressure budget.

Actual pump selection should also take into account the coolant flow requirements of the thermal subsystem (see TASK 6). From a programmatic viewpoint, the same pump assembly should be selected for all applications. One potential candidate is a pump assembly being used in the Shuttle Galley currently under development by GE for NASA-JSC. This pump is a magnetically coupled gear pump supplied by Micropump, Concord, Ca. An outline dwg. is shown in the Appendix, Section 5.3.

As shown in Figure 4, use of this specific pump will result in a circulation flow rate of $1420 \text{ cm}^3/\text{min}$. (0.375 gpm) and a system operating pressure of 15 psi. At this flow rate and an estimated dielectric fluid volume of 275 cm^3 (Table 1), a 26 volume purge can be accomplished during the 5 minute period assumed available between each individual AGCE experiment. This should be more than ample to maintain the dielectric fluid in a dust free condition. Note that pump capacity can be increased/decreased by selecting a higher/lower rpm pump motor.

3.3 Particulate Filter

The task guidelines, Section 5.1, specify that the dust removal capability must maintain particulate concentrations in the dielectric fluid to less than 10 particles/ cm^3 for particles exceeding 0.5 micron in diameter with the maximum particle size not to exceed 1.0 micron. A disposable depth type filter tube available from Balston, Inc., Lexington, Ma. appears to be a suitable candidate.

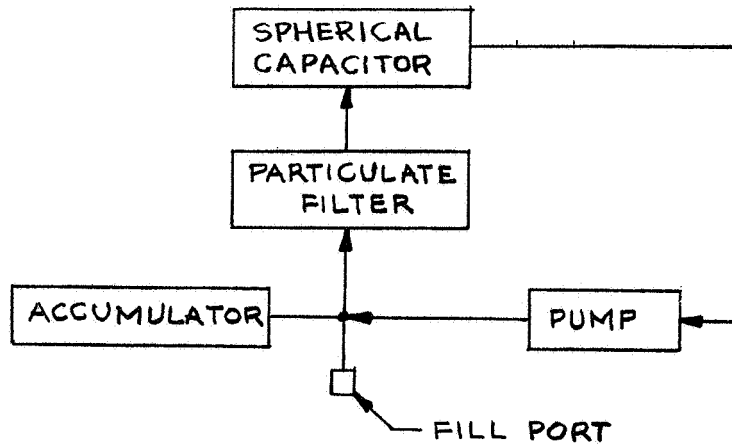


FIGURE 3 FILTRATION AND CIRCULATION LOOP
BLOCK DIAGRAM

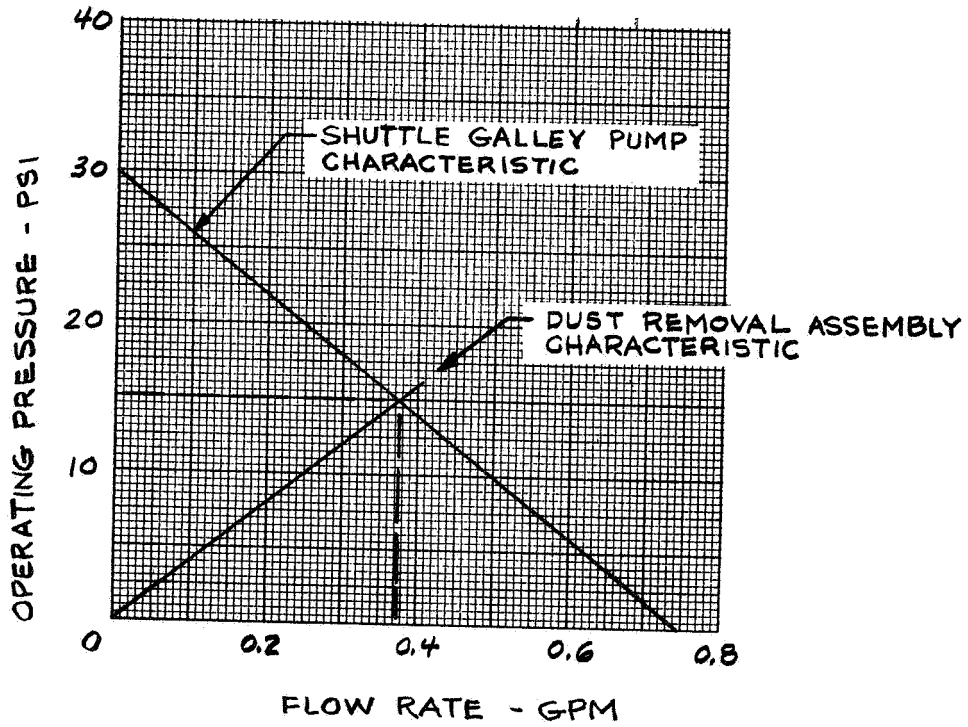


FIGURE 4 DIELECTRIC FLUID FLOW RATE USING
SHUTTLE GALLEY PUMP ASSEMBLY

TABLE 1 DIELECTRIC FLUID VOLUME

ITEM	EST. FLUID VOLUME
CAPACITOR*	224 cm ³
PLUMBING	14
PUMP	5
ACCUMULATOR	17
FILTER	<u>5</u>
TOTAL	275 cm ³

*From N Pole to 10°S latitude

TABLE 2 PRESSURE BUDGET

ITEM	ESTIMATED PRESSURE LOSS*		
	0.1 gpm	0.2 gpm	0.3 gpm
FILTER	3.57 psi	7.14 psi	10.71 psi
CAPACITOR	0.01	0.06	0.13
PLUMBING	<u>0.12</u>	<u>0.77</u>	<u>0.82</u>
TOTAL	3.70 psi	7.97 psi	11.55 psi

*Assuming fluid viscosity = 1.0 centipoise.

Balston standard filter tube, type AAQ, 1/2 inch diameter by 2 1/4 inch long is rated at 99.9% efficiency for removing particles 0.5 micron and larger. Filter material is flouorocarbon bonded glass fibers, See Section 5.4. Sintered teflon (See Section 5.3), and sintered or woven stainless steel fiber media are also available as alternate candidate filter media.

Figure 5 shows typical construction details for the filter assembly.

3.4 Accumulator

The function of the accumulator is to compensate for the change in dielectric fluid volume due to changes in fluid temperature occuring during AGCE activity. As shown in Table 3, the maximum temperature range occurs during transportation conditions. Thus, assuming an internal dielectric fluid volume of 275 cm³ and assuming a coefficient of expansion equivalent to that for DMSO (0.00088%/°C), the accumulator must accomodate a thermal expansion of 0.18 cm³. Assuming an accumulator design as shown in Figure 6, variation in system operating pressure due to this expansion will be a minimal +4.1 psi.

3.5 Weight/Power

Table 4 shows an estimated weight breakdown for the dust removal capability. Estimated total weight is 1.7 Kg. Power is estimated at 35 watts. Neither would appear to have a significant impact.

3.6 Materials Compatibility

No materials compatibility problem is anticipated. Expected materials in direct contact with the dielectric fluid will probably be stainless steel, fluorocarbons and glass (See Table 5), all very tolerant of most fluids.

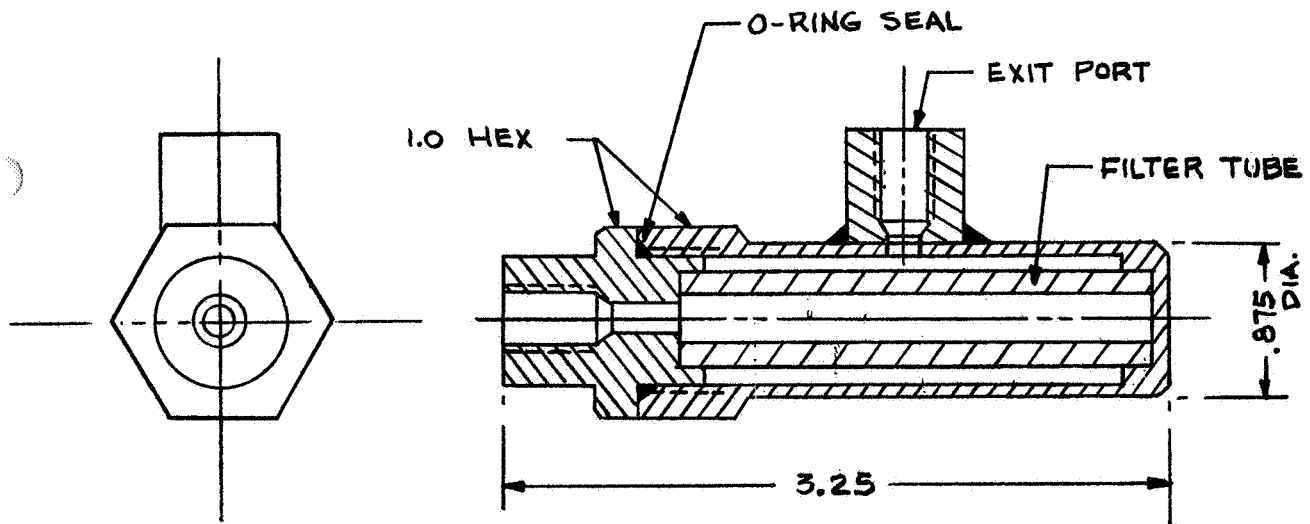


FIGURE 5 FILTER ASSEMBLY CONSTRUCTION DETAILS (NOT TO SCALE, MOUNTING BRACKET NOT SHOWN)

ORIGINAL PAGE IS
OF POOR QUALITY

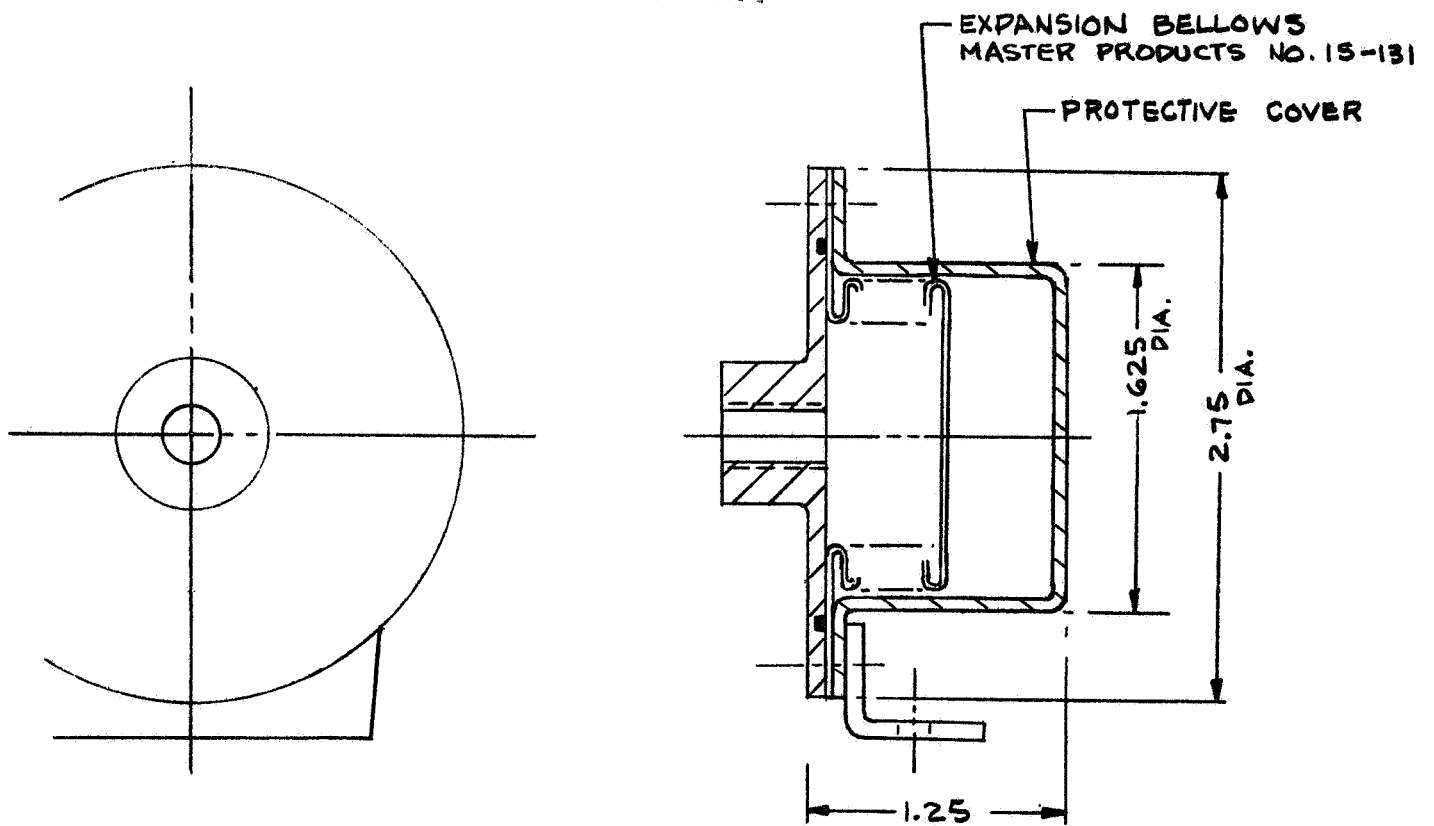


FIGURE 6 ACCUMULATOR CONSTRUCTION DETAILS (NOT TO SCALE)

TABLE 3 ESTIMATED OPERATING/NON-OPERATING TEMPERATURE
EXTREMES FOR AGCE DIELECTRIC FLUID

Condition	Temperature Extremes
Non-Operating	
launch site environment integration*	18 to 25°C
transportation*	-10 to 55°C
factory environment	15 to 25°C
Operating	15 to 35°C

*From SLP/2104, Section 5.0

TABLE 4 WEIGHT BREAKDOWN

Component	Estimated Weight
dielectric fluid*	0.04 kg
filter	0.16
pump	0.68
accumulator	0.19
plumbing	<u>0.43</u>
Sub-total	1.50 kg
Growth Contingency	<u>0.21</u>
TOTAL	1.71 kg

*Extra fluid required to accomodate dust removal capability hardware

TABLE 5 COMPONENT MATERIAL USAGE

DUST REMOVAL HARDWARE ELEMENT	MATERIAL*
Filter	Glass fibers (fluorocarbon binder), Stainless steel
Accumulator	Stainless Steel
Pump	Stainless Steel, teflon
Plumbing	Stainless Steel (fluorocarbon seals)

*In contact with dielectric fluid

3.7 Leakage

Leakage of dielectric fluid from the dust removal hardware is not expected to be a problem. The suggested pump assembly is a magnetically coupled type, thus eliminating a rotating pump seal. O-seal tube fittings, tube to male straight thread, such as supplied by Combination Pump Valve Company, Philadelphia, Pa., are reliably leak tight and reusable, see Section 5.5

4.0 CONCLUSIONS/RECOMMENDATIONS

Incorporating a hardware capability for removal of particulate contaminants from the dielectric fluid after assembly of the AGCE system appears feasible. The addition has a minor impact on the design of system and the spherical capacitor assembly in particular. Suitable hardware elements are available; weight and power impact on the system are minor. Materials compatibility with the dielectric fluid should not be a problem but must be re-evaluated against the dielectric fluid finally selected.

Operation of the dust removal capability during AGCE final assembly, acceptance test, pre-launch checkout and on-orbit operations is recommended as follows:

a) Final Assembly

After vacuum filling the system with precleaned and deaerated dielectric fluid, operate the dust removal pump, with electric field applied at full voltage, for TBD minutes (actual time based on laboratory development tests).

b) Acceptance Test

As part of acceptance test activity, operate dust removal pump, with electric field applied, for TBD minutes.

c) Pre-launch checkout

As part of pre-launch checkout testing, operate dust removal pump, with electric field applied, for TBD minutes.

d) On-Orbit

At on-orbit AGCE initialization, operate dust removal pump, with electric field applied for TBD minutes. Also as a final precautionary measure, the dust removal pump could be operated for a short period between each individual AGCE experiment sequency.

Note that the purge time can be relatively short, e.g. a 50 volume purge can be accomplished within 10 minutes. Even with a poor flush flow pattern in the spherical capacitor fluid volume, by the time on-orbit testing is started, the fluid should be "squeaky" clean.

5.0 APPENDIX

The following are attached hereto as supplemental information.

- 5.1 PIR 1254-AGCE-005, "Dust Removal Design Requirements".
- 5.2 Porex Porous Plastics Bulletin.
- 5.3 Pump outline dwg. from GE specification 47A231867.
- 5.4 Balston, Inc. Microfibre Filter tube bulletin.
- 5.5 Combination Pump Valve Company Bulletin.
- 5.6 Master Products Metal Bellows Bulletin.

GENERAL ELECTRIC

SPACE DIVISION
PHILADELPHIA

*CLASS. LTR. U	OPERATION 1254	PROGRAM AGCE	SEQUENCE NO. 005	REV. LTR.
-------------------	-------------------	-----------------	---------------------	-----------

PIR NO.

*USE "C" FOR CLASSIFIED AND "U" FOR UNCLASSIFIED

PROGRAM INFORMATION REQUEST / RELEASE

FROM G. L. FOGAL <i>GLF</i>	TO DISTRIBUTION
--------------------------------	--------------------

DATE SENT 1/26/81	DATE INFO. REQUIRED	PROJECT AND REQ. NO.	REFERENCE DIR. NO.
----------------------	---------------------	----------------------	--------------------

SUBJECT
TASK 3 - DUST REMOVAL DESIGN REQUIREMENTS

INFORMATION REQUESTED/RELEASED

The attached AGCE dust removal capability key design requirements have been generated as the first step in assessing the feasibility of incorporating into the AGCE a hardware capability for programmed circulation and filtration of the dielectric fluid.

**ORIGINAL PAGE IS
OF POOR QUALITY**

cc: L. Eaton
S. Neste
G. Fogal

PAGE NO. <u>1</u> OF <u>3</u>	RETENTION REQUIREMENTS	
	COPIES FOR	MASTERS F
<input type="checkbox"/> 1 MO.	<input type="checkbox"/> 3 MOS.	
<input type="checkbox"/> 3 MOS.	<input type="checkbox"/> 6 MOS.	
<input type="checkbox"/> 6 MOS.	<input type="checkbox"/> 12 MOS.	
<input type="checkbox"/> MOS.	<input type="checkbox"/> MOS.	
<input type="checkbox"/>	<input type="checkbox"/> DO NOT DESTROY	

TASK 3 - DUST REMOVAL DESIGN REQUIREMENTS

1.0 SCOPE

The dust removal design requirements are intended as guidelines to be used in the assessment of the feasibility of incorporating a hardware capability into the AGCE for programmed circulation and filtration of the dielectric fluid.

2.0 GENERAL

The dust removal design requirements are based on GFFC experience, Spacelab Payloads Accomodation Handbook SLP/2104 and a current estimate of the AGCE flight design.

3.0 PERFORMANCE REQUIREMENTS

3.1 General

Provide programmed circulation and filtration between experimental sequence as a means of controlling particulate concentration in the dielectric fluid.

3.2 Particulate Concentration

Maintain particulate concentration in the dielectric fluid to less than 10 particles/cm³ for particles exceeding 0.5 micron in diameter with the maximum particle size not to exceed 1.0 micron in diameter.

4.0 INTERFACES

4.1 Mechanical

The dust removal hardware shall be compatible with a 5.0 ± 1.0 cm inner sphere radius and a 1.0 cm spacing, for the dielectric fluid, between the inner and outer spheres.

4.2 Electrical

The dust removal hardware shall operate on Spacelab DC power supplied via the AGCE controller in accordance with stored timeline commands.

4.3 Thermal

The thermal load generated by the dust removal hardware shall be dissipated to the rotating platform.

4.4 Dielectric Fluid

The dust removal hardware shall be compatible with a dielectric fluid of specific gravity range of 1.0 to 1.5 and a viscosity range of 0.8 to 2.0 centipoise.

5.0 FLIGHT OPERATIONS

The dust removal hardware shall be operated on a preprogrammed basis between experimental sequences. Each filtration operational period shall not exceed 5.0 minutes (shorter time desired).

6.0 SAFETY

The dust removal hardware shall be located within the confines of the gaseous nitrogen filled outer sealed enclosure.

7.0 LIFE

The dust removal hardware shall have a minimum useful operating life of 120 hours (ground test plus mission operations).

Approved by: 
AGCE Program Manager

/amb

ORIGINAL PAGE IS
OF POOR QUALITY

POREX

PTFE

Porous Teflon Membrane

POREX PTFE

A porous Teflon* membrane of unique properties having a wide range of applications in industry and medicine.

GENERAL CHARACTERISTICS

- Pliable white sheet of varying degrees of softness.
- Lightweight. Specific gravity from 0.2 to 0.8; approximately 0.4 oz per sq. ft.
- Chemically inert.
- Heat stable. Withstands temperatures from -400° to 550° for extended periods.
- Excellent dielectric.
- Highly hydrophobic.
- Permanently fire retardent.
- Low co-efficient of friction.
- Heat sealable.

STANDARD SIZES

Porex PTFE membrane No. P2500 is available in 12" strips up to 100' long. Standard dimensions for all other membranes are 12" x 48."

INDUSTRIAL AND SCIENTIFIC APPLICATIONS

- Manufacturing chemicals requiring inert material in hostile environment.
- Chemical processing
- Filtering concentrated acids, bases, solvents, and hazardous chemicals.
- Filter media for laboratory apparatus.
- Cable wrap and wire insulation.
- Liquid and gas chromatography.
- Fuel cells.
- Battery separators.
- Catalyst matrices.
- High temperature air sampling.
- Vacuum dust bag for spacecraft.
- Protective clothing.
- Liquid gas separation.
- Aeration for bubbling or air agitation.
- Insulation and cushioning in cryogenic applications.
- Oxygenators.
- Bandages.
- Air venting.
- Any medical sheet application where strong solutions or autoclaving is necessary.

Porex PTFE material is also being manufactured with various fillers to obtain electrical conductivity, wettability, and other specific traits. Possibilities for its use are constantly developing, not only in new areas, but in the re-

placement of other materials which may cost more, have a shorter life, or perform less satisfactorily. Glasrock has worked in numerous areas of application and may have the answer you need for your problem.



GLASROCK PRODUCTS, INC.
PLASTICS GROUP

Fairburn, Georgia 30213 • 404-964-1421
TWX 810-766-1505

STANDARD MEMBRANES WITH FILTER DATA

MATERIAL	THICKNESS (Mils)	PORE SIZE (μm)	PORE VOLUME (%)	AIR FLOW		WATER FLOW ⁽³⁾ (ml)	METHANOL BUBBLE POINT ⁽⁴⁾		WATER INITIATION PRESSURE ⁽⁵⁾	
				Secs ⁽¹⁾	Secs ⁽²⁾		(psi)	(kg/cm ²)	(psi)	(1c/cm ²)
P 8000	10	8	80	29	45	275	0.75	0.052	2.0	0.14
P 1200	15	12	90	16	25	430	0.7	0.049	1.44	0.10
P 2500	15	25	85	8	12	1,100	0.33	0.023	1.0	0.07
P 1000	25	10	80	83	125	90	0.60	0.042	1.4	0.098
P 800	10	.8	70	74 ⁽⁶⁾	11.5 ⁽⁷⁾	1.15 ⁽⁸⁾	8.36	0.587	23.0	1.60

Notes:

- (1) Time required for 100 milliliters of air to flow through 1 sq. cm. filter area at 20°C with a differential pressure of 3.1 cm. water (0.043 psi).
- (2) Using a Gurley Densometer, time required for 100 milliliters of air to flow through a 0.1 sq. in. orifice with a 5 oz. cylinder. Pressure differential of 3.1 cm water (0.043 psi).
- (3) Water flow rates are milliliters per min. per cm² with a differential pressure of 52 cm Hg (10 psi).
- (4) Pressure required to force air through a methanol-wet membrane.
- (5) Pressure required to force water through the membrane.
- (6) Time required for 10 milliliters of air to pass through 1 sq. cm filter area at 20°C with a differential pressure of 31 cm water (0.44 psi).
- (7) Using a High Pressure Gurley Densometer, time required for 10 milliliters of air to flow through 1 sq. in. orifice with a differential pressure of 31 cm water (0.44 psi).
- (8) Filter was initially wetted with methanol prior to water flow.

**ORIGINAL PAGE IS
OF POOR QUALITY**

SIZE
A

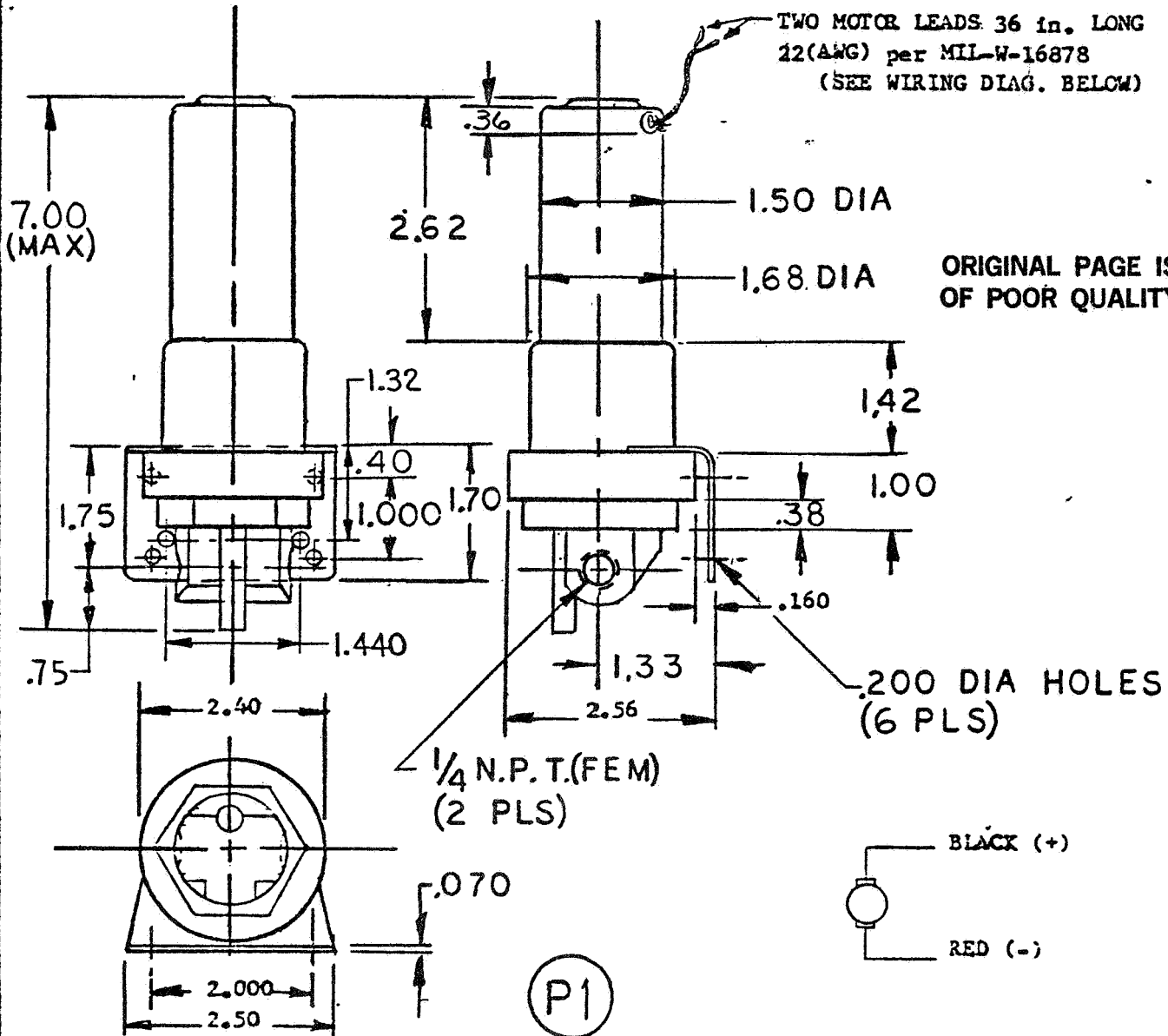
47A231867

SHEET
6

REV
A

REVISIONS

LTR	DESCRIPTION	DATE	APPROVE



APPROVED SOURCE OF SUPPLY

MFG'R- MICROPUMP CORP. PART NO. FSCM
CONCORD, CALIF. 5410-03 32042

GE PART NO. 47A231867 P1

UNLESS OTHERWISE SPECIFIED
DIMENSIONS ARE IN INCHES.
TOLERANCES ON:

FRACTIONS DECIMALS ANGLES
+ .XX +.06 +
XXX .010 ✓
ALL SURFACES

MATL-

SIGNATURES		DAY	MO	YR
DRAWN	<i>E. Pech</i>	29	5	79
CHECKED				
ISSUED				
ENGRG				
MFG				
MATLS				

GENERAL ELECTRIC
DEPT LOC

PUMP/MOTOR ASSEMBLY (UMS)

SIZE CODE IDENT NO. 47A231867
A 23991

SCALE SHEET 6 OF 6

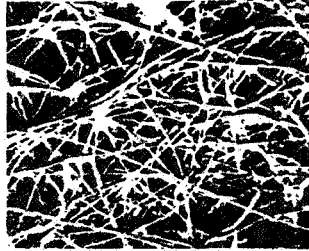
FN-901.F (9-64) REV PRINTED IN U.S.A.

UMS-2
DIST TO

BALSTON

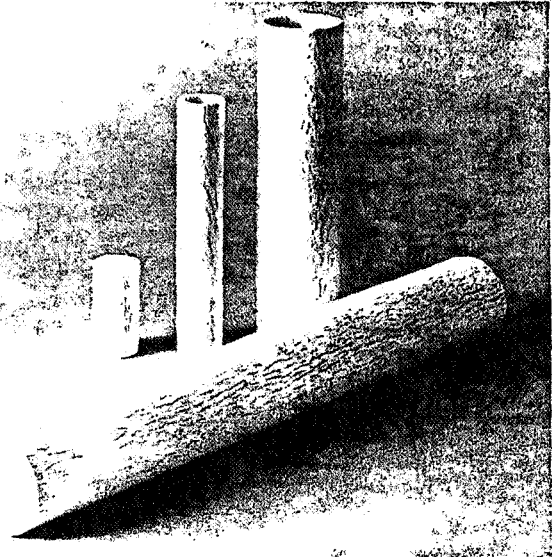
ORIGINAL PAGE IS
OF POOR QUALITY

Microfibre[®] Filter Tubes



*Unique microfibre
filter medium of
glass microfibers
bonded with resin.*

*Balston Microfibre Filter
Tubes are available
in a variety of
diameters and lengths.*



GENERAL PROPERTIES (Detailed Properties are given on Pages 2, 3 and 4)

Balston[®] Microfibre Filter Tubes are high efficiency disposable cartridge filters. Each Microfibre Filter Tube is composed of borosilicate glass microfibers, bonded into a cylinder with 1/8-inch thick walls. Fluorocarbon resin or other binders provide resistance to the most severe corrosion and temperature conditions. Used for either liquid or gas filtrations, Balston Microfibre Filters provide an unusual combination of fine filtration and high flow rate:

- *Retention Efficiencies* – Five grades of filters: in *Liquid Filtration* from 25 micron to 0.3 micron retention; in *Gas Filtration* from 90% to 99.9999+% of 0.6 micron particles (the two finer grades are gas-sterilizing filters).
- *Flow Rates* – One 2-inch diameter by 9-inch long Microfibre Filter Tube can filter up to 38 GPM of water, or up to 885 SCFM of air.

Other advantages of Microfibre Filter Tubes include:

- Temperature resistance to 1000 F in dry gas or up to 310 F in steam (60 psig steam.)

- Excellent resistance to virtually all chemicals except hydrofluoric acid.
- They are unaffected by water or oil, and will remove oil and water droplets from air with the same efficiency as solid contaminants.

Microfibre Filter Tubes are self-gasketing; they are sealed into place simply by compression against any flat surface. No resilient gaskets or end caps are required for the filter cartridges. The Microfibre Filter Tubes are self-supporting in applications in which the pressure drop across the filter is moderate, including most gas filtrations. When a high pressure drop is anticipated, a permanent support core is used. When the filter tube is changed, only the filter medium and none of the hardware is replaced. Therefore, the Microfibre Filter Tubes are much more economical than any other cartridge filter with comparable performance, and their simple design results in a remarkably rugged and convenient high efficiency filter system.

APPLICATIONS

Gas Filtration

- Removal of dirt, oil, and water from plant air supplies, at flow rates to 45,000 SCFM. (A-1)*
- Essentially complete coalescing of oil from air for critical applications, such as instrument air, air to fluidic control systems, breathing air (A-1)
- Removal of suspended solids and liquid droplets from gas samples to analyzers, such as automobile emission analyzers or stack gas analyzers. (A-2)
- Sterilization of air and other gases – and the filter tubes may be repeatedly steam-sterilized. (T1-63)
- Filtration of vacuum pump exhaust to remove oil mist, smoke, haze. (A-3)
- Removal from room air of oil mist being generated by spray lubricators or flood coolants on metal fabricating machines (A-3)
- Filtration of steam to autoclaves. (A-5)

*The numbers in parentheses refer to a detailed Balston Technical Information Bulletin on the application.

Liquid Filtration

- Protection of reverse osmosis and dialysis membranes and membrane filters. (A-4)*
- Final filtration of 18 meg-ohm deionized water (A-4)
- Clarification of solvents and corrosive solutions used in chemical processes, plating, manufacture of electronic components.
- Recovery of trace quantities of precious metals and other valuable solids from liquids.
- Final filtration of high performance hydraulic fluids, lubricants, and fuels.
- High efficiency separation of small quantities of water from organic liquids, or small quantities of organic liquids from water
- Removal of suspended solids and immiscible liquids from liquid samples to analyzers, such as boiler feedwater analyzers or effluent analyzers. (A-2)
- Recovery of bacteria or viruses from water samples for quantitative analysis. (A-2)

FILTRATION EFFICIENCIES

Microfibre Filter Tubes are manufactured in five retention efficiencies. Since flow resistance increases with increasing retention efficiency, it is a good practice to specify the coarsest filter which will satisfy the requirements, rather than overspecify to be "safe." Detailed recommendations on filter tube selection for specific applications may be

obtained from the Balston Technical Information sheets or by contacting Balston Technical Representatives.

A given grade of Microfibre Filter Tube is more efficient in gas (or air) filtration than in liquid filtration. Therefore, each grade of filter tube has two retention ratings, one for gas filtration and one for liquid filtration.

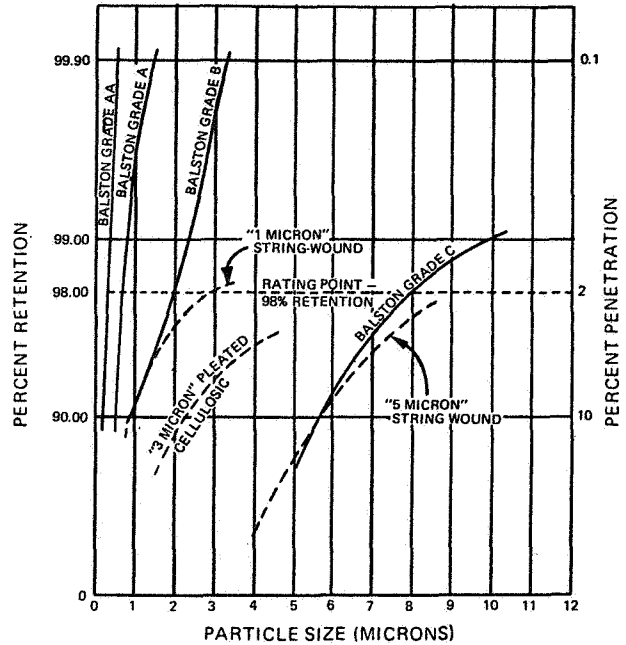
LIQUID FILTRATION

The retention characteristics of Balston Microfibre Filters in liquids are shown on the chart, which plots percent retention efficiency for a given size particle versus particle size. For example, Balston Grade B Filters will retain about 90% of 1 micron particles, 98% of 2 micron particles, and 99.9% of 3.3 micron particles. For liquid filtration, Balston Filters are rated at the particle size corresponding to 98% retention, and therefore the rating for Grade B is 2 microns.

When comparing retention ratings of filters of different manufacturers, it is important to note the efficiency at which the filter is rated. Many manufacturers rate filters at their 90% retention efficiency particle size. If Grade B were rated at its 90% efficiency point, it would be a "1 micron" filter. In fact, as shown by the curve, Grade B, rated at 2 microns, is a finer filter than another type of cartridge filter which is rated by the manufacturer at "1 micron." Since there is no accepted industry-wide standard rating method, comparison of published ratings between different manufacturers can be misleading. The safest method for selecting the proper filter tube grade is to test under actual use conditions. Balston Representatives will be happy to supply sample filter tubes for test.

Balston Filters, particularly Grades A and AA, have relatively sharp particle cut-off characteristics compared with other types of cartridge filters. The Balston Grade AA Filter, although a depth filter, approaches the retention characteristics of an "absolute" filter and may be used for bacteria filtration in many applications.

RETENTION VS. PARTICLE SIZE (IN WATER)



(NOTE: See page 4 for Microfibre Filter Tube Retention Efficiency Ratings.)

GAS FILTRATION

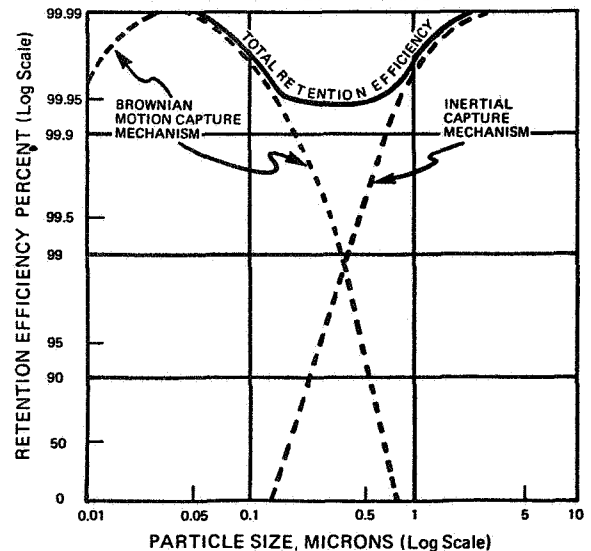
In gas filtration, as in liquid filtration, a particle is captured by a Balston Filter when the particle collides with a fiber. The forces holding the particle to the fiber are intermolecular (Van der Waals) forces and are essentially independent of the particle composition or of external conditions, such as relative humidity or temperature. The filter is designed to maximize the chance for a particle to collide with a fiber. The exact sizes or shapes of the spaces between fibers is not significant, and therefore it is not meaningful to characterize the filter by "pore size."

In liquid filtration, particle capture is entirely by the inertial or interception mechanisms, which are less effective as the contaminant particle size decreases. In contrast with liquid filtration, gas filtration also benefits from the Brownian motion capture mechanism, which is most effective for particles in the 0.05 to 0.1 micron range. As shown on the chart, these mechanisms for particle capture in gases result in a minimum retention efficiency for 0.3 to 0.6 micron particles, with higher retention efficiencies for both larger and smaller particles.

Standard test methods for high efficiency filters (DOP Test and Sodium Flame Test) are designed to rate filters under the most severe conditions—capture of particles in the 0.3 to 0.6 micron range. The ratings for the Balston Microfibre Filters for gas filtration are shown on the right.

RETENTION EFFICIENCY VS. PARTICLE SIZE FOR HIGH EFFICIENCY COALESCING FILTER

NOTE: GENERALIZED REPRESENTATION



The filters will be more efficient than the rating for both larger and smaller particles. Grades A and AA are sterile filters for gases.

Filter Tube	Gas Filtration Efficiency (Retention of 0.6 micron particles)
Grades D & DX	90%
Grades C & CX	95%
Grades B & BX	99.99%
Grade A	99.9999+%
Grade AA	99.9999+%

DIFFERENT TYPES OF MICROFIBRE FILTER TUBES

Balston Microfibre Filter Tubes are composed of borosilicate glass microfibers with a resinous binder. Four different binder types are available:

BINDER RESIN	TUBE TYPE DESIGNATION
Epoxy	No Suffix letter
Fluorocarbon	Q-Type
High temperature organic	L-Type
Inorganic	H-Type

The Q-Type tubes are an important recent Balston development. They are resistant to: essentially all solvents (including fluorinated solvents), all acids except hydrofluoric acid, sodium hydroxide and potassium hydroxide up to about 45% concentration, steam to 60 psig, liquid or gaseous ammonia, liquid or gaseous chlorine, liquid or gaseous ethylene oxide, hydrogen peroxide, and virtually any other chemical that does not attack borosilicate glass. In addition, the Q-Type tubes have higher burst strengths than the other types of Microfibre Filter Tubes (please refer to detailed data on next page) and also have better field handling characteristics. Q-Type filter tubes are now recommended for all compressed air and gas filtrations below 300F, all sample filtrations below 300F, and all liquid filtrations.

For air or gas filtrations at temperatures above 300F, L-Type tubes are recommended for the 300F to 600F range, and H-Type tubes are recommended for the 600F to 1000F range. In particular, H-Type tubes are recommended for high temperature stack gas sample filtration.

The epoxy-binder tubes, which are less expensive than the other types of filter tubes, should be used in all existing applications in which they have proven satisfactory. In addition, epoxy-binder tubes are recommended for new applications in which the superior physical properties of the higher cost Q-Type tubes are not required; for example, in removing visible smoke from air at atmospheric pressure.

Special-design filter tubes are continually being developed for specific applications. Examples include a two-stage filter tube, designated -X, for coalescing and removing large quantities of suspended liquids from compressed air; and filter tubes with integral prefilters for certain applications in which high solids loadings are expected (such as filtration of welding fumes). Detailed information and recommendations on the special-design filter tubes may be found in the literature pack for each specific application.

BALSTON FILTER HOUSINGS

Balston Filter Housings are designed to take advantage of the unique properties of Balston Microfibre Filter Tubes, with minimum field maintenance.

Housings are available for liquid or gas filtrations in pressure ranges to 5000 psig, in a wide range of sizes, from single cartridge miniature units to multiple cartridge, heavy-duty filters, and in a variety of materials, including: anodized aluminum, stainless steel, polycarbonate, polypropylene, Teflon, Pyrex glass, carbon steel and epoxy-coated steel.

Flow capacities range from a few gallons per hour to hundreds of gallons per minute and thousands of CFM.

Balston also offers selected accessories, including pressure regulators and gages, adaptors for using Balston Microfibre Filter Tubes in non-Balston housings, and a full array of manual and automatic drain valves.

Please refer to the section below for instructions on obtaining detailed information on Balston Filter Housings for each application area of interest.

USE OF BALSTON MICROFIBRE FILTER TUBES IN FILTER HOUSINGS OF OTHER MANUFACTURERS

With the use of Balston 10Z33 or 20Z33 support cores, Balston Filter Tubes may be installed in almost all cartridge filter housings designed for nominal 10-inch or 20-inch-long filter tubes, without any modification to the housing.

Balston supplies special filter tubes to other filter manu-

facturers for incorporation into filter cartridges of their own design. Balston will provide, on a confidential basis, any technical assistance requested to ensure that the particle retention and flow properties of the Microfibre Filter Tubes are efficiently utilized in the new designs. Please contact the Balston office for information.

PATENTS

Microfibre Filter Tubes are the exclusive development of Balston, Inc., (Lexington, Mass.) and Balston, Ltd. (Maid-

stone, England), and are protected by numerous patents issued in the U.S., Canada, U.K., and other countries.

WOULD YOU LIKE ADDITIONAL INFORMATION?

Balston technical information is organized in Application Packs, each of which contains: complete product data on the filter housings used in that application, flow rate charts, technical information on selection of the proper filter system, and prices. Please request the appropriate Application Pack for each filter application area of interest:

- Pack #1 - Coalescing filters for compressed air and other gases
- Pack #2 - Filtration of samples to analyzers
- Pack #3 - Oil mist removal from low pressure air
- Pack #4 - High efficiency filtration of liquids
- Pack #5 - Filtration of steam to autoclaves

Complete catalogs, which combine the information of the five Application Packs, are also available on request.

Balston publishes "Filter Forum," a quarterly technical newsletter which describes solutions to specific filtration

requirements and also discusses in detail filtration topics of general interest, such as removal of oil from compressed air. To obtain "Filter Forum" and Balston new product information as it is issued, please request that your name be placed on our mailing list. Your local Balston Technical Representative can provide copies of all the technical information listed above and can arrange for your name to be placed on our mailing list.

Your Balston Technical Representative can give you a working demonstration in your office of the Balston filter in an actual test in comparison with your present filter or any other filter. He is factory-trained to make specific recommendations on your filter requirements, and he maintains a complete local stock of Balston filter housings and Microfibre Filter Tubes. Please contact our office for the name of your nearest Technical Representative.

PROPERTIES OF BALSTON MICROFIBRE FILTER TUBES

COMPOSITION AND PROPERTIES

(Please refer to p. 3 for recommended applications of the different types of filter tubes)

Fiber in all Types		Borosilicate Glass Microfibers	
Tube Type	Binder Resin Composition	Max. Temp. in Dry Gas	Max. Steam Pressure
No Suffix	Epoxy	400 F	20 psig
Q- & X-Type	Fluorocarbon	300 F	60 psig
L-Type	High Temperature Organix	600 F	40 psig
H-Type	Inorganic	1000 F	Not Recommended

Chemical and Solvent Resistance, Q-Type and X-Type:

Excellent - All solvents, all oxidizing and non-oxidizing acids except hydrofluoric, sodium hydroxide and potassium hydroxide to about 45% concentration, liquid or gaseous ammonia, liquid and gaseous chlorine, liquid or gaseous ethylene oxide.

Not Recommended - Concentrated fluoride salt solutions, hydrofluoric acid, sodium hydroxide and potassium hydroxide above about 50% concentration.

Chemical and Solvent Resistance, All Types Except Q- & X-Type:

	Epoxy	L-Type	H-Type
Cold Water	Good	Excellent	Fair
Hot Water	Fair-Poor	Good	Poor
Non-oxidizing acids	Excellent	Excellent	Excellent
Oxidizing acids	Poor	Good	Excellent
Dilute caustic (below 1%)	Excellent	Fair	Fair
Moderate Caustic (1-20%)	Good	Poor	Poor
Concentrated Caustic (above 20%)	Fair	Poor	Poor
Ketones	Good-Fair	Poor	Excellent
Chlorinated Solvents	Fair-Poor	Poor	Excellent
Aromatic hydrocarbons	Excellent	Good	Excellent
Other hydrocarbons	Excellent	Good	Excellent
Hydrofluoric acid and fluorides	Poor	Poor	Poor

STANDARD SIZES OF BALSTON FILTER TUBES

Inside Diameter and Length	Order No.
½" x 1¼"	050-05
½" x 2¼"	050-11
1" x 2½"	100-12
1" x 7"	100-25
1½" x 6"	150-19
2" x 3½"	200-16
2" x 9"	200-35
2" x 18¼"	200-80

FILTER TUBE ORDERING INFORMATION

When ordering Microfibre Filter Tubes, please specify:

Size - The Order No. code for standard sizes is shown above. For example, 1" diameter x 2½" long is code 100-12.

Retention Efficiency Grade - For example, Grade A.

Type of Filter Tube - If the epoxy binder is wanted, no type designation is used. If the Q, L, or H-Type is wanted, the appropriate letter should follow the grade designation.

STOCKING AND DELIVERY INFORMATION

Standard Balston Filter Tubes and filter housings are stocked at more than thirty locations in the U.S. and Canada by Balston Technical Representatives. Please request the name of the nearest stocking Representative. In addition, all Microfibre Filter Tubes and Balston filter housings are stocked in Andover, Massachusetts and Mississauga, Ontario. Off-the-shelf delivery usually can be made

FILTRATION EFFICIENCY

Filter Tube	Gas Filtration Efficiency (Retention of 0.6 micron particle)	Liquid Filtration Efficiency (98% retention particle size)
Grades D & DX	90.0%	25 microns
Grades C & CX	95%	8 microns
Grades B & BX	99.99%	2 microns
Grade A	99.9999+%	0.9 micron
Grade AA	99.9999+%	0.3 micron

FLOW RATES FOR 2" x 9" FILTER TUBE

	Filter Tube Grade			
	C	B	A	AA
Air Flow, SCFM at 2 psi drop:				
100 psig line pressure	885	149	67	17.2
50 psig	499	84	38	9.7
0 psig	113	19	9	2.2
Water Flow, gal. per min. at 5 psi drop	38.0	6.9	4.3	2.1

NOTES:

- Flow rates are for the filter tubes only and do not take into account pressure drop of the housing. Please refer to the product data sheet for flow rate in a particular Balston housing. Flow rates for Grade D are not included because they are primarily determined by the housing characteristics.
- Pressure drop is proportional to flow rate. For example, if the flow rate through 2" x 9" Grade B at 50 psig is 21 SCFM, rather than 84 SCFM as shown on the table, the pressure drop will be 21/84 x 2 psi = 0.5 psi.
- In liquid filtration, pressure drop for liquids other than water will not be proportional to viscosity.

MAXIMUM RECOMMENDED PRESSURE DIFFERENTIALS

Tube Diameter	Q-TYPE TUBE		OTHER TUBE TYPES	
	Inside-to-Outside Flow	Outside-to-Inside Flow	Inside-to-Outside Flow	Outside-to-Inside Flow
½"	80 psi	20 psi	60 psi	20 psig
¾"	80	13	40	13
1"	80	10	25	10
1½"	80	7	20	7
2"	80	5	15	5

NOTES:

- Maximum recommended pressure differential with support core, outside-to-inside flow, all diameters, except ½", = 70 psi, for ½" = 150 psi.
- For Grades DX, CX and BX, maximum recommended pressure differential for inside-to-outside flow is 100 psi.

- EXAMPLE: The designation for 1" x 2½", Grade A, Q-Type, is 100-12-AQ.
- EXAMPLE: The designation for 2" x 9", Grade B, epoxy binder is 200-35-B.

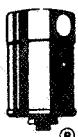
Standard packing is ten tubes per box. Please order complete boxes whenever possible. For less than one box quantities, an additional charge of 40% is made to the tube price.

A range of special sizes can be supplied on request. Please contact Balston, Inc., for detailed information.

on any catalog item.

Balston manufactures Microfibre Filter Tubes at plants in Andover, Massachusetts, and Maidstone, England. For price and delivery information in locations outside North America and South America, please contact: Balston, Ltd., Springfield Mill, Maidstone, England.

BALSTON® Filter Products



BALSTON, INC.
P.O. Box C, 703 Massachusetts Ave.
Lexington, Mass. 02173
Tel. 617-861-7240 • 862-7455
Telex: 92-3481

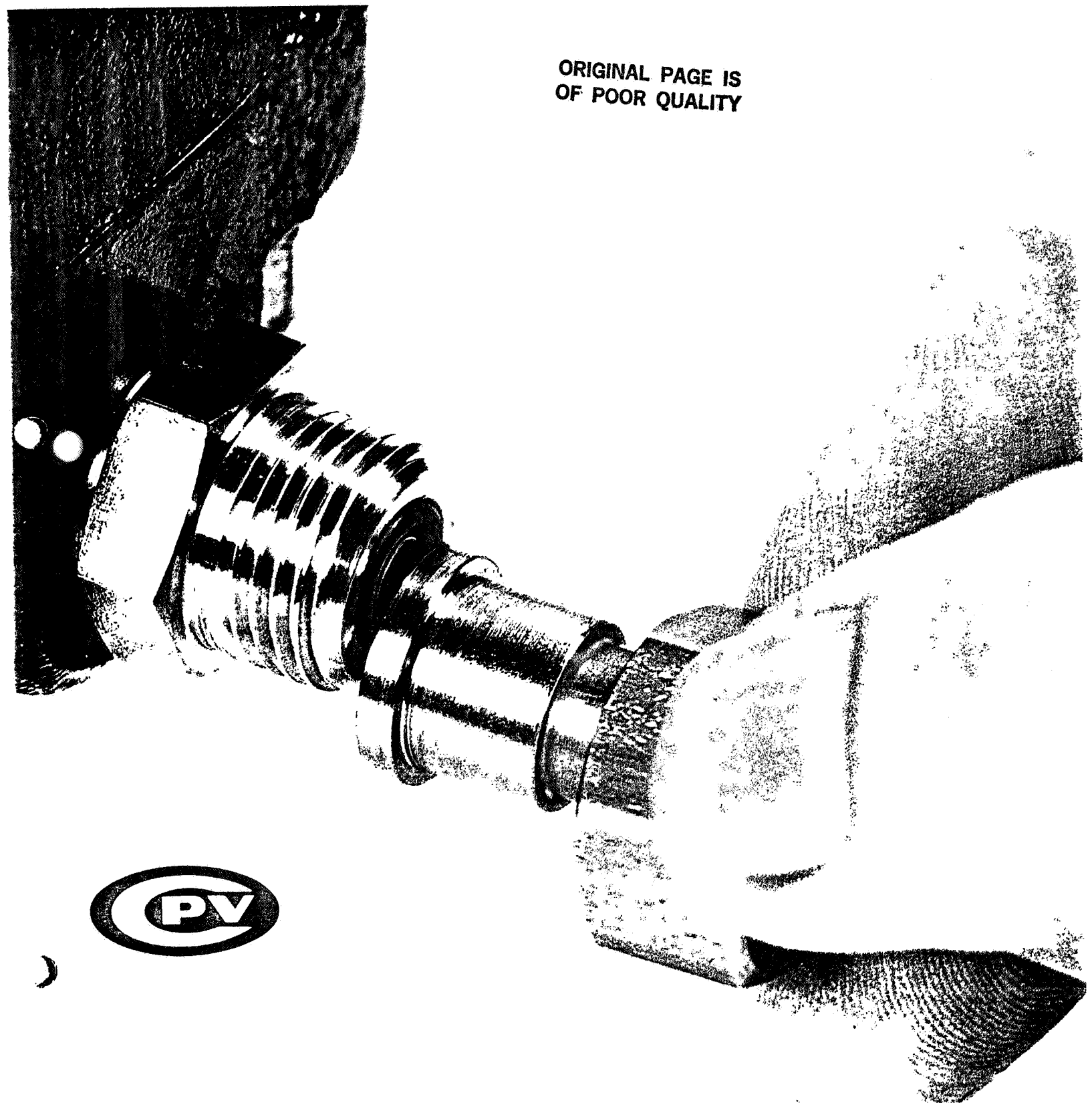
BALSTON CANADA LTD.
1938 Mattawa Avenue
Mississauga, Ontario L4X 1K1
Tel. 416-272-1516

ORIGINAL PAGE IS
OF POOR QUALITY

Bulletin 101-H
©Balston, Inc., 1975, 1977, 1979
Printed in U.S.A.

MARK VIII O-SEAL Tube Fittings

ORIGINAL PAGE IS
OF POOR QUALITY



the leakproof, fully separable, heat-sealed tube fittings that resist vibration and never need retightening

CPV has developed the closest thing to the perfect line of tube fittings yet: Mark VIII O-SEAL. These unique components combine the most desirable, most important characteristics of any tube fittings: **totally leakproof reliability** in liquid or gas service from vacuum to 3000 psi . **maximum resistance to vibration** (they won't loosen even with extreme system vibration or line pressure fluctuations) . **no maintenance** (they never have to be retightened) . **unlimited break-remake flexibility** (you can break and remake connections at will and slip components in and out of the system without springing or cutting the line) . and **complete design freedom** (wide choice of fittings to connect components to any system).

The Big Difference

Unlike Mark VIII O-SEAL, ordinary tube fittings—compression, flareless, flared tube, etc.—rely on external force or torquing of the nut to seal. This force must be sufficient to deform the tube wall to achieve even a passable seal. Consequently, the sealing area is actually the weakest portion of these fittings. Any vibration or pressure fluctuation loosens the seal and makes it necessary to retighten the nut again and again until the fitting fails or the tube collapses. And when these fittings do fail, the entire tube section, not just the fitting, must be replaced, greatly increasing downtime and operating costs.

The Mark VIII O-SEAL System

The basic Mark VIII O-SEAL connector comprises a body and a tailpiece, with a resilient O-ring recessed in a close tolerance groove in the body. These two flat-faced components are joined by a union nut, which compresses the captive O-ring to form an initial, leaktight seal. Light wrenching completes the installation to assure a leakproof connection that will not vibrate loose. The flat-faced construction of Mark VIII O-SEAL fittings eliminates any concern about critical torque or positioning of the nut. Internal line pressure actually increases the sealing effectiveness of these unique fittings.

Low Torque Assembly

Unlike conventional fittings which require a great deal of torque to effect a seal, Mark VIII O-SEAL fittings require a minimal amount of torque to achieve a seal that never needs to be retightened. A typical ½" Mark VIII O-SEAL fitting, for example, requires just 36 in.-lbs. of torque for proper assembly, while a conventional bite-type fitting of the same size requires more than 500 in.-lbs.

Heat-Sealed Tube Connection — Welded or Brazed

All Mark VIII O-SEAL fittings are furnished complete, ready for installation. Tube end connections are permanently heat sealed (either welded or brazed) and are not subject to failure when breaking or remaking connections. See page 18 for methods of installation. This complete system of engineered fittings—including unions, connectors, tees, elbows and crosses in O.D. tube sizes from ¼" to 2" and reducers down to ⅛"—is ideal for any fluid system at pressures from vacuum to 3000 psi. Temperature rating and fluid compatibility are limited only by the O-ring material employed.

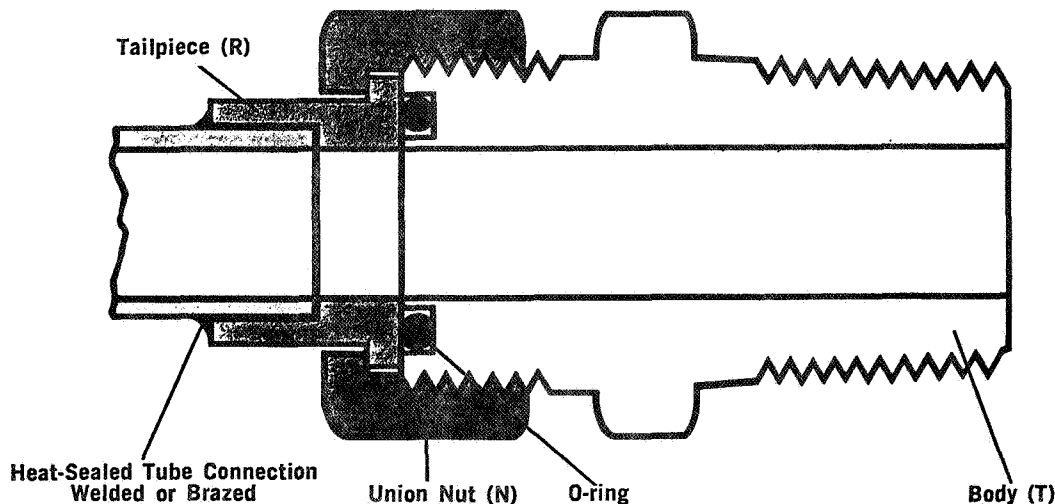
Vibration Resistance

The unique construction of Mark VIII O-SEAL fittings assures maximum resistance to the effects of vibration, flexural stresses or pressure surges. Essentially, the Mark VIII system is a compact, lightweight version of the famed CPV O-SEAL fittings which have been providing leakproof connections for more than 25 years—even in systems with severe vibration and other cyclic stresses. Like the O-SEAL SYSTEM, Mark VIII O-SEAL fittings employ a resilient O-ring that maintains its positive sealing regardless of system pressure fluctuations or vibration.

Uniquely Superior

If you want to build a "dry machine" with inherent vibration resistance and complete flexibility, put the unrivaled capabilities of Mark VIII O-SEAL fittings to work for you. They'll never let you down.

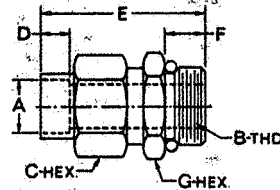
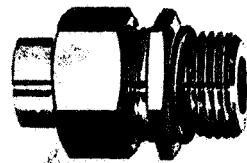
Typical Mark VIII Male Connector (H854)



ORIGINAL PAGE IS
OF POOR QUALITY

MALE CONNECTOR — H859
Tube to Male Straight Thread

Part No.	Tube	Male	C-Hex.	D	E	F	G-Hex.
	O.D.	Str. Thd.					
	A	B					
H859-2-2	1/8	5/16-24	1/2	3/16	13/8	.36	1/2
H859-2-4	1/8	7/16-20	5/8	3/16	17/16	.41	5/8
H859-4-4	1/4	7/16-20	5/8	3/16	17/16	.41	5/8
H859-4-6	1/4	9/16-18	13/16	3/16	17/16	.43	3/4
H859-4-8	1/4	3/4-16	15/16	3/16	111/16	.47	7/8
H859-6-6	3/8	9/16-18	13/16	1/4	15/8	.43	3/4
H859-6-8	3/8	3/4-16	15/16	1/4	13/4	.47	7/8
H859-6-10	3/8	7/8-14	11/8	1/4	115/16	.53	11/16
H859-8-8	1/2	3/4-16	15/16	5/16	113/16	.47	7/8
H859-8-10	1/2	7/8-14	11/8	5/16	2	.53	11/16
H859-8-12	1/2	11/16-12	13/8	5/16	23/16	.63	13/8
H859-10-10	5/8	7/8-14	11/8	3/8	21/16	.53	11/16
H859-10-12	5/8	11/16-12	13/8	3/8	21/4	.63	13/8
H859-12-12	3/4	11/16-12	13/8	7/16	25/16	.63	13/8
H859-12-16	3/4	15/16-12	15/8	7/16	21/2	.63	15/8
H859-16-16	1	15/16-12	15/8	1/2	27/16	.63	15/8
H859-20-20	1 1/4	15/8-12	2	5/16	211/16	.63	17/8
H859-24-24	1 1/2	17/8-12	2 3/8	5/8	213/16	.63	2 1/4
H859-32-32	2	2 1/2-12	3 1/4	7/8	3 1/4	.63	3



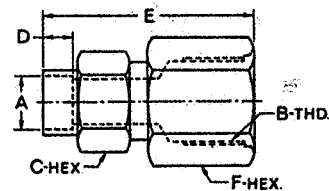
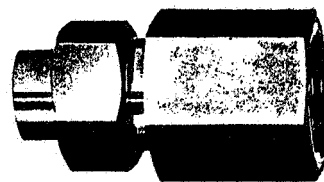
ORIGINAL PAGE IS
 OF POOR QUALITY

The A dimension can be reduced to any line size. See page 17 for details.



FEMALE CONNECTOR — H864
Tube to Female Straight Thread

Part No.	Tube	Female	C-Hex.	D	E	F-Hex.
	O.D.	Str. Thd.				
	A	B				
H864-2-4	1/8	3/16-20	5/8	3/16	1 1/2	3/4
H864-4-4	1/4	3/16-20	5/8	3/16	1 1/2	3/4
H864-4-6	1/4	3/16-18	13/16	3/16	1 11/16	3/8
H864-4-8	1/4	3/4-16	15/16	3/16	1 7/8	1 1/16
H864-6-6	3/8	3/16-18	13/16	1/4	1 3/4	7/8
H864-6-8	3/8	3/4-16	15/16	1/4	1 15/16	1 1/16
H864-6-10	3/8	7/8-14	1 1/8	1/4	2 1/4	1 1/8
H864-8-8	1/2	3/4-16	15/16	5/16	2	1 1/16
H864-8-10	1/2	7/8-14	1 1/8	5/16	2 3/16	1 1/8
H864-8-12	1/2	1 1/16-12	1 3/8	5/16	2 3/16	1 3/8
H864-10-10	5/8	7/8-14	1 1/8	3/8	2 3/8	1 1/8
H864-10-12	5/8	1 1/16-12	1 3/8	3/8	2 1/2	1 3/8
H864-12-12	3/4	1 1/16-12	1 3/8	7/16	2 5/16	1 3/8
H864-12-16	3/4	1 5/16-12	1 5/8	7/16	2 13/16	1 5/8
H864-16-16	1	1 5/16-12	1 5/8	1/2	2 7/8	1 5/8
H864-20-20	1 1/4	1 5/8-12	2	5/16	3	2
H864-24-24	1 1/2	1 7/8-12	2 3/8	5/8	3 1/4	2 1/4



The A dimension can be reduced to any line size. See page 17 for details.

Combination Pump Valve Co.
 851 Preston St., Philadelphia, Pa. 19104

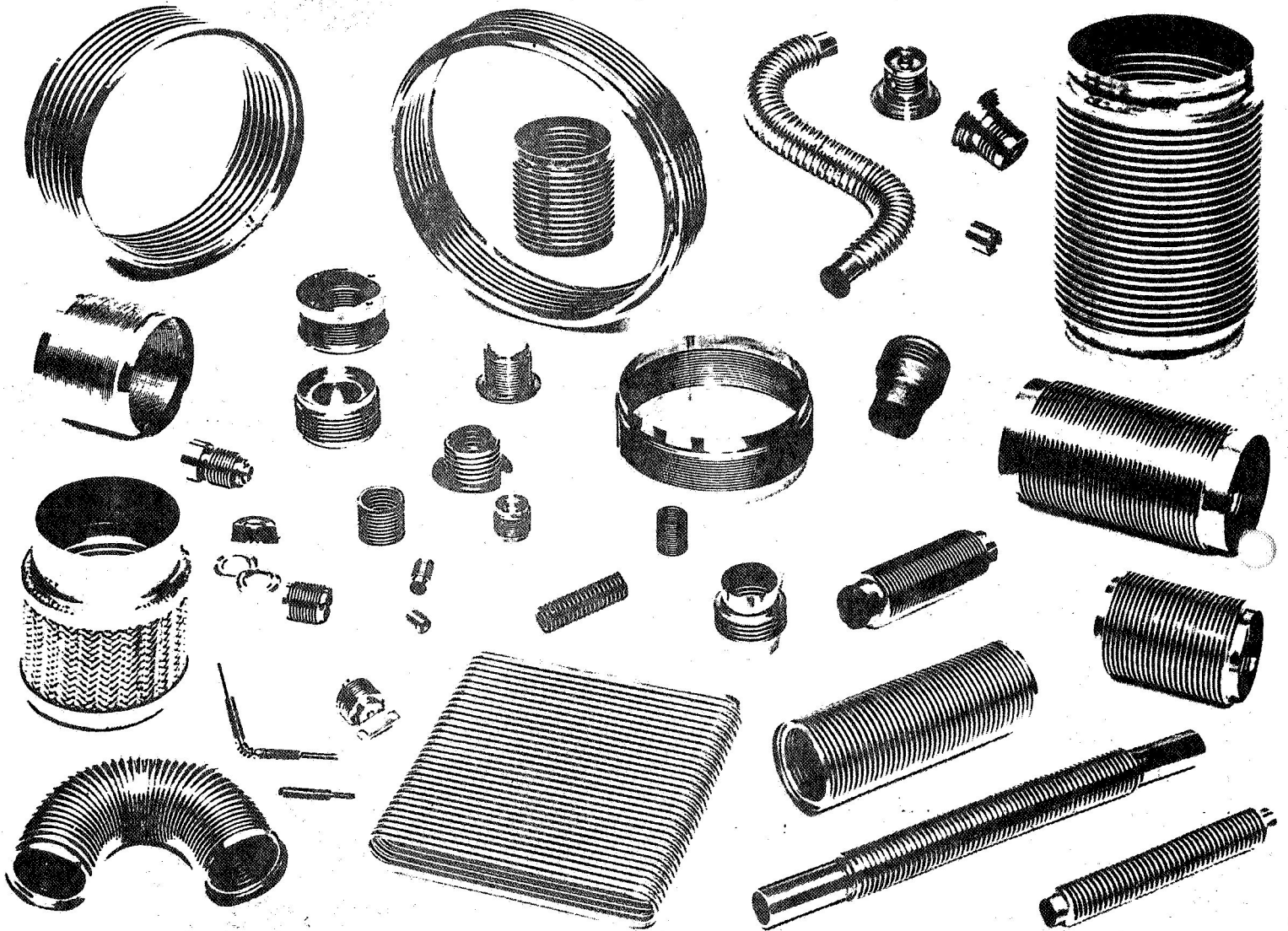
For ordering information, see page 4.

MASTER PRODUCTS

Specialists in...

ORIGINAL PAGE IS
OF POOR QUALITY

METAL BELLOWS • BELLOWS ASSEMBLIES • COMPONENTS



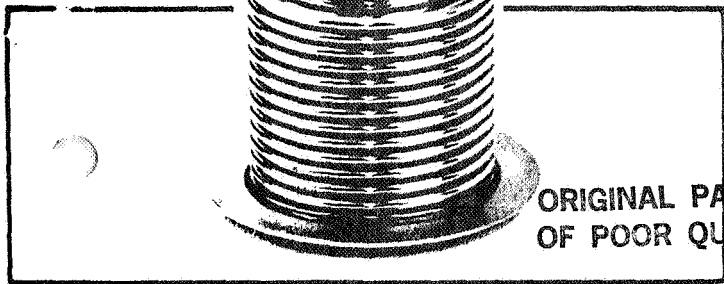
THIS brochure presents a summary of the capabilities and past performances of Master Products Manufacturing Co. as a leader in the design and manufacture of convoluted metal structures, related component parts, and assemblies.

Present usages of convoluted structures are generally so inextricably involved with engineering problems that stock bellows are largely a thing of the past. In many instances, design research and experimental studies, possibly including prototypes, are necessary to meet requirements in this era of space exploration and missile development. Our personnel drawing on the skill that comes only from years of ex-

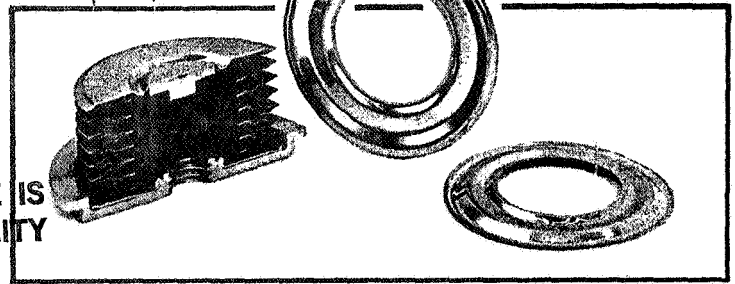
perience, and making use of our specialized equipment and facilities, are uniquely qualified to provide the customer with services unsurpassed in this field.

Master Products has for many years specialized in the manufacture of instrument quality metal structures and assemblies involving such structures, for aircraft, missile, and many industrial applications.

Basically, we manufacture bellows by two processes. Most bellows are formed from tubing of the proper size by mechanical, hydraulic, or pneumatic means and may be of one of



ORIGINAL PAGE IS
OF POOR QUALITY



FORMED BELLOWS

Shown is a two ply lap seam welded bellows made from 321 stainless steel .003 wall thickness. Spring rate is 40 lbs. per inch. The flange is heliarc welded to the open end. The cap is seam welded to the closed end.

STACKED BELLOWS (WELDED)

A cutaway illustration of a stacked bellows or one where discs are welded around the inner and outer periphery of each convolution. Made of AM 350 single ply .002 wall thickness. Spring rate 14 lbs. per inch. All welding is heliarc. Flange and cap are 321 stainless.

DIMENSIONS & CHARACTERISTICS—FORMED STAINLESS STEEL BELLOWS

1	2	3	4	5	6	7	8	9
REFERENCE NUMBER	INSIDE DIAMETER (Inches)	OUTSIDE DIAMETER (Inches)	PITCH (Inches)	MAXIMUM DEFLECTION (In/Conv.)	EFFECTIVE AREA (Sq. In.)	SPRING RATE (#/In/Conv.)	DEFLECTION PER P.S.I. (In./Conv.)	MAXIMUM INTERNAL PRESSURE (P.S.I.)
300 SERIES STAINLESS (1 PLY) LAP-WELDED, BUTT-WELDED OR SEAMLESS								
1S-13	1/8	1/4	.031	.005	.025	500	.00005	1,000
1S-25	1/4	13/32	.062	.019	.085	2,000	.000043	1,100
1S-31	5/16	15/32	.062	.019	.120	1,660	.000072	630
1S-37	3/8	9/16	.093	.019	.172	960	.00018	800
1S-48	15/32	3/4	.093	.023	.294	715	.00041	405
1S-50	1/2	3/4	.093	.023	.293	370	.0008	310
1S-61	5/8	7/8	.093	.023	.424	540	.00078	350
1S-67	11/16	29/32	.093	.023	.487	480	.00101	250
1S-72	3/4	31/32	.125	.031	.567	1,000	.00056	460
1S-87	7/8	1-1/8	.125	.031	.785	810	.00097	400
1S-91	29/32	1-5/32	.125	.031	.841	700	.0012	375
1S-98	31/32	1-5/16	.125	.031	1.020	370	.00275	175
1S-100	1.00	1-9/32	.125	.031	1.015	1,575	.00064	295
1S-125	1-1/4	1-11/16	.125	.031	1.767	300	.0058	170
1S-131	1-5/16	1-9/16	.125	.031	1.622	600	.0027	190
1S-136	1-3/8	1-21/32	.125	.031	1.805	505	.0036	175
1S-150	1-1/2	1-29/32	.187	.045	2.270	875	.0026	200
1S-162	1-5/8	2-1/8	.187	.045	2.761	725	.0038	170
1S-175	1-3/4	2-3/16	.187	.045	3.141	600	.0052	160
1S-200	2.00	2-1/2	.250	.050	3.932	960	.0041	130
1S-237	2-3/8	2-7/8	.250	.050	5.412	1,675	.0032	110
1S-250	2-1/2	2-7/8	.250	.050	5.670	1,550	.0036	95
1S-300	3.00	3-1/2	.250	.050	8.294	1,080	.0077	65
1S-325	3-1/4	3-3/4	.250	.050	9.621	2,250	.0043	75
1S-350	3-1/2	4-1/8	.250	.050	11.412	1,900	.006	80
1S-400	4.00	4-3/4	.300	.075	14.862	910	.0163	45
1S-431	4-5/16	4-15/16	.300	.075	16.799	930	.018	42
1S-443	4-7/16	5.00	.300	.075	17.475	6,150	.0282	75
1S-450	4-1/2	4-25/32	.300	.075	16.941	6,000	.0282	80
1S-500	5.00	6.00	.375	.078	23.758	2,350	.0101	45
1S-550	5-1/2	6-1/2	.375	.078	28.274	800	.0353	25
1S-600	6.00	6-21/32	.375	.078	31.416	1,060	.0296	50
1S-700	7.00	8.00	.375	.078	44.178	1,250	.035	40
1S-800	8.00	9.00	.375	.078	56.745	1,500	.038	32
1S-900	9.00	10.00	.375	.078	70.882	1,725	.0415	25
1S-1000	10.00	11-1/2	.375	.078	90.760	7,900	.0114	105
1S-1100	11.00	12-1/2	.375	.078	108.430	9,000	.0120	90
1S-1275	12-3/4	14-1/2	.375	.078	145.800	10,750	.0135	75



*CLASS. LTR.	OPERATION	PROGRAM	SEQUENCE NO.	REV. LTR.
PIR NO. U	- 1254	- AGCE	- 019	
*USE "C" FOR CLASSIFIED AND "U" FOR UNCLASSIFIED				

PROGRAM INFORMATION REQUEST / RELEASE

FROM S.L. Neste	TO Distribution
--------------------	--------------------

DATE SENT 4/6/81	DATE INFO. REQUIRED	PROJECT AND REQ. NO.	REFERENCE DIR. NO.
---------------------	---------------------	----------------------	--------------------

SUBJECT
 DIELECTRIC MATERIAL FOR THE AGCE BAFFLE

INFORMATION REQUESTED/RELEASED

1.0 SUMMARY

A potential source of high dielectric constant material for the baffle in the AGCE assembly has been identified. Trans-Tech, Inc. of Gaithersburg, MD can provide ceramic dielectric material with any value of dielectric constant between 14 and 140 on request. They will also machine the material to customer specified configurations. The person to contact for information beyond that provided below is Russell G. West (301) 948-3800, Senior Staff Engineer at Trans-Tech, Inc.

2.0 BACKGROUND

In the construction of the AGCE assembly, an equatorial baffle may be required in the lower hemispherical section of the convection cell to prevent fluid circulation in that region (PIR 1254-AGCE-016). The dielectric constant of the baffle material should match that of the dielectric fluid to minimize distortion of the electric field. For the GFFC assembly, teflon with a dielectric constant of 2.2 was used which conveniently matched that of the DC Silicone Oil (i.e., 2.18). In the case of the AGCE, fluids with dielectric constants of 40 or more may be used. During the AGCE Program review held at GE in early February, a question arose as to the availability of material for the baffle which had this large a dielectric constant. As a result of that concern GE informally agreed to investigate this potential problem and to identify sources of high dielectric constant material.

3.0 RESULTS AND CONCLUSIONS

Trans-Tech, Inc. a producer of ceramic dielectrics was contacted and asked to provide information on the availability of high dielectric materials. Data sheets giving complete specifications for several compounds were sent and are given in the Appendix. Although the values of dielectric constant given for each compound were measured at several GHz, the values at AGCE frequencies of ~300 Hz will not be appreciably different (probably slightly higher).

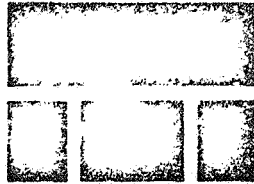
G. Fogal R. Homsey S. Neste	PAGE NO.	RETENTION REQUIREMENTS	
	1 OF 2	COPIES FOR	MASTERS FOR
		<input type="checkbox"/> 1 MO.	<input type="checkbox"/> 3 MOS.
		<input type="checkbox"/> 3 MOS.	<input type="checkbox"/> 6 MOS.
		<input type="checkbox"/> 6 MOS.	<input type="checkbox"/> 12 MOS.
		<input type="checkbox"/> MOS.	<input type="checkbox"/> MOS.
		<input type="checkbox"/>	<input type="checkbox"/> DONOT DESTROY

Of particular interest for AGCE applications is the Magnesium Calcium Titanite (MCT) Series which are pure ceramic dielectric materials developed with the exacting requirements of the microwave industry in consideration. Any value of dielectric constant between 14 and 140 is available on request. A list of compositions representative of the MCT Series is given on the last page of the Appendix.

Based on the information obtained to date, procurement of a dielectric baffle material to match the dielectric constant of the fluid seems quite feasible. Additional information regarding characteristics of these materials and their potential application to the AGCE can be obtained from Trans-Tech, Inc.

APPENDIX
DIELECTRIC SPECIFICATION BULLETINS

TRANS-TECH, INC.
GARNETS • FERRITES • ALUMINA
DIELECTRICS • CUSTOM R & D



SPECIFICATION BULLETIN

TRANS-TECH™ Brand Electronic Ceramics

TYPE D-4
Cordierite

DIELECTRIC
BULLETIN NO. 59-71

CHARACTERISTICS

Specific Gravity — g/cc	2.30
Color	White
Thermal Conductivity — cal./cm ² /cm/sec./°C	0.007
Hardness — Mohs' Scale	7 — 8
Coefficient of Thermal Expansion — Per °C	2 x 10 ⁻⁶
Dielectric Strength — volts per mil	40 — 230
Dielectric Constant at: 10 GHz — ε'	4.3 ± 0.3
Dielectric Loss Tangent at: 10 GHz — ε''/ε'	<0.0002
Temperature Coef. of dielectric constant/°C	+55 x 10 ⁻⁶

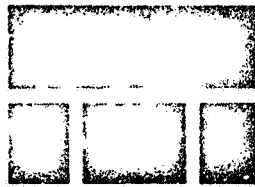
D-4 is a single phase ceramic dielectric material developed and produced with the exacting requirements of the microwave industry in consideration. Every effort has been made to produce and keep the microwave losses to a minimum. Very constant characteristics are assured, both with frequency and temperature variations.

D-4 is intended to be used as a r.f. matching medium for ferrites and garnets when a dielectric constant of 4 is needed, but this is not the limitation of use. Whenever a very low loss dielectric exhibiting a small coefficient of linear thermal expansion is required, D-4 is indicated.

**ORIGINAL PAGE IS
 OF POOR QUALITY**

Specifications subject to change without notice.
 Unless otherwise indicated, all data is nominal

AUGUST 1, 1972



TRANS-TECH™ Brand Electronic Ceramics

TYPE DS-6
Forsterite-High Purity

DIELECTRIC
BULLETIN NO. 60-67

CHARACTERISTICS

Water Absorption - %	0.6
Specific Gravity - g/cc	2.89
Color	Cream
Thermal Conductivity - cal./cm ² /cm/sec./°C	0.009
Hardness - Mohs' Scale	7.5
Tensile Strength - PSI	9000
Compressive Strength - PSI	85,000
Flexural Strength - PSI	20,000
Resistance to Impact - Inch-Pounds	5.1
Coefficient of Thermal Expansion - Per °C	1 x 10 ⁻⁵
Dielectric Strength - volts per mil	200
Te - °C	1000
Dielectric Constant at: 10 GHz - ε'	6.3 + 0.3
Dielectric Loss Tangent at: 10 GHz - ε''/ε'	<0.0002
Temperature Coef. of dielectric constant/°C	+107 x 10 ⁻⁶

DS-6 is a single phase ceramic dielectric material developed and produced with the exacting requirements of the microwave industry in consideration. Every effort has been made to produce and keep the microwave losses to a minimum. Very constant characteristics are assured, both with frequency and temperature variations.

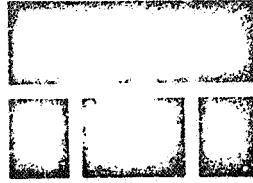
DS-6 is intended to be used as a r.f matching medium for ferrites and garnets when a dielectric constant of 6 is needed, but this is not a limitation of use. Whenever a very low loss and stable dielectric material is required, DS-6 is indicated.

ORIGINAL PAGE IS
 OF POOR QUALITY

Specifications subject to change without notice.
 Unless otherwise indicated, all data is nominal

AUGUST 1, 1972

TRANS-TECH, INC.
GARNETS • FERRITES • ALUMINA
DIELECTRICS • CUSTOM R & D



SPECIFICATION
BULLETIN

TRANS-TECH™ Brand Electronic Ceramics

TYPE DA-9
Alumina -99.7%

DIELECTRIC
BULLETIN NO. 61-67

CHARACTERISTICS

Water Absorption - %	0.000 Impervious
Specific Gravity - g/cc	3.85 to 3.89
Color	Pink
Thermal Conductivity - cal./cm ² /cm/sec./°C	0.045
Hardness - Mohs' Scale	9
Tensile Strength - PSI	30,000
Compressive Strength - PSI	375,000
Flexural Strength - PSI	60,000
Resistance to Impact - Inch-Pounds	7.5
Coefficient of Thermal Expansion - Per °C	5 x 10 ⁻⁶
Dielectric Strength - volts per mil	300
Te - °C	1100
Dielectric Constant at 10 GHz ε'	9.5±0.3
Dielectric Loss Tangent at: 10 GHz ε''/ε'	< 0.000i
Temperature Coef. of dielectric constant/°C	+113 x 10 ⁻⁶

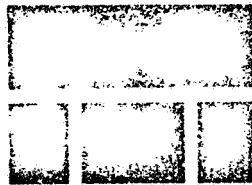
DA-9 is a single phase ceramic dielectric material developed and produced with the exacting requirements of the microwave industry in consideration. Every effort has been made to produce and keep the microwave losses to a minimum. Very constant characteristics are assured, both with frequency and temperature variations.

DA-9 is intended to be used as a r.f. matching medium for ferrites and garnets when a dielectric constant of 9 is needed, but this is not a limitation of use. Whenever a very low loss and stable dielectric material is required, DA-9 is indicated.

ORIGINAL PAGE IS
OF POOR QUALITY

Specifications subject to change without notice.
 Unless otherwise indicated, all data is nominal

AUGUST 1, 1972



TRANS-TECH™ Brand Electronic Ceramics

TYPE D-13
Magnesium-Titanate

DIELECTRIC
BULLETIN NO. 62-67

CHARACTERISTICS

Water Absorption – %0000 Impervious
Specific Gravity – g/cc	3.40
Color	Ivory
Thermal Conductivity – cal./cm ² /cm/sec./°C	0.01
Hardness – Mohs' Scale	7
Coefficient of Thermal Expansion – Per °C	8 x 10 ⁻⁶
Dielectric Strength – volts per mil	300
Dielectric Constant at: 10 GHz – ε'	13.0 ± 0.5
Dielectric Loss Tangent at: 10 GHz ε''/ε'	< 0.0002
Temperature Coef. of dielectric constant/°C	+135 x 10 ⁻⁶

D-13 is a single phase ceramic dielectric material developed and produced with the exacting requirements of the microwave industry in consideration. Every effort has been made to produce and keep the microwave losses to a minimum. Very constant characteristics are assured, both with frequency and temperature variations.

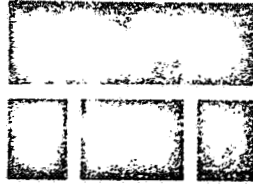
D-13 is intended to be used as a r.f. matching medium for ferrites and garnets when a dielectric constant of 13 is needed, but this is not a limitation of use. Whenever a very low loss and stable dielectric material is required, D-13 is indicated.

**ORIGINAL PAGE IS
 OF POOR QUALITY**

Specifications subject to change without notice.
 Unless otherwise indicated, all data is nominal

AUGUST 1, 1972

TRANS-TECH, INC.
GARNETS • FERRITES • ALUMINA
DIELECTRICS • CUSTOM R & D



SPECIFICATION
BULLETIN

TRANS-TECH™ Brand Electronic Ceramics

TYPE D-16
Magnesium-Titanate

DIELECTRIC
BULLETIN NO. 63-67

CHARACTERISTICS

Water Absorption — %	0.000	Impervious
Specific Gravity — g/cc	3.60	
Color	Ivory	
Thermal Conductivity — cal./cm ² /cm/sec./°C	0.01	
Hardness — Mohs' Scale	7	
Coefficient of Thermal Expansion — Per °C	7.5 x 10 ⁻⁶	
Dielectric Strength — volts per mil	300	
Dielectric Constant at: 10 GHz — ε'	16.0 ± 0.5	
Dielectric Loss Tangent at 10 GHz — ε''/ε'	< 0.0002	
Temperature Coef. of dielectric constant/°C	+98 x 10	

D-16 is a single phase ceramic dielectric material developed and produced with the exacting requirements of the microwave industry in consideration. Every effort has been made to produce and keep the microwave losses to a minimum. Very constant characteristics are assured, both with frequency and temperature variations.

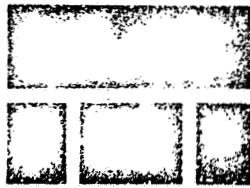
D-16 is intended to be used as a r.f. matching medium for ferrites and garnets when a dielectric constant of 16 is needed, but this is not a limitation of use. Whenever a very low loss and stable dielectric material is required, D-16 is indicated.

ORIGINAL PAGE IS
 OF POOR QUALITY

Specifications subject to change without notice.
 Unless otherwise indicated, all data is nominal

AUGUST 1, 1972

TRANS-TECH, INC.
GARNETS • FERRITES • ALUMINA
DIELECTRICS • CUSTOM R & D
 TRANS-TECH™ Brand Electronic Ceramics



SPECIFICATION BULLETIN

TYPE D-30
Nickel-Aluminum-Titanate

DIELECTRIC
BULLETIN NO. 64-70

CHARACTERISTICS

Water Absorption — %	0.8
Specific Gravity — g/cc	3.9 — 4.0
Color	Green
Dielectric Constant at: 10 GHz — ϵ'	31.0 ±5%
Dielectric Loss Tangent at: 10 GHz — ϵ''/ϵ'	< 0.0002
Temperature Coef. of dielectric constant/°C	-387 x 10 ⁻⁶
Coefficient of Thermal Expansion — Per °C	9 x 10 ⁻⁶

D-30 is a ceramic dielectric material developed and produced with the exacting requirements of the microwave industry in consideration. Every effort has been made to produce and keep the microwave losses to a minimum. Very constant characteristics are assured, both with frequency and temperature variations.

D-30 is intended to be used as a phaser toroid loading and a r.f. matching medium for ferrites and garnets when a dielectric constant of 30 is needed, but this is not a limitation of use. Whenever an extremely low loss moderately high permittivity dielectric material is required, D-30 is indicated.

ORIGINAL PAGE IS
 OF POOR QUALITY

Specifications subject to change without notice.
 As otherwise indicated, all data is nominal

AUGUST 1, 1972

TRANS-TECH, INC.
GARNETS • FERRITES • ALUMINA
DIELECTRICS • CUSTOM R & D

TRANS-TECH™ Brand Electronic Ceramics



SPECIFICATION BULLETIN

**DIELECTRIC
 BULLETIN NO. 65-70**

**TYPE D-100
 Titania**

CHARACTERISTICS

Water Absorption — %	0.1
Specific Gravity — g/cc	3.9 — 4.0
Color	Cream
Thermal Conductivity — cal./cm ² /cm/sec./°C	0.01
Hardness — Mohs' Scale	6
Coefficient of Thermal Expansion — Per °C	7.5 x 10 ⁻⁶
Dielectric Strength — volts per mil	150
Dielectric Constant at: 6 GHz — ε'	96 ±5%
Dielectric Loss Tangent at: 6 GHz — ε''/ε'	Less than 0.001
Temperature Coef of dielectric constant/°C	-575 x 10 ⁻⁶

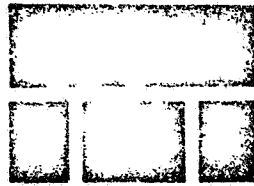
D-100 is a single phase ceramic dielectric material developed and produced with the exacting requirements of the microwave industry in consideration. Every effort has been made to produce and keep the microwave losses to a minimum. Very constant characteristics are assured, both with frequency and temperature variations.

D-100 is intended to be used as a r.f. matching medium for ferrites and garnets when a high dielectric constant is needed, but this is not a limitation of use. Whenever a low loss high dielectric material is required, D-100 is indicated.

**ORIGINAL PAGE IS
 OF POOR QUALITY**

Specifications subject to change without notice.
 Unless otherwise indicated, all data is nominal

AUGUST 1, 1972



TRANS-TECH™ Brand Electronic Ceramics

TYPE D-38
Barium Tetratitanate

DIELECTRIC
BULLETIN NO. 66-70

CHARACTERISTICS

Water Absorption – %	0.30
Specific Gravity – g/cc	4.40
Color	tan
Hardness – Mohs' Scale	7
Coefficient of Thermal Expansion – Per °C	9.4×10^{-6}
Dielectric Constant at 6 GHz – ϵ'	$37.0 \pm 5\%$
Dielectric Loss Tangent at 6 GHz – ϵ''/ϵ'	< 0.0005
Temperature Coef of dielectric constant/°C	-25×10^{-6}

D-38 is a single phase ceramic dielectric material developed and produced with the exacting requirements of the microwave industry in consideration. Every effort has been made to produce and keep the microwave losses to a minimum. Very constant characteristics are assured, both with frequency and temperature variations.

D-38 is intended to be used as a phaser toroid loading and a r.f. matching medium for ferrites and garnets when a dielectric constant of 37 is needed, but this is not a limitation of use. Whenever a low loss moderately high permittivity dielectric material, exhibiting a small temperature coefficient of dielectric constant is required, D-38 is indicated.

ORIGINAL PAGE IS
OF POOR QUALITY

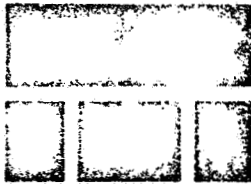
Specifications subject to change without notice.
 unless otherwise indicated, all data is nominal

NOVEMBER 1, 1980

TRANS-TECH, INC.

GARNETS • FERRITES • ALUMINA
DIELECTRICS • CUSTOM R & D

TRANS-TECH™ Brand Electronic Ceramics



ORIGINAL PAGE IS
OF POOR QUALITY

SPECIFICATION BULLETIN

TYPE D-15
Magnesium-Titanate

DIELECTRIC
BULLETIN NO. 67-71

CHARACTERISTICS

Water Absorption — %	0.000	Impervious
Specific Gravity — g/cc	3.50	
Color	Ivory	
Thermal Conductivity — cal./cm ² /cm/sec./°C	0.009	
Hardness — Mohs' Scale	7	
Coefficient of Thermal Expansion — Per °C	7.5 x 10 ⁻⁶	
Dielectric Strength — volts per mil	300	
Dielectric Constant at: 10 GHz — ϵ'	15.0 ± 0.5	
Dielectric Loss Tangent at: 10 GHz — ϵ''/ϵ'	< 0.0002	
Temperature Coef. of dielectric constant/°C	+98 x 10 ⁻	

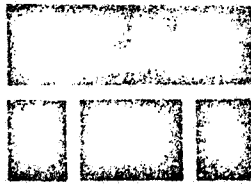
D-15 is a single phase ceramic dielectric material developed and produced with the exacting requirements of the microwave industry in consideration. Every effort has been made to produce and keep the microwave losses to a minimum. Very constant characteristics are assured, both with frequency and temperature variations.

D-15 is intended to be used as a r.f. matching medium for ferrites and garnets when a dielectric constant of 15 is needed, but this is not a limitation of use. Whenever a very low loss and stable dielectric material is required, D-15 is indicated.

ORIGINAL PAGE IS
OF POOR QUALITY

Specifications subject to change without notice.
Unless otherwise indicated, all data is nominal

AUGUST 1, 1972



TRANS-TECH T.M. BRAND ELECTRONIC CERAMICS

TYPE S-71
SPINEL

ORIGINAL PAGE IS
OF POOR QUALITY

DIELECTRIC
BULLETIN NO. 91 - 76

CHARACTERISTICS

Dielectric Constant at 10GHz — ϵ'	8.0 ± 5%
Dielectric Loss Tangent at 10GHz — ϵ''/ϵ'	<0.0002
Coefficient of Thermal Expansion — per °C	7.1 x 10 ⁻⁶ (1)
Specific Gravity — g/cc	3.53
Color	White
Water Absorption — %	< 0.2%
Temperature Coefficient of dielectric constant — per °C	+100 x 10 ⁻⁶

(1) Range 25°C — 300°C., see reverse side for broader temperature range.

S-71 is one of a series of pure ceramic dielectric materials developed with the exacting requirements of the microwave industry in consideration. The temperature coefficient of linear thermal expansion has been adjusted within this

series to match those of microwave ferrites and garnets. Whenever an extremely low loss dielectric material of controllable thermal expansion is required, the spinel series is indicated.

TYPICAL THERMAL EXPANSION VALUES OF POLYCRYSTALLINE FERRITES AND GARNETS (2):

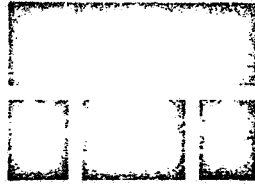
<u>Composition Type</u>	<u>Coefficient of expansion (°C⁻¹)</u>	
	<u>20°C to 120°C</u>	<u>20°C to 720°C</u>
YIG, YA1IG, YGdIG	8.0 x 10 ⁻⁶	10.5 x 10 ⁻⁶
MgMn Ferrite, MgMnAl Ferrite	8.2 x 10 ⁻⁶	11.0 x 10 ⁻⁶
Ni Ferrite, NiAl Ferrite	7.6 x 10 ⁻⁶	10.6 x 10 ⁻⁶

(2) F.G. Peters, IEEE Trans. on Mag. Vol. MAG-4, page 480, Sept. 1968

Specifications subject to change without notice.
 unless otherwise indicated, all data is nominal.

AUGUST 1, 1976

TRANS-TECH, INC.
 GARNETS • FERRITES • ALUMINA
 DIELECTRICS • CUSTOM R & D



**SPECIFICATION
 BULLETIN**

TRANS-TECH T.M. BRAND ELECTRONIC CERAMICS

**TYPE S-78
 SPINEL**

ORIGINAL PAGE IS
 OF POOR QUALITY

DIELECTRIC
 BULLETIN NO. 92 - 76

CHARACTERISTICS

Dielectric Constant at 10GHz - ϵ'	8.2 ± 5%
Dielectric Loss Tangent at 10GHz - ϵ''/ϵ'	<0.0002
Coefficient of Thermal Expansion - per °C	7.8 x 10 ⁻⁶ (1)
Specific Gravity - g/cc	3.52
Color	White
Water Absorption - %	< 0.2%
Temperature Coefficient of dielectric constant - per °C	+100 x 10 ⁻⁶

(1) Range 25°C - 300°C., see reverse side for broader temperature range.

S-78 is one of a series of pure ceramic dielectric materials developed with the exacting requirements of the microwave industry in consideration. The temperature coefficient of linear thermal expansion has been adjusted within this

series to match those of microwave ferrites and garnets. Whenever an extremely low loss dielectric material of controllable thermal expansion is required, the spinel series is indicated.

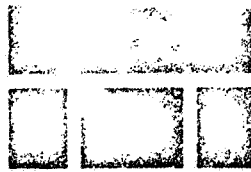
TYPICAL THERMAL EXPANSION VALUES OF POLYCRYSTALLINE FERRITES AND GARNETS ⁽²⁾:

<u>Composition Type</u>	<u>Coefficient of expansion (°C⁻¹)</u>	
	<u>20°C to 120°C</u>	<u>20°C to 720°C</u>
YIG, YA1IG, YGdIG	8.0 x 10 ⁻⁶	10.5 x 10 ⁻⁶
MgMn Ferrite, MgMnAl Ferrite	8.2 x 10 ⁻⁶	11.0 x 10 ⁻⁶
Ni Ferrite, NiAl Ferrite	7.6 x 10 ⁻⁶	10.6 x 10 ⁻⁶

(2) F.G. Peters, IEEE Trans. on Mag. Vol. MAG-4, page 480, Sept. 1968

Specifications subject to change without notice.
 Unless otherwise indicated, all data is nominal.

AUGUST 1, 1976



TECH T.M. BRAND ELECTRONIC CERAMICS

TYPE S-98
SPINEL

ORIGINAL PAGE IS
 OF POOR QUALITY

DIELECTRIC
BULLETIN NO. 93 - 76

CHARACTERISTICS

Dielectric Constant at 10GHz - ϵ'	8.8 ± 5%
Dielectric Loss Tangent at 10GHz - ϵ''/ϵ'	< 0.0002
Coefficient of Thermal Expansion - per °C	9.8 x 10 ⁻⁶ (1)
Specific Gravity - g/cc	3.51
Color	White
Water Absorption - %	< 0.2%
Temperature Coefficient of dielectric constant - per °C	+100 x 10 ⁻⁶

(1) Range 25°C. - 300°C., see reverse side for broader temperature range.

S-98 is one of a series of pure ceramic dielectric materials developed with the exacting requirements of the microwave industry in consideration. The temperature coefficient of linear thermal expansion has been adjusted within this

series to match those of microwave ferrites and garnets. Whenever an extremely low loss dielectric material of controllable thermal expansion is required, the spinel series is indicated.

TYPICAL THERMAL EXPANSION VALUES OF POLYCRYSTALLINE FERRITES AND GARNETS (2) :

<u>Composition Type</u>	<u>Coefficient of expansion (°C⁻¹)</u>	
	<u>20°C to 120°C</u>	<u>20°C to 720°C</u>
YIG, YA1IG, YGdIG	8.0 x 10 ⁻⁶	10.5 x 10 ⁻⁶
MgMn Ferrite, MgMnAl Ferrite	8.2 x 10 ⁻⁶	11.0 x 10 ⁻⁶
Ni Ferrite, NiAl Ferrite	7.6 x 10 ⁻⁶	10.6 x 10 ⁻⁶

(2) F.G. Peters, IEEE Trans. on Mag. Vol. MAG-4, page 480, Sept. 1968

Specifications subject to change without notice.
 Unless otherwise indicated, all data is nominal.

AUGUST 1, 1976

TRANS-TECH T.M. BRAND ELECTRONIC CERAMICS

**TYPE S-110
 SPINEL**

ORIGINAL PAGE IS
 OF POOR QUALITY

**DIELECTRIC
 BULLETIN NO. 94 - 76**

CHARACTERISTICS

Dielectric Constant at 10 GHz - ϵ'	9.0 ± 5%
Dielectric Loss Tangent at 10 GHz - ϵ''/ϵ'	<0.0002
Coefficient of Thermal Expansion - per °C	11.0 x 10 ⁻⁶ (1)
Specific Gravity - g/cc	3.49
Color	White
Water Absorption - %	<0.2%
Temperature Coefficient of dielectric constant - per °C	+100 x 10 ⁻⁶

(1) Range 25°C - 300°C., see reverse side for broader temperature range.

S-110 is one of a series of pure ceramic dielectric materials developed with the exacting requirements of the microwave industry in consideration. The temperature coefficient of linear thermal expansion has been adjusted within this

series to match those of microwave ferrites and garnets. Whenever an extremely low loss dielectric material of controllable thermal expansion is required, the spinel series is indicated.

TYPICAL THERMAL EXPANSION VALUES OF POLYCRYSTALLINE FERRITES AND GARNETS⁽²⁾:

<u>Composition Type</u>	<u>Coefficient of expansion (°C⁻¹)</u>	
	<u>20°C to 120°C</u>	<u>20°C to 720°C</u>
YIG, YA1IG, YGdIG	8.0 x 10 ⁻⁶	10.5 x 10 ⁻⁶
MgMn Ferrite, MgMnAl Ferrite	8.2 x 10 ⁻⁶	11.0 x 10 ⁻⁶
Ni, NiAl Ferrite	7.6 x 10 ⁻⁶	10.6 x 10 ⁻⁶

(2) F.G. Peters, IEEE Trans. on Mag. Vol. MAG-4, page 480, Sept. 1968

Specifications subject to change without notice.
 Unless otherwise indicated, all data is nominal.

AUGUST 1, 1976

ORIGINAL PAGE IS
 OF POOR QUALITY

**DIELECTRIC
 BULLETIN NO. 75-71 thru 87-77**

TYPE MCT SERIES

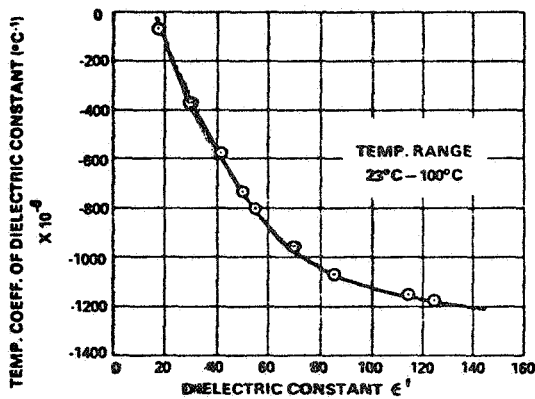
CHARACTERISTICS

Bulletin No.	Composition No.	Dielectric* Constant ϵ'	Dielectric* Loss Tangent $\tan \delta$	Density (g/cm ³)	Water Absorption (%)
75-71	MCT-18	18 ± 3%	<0.002	3.47	0.1
86-77	MCT-20	20 ± 5%	<0.002	3.50	0.1
87-77	MCT-25	25 ± 5%	<0.002	3.54	0.1
76-71	MCT-30	30 ± 5%	<0.002	3.59	0.1
77-71	MCT-40	40 ± 5%	<0.002	3.62	0.1
78-71	MCT-50	50 ± 5%	<0.002	3.65	0.1
79-71	MCT-55	55 ± 5%	<0.002	3.68	0.1
80-71	MCT-70	70 ± 5%	<0.002	3.70	0.1
81-71	MCT-85	85 ± 5%	<0.002	3.75	0.1
82-71	MCT-100	100 ± 5%	<0.002	3.78	0.1
83-71	MCT-115	115 ± 5%	<0.002	3.80	0.1
84-71	MCT-125	125 ± 5%	<0.002	3.83	0.1
85-71	MCT-140	140 ± 10%	<0.002	3.85	0.1

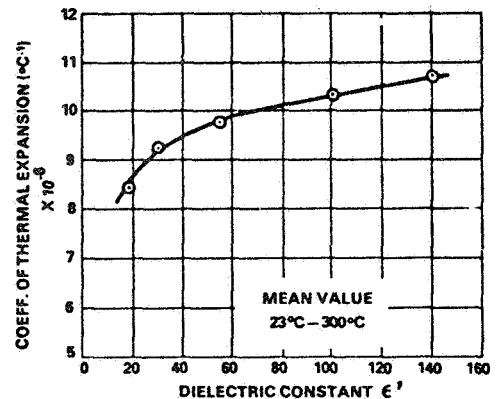
*measured at C-band microwave frequencies

The MCT Series are pure ceramic dielectric materials developed with the exacting requirements of the microwave industry in consideration. Any value of dielectric constant between 14 and 140 is available on request. The above listed compositions have been developed as representative of the MCT Series and are available on a production basis.

The MCT Series is intended for use in microwave devices where moderate dielectric loss can be tolerated and the inherent stability of a pure ceramic dielectric is beneficial.



Temperature Coefficient of dielectric constant vs. dielectric constant for composition in the MCT Series



Coefficient of thermal expansion vs. dielectric constant for compositions in the MCT Series

Specifications subject to change without notice.
 Unless otherwise indicated, all data is nominal.

JUNE 15, 1977



)

*CLASS. LTR.	OPERATION	PROGRAM	SEQUENCE NO.	REV. LTR.
U	1254	AGCE	026	

PROGRAM INFORMATION REQUEST / RELEASE

PIR NO. U - 1254 - AGCE - 026
 *USE "C" FOR CLASSIFIED AND "U" FOR UNCLASSIFIED

FROM S. L. Neste	TO Distribution
---------------------	--------------------

DATE SENT 5/29/81	DATE INFO. REQUIRED	PROJECT AND REQ. NO.	REFERENCE DIR. NO.
----------------------	---------------------	----------------------	--------------------

SUBJECT
 COST OF MATERIAL FOR THE AGCE BAFFLE

INFORMATION REQUESTED/RELEASED

The availability of high dielectric constant material for the AGCE baffle was addressed in PIR No. 1254-AGCE-019. The attached quotation from Trans-Tech, Inc. provides an estimate of cost and delivery time for a ring configuration (8 in OD x 6 in ID x 1 in thickness) using material having a dielectric constant of 20. Costs for the exact configuration and material composition required by the AGCE should not differ greatly from these values. Although the maximum thickness available in large diameters is approximately 1 inch, multiple pieces can be used to achieve any desired thickness.

G. Fogal R. Homsey	PAGE NO. 1 OF 2	RETENTION REQUIREMENTS	
		COPIES FOR	MASTERS FOR
		<input type="checkbox"/> 1 MO.	<input type="checkbox"/> 3 MOS.
		<input type="checkbox"/> 3 MOS.	<input type="checkbox"/> 6 MOS.
		<input type="checkbox"/> 6 MOS.	<input type="checkbox"/> 12 MOS.
		<input type="checkbox"/> MOS.	<input type="checkbox"/> MOS.
		<input type="checkbox"/>	<input type="checkbox"/> DO NOT DESTROY



PROGRAM INFORMATION REQUEST / RELEASE

*CLASS. LTR.	OPERATION	PROGRAM	SEQUENCE NO.	REV. LTR.
U	1254	AGCE	09	
PIR NO. _____				
*USE "C" FOR CLASSIFIED AND "U" FOR UNCLASSIFIED				

FROM DR. S. L. NESTE	TO DISTRIBUTION
-------------------------	--------------------

DATE SENT 1-29-81	DATE INFO. REQUIRED	PROJECT AND REQ. NO.	REFERENCE DIR. NO.
----------------------	---------------------	----------------------	--------------------

SUBJECT
TASK 8 - REQUIREMENTS FOR OUTER SPHERE MATERIAL

INFORMATION REQUESTED/RELEASED

The attached requirements for the outer sphere are provided for use in determining the availability of suitable material.

TASK 8 - REQUIREMENTS FOR OUTER SPHERE MATERIAL

1.0 SCOPE

A survey of vendors will be performed to determine the availability of suitable material for the outer sphere. The requirements listed below will be used as guidelines for this effort.

2.0 GENERAL

The requirements for the outer sphere material are based on GFFC experience and the AGCE statement of work.

3.0 REQUIREMENTS

3.1 Size

A nominal value of 12 cm will be assumed for the inner diameter of the sphere. Thickness of the hemispherical shell will be determined by thermal considerations and by the strength required for machining operations. Sphere diameters of 8 cm and 15 cm will also be considered to bracket the nominal value.

3.2 Optical Axis

Optical axis will be specified parallel to the axis of rotation to within $\pm 5^\circ$ to minimize birefringent effects (refer to Tasks 4 and 5).

L. R. Eaton G. Fogal S. Neste W. Yager	PAGE NO.	<input checked="" type="checkbox"/> RETENTION REQUIREMENTS	
	1 OF 2	COPIES FOR	MASTERS FOR
		<input type="checkbox"/> 1 MO.	<input type="checkbox"/> 3 MOS.
		<input type="checkbox"/> 3 MOS.	<input type="checkbox"/> 6 MOS.
		<input type="checkbox"/> 6 MOS.	<input type="checkbox"/> 12 MOS.
		<input type="checkbox"/> MOS.	<input type="checkbox"/> MOS.
		<input type="checkbox"/>	<input type="checkbox"/> DO NOT DESTROY

3.3 Surface Quality

Fabrication tolerances to be assumed are:

Radii : ± 0.1 mm for 60 mm diameter sphere

Surface Figure : 1 ring power, 1/2 ring irregularity over 25 mm at 5899 Å.
Scratch and dig : 80/50

Approved by: *L R Paton*
AGCE Program Manager

PROGRAM INFORMATION REQUEST / RELEASE

*CLASS. LTR.	OPERATION	PROGRAM	SEQUENCE NO.	REV. LTR.
U	-1254	AGCE	020	
*USE "C" FOR CLASSIFIED AND "U" FOR UNCLASSIFIED				

FRC	S.L. Neste	TO	Distribution
DATE SENT	DATE INFO. REQUIRED	PROJECT AND REQ. NO.	REFERENCE DIR. NO.
4/24/81			

SUBJECT
TASK 8 - MATERIAL FOR THE OUTER SPHERE

INFORMATION REQUESTED/RELEASED

1.0 SUMMARY

Crystal Systems, Inc. was identified as the only producer of large sapphire boules of the size required for the AGCE. Presently, material to fabricate hemispherical shells with up to 4 cm inner radius can be provided with the optic axis and the centerline co-linear, while shells with inner radius of 7.5 cm can be made with the optic axis perpendicular to the centerline. Although larger boules may be available in the future, and permit construction of larger shells with co-linear optic axis and centerline, it is recommended that the need for co-linearity be assessed. Cost estimates for the sapphire boules range from \$6,000 (4 cm inner radius) to \$17,000 (7.5 cm inner radius).

Machining of the boules into hemispherical shells can be performed by either Insaco, Inc. or Frank Cooke, Inc., although better surface quality is guaranteed by Frank Cooke (+1 fringe power and 1/2 fringe irregularity vs. +5 fringe power and 2 fringe irregularity). The machining costs for the smallest hemisphere (4 cm inner radius) are \$12,000 and \$20,000 as estimated by Insaco and Cooke, respectively. For the largest size (7.5 cm inner radius) the respective costs are \$20,000 and \$30,000. It is recommended that an assessment of surface quality requirements be performed and used as the basis for selection of the machinist.

G. Fogal J. Homsey S. Neste W. Yager	PAGE NO.	<input checked="" type="checkbox"/> RETENTION REQUIREMENTS	
	OF	COPIES FOR	MASTERS FOR
		<input type="checkbox"/> 1 MO.	<input type="checkbox"/> 3 MOS.
		<input type="checkbox"/> 3 MOS.	<input type="checkbox"/> 6 MOS.
		<input type="checkbox"/> 6 MOS.	<input type="checkbox"/> 12 MOS.
		<input type="checkbox"/> MOS.	<input type="checkbox"/> MOS.
		<input type="checkbox"/>	<input type="checkbox"/> DO NOT DESTROY

Delivery time for the finished hemispherical shell will approach one year or more, depending on the specified size of the shell and the orientation of the optic axis.

2.0 BACKGROUND

The success of the AGCE experiment depends on being able to make flow velocity and temperature measurements in the relatively small, confined volume of fluid between the two concentric spherical shells. In the Geophysical Fluid Flow Cell (GFFC), which is conceptually similar to the AGCE, the outer and inner radii of the smaller and larger spheres were approximately 3.30 and 4.50 cm respectively. These dimensions provided a gap of about 1.20 cm in which the fluid was confined.

For AGCE applications it is desirable to increase the radii of the spheres while keeping the gap constant. This will facilitate flow measurement and reduce the effect of the radial variation of the electrostatic gravity. Since the observational and thermal requirements of the outer sphere will necessitate the use of a material such as sapphire, or spinel, the question arises as to whether or not such material is available in the dimensions required. The availability of material for the AGCE outer sphere, the limits on optical and surface quality and budgetary cost estimates for material and machining are provided in Section 3.0.

3.0 TASK IMPLEMENTATION

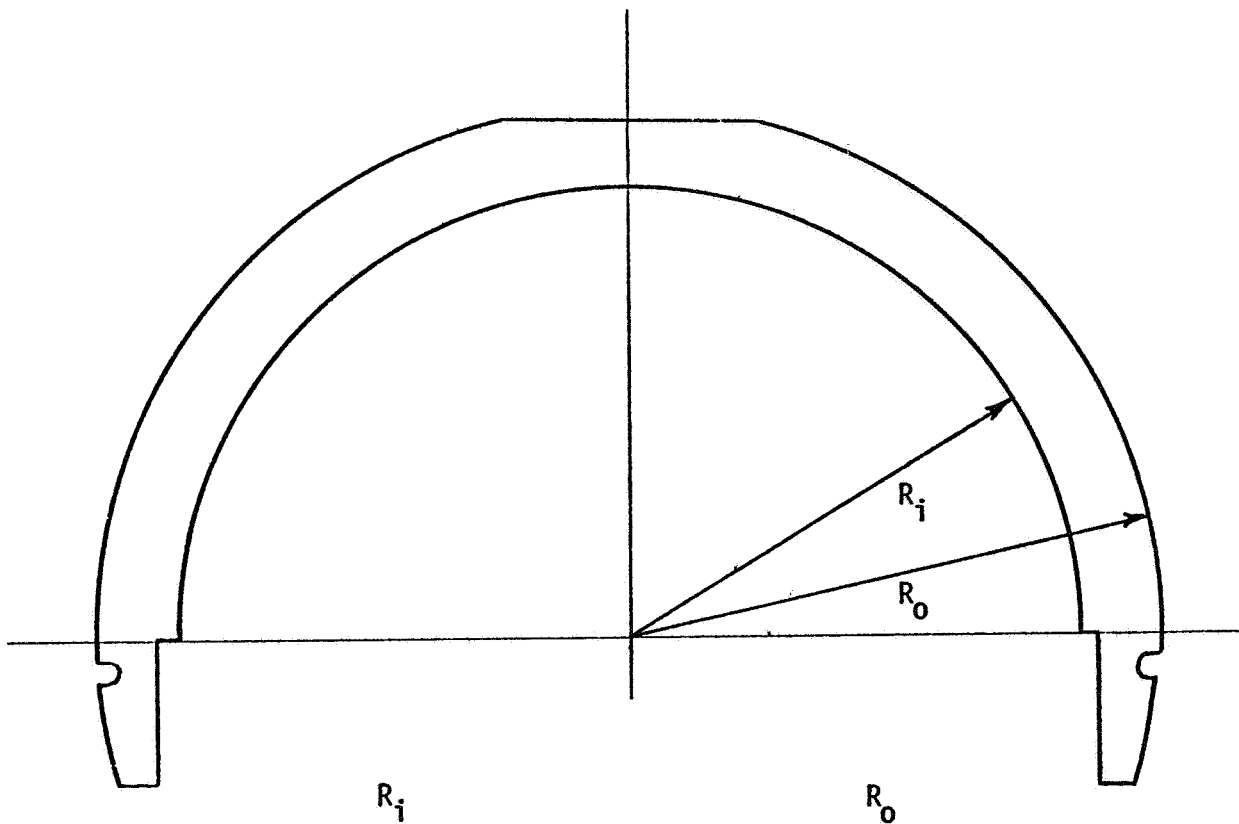
Letters were sent to Insaco, Inc. and Frank Cooke, Inc. who both specialize in machining of sapphire and are familiar with potential sources of large sapphire boules. Copies of the letters and their responses are given in Appendices A and B. This correspondence was also supplemented by telephone conversations with Mr. Frank Cooke and Mr. John Coleman (Insaco, Inc.). The size and optical requirements

specified to the vendors are given in Figure 1. The three hemisphere sizes were intended to span the range of sizes desired for the AGCE and to provide a trend of cost versus size. The specified optical requirements were the same as those stated for the GFFC outer hemispheres. Spinel was not considered as a potential material for the AGCE since both Mr. Cooke and Mr. Coleman stated that it would not provide the optical quality of sapphire, nor was it available in the large sizes required.

The results obtained from Cooke and Insaco are summarized in Table 1. Both stated that the only known supplier of large sapphire boules is Crystal Systems, Inc. (Appendix C). Although this supplier has recently encountered difficulties in producing larger boules of "good" optical quality, both Cooke and Insaco feel that in the future Crystal Systems may be able to produce the large sizes desired. The material costs in Table 1 are based on estimates obtained from Crystal Systems by Insaco, Inc.

Table 1
Cost Estimates for Material and Machining
of the AGCE Outer Hemisphere

	Hemisphere Size		Cost Quotes		
			Sapphire Material	Machining	
	Inner Radius	Outer Radius	Crystal Systems, Inc.	Insaco, Inc.	Frank Cooke, Inc.
1	4 cm	5 cm	\$ 6,000	\$12,000	\$20,000
2	6 cm	7 cm	\$10,250	\$13,750	\$25,000
3	7.5 cm	8.5 cm	\$17,000	\$20,000	\$30,000
4	5.35 cm	6.35 cm	\$ 9,100	\$13,900	-
5	6 cm	7 cm	\$11,000	\$15,000	-
6	6.6 cm	7.6 cm	\$15,000	\$19,000	-



Case 1.	4.00 cm \pm 0.01 cm	5.00 cm \pm 0.01 cm
Case 2.	6.00 cm \pm 0.01 cm	7.00 cm \pm 0.01 cm
Case 3.	7.50 cm \pm 0.01 cm	8.50 cm \pm 0.01 cm

REQUIREMENTS:

1. Edges and bevels to be fine grind.
2. Materials: synthetic sapphire, optical quality. No imperfections or inclusions larger than .010 in diameter permitted. Crystal axis co-linear with indicated centerline within 5°.
3. Scratch and dig 80-50. There shall be no evidence of grayness or stain on optical surfaces.
4. Surfaces of clear aperture shall be test plate fit within 1 fringe power and 1/2 fringe irregularity over a one inch diameter area using a standard mercury source.
5. Clear aperture: I.D. and O.D.

Figure 1. Hemisphere Size and Optical Requirements Used to Obtain Cost Estimates.

Based on the present capabilities of Crystal Systems only the smallest size (Case #1) in Table 1 is reliably expected to be available with the "C" or optical axis co-linear with the centerline. The other cases in Table 1 would have the C axis perpendicular to the centerline.

Nominal time required to produce these boules would be ~24 weeks. In the future, material may be available to produce hemispheres up to 7.6 cm outer radius in zero orientation (C axis parallel to centerline), but the delivery time for these large boules would increase to as much as 48 weeks. The machining time, which is fairly independent of size varies from ~12-15 weeks (Insaco, Inc.) to ~26 weeks (Frank Cooke, Inc.). Thus, the total procurement time for the AGCE outer hemisphere may approach or exceed a year. If the boule is broken during fabrication, both machinists will absorb the cost of labor, but the customer assumes the cost of replacing the material.

Mr. Cooke indicated that his machining costs could be reduced by ~\$5,000 if the "hemisphere" was made in two parts, a true hemisphere and an "attachment ring", which could then be bonded together. However, he felt the additional cost was worthwhile to avoid the bonding requirement and any problems which could result.

Both Mr. Cooke and Mr. Coleman (Insaco) pointed out that the changing crystal orientation and associated variation in material hardness around the circumference of the hemisphere make it difficult to achieve uniform surface quality over the entire hemisphere. Mr. Coleman, therefore, would only agree to a surface quality specification of ± 5 fringes power and 2 fringe irregularity, but stated that the surface quality would vary in a predictable manner and selected areas would have much better surface quality. Mr. Cooke, stated that although it would be difficult, he could meet the specifications of 1 fringe power and 1/2 fringe

irregularity as given in the letter request for quote.

4.0 CONCLUSIONS AND RECOMMENDATIONS

Presently, the only source for the large sapphire boules required for the AGCE is Crystal Systems, Inc. of Salem, MA, (617)745-0088. This was confirmed by both firms which were contacted to provide quotes for machining of the hemisphere. The ultimate size available with the centerline and "C" or optic axis co-linear cannot be firmly established at this time. However, if the birefringent effects associated with material in which the C axis is perpendicular to the centerline can be compensated by data processing, then obtaining the large hemispheres required is feasible. It is, therefore, recommended that the impact of this orientation be assessed to establish if co-linear optic axis and centerline are necessary.

Fabrication of the sapphire hemisphere can be performed by either Insaco, Inc. of Quakertown, PA, (215)536-3500 or Frank Cooke, Inc. of North Brookfield, MA, (617)867-2892. Although machining costs submitted by Insaco are considerably less, final selection should be based on an evaluation of the surface quality requirements. If the optimum optical surface is required, then Frank Cooke, Inc. should be selected. Mr. Cooke has a very good reputation for producing quality optical elements and was recommended by John Coleman of Insaco.

Delivery time for the finished hemispherical shell can be as long as a year, or more. Thus, high priority should be given to establishing the optical and size requirements of the hemisphere so that its procurement can be initiated early in any instrument development program.

APPENDIX A
CORRESPONDENCE WITH INSACO, INC.

GENERAL ELECTRIC

SPACE DIVISION

GENERAL ELECTRIC COMPANY

VALLEY FORGE SPACE CENTER

KING OF PRUSSIA PARK, P.O. BOX 8661, PHILADELPHIA, PENNA. 19101. TEL (215) 962-2000

18 February 1981

Mr. John Coleman
Insaco, Inc.
P.O. Box 422
Quakertown, PA 18951

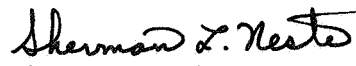
Dear Mr. Coleman:

As per our telephone conversation of 18 February 1981, I am requesting a budgetary estimate of the costs associated with material procurement and machining of a sapphire "hemispherical" shell meeting the nominal shape, dimensional and optical requirements specified on the attached sketch. In addition, it would be most helpful to us if you could provide an indication of the cost impact of the following:

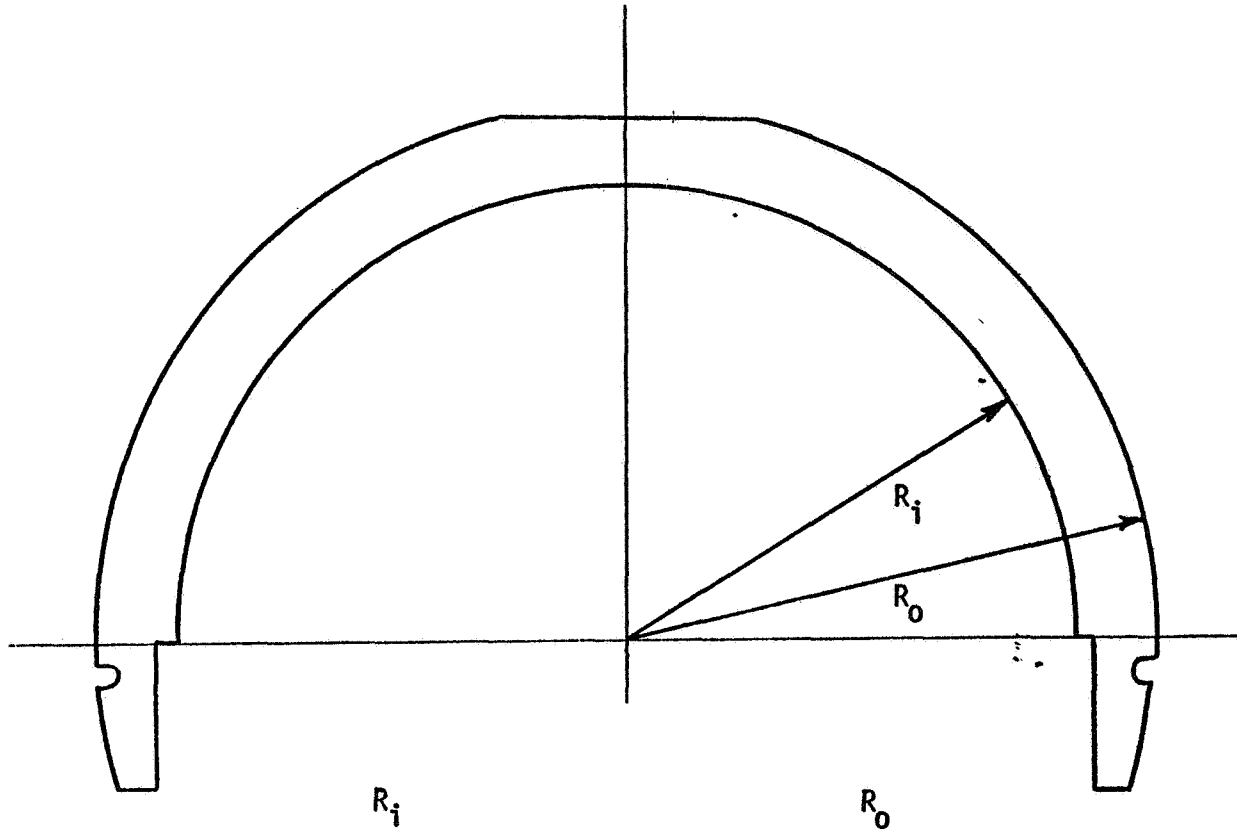
- | | | |
|--|---|---|
| 1) radii tolerance | } | assess increases and
decreases relative to
nominal values |
| 2) scratch and dig tolerance | | |
| 3) surface irregularity | | |
| 4) shell thickness | | |
| 5) producing a hemispherical shell with
crystal axis perpendicular to centerline. | | |

If a risk factor associated with unacceptable boule, or accidental breakage during machining is included, please specify. Do not hesitate to contact me for additional information or clarification if required.

Sincerely,


Sherman L. Neste
Senior Scientist
(215) 962-2153

SLN/jan
Encl.



Case 1.	4.00 cm \pm 0.01 cm	5.00 cm \pm 0.01 cm
Case 2.	6.00 cm \pm 0.01 cm	7.00 cm \pm 0.01 cm
Case 3.	7.50 cm \pm 0.01 cm	8.50 cm \pm 0.01 cm

REQUIREMENTS:

1. Edges and bevels to be fine grind.
2. Materials: synthetic sapphire, optical quality. No imperfections or inclusions larger than .010 in diameter permitted. Crystal axis co-linear with indicated centerline within 5°.
3. Scratch and dig 80-50. There shall be no evidence of grayness or stain on optical surfaces.
4. Surfaces of clear aperture shall be test plate fit within 1 fringe power and 1/2 fringe irregularity over a one inch diameter area using a standard mercury source.
5. Clear aperture: I.D. and O.D.

PRICE QUOTATION



**INSACO
INCORPORATED**

P O. Box **460**/Quakertown Pa. 18951 / Phone: 536-3500 (Area Code 215)

TWX Number: 510-661-5943

To

Mr. Sherman L. Neste
General Electric Co
Valley Forge Space Center
P. O. Box 8555
Philadelphia, Pa 19101

Date March 16, 1981

RFQ # Letter dated 2/18/81

QUOTE # 32688

We are pleased to quote on the following, subject to the terms herein:

QUANTITY	DESCRIPTION	UNIT PRICE
1 ea	Sapphire "Hemispherical" Shell 4 cm I.R. x 5 cm O.R. <u>#1</u> (1.575" I.R. x 1.9685" O.R.)	\$18,000.00 ea
1 ea	Sapphire "Hemispherical" Shell 6 cm I.R. x 7 cm O.R. <u>#2</u> (2.362" I.R. x 2.756" O.R.)	\$24,000.00 ea
1 ea	Sapphire "Hemispherical" Shell 7.5 cm I.R. x 8.5 cm O.R. <u>#3</u> (2.953" I.R. x 3.346" O.R.)	\$37,000.00 ea
1 ea	Sapphire "Hemispherical" Shell 5.35 cm I.R. x 6.35 cm O.R. <u>#4</u> (2.106" I.R. x 2.50" O.R.)	\$23,000.00 ea
1 ea	Sapphire "Hemispherical" Shell 6 cm I.R. x 7.00 cm O.R. <u>#5</u> (2.35" I.R. x 2.756" O.R.)	\$26,000.00 ea
1 ea	Sapphire "Hemipsheral" Shell 6.6 cm I.R. x 7.60 cm O.R. <u>#6</u> (2.6" I.R. x 2.992" O.R.)	\$39,000.00 ea \$34,000.00 ea
<p><u>Notes:</u> 1. Quote is Budgetary and will be firmed upon agreement of all requirements.</p> <p>Continued on next page This Price remains firm for 60 days</p>		


Delivery _____ Terms: Net 30 days — F.O.B. Point: Quakertown, Pa.

The prices and terms on this quotation are not subject to verbal changes or other agreements unless approved in writing by the Home Office of the Seller. All quotations and agreements are contingent upon strikes, accidents, fires, availability of materials and all other causes beyond our control. Prices are based on costs and conditions existing on date of quotation and are subject to change by the Seller before final acceptance.

Typographical and stenographic errors subject to correction. Purchaser agrees to accept either overage or shortage not in excess of ten percent to be charged for pro-rata. Purchaser assumes liability for patent and copyright infringement when goods are made to Purchaser's specifications. When quotation specifies material to be furnished by the purchaser, ample allowance must be made for reasonable spoilage and material must be of suitable quality to facilitate efficient production.

Conditions not specifically stated herein shall be governed by established trade customs. Terms inconsistent with those stated herein which may appear on Purchaser's formal order will not be binding on the Seller.

WE THANK YOU FOR YOUR INQUIRY, MAY WE HAVE THE PLEASURE OF SERVING YOU?


Name John H. Coleman, Sales
Title _____

PRICE QUOTATION



**INSACO
INCORPORATED**

P.O. Box 460/Quakertown Pa. 18951 / Phone: 536-3500 (Area Code 215)

TWX Number: 510-661-5943

To

Sherman L. Neste
General Electric Co
Philadelphia, Pa 19101

Date March 16, 1981

RFQ# _____

QUOTE# 32688

We are pleased to quote on the following, subject to the terms herein:

QUANTITY	DESCRIPTION	UNIT PRICE
	<p>Notes: Continued from first page</p> <ol style="list-style-type: none"> 2. Material will average quality which will have some light scatter when viewed under polarized light. Material will be state of the art quality and is available from only one source. Only for <u>Case #1</u> will material be available with the "C" or optic axis co-linear with centerline. 3. Quote is based on customer assuming cost of material if part is broken during fabrication. Insaco will absorb cost of labor if loss occurs during fabrication. 4. Delivery will be approx. 12 weeks AROM, material will require approx 24 weeks from date of order. Therefore final delivery is expected to be 36 weeks ARO. 5. Your Note #4 with respect 1 fringe power and 1/2 fringe irregularity will be held to ± 5 fringes power (using nominal size test glass) and 2 fringe irregularity. 6. Material may be available for up to 3.00" outside radius in zero orientation (C axis parallel to optic axis of lense). however delivery may be as long as 48 weeks for material plus 12 to 15 weeks for This Price remains firm for 60 days machining or greater than 1 year delivery ARO. 	

Delivery _____

Terms: Net 30 days — F.O.B. Point: Quakertown, Pa.

The prices and terms on this quotation are not subject to verbal changes or other agreements unless approved in writing by the Home Office of the Seller. All quotations and agreements are contingent upon strikes, accidents, fires, availability of materials and all other causes beyond our control. Prices are based on costs and conditions existing on date of quotation and are subject to change by the Seller before final acceptance.

Typographical and stenographic errors subject to correction. Purchaser agrees to accept either overage or shortage not in excess of ten percent to be charged for pro-rata. Purchaser assumes liability for patent and copyright infringement when goods are made to Purchaser's specifications. When quotation specifies material to be furnished by the purchaser, ample allowance must be made for reasonable spoilage and material must be of suitable quality to facilitate efficient production.

Conditions not specifically stated herein shall be governed by established trade customs. Terms inconsistent with those stated herein which may appear on Purchaser's formal order will not be binding on the Seller.

WE THANK YOU FOR YOUR INQUIRY, MAY WE HAVE THE PLEASURE OF SERVING YOU?

John A. Chum
Name _____
Title _____

APPENDIX B
CORRESPONDENCE WITH FRANK COOKE, INC.

GENERAL ELECTRIC

SPACE DIVISION

GENERAL ELECTRIC COMPANY

VALLEY FORGE SPACE CENTER

KING OF PRUSSIA PARK, P.O. BOX 8661, PHILADELPHIA, PENNA. 19101. TEL (215) 962-2000

25 March 1981

Frank Cooke, Inc.
59 Summer Street
North Brookfield, MA 01535

Dear Mr. Cooke:

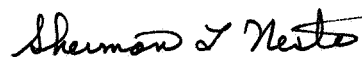
As per our telephone conversation of 25 March 1981, I am requesting a budgetary estimate of the costs associated with material procurement and machining of a sapphire "hemispherical" shell meeting the nominal shape, dimensional and optical requirements specified on the attached sketch. In addition, it would be most helpful to us if you could provide an indication of the cost impact of the following:

- | | | |
|--|---|---|
| 1) radii tolerance | } | assess increases and
decreases relative to
nominal values |
| 2) scratch and dig tolerance | | |
| 3) surface irregularity | | |
| 4) shell thickness | | |
| 5) producing a hemispherical shell with
crystal axis perpendicular to centerline. | | |

If a risk factor associated with unacceptable boule, or accidental breakage during machining is included, please specify.

In addition, if you feel there is a "reasonable" potential for producing larger hemispheres built up from segments, we would also be interested in your concepts and an ROM cost estimate for that. Do not hesitate to contact me for additional information or clarification if required.

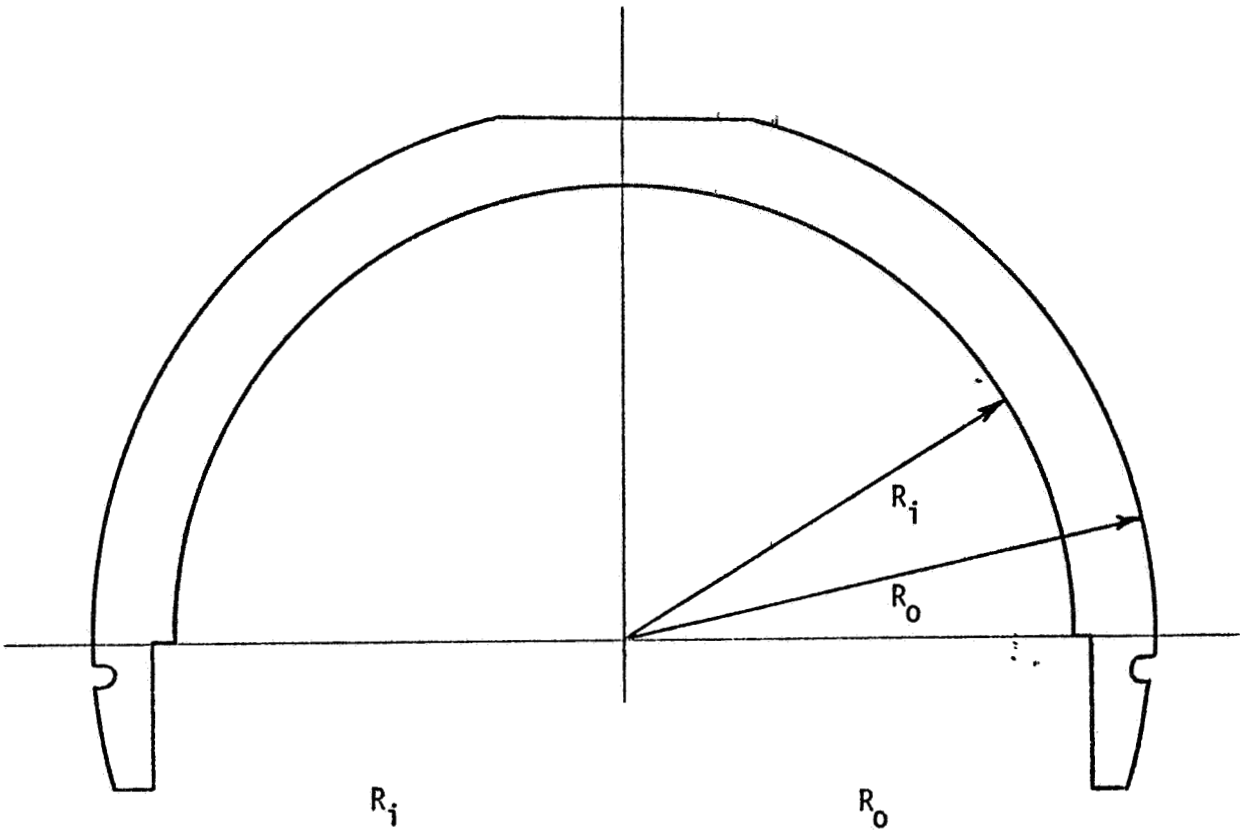
Sincerely,



Sherman L. Neste
Senior Scientist
(215) 962-2153

SLN/jan

Enclosure



Case 1.	4.00 cm \pm 0.01 cm	5.00 cm \pm 0.01 cm
Case 2.	6.00 cm \pm 0.01 cm	7.00 cm \pm 0.01 cm
Case 3.	7.50 cm \pm 0.01 cm	8.50 cm \pm 0.01 cm

REQUIREMENTS:

1. Edges and bevels to be fine grind.
2. Materials: synthetic sapphire, optical quality. No imperfections or inclusions larger than .010 in diameter permitted. Crystal axis co-linear with indicated centerline within 5°.
3. Scratch and dig 80-50. There shall be no evidence of grayness or stain on optical surfaces.
4. Surfaces of clear aperture shall be test plate fit within 1 fringe power and 1/2 fringe irregularity over a one inch diameter area using a standard mercury source.
5. Clear aperture: I.D. and O.D.

FRANK COOKE, INC.

59 Summer Street
North Brookfield, Massachusetts 01535

Optics for the Infrared
Special Optical Elements
Optical Machinery

617-867-2892
617-867-9210

April 7, 1981

General Electric Company
Valley Forge Space Center
P.O. Box 8555
Philadelphia, Pa. 19101

Att: Sherman L. Neste -Senior Scientist

Dear Mr. Neste: Re: Letter of 25 March 1981

We are willing and able to make this sapphire dome covered by your above subject letter.

While not poor we do not have sufficient capital to cover the cost of this sapphire boule.

By using a design similar to a modern geodesic dome almost any Sapphire Dome can be made. The problem of estimating the cost of this construction is beyond us but we know it can be done.

It would greatly facilitate if the dome stopped at the equator instead of a hyper-hemisphere. Can this be done?

An early reply would be appreciated.

Sincerely,

FC
Frank Cooke *FC*

FC/s



SPACE DIVISION

GENERAL ELECTRIC COMPANY VALLEY FORGE SPACE CENTER
(MAIL P. O. BOX 8555, PHILADELPHIA, PENNSYLVANIA 19101), Phone (215) 962-2000

10 April 1981

Frank Cooke, Inc.
59 Summer Street
North Brookfield, MA 01535

Dear Mr. Cooke:

Re: Letter of 7 April 1981

We have considered your comments regarding termination of the sapphire dome at the equator as opposed to extending it as indicated in the sketch. The portion of the dome below the equator is required to provide an attachment surface for mating the dome to the main experiment apparatus, but it need not be optical quality material. The possibility exists for making the dome in two pieces: (1) a hemisphere and (2) an "attachment ring" of a shape similar to that portion of the dome extending below the equator. However, it must be possible to achieve a leak free bond between the two pieces and maintain thermal continuity across the boundary. It may also be possible to use a material other than sapphire for the attachment ring if that is simpler from a machining standpoint and if the above conditions can be met.

We would appreciate a cost estimate for both approaches as well as your assessment of the problems involved in material procurement and machining, and the quality of the end product, in each case. Please call me if additional information is required.

Sincerely,

A handwritten signature in cursive script that reads "Sherman L. Neste".

Sherman L. Neste
Environmental Physicist
Room M9521, 215-962-2153

SLN/grv

FRANK COOKE, INC.

59 Summer Street
North Brookfield, Massachusetts 01535

Optics for the Infrared
Special Optical Elements
Optical Machinery

617-867-2892
617-867-9210

April 17, 1981

General Electric Company
P.O. Box 8555
Philadelphia, Pa. 19101

Att: Sherman L. Neste - Environmental Physicist

Dear Mr. Neste: Re: Letter of 10 APRIL

In reply to your above subject letter concerning sapphire domes, if the dome is being used in a high temperature environment what cement should we use for the attachment ring?

If G. E. would furnish the material we would be willing to make a dome of Case I for approximately\$15,000.00.

We note a flat at the apex of the convex side. Is this intentional?

The above price is less coating.

Sincerely,

Frank Cooke

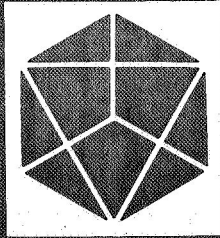


FC/s

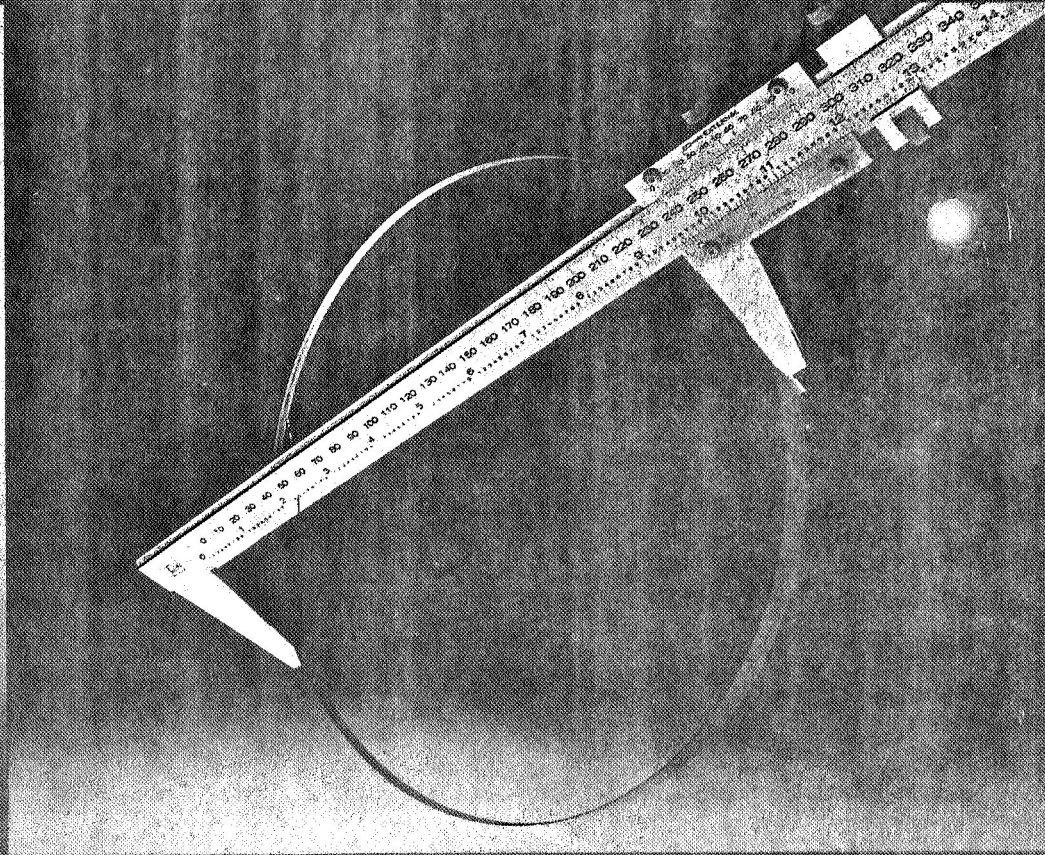
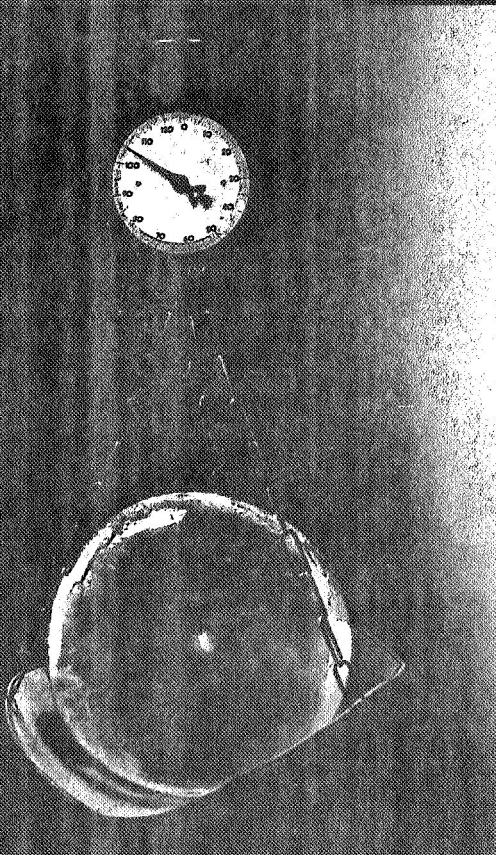
APPENDIX C

DATA SHEETS FROM CRYSTAL SYSTEMS, INC.

**CRYSTAL
SYSTEMS**



ORIGINAL PAGE IS
OF POOR QUALITY



**Largest sapphire in the world
being produced economically and
light-scatter free by
the Heat Exchanger Method**

PROPERTIES OF SAPPHIRE

PHYSICAL

Chemical formula
Crystal structure
Unit cell dimension
Density
Hardness

Melting point
Boiling point

Al_2O_3
Hexagonal system (Rhombohedral)
 $a = 4.758 \text{ \AA}$, $c = 12.991 \text{ \AA}$
 3.98 gm/cm^3
9 mohs
1525-2000 Knoop
2040°C
2980°C

ORIGINAL PAGE IS
OF POOR QUALITY

MECHANICAL

Tensile strength
at 25°C
at 500°C
at 1000°C

Bulk modulus
Young's modulus (60° to c)
Modulus of rigidity
Modulus of rupture
Poisson's ratio

60,000 psi (design criterion)
40,000 psi (design criterion)
50,000 psi (design criterion)
 35×10^6
 50×10^6 psi
 21.5×10^6 psi
65,000 - 100,000 psi
0.25

THERMAL

Thermal conductivity (60° to c) at 25°C
Thermal expansion coefficient
(60° to c) 25° - 800°C
Specific heat at 25°C
Heat capacity at 25°C

0.065 cal/cm-sec-°C
 8.40×10^{-6} per °C
0.10 cal/gm
18.6 cal/°C-mole

ELECTRICAL

Volume resistivity
Dielectric strength
Dielectric constant (E ⊥ c)
(E || c)
Dissipation factor, tan δ

10^{14} ohm-cm
48,000 volt/cm
9.4
11.5
 10^{-4}

OPTICAL

Transmission is dependent on the reflection and absorption losses as shown:

$$\text{Reflection at one surface } r = \frac{(n-1)^2}{(n+1)^2}, \text{ } n \text{ refractive index (Table I)}$$

For transmission through two surfaces without absorption

$$T = (1-r)^2$$

For wavelengths and thickness x where absorption occurs

$$T = \frac{(1-r)^2 e^{-\alpha x}}{1-r^2 e^{-2\alpha x}}, \text{ } \alpha \text{ absorption coefficient (Figure 1)}$$

WAVELENGTH (Microns)	Refractive Index, Ordinary Ray (at 24°C)
0.26520	1.83360
0.28035	1.82427
0.29673	1.81695
0.3130	1.80906
0.34662	1.79815
0.365015	1.79358
0.404656	1.78582
0.546071	1.77078
0.579066	1.76871
0.64385	1.76547
0.706519	1.76303
0.89440	1.75796
1.01398	1.75547
1.12866	1.75339
1.6932	1.74368
2.24929	1.73232
3.3026	1.70231
4.2553	1.66371
5.577	1.58642

TABLE I. Index of Refraction n for Sapphire vs. Wavelength. Index of Extraordinary ray approximately 0.008 less than for ordinary ray ¹

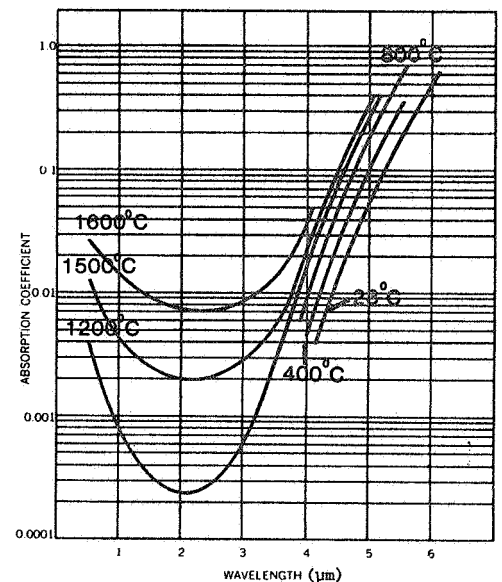


Figure 1 Absorption Coefficient α for Sapphire in the Infrared as a Function of Temperature. ¹

Note 1 Compiled from J. Opt. Soc. Amer. I.H. Malitson, 52 (12) 1377 (1962); B. A. Burch, 59, 625 (1965).

APPLICATIONS OF SAPPHIRE

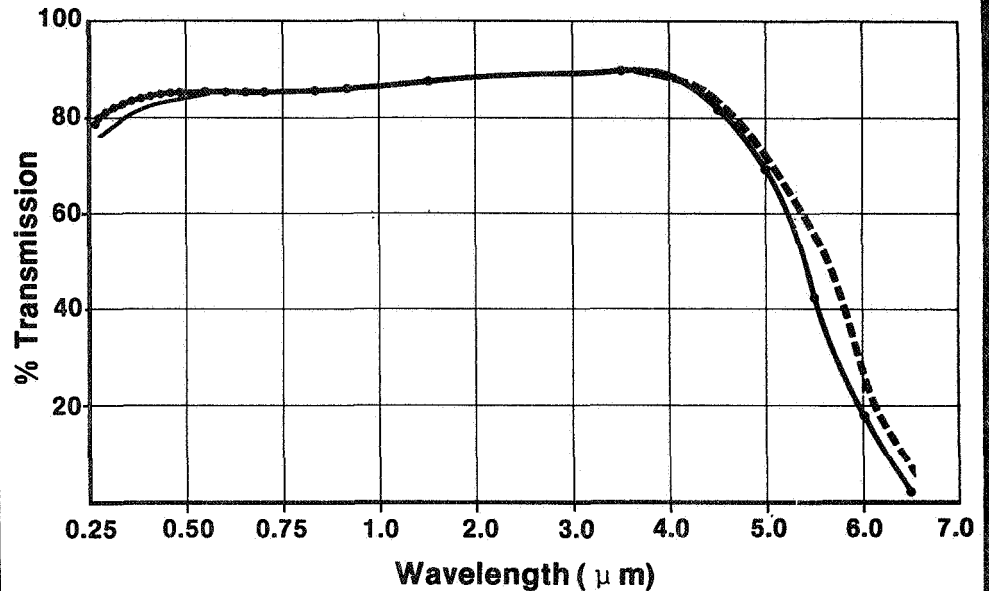
Sapphire, free of light scatter, is available only from Crystal Systems. Boules up to 12 inches diameter, 5 inches thick, can be provided in (1120), (10 $\bar{1}$ 0) and (1 $\bar{1}$ 02) orientations. For zero birefringence optics, (0001) orientation, up to 5-inch diameter rods are available. Large crystals can be fabricated to satisfy a variety of technological needs.

OPTICAL

Sapphire's size availability with zero light scatter, coupled with its broad optical transmission band, high strength, hardness, and chemical stability even at high temperature, makes it an exceptional optical material.

It is a choice window material for high temperature and severe environments. A high melt point, good thermal conductivity and low expansion permit high temperature use and rapid temperature change. In addition, it is nearly insoluble in water and common acids, and has excellent rain erosion resistance. Typical applications are IR, visible, UV, high pressure and high temperature windows, optical lenses, prisms, filters, and beam-splitters.

TRANSMISSION OF
CRYSTAL SYSTEMS HEM SAPPHIRE



— 3 mm thickness, 5 Å rms roughness (TIS) - - - 3 mm thickness, 100 Å rms roughness (TIS) ···· 2.25 mm thickness, 100 Å rms roughness (TIS)

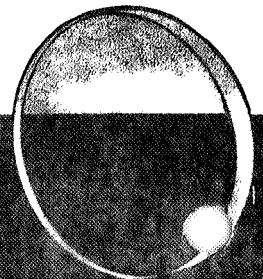
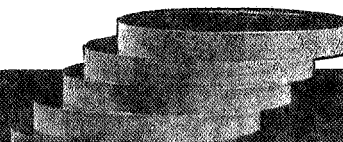
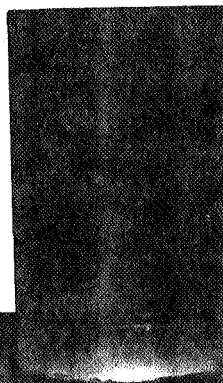
ELECTRONIC MECHANICAL

Sapphire is also an ideal material for electronic substrates, having zero porosity, high dielectric strength and low loss. Applications are SOS, MIC, and hybrid substrates.

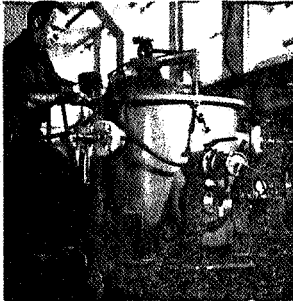
This extremely hard material, third only to diamond, can be polished to a pore- and scratch-free surface for low friction wear surfaces. Typical applications are jewel and precision bearings, nozzles and wear flats.

Sapphire components custom fabricated are acoustic rods, tubes for maser cavities, transparent armor, point-of-sale windows, and optical flats.

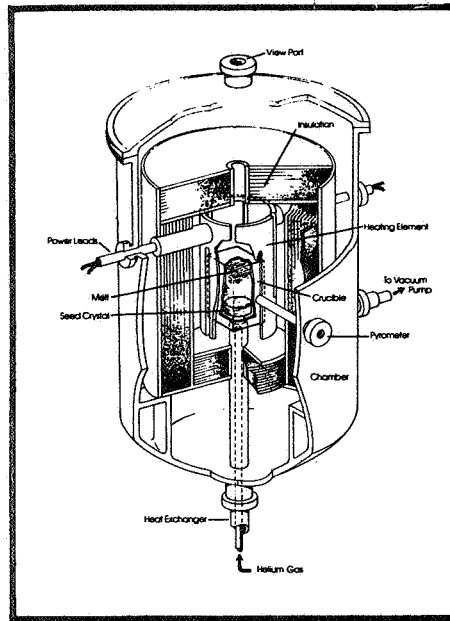
ORIGINAL PAGE IS
OF POOR QUALITY



ORIGINAL PAGE IS
OF POOR QUALITY



Crystal Systems uses its patented Heat Exchanger Method (HEM) to grow large crystals. By this unique motionless crystal growth process, temperature fluctuations are minimized promoting highly uniform growth and high crystal-line perfection.



HEM FURNACE

Scatter-free crystals result from the unique ability to grow in a vacuum environment. **In situ** growth permits post-solidification anneal and controlled cool-down of very large crystals.

Because of HEM's simplicity, higher quality crystals can now be grown to larger size at reduced cost.

R & D DIVISION

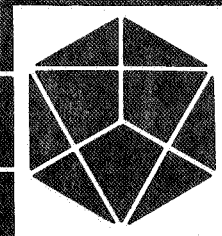
Crystal Systems R&D Division has successfully adapted the unique Heat Exchanger Method (HEM) to commercial production of silicon for solar and optical application. It has a proven capability to extend R&D developments to the production and marketing of important industrial crystals.

A new slicing method—FAST (Fixed Abrasive Slicing Technique)—has been developed for wafering of expensive materials, with minimum thickness, kerf and surface damage.

For contract research on sapphire, silicon, and other materials, direct your inquiry to Crystal Systems R&D Division.

For any of your sapphire requirements—rod stock, bar stock or finished components—contact Crystal Systems.

CRYSTAL SYSTEMS INC.
SHETLAND INDUSTRIAL PARK
35 CONGRESS STREET, SALEM, MA 01970
(617) 745-0088



3.2 OPTICS FOR DATA RETRIEVAL

	<u>PIR NO.</u>
Task 4 and 5: Flying Spot Scanner Design Requirements	-007
Final Report: Task 4 and 5, AGCE Feasibility Study	-011
Effect of Thermal Gradient in the Sapphire Shell	-024
Effects of Birefringence in the Sapphire Shell	-027
Futher Note on Sapphire Birefringence	-033

)

)

)

GENERAL ELECTRIC

SPACE DIVISION
PHILADELPHIA

PROGRAM INFORMATION REQUEST / RELEASE

*CLASS. LTR.	OPERATION	PROGRAM	SEQUENCE NO.	REV. LTR.
U	1254	AGCE	07	

PIR NO. U - 1254 - AGCE - 07
*USE "C" FOR CLASSIFIED AND "U" FOR UNCLASSIFIED

FROM	TO
W. C. Yager M9423, x4235	DISTRIBUTION

DATE SENT	DATE INFO. REQUIRED	PROJECT AND REQ. NO.	REFERENCE DIR. NO.
1/29/81			

SUBJECT
TASK 4 and 5: FLYING SPOT SCANNER DESIGN REQUIREMENTS

INFORMATION REQUESTED/RELEASED

See attached text.

L. R. Eaton G. Fogal S. Neste W. Yager	PAGE NO. 1 OF 6	RETENTION REQUIREMENTS	
		COPIES FOR	MASTERS FOR
		<input type="checkbox"/> 1 MO.	<input type="checkbox"/> 3 MOS.
		<input type="checkbox"/> 3 MOS.	<input type="checkbox"/> 6 MOS.
		<input type="checkbox"/> 6 MOS.	<input type="checkbox"/> 12 MOS.
		<input type="checkbox"/> MOS.	<input type="checkbox"/> MOS.
		<input type="checkbox"/>	<input type="checkbox"/> DO NOT DESTROY

ORIGINAL PAGE IS
OF POOR QUALITY

TASK 4 AND 5

1.0 SCOPE

This document sets forth some preliminary specifications for the optical and electro-optical design of the flying-spot scanner (FSS) subsystem of the AGCE. These are tentative, and are intended only for guidance in preliminary design and feasibility assessment.

2.0 GENERAL

The FSS is intended to scan the surface of the AGCE test cell, detect the presence of drifting marker dots, and measure the two non-radial components of thermal gradient in the interstitial fluid. The FSS also supplies a latitude encoder signal that, in combination with a test cell longitude encoder, locates the scanner spot on the surface of the test cell. The FSS is intended to deliver marker, gradient, and latitude signals to a signal processor for subsequent conditioning (which may include digitization) and electronic recording.

3.0 PERFORMANCE SPECIFICATION

3.1 Test Cell Fabrication

The geometry of the rotating test cell that must be scanned is assumed to be as shown in Figure 1. Fabrication tolerances to be assumed are:

radii : +/- 0.1 mm

surface figure : 1 ring power, $\frac{1}{2}$ ring irregularity, over
25 mm diameter at 5893A

scratch and dig : 80/50

The outer shell of the test cell shown in Figure 1 will be fabricated from synthetic sapphire. The optical axis will be assumed parallel to the axis of rotation within 5° . Optical properties to be assumed for sapphire are those tabulated in the OSA Handbook of Optics.

The inner sphere will be assumed to be specularly reflective and to exhibit the reflectivity of aluminum (85%).

The interstitial fluid will be assumed to exhibit a refractive index of $n_D = 1.478$.

The inner surface of the sapphire shell will be assumed to be coated with a transparent conductive coating.

3.2 Test Cell Rotation

The maximum rate of test cell rotation will be assumed to be 3.0 radians/sec. The minimum rate will be assumed to be 0.25 radians/sec.

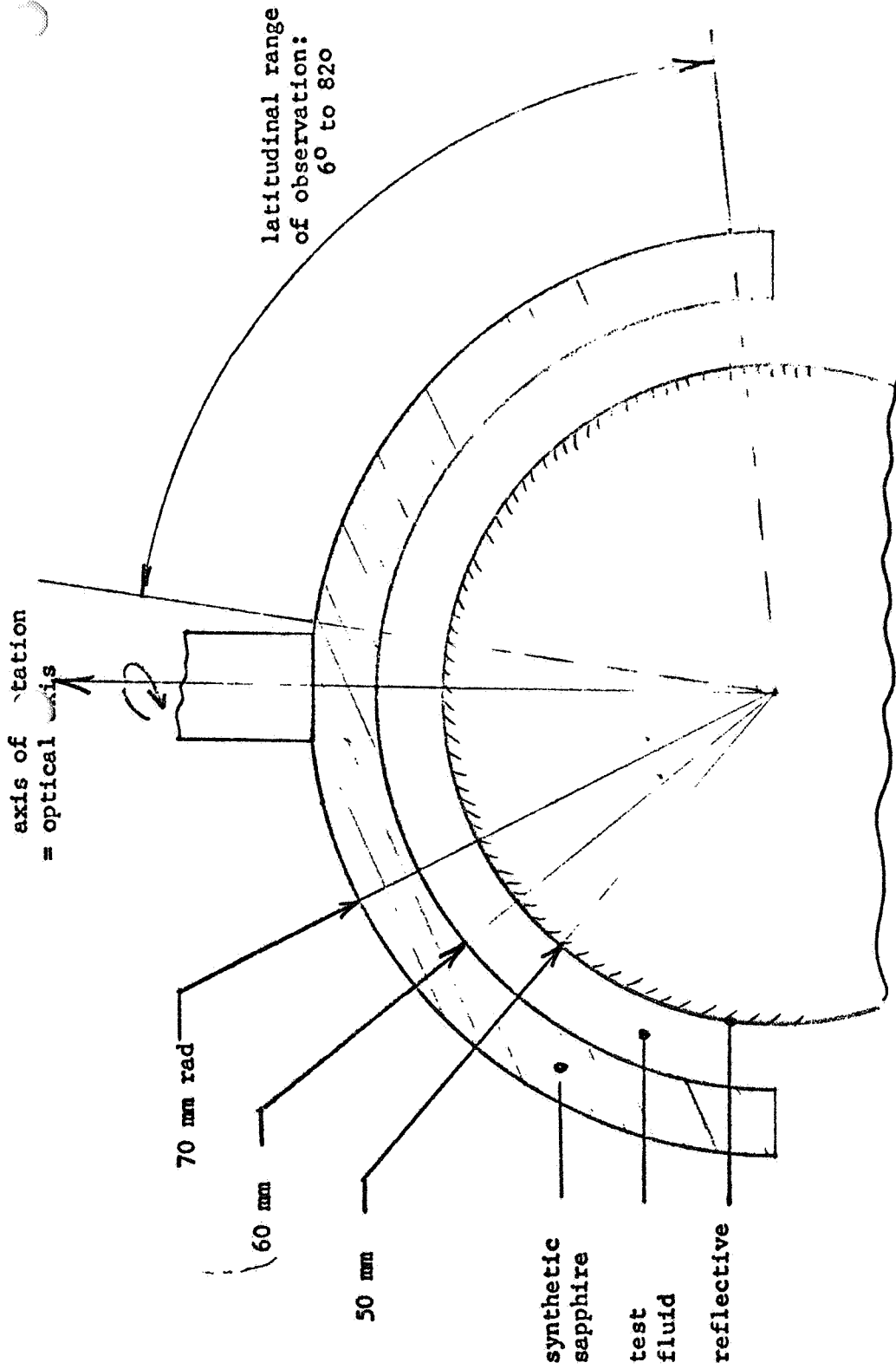


FIGURE 1. ASSUMED BASIC LAYOUT OF AGCE TEST CELL

3.3 Scan Pattern

The FSS will be assumed to scan in meridional arcs from latitude 82° to latitude 6° , covering most of a full hemisphere in one revolution. The scanner itself will provide only motion along the meridian. Motion transverse to the meridian will be provided by rotation of the test cell. It is assumed the scan rate will be adjusted to the rotation rate so as to provide a geometrical pattern of scan that is independent of the cell rotation rate.

3.4 Scanner Spot Size

The scanner will be designed to produce a spot of light on the inner reflective sphere a nominal 1 mm in diameter.

3.5 Scanner Optical Design

The scanner optics will be designed for a spectrum centered on the sodium D line, 5893A. Insofar as possible, all materials will be glass, selected from among the preferred glass types of the Schott catalog. Constructional tolerances for the scanner optics will be identical to those for the test cell (3.1, above).

3.6 Dynamic Range

The FSS will be potentially able to measure index gradients in the interstitial fluid from 0.0005 cm^{-1} to 0.00005 cm^{-1} . Assuming an index thermal coefficient of $0.0005/^{\circ}\text{C}$, this will represent a thermal gradient of from $1^{\circ}/\text{cm}$ to $0.1^{\circ}/\text{cm}$.

3.7 Gradient Sensitivity

The design goal will be a noise-equivalent gradient of 10% of the lower limit of the dynamic range, above.

3.8 Spot Detection Sensitivity

It will be a design goal that the scanner be able to detect the presence of a photochromic marker dot whose opacity is sufficient to reduce transmitted light to 80% of its value in the absence of the dot.

4.0 INTERFACE REQUIREMENTS

4.1 Mechanical Interface

The minimum clearance between the rotating sphere and the FSS will be 1 mm.

4.2 Power Interface

The power requirements of the FSS, including light source, detector/preamplifier, motor and encoder, must be compatible with the AGCE power supply.

4.3 Signal Interface

The gradient detector signal will be an analog voltage, linearly proportional to gradient. The marker dot detector signal will be a pulse. The latitude encoder signal will be digital. All signal levels will be compatible with AGCE control and data handling electronics.

Approved by: _____
AGCE Program Manager

GENERAL ELECTRIC

SPACE DIVISION
PHILADELPHIA

*CLASS. LTR.	OPERATION	PROGRAM	SEQUENCE NO.	REV. LTR.
U	_ 1254	_ AGCE	_ 11	

PIR NO.

*USE "C" FOR CLASSIFIED AND "U" FOR UNCLASSIFIED

PROGRAM INFORMATION REQUEST / RELEASE

M

W. C. Yager M9423 x4235

TO

L. R. Eaton

DATE SENT 2/24/81	DATE INFO. REQUIRED	PROJECT AND REQ. NO.	REFERENCE DIR. NO.
----------------------	---------------------	----------------------	--------------------

SUBJECT
FINAL REPORT: TASKS 4 and 5, AGCE FEASIBILITY STUDY

INFORMATION REQUESTED/RELEASED
See attached text.

Distribution: L. Eaton
G. Fogal
C. Mosley
S. Neste
W. Yager

PAGE NO.

121 pp

OF

RETENTION REQUIREMENTS

COPIES FOR	MASTERS FOR
<input type="checkbox"/> 1 MO.	<input type="checkbox"/> 3 MOS.
<input type="checkbox"/> 3 MOS.	<input type="checkbox"/> 6 MOS.
<input type="checkbox"/> 6 MOS.	<input type="checkbox"/> 12 MOS.
<input type="checkbox"/> MOS.	<input type="checkbox"/> MOS.
<input type="checkbox"/>	<input type="checkbox"/> DONOT DESTROY

ORIGINAL PAGE IS
OF POOR QUALITY

CONTENTS

1.0	SUMMARY.....	1
2.0	BACKGROUND.....	2
3.0	TASK IMPLEMENTATION.....	3
3.1	Design Concept.....	3
3.2	Elimination of Birefringence...	11
3.3	Assumptions and Constraints....	13
3.4	Effects of Thermal Gradient....	18
3.5	Preliminary Design.....	41
3.6	Performance Analysis.....	64
3.7	Alternative Video Methods.....	96
4.0	CONCLUSIONS & RECOMMENDATIONS..	98
5.0	APPENDICES.....	101

1.0 SUMMARY

This study has shown that the measurement requirements of the AGCE can be met by a relatively simple instrument of the flying-spot scanner type. A preliminary design--by no means optimized--has been shown capable of surveying one hemisphere of the rotating test cell at 1° resolution over a 69° span of latitude. This scanner can observe and measure the two non-radial components of thermal gradient in the test fluid with $0.01^\circ\text{C}/\text{cm}$ resolution at a SNR of at least 6. Photochromic marker dots can be observed simultaneously with a SNR in the hundreds. The same detectors can also feed a CCTV display for the payload specialist, with a similar SNR in the hundreds. With further design effort, both scan angle and SNR can be significantly improved.

This flying-spot scanner instrument is fundamentally simple in design, and should be realizable at modest cost. Volume and weight will be small in comparison with the rest of the experimental apparatus. The preliminary optical design developed for this study has been shown through raytracing to exhibit outstanding image quality and to yield a signal that is linear with thermal gradient over at least two decades of dynamic range. The study has also shown what direction to take in further improving the design, especially with respect to increasing the latitude scan angle and the signal-to-noise ratio.

2.0 BACKGROUND

As with its predecessor, the GFFC, the general objectives of the AGCE are to generate time-sequential maps of both fluid circulation and thermal gradient over substantially a full hemisphere of a rotating test cell that models the earth's atmosphere. Given that electronic data recording is allowed to replace the photographic recording used in the GFFC, the General Electric Company has argued that both of these objectives can be realized with a single small instrument, basically a flying spot scanner. General Electric has also argued that the signals from this same instrument can serve to feed a slow-scan TV system that can provide a payload specialist with a real-time synoptic view of the rotating model. All these functions are possible, it has further been argued, while also providing better quality data and major cost savings in data reduction.

It is the purpose of this task (contract tasks 4 and 5 combined) to develop a preliminary design of such a flying spot scanner instrument and demonstrate analytically that it does indeed have the potential that has been claimed for it.

3.0 TASK IMPLEMENTATION

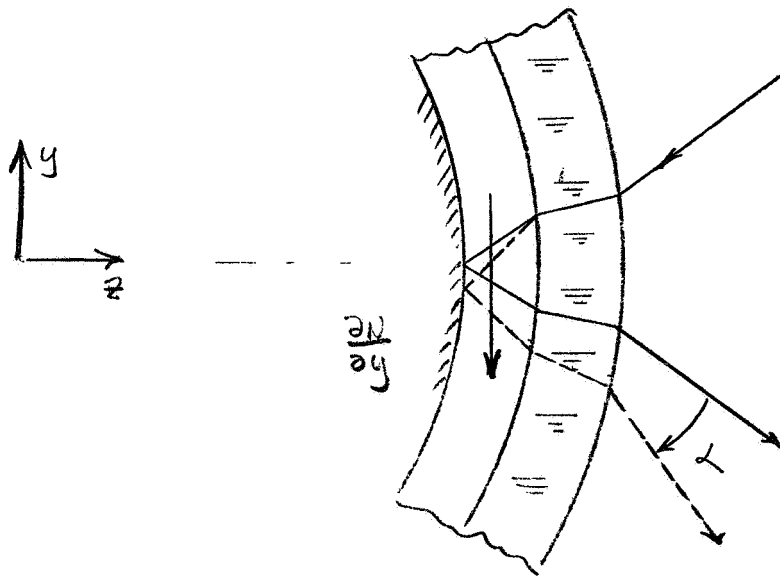
3.1 Design Concept

When electronic data recording is considered as an alternative to photographic data recording, the implications are much more general than simply replacing one medium with another. Since to be recorded electronically the data must be in the form of electrical signals, it makes sense to enquire whether the basic observational data can be generated in electrical form originally. If this is possible, the entire experimental apparatus might be drastically simplified and the performance itself improved by eliminating unnecessary stages of data conversion.

In the GFFC apparatus, a fixed, extended source is brought to a focus at the reflective surface of the inner sphere. As shown in Figure 1, an index gradient in the enclosed fluid will cause the incident rays to be deviated. This deviation is rendered visible as a (moire) pattern of geometrical interference between gratings, photographically recorded. Thermal gradient and its surface locus are then determined by decoding the photograph.

Photographic methods such as this are needed when ray deviation and surface locus cannot be determined directly. When electronic recording is admitted, however, the way is open to determine both

ORIGINAL PAGE IS
OF POOR QUALITY

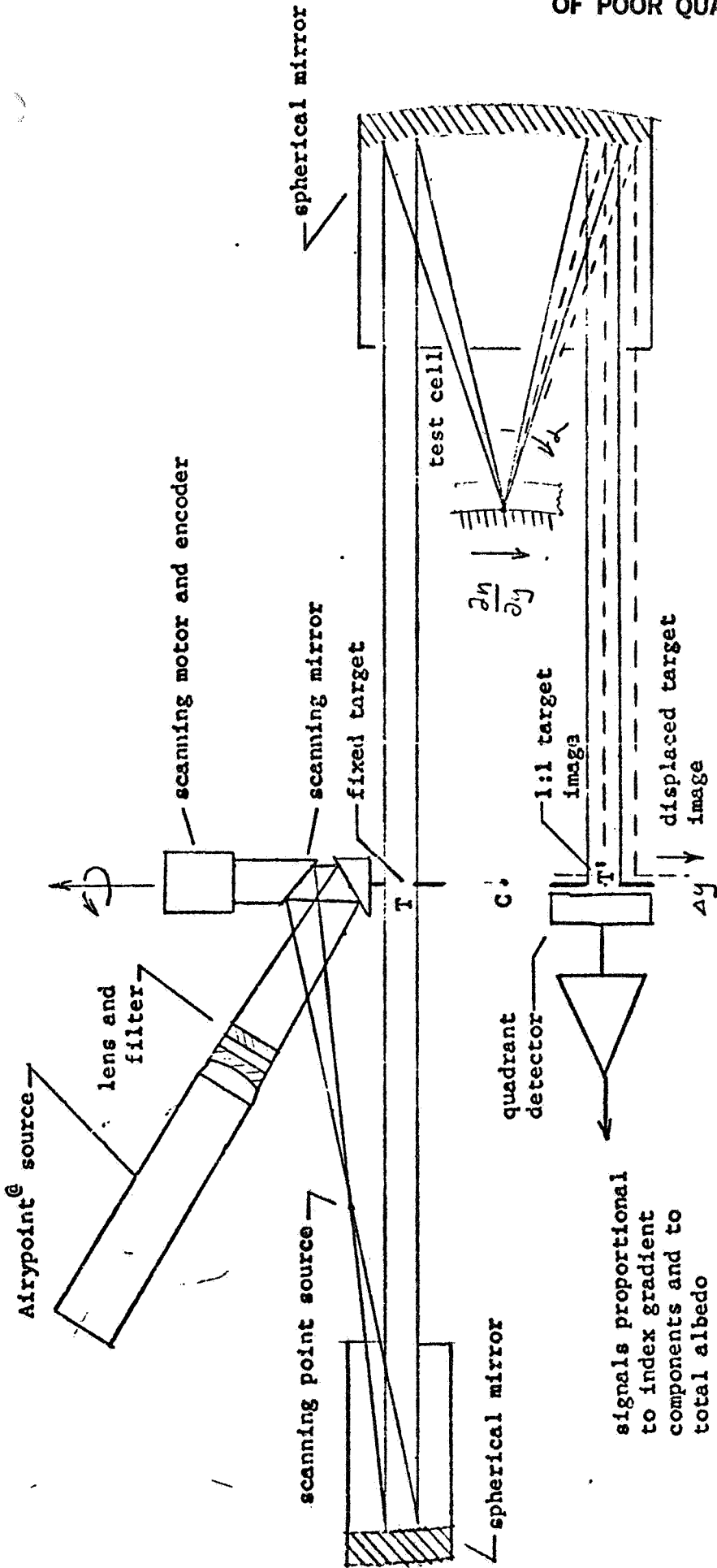


ANGULAR RAY DEVIATION DUE TO INDEX GRADIENT

Figure 1

directly by relatively simple means, and the artifice of schlieren photography becomes unnecessary. A great deal of data reduction effort is avoided by eliminating the schlieren photograph stage.

A more direct and accurate method of thermal mapping would employ a flying spot scanner, one possible form of which is illustrated in Figure 2. In this system the virtual image of the reflective inner surface is projected to infinity by a second, concentric mirror. It has been shown by Offner (see References 12 through 15) that such a monocentric pair can image a target near the common center at unit magnification in a manner substantially free of all third order aberrations. If now this target is illuminated by a rotating collimator sharing the same vertical axis, the light passing through the target will be brought to a sharply focussed spot on the inner reflective sphere, then returned to the target image. As the illuminator rotates, the scanning spot will sweep out a thin arc of a great circle on the surface of the inner sphere. If thermal gradients (manifested as refractive index gradients) are present in the fluid, the light passing through the focussed spot will be significantly deviated in direction, but the location of the spot



THERMAL GRADIENT MEASUREMENT CONCEPT (unfolded)

Figure 2

will be only slightly affected. The result is that the direction of the rays returning to the target image will be altered only very slightly, but the target image itself will translate significantly. This translation is two-dimensional and directly related to the index gradient vector in the fluid. For the changes expected here it is also directly proportional to the magnitude of the thermal gradient vector. Two orthogonal components of the index gradient vector can be measured directly, in terms of image displacement, by a suitable detector array placed at the target image position. Since simultaneous encoder readings identify the surface location of the flying spot, all information needed to develop a surface thermal map is available directly in electrical form, suitable for electronic recording.

A thermal mapping instrument like that of Figure 2 offers many advantages that commend it for application to this problem. First of all, it completely bypasses the need for intermediate coding of gradient and locus, which photographic methods are designed to achieve, and consequently saves much time and effort in data reduction. All mapping information is in electrical form and can be recorded

**ORIGINAL PAGE IS
OF POOR QUALITY**

directly for subsequent automatic processing or plotting. Second, performance measured in coverage, resolution and dynamic range will generally exceed that available by schlieren photographic methods. Finally, the instrument itself is very compact and lightweight, and can be expected to use little power.

Apart from these attractive features for thermal mapping, this instrument has the further very great advantage that it can also perform the surface flow mapping at the same time it does the thermal mapping. It thus offers the attractive possibility of doing all the experimental data gathering and recording with a single very small instrument.

In this experiment surface flow is described entirely in terms of the drift of photochromic markers in the fluid. Any means of locating a marker dot in both surface coordinates and time can therefore accomplish flow mapping. The flying spot scanner just described can do exactly that. In this case one would make use of the total return at the detector, whose magnitude is a measure of surface albedo. A sudden drop in that total signal, detected by a differentiation circuit, identifies

the presence of an opaque marker dot at the locus of the scanner spot. If then both deflection signals and total signal derivative are recorded simultaneously with scanner and model encoder signals, both surface flow and surface thermal maps will have been recorded in a form lending itself to subsequent automatic processing and plotting.

The data normally written on the film along with the schlieren or surface images in the GFFC are of course available in electrical form and can be recorded electronically along with the detector output. With electronic recording there is no need to go through the extra stage of converting these electrical signals to images.

The flying spot scanner can also furnish the payload specialist with a substantially real-time synoptic view of the surface. The scanner sweeps an entire hemisphere in the form of thin meridional zones. Each scan can be displayed as a single vertical line on a video display that is scrolled sideways at a rate corresponding to the model rotation. The payload specialist would then see on the screen a slowly scrolling display of the entire hemispherical surface in cylindrical equal-spaced projection. This has the merit that it uses essentially

**ORIGINAL PAGE IS
OF POOR QUALITY**

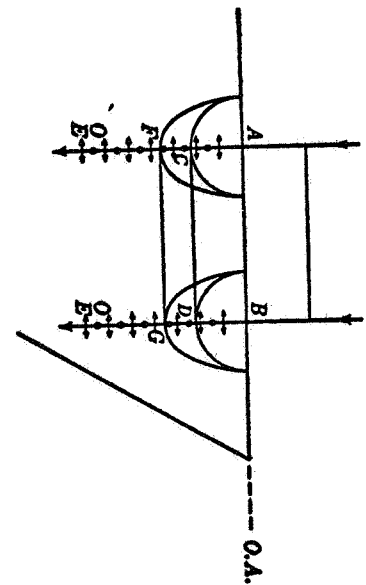
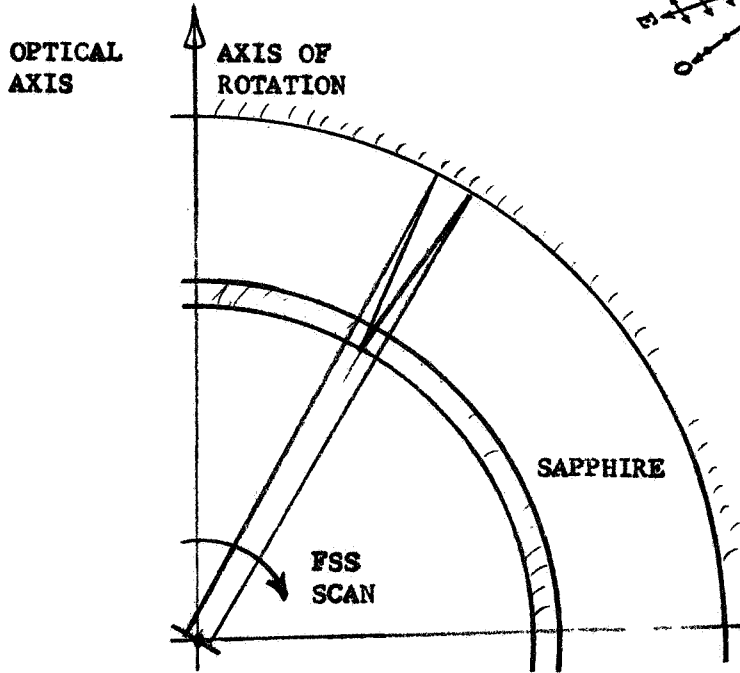
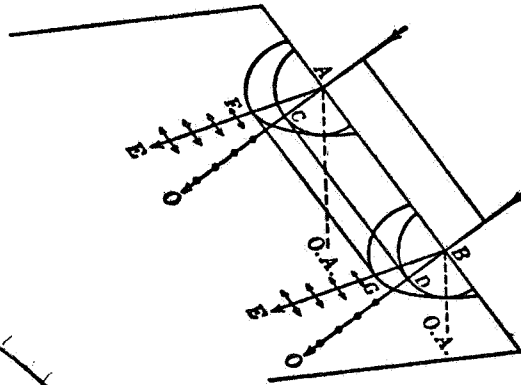
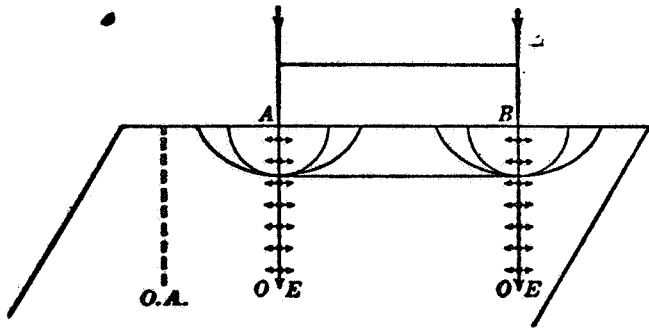
raw signal, conditioned only enough to match the display electronics. If for human engineering or other reasons another type of projection or display is preferred, the raw signal can of course be processed locally to provide it.

3.2 Elimination of Birefringence Effects

One source of optical difficulty for any AGCE apparatus is that for thermal reasons the outer shell of the test cell must be made of sapphire, and sapphire is birefringent. Birefringence can produce effects that mimic thermal gradients, so it is most desirable to eliminate birefringence as a factor in design.

The flying spot scanner sweeps the test cell always in thin meridional arcs. This fact can be turned to advantage in eliminating birefringent effects. It will be necessary only to orient the optical axis of the crystal so it parallels the axis of rotation. Since all scanning rays are substantially in the meridional plane, they must also then lie in the principal plane of the crystal. If we then polarize the scanning beam perpendicular to the scanning plane, which is technically easy to do, all rays will appear to the crystal as ordinary rays, and birefringent effects will have been eliminated. This approach is illustrated in Figure 3.

ELIMINATION OF BIREFRINGENCE EFFECTS



1. Optical axis = axis of rotation
2. FSS meridional scan is always in a principal plane of the crystal
3. Scanning beam can be polarized perpendicular to the optical axis
4. All light passing thru the crystal is representable as an ordinary ray

Figure 3

3.3 Assumptions and Constraints

In order to proceed with a preliminary design and performance evaluation, it is necessary to assume certain facts and constraints relating to the physical character of the test cell and to scanner design requirements, that might eventually be imposed. The most important of these are detailed below.

3.3.1 Test Cell Fabrication

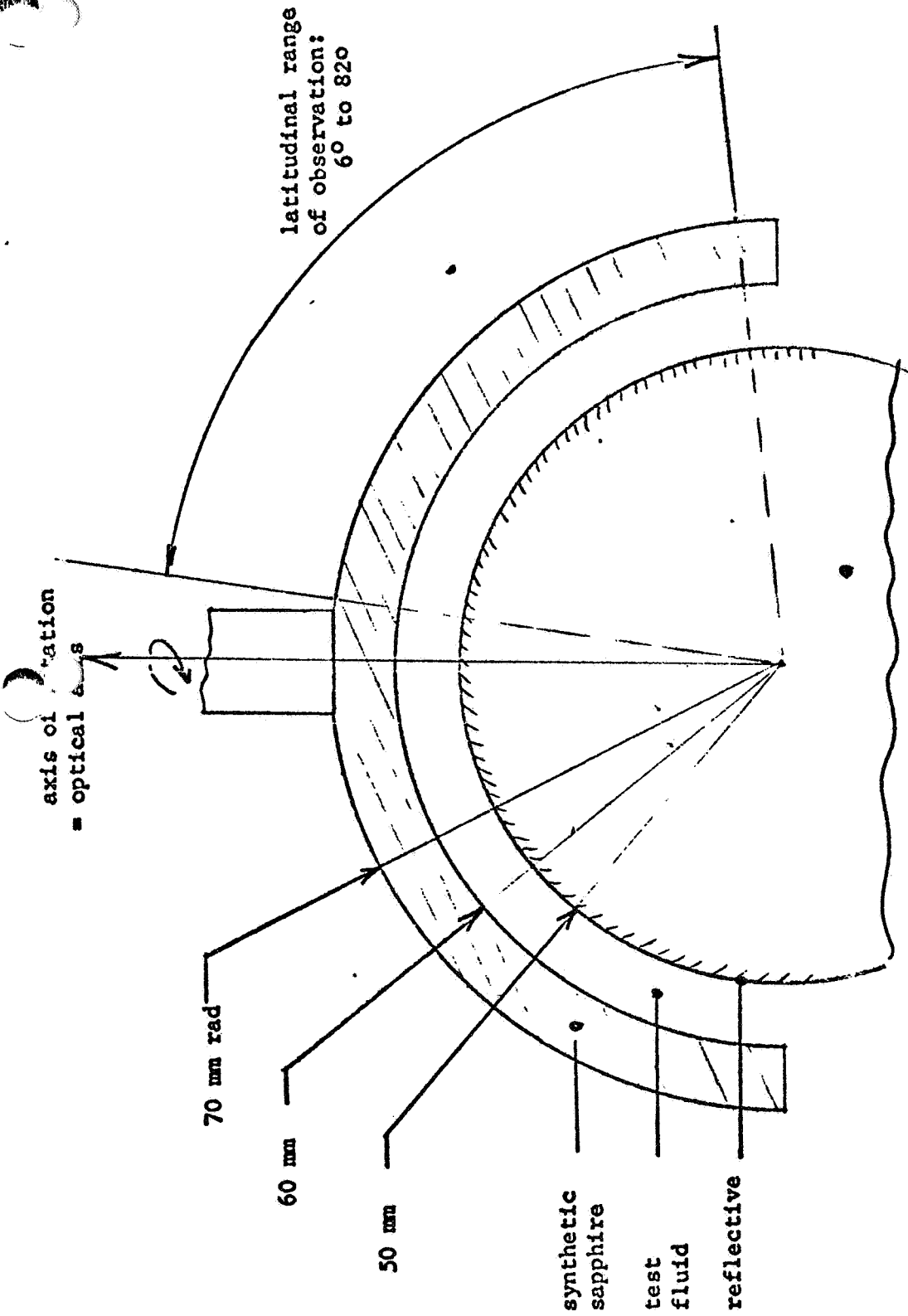
The geometry of the test cell that must be scanned is assumed to be as shown in Figure 4. Fabrication tolerances are assumed to be:

radii:	± 0.1 mm
surface figure:	1 ring power $\frac{1}{2}$ ring irregularity over 25 mm diameter at 5893A
scratch and dig:	80/50

The outer shell of the test cell illustrated will be fabricated from synthetic sapphire. The optical axis will be assumed parallel to the axis of rotation within 5° . Optical properties to be assumed for sapphire will be those tabulated in the OSA Handbook of Optics.

The inner sphere will be assumed to be specularly reflective and to exhibit the reflectivity of silver.

~~14~~
13



ASSUMED BASIC LAYOUT OF ACCE TEST CELL

Figure 4

The interstitial test fluid will be assumed to possess the properties of DMSO, equivalent to a glass type 478275.

The inner surface of the sapphire shell will be assumed to be coated with a transparent conductive coating.

3.3.2 Test Cell Rotation

The maximum rate of test cell rotation will be assumed to be 3.0 radians/sec. The minimum rate will be assumed to be 0.25 radians/sec..

3.3.3 Scan Pattern

A design goal for the flying spot scanner is to scan in meridional arcs from latitude 82° to latitude 6° , covering most of a full hemisphere in one revolution. The scanner itself will provide only motion along the meridian. Motion transverse to the meridian will be provided by the test cell. It is assumed that the scan rate will be adjusted to the rotation rate so as to provide a geometrical pattern of scan that is independent of the cell rotation rate. This scan pattern should be such as to cover exhaustively all surface area within the latitudinal range of scan.

3.3.4 Scanner Spot Size

The scanner will be designed to produce a spot of light on the inner reflective sphere

**ORIGINAL PAGE IS
OF POOR QUALITY**

nonically subtending 1° at the center of the sphere.

3.3.5 Scanner Optical Design

The scanner optics will be designed for the normal visible spectrum, assumed centered on the sodium D-line, 5893A. Insofar as possible, all materials used will be glass, selected from current manufacturer's catalogs. Constructional tolerances for the scanner optics will be assumed identical to those for the test cell (3.3.1, above).

3.3.6 Dynamic Range

It will be a design goal that the scanner be able to measure index gradients in the interstitial fluid from 0.0005 cm^{-1} to 0.00005 cm^{-1} . Assuming an index thermal coefficient of $0.0005 \text{ }^\circ\text{C}^{-1}$, this will represent a thermal gradient of from $1^\circ\text{C}/\text{cm}$ to $0.1^\circ\text{C}/\text{cm}$.

3.3.7 Gradient Sensitivity

The design goal will be a least detectable gradient equal to 10% of the lower limit of the dynamic range, above.

3.3.8 Spot Detection Sensitivity

It will be a design goal that the scanner be able to detect the presence of a photochromic marker dot whose opacity is sufficient to reduce transmitted light to 80% of its value in the absence of the dot.

3.3.9 Mechanical Interface

The minimum clearance between the rotating sphere and the flying spot scanner shall be 1 mm.

3.3.10 Power Interface

The power requirements of the flying spot scanner, including light source, detector/preamplifier, motor and encoder, must be compatible with the AGCE power supply.

3.3.11 Signal Interface

The gradient detector signal will be an analog voltage, linearly proportional to gradient. The marker dot detector signal will be a pulse. The latitude encoder signal will be digital. All signal levels and frequencies must be compatible with AGCE control and data handling electronics.

3.4 Effects of Thermal Gradient

3.4.1 Relation of Thermal Gradient to Index Gradient

The thermal gradient in the test fluid cannot, of course, be observed directly by optical means. What can be made visible is a refractive index gradient. To detect and measure thermal gradient, we rely upon the physical fact that a temperature change produces a change in density and consequently a change in refractive index, which basically is density related. Over the temperature range of interest here, index change is linearly related to temperature change. Therefore a refractive index gradient, which is optically observable and measurable, may be taken as equal, except for a scale factor, to the thermal gradient.

At this point the final choice of test fluid has not been made, and the optical properties of that fluid are therefore not known. For preliminary design purposes we have assumed that the fluid will be DMSO or something closely similar to it chemically. We will therefore assume that the optical properties of DMSO are the optical properties of the test fluid. Published data (Reference 9) indicate that the refractive index of DMSO at the sodium D-line is 1.478, that its Abbe V-number is 27.5, and that the rate of change of index with temperature is

ORIGINAL PAGE IS
OF POOR QUALITY

$$dn/dT = -.00046 \text{ } ^\circ\text{C}^{-1}$$

Allowing for uncertainties, we will here round this figure to $-.0005$. A thermal gradient of $1 \text{ } ^\circ\text{C/cm}$ will therefore translate into a refractive index gradient of

$$dn/dx = .00005 \text{ mm}^{-1}$$

Our analysis will be based on gradients in this numerical neighborhood.

3.4.2 Theory of Gradient Index Refraction

The theory of refraction in an inhomogeneous medium has been treated at length in the literature (see e.g. References 1 to 8). For present purposes it is convenient to work in vector notation. In what follows let N be the refractive index, and let

$$\nabla \equiv \hat{i} \frac{\partial}{\partial x} + \hat{j} \frac{\partial}{\partial y} + \hat{k} \frac{\partial}{\partial z}$$

the gradient operator

$$\nabla N \equiv \hat{i} \frac{\partial N}{\partial x} + \hat{j} \frac{\partial N}{\partial y} + \hat{k} \frac{\partial N}{\partial z}$$

the index gradient

$$d\vec{s} \equiv \hat{i} dx + \hat{j} dy + \hat{k} dz$$

a ray path element

$$d\vec{\theta} \equiv \hat{i} d\theta_x + \hat{j} d\theta_y + \hat{k} d\theta_z$$

the differential rotation of the ray path

The general vector law of differential refraction in an inhomogeneous medium may then be written

$$d\vec{\theta} = \frac{1}{N} d\vec{s} \times \nabla N$$

Expanding this vector differential equation yields three component scalar differential equations

$$\begin{aligned}d\theta_x &= \frac{1}{N} \left(\frac{\partial N}{\partial z} \right) dy - \frac{1}{N} \left(\frac{\partial N}{\partial y} \right) dz \\d\theta_y &= \frac{1}{N} \left(\frac{\partial N}{\partial x} \right) dz - \frac{1}{N} \left(\frac{\partial N}{\partial z} \right) dx \\d\theta_z &= \frac{1}{N} \left(\frac{\partial N}{\partial y} \right) dx - \frac{1}{N} \left(\frac{\partial N}{\partial x} \right) dy\end{aligned}$$

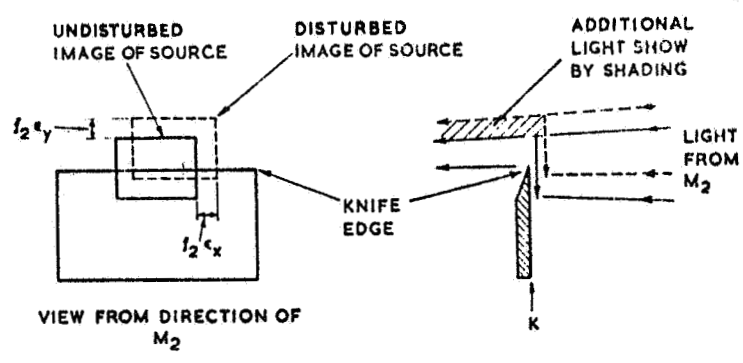
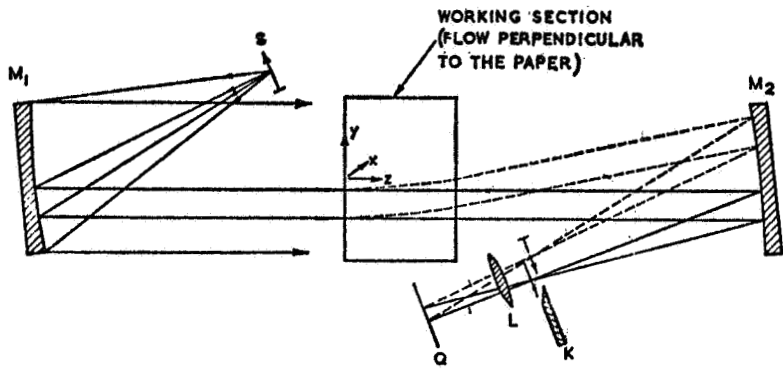
These equations, in finite difference form, are the basis of our design and analysis.

3.4.3 Detection and Measurement of Index Gradients

Index gradients in transparent media are conventionally observed by some type of schlieren apparatus. The basic principle of a schlieren apparatus is that when an image is formed from rays that have passed through an inhomogeneous medium, the lateral deflection of the image is a measure of the rotation of the ray path in the medium, in turn attributable to the index gradient in the medium (Figure 5).

Most commonly in a schlieren apparatus the rays that traverse the medium are collimated. If the gradient is uniform over the beam, all rays are affected uniformly. In the present case the gradient is not uniform, and this spatial non-uniformity is one of the things we seek to observe. We must

ORIGINAL PAGE IS
OF POOR QUALITY



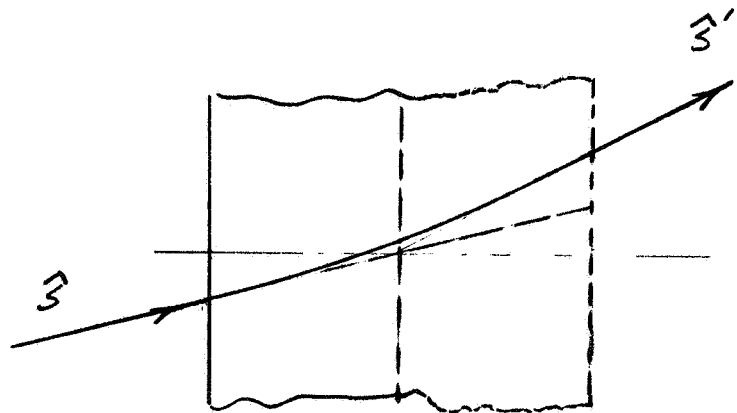
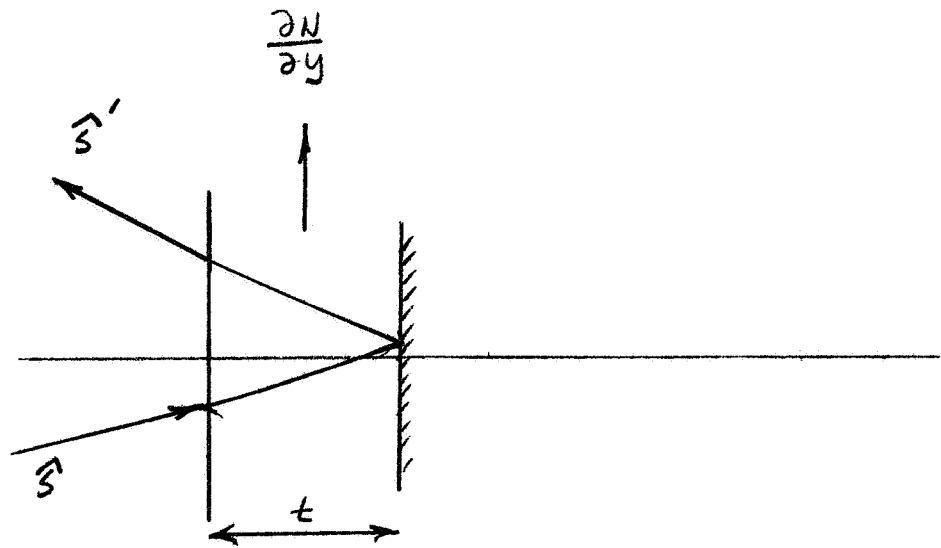
A CONVENTIONAL SCHLIEREN APPARATUS
(From Reference 1)

Figure 5

therefore localize and restrict the volume of fluid that is allowed to act upon the ray bundle from which our image will be formed. We do this by bringing this light to a point focus at the midpoint of its path through the fluid, corresponding to the reflective surface of the inner sphere. We will aim for a spot size of about 0.9 mm at that surface, corresponding to a spatial resolution of about 1° in mapping the thermal gradient over the surface of the test cell.

Refraction in the presence of an index gradient in the test fluid is most easily visualized for a gradient vector in the meridional plane. If we draw a tunnel diagram for the liquid shell (Figure 6) we can treat refraction through the shell as refraction through a plate of twice the shell thickness. Refraction for a ray incident normally is shown in Figure 7, for a ray incident non-normally in Figure 8.

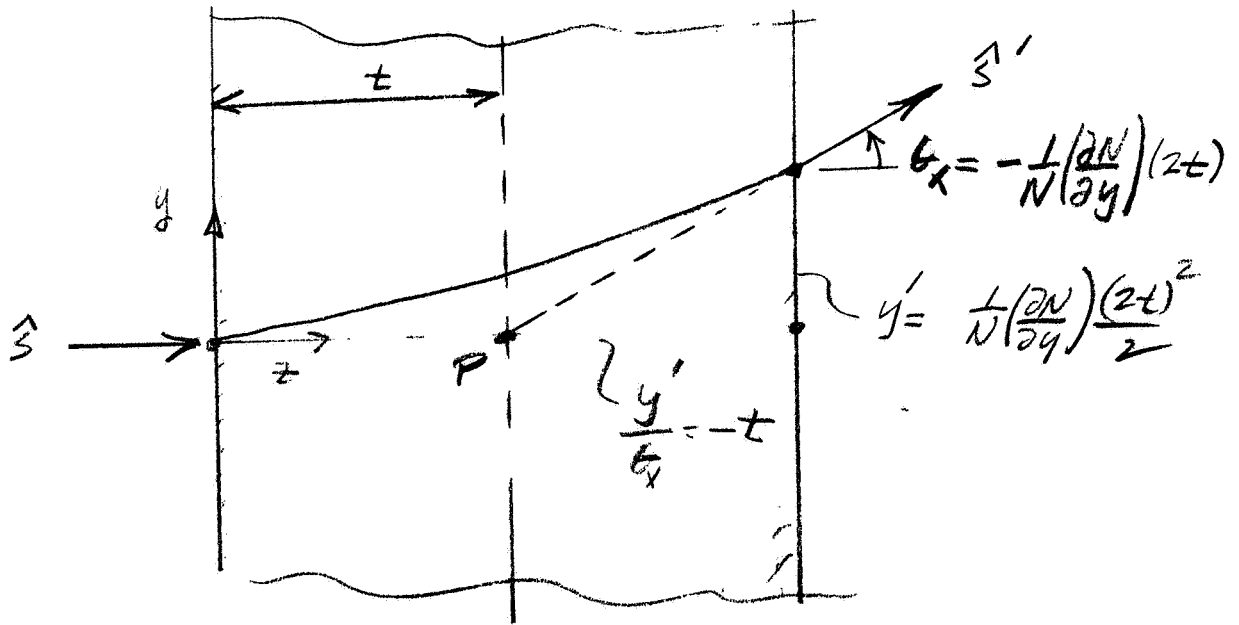
The key insight to be gained from these sketches is that for small effects the ray path is parabolic. As illustrated in these figures, the slope of a leaving ray has been changed, but its virtual source--the reflective inner sphere--has not been changed. This means that in an Offner relay



TUNNEL DIAGRAM OF REFRACTIVE FLUID SHELL

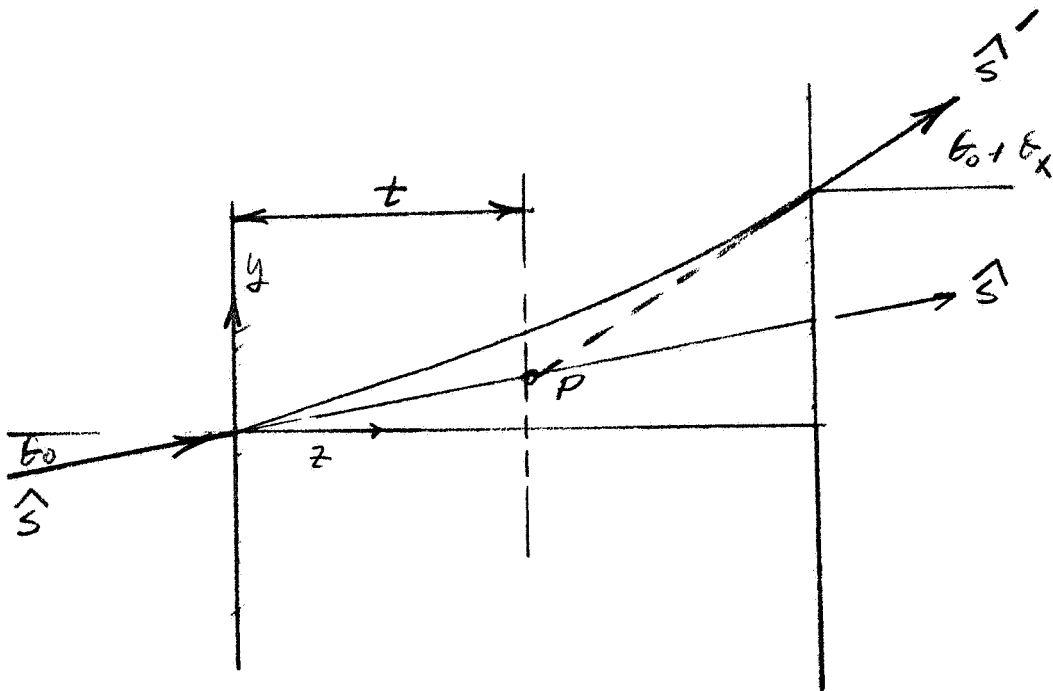
Figure 6

ORIGINAL PAGE IS
OF POOR QUALITY



$$\hat{S} = \hat{k}$$

Figure 7



$$\hat{S} = m \hat{j} + m \hat{k}$$

Figure 8

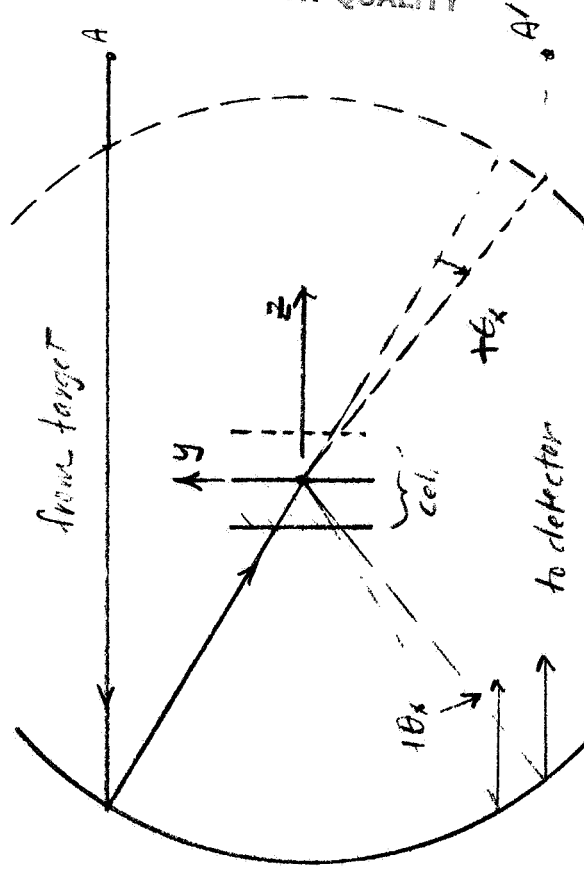
REFRACTION IN FLUID SHELL WITH GRADIENT

the image position (which depends on ray angle) will shift but the final ray direction (which depends on the location of the virtual source) will not. The target image will therefore translate in the self-conjugate plane of the relay by an amount proportional to that component of index gradient to which the instrument is sensitive. We next need to understand how the three components of index gradient contribute to this image translation, and how we can design the detector array to measure these components independently.

Figures 9 and 10 further illustrate how image shifts occur in the Offner relay in the presence of an index gradient. From the scalar differential equations of gradient index refraction we can see that in general all three components of the index gradient vector contribute to translations in the detector plane of the relay. With a suitable detector arrangement, therefore, it should be possible to measure all three of these components. The sensitivity to the transverse components of the index gradient vector will be much greater than to the radial component, however, because, as can be seen from the basic equation

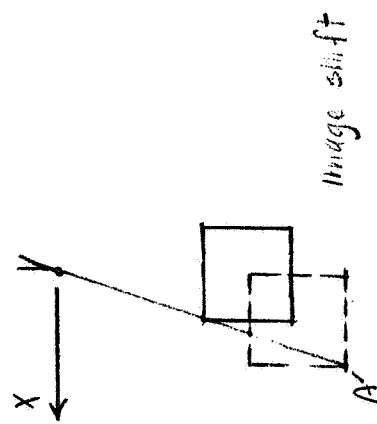
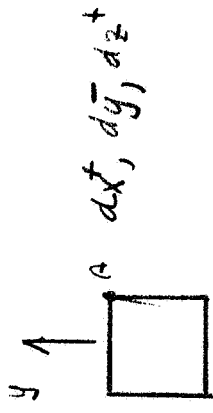
$$d\theta = \frac{1}{n} dS \times \nabla n$$

ORIGINAL PAGE IS
OF POOR QUALITY



GEOMETRY OF TARGET IMAGE
DEFLECTION BY INDEX GRADIENT

Figure 9

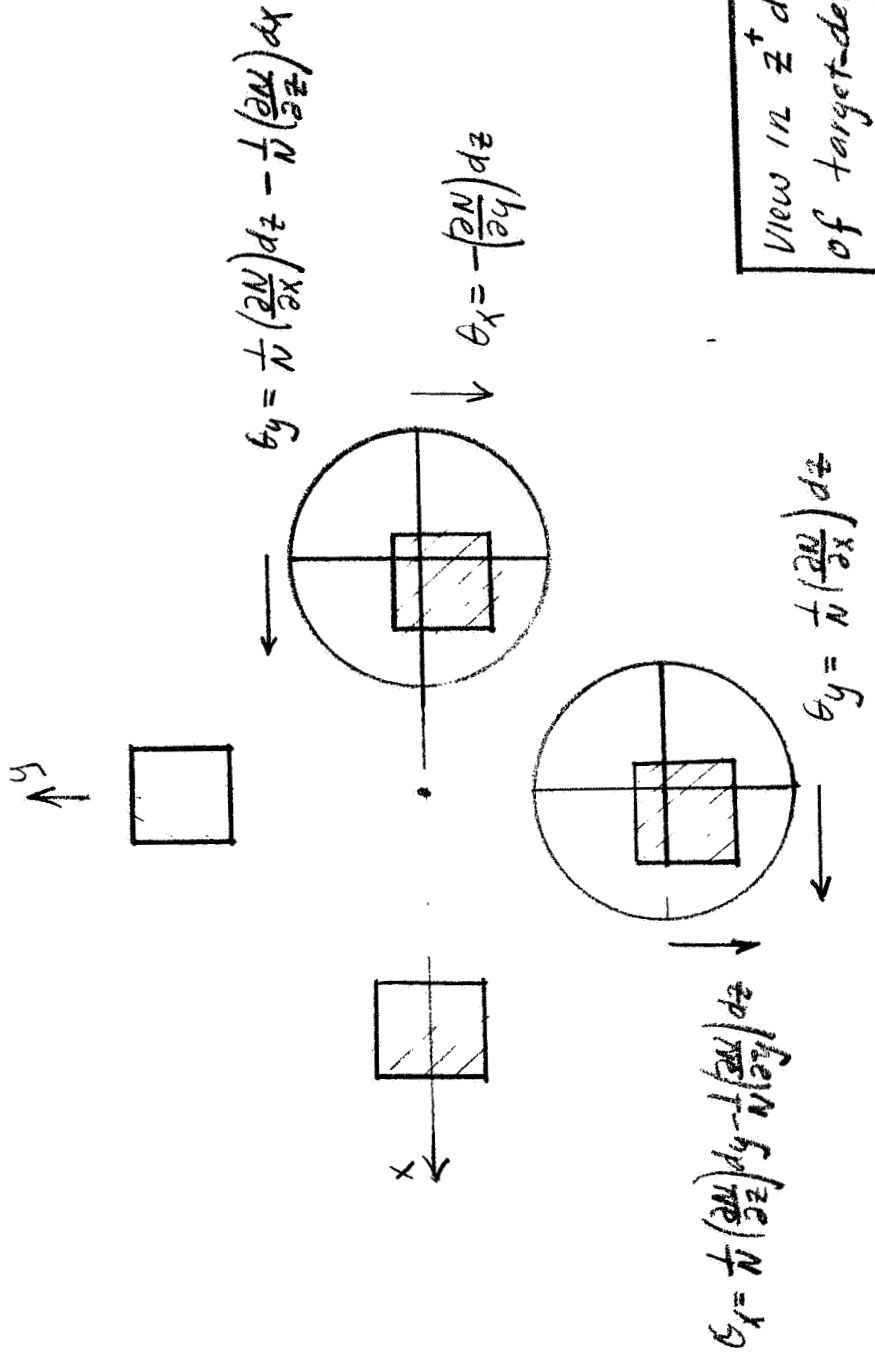


target-detector
P.O.

$$d\epsilon_x = \frac{1}{N} \left(\frac{\partial N}{\partial z} \right) dz - \frac{1}{N} \left(\frac{\partial N}{\partial y} \right) dy + \frac{\partial p}{\partial z}$$

$$d\epsilon_y = \frac{1}{N} \left(\frac{\partial N}{\partial x} \right) dx - \frac{1}{N} \left(\frac{\partial N}{\partial z} \right) dz + \frac{\partial p}{\partial x}$$

ORIGINAL PAGE IS
OF POOR QUALITY



MEASUREMENT OF INDEX
GRADIENT COMPONENTS FROM
TARGET IMAGE SHIFTS

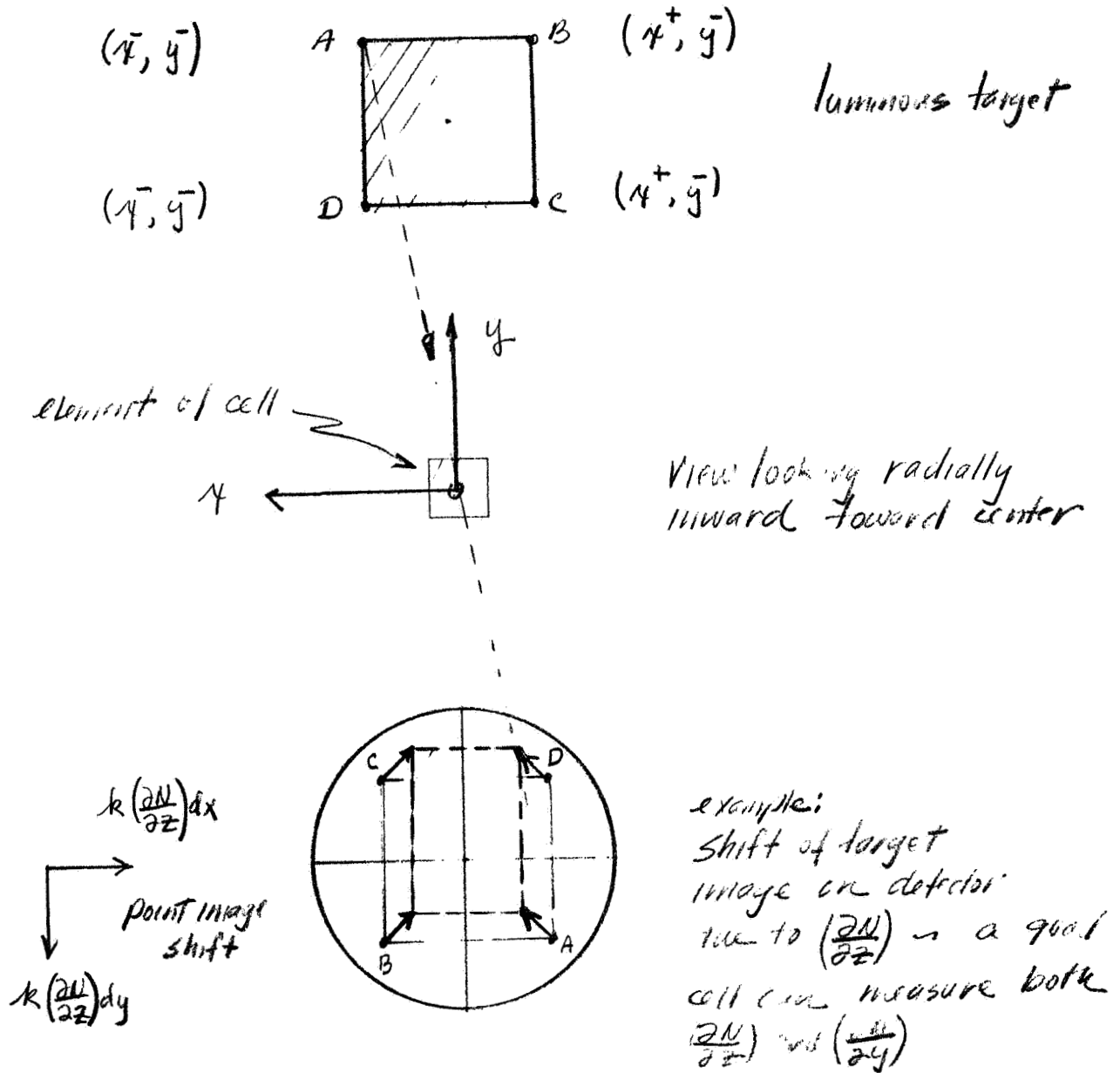
Figure 10-

the components of ray rotation must be orthogonal to the ray direction \hat{s} . Since the rays are incident on the fluid almost radially, most of the ray rotation must be about axes that are transverse to the radius. Nevertheless, a sensitivity to radial gradient does exist and must be taken into account in designing the detector array. Figure 11 illustrates the image shift to be expected from a purely radial index gradient.

From the foregoing illustrations and examples we can make a number of inferences that have a bearing on detector design. These inferences are summarized in Figure 12.

We are specifically required here to detect and measure the two transverse components of index gradient only. An arrangement of detectors that will yield these two components independently of all others is shown in Figure 13. This is the configuration we will use for this preliminary design. It is shown later that the compact arrangement of a centered quadrant detector is more advantageous in terms of scan angle, but we have ruled it out for this exercise because of central obscuration by the opaque strip needed to block a ghost image and because it entails the use of a target/detector beamsplitter to effect superposition, with consequent loss of light.

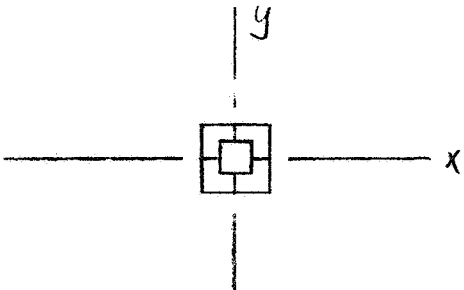
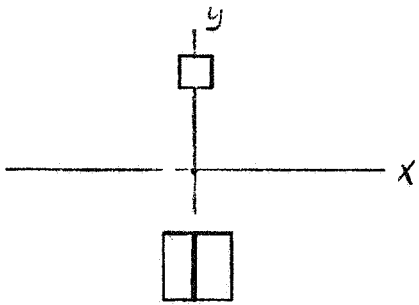
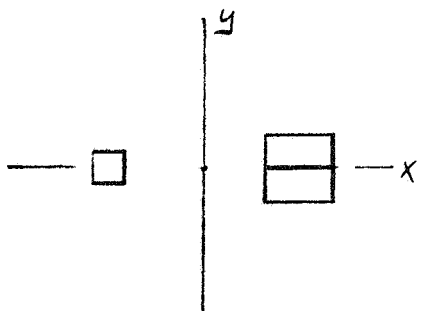
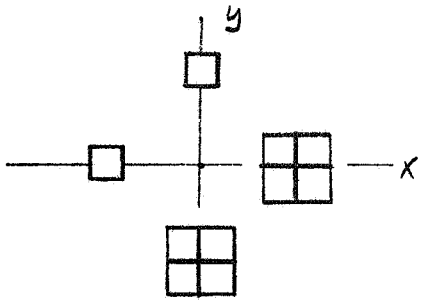
ORIGINAL PAGE IS
OF POOR QUALITY



SENSITIVITY TO RADIAL GRADIENT

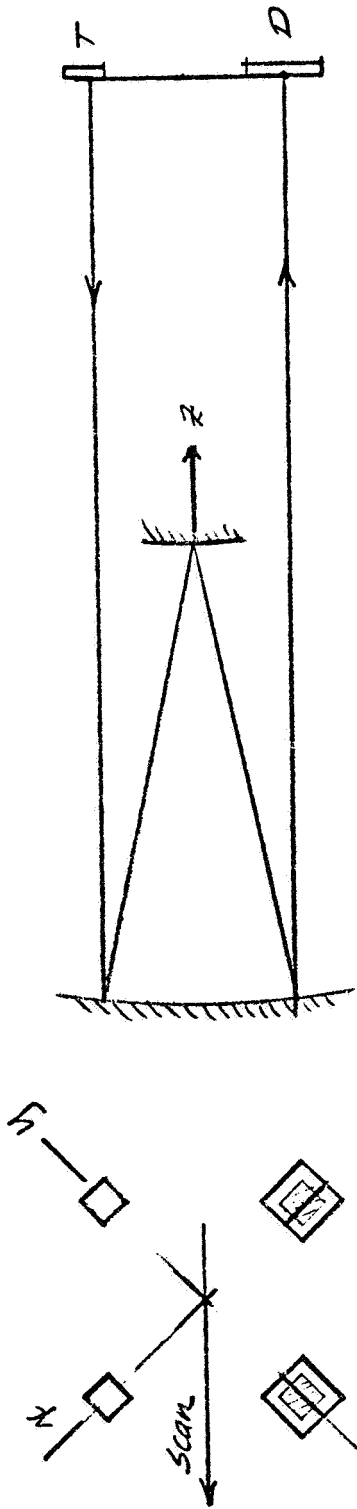
Figure 11

ORIGINAL PAGE IS
OF POOR QUALITY

Configuration	Quad Cell	Dual Cell
	$\frac{\partial N}{\partial x}$ $\frac{\partial N}{\partial y}$	
		$\frac{\partial N}{\partial x}$
		$\frac{\partial N}{\partial y}$
	$\frac{\partial N}{\partial x}$ $\frac{\partial N}{\partial y}$ $\frac{\partial N}{\partial z}$	

POSSIBLE INDEPENDENT MEASURES OF GRADIENT

Figure 12



$$d\theta_x = -\frac{1}{N} \left(\frac{\partial N}{\partial y} \right) dz \quad d\theta_y = -\frac{1}{N} \left(\frac{\partial N}{\partial x} \right) dz$$

SELECTED TARGET-DETECTOR CONFIGURATION FOR PRELIMINARY DESIGN

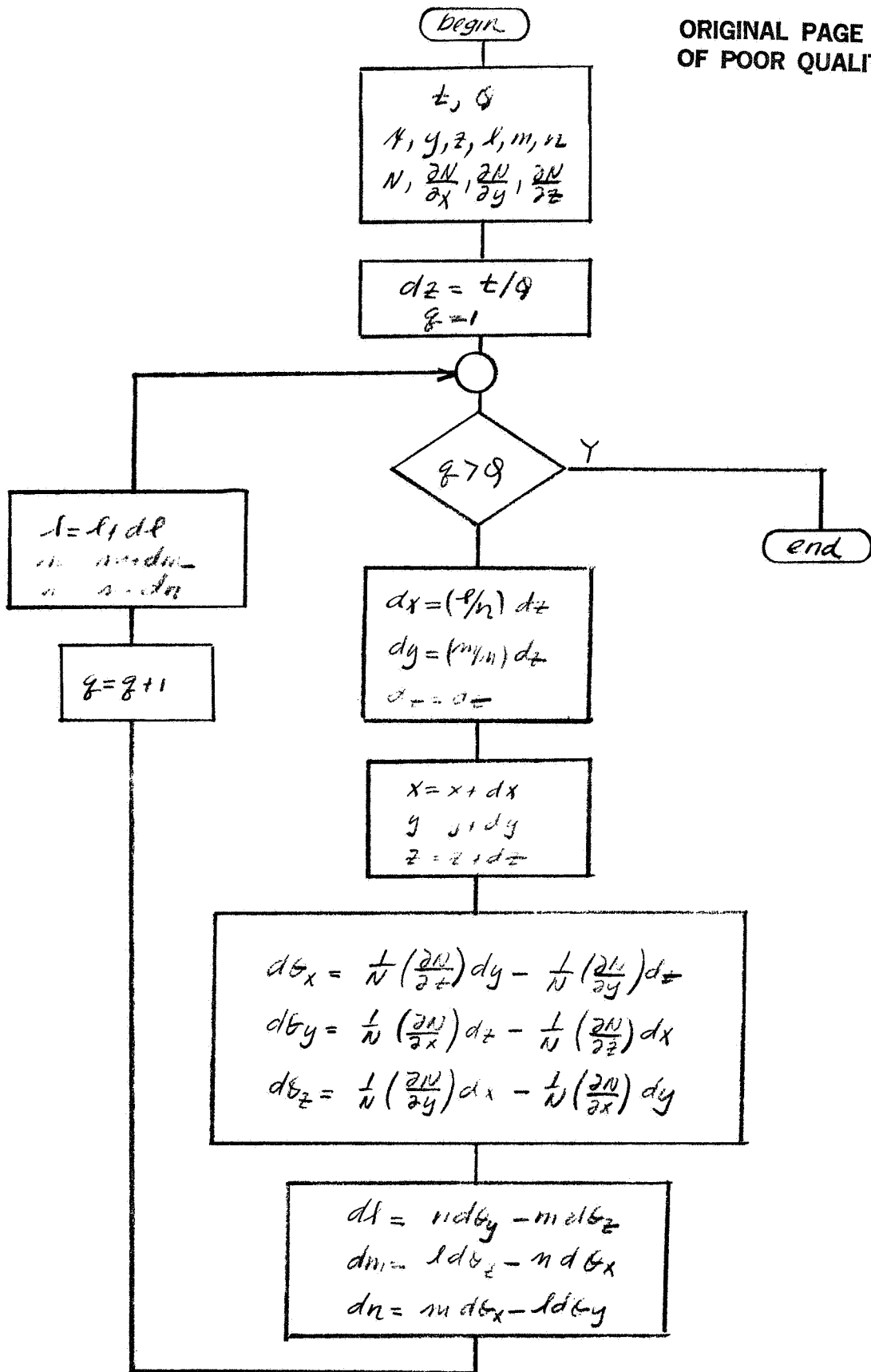
Figure 13

3.4.4. Index Gradient Refraction Algorithm

In order to design and evaluate the flying-spot scanner, it is necessary actually to trace rays through the relay in the presence of a (thermally induced) refractive index gradient in the test fluid. The first step was therefore to devise a computational algorithm for doing this.

The basic approach taken is that of finite difference approximation to the differential equations of refraction, followed by numerical integration along the path. The total thickness of the gradient index medium is divided up into a large number of very thin layers, within each of which the ray propagation may be considered uniform, directional changes due to the index gradient being assumed to occur only at layer boundaries. The algorithm, shown in Figure 14, follows in a straightforward manner from the three scalar differential equations given earlier.

To test this algorithm, it was first written as a TI-59 calculator program (see Appendix) and with it rays were traced through 20 mm of test fluid with an index gradient of 0.00005 mm^{-1} . The results, shown in Figure 15, were completely consistent with expectation. Twenty steps of 1 mm each were



RAYTRACE THROUGH GRADIENT INDEX MEDIUM

Figure 14

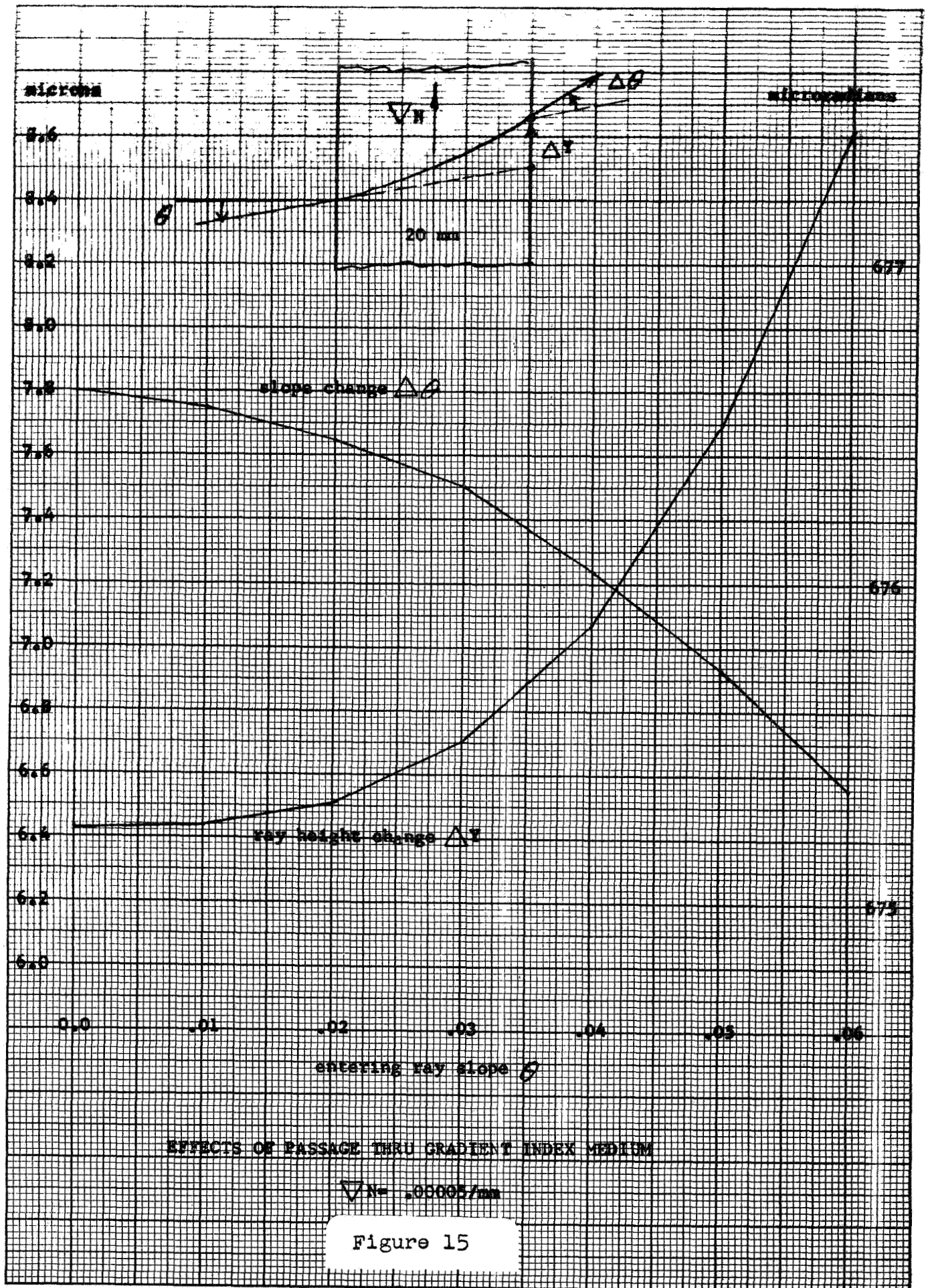


Figure 15

K&E 10 X 10 TO THE 1/2 INCH 359-11
 KEUFFEL & ESSER CO. MADE U.S.A.

found to give ample accuracy. Beyond 40 steps of 0.5 mm each no changes in computational results could be observed.

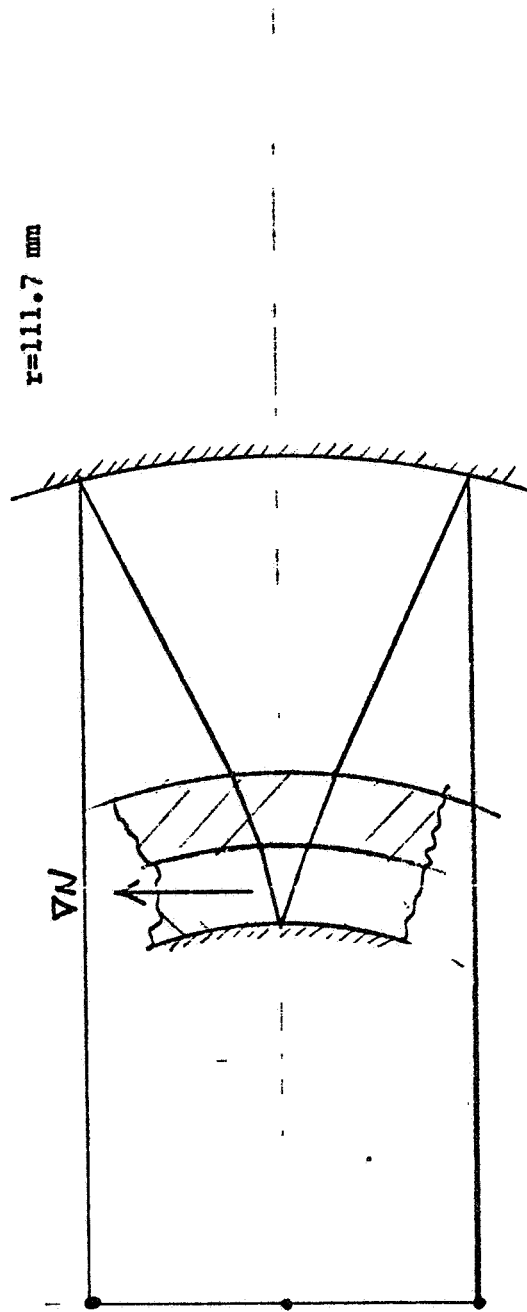
3.4.5 Index Gradient Effects in the Flying-Spot Scanner

To further confirm that the flying-spot scanner is capable of measuring index gradients, we incorporated the refraction algorithm of the previous section into a raytrace computer program as a subroutine and traced a simple version of the proposed instrument. The optical system traced (Figure 16) is the basic Offner relay without folding. The expected image translation is shown in Figure 17.

We first sought to prove that the image quality of the Offner relay, even in the presence of an index gradient, was completely satisfactory. A small bundle of eight rays was therefore traced from each corner of a 2mm x 2mm square target centered on the instrument axis. The image coordinates, shown in Figure 18, indicate

- 1) that the mean image of each point is within .01 micron of its geometric location; and
- 2) that the RMS spot size is on the order of .1 micron in diameter.

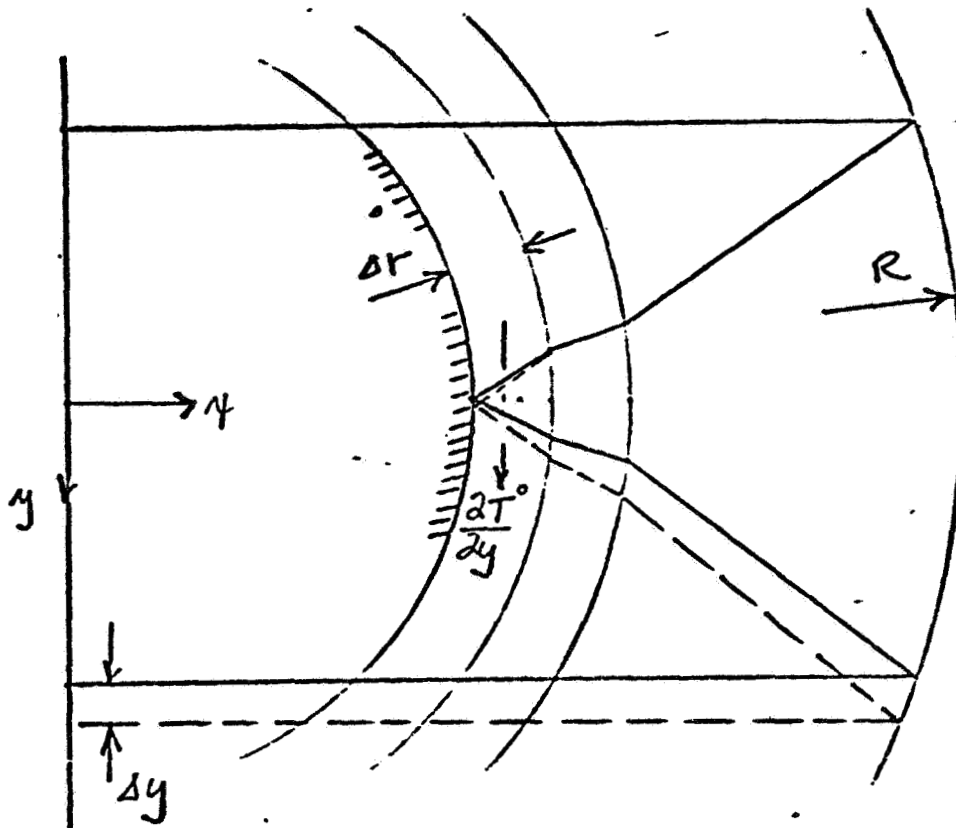
ORIGINAL PAGE IS
OF POOR QUALITY



INITIAL SYSTEM FOR RAYTRACE

Figure 16

ORIGINAL PAGE IS
OF POOR QUALITY



$$\Delta y = \left(\frac{\partial n}{\partial T^{\circ}} \right) \left(\frac{\partial T^{\circ}}{\partial y} \right) (2\Delta r) (R/2)$$

for a typical organic fluid $\left(\frac{\partial n}{\partial T^{\circ}} \right) = -5 \times 10^{-4} \text{ } ^{\circ}\text{C}^{-1}$

then for a typical thermal gradient of $1 \text{ } ^{\circ}\text{C}/\text{cm}$ and
the recommended design geometry

$$\Delta y = (-5 \times 10^{-4}) (0.1) (20) (156)$$

$$\Delta y = -0.056 \text{ mm}$$

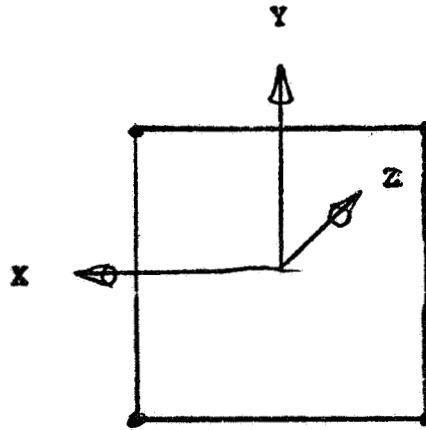
EXPECTED MAGNITUDE OF IMAGE SHIFT

Figure 17

CALCULATED CORNER POSITIONS FOR 2 x 2 mm SQUARE

GRADIENT .00005 mm⁻¹

X	Y		X	Y
-1.0000087	-.94499315	mean	1.0000087	-.94499315
.000043094	.000050709	σ	.000043094	.000050709



-.99999041	1.0550061	mean	.99999041	1.0550061
.000043095	.000039641	σ	.000043095	.000039641

(based on 8 rays per point)

Figure 18

We conclude from these results that imagery in this Offner relay may be considered diffraction limited.

We next sought to determine whether an index gradient image shift would be linearly proportional to the index gradient. For this test axial rays were traced from eight points around the periphery of a 2mm x 2mm centered target for three values of index gradient:

$$|\nabla N| = \begin{cases} .0005 \\ .00005 \\ .000005 \end{cases} \text{ mm}^{-1}$$

corresponding to thermal gradients of:

$$|\nabla T| = \begin{cases} 10.0 \\ 1.0 \\ 0.1 \end{cases} \text{ }^{\circ}\text{C/cm}$$

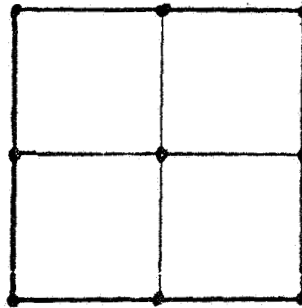
respectively. The resulting image shifts, shown in Figure 19, indicate that image translation is indeed linearly proportional to index gradient over at least two decades. These results make it clear that the flying spot scanner instrument proposed has the potential to detect index gradients in a manner amenable to very accurate measurement.

-.4500
-.9450
-.9945

-.4500
-.9450
-.9945

-.4500
-.9450
-.9945

.5500
.0550
.0055



.5500
.0550
.0055

1.5500
1.0550
1.0055

1.5500
1.0550
1.0055

1.5500
1.0550
1.0055

CALCULATED IMAGE POSITIONS FOR THREE VALUES OF GRADIENT

$$|\nabla N| = \begin{cases} .0005 \text{ mm}^{-1} \\ .00005 \\ .000005 \end{cases}$$

Figure 19

3.5 Preliminary Design

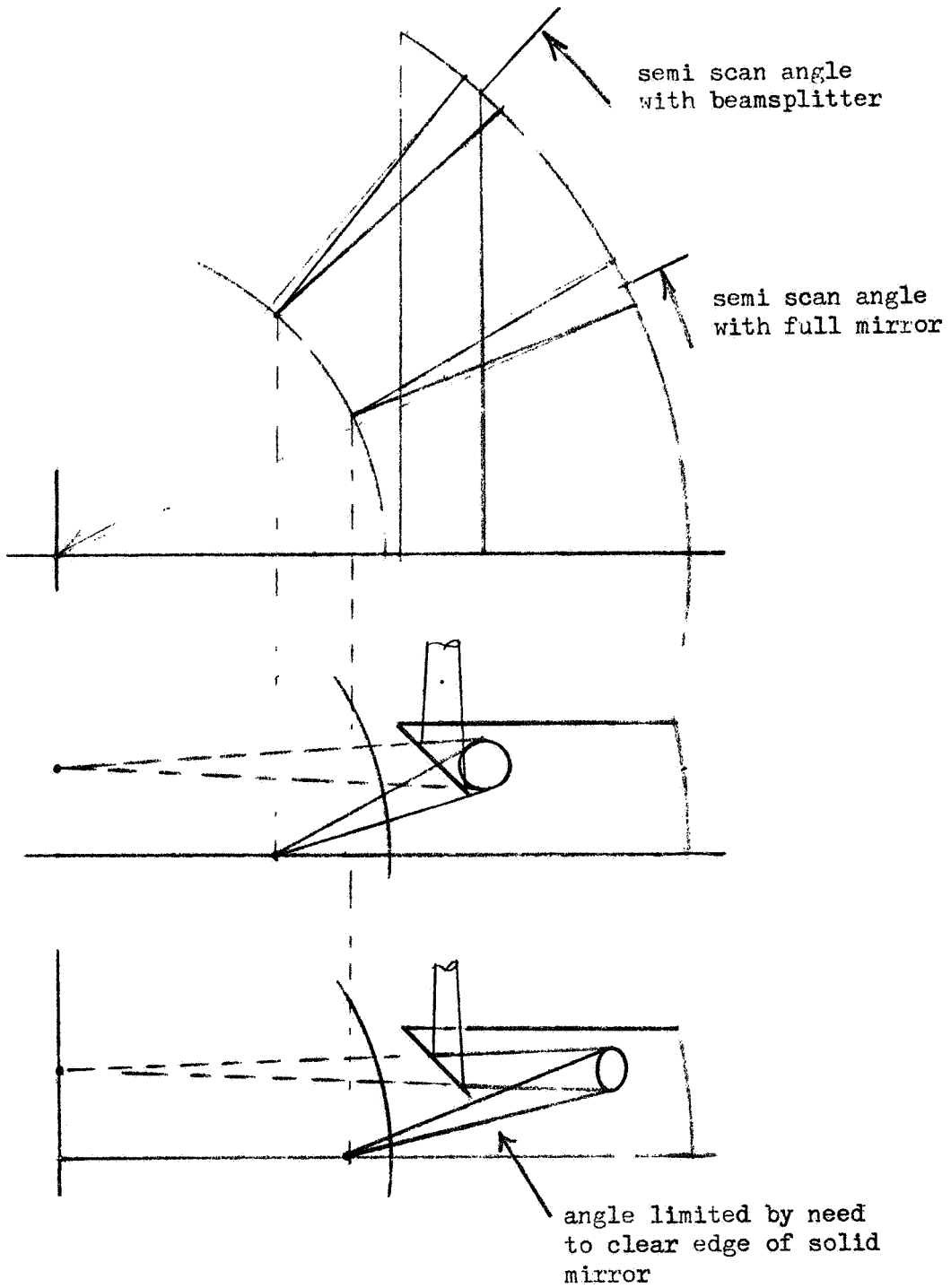
3.5.1 Folding

The flying-spot scanner of Figure 2 is based on the monocentric (Offner) relay. Obviously the optical path must be folded away from the test cell itself, which otherwise would physically interfere. The folding mirror (or mirrors) could be either completely reflective or semi-reflective. We have chosen here to use a semi-reflective mirror, for several reasons. The most important of these is that, as shown in Figure 20, a semi-reflective mirror maximizes the scan angle. A semi-reflective mirror also allows the scanning beam to pass through the test fluid almost radially. This is important for minimizing the volume of fluid intercepted by the scanning beam and therefore maximizing the spatial resolution of the instrument. On the other hand, a semi-reflective folding mirror will entail a substantial loss of light and will introduce ghosts that must be blocked or absorbed. Since the optical system is specular, the loss of light need not be significant, but care must be taken to eliminate the ghosts.

3.5.2 Choice of Solid Construction

A monocentric relay with a semi-reflective folding mirror could be realized as a solid assembly

ORIGINAL PAGE IS
OF POOR QUALITY



INCREASING SCAN ANGLE WITH SEMI-TRANSPARENT MIRROR

Figure 20

or as an open assembly. We have chosen here to use the solid design because it results in a smaller and more stable instrument, because it is easier to realize the semi-reflective folding mirror as a buried-surface beamsplitter, and because fresnel losses can be better controlled in such a design. On the debit side of the ledger, it must be admitted that a solid system is generally harder to make, will reduce the deflection produced by any given thermal gradient, will reduce the available scan angle, and may introduce problems of chromatic aberration. On balance, however, we favor the solid design.

3.5.3 Design of a Zero-Power Interface

To realize a solid system while yet allowing for motion of the test cell and the scanner head, we can introduce a zero-power, air lens at the two interfaces where relative motion will occur:

- 1) between the scanner assembly and the test cell, and
- 2) between the scanner head and the scanner body.

We visualize each interface as two concentric spherical surfaces separated by a small air gap of about 1 mm. The glasses are to be chosen so that the optical power of the thin air lens is zero.

The power ϕ of an air lens is given by

ORIGINAL PAGE IS
OF POOR QUALITY

$$\phi = \phi_1 + \phi_2 - \phi_1 \phi_2 t$$

in which the meaning of the terms is as indicated in Figure 21. If the net power ϕ is to equal zero, then this implies

$$t = \frac{1}{\phi_1} + \frac{1}{\phi_2}$$

Writing this in terms of refractive indices and dimensional parameters, we obtain:

$$t = \frac{r}{n_1 - 1} - \frac{r + t_1}{n_2 - 1}$$

This relation may be cast in any of several forms, depending on which variable we choose to regard as dependent:

$$t = \frac{(n_2 - n_1)}{n_2(n_1 - 1)} r$$

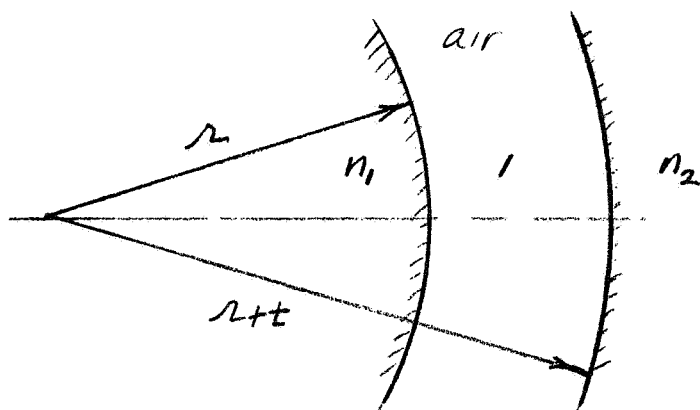
$$r = \frac{n_2(n_1 - 1)}{(n_2 - n_1)} t$$

$$(n_1 - 1) = \left(\frac{r}{r + n_2 t} \right) (n_2 - 1)$$

$$(n_2 - 1) = \frac{(r + t)}{(r + t - n_1 t)} (n_1 - 1)$$

A zero-power interface is easily designed with this set of equations. Usually one or two iterations will be necessary to satisfy dimensional constraints with real glasses.

ORIGINAL PAGE IS
OF POOR QUALITY



$$\text{power } \phi_1 = \frac{1-n_1}{-(r)}$$

$$\text{power } \phi_2 = \frac{n_2-1}{-(r+t)}$$

$$\text{power of combination } \phi = \phi_1 + \phi_2 - \phi_1 \phi_2 t$$

$$\text{for } \phi = 0 \quad t = \frac{1}{\phi_1} + \frac{1}{\phi_2}$$

DESIGN OF ZERO POWER CONCENTRIC INTERFACE

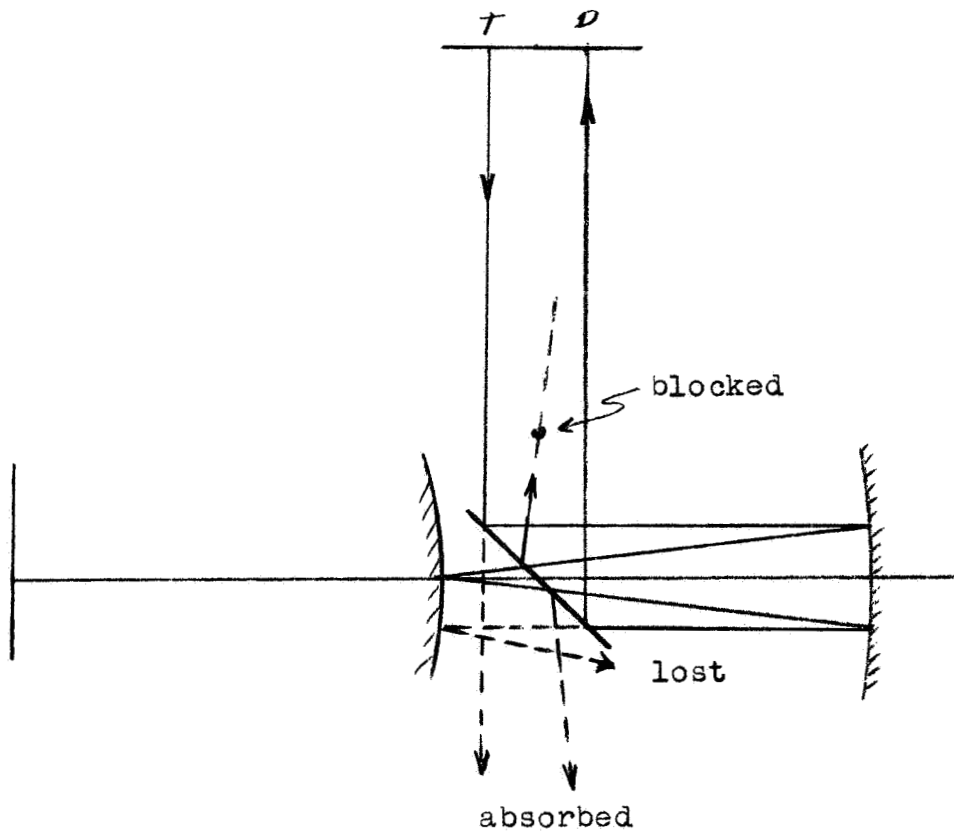
Figure 21

3.5.4 Provision for Ghosts

The price paid for the advantages of the semi-reflective folding mirror is the presence of ghosts. These are not difficult to eliminate, however. The principal ghosts are shown in Figure 22. These are the ones associated with the folding mirror. Minor ghosts are created at the zero-power interfaces, but these can be suppressed by AR coatings on the air-glass surfaces.

Ghosts created by the folding mirror can be diverted, absorbed or blocked. The choice of folding angle encourages the loss of some ghost light. Other ghosts can be absorbed by black velvet paint or a layer of absorbent glass on the outer surfaces. The most important ghost is a replica of the focussed spot that appears at the ghost image of the inner reflective sphere. This could be eliminated very simply by placing the scanner head interface at that ghost image and physically blocking the light with a black spot on the glass. In the present case this would make the scanner head larger than is desirable for dynamic reasons, so instead we can provide a buried surface at that point and block the ghost with a black absorbent stripe on that surface. The zero-power interface can then be placed so as to minimize the size of the scanner head.

ORIGINAL PAGE IS
OF POOR QUALITY



GHOST LIGHT IN THE SCANNER SYSTEM USING
SEMI REFLECTIVE MIRROR

Figure 22

3.5.5 Detector Plane Constraints

Before proceeding to the layout of the scanner, we must consider the geometrical constraints at the self-conjugate detector plane. Practical detectors to be considered for the configuration of Figure 13 include the following, both available as chips:

UPT PIN Spot/2D

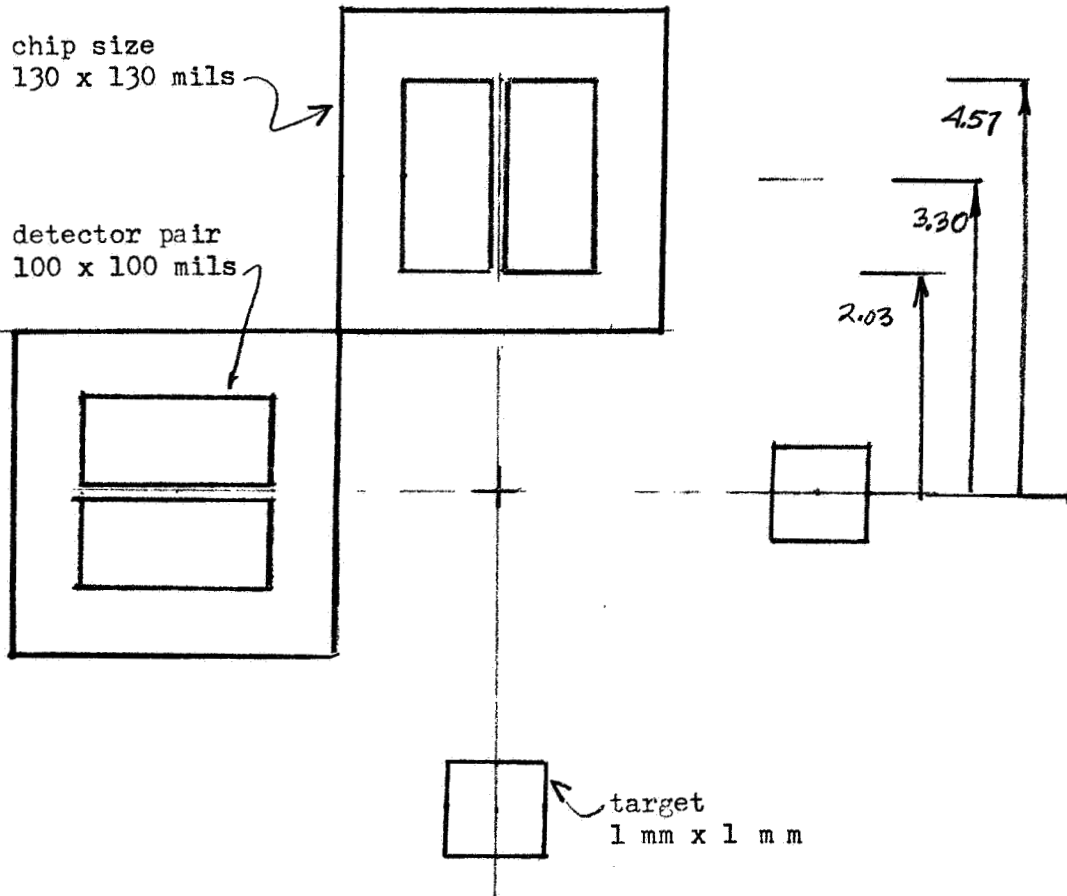
Hughes HPIN 100D

Data sheets for these detectors are included in the Appendix. Both have very similar geometry. The basic design constraint is the chip size. The two chips must be mounted so as to clear each other physically. This implies that the most compact layout, providing the nearest thing to radially incident light at the test cell, is that of Figure 23. From this figure we see that the image height at the center of the image is 3.30 mm, and that the upper and lower marginal ray heights are 4.57 and 2.03 mm, respectively. These figures will enter into the layout raytrace and achromatization.

3.5.6 Achromatization

The solid Offner relay will be designed to be achromatic over the normal visible spectrum. The nominal relay design will be based on the mid-image

ORIGINAL FACE
OF POOR QUALITY



LAYOUT IN TARGET-DETECTOR PLANE

Figure 23

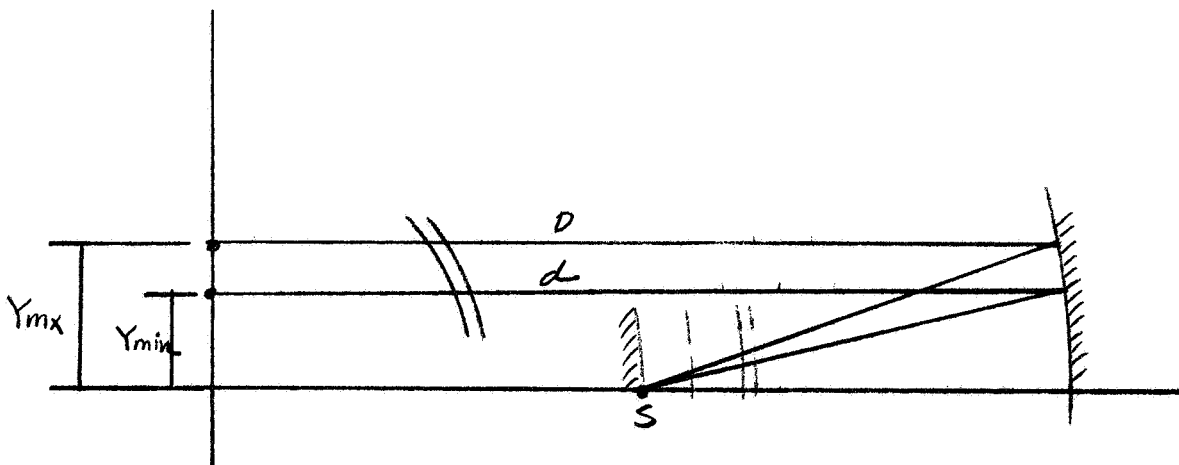
height (3.30 mm) and the sodium D-line ($5893 \overset{\circ}{\text{Å}}$).

This nominal design results in a selection of glasses on the basis of sodium D-line index n_D . Normally several glasses will be available with very nearly the same n_D but with different dispersive properties, expressed in terms of the Abbe V-number.

To achromatize, we may regard the relay as a collimator and apply Conrady's (D-d) method (see Reference 15). Referring to Figure 24, we put a chromatic source at point S and trace an upper and a lower marginal ray through the system. Let D represent the length of the upper marginal ray in any element, and d the length of the lower marginal ray. Then if we require that

$$\sum \frac{(D-d)(n_D-1)}{V} = 0$$

over all elements, the system will be satisfactorily achromatized. We satisfy this requirement by selecting from among glasses with the same n_D those with Abbe V-numbers that will reduce the above sum to zero, or close to it. The residual value of this sum is the wavefront aberration, and in this optical system, where the upper and lower marginal rays differ only slightly, it should be easy to reduce this residual aberration to insignificance.



$$\sum \frac{(D-d)(n_0-1)}{V} = 0$$

ACHROMATIZATION BY CONRADY'S (D-d) METHOD

Figure 24

3.5.7 General Layout Procedure

The layout of the solid Offner relay can be completed in a systematic and straightforward manner. It is sufficient for this purpose to use a meridional raytrace calculator program and execute the following steps in sequence:

- 1) From the optical invariant of the system determine the angle of incidence at the inner reflective sphere for a ray parallel to the axis passing through the center of the detector.

- 2) Launch a ray outward from this point at the angle thus determined and trace it through the fluid and the sapphire shell.

- 3) Design the first zero power interface, between sapphire and scanner, and continue the raytrace through that interface.

- 4) Locate the virtual source seen by the primary mirror and size the primary mirror to collimate rays emanating from that source.

- 5) Locate the second zero-power interface as close to the self-conjugate plane as is practical so as to minimize the inertia of the spinning scanner head, and design this interface as a zero power air lens.

- 6) Complete the trace to the self-conjugate plane.

7) Trace upper and lower marginal rays through the system and compute (D-d) for each element.

8) Select glasses to achromatize by Conrady's (D-d) method.

9) Iterate as necessary to realize the system with standard catalog glasses.

3.5.8 Completed Relay Design

The result of the steps just described is the layout of Figure 25, representing the complete preliminary design of the scanner relay optics. Information developed to this point is sufficient to permit reliable predictions of optical performance.

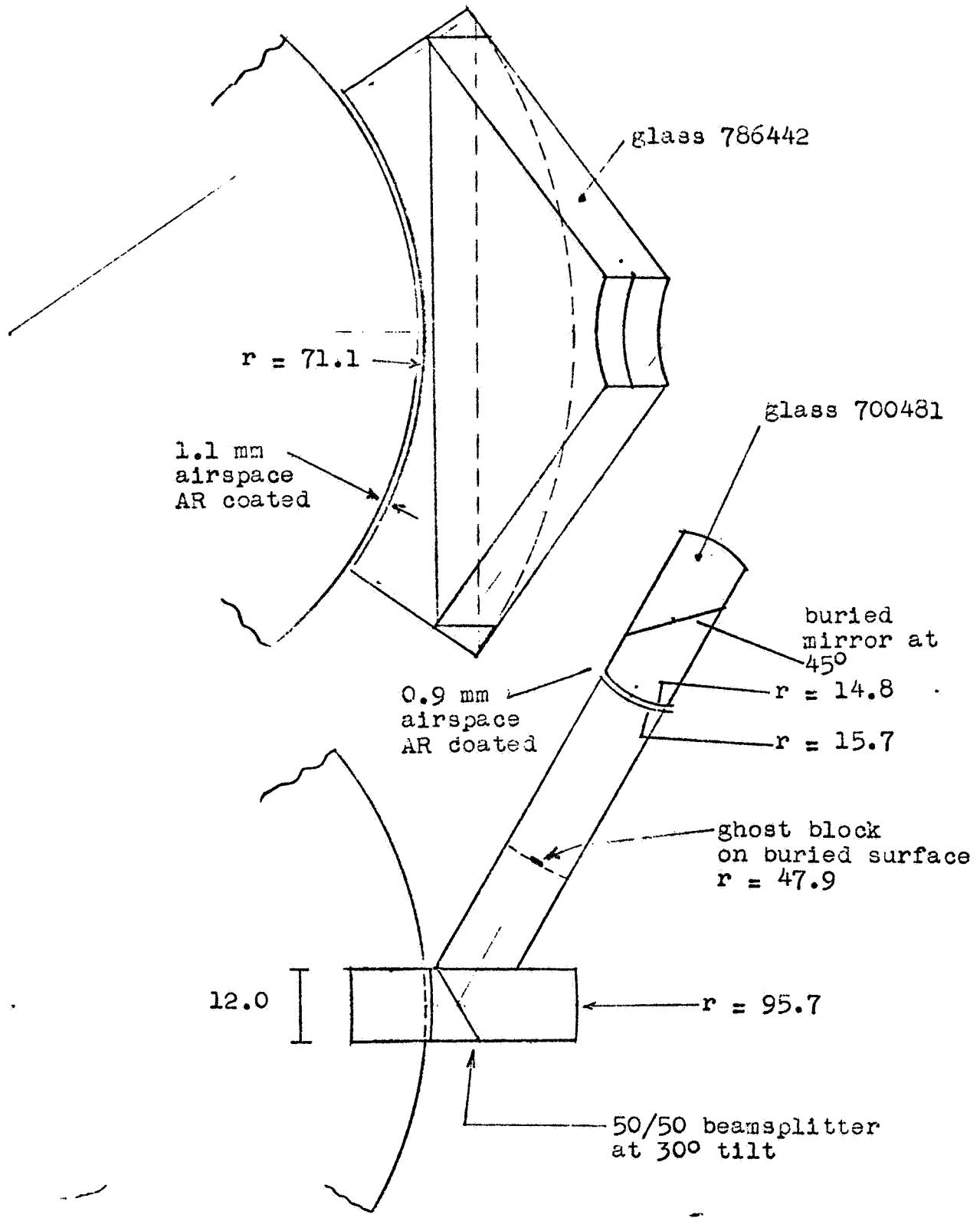
3.5.9 Constraints on Illuminator

Our objective here is to produce a spot of light on the inner reflective sphere that subtends one degree at the center. For a 50 mm radius this represents a spot $100 \pi / 360 = 0.87$ mm in diameter. This corresponds (in glass) to an angular beamspread of 0.018 radians. In air this beamspread would be 0.032 radians. The illuminator must therefore be constrained to pass light through the target that is collimated to this degree.

3.5.10 Constraints on Scan Angle

For a beamwidth of 0.018 radians in glass, a point source on the target would illuminate a

ORIGINAL PAGE IS
OF POOR QUALITY

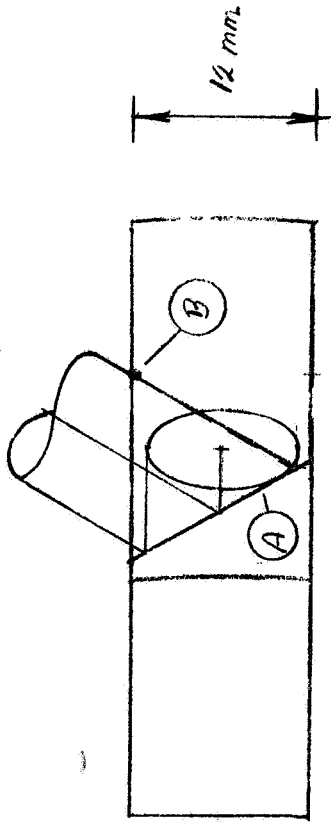


FOLDED SCANNER RELAY

Figure 2b

spot 1.7 mm in diameter on the primary mirror. A 1 x 1 mm target would illuminate a spot 2.7 x 2.7 mm on the primary mirror. Allowing for beam motion due to index gradients, the ray envelope for the target/detector layout of Figure 23 is a circle 10 mm in diameter at the primary mirror. The basic constraints on scan angle are, as shown in Figure 26, 1) that all light must reach the primary mirror via the folding beamsplitter and 2) that the lowermost edge of the ray envelope must clear the primary mirror. The arrangement of Figure 26 is close to optimum for the target/detector array considered, but provides an unobstructed scan of only 69° , less than that sought. We therefore need to understand how this could be improved.

If the target/detector array were more compact, the ray envelope would be smaller. Other things being equal, this alone would increase the scan angle. If the primary mirror radius were larger, the sagittal gap between mirror and beamsplitter would be larger, and this also would increase the scan angle. The mirror radius depends on the refractive index of the glass forming the main body of the relay. If the index is lowered, the mirror radius increases. In the limit, substituting air for glass (Figure 16), the sagittal gap increases by 16 mm. In a solid system only a fraction of this can be realized, but significant improvement is possible.

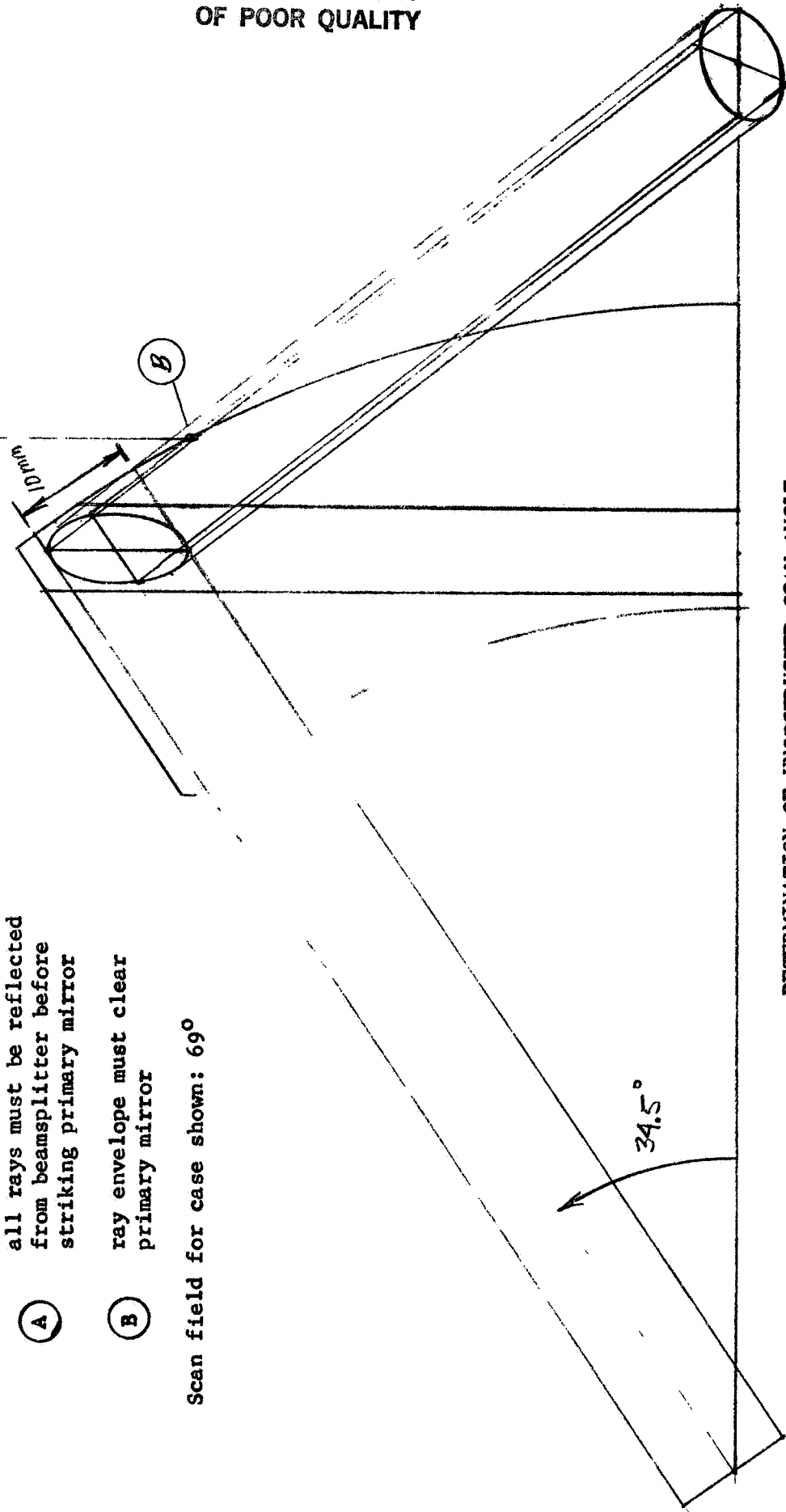


Case shown: mirror tilt 30°
ray envelope at mirror 10 mm

Constraints:

- (A) all rays must be reflected from beamsplitter before striking primary mirror
- (B) ray envelope must clear primary mirror

Scan field for case shown: 69°



DETERMINATION OF UNOBSTRUCTED SCAN ANGLE

Figure 26

3.5.11 Scanner Head Design

We have shown that accurate measurement of index gradient is possible if source and detector are placed symmetrically about the common center in the self-conjugate plane of an Offner relay. We next must show how source and detector can be put there if the scanner head must rotate.

To scan the surface of the test cell with a 1-degree raster while the cell is rotating at its maximum rate of 3 rad/sec requires that the scanner head must rotate

$$3 \times (180/\pi) = 172 \text{ rps} = 10,300 \text{ rpm}$$

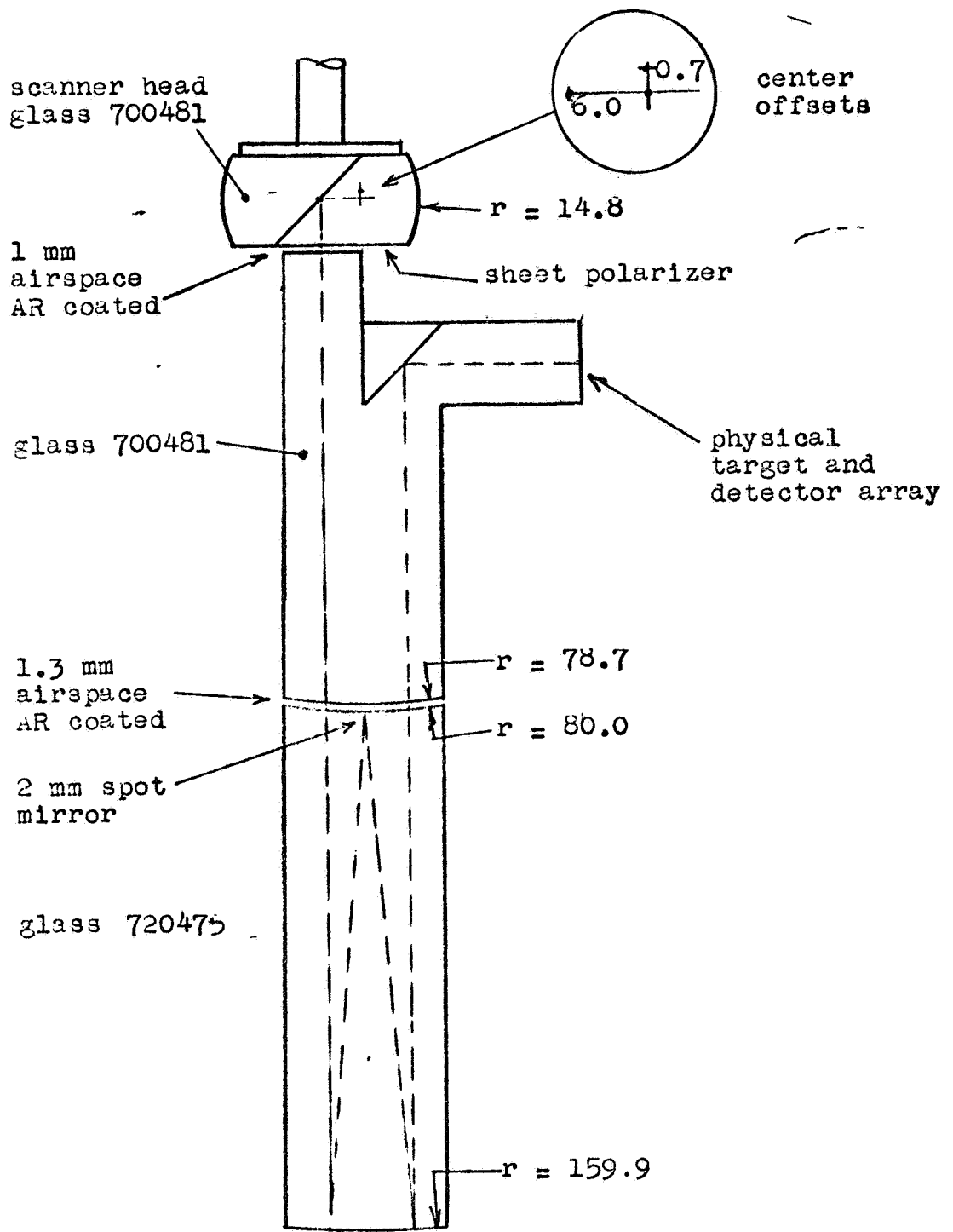
if it makes only a single scan per revolution. At this rate it is out of the question to consider anything but continuous motion for the scanner head. Small instrument motors are available to spin the scanner at this rate, but it would be impractical to consider putting electrical power in or taking electrical signals out. The detector cannot therefore be physically mounted on the scanner head. Instead, some form of optical coupling is indicated.

We propose to put at the self-conjugate plane of the relay, not a physical source/detector array, but an image of such an array. A reasonable scheme

is that shown in Figure 27.

Since we have already shown how to design a high-quality solid Offner relay for the scanner itself, it is natural to use very similar solid Offner relays to put the images of source and detector into the scanner head. As shown in Figure 27, the scanner head will incorporate a fully reflective buried folding mirror that will rotate these images into the self-conjugate plane. There they will function exactly as would physical sources and detectors. The only part that moves, now, is the small glass scanner head, which should be made symmetrical for dynamic balance.

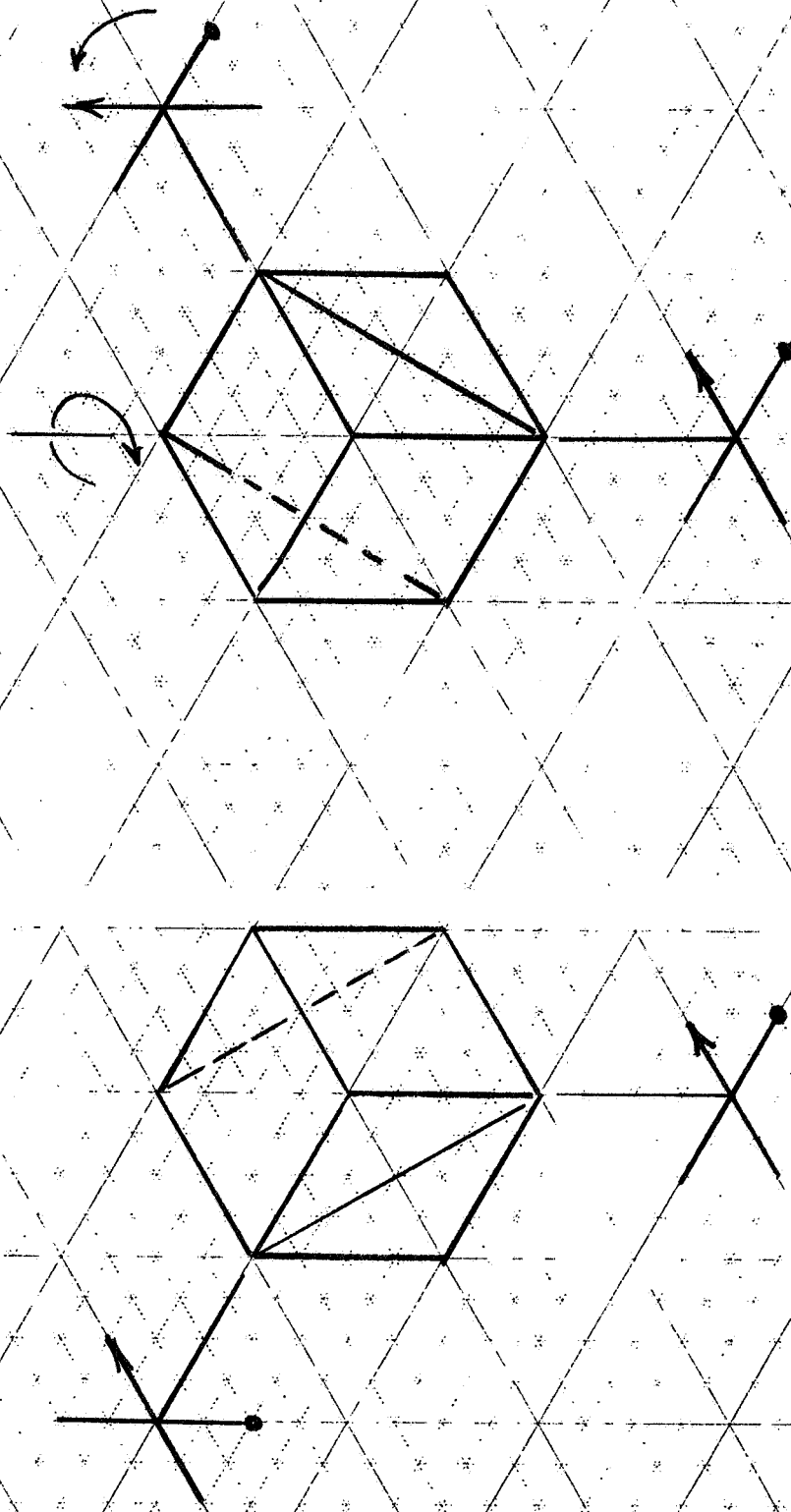
The scheme of Figure 27 solves the optical coupling problem neatly enough, but at the price of a further computational requirement. If the source/detector assembly is fixed, as we would recommend it be, the apparent orientation of this array changes as the scanner head rotates. As shown in Figure 28, the array that is used to measure gradient rotates at the same rate as the scanner head. The detectors continue to record two orthogonal components of gradient, but the reference axes rotate over the course of the scan. This rotation of axes is systematic, however, and is known a priori very accurately. Since an encoder signal will record scan latitude, the same encoder is also recording



INPUT RELAY TO SCANNER

Figure 27

ORIGINAL PAGE IS
OF POOR QUALITY



ROTATION OF DETECTOR AXES

Figure 28

ORIGINAL PAGE IS
OF POOR QUALITY

the rotation of the array axes. Hence there should be no trouble in transforming indicated components to any axes desired, as part of the normal reduction process.

The scheme of Figure 27 requires that the two Offner relays be carefully aligned, because misalignment will produce a spurious gradient signal as the scanner rotates. On the other hand, this same spurious signal can be used advantageously during setup to achieve alignment. The relative positions of the relays are simply adjusted until spurious signals disappear: the two relays are then aligned.

We have supposed here only one scan per scanner head revolution. It is quite possible to have more than one, however, thereby reducing the required scan rate. Advantage can be taken of the symmetry of the scanner head to position input relays at both top and bottom of the scanner head, thereby producing two scans per scanner head revolution. Of course this would require multiple source/detector arrays and would result in a generally more complex instrument. It is equally possible to as much as double the meridional scan angle by butting two scanners together at the edge or by arranging them in echelon.

3.5.12 Polarizer

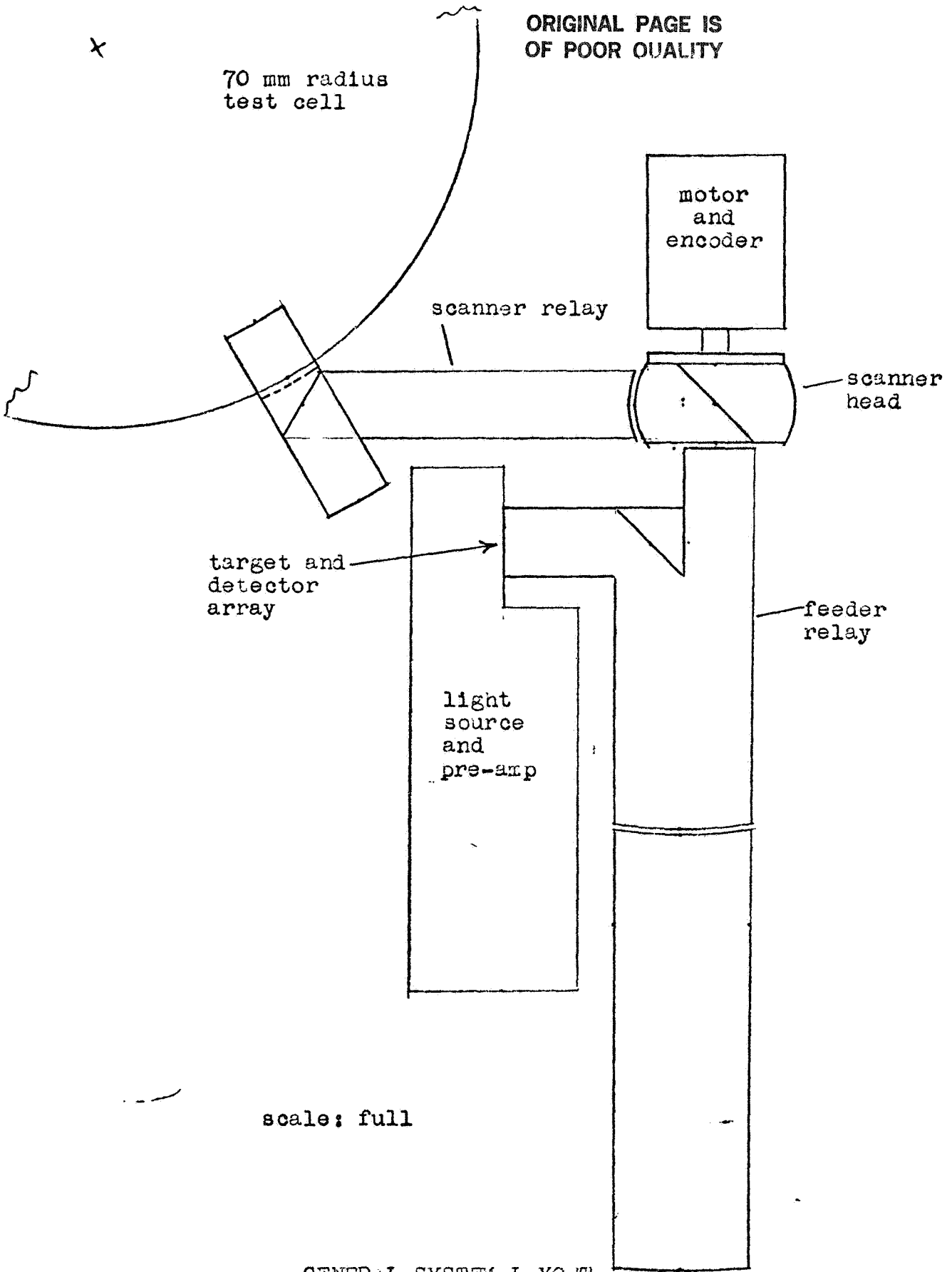
It was said earlier that to eliminate birefringence in the sapphire shell it was necessary only to polarize the incident light perpendicular to the scanning plane. This is easily done by incorporating a polarizer into the scanning head. Due attention must be given to polarization-by-reflection effects that may occur elsewhere in the optical path. These effects can be minimized by using metal reflectors throughout the instrument.

3.5.13 Complete Preliminary Design of Scanner

Applying the procedures and considerations detailed above, we have arrived at the complete preliminary scanner design shown in Figure 29. This instrument promises to be realizable at reasonable cost, to be stable and reliable in use, and to yield the results desired.

ORIGINAL PAGE IS
OF POOR QUALITY

70 mm radius
test cell



target and
detector
array

light
source
and
pre-amp

feeder
relay

scale: full

GENERAL SYSTEM LAYOUT

Figure 29

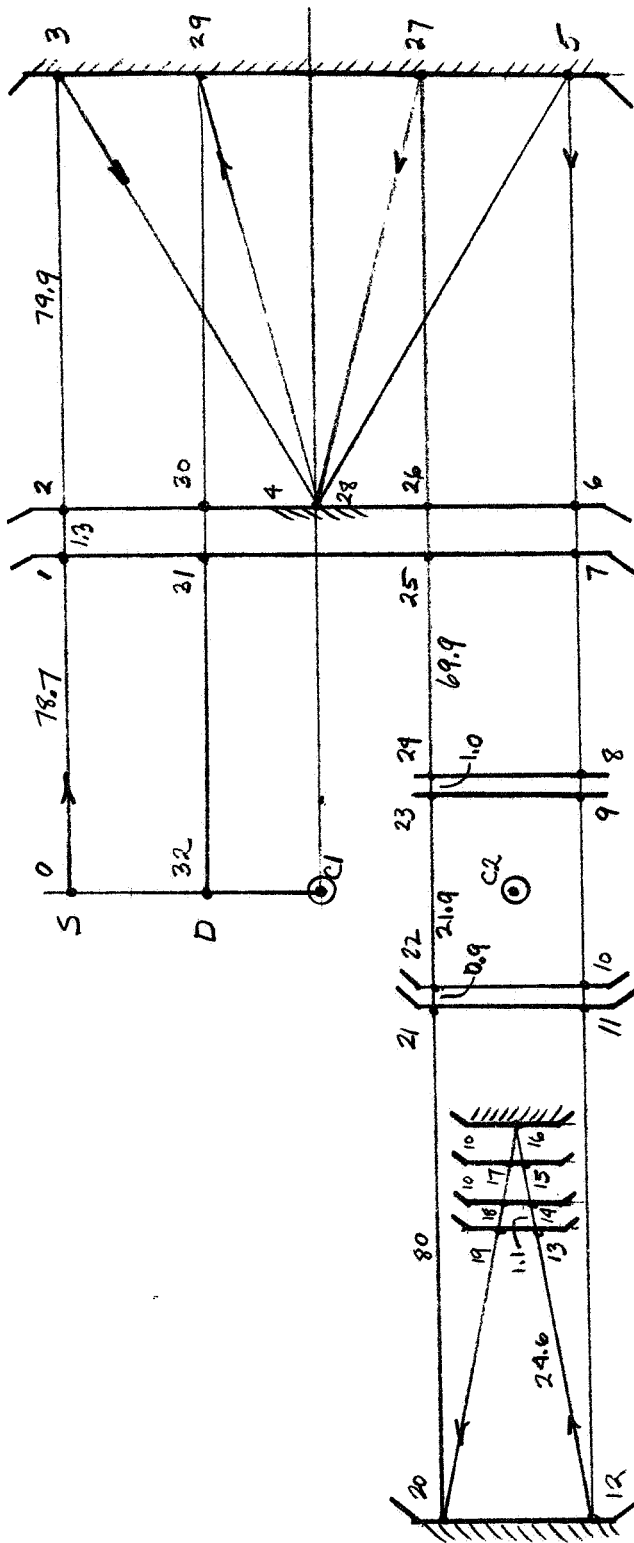
3.6 Performance Analysis

It was shown earlier that the image quality in the Offner relay is excellent in general. It is now necessary to examine in similar fashion the completed preliminary design of the scanner to ascertain whether the image quality in this more complex construction is still satisfactory and whether the sensitivities to thermal gradient and marker dot opacity are consistent with design goals. As before, image quality will be verified by raytracing. Instrumental sensitivity will be determined by photometric analysis.

3.6.1 System Raytrace

The preliminary design consists of two solid Offner relays in cascade. Neglecting folds, a ray must pass through 32 surfaces in going from target to detector. These surfaces are shown schematically in Figure 30. The same system is shown again in Figure 31, this time projected into the plane perpendicular to that of the previous figure. The target/detector array is shown, as is the path of rays from one target to its final image at its conjugate detector.

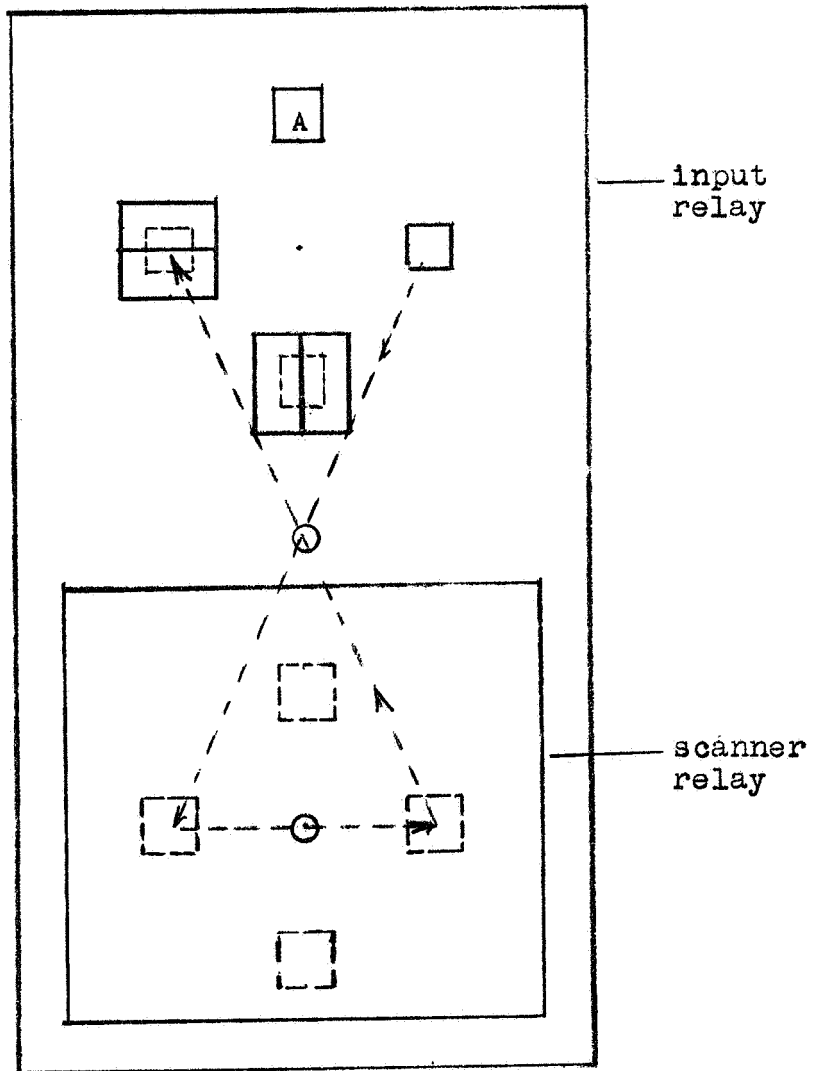
The raytrace for this full system was essentially similar to that carried out earlier for the simpler single relay. To test for image quality, a bundle



SURFACE TRAVAILS IN THE SCANNER SYSTEM

Figure 30

ORIGINAL PAGE IS
OF POOR QUALITY



PROJECTION OF SCANNER SYSTEM TRANSVERSE TO AXIS

Figure 31

ORIGINAL PAGE IS
OF POOR QUALITY

of nine rays was traced from each of eight peripheral points of target "A" in Figure 31 to the conjugate detector. For each bundle a mean position and RMS spot size were then calculated. This was done for a gradient of 0.00005 mm^{-1} , corresponding to the baseline thermal gradient of $1^\circ\text{C}/\text{cm}$. The objective here was to show that even with an index gradient in the fluid the image quality was consistent with the performance requirements of the instrument.

To test for gradient sensitivity and linearity, rays parallel to the axis were traced from each of eight peripheral points of target "A" for gradients of 0.0005 , 0.00005 and 0.000005 mm^{-1} . The objective here was to demonstrate that the entire image translated as a whole in the presence of an index gradient and that this translation was linearly proportional to gradient over at least these two decades of dynamic range.

As further checks, bundles of rays much wider than necessary were traced from selected object points, to see how well image quality was preserved, and some image shift calculations were repeated for gradient components orthogonal to those assumed for the primary calculations.

Descriptive parameters for the computer raytrace are illustrated and explained in Figure 32. The system prescription as actually input to the computer is displayed in Figure 33. Because system achromatization was not complete, the scanner system was traced only in sodium D light.

3.6.1.1 Raytrace Results

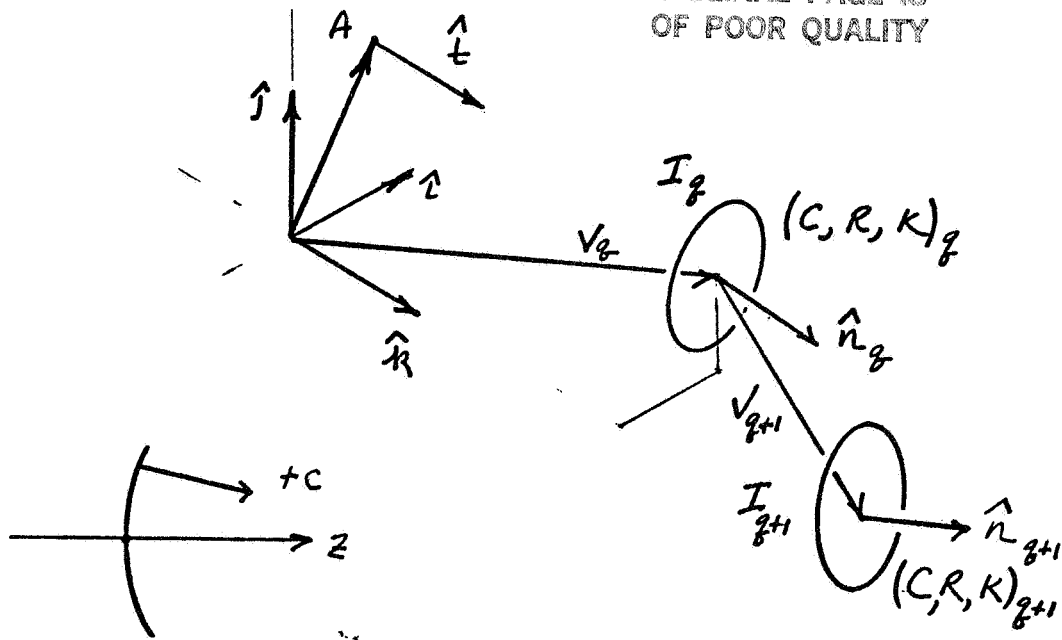
An illustrative all-surface printout is shown in Figure 34 for a preliminary case with no gradient present, and another in Figure 35 for a later case when a gradient was present.

Figure 36 shows the mean image shifts for eight points around the boundary of target "A", plus RMS spot sizes, for an f/50 bundle of rays and an index gradient of 0.00005 mm^{-1} . It can be seen here that lateral image shifts are identical to within 0.05 microns and that the geometrical RMS blur is only 0.04 microns at its worst. By comparison the diffraction blur for this case is

$$B = \frac{(2.44)(0.6)}{(1.70)(60)} = 43 \mu$$

Hence the system is clearly diffraction limited. Since f/50 is almost pinhole optics, we would expect this. The large diffraction blur relative to the small geometric blur implies that in the final design tolerances can be made fairly loose.

ORIGINAL PAGE IS
OF POOR QUALITY



A = object point position vector

\hat{z} = ray direction vector

V = surface vertex position vector

\hat{n} = surface vertex normal

C = surface vertex curvature (scalar)

K = surface conic constant (scalar)

R = surface reflectivity (scalar: 0 or 1)

I = refractive index on input side

DESCRIPTIVE PARAMETERS FOR COMPUTER RAYTRACE

ORIGINAL PAGE IS
OF POOR QUALITY

PROGRAM RAYTRACE, BY W. L. YOCER

DO YOU WISH INSTRUCTION (Y OR N)?

SYSTEM SPECIFICATION

NUMBER OF SURFACES, INCLUDING STOPS AND IMAGE PLANE=332
NUMBER OF COLORS TO BE TRACED=3

ENTER DATA FOR SURFACE 1

V(X), V(Y), V(Z)=20,0,78.7

N(X), N(Y)=20,0

C=2.0 270.43

K=20

R=20

ENTER, ONE AT A TIME, REFRACTIVE INDEXES I(W)

21.700

ENTER DATA FOR SURFACE 2

V(X), V(Y), V(Z)=20,0,1.3

N(X), N(Y)=20,0

C=2.0 125

K=20

R=20

ENTER, ONE AT A TIME, REFRACTIVE INDEXES I(W)

21.0

SYSTEM PRESCRIPTION INPUT TO COMPUTER

Figure 33

70

ENTER DATA FOR SURFACE 3
V(X),V(Y),V(Z)=70,0,79.9
N(X),N(Y)=70,0
C=1.006253909
K=70
R=71
ENTER, ONE AT A TIME, REFRACTIVE INDEXES I(W)
71.720

ENTER DATA FOR SURFACE 4
V(X),V(Y),V(Z)=70,0,79.9
N(X),N(Y)=70,0
C=7.0177
K=70
R=71
ENTER, ONE AT A TIME, REFRACTIVE INDEXES I(W)
71.720

ENTER DATA FOR SURFACE 5
V(X),V(Y),V(Z)=70,0,79.9
N(X),N(Y)=70
illegal input, retype 70,0
C=1.006253909
K=70
R=71
ENTER, ONE AT A TIME, REFRACTIVE INDEXES I(W)
71.720

ENTER DATA FOR SURFACE 6
V(X),V(Y),V(Z)=70,0,79.9
N(X),N(Y)=70,0
C=7.0177
K=70
R=70
ENTER, ONE AT A TIME, REFRACTIVE INDEXES I(W)
71.720

ENTER DATA FOR SURFACE 7
V(X),V(Y),V(Z)=70,0,79.9
N(X),N(Y)=70,0
C=7.01770448
K=70
R=70
ENTER, ONE AT A TIME, REFRACTIVE INDEXES I(W)
71.0

ENTER DATA FOR SURFACE 8
V(X),V(Y),V(Z)=70,0,69.9
N(X),N(Y)=70,0
C=70
K=70
R=70
ENTER, ONE AT A TIME, REFRACTIVE INDEXES I(W)
71.700

ENTER DATA FOR SURFACE 9

V(X),V(Y),V(Z)=70,0,-1.0

N(X),N(Y)=70,0

C=70

K=70

R=70

ENTER, ONE AT A TIME, REFRACTIVE INDEXES I(W)

P1.0

ENTER DATA FOR SURFACE 10

V(X),V(Y),V(Z)=70,-6.0,-21.9

N(X),N(Y)=70,0

C=7.067567567

K=70

R=70

ENTER, ONE AT A TIME, REFRACTIVE INDEXES I(W)

P1.700

ENTER DATA FOR SURFACE 11

V(X),V(Y),V(Z)=70,0,-9

N(X),N(Y)=70,0

C=7.043694267

K=70

R=70

ENTER, ONE AT A TIME, REFRACTIVE INDEXES I(W)

P1.0

ENTER DATA FOR SURFACE 12

V(X),V(Y),V(Z)=70,0,-80.0

N(X),N(Y)=70,0

C=7.01044932

K=70

R=71

ENTER, ONE AT A TIME, REFRACTIVE INDEXES I(W)

P1.785

ENTER DATA FOR SURFACE 13

V(X),V(Y),V(Z)=70,0,24.4

N(X),N(Y)=70,0

C=7.014064697

K=70

R=70

ENTER, ONE AT A TIME, REFRACTIVE INDEXES I(W)

P1.785

ENTER DATA FOR SURFACE 14

V(X),V(Y),V(Z)=70,0,1.1

N(X),N(Y)=70,0

C=7.014285714

K=70

R=70

ENTER, ONE AT A TIME, REFRACTIVE INDEXES I(W)

P1.0

ENTER DATA FOR SURFACE 15
V(X),V(Y),V(Z)=?0,0,10.0
N(X),N(Y)=?0,0
C=?016666667
K=?0
R=?0
ENTER, ONE AT A TIME, REFRACTIVE INDEXES I(W)
?1.764

ENTER DATA FOR SURFACE 16
V(X),V(Y),V(Z)=?0,0,10.0
N(X),N(Y)=?0,0
C=?02
K=?0
R=?1
ENTER, ONE AT A TIME, REFRACTIVE INDEXES I(W)
?1.478

ENTER DATA FOR SURFACE 17
V(X),V(Y),V(Z)=?0,0,-10.0
N(X),N(Y)=?0,0
C=?016666667
K=?0
R=?0
ENTER, ONE AT A TIME, REFRACTIVE INDEXES I(W)
?1.478

ENTER DATA FOR SURFACE 18
V(X),V(Y),V(Z)=?0,0,-10.0
N(X),N(Y)=?0,0
C=?014285714
K=?0
R=?0
ENTER, ONE AT A TIME, REFRACTIVE INDEXES I(W)
?1.764

ENTER DATA FOR SURFACE 19
V(X),V(Y),V(Z)=?0,0,-1.1
N(X),N(Y)=?0,0
C=?014064697
K=?0
R=?0
ENTER, ONE AT A TIME, REFRACTIVE INDEXES I(W)
?1.0

ENTER DATA FOR SURFACE 20
V(X),V(Y),V(Z)=?0,0,-24.6
N(X),N(Y)=?0,0
C=?01044932
K=?0
R=?1
ENTER, ONE AT A TIME, REFRACTIVE INDEXES I(W)
?1.785

ORIGINAL PAGE IS
OF POOR QUALITY

ENTER DATA FOR SURFACE 21

V(X),V(Y),V(Z)=20,0,0.0

N(X),N(Y)=20,0

C=.063694267

K=20

R=20

ENTER, ONE AT A TIME, REFRACTIVE INDEXES I(W)

?1.785

ENTER DATA FOR SURFACE 22

V(X),V(Y),V(Z)=20,0,.9

N(X),N(Y)=10,0

C=.067567567

K=20

R=20

ENTER, ONE AT A TIME, REFRACTIVE INDEXES I(W)

?1.0

ENTER DATA FOR SURFACE 23

V(X),V(Y),V(Z)=20,6.0,21.9

N(X),N(Y)=20,0

C=20

K=20

R=20

ENTER, ONE AT A TIME, REFRACTIVE INDEXES I(W)

?1.700

ENTER DATA FOR SURFACE 24

V(X),V(Y),V(Z)=20,0,1.0

N(X),N(Y)=20,0

C=20

K=20

R=20

ENTER, ONE AT A TIME, REFRACTIVE INDEXES I(W)

?1.0

ENTER DATA FOR SURFACE 25

V(X),V(Y),V(Z)=20,0,69.9

N(X),N(Y)=10,0

C=.01270648

K=20

R=20

ENTER, ONE AT A TIME, REFRACTIVE INDEXES I(W)

?1.700

ENTER DATA FOR SURFACE 26

V(X),V(Y),V(Z)=20,0,1.3

N(X),N(Y)=20,0

C=.0125

K=20

R=20

ENTER, ONE AT A TIME, REFRACTIVE INDEXES I(W)

?1.0

ENTER DATA FOR SURFACE 27

V(X),V(Y),V(Z)=20,0,79.9

N(X),N(Y)=20,0

C=.006253909

K=20

R=21

ENTER, ONE AT A TIME, REFRACTIVE INDEXES I(W)

?1.720

Figure 33
(cont'd)

ENTER DATA FOR SURFACE 28

V(X),V(Y),V(Z)=70,0,-79.9

N(X),N(Y)=70,0

C=7-.0125

K=70

R=71

ENTER, ONE AT A TIME, REFRACTIVE INDEXES I(W)

71.720

ENTER DATA FOR SURFACE 29

V(X),V(Y),V(Z)=70,0,79.9

N(X),N(Y)=70,0

C=7-.0062539086

illegal input. retype 7-.0062539086

illegal input. retype 7-.006253909

K=70

R=71.0

ENTER, ONE AT A TIME, REFRACTIVE INDEXES I(W)

71.720

ENTER DATA FOR SURFACE 30

V(X),V(Y),V(Z)=70,0,-79.9

N(X),N(Y)=70,0

C=7-.0125

K=70

R=70

ENTER, ONE AT A TIME, REFRACTIVE INDEXES I(W)

71.720

ENTER DATA FOR SURFACE 31

V(X),V(Y),V(Z)=70,0,-1.3

N(X),N(Y)=70,0

C=7-.01270648

K=70

R=70

ENTER, ONE AT A TIME, REFRACTIVE INDEXES I(W)

71.0

ENTER DATA FOR SURFACE 32

V(X),V(Y),V(Z)=70,0,-78.7

N(X),N(Y)=70,0

C=70

K=70

R=70

ENTER, ONE AT A TIME, REFRACTIVE INDEXES I(W)

71.700

PROGRAM?RAYTRACE

GENERAL RAYTRACE

ENTER COLOR NUMBER W=71

ENTER OBJECT POINT A(X),A(Y)=70,8.3

ENTER RAY COMPONENTS T(X),T(Y)=70,0

PRINT ALL SURFACES (Y OR N)?Y

INSTRUCTION?TRACE

INSTRUCTION TRACE

RUN INPUT DATA, TRACE 2

A= 0 8.3 0
T= 0 0 1
BACKFOCUS= 78.7

SURFACE= 1 COLOR= 1
A= 0 8.3 -.4385981
T= 0 -.0745337 .9972185

SURFACE= 2 COLOR= 1
A= 0 8.201537 -.4215178
T= 0 -2.45194e-25 1

SURFACE= 3 COLOR= 1
A= 0 8.199573 -.210372
T= 0 -.1024442 -.9947384

SURFACE= 4 COLOR= 1
A= 0 -.0077714 9.53674e-07
T= 0 -.1024442 .9947188

SURFACE= 5 COLOR= 1
A= 0 -8.230198 -.119484
T= 0 .0001877 -1

SURFACE= 6 COLOR= 1
A= 0 -8.21579 -.4230919
T= 0 .0745445 -.9972332

SURFACE= 7 COLOR= 1
A= 0 -8.31500 -.4404914
T= 0 .0001918 -1

SURFACE= 8 COLOR= 1
A= 0 -8.30160 0
T= 0 .000315 -1

SURFACE= 9 COLOR= 1
A= 0 -8.30136 0
T= 0 .0001918 -1

SURFACE= 10 COLOR= 1
A= 0 -2.297194 .1793675
T= 0 .11286 -.9937889

SURFACE= 11 COLOR= 1
A= 0 -2.19357 .1539956
T= 0 -.0001991 -1

ILLUSTRATIVE ALL-SURFACE
RAYTRACE WITH NO GRADIENT

Figure 34

SURFACE=	12	COLOR=	1		
A=	Ø		-2.209523		.0255108
T=	Ø		.0459648		.9989432
SURFACE=	13	COLOR=	1		
A=	Ø		-1.078389		.0081782
T=	Ø		.0701389		.9975381
SURFACE=	14	COLOR=	1		
A=	Ø		-1.001126		.0071593
T=	Ø		.0459564		.9989436
SURFACE=	15	COLOR=	1		
A=	Ø		-.5412931		.0024416
T=	Ø		.0531021		.9985893
SURFACE=	16	COLOR=	1		
A=	Ø		-.009652		7.15256e-07
T=	Ø		.0527165		-.9986098
SURFACE=	17	COLOR=	1		
A=	Ø		.5181291		.0022372
T=	Ø		.0455707		-.9989613
SURFACE=	18	COLOR=	1		
A=	Ø		.9741032		.006778
T=	Ø		.0697497		-.9975653
SURFACE=	19	COLOR=	1		
A=	Ø		1.050942		.0077675
T=	Ø		.0455792		-.9989609
SURFACE=	20	COLOR=	1		
A=	Ø		2.172584		.0246642
T=	Ø		.000187		1
SURFACE=	21	COLOR=	1		
A=	Ø		2.187568		.1531487
T=	Ø		.1116696		.9937461
SURFACE=	22	COLOR=	1		
A=	Ø		2.291549		.1784815
T=	Ø		.0005779		1
SURFACE=	23	COLOR=	1		
A=	Ø		-3.695899		-2.38419e-07
T=	Ø		.0009824		1
SURFACE=	24	COLOR=	1		
A=	Ø		-3.694916		-1.49012e-08
T=	Ø		.0005779		1
SURFACE=	25	COLOR=	1		
A=	Ø		-3.654573		-.0848999
T=	Ø		.0035493		.9994377

ORIGINAL PAGE IS
OF POOR QUALITY

SURFACE=	26	COLOR=	1	
A=	0		-3.610821	.0815292
T=	0		.000176	1
SURFACE=	27	COLOR=	1	
A=	0		-3.564651	-.0397387
T=	0		.0451519	-.9859804
SURFACE=	28	COLOR=	1	
A=	0		.0442728	.14441e-05
T=	0		.0462715	.9989292
SURFACE=	29	COLOR=	1	
A=	0		3.743982	-.0438375
T=	0		.0005445	-1
SURFACE=	30	COLOR=	1	
A=	0		3.700472	-.0856295
T=	0		.0024201	-.9994754
SURFACE=	31	COLOR=	1	
A=	0		3.742762	-.0890482
T=	0		-.000544	-1
SURFACE=	32	COLOR=	1	
A=	0		3.7	0
T=	0		-.000144	-1

INSTRUCTION?

Figure 34 (cont'd)

ORIGINAL PAGE IS
OF POOR QUALITY

TRACE

```

RUN INPUT DATA, TRACE      86
A=          0              8.8              0
T=          0              0                1
BACKFOCUS=-78.7

SURFACE=    1 COLOR=      1
A=          0              8.8              -.4935417
T=          0              -.0751186         .9968652

SURFACE=    2 COLOR=      1
A=          0              8.695268         -.4739519
T=          0              -3.02610e-05        1

SURFACE=    3 COLOR=      1
A=          0              8.692842         -.2364655
T=          0              -.1085978         -.9940858

SURFACE=    4 COLOR=      1
A=          0              -.0099109              0
T=          0              -.1088441              .9940589

SURFACE=    5 COLOR=      1
A=          0              -8.732402             -.2386227
T=          0              .0002175              -1

SURFACE=    6 COLOR=      1
A=          0              -8.714971             -.4761076
T=          0              -.0788716             -.9968851

SURFACE=    7 COLOR=      1
A=          0              -8.819377             -.4957252
T=          0              .0002478              -1

SURFACE=    8 COLOR=      1
A=          0              -8.80218              9.53674e-07
T=          0              .0004212              -1

SURFACE=    9 COLOR=      1
A=          0              -8.801759             1.49012e-08
T=          0              .0002478              -1

SURFACE=   10 COLOR=      1
A=          0              -2.796399             .2665849
T=          0              .1369715              -.9905823

SURFACE=   11 COLOR=      1
A=          0              -2.666682             .2281285
T=          0              .102445e-06           -1

```

ILLUSTRATIVE ALL-SURFACE
RAYTRACE WITH GRADIENT

$$\frac{2n}{2x} = .00005 \text{ mm}^{-1}$$

Figure 35

ORIGINAL PAGE IS
OF POOR QUALITY

SURFACE=	12	COLOR=	1		
A=	Ø		-2.666764		.Ø371637
T=	Ø		.Ø557ØØ.		.9984472
SURFACE=	13	COLOR=	1		
A=	Ø		-1.2956Ø4		.Ø118Ø53
T=	Ø		.Ø85118L		.9963714
SURFACE=	14	COLOR=	1		
A=	Ø		-1.2Ø176		.Ø1Ø3167
T=	Ø		.Ø55696.		.9984478
SURFACE=	15	COLOR=	.		
A=	Ø		-.6442939		.ØØ34593
T=	Ø		.Ø64953		.9979247
SURFACE=	16	COLOR=	1		
A=	.ØØ16549		.ØØØ7799		3.347Ø1e-Ø8
T=	.ØØØ4Ø49		.Ø644269		-.9979226
SURFACE=	17	COLOR=			
A=	.ØØ73662		.6461657		.ØØ348
T=	.ØØØ6433		.Ø557295		-.9984458
SURFACE=	18	COLOR=	1		
A=	.Ø138Ø43		1.2Ø3944		.Ø1Ø3555
T=	.ØØØ9338		.Ø551493		-.9963682
SURFACE=	19	COLOR=	1		
A=	.Ø14889		1.297822		.Ø118474
T=	.ØØØ6434		.Ø5574Ø2		-.9984453
SURFACE=	20	COLOR=	1		
A=	.Ø3Ø7244		2.669749		.Ø372515
T=	1.529Ø8e-Ø6		3.22266e-Ø5		1
SURFACE=	21	COLOR=	1		
A=	.Ø3Ø847		2.667165		.2282419
T=	.ØØ15866		.156891		.99Ø5856
SURFACE=	22	COLOR=	1		
A=	.Ø3235Ø1		2.79e353		.2667Ø82
T=	4.4Ø815e-Ø6		.ØØ62165		1
SURFACE=	23	COLOR=	1		
A=	.Ø324455		-3.198464		-2.38419e-Ø7
T=	7.49385e-Ø6		.ØØØ368		1.ØØØØØ1

Figure 35 (cont'd)

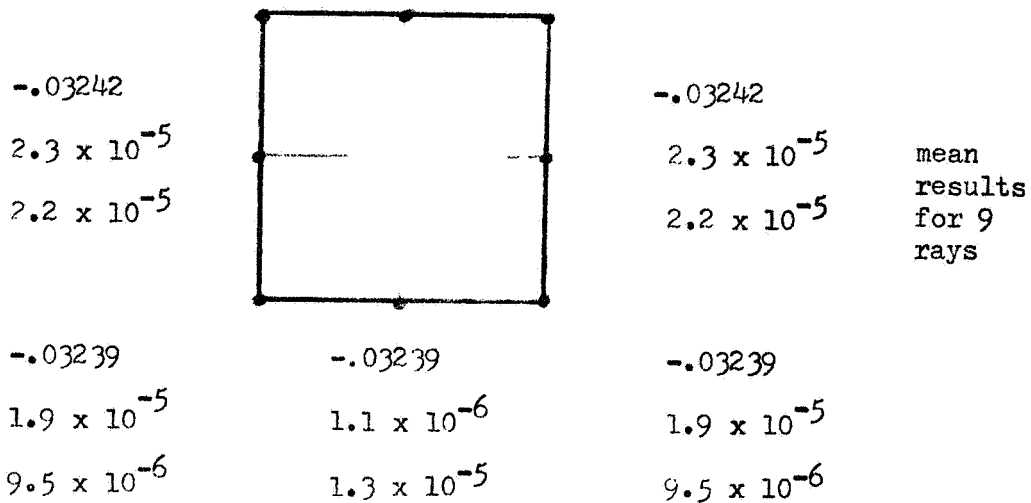
ORIGINAL PAGE IS
OF POOR QUALITY

SURFACE=	24	COLOR=	1		
A=	.032453		-3.198096		0
T=	4.40815e-06		.0002165		1
SURFACE=	25	COLOR=	1		
A=	.0327608		-3.182978	-.0644007	
T=	-.0002843		.028719	.9995882	
SURFACE=	26	COLOR=	1		
A=	.0323903		-3.145556	-.0618712	
T=	4.41684e-06		.0002156		1
SURFACE=	27	COLOR=	1		
A=	.0327434		-3.128321	-.0306072	
T=	-.0004051		.0393364	-.9992262	
SURFACE=	28	COLOR=	1		
A=	.0003671		.0158893	-9.53674e-07	
T=	.0003959		.0397334	.9992106	
SURFACE=	29	COLOR=	1		
A=	.0312761		3.191826	-.0318632	
T=	-4.76119e-06		-.0001816		-1
SURFACE=	30	COLOR=	1		
A=	-.0316567		3.177309	-.0631256	
T=	.0002935		.0285219	-.9996	
SURFACE=	31	COLOR=	1		
A=	.0320391		3.214214	-.0656703	
T=	-4.76987e-06		-.0001803		-1
SURFACE=	32	COLOR=	1		
A=	.0324142		3.2		0
T=	-4.76987e-06		-.0001803		-1

Figure 35 (cont'd)

ORIGINAL PAGE IS
OF POOR QUALITY

$\Delta x =$	$-.03244$	$-.03244$	$-.03244$
$\Delta y =$	2.7×10^{-5}	1.4×10^{-6}	2.7×10^{-5}
Blur =	4.1×10^{-5}	1.7×10^{-5}	4.1×10^{-5}



(all dimensions mm)

GEOMETRIC IMAGE SHIFTS AND BLUR FOR GRADIENT

$$\left(\frac{\partial N}{\partial x}\right) = .00005 \text{ mm}^{-1}$$

Figure 35

For comparison, Figure 37 shows the geometric image blur for two selected target points for an $f/5$ ray bundle--ten times larger. The geometric blur is seen to be about 4.6 microns, while the diffraction blur for this case would be 4.3 microns. Even for this extreme case the optics may be considered to be close to diffraction limited.

Figure 38 shows the image shifts around the target image boundary for three values of index gradient. These shifts can be seen to both uniform and linear to one part in a thousand over the full two decades of dynamic range.

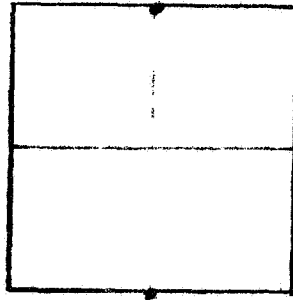
In Figure 39 the shifts produced by two orthogonal gradient components are compared. It can be seen that they also are equal to one part in a thousand.

These raytrace results may be considered very satisfactory and consistent with expectation. They imply that if the 1 x 1 mm target is uniformly illuminated, the light distribution at the detector will be as shown in Figure 40. The maximum image movement accurately measurable will be 414 microns, corresponding to a thermal gradient of

$$(.414 / .3226) (10) = 12.8 \text{ } ^\circ\text{C/cm}$$

ORIGINAL PAGE IS
OF POOR QUALITY

$$\begin{aligned}\Delta x &= < 10^{-8} \\ \Delta y &= -7.5 \times 10^{-6} \\ \text{Blur} &= 4.7 \times 10^{-3}\end{aligned}$$



mean results
of 9 rays

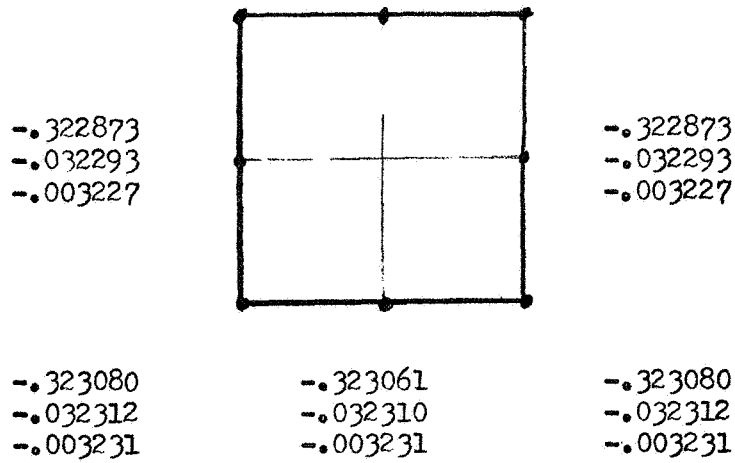
$$\begin{aligned}\Delta x &= < 10^{-8} \\ \Delta y &= 1.8 \times 10^{-5} \\ \text{Blur} &= 4.5 \times 10^{-3}\end{aligned}$$

GEOMETRIC IMAGE SHIFTS FOR AN 0.20 RAY BUNDLE (mm)
(no gradient)

Figure 37

ORIGINAL PAGE IS
OF POOR QUALITY

$$\Delta y = \begin{cases} -.322630 & -.322610 & -.322630 \\ -.032270 & -.032267 & -.032270 \\ -.003228 & -.003227 & -.003228 \end{cases}$$



(dimensions in mm)

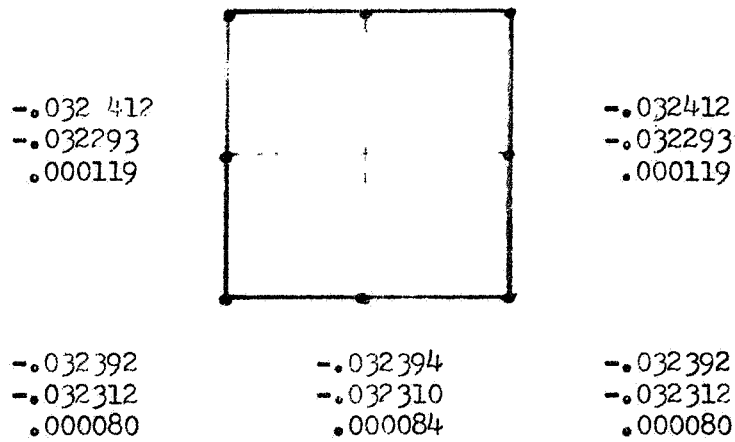
GEOMETRIC IMAGE SHIFTS FOR THREE VALUES OF GRADIENT

$$|\nabla N| = \begin{cases} .0005 \\ .00005 \\ .000005 \end{cases} \text{ mm}^{-1}$$

Figure 38

ORIGINAL PAGE IS
OF POOR QUALITY

$\Delta x =$	-.032437	-.032439	-.032437
$\Delta y =$	-.032270	-.032267	-.032770
diff =	.000167	.000172	.000167



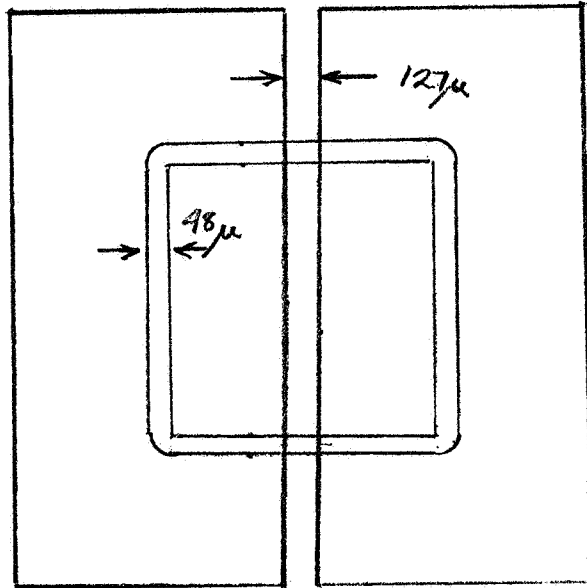
(all dimensions in mm)

COMPARISON OF GEOMETRIC IMAGE SHIFTS FOR

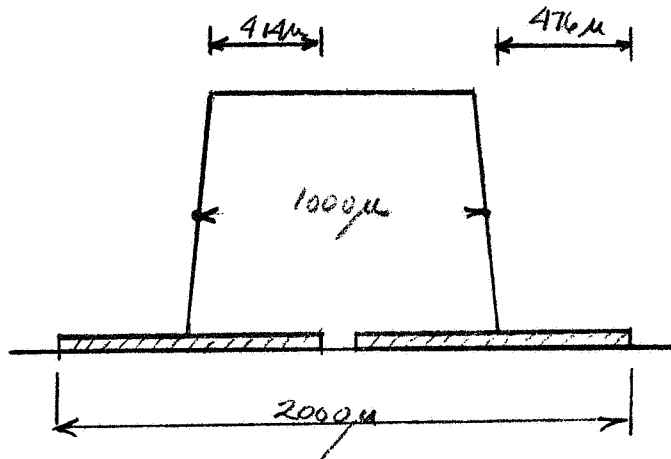
$$\left\{ \begin{array}{l} \frac{\partial n}{\partial x} \\ \frac{\partial n}{\partial y} \end{array} \right\} = .00005 \text{ mm}^{-1}$$

Figure 39

$$\text{diffraction blur } B = \frac{2.44(0.6\mu)}{1.700(0.018)} = 98\mu$$



assumed
detector
2 x 2 mm



PREDICTED LIGHT DISTRIBUTION AT DETECTOR

Figure 40

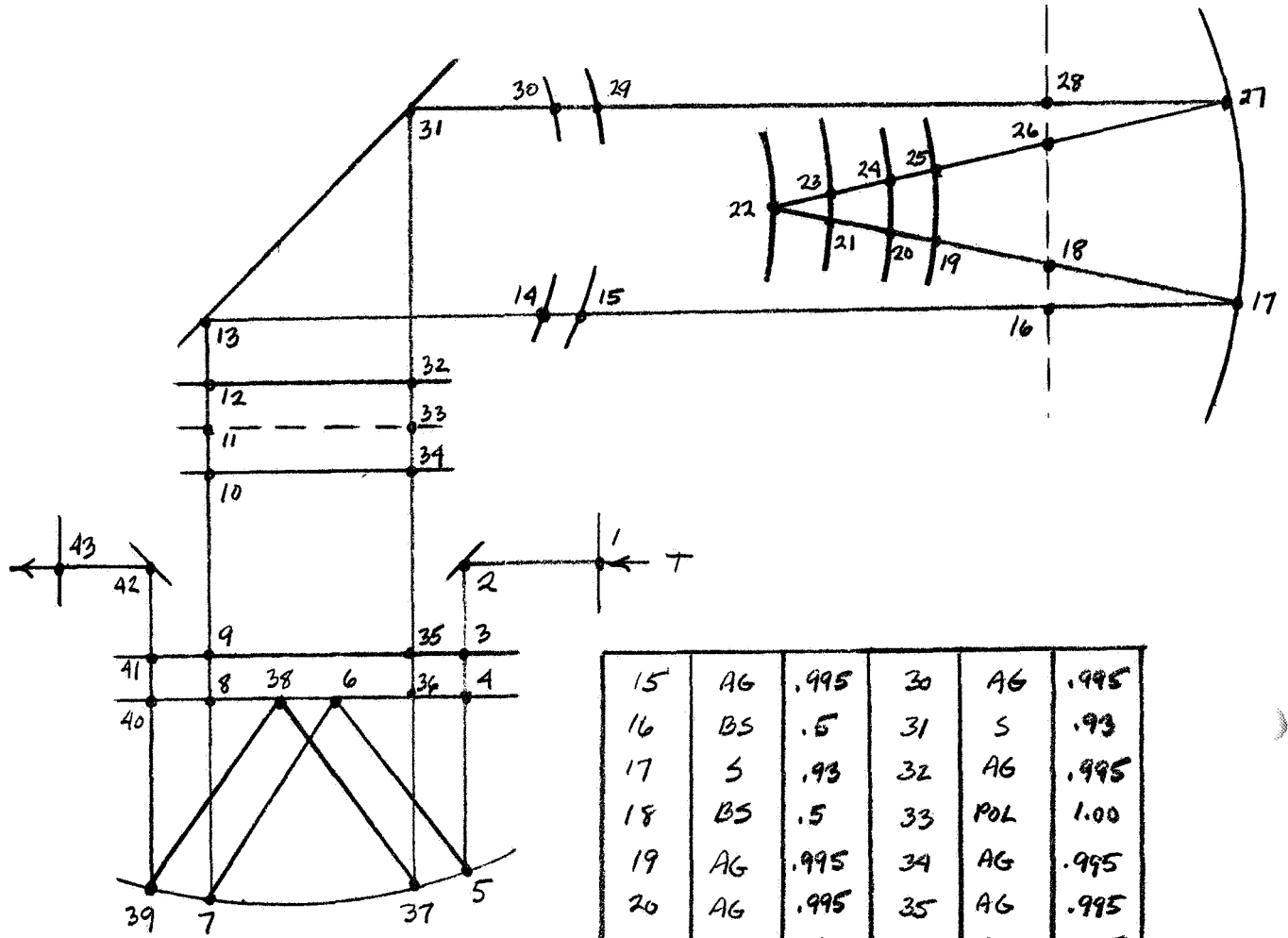
3.6.2 Photometric Analysis

Photometric analysis is necessary to estimate the available (or potential) signal-to-noise ratio in the detectors. Knowing the SNR, we can then estimate the ability of the scanner to detect increments in thermal gradient and the presence of marker dots.

3.6.2.1 System Transmission

The first step is to estimate the optical transmission of the scanner. We assume here the double Offner relay design. All sources of loss in this system are identified in Figure 41, and transmission estimates are given for each. Anti-reflection coatings have been assumed for all air/glass surfaces. To minimize unwanted polarization effects, all internal reflections are assumed to be from metal. For maximum reflectivity, this is assumed to be silver. Input light is assumed to be unpolarized, and a polarizer at the scanner head is assumed to absorb 50% of this input. From the calculations of Figure 41 we conclude that the overall transmission of the scanner is 1.07% from source to detector.

ORIGINAL PAGE IS
OF POOR QUALITY



1	AG	.995	8	AG	.995	15	AG	.995	30	AG	.995
2	S	.93	9	AG	.995	16	BS	.5	31	S	.93
3	AG	.995	10	AG	.995	17	S	.93	32	AG	.995
4	AG	.995	11	POL	.5	18	BS	.5	33	POL	1.00
5	S	.93	12	AG	.995	19	AG	.995	34	AG	.995
6	S	.93	13	S	.93	20	AG	.995	35	AG	.995
7	S	.93	14	AG	.995	21	FS	.99	36	AG	.995
						22	S	.93	37	S	.93
						23	FS	.99	38	S	.93
						24	AG	.995	39	S	.93
						25	AG	.995	40	AG	.995
						26	BS	.5	41	AG	.995
						27	S	.93	42	S	.93
						28	BS	.5	43	AG	.995
						29	AG	.995			

$$T = (.995)^{22} (.93)^{13} (.5)^5 (.99)^2 (1.00) = 0.0107$$

CALCULATED TRANSMISSION OF SCANNER SYSTEM

Figure 41

3.6.2.2 Signal Bandwidth

We may estimate the signal bandwidth from the conventional approximation for television:

$$\Delta f = \frac{1}{2} N_h N_v F_p$$

where N_h = number of horizontal picture elements
 N_v = number of vertical picture elements
 F_p = picture repetition rate

We assume here that the scanning spot is 1° in diameter and that we require exhaustive coverage at the equator, representing the worst case. We assume that the maximum rotation rate of the test sphere is 3 rad/sec. For this worst case, then

$$\begin{aligned} N_h &= 360 \\ N_v &= 360 \\ F_p &= 3/(2\pi) \end{aligned}$$

whence

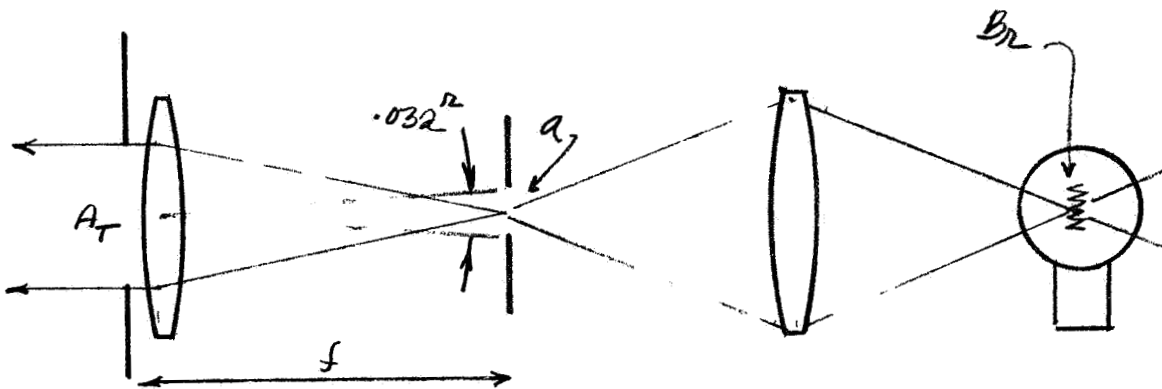
$$\Delta f = \frac{1}{2}(360)(360)(1.5/\pi)$$

$$\Delta f = 30,940 \text{ Hz}$$

3.6.2.3 Source Selection

We would propose to illuminate the 1 mm^2 target with a miniature collimator having the general form of that sketched in Figure 42. From References 10 and 11 we infer that for a typical small 10 watt tungsten lamp, such a collimator can deliver into the target aperture approximately 42 microwatts within the 0.5 to 0.7 micron bandpass. This estimate is consistent with published specifications of commercial devices of this type (see Appendix).

ORIGINAL PAGE IS
OF POOR QUALITY



$$P = B_D \left(\frac{a}{f^2} \right) A_T$$

$$B_D = .052 \text{ w/ster-mm}^2$$

$$A_T = 1 \text{ mm}^2$$

$$\frac{a}{f^2} = \frac{\pi}{4} (.032)^2$$

$$P = 42 \mu\text{W}$$

TYPICAL TARGET ILLUMINATOR

Figure 42

ORIGINAL PAGE IS
OF POOR QUALITY

3.6.2.4 Signal-to-Noise Ratio

Of the 42 microwatts, half will normally be directed toward a single detector in the dual detector array. The NEP of the UDT PIN Spot/2 (see Appendix) is given as $9 \times 10^{-14} \text{ W(Hz)}^{-\frac{1}{2}}$ at the peak wavelength of 0.9 micron. Converted to the intended midband wavelength of 0.6 microns this becomes $1.3 \times 10^{-13} \text{ W(Hz)}^{-\frac{1}{2}}$. For a system transmission of 1.07% and a system bandpass of 30,940 Hz, the indicated SNR is

$$\text{SNR} = \frac{PT}{\text{NEP} \sqrt{\Delta f}}$$
$$\text{SNR} = \frac{(21 \times 10^{-6})(.0107)}{(1.3 \times 10^{-13}) \sqrt{30,940}} = 9827$$

This represents the SNR for the full signal falling on a detector.

3.6.2.5 Thermal Gradient Sensitivity

We have seen that in glass the image shift produced by a 1°C/cm gradient component is about 32 microns. The desired least-detectable gradient of 0.01°C/cm will produce an image shift of 0.32 microns. A shift of 0.32 microns on the detector represents a relative signal change of $0.32/500 = 6.4 \times 10^{-4}$. Such a shift should therefore be detectable with a SNR of

$$\text{SNR} = (6.4 \times 10^{-4})(9.83 \times 10^3) = 6.3$$

It should be pointed out that the signal bandpass assumed here is larger than is necessary, so this figure is on the conservative side. The bandpass assumed (31 KHz) is appropriate for generating a television picture in which the details subtend about 1° , but the maximum spatial frequency for thermal gradient is likely to be 0.1 cycle/degree. The electrical bandpass could therefore be reduced by a factor of about 5 if desired, implying a SNR for minimum gradient closer to 14 than to 6. This is a healthy SNR and leads us to conclude that the goal of a minimum detectable thermal gradient of $0.01^\circ\text{C}/\text{cm}$ is certainly realizable in this instrument.

3.6.2.6 Marker Spot Sensitivity

The absorption spectrum of a marker spot is considerably narrower than the $200\text{ m}\mu$ bandpass assumed here for the illuminator. If we suppose for the present that this absorption spectrum is $10\text{ m}\mu$ wide, then only about 1/20 of the incident light can be affected by the marker spot. At full opacity the spot will produce a relative signal change of 0.05. In this case the full 31 KHz bandpass is necessary, so the SNR in this case is

$$\text{SNR} = (0.05)(9.83 \times 10^3) = 492$$

If the two-way opacity of the spot is reduced to only 10%, the SNR is still

$$SNR = (5 \times 10^3)(9.83 \times 10^3) = 49$$

We may infer then that the design goal for marker dot sensitivity can probably be met in this instrument rather easily.

3.6.2.7 Increasing Signal-to-Noise Ratio

The detector SNR for either gradient or marker spot detection is proportional to the power put through the target by the illuminator. We have assumed here a very conservative model of a tungsten source. By various means (reflexive mirror, increasing voltage) it would be easy to at least double the power available from this same source, which means doubling the SNR. A small Xenon arc would dramatically increase the SNR still further. A small unpolarized laser, if spectrally suitable, could yield an even greater increase. The problem with the laser, however, is that its spectrum must overlap the absorption spectrum of the photochromic dye in the fluid, which is narrow. The general point to be made here is that the SNR in this instrument can easily be brought by various means to a very healthy level, ample for any measurement of interest in this experiment.

It should be pointed out here also that considerable further improvement is possible through optimum matching of target to detector. This preliminary design was based on a nominal 1 x 1 mm target and a nominal 2 x 2 mm detector. In fact the detector is 2.54 x 2.54 mm. A better target design for this detector would be 1.33 x 3.00 mm. Such a change would have the following effects, all in the right direction:

1) The power into each detector is increased by a factor of 3.38, from $21 \mu\text{W}$ to $71 \mu\text{W}$.

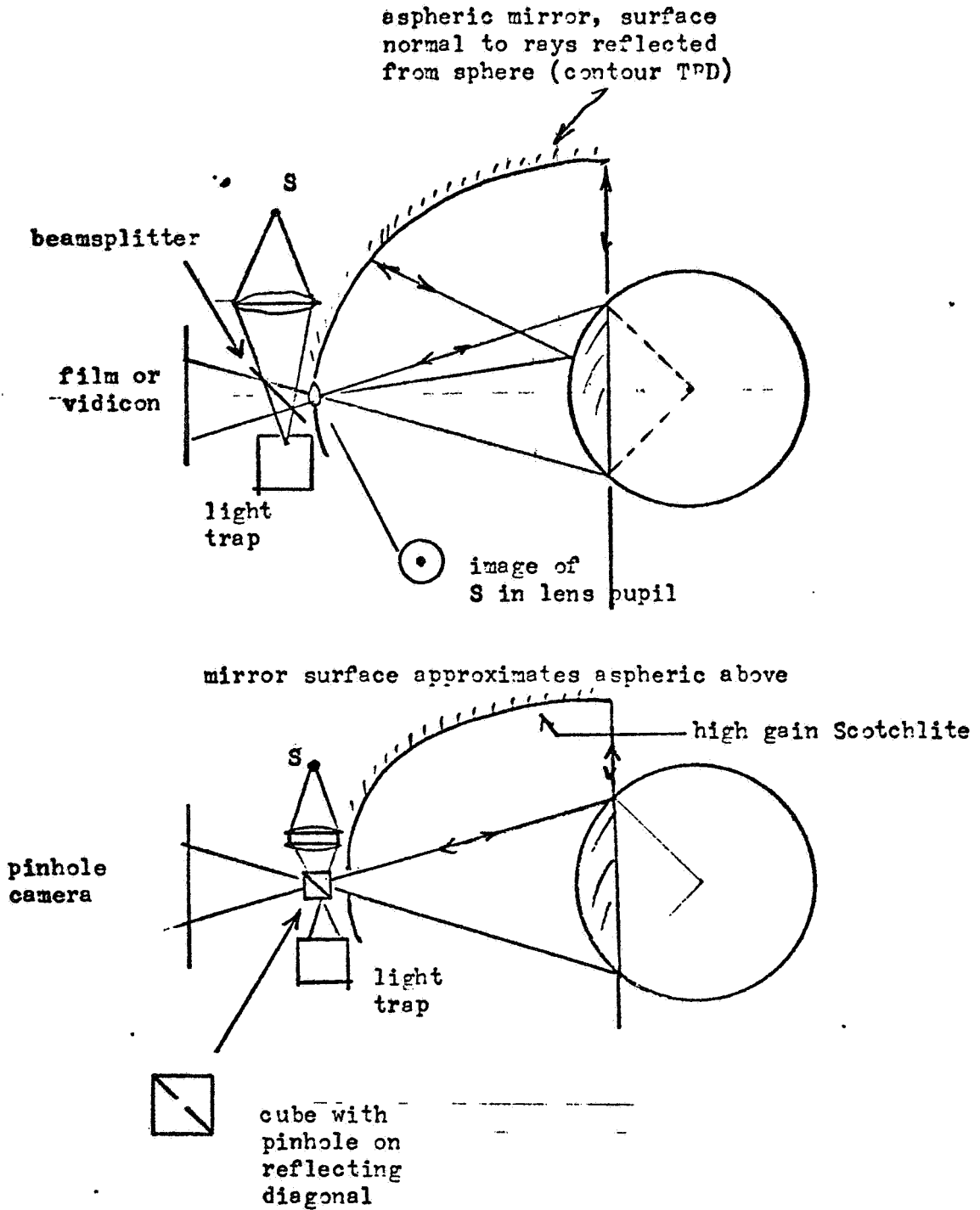
2) The SNR at null is increased by this same factor of 3.38.

3) The SNR for a least detectable difference of $0.01^\circ\text{C}/\text{cm}$ is increased by a factor of 2.8, from 6.2 to 17.6.

4) The maximum detectable gradient is increased by a factor of 1.46, from 12.8 to $17.6^\circ\text{C}/\text{cm}$.

3.7 Alternative Video Methods

We have argued above that the total return signal in the detector array represents a measure of surface albedo and can be used, with minimal processing, as a video input signal for the payload specialist's display. If for human engineering reasons the scrolling display is undesirable and, for instance, a strobe display is desired instead, this can be provided without great difficulty. Two simple ways to view a 90° spherical sector by strobe TV are shown in Figure 43. The key optical requirements here are bright-field illumination and extreme depth of field. The first is achieved by using a retroreflective illuminator; the second by stopping down the camera severely. In fact, given specular bright-field illumination, as shown in Figure 43, pinhole optics should be perfectly satisfactory for observing opaque marker dots. The light source would be a flashlamp strobed at whatever update frequency is desired.



SIMPLE METHODS OF IMAGING 90° SPHERICAL
SECTOR

Figure 43

4.0 CONCLUSIONS AND RECOMMENDATIONS

This study has clearly shown the feasibility of performing all necessary AGCE measurements with an instrument of the flying-spot scanner type. The claims made for such an instrument have been shown to be justified. The design evaluated was only a preliminary design, however, and some details chosen were not optimum. It is clear that a re-examination of glass choices would be advantageous, for instance.

The design examined in this study proved to have a smaller scan angle than desired. This followed from the choice of detector configuration and from the fact that high-index materials were used for the components of the solid scanner relay. High index materials were used because of an early design decision that the interface between scanner and rotating test cell should be a zero-power interface. This made it necessary to use a higher index on the scanner side of the interface than that of the sapphire, which was already high. If, on the other hand, the design had begun from the premise that the first interface did not have to be zero-power, then low index materials could have been used in the scanner, the primary mirror radius would have been larger, there would have been more room for the folding mirror, the scan angle would have been larger, and the image displacement for a given

**ORIGINAL PAGE IS
OF POOR QUALITY**

gradient would have been larger. In this preliminary design effort, intended only to establish feasibility, there was no time to explore more than one design approach, and the zero-power interface was the approach chosen. There also was no time in this study to choose the glass types most advantageously for achromatization. This must of course be done before any design can be called final.

A most important aspect of this optical design that has not been touched is that of tolerance and sensitivity analysis. It must be determined by raytracing just how sensitive the performance of this system is to variations in radii and glass indexes. From such analysis it will be possible to allocate manufacturing errors according to cost. It would be very desirable from a cost standpoint, for instance, to loosen tolerances on the sapphire shell, where overspecification is expensive, if the effect can be made up by tightening tolerances on the scanner head, where overspecification is much less expensive. This cannot be done without a sensitivity analysis, however.

On the basis of study results, and the further comments above, we make the following recommendation with respect to further work on the preliminary optical design of the flying spot scanner:

1) That there be further design iteration to optimize the target-detector configuration, to complete achromatization, and to extend as far as possible what advantage can be gained through substitution of glasses.

2) That there be a general sensitivity and tolerance analysis of the system, to establish limits on performance expectation and to provide the basis for a cost-effective allocation of manufacturing errors;

3) That there be an examination of instrument configurations based on multiple scanners to ascertain whether increased scan angle, reduced scan rate, or improved information can be obtained cost-effectively in this way; and finally,

4) That the question of polarization, basically ignored here except for certain general statements, be given further attention.

C-4

3.0 APPENDICES

APPENDIX A - References

Gradient Index Optics

1. D. W. Holder and R. J. North, Schlieren Methods, London, HMSO, 1963
2. O. N. Stavroudis, Optics of Rays, Wavefronts and Caustics, NY Academic Press, 1972
3. S. Wolin, "Ray Deflection Through a Medium Having a Continuously Varying Refractive Index," JOSA 43, 373 (1953)
4. D. T. Moore, "Raytracing in Gradient-Index Media," JOSA 65, 451 (1975)
5. L. Montaluno, "Raytracing in Inhomogeneous Media," JOSA 58, 1667 (1968)
6. K. W. Beach et. al., "Light Deflection Effects in the Interferometry of One-Dimensional Refractive Index Fields," JOSA 63, 559 (1973)
7. Y. Aoki, "Light Rays in Lens-like Media," JOSA 56, 1648 (1966)
8. R. J. Goldstein, "Optical Techniques for Temperature Measurement," in E. R. G. Eckert and R. J. Goldstein, eds., Measurements in Heat Transfer, Washington, Hemisphere Pub., 1976

DMSO

9. H. L. Clever and M. L. Taylor, "Refractive Indexes of Dimethylsulfoxide...", J. Chem & Engr. Data 16, 91 (1971)

Tungsten Sources

10. F. E. Carlson and C. N. Clark, "Light Sources for Optical Devices," in R. Kingslake, ed., Applied Optics and Optical Engineering, V.1, NY, Academic Press, 1965
11. L. E. Barrow, "Memorandum on a Procedure for Obtaining Spectral Radiant Intensities of Tungsten Filament Lamps, 400-700 m μ ," JOSA 49, 1122 (1959)

The Monocentric Relay

12. A. Offner, "New Concepts in Projection Mask Aligners," Optical Engineering 14, 130 (1975)
13. D. R. Shafer, "Four-mirror Unobscured Anastigmatic Telescopes with All-Spherical Surfaces," AO 17, 1072 (1978)
14. C.S. Ih and K. Yen, "Imaging and Fourier Transform Properties of an All-Spherical Mirror System," AO 19, 4196 (1980)
15. R. Kingslake, Lens Design Fundamentals, NY, Academic Press, 1978

ORIGINAL PAGE IS
OF POOR QUALITY

starting coordinates			
00	76	L10L	
	11	A	
5	01	1	
	42	STO	
	00	00	
	91	R/S	
10	42	STO	
	01	01	X → 01
	02	2	
	42	STO	
	00	00	
	91	R/S	
15	42	STO	
	02	02	Y → 02
	03	3	
	42	STO	
	00	00	
	91	R/S	
20	42	STO	
	03	03	Z → 03
	92	INV SQR	

display 1, enter x

display 2, enter y

display 3 enter z

TI-59 CALCULATOR
PROGRAM FOR GRADIENT
INDEX REFRACTION

Starting directory			
	76	L/DL	
	02	B	
	01	1	
	42	STO	
25	00	00	
	91	R/B	
	42	STO	
	04	04	$l \rightarrow 04$
	02	2	
30	42	STO	
	00	00	
	91	R/B	
	42	STO	
	05	05	$m \rightarrow 05$
35	33	14^2	
	85	+	
	43	RCL	
	04	04	l
	33	14^2	
40	75	-	
	01	1	
	95	=	
	94	\pm	
	34	$\sqrt{\quad}$	
45	42	STO	
	06	06	$n \rightarrow 06$
	92	INV/SB2	

display 1, enter l

display 2, enter m

$$n = \sqrt{1 - m^2 - l^2}$$

	Index a. d. u. d. e. s.		
	76	L1BL	
	13	C	
50	01	1	
	42	STD	
	00	00	
	91	R/S	
	42	STD	
55	07	07	$N \rightarrow 01$
	02	-	
	42	STD	
	00	00	
	91	R/S	
60	42	STD	$ V_N \rightarrow 08$
	08	08	
	06	3	
	42	STD	
	00	00	
65	91	R/S	
	65	X	
	43	R/L	
	08	08	$ V $
	95	=	
70	42	STD	$\frac{dV}{dx} \rightarrow 09$
	09	09	
	04	A	
	42	STD	
	00	00	
75	91	R/S	

display 1, enter N

display 2, enter $|V_N|$
(cm^{-1})

display 3, enter f_N

display 4, enter m_N

ORIGINAL PAGE IS
OF POOR QUALITY

	65	X	
	43	RCL	
	08	08	
	95	=	
80	42	STD	$\frac{2N}{24} \rightarrow 10$
	10	10	
	33	4.2	
	85	+	
	43	RCL	$\frac{2N}{2X}$
85	09	09	
	33	4.2	
	75	-	
	43	RCL	N
	08	08	
90	33	4.2	
	95	=	
	94	+/-	
	34	$\sqrt{\quad}$	
	42	STD	$\frac{2N}{27} \rightarrow 11$
95	11	11	
	92	INV. SQR	

ORIGINAL PAGE IS
OF POOR QUALITY

medium thickness			
	76	LBL	
	19	0	
160	01	1	
	42	STO	
	00	00	
	91	R/S	
105	42	STO	$t_z \rightarrow 12$
	12	12	
	02	2	
	42	STO	
	00	00	
	91	R/S	
110	42	STO	
	13	13	$z \rightarrow 13$
	43	RCL	
	12	12	t_z
	55	÷	
115	43	RCL	
	13	13	z
	95	=	
	42	STO	
	14	14	$\Delta z \rightarrow 14$
	92	INV SP/R	

display 1, enter t_z
(thickness of medium)
(cm)

display 2, enter z
(number of steps)

$$\Delta z = \frac{t_z}{z}$$

E-1/6

120	76 15	LBL E	
	43 13 85	RCL 13 +	q
125	01 95	1 =	
	32	X \rightarrow t	
	01	1	
130	42 17	STD 17	K \rightarrow 17
	76 90	LBL LIST	loop 1114
	43 17	RCL 17	K
135	77 99	X \rightarrow t PRT	loop exit
	43 04 55 43	RCL 04 ÷ RCL	p
140	06 65 43	06 x RCL	m
	14 95	14 =	ΔZ
145	42 15	STD 15	$\Delta X \rightarrow 15$

q+1 \rightarrow t

K=1

IF K \geq q+1 GOTO PRT
ELSE CONTINUE

$$\Delta X = \left(\frac{p}{n}\right) \Delta Z$$

ORIGINAL PAGE IS
OF POOR QUALITY

150	43	RCL	
	05	05	m
	55	÷	
	43	RCL	
	86	06	m
155	65	x	
	43	RCL	
	14	14	Δz
	95	=	
	42	STD	
160	16	16	Δy → 16
	44	SUM	
	02	02	
	43	RCL	
	15	15	Δx
165	44	SUM	
	01	01	
	43	RCL	
	14	14	Δz
	44	SUM	
170	03	03	
	43	RCL	
	11	11	$\frac{\partial M}{\partial z}$
	65	x	
	43	RCL	
175	16	16	Δy
	75	-	
	43	RCL	
	10	10	$\frac{\partial N}{\partial y}$
	65	x	
180	43	RCL	
	14	14	Δz
	95	=	

$$\Delta y = \left(\frac{M}{n}\right) \Delta z$$

$$y = y + \Delta y$$

$$x = x + \Delta x$$

$$z = z + \Delta z$$

	55	÷	
	43	RCL	
	07	07	N
	95	=	
185	42	STB	
	18	18	$d\theta_x \rightarrow 18$
	43	RCL	
	09	09	$\frac{\partial N}{\partial x}$
	65	X	
190	43	RCL	
	14	14	Δz
	75	-	
	43	RCL	$\frac{\partial N}{\partial z}$
	11	11	
195	65	X	
	43	RCL	
	15	15	Δx
	95	=	
	55	÷	
200	43	RCL	
	07	07	N
	95	=	
	42	STB	
	19	19	$d\theta_y \rightarrow 19$

$$d\theta_x = \frac{1}{N} \left[\left(\frac{\partial N}{\partial z} \right) dy - \left(\frac{\partial N}{\partial y} \right) dz \right]$$

$$d\theta_y = \frac{1}{N} \left[\left(\frac{\partial N}{\partial x} \right) dz - \left(\frac{\partial N}{\partial z} \right) dx \right]$$

ORIGINAL PAGE IS
OF POOR QUALITY

205	43	RCL	$\frac{\partial N}{\partial y}$
	10	10	
	65	X	
	43	RCL	
210	15	15	Δx
	75	-	
	43	RCL	$\frac{\partial N}{\partial x}$
	09	09	
65	X		
43	RCL		
215	16	16	Δy
	95	=	
	55	o	
	43	RCL	
220	07	07	N
	95	=	
	42	STD	$d\theta_2 \rightarrow 20$
	20	20	
225	43	RCL	n
	06	06	
	65	X	
	43	RCL	
230	19	19	$d\theta_y$
	75	-	
	43	RCL	m
	05	05	
65	X		
43	RCL		
235	20	20	$d\theta_z$
	95	=	
	44	SUM	
	09	09	

$$d\theta_z = \frac{1}{N} \left[\left(\frac{\partial N}{\partial y} \right) dx - \left(\frac{\partial N}{\partial x} \right) dy \right]$$

$$dI = n d\theta_y - m d\theta_z$$

$$I = \int dI$$

ORIGINAL PAGE IS
OF POOR QUALITY

240	43	RCL	f
	04	04	
	65	x	
	43	RCL	
	20	20	
	75	-	
245	43	RCL	n
	06	06	
	65	x	
	43	RCL	
	18	18	
250	95	=	dBx
	44	SUM	
	05	05	
255	43	RCL	m
	05	05	
	65	x	
	43	RCL	
	18	18	
	75	-	
	43	RCL	
260	04	04	f
	65	x	
	43	RCL	
	17	19	
	95	=	
	44	Sum	dBg
	06	06	

$$dn = f dB_z - n dB_x$$

$$m = m + dn$$

$$dn = m dB_x - f dB_y$$

$$m = m + dn$$

ORIGINAL PAGE IS
OF POOR QUALITY

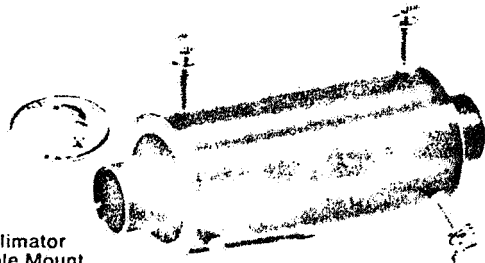
265	43	RCL	
	17	17	
	66	PAUSE	
270	85	+	
	01	1	
	95	=	
	42	STD	
	17	17	
275	61	GTO	
	90	LIST	
	76	LBL	Results
	99	PRT	Display
280	43	RCL	
	01	01	X
	91	R/S	
	43	RCL	
	02	02	Y
	91	R/S	
285	43	RCL	
	03	03	Z
	91	R/S	
	43	RCL	
	04	04	P
290	91	R/S	
	43	RCL	
	05	05	m
	91	R/S	
	43	RCL	
	06	06	n
	93	INVSBR	

ORIEL MINIPOINT COLLIMATORS

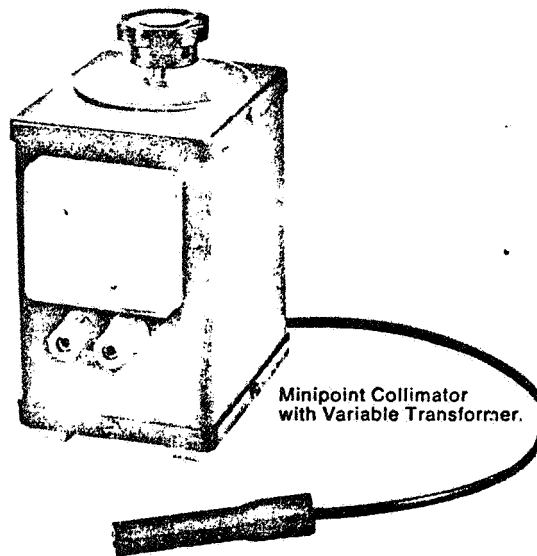
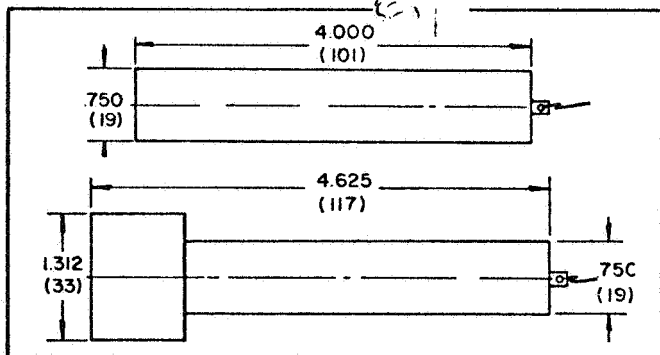
The Oriel Minipoint Collimators project a collimated beam from a small circular aperture and condensing lens. The entire unit is housed in an extremely compact cylindrical housing only $\frac{3}{4}$ inch diameter 4 inch length.

The Model 6545 Minipoint Collimator has an inter-

changeable internal aperture allowing a trade off of beam collimation angle with light output. The larger apertures provide more light output but create beams with greater divergence angles. An optional filter holder mounts onto the output port and accepts any 1 inch or 25 mm diameter filters up to 0.375 inch (9.5 mm) thick.



Minipoint Collimator with Adjustable Mount.



Minipoint Collimator with Variable Transformer.

SPECIFICATIONS

Housing diameter: 0.75 in. (19 mm)

Housing length: 4.0 inch

Lamp: 6 volt, 1 1/2 ampere

Color temperature: 2750°K

Lamp life: 500 hours

Focal length: 50 mm (2 inch)

Beam Diameter: 15 mm (.59 in.). Can be stopped down with optional apertures to 10, 5, or 2 mm (0.39, 0.20, or 0.08 inch).

Interchangeable Beam Divergence Inserts

Model No.	Angular Divergence		Approx. Light Beam Power* Microwatts
	Arc Minutes	Milliradians	
6546	75	21.8	3500
6546-1	30	8.7	720
6546-2	15	4.4	190
6546-3	6	1.75	45

*At full 15 mm beam diameter.

LIGHT SENSING MINI PROBES: These high sensitivity silicon probes measure reflected or emitted radiant power within small fields of view.

Near Field Probes: measure a field 1.5 mm (0.060 inch) diameter at a working distance of 25.4 mm (1 inch).

Far Field Probes: measure an angular field of 3°

See Page F-20 for details.

ORDERING INFORMATION

6545 Minipoint Collimator with lamp without transformer
Beam Divergence Inserts and Beam Diameter Apertures not included - order from below. \$518.00

Beam Divergence Inserts

Model No.	Divergence	Price
6546	75 arc min.	\$72.00
6546-1	30 arc min.	\$72.00
6546-2	15 arc min.	\$72.00
6546-3	6 arc min.	\$72.00

Beam Diameter Aperture

Model No.	Beam Diameter	Price
6549	15 mm	None required
6549-1	10 mm	\$13.00
6549-2	2 mm	\$13.00

6552 Optional Filter Holder: This holds 1 inch or 25 mm filters up to $\frac{3}{8}$ inch (9.5 mm) thick. It mounts onto the beam port \$39.00

6532 Variable Transformer for the Mini Collimator with meter and control knob. \$ 95.00
Output: 4.5 to 6.5 volts
Input: 115 or 130 volts, 50/60 Hz.

6553 Adjustable Mount for Mini Collimators and Light Sensing Probes. \$59.00
- Rod mounted. Order rod below.

1231 Rod - 14.3 mm dia., 41.5 mm long \$ 5.75

1232 Rod - 14.3 mm dia., 70 mm long \$ 6.50

1233 Rod - 14.3 mm dia., 98.5 mm long \$ 7.00

Oriel MiniPoint Sources

ORIGINAL PAGE IS
OF POOR QUALITY

The Oriel MiniPoints create extremely small, highly intense, spatially stable "point" sources of light. The source image is actually projected in front of the housing by an internal optical system.

The 6530 source consists of a small low voltage tungsten lamp, an imaging optical system and internal interchangeable aperture inserts. Inserts are available to produce projected "points" of 1.0, 0.4, 0.2, 0.1 and 0.05 mm (0.040, 0.016, 0.008, 0.004 and

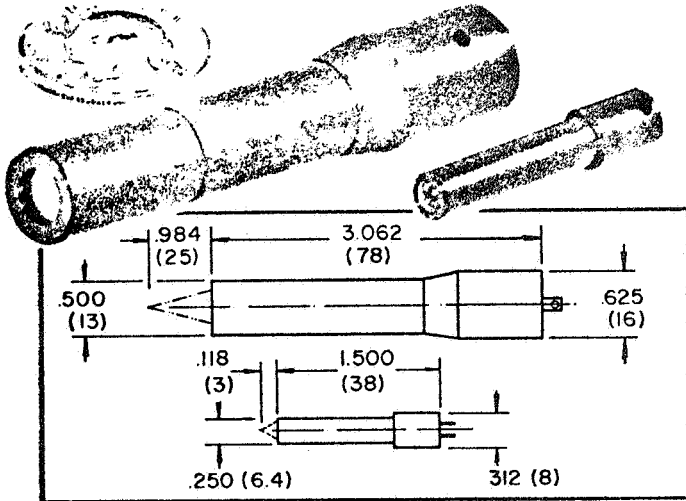
0.002 inch) diameter at a 25 mm (1 inch) working distance.

In addition three fixed aperture sources produce projected points of 0.050, 0.025 or 0.01 mm (0.002, 0.001 or 0.0004 inch) diameter at a 3 mm (0.1278 inch) working distance.

Adapters are available to mount these sources in rod mounted X-Y adjustable mounts.

APPLICATIONS

- High intensity point illumination
- Artificial star for optical testing
- Critical alignments
- High resolution position measurement or control
- Optical scanning



SPECIFICATIONS

Model 6530 MINIPOINT SOURCE with Interchangeable Inserts
 Working distance to point: 25 mm
 Beam f/no: 3.5
 Lamp: 5 volt, 0.75 ampere filament lamp
 Color Temperature: 2525° K
 Lamp Life: 5000 hours

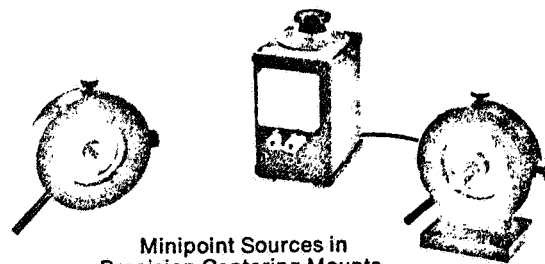
Interchangeable inserts: produce projected points of these diameters and these approximate beam power levels.

Insert Model No.	Diameter of Projected Point mm (inches)	Approximate Beam Power microwatts
6531	1.0 (0.040)	750
6531-1	0.4 (0.016)	140
6531-2	0.2 (0.008)	32
6531-3	0.1 (0.004)	9
6531-4	0.05 (0.002)	3.5

FIXED MINIPOINT SOURCES

Working Distance to point: 3 mm
 Beam f/no: 2.7
 Lamp: 5 volt, 0.11 ampere filament lamp
 Color Temperature: 2100° K
 Lamp Life: 40,000 hours
 These three fixed models are available:

Model No.	Diameter of Projected Point mm (inches)	Approximate Beam Power (microwatts)
6537	0.05 (0.002)	2
6538	0.025 (0.001)	0.5
6539	0.01 (0.0004)	0.1



MiniPoint Sources in Precision Centering Mounts.

ORDERING INFORMATION

6530 Interchangeable MiniPoint Source \$278.00
 with lamp—without transformer.
 Insert not included. Order from list below.

Interchangeable Inserts for the MiniPoint Source

Model No.	Diameter of Projected Point mm (inch)	Price
6531	1.0 (0.040)	\$72.00
6531-1	0.4 (0.016)	\$72.00
6531-2	0.2 (0.008)	\$72.00
6531-3	0.1 (0.004)	\$72.00
6531-4	0.05 (0.002)	\$72.00

6537 Fixed MiniPoint Source with 0.050 mm (0.002 inch) projected point with lamp, without transformer. \$202.00
 6538 Fixed MiniPoint Source with 0.025 mm (0.001 inch) projected point with lamp, without transformer. \$218.00
 6539 Fixed MiniPoint Source with 0.010 mm (0.0004 inch) projected point with lamp, without transformer. \$262.00

6532 Variable Transformer for any of the MiniPoint sources above with meter and control knob. \$ 95.00
 Output: 4.5 to 6.5 volts, 3.3 amperes max.
 Input: 115 or 230 volts, 50/60 Hz

1733 Precision Centering Mount – rod mounted provides ± 6 mm (0.25 in.) adjustment with fine pitch screws in the plane perpendicular to the optical axis, page C-28. Order adapter and rod below. \$118.00

1231 Rod – 14.3 mm dia., 4.15 mm long \$ 5.75
 1232 Rod – 14.3 mm dia., 70 mm long \$ 6.50
 1233 Rod – 14.3 mm dia., 98.5 mm long \$ 7.00

1737 Precision Centering Mount – base mounted similar to the 1733 above with base mount. See page C-28 for details. Order adapter below. \$139.00

6541 Adapter for Precision Centering Mount for 6530 Interchangeable MiniPoint Source. \$ 27.00

6542 Adapter for Precision Centering Mount for 6537, 6538 or 6539 Fixed MiniPoint Sources. \$ 29.00

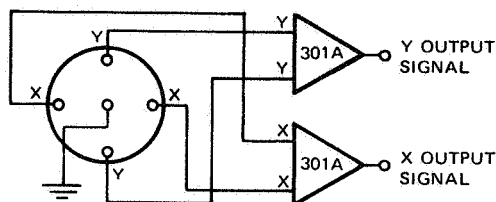
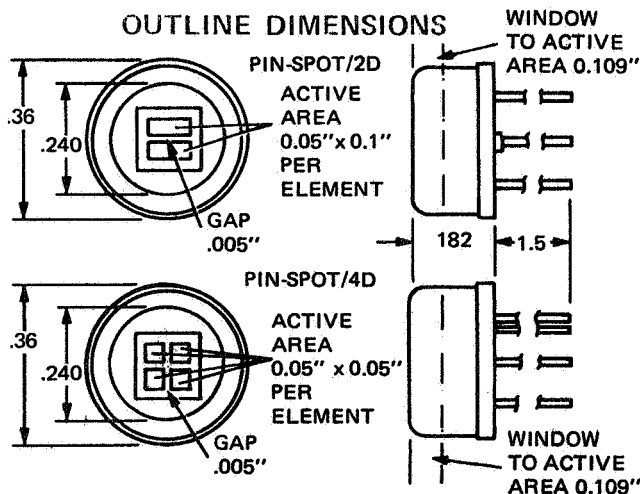
ELECTRICAL CHARACTERISTICS

PARAMETER AND (UNITS)	PIN-Spot/2D			PIN-Spot/4D		
	MIN	TYP	MAX	MIN	TYP	MAX
Recommended Mode of Operation	Photovoltaic/Photoconductive			Photovoltaic/Photoconductive		
Spectral Range @ 5% Peak (nm)	350-1100			350-1100		
Responsivity at Peak λ (amps/watt)	0.4	0.5	-	0.4	0.5	-
Uniformity of Response (with 1 mm spot dia)	-	$\pm 2\%$	$\pm 5\%$	-	$\pm 2\%$	$\pm 5\%$
Dark Current per element (μ a)	@ 10V Bias	0.002	0.05	-	0.002	0.05
	@ 50V Bias	0.006	0.15	-	0.006	0.15
Source Resistance per element (M Ω)	-	60	-	-	70	-
Breakdown Voltage @ 10 μ a (volts)	50	100	-	50	100	-
Capacitance per element (pF)	@ 0V Bias	54	81	-	29	44
	@ 10V Bias	15	22	-	7	10
	@ 50V Bias	6.7	10	-	4	6
Rise Time at 632.8 nm 10%-90% (ns)	@ 10V Bias	10.0	-	-	10	-
	@ 50V Bias	10.0	-	-	10	-
Fall Time at 632.8 nm 90%-10% (ns)	@ 10V Bias	10.0	-	-	10	-
	@ 50V Bias	10.0	-	-	10	-
Frequency Response at 632.8 nm into 50 Ω Load (MHz)	@ 10V Bias	35	-	-	35	-
	@ 50V Bias	35	-	-	35	-
Max. Output for 10% Linearity (ma)	@ 0V Bias	0.2	-	-	0.5	-
	@ 10V Bias	0.25	-	-	1.0	-
NEP @ Peak λ , 1 kHz, 10V (w/Hz $^{1/2}$)	-	9×10^{-14}	-	-	9×10^{-14}	-
Noise Current (rms amp/ Hz $^{1/2}$) @ 1 kHz	@ 0V Bias	2×10^{-14}	-	-	2×10^{-14}	-
	@ 10V Bias	3×10^{-14}	-	-	3×10^{-14}	-
	@ 50V Bias	5×10^{-14}	-	-	5×10^{-14}	-
Forward Resistance (Ω)	-	45	-	-	55	-

MECHANICAL SPECIFICATIONS

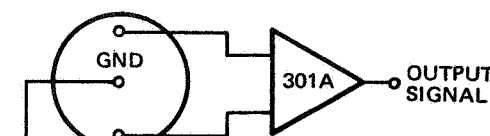
SPECIFICATION	PIN-Spot/2D	PIN-Spot/4D
Active Area/Element		
Area (cm 2)	0.032	0.016
Dimensions (in.)	0.05x0.1	0.05x0.05
Package		
Type	TO-5	TO-5
Window	Glass	Glass
Field of View		
Full Angle	96 $^\circ$	96 $^\circ$
Temperature Range		
Operating ($^\circ$ C)	-55 to +125	-55 to +125
Storage ($^\circ$ C)	-55 to +125	-55 to +125

OUTLINE DIMENSIONS



TYPICAL CONNECTIONS FOR PIN-SPOT/4D TO MODIFIED UDT 301A AMPLIFIER*

SCHMATIC DIAGRAMS



TYPICAL CONNECTIONS FOR PIN-SPOT/2D SINGLE AXIS DETECTOR TO UDT 301A AMPLIFIER

*AMPLIFIER BIAS POLARITY MUST BE CHANGED

SPECIFICATIONS SUBJECT TO CHANGE WITHOUT NOTICE

D-017-0777



MOSBY 116

HUGHES

HUGHES AIRCRAFT COMPANY

INDUSTRIAL PRODUCTS DIVISION
CARLSBAD, CALIFORNIA

PHOTODETECTOR SERIES
PIN PHOTODETECTORS

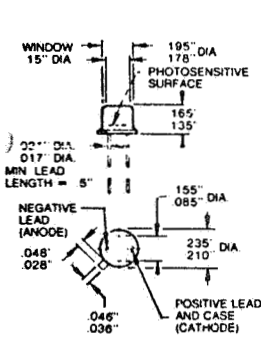
Hughes now offers OEM manufacturers the HPIN series of photodetector devices featuring the highest responsivity of any commercially available devices. Because of their fast response time, this series is effective over a broad frequency range. Hughes HPIN Series Photodetectors have many applications in instrumentation using lasers, as well as in fiber optic communication and data links.

The p on n variety of PIN photodetectors uses intrinsic silicon grown and processed to provide uniform

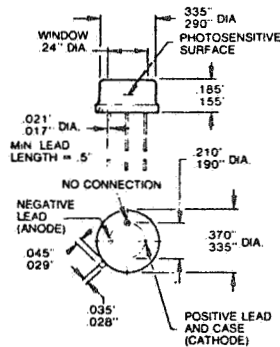
carrier concentration levels throughout the active volume. The devices are ion implanted for high uniformity and response, low temperature processed for high quantum efficiency, and silicon nitride passivated for low leakage and stability.

A complete range of custom PIN photodetector devices is also available, and we will be happy to provide customer assistance for evaluating proposed applications. Contact us for your special requirements.

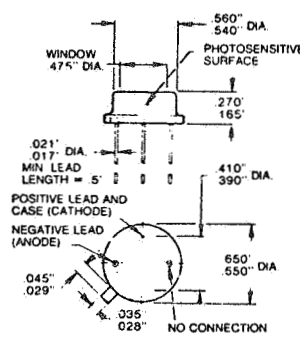
CATALOG DEVICES FOR PIN COMPATIBLE REPLACEMENTS IN EXISTING APPLICATIONS



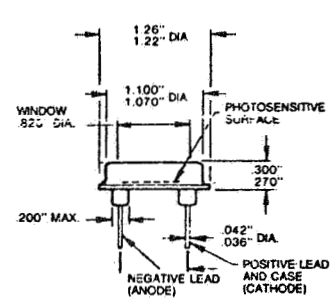
TO-18 PACKAGE
HPIN002
HPIN040



TO-5 PACKAGE
HPIN100



TO-8 PACKAGE
HPIN200



30-mm PACKAGE
HPIN444

Part Number	HPIN002	HPIN040	HPIN100	HPIN200	HPIN444
Geometry (mils)	2 (dia.)	40 x 33	100 (dia.)	200 (dia.)	444 (dia.)
Area (mm ²)	.0025	.852	5.07	20.3	100
Responsivity (A/W) @ 900 nm	63	63	63	63	63
Quantum Efficiency (%) @ 900 nm	87	87	87	87	87
Dark Current (nA) @ 50V	0.7	4	20	70	300
Capacitance (pF) @ 50V	1	3	6	17	70
Rise Time (nsec) @ 50V 50 ohms	3	3	5	7	12
NEP (W/√Hz) @ 900 nm, 50V	2.4x10 ⁻¹⁴	5.7x10 ⁻¹⁴	1.4x10 ⁻¹³	2.8x10 ⁻¹³	5.7x10 ⁻¹³
Min. Breakdown Voltage (volts) @ 10 μA	200	200	200	200	200
Package Type	TO-18	TO-18	TO-5	TO-6	30-mm

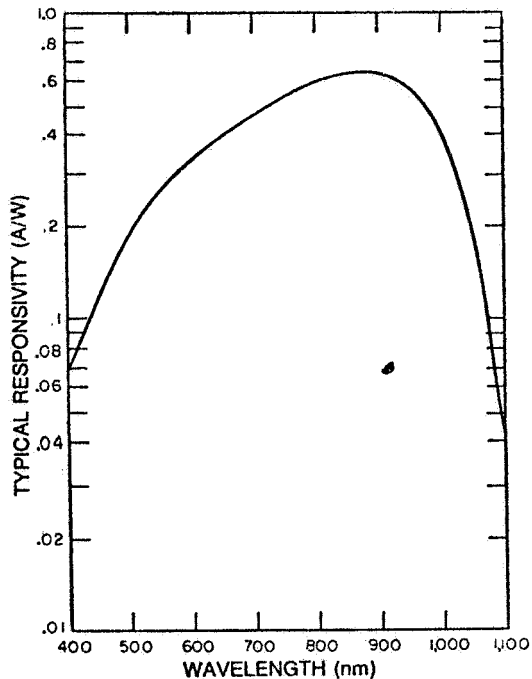


Fig. 1 - Typical Spectral Responsivity vs. Wavelength.

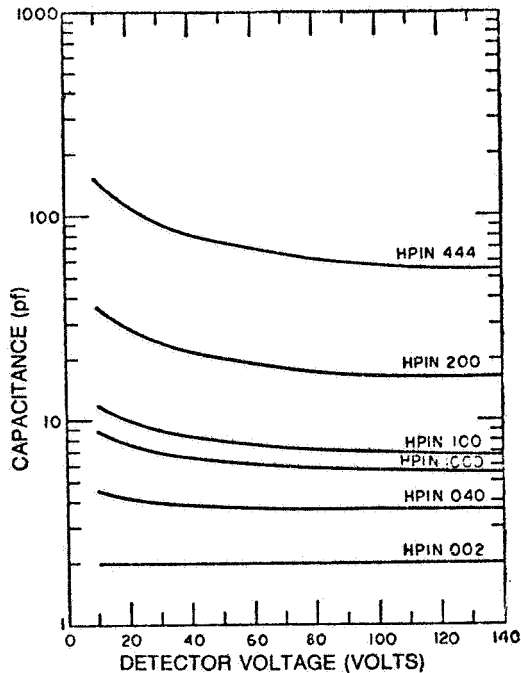


Fig. 2 - Typical Capacitance vs. Detector Voltage.

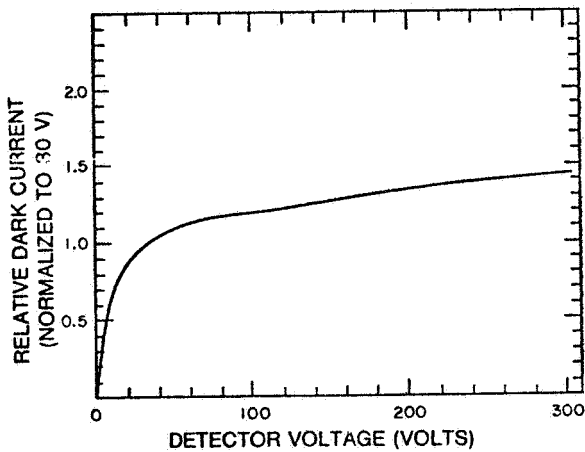


Fig. 3 - Typical Relative Dark Current vs. Detector Voltage.

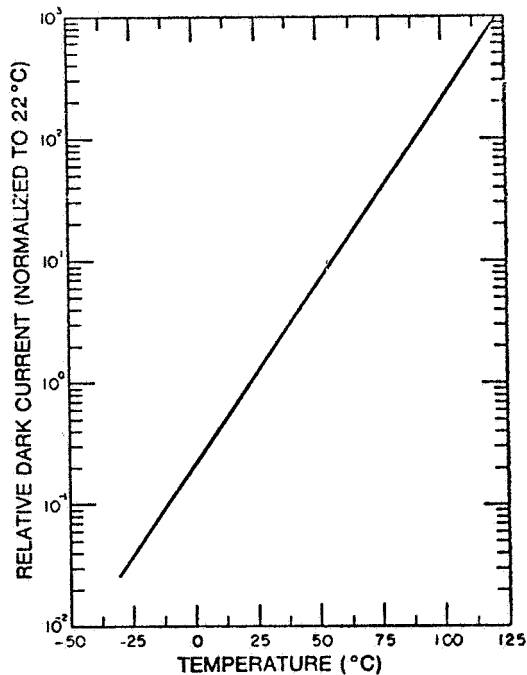


Fig. 4 - Typical Relative Dark Current vs. Temperature.

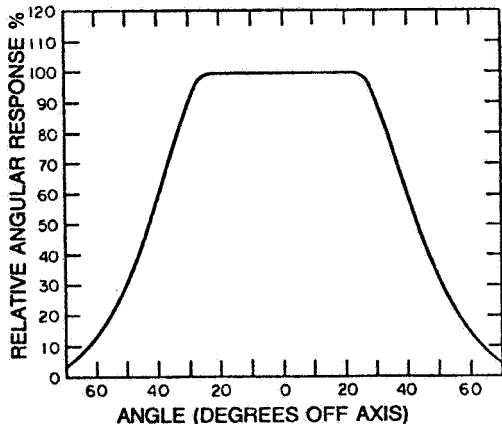


Fig. 5 - Typical Relative Angular Response vs. Angle for TO-18 Packages.



HUGHES AIRCRAFT COMPANY Industrial Products Division
Image and Display Products • 6155 El Camino Real, Carlsbad, CA 92008
Phone (714) 438-9191 • TWX: 910-322-1393

HPIN SERIES PIN PHOTODETECTOR ARRAYS

ORIGINAL PAGE IS
OF POOR QUALITY

HUGHES
HUGHES AIRCRAFT COMPANY
INDUSTRIAL PRODUCTS DIVISION
CARLSBAD, CALIFORNIA

Hughes supplies OEM manufacturers with dual, quadrant, linear, and matrix PIN photodetector arrays which complement its single element photodetectors. These high reliability arrays are made by the advanced planar techniques of the single element line, including ion implantation processes and the use of silicon oxide and nitride layers for maximum spectral response and low noise.

While the widely accepted devices described below are representative of the Hughes capability, a complete line of custom arrays is also available. We will be pleased to provide customer assistance and alternate configurations to fill your particular application.

HPIN MONOLITHIC ARRAYS

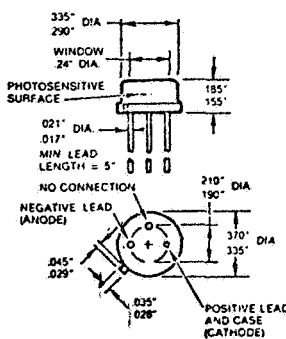
DIMENSIONS

ARRAY	HPIN100D	HPIN200Q	HPIN444Q	HPIN444M	HPIN700L
Type	dual	quadrant	quadrant	5 x 5 matrix	1 x 16 linear
Number of Elements	2	4	4	25	16
Chip Size (mil ²)	130 x 130	247 x 247	499 x 499	499 x 499	751 x 247
Element Size (mils)	100 x 50	100R quadrant	222R quadrant	85 x 85	180 x 41
Active Area per Element (in ²) (mm ²)	.005 3.2	.0079 5.1	.039 25.0	.0072 4.6	.0074 4.8
Transition Zone (mils)	5	4.4	6	3.6	2.4

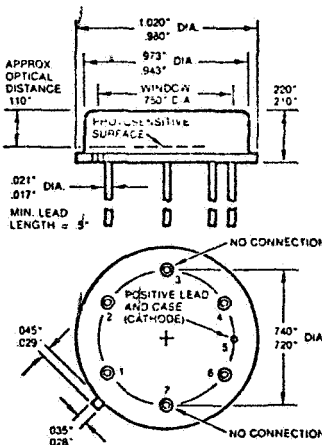
ELECTRICAL SPECIFICATIONS

All values are typical and measured at a wavelength of 900nm and at 50 volts.

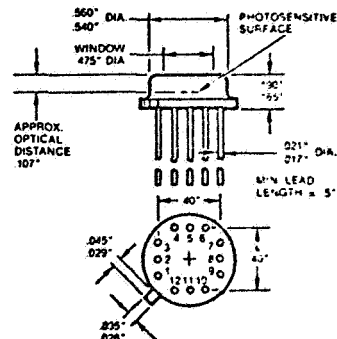
PARAMETER	HPIN100D	HPIN200Q	HPIN444Q	HPIN444M	HPIN700L
Responsivity (A/W)	0.6	0.6	0.6	0.6	0.6
Crosstalk (%)	< 1	< 1	< 1	< 2	< 2
Quantum Efficiency (%)	87	87	87	87	87
Capacitance (pF) per Element	2.8	4.4	22.0	4.0	4.2
Dark Current (nA) per Element	16	50	125	50	50
Rise Time (ns) (R _L = 50 Ω)	6	6	8	6	6
Bandwidth (Hz)	12	15	33	14	15
Breakdown Voltage (V)	> 200	> 200	> 200	> 200	> 200
Package Type	TO-5	TO-8	25mm	44 pin plug-in	24 pin DIP



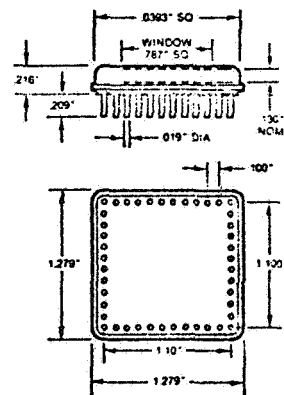
HPIN100D
Modified 12-Lead
TO-5 package



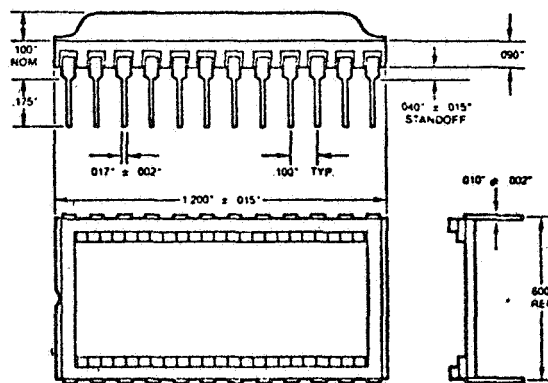
HPIN444Q
25mm package



HPIN200Q
Modified 12-Lead
TO-8 package



HPIN444M
44 pin package



HPIN700L
24 pin package

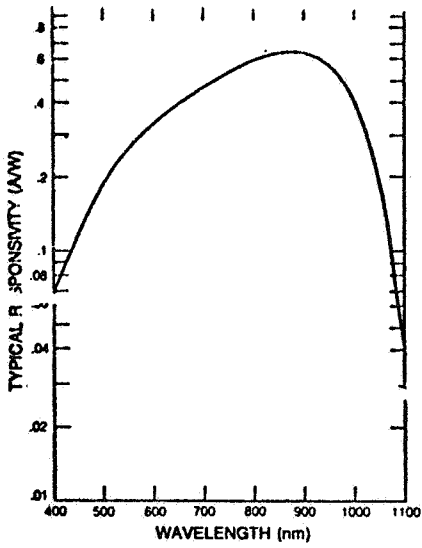


Fig. 1 - Typical Spectral Responsivity vs. Wavelength.

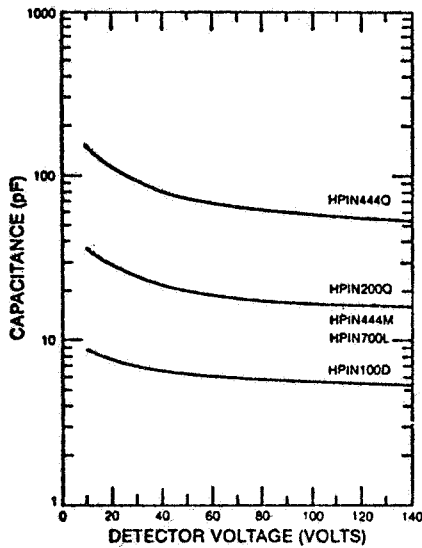


Fig. 2 - Typical Capacitance vs. Voltage Curve for Each Element in the Specified Array.

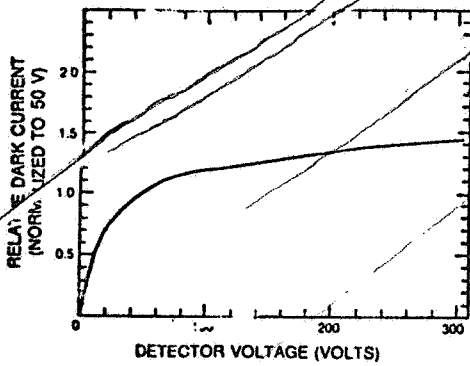


Fig. 3 - Typical Relative Dark Current vs. Detector Voltage.

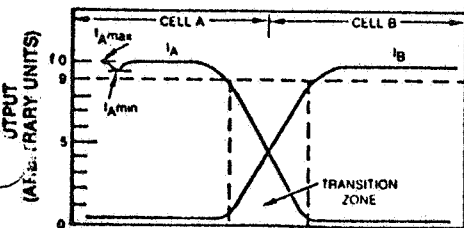
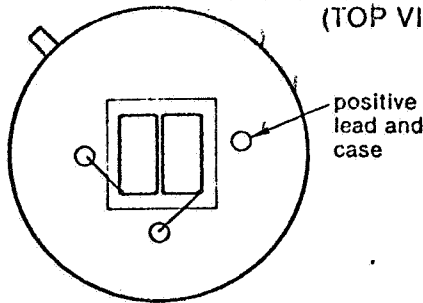
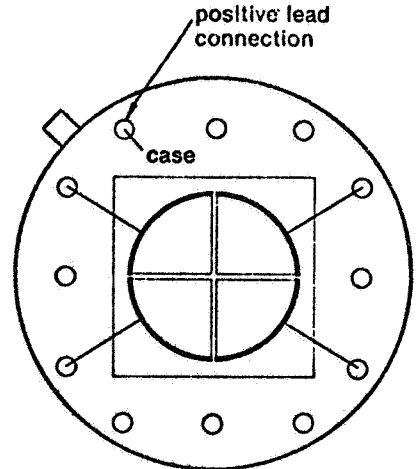


Fig. 4 - Curve Depicting Crosstalk (HPIN200Q, HPIN444Q, HPIN700L).

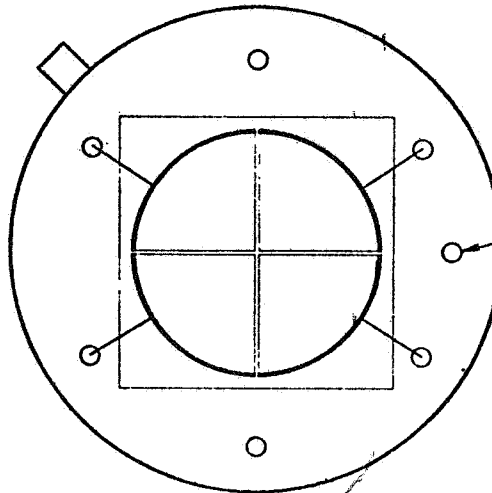
DETECTOR OUTLINES
(TOP VIEWS)



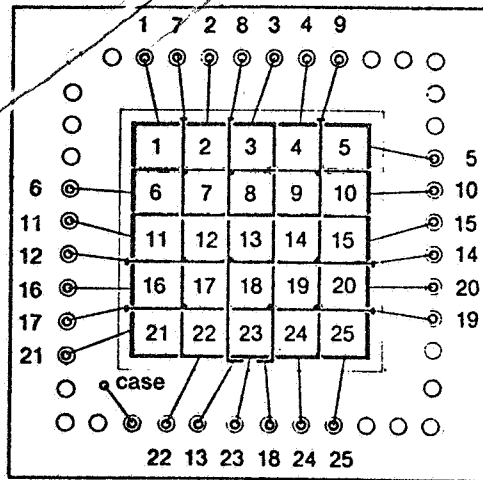
HPIN100D PHOTODIODE
DUAL ELEMENT ARRAY
Modified 12-Lead
TO-5 package



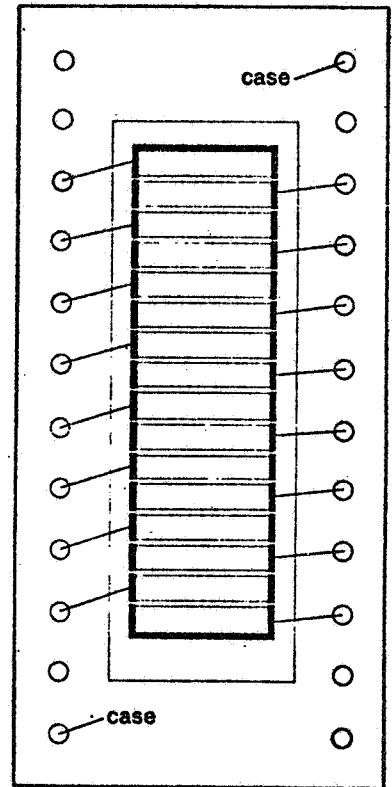
HPIN200Q PHOTODIODE
QUADRANT ARRAY
Modified 12-Lead
TO-8 package



HPIN444Q PHOTODIODE
QUADRANT ARRAY
25 mm package



HPIN444M PHOTODIODE ARRAY
44 pin package



HPIN700L PHOTODIODE
LINEAR ARRAY
24 pin package



APPENDIX E (cont'd)

Revision • Solid State Products Sales
4J 438-9191 • TWX: 910-322-1393

PROGRAM INFORMATION REQUEST / RELEASE

	*CLASS. LTR.	OPERATION	PROGRAM	SEQUENCE NO.	REV. LTR.
PIR NO.	U	1254	AGCE	024	

*USE "C" FOR CLASSIFIED AND "U" FOR UNCLASSIFIED

FROM	TO
W. C. Yager M9423 x4235	R. J. Homsey M9415

DATE SENT	DATE INFO. REQUIRED	PROJECT AND REQ. NO.	REFERENCE DIR. NO.
5/11/81		AGCE Task 4/5	

SUBJECT

EFFECT OF THERMAL GRADIENT IN THE SAPPHIRE SHELL

INFORMATION REQUESTED/RELEASED

See attached text.

Distribution: R. J. Homsey
G. Fogal
S. Nexte
T. Scollon
W. Yagef

PAGE NO.	RETENTION REQUIREMENTS	
	COPIES FOR	MASTERS FOR
OF	<input type="checkbox"/> 1 MO.	<input type="checkbox"/> 3 MOS.
	<input type="checkbox"/> 3 MOS.	<input type="checkbox"/> 6 MOS.
	<input type="checkbox"/> 6 MOS.	<input type="checkbox"/> 12 MOS.
	<input type="checkbox"/> MOS.	<input type="checkbox"/> MOS.
	<input type="checkbox"/>	<input type="checkbox"/> DO NOT DESTROY

EFFECT OF THERMAL GRADIENT IN THE SAPPHIRE SHELL

Introduction

This note considers how a thermal gradient in the sapphire shell can perturb the AGCE by mimicking a thermal gradient in the fluid. The objective here is to establish the scale of the effect and indicate in general how it can be compensated in the experiment.

Analysis

The temperature distribution in the sapphire shell was studied for a number of cases in PIR 1R54-AGCE-023. The division of the shell into cells is shown in Figure 1 (taken from this PIR), and the calculated temperature distribution for a typical case in Figure 2 (also from this PIR). From Figure 2 we can calculate the average gradient from cell 2 to cell 9 as

$$\frac{\Delta T}{\Delta y} = \frac{34.62 - 28.52}{6.5 \times \frac{70}{180}} = .768 \text{ } ^\circ\text{C}/\text{cm}$$

For comparison, maximum and minimum gradients in this same range are calculated as 1.00 and .593 $^\circ\text{C}/\text{cm}$, respectively.

The thermal coefficient of refractive index for sapphire averages $0.000013/^\circ\text{C}$ over the visible range (Reference 1). On the other hand, the thermal coefficient of refractive index for a typical organic fluid is $-.0005/^\circ\text{C}$. In passing from source to detector, light passes (in the present design) through equal thicknesses of sapphire and fluid. Gradient effects in

ORIGINAL PAGE IS
OF POOR QUALITY

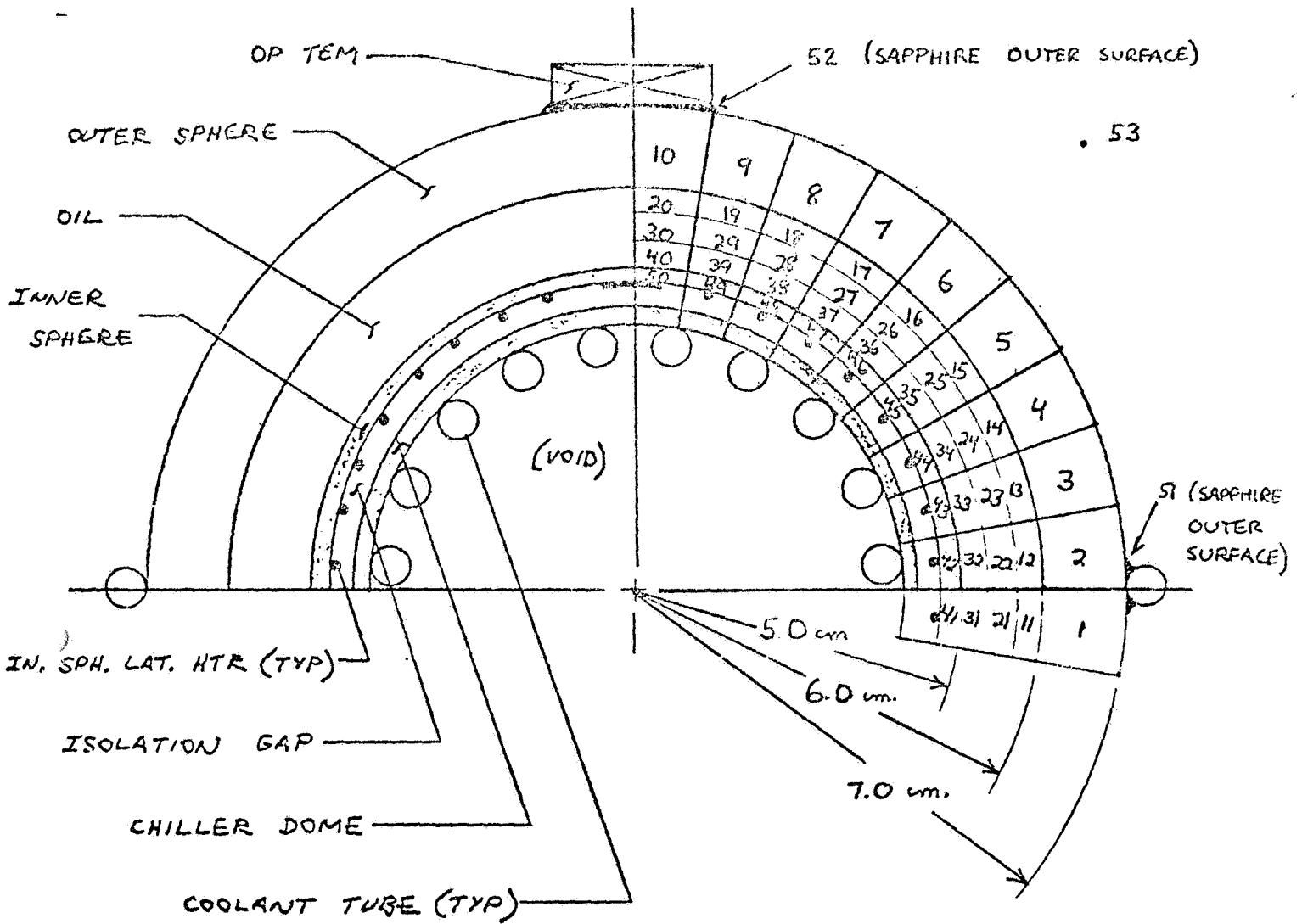


Fig. 1 AGCE CELL MODEL

Fig. 2 CASE IIIA

TEMPERATURE PROFILE AND THERMAL LOADS

TEMPERATURE PROFILE (°C)

										<u>NODES</u>	
										10 ← 1	20 ← 11
										30 ← 21	40 ← 31
										50 ← 41	
26.40	28.52	29.53	30.26	30.89	31.56	32.43	33.49	34.62	34.87		
26.82	28.66	29.07	28.90	28.01	25.47	26.87	31.19	30.82	33.82		
28.31	27.74	27.82	26.98	24.87	22.54	21.53	22.22	22.25	25.57		
25.76	22.07	24.21	24.99	21.28	18.86	17.37	16.86	16.77	17.53		
15.00	15.00	15.00	15.00	15.00	15.00	15.00	15.00	15.00	15.00		

INNER SPHERE LOADS
PER LATITUDE (WATTS)

0.64137877E 00
0.45723748E 00
0.46625214E 00
0.56456404E 00
0.83907994E 00
0.11852586E 01
0.15389075E 01
0.10430537E 01
0.48914090E 00
0.26163701E 00

NODES

<u>FLUID</u>	<u>INNER SPHERE</u>
31	41
32	42
33	43
34	44
35	45
36	46
37	47
38	48
39	49
40	50

LATITUDE

-10 → 0°
0 → 10°
10 → 20°
20 → 30°
30 → 40°
40 → 50°
50 → 60°
60 → 70°
70 → 80°
80 → 90°

POLE

INNER SPHERE
TOTAL COOLING LOAD (WATTS) = 0.74865102E 01

HEAT REQUIRED AT EQUATOR (WATTS) = 0.13900729E 02

COOLING REQUIRED AT POLE (WATTS) = 0.32965379E 01

HEAT LOSS TO AMBIENT (WATTS) = 0.16678249E 01

the two media can therefore be directly compared in terms of temperature coefficient of refractive index. A gradient in the sapphire will produce a signal that is $.000013/(-.0005)=-.026$ as great as the same gradient in the fluid would produce. The average gradient in sapphire will therefore have the same effect on the signal as would a fluid thermal gradient of $(-.026)(.768) = -.02^{\circ}\text{C}/\text{cm}$.

We have seen earlier that the AGCE scanner has the capability of detecting a $0.01^{\circ}\text{C}/\text{cm}$ gradient in the fluid with a SNR of at least 6. The gradient in the sapphire will therefore be detectable. The resulting signal will be both small and systematic. It should therefore be satisfactory to correct for this perturbation by simply adding (or subtracting) calculated values to the raw signal.

References

1. I. H. Malitson, "Refraction and Dispersion of Synthetic Sapphire," JOSA 43, 1377 (1962).
2. G. Andres, "Task 6.2 AGCE Thermal Feasibility/Design Study," PIR 1R54-AGCE-023.

ORIGINAL PAGE IS
OF POOR QUALITY



)

)

CLASS. LTR. U	OPERATION 1254	PROGRAM AGOE	SEQUENCE NO. 027	REV. LTR.
------------------	-------------------	-----------------	---------------------	-----------

PROGRAM INFORMATION REQUEST / RELEASE

PIR NO. _____
 *USE "C" FOR CLASSIFIED AND "U" FOR UNCLASSIFIED

JM	FROM W. C. Yager	TO R. Homsey
----	---------------------	-----------------

DATE SENT 6/09/61	DATE INFO. REQUIRED	PROJECT AND REQ. NO.	REFERENCE DIR. NO.
----------------------	---------------------	----------------------	--------------------

SUBJECT
 EFFECTS OF BIREFRINGENCE IN THE SAPPHIRE SHELL

INFORMATION REQUESTED/RELEASED
 See attached text..

PAGE NO. OF	RETENTION REQUIREMENTS		
	COPIES FOR	MASTERS FOR	
<input type="checkbox"/>	1 MO.	<input type="checkbox"/>	3 MOS.
<input type="checkbox"/>	3 MOS.	<input type="checkbox"/>	6 MOS.
<input type="checkbox"/>	6 MOS.	<input type="checkbox"/>	12 MOS.
<input type="checkbox"/>	MOS.	<input type="checkbox"/>	MOS.
<input type="checkbox"/>		<input type="checkbox"/>	DO NOT DESTROY

ORIGINAL PAGE IS
OF POOR QUALITY

EFFECTS OF BIREFRINGENCE IN THE SAPPHIRE SHELL.

SUMMARY

INTRODUCTION

BASIC PHYSICS OF REFRACTION

RAYTRACING THE EXTRAORDINARY RAY

PRELIMINARY ESTIMATE OF BIREFRINGENCE EFFECTS

COMPUTER RAYTRACE

ORIGINAL PAGE IS
OF POOR QUALITY

SUMMARY

The significance of birefringence in the sapphire shell is considered in this note. It is shown that this birefringence will produce image shifts at the detector that can mimic large index gradients. These image shifts are completely predictable functions of latitude and longitude, however, and can be removed through a calibration procedure.

INTRODUCTION

The sapphire sphere in the AGCE apparatus is birefringent, sapphire being physically a negative uniaxial crystal. Unpolarized light incident on the sapphire shell will therefore be separated on entering the crystal into two rays of orthogonal polarization: the ordinary ray and the extraordinary ray. Since this separation of rays in the crystal can lead to two separate images at the detector, one of which may be displaced from the other, and since image displacement is what is being measured in the FSS, it is evident that birefringence can to this extent mimic index gradients, and must therefore be eliminated or accounted for. In the baseline design birefringence was sidestepped by requiring the optical axis to be parallel to the axis of rotation, then polarizing the incident light so all rays would be ordinary rays. For technical reasons a sphere made with this orientation is limited in size. A sphere made with the optical axis in the equatorial plane can be made larger, however, and since a larger test cell is generally desirable, this method of construction will be preferred, provided the effects of birefringence can be dealt with. It is the purpose of this note to examine these effects qualitatively and quantitatively and assess the problem generally.

BASIC PHYSICS OF REFRACTION

A conventional approach to understanding the propagation and refraction of light waves is to apply Huygens' Principle. This principle states that if the locus of an advancing wavefront is known at time t , its locus at a subsequent time $(t + \Delta t)$, where Δt is very short, may be found by regarding each point on the wavefront as a source of secondary wavelets that commence at time t and expand for the time Δt at a velocity c/n , where c is the velocity of light and n is the local index of refraction. The wavefront at time $(t + \Delta t)$ is then taken to be the envelope of those secondary wavelets in the forward direction. When the medium is isotropic, these wavelets are spherical, as shown in Figure 1. In the case of a uniaxial crystal, however, the wavelets are spherical for the ordinary ray but ellipsoidal for the extraordinary ray.

Figure 2 illustrates the application of Huygens' Principle to e-wave refraction in a negative uniaxial crystal (e.g., sapphire). Illustrated is the special case for which the optical axis lies in the plane of incidence. The e-ray \hat{e} is defined as that ray from the origin of the ellipsoidal wavelets to the point of tangency with the wavelet envelope. The wave normal \hat{s} is that vector perpendicular to the envelope.

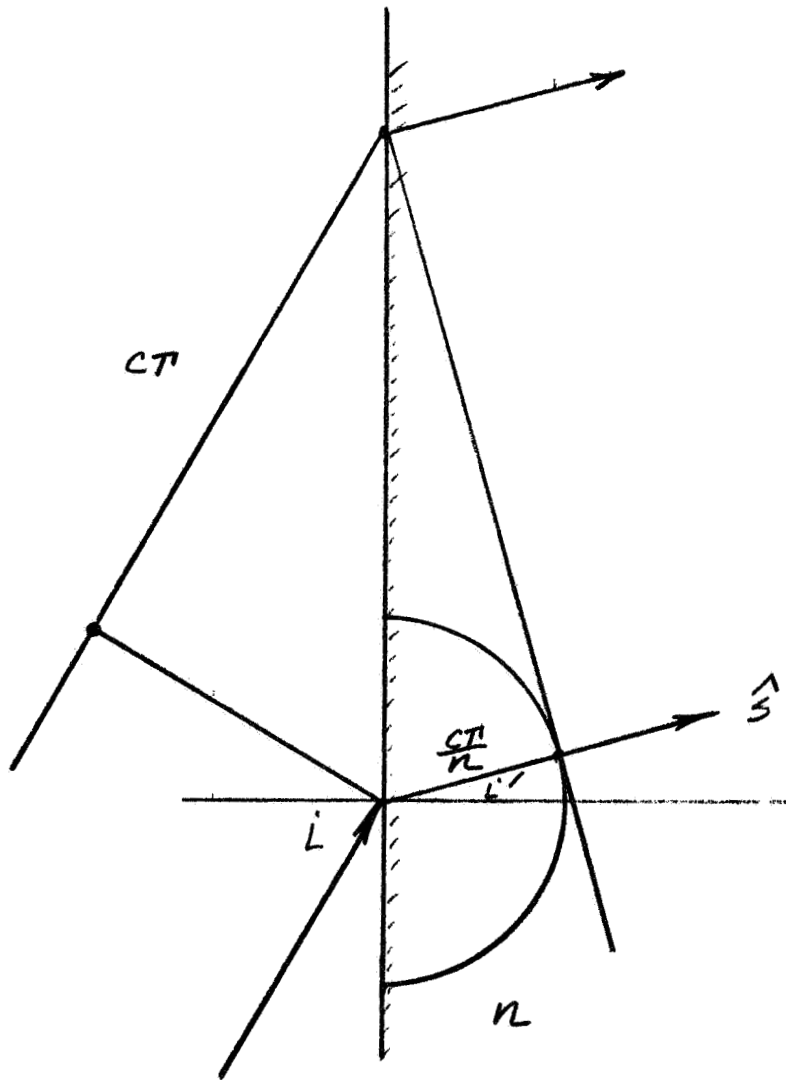


Figure 1 Huygens' Principle for Isotropic Media

ORIGINAL PAGE IS
OF POOR QUALITY

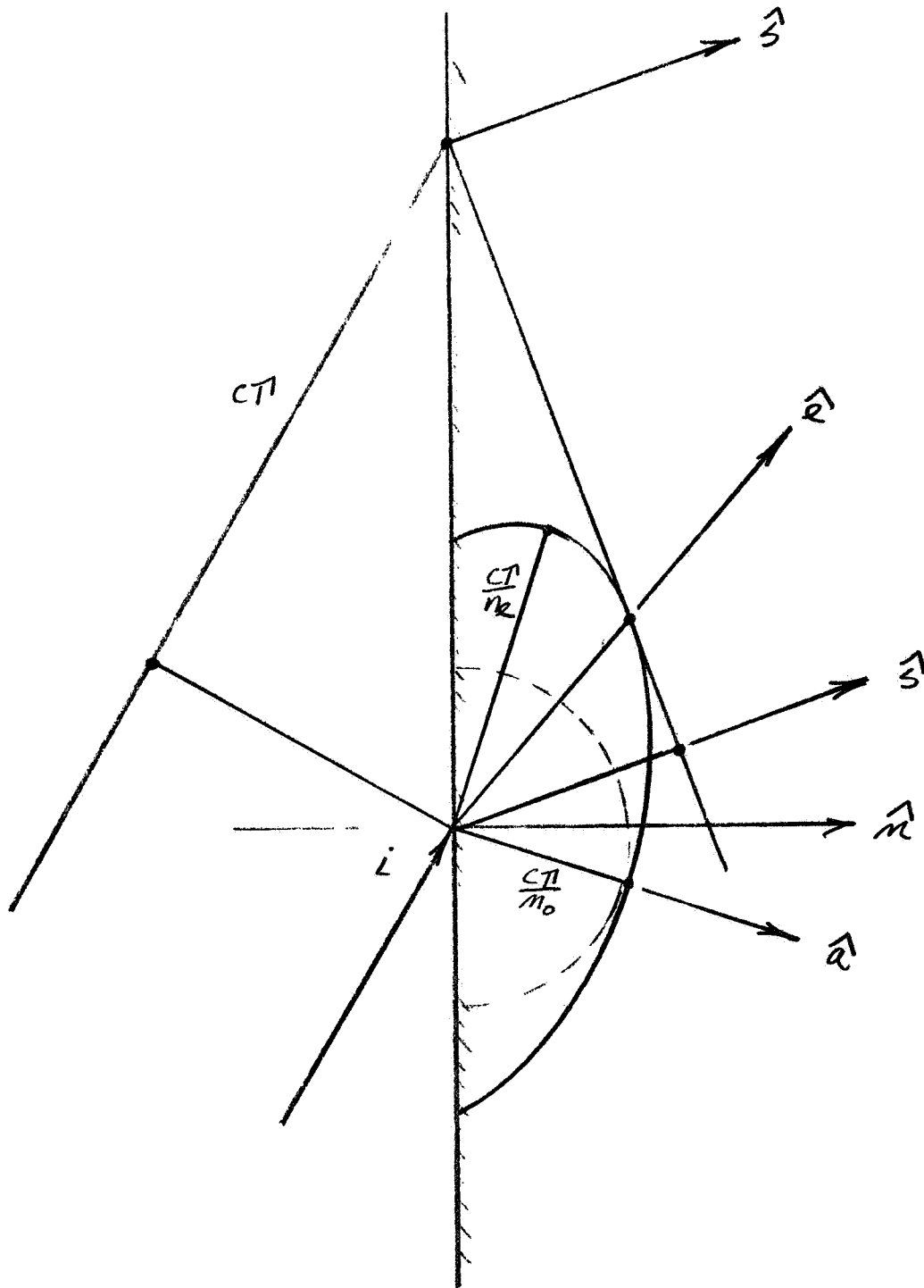


Figure 2- Huygens' Principle for Anisotropic Media

The major and minor axes of the elliptical section of the ellipsoidal wavelet are proportional to $(1/n_e)$ and $(1/n_o)$, where n_o and n_e are respectively the ordinary and extraordinary refractive indexes of the crystal. The effective refractive index for the e-ray is derived in Figure 3 from the basic analytic geometry of the ellipse and is there shown to be given by

$$n_e = n_e^2 + (n_o^2 - n_e^2) \cos^2 \beta$$

where β is the angle between the e-ray \hat{e} and the optical axis \hat{a} . The wavefront normal \hat{s} at the point of tangency to the ellipsoid must of course be normal to the elliptical section at that point. The relation between \hat{e} and \hat{s} is derived in Figure 4, where it is shown that

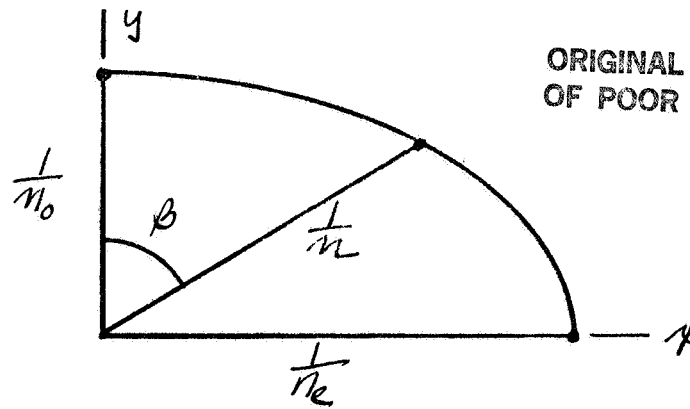
$$\tan \alpha = \left(\frac{n_e}{n_o} \right)^2 \tan \beta$$

the angle α now being the angle between the e-wave normal \hat{s} and the optical axis \hat{a} .

Given this relation between α and β , it is then possible to calculate the effective index for the e-wave normal \hat{s} . This is derived in Figure 5 and shown to be given by

$$n_s = \frac{n_o n_e}{\sqrt{n_o^2 + (n_e^2 - n_o^2) \cos^2 \alpha}}$$

ORIGINAL PAGE IS
OF POOR QUALITY



equation of the ellipse

$$\frac{x^2}{a^2} + \frac{y^2}{b^2} = 1$$

for the Huygens wavelet

$$\frac{\left(\frac{1}{n} \sin \beta\right)^2}{\left(\frac{1}{n_e}\right)^2} + \frac{\left(\frac{1}{n} \cos \beta\right)^2}{\left(\frac{1}{n_0}\right)^2} = 1$$

$$\left(\frac{1}{n}\right)^2 (n_e^2 \sin^2 \beta + n_0^2 \cos^2 \beta) = 1$$

whence

$$n^2 = n_e^2 \sin^2 \beta + n_0^2 \cos^2 \beta$$

or

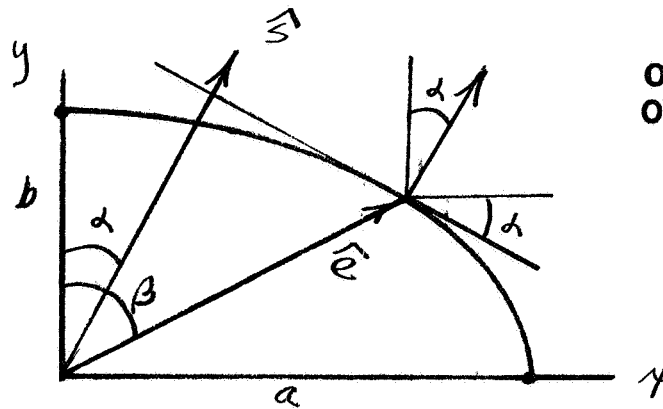
$$n^2 = n_0^2 + (n_e^2 - n_0^2) \sin^2 \beta$$

or

$$n^2 = n_e^2 - (n_e^2 - n_0^2) \cos^2 \beta$$

Figure 3 Effective Index for the E-Ray

ORIGINAL PAGE IS
OF POOR QUALITY



the equation of the ellipse

$$\frac{x^2}{a^2} + \frac{y^2}{b^2} = 1$$

differentiating

$$\frac{2x dx}{a^2} + \frac{2y dy}{b^2} = 0$$

whence

$$\frac{dy}{dx} = -\frac{x}{y} \frac{b^2}{a^2}$$

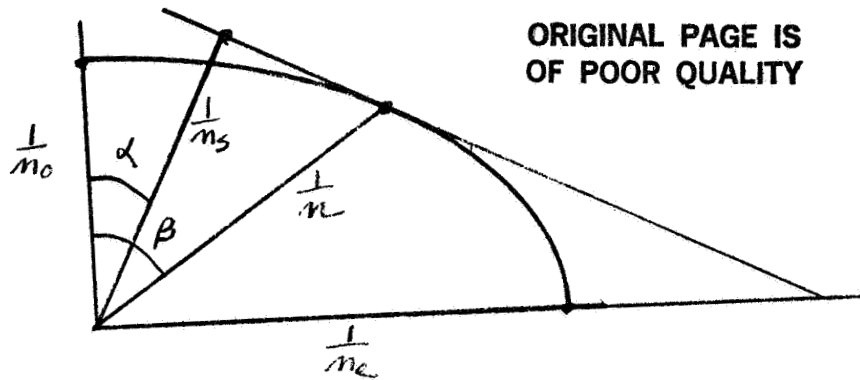
but $\frac{dy}{dx} = -\tan \alpha$, $\frac{x}{y} = \tan \beta$, $b = \frac{1}{m_0}$, $a = \frac{1}{m_e}$

hence $\tan \alpha = \left(\frac{m_0}{m_e}\right)^2 \tan \beta$

or $\tan \beta = \left(\frac{m_0}{m_e}\right)^2 \tan \alpha$

Figure A Relation Between E-Ray and
E-wave Normal

ORIGINAL PAGE IS
OF POOR QUALITY



for the e-ray

$$\frac{1}{n} = \frac{1}{\sqrt{n_e^2 \sin^2 \beta + n_0^2 \cos^2 \beta}}$$

for the e-wave normal

$$\frac{1}{n_s} = \frac{1}{n} \cos(\beta - \alpha)$$

whence

$$\frac{1}{n_s} = \frac{\cos \beta \cos \alpha - \sin \beta \sin \alpha}{\sqrt{n_e^2 \sin^2 \beta + n_0^2 \cos^2 \beta}}$$

$$\text{or } \frac{1}{n_s} = \frac{\cos \alpha + \tan \beta \sin \alpha}{\sqrt{n_e^2 \tan^2 \beta + n_0^2}}$$

$$\text{but } \tan \beta = \left(\frac{n_e}{n_0}\right)^2 \tan \alpha$$

substituting and clearing leads to

$$n_s = \frac{n_0 n_e}{\sqrt{n_0^2 + (n_e^2 - n_0^2) \cos^2 \alpha}}$$

Figure 5 Effective Index for E-wave Normal

ORIGINAL PAGE IS
OF POOR QUALITY

We have considered here what we described as the special case of the optical axis in the plane of incidence. Textbooks usually stop their discussion of birefringence at this point. This same analysis can be shown to be much more general than is usually implied, however. To illustrate: in Figure 6, holding α constant, let the optical axis \hat{a} be rotated about the e-wave normal \hat{s} . Clearly the wavelet envelope and the e-wave normal are unaffected. We may conclude, then, that the e-wave normal \hat{s} always lies in the plane of incidence, its orientation in that plane depending only on the angle α and not on the position of \hat{a} relative to the plane of incidence. We may further conclude that as the optical axis rotates about \hat{s} , holding α constant, the vectors \hat{a} , \hat{s} , and \hat{e} remain coplanar and in the same relation to each other as obtains in the elliptical section of Figure 2, representing the special case of optical axis in the plane of incidence. We conclude that the direction of the e-ray \hat{e} does depend on the direction of the optical axis \hat{a} , and that in fact \hat{e} is representable as a linear combination of \hat{a} and \hat{s} : specifically,

$$\hat{e} = \left(\frac{\sin \beta}{\sin d} \right) \hat{s} - \left(\frac{\sin(\beta-d)}{\sin d} \right) \hat{a}$$

ORIGINAL PAGE IS
OF POOR QUALITY

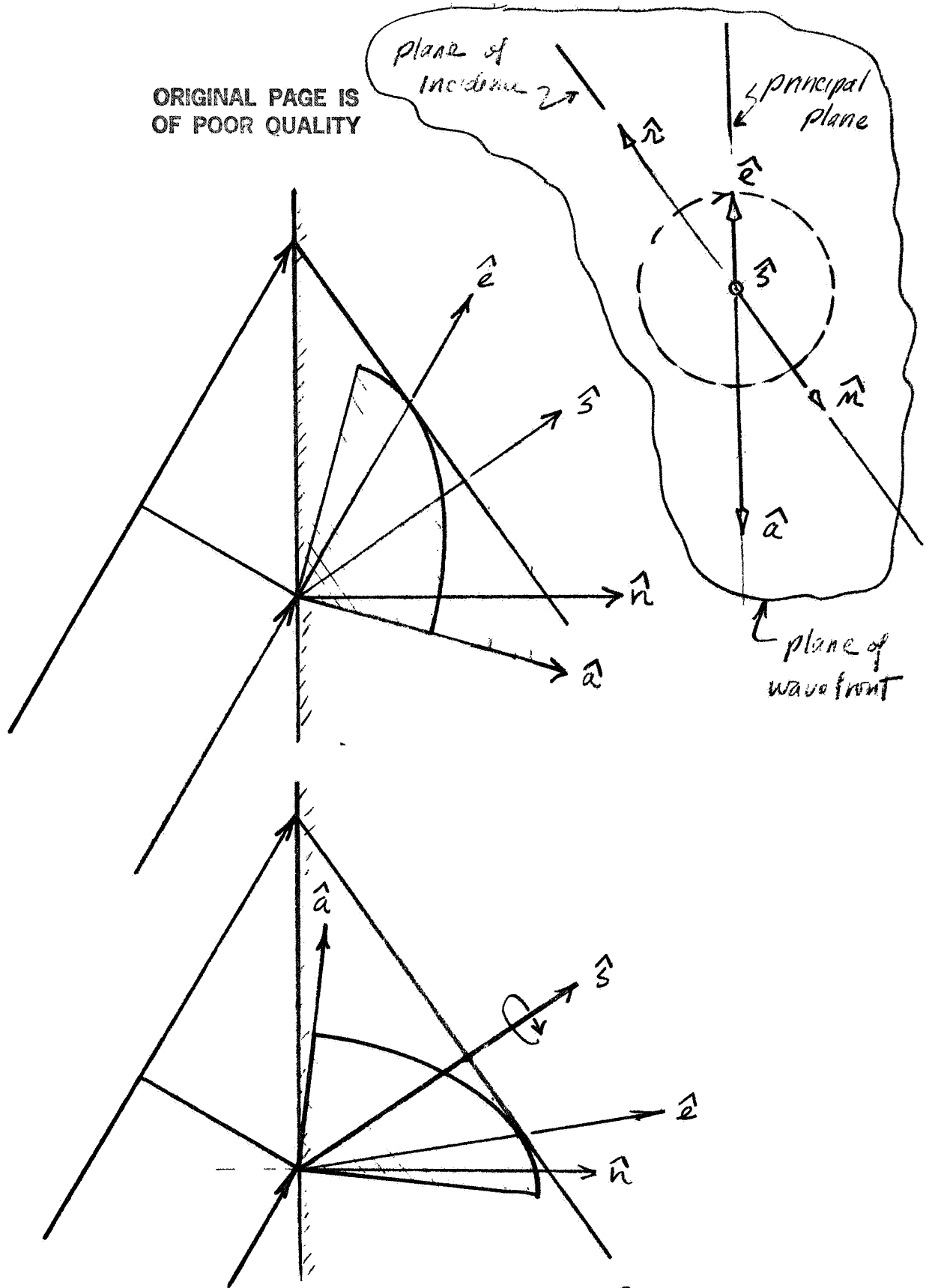


Figure 6 Relations Among Planes in Crystal Refraction

ORIGINAL PAGE IS
OF POOR QUALITY

We may further conclude from the above that the e-wave normal \hat{s} obeys Snell's Law, since it lies in the plane of incidence and since its direction in that plane is determined by a formula equivalent to Snell's Law:

$$n_1 \sin i = n_2(\alpha) \sin L'$$

We may also conclude that the e-ray \hat{e} always lies in the principal plane containing the e-wave normal \hat{s} , and that its direction in that plane is determined by a relation that for small angles, at least, has a formal similarity to Snell's Law:

$$n_e^2 \tan \beta = n_o^2 \tan \alpha$$

RAYTRACING THE EXTRAORDINARY RAY

The geometrical optics of the extraordinary ray in a uniaxial crystal may be understood in terms of the diagram of Figure 1. The incident ray \hat{r} and the surface normal \hat{n} define the plane of incidence. The extraordinary wave normal (e-wave normal) \hat{s} lies in this plane and is refracted according to Snell's Law, the crystal refractive index being taken as

$$n(\alpha) = \frac{n_o n_e}{\sqrt{n_o^2 + (n_e^2 - n_o^2) \cos^2 \alpha}}$$

in which n_o is the ordinary refractive index, n_e is the extraordinary refractive index, and $\cos(\alpha) = \hat{a} \cdot \hat{s}$, \hat{a} being the optical axis of the crystal. The position of \hat{s} is determined iteratively, since it depends on the index n , which in turn depends on the position of \hat{s} . The e-wave normal \hat{s} and the optical axis \hat{a} together define a principal plane of the crystal. The extraordinary ray \hat{e} (e-ray) will lie in this principal plane, displaced from \hat{a} by an angle β such that

$$\tan \beta = \left(\frac{n_o}{n_e} \right)^2 \tan \alpha$$

ORIGINAL PAGE IS
OF POOR QUALITY

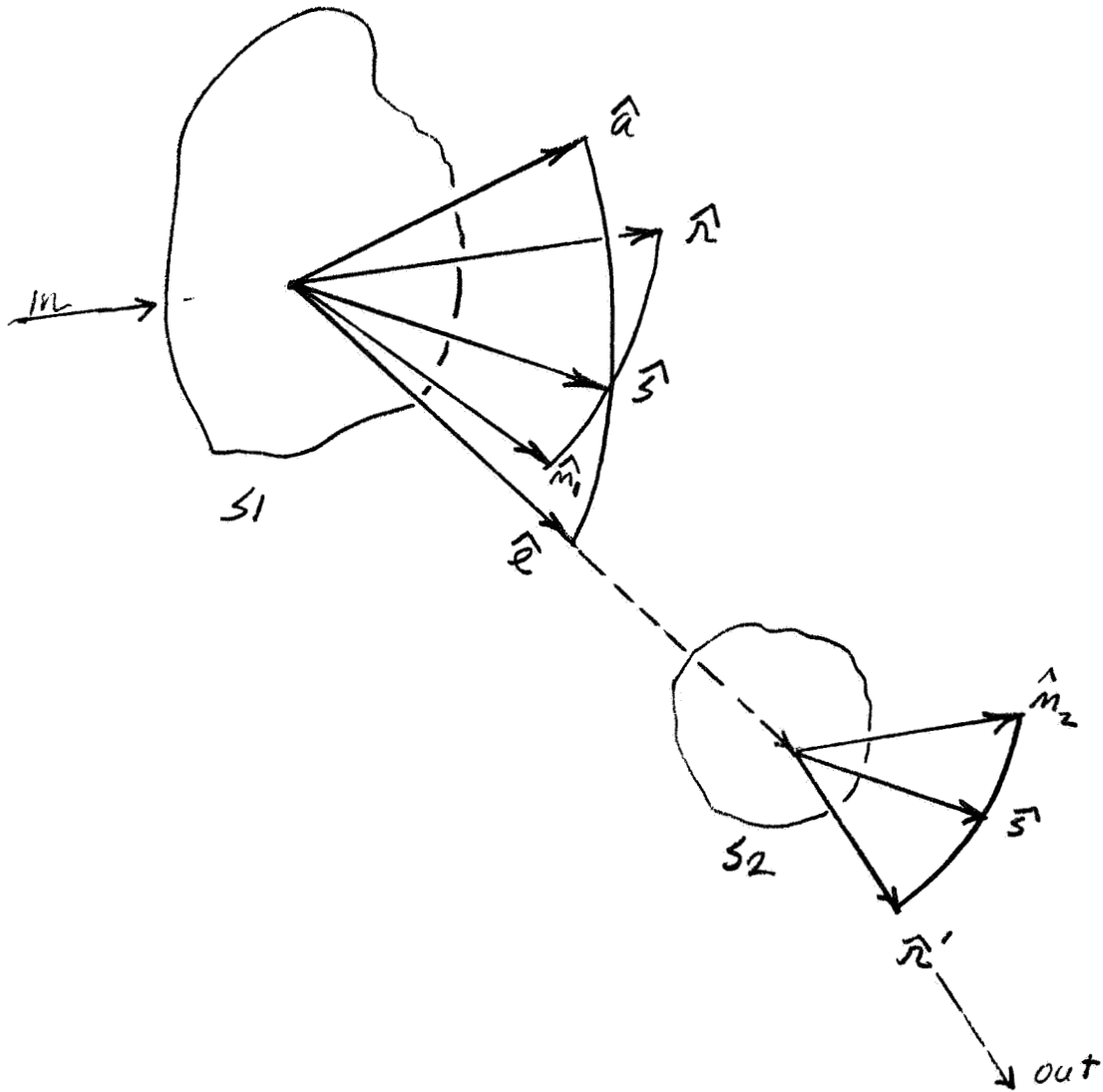


Figure 7 Transmission of Light Through a Crystal

ORIGINAL PAGE IS
OF POOR QUALITY

The e-ray \hat{e} , since it lies in the (\hat{a}, \hat{s}) plane, is expressible as a linear combination of \hat{a} and \hat{s} . The e-normal \hat{s} , since it lies in the (\hat{r}, \hat{n}) plane, is itself expressible as a linear combination of \hat{r} and \hat{n} . Hence the e-ray \hat{e} , as well as all other vectors in this problem, must be expressible in terms of the triad $(\hat{r}, \hat{n}, \hat{a})$, which represents a natural base-vector set for this problem.

Once both \hat{s} and \hat{e} are found, raytracing proceeds by projecting the ray \hat{e} until it intersects the next surface. At that point the e-normal \hat{s} is substituted for \hat{e} and refraction out of the crystal executed using Snell's Law, the crystal index $n(\downarrow)$ being the same as that used for refraction into the crystal. Outside the crystal, of course, \hat{e} and \hat{s} become identically \hat{r} , which is traced further by conventional means.

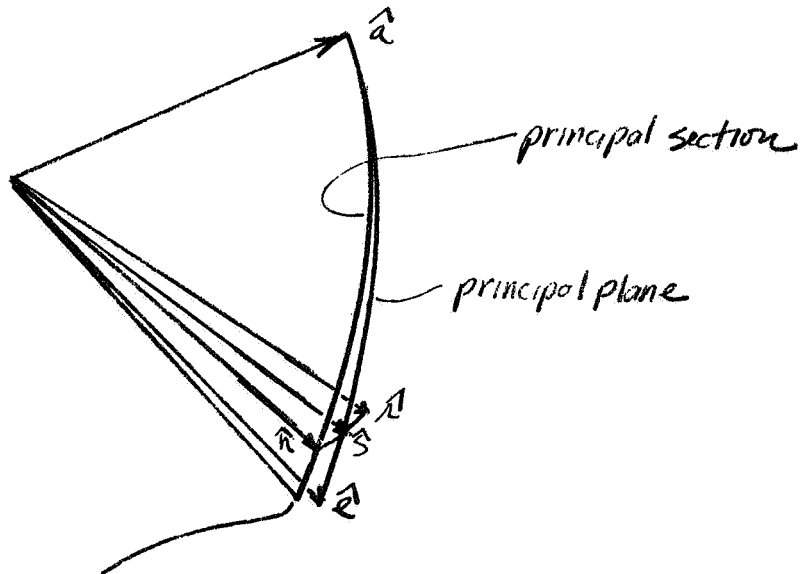
PRELIMINARY ESTIMATE OF BIREFRINGENCE EFFECTS

Before embarking upon a general raytracing exercise, it is possible to get a good idea of what to expect by relatively simple means. We can do this by taking advantage of the fact that in the FSS all rays are incident very close to normally on the sapphire sphere. Because of this the general vector diagram of Figure 7 in the present case looks like Figure 8. Since the incident ray \hat{r} , the e-wave normal \hat{s} , and the surface normal \hat{n} are all very close together, it follows that (except when α is very small) the (\hat{a}, \hat{s}) principal plane will be very nearly coincident with the (\hat{a}, \hat{n}) plane, which is called the principal section. Except for α very small, we may therefore to a good approximation consider the e-ray \hat{e} to lie in the principal section, displaced from the normal \hat{n} by the angle $\delta = (\beta - \alpha)$. For a weakly birefringent crystal like sapphire, we know this angle δ must be small. From the argument of Figure 9 we deduce that for sapphire this angle is given by

$$\delta = .00911 \sin \alpha \cos \alpha$$

in which α may now be taken as the angle between \hat{a} and \hat{n} .

ORIGINAL PAGE IS
OF POOR QUALITY



for small incidence angles,
assume $\hat{e} \parallel$ principal section
instead of principal plane

Figure 8 Approximations for Small Incidence Angles

in general $\tan \rho = \left(\frac{n_0}{n_e}\right)^2 \tan \alpha$

for $(\beta - \alpha)$ small, $\tan \alpha + \Delta(\tan \alpha) = \left(\frac{n_0}{n_e}\right)^2 \tan \alpha$

whence $\Delta(\tan \alpha) = \left(\left(\frac{n_0}{n_e}\right)^2 - 1\right) \tan \alpha$

but from the differential \rightarrow arcs

$$\Delta(\tan \alpha) = \sec^2 \alpha (\Delta \alpha)$$

equating these two expressions for $\Delta(\tan \alpha)$

$$\sec^2 \alpha (\Delta \alpha) = \left(\left(\frac{n_0}{n_e}\right)^2 - 1\right) \tan \alpha$$

whence $\Delta \alpha = \left(\left(\frac{n_0}{n_e}\right)^2 - 1\right) \sin \alpha \cos \alpha$

but $\Delta \alpha = (\beta - \alpha) = \delta$

hence $\delta = \left(\left(\frac{n_0}{n_e}\right)^2 - 1\right) \sin \alpha \cos \alpha$

for suppre $n_0 = 1.768$, $n_e = 1.760$

hence $\delta = .00911 \sin \alpha \cos \alpha$

for large α , $\delta = .00911 \eta$ [$\eta = 90 - \alpha$]

Figure 9 Angular Deviation of the E-Ray

ORIGINAL PAGE IS
OF POOR QUALITY

In a centered optical system a ray deflection in the (\hat{a}, \hat{n}) plane can be expected to produce an image shift parallel to that plane. The image at the detector plane formed by e-rays can therefore be expected to be displaced along the direction of the optical axis as projected into the (x, y) plane. Such displacement is illustrated in Figure 10.

We now know the general nature and direction of the image shift: it remains to determine its magnitude. We can do this easily by considering the particular case in which the optical axis lies in the meridional plane, then performing a paraxial raytrace. Such a raytrace is shown in Figure 11. For this example the optical axis was taken to be

$$\hat{a} = -(0.707)\hat{j} + (0.707)\hat{k}$$

and the calculated image deflection was -0.16 mm. We deduce, then, that in general the image deflection will be in the direction of the optical axis as projected into the detector plane and of a magnitude

$$\Delta = 0.32 (\sin d \cos d) \text{ mm}$$

Subsequent computer raytracing has confirmed this to be a very accurate estimate of image displacement, except for very small values of the angle d .

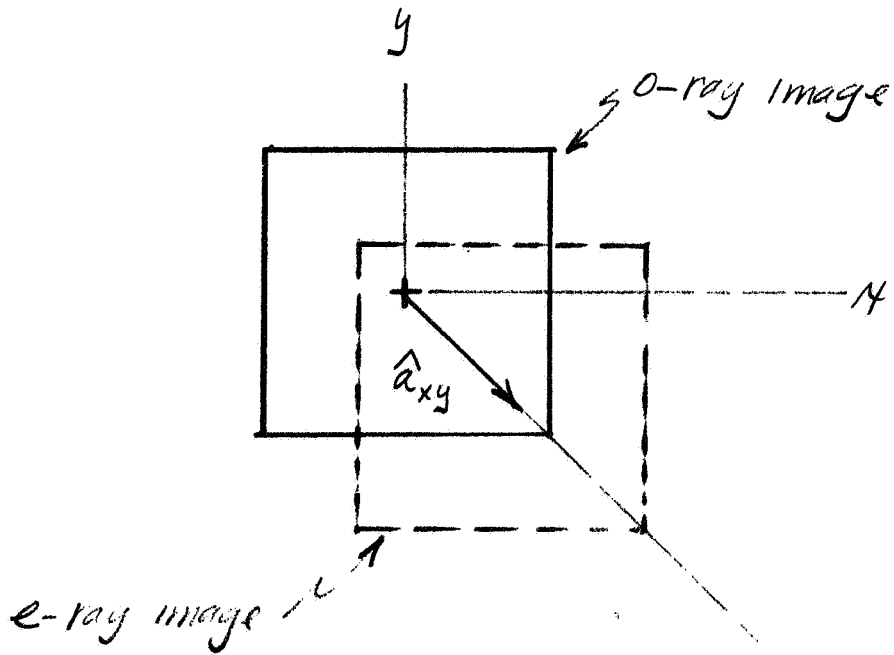


Figure 10 Expected E-ray Image Displacement

ORIGINAL PAGE IS OF POOR QUALITY

n	1.0	\emptyset	1.0	\emptyset	1.0	\emptyset	1.478	index
t/m	118.46835		48.76825		10/1.764		10/1.478	radius
y	3	4	4	.54525368	4	.178842	4	height
nu	0	4	-0.05064644	4	-0.0565973	4	-0.05574977	reduced slope
$-\phi$			-0.016888146	-0.0109142		.00476607		surface power

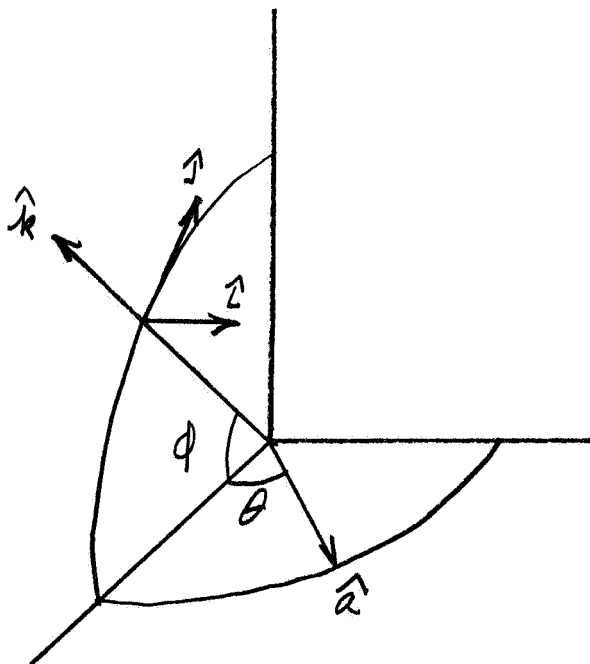
n	1.478	\emptyset	1.764	\emptyset	1.0	\emptyset	1.0	8
t/m	10/1.478		10/1.764		48.76825			
y	4	4	4	-1.0014105	4	-3.596817	4	-3.1655
nu	-0.06746575	-0.07058985	-0.080035	-0.0109143	-0.05959274			$\Delta = -0.16mm$
$-\phi$.05912	.00476607				-0.06582146		

$$y' = (nu) \left(\frac{t}{r} \right) + y \quad (nu)' = -\phi y' + (nu)$$

boxed terms -0.080035 represent $n\delta = 1.764(-0.00911)(.707)(.707)$

Figure 11 Paraxial Raytrac of System for $\bar{a} = -0.707j + 0.707k$

For a rotating sphere with an optical axis in the equatorial plane, this deflection formula is easily expressed in terms of latitude ϕ and longitude θ , as shown in Figure 12.



$$\Delta x = 0.32 (\cos \theta \cos \phi) \sin \theta$$

$$\Delta y = 0.32 (\cos \theta \cos \phi) \cos \theta \sin \phi$$

Figure 12 Image Displacement Formulas

ORIGINAL PAGE IS
OF POOR QUALITY

When the angle α is small, the deflection is still given correctly by the above expression, but this deflection may no longer with accuracy be assumed to lie in the principal section. For α small, the index $n(\alpha) \approx n_0$. The e-wave normal \hat{s} becomes coincident with the ordinary ray \hat{t} , and the deflection of each e-ray will be in the principal plane defined by \hat{a} and the ordinary ray \hat{t} . The magnitude of the shift now becomes $\Delta \approx 0.32\alpha$ mm where α is now to be taken angle between the optical axis \hat{a} and the ordinary ray \hat{t} .

In the FSS the lower limit for accurate measurement is a deflection of 0.32 microns.

An e-ray image shows this much deflection at only

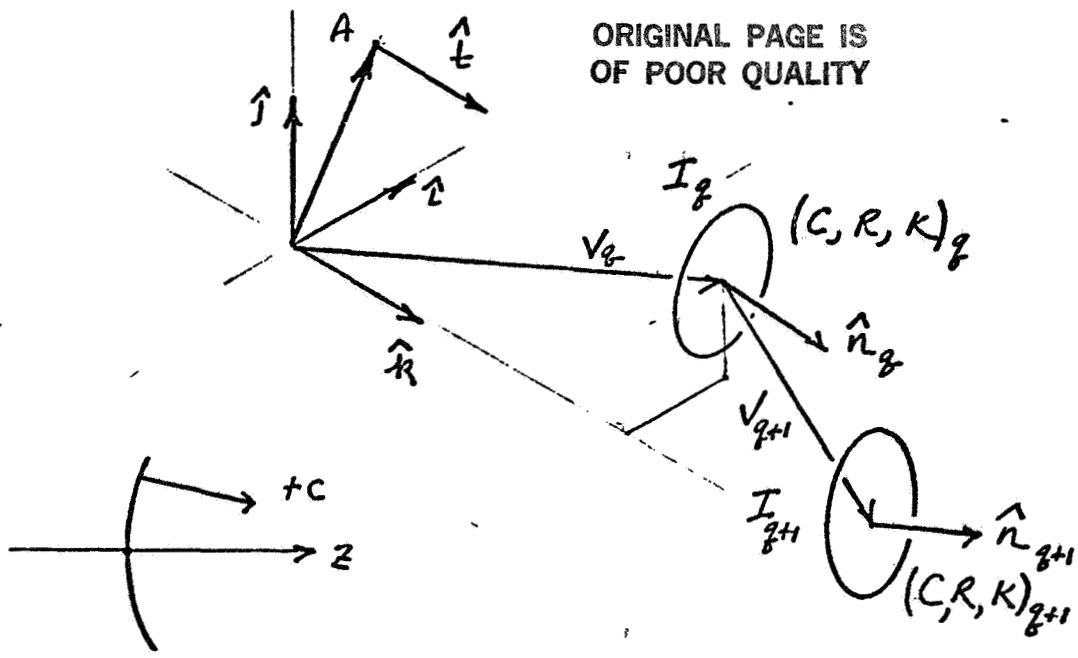
$\alpha = .001$. Since the o-ray in the FSS averages about .050 from the normal, it appears impossible to avoid significant e-ray image displacement at the detector no matter how the optical axis is oriented, if unpolarized light is used.

COMPUTER RAYTRACE

To verify the foregoing analysis and the expectations derived from it, a simplified version of the FSS was raytraced, taking into account the birefringence of the sapphire shell. The same program used earlier to raytrace the baseline design was used here, except that the program was modified to trace the e-ray as well as the o-ray. An explanation of the system parameters is given in Figure 13. The system description in terms of these parameters is given in Figure 14. The basic algorithm for accommodating the e-ray in the program is described in Figure 15.

The particular cases studied are tabulated in Figure 16. For each of these cases rays were traced from eight points around the periphery of a 2 x 2 mm target to the image plane. All results confirmed the displacement expectations described earlier. Typical of these results is the case shown in Figure 17. The entire e-ray image translates as a whole; the translation is in the direction of the x,y projection of the optical axis \hat{a} and is of a magnitude accurately representable by the relation derived earlier:

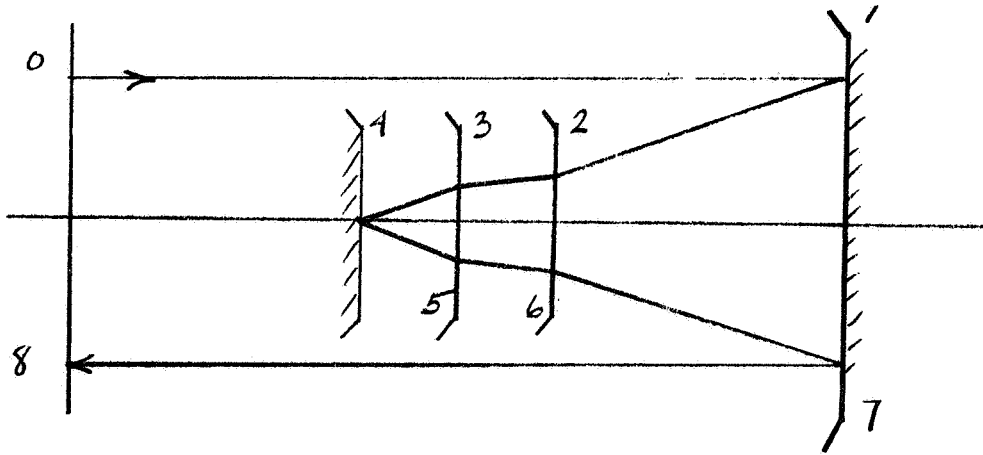
$$A = .32 (\sin d \cos d) \text{ mm}$$



- A = object point position vector
- \hat{E} = ray direction vector
- V = surface vertex position vector
- \hat{N} = surface vertex normal
- C = surface vertex curvature (scalar)
- K = surface conic constant (scalar)
- R = surface reflectivity (scalar: 0 or 1)
- I = refractive index on input side

Figure 13 - Descriptive Parameters for Computer Raytrace

ORIGINAL PAGE IS
OF POOR QUALITY



① V 0,0,111.8
N 0,0
C -0.0089445
K 0
R 1
I 1.0

④ V 0,0,-10.0
N 0,0
C -0.02
K 0
R 1
I 1.468

⑦ V 0,0,41.8
N 0,0
C -0.0089445
K 0
R 1
I 1.0

② V 0,0,-41.8
N 0,0
C -0.014286
K 0
R 0
I 1.0

⑤ V 0,0,10.0
N 0,0
C -0.016667
K 0
R 0
I 1.478

⑧ V 0,0,-111.8
N 0,0
C 0
K 0
R 0
I 1.0

③ V 0,0,-10.0
N 0,0
C -0.016667
K 0
R 0
I 1.768

⑥ V 0,0,10.0
N 0,0
C -0.014286
K 0
R 0
I 1.768

Figure 1A Parametric Description of System Traced

ORIGINAL PAGE IS
OF POOR QUALITY

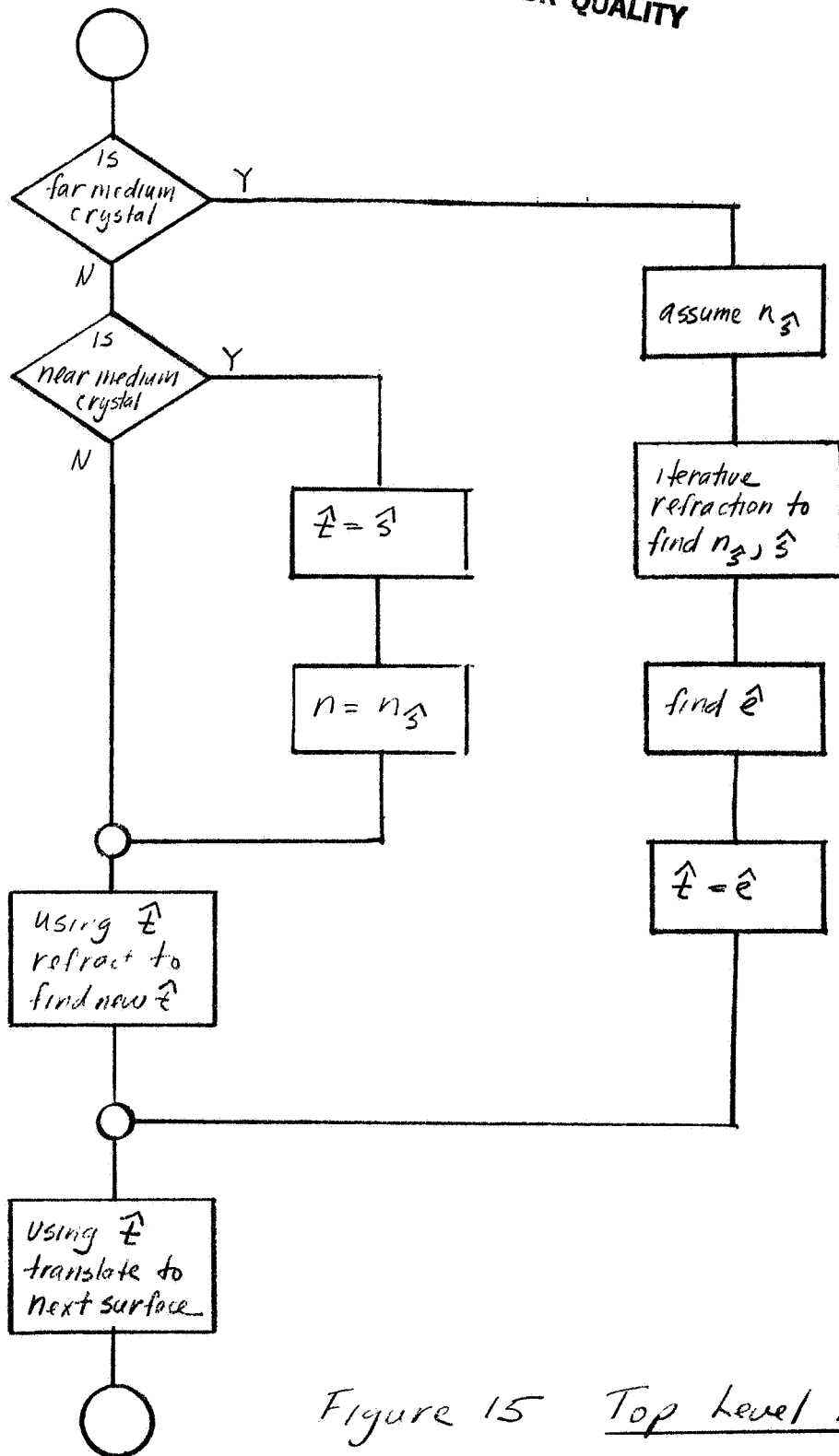


Figure 15 Top Level Algorithm
for E-ray Trace

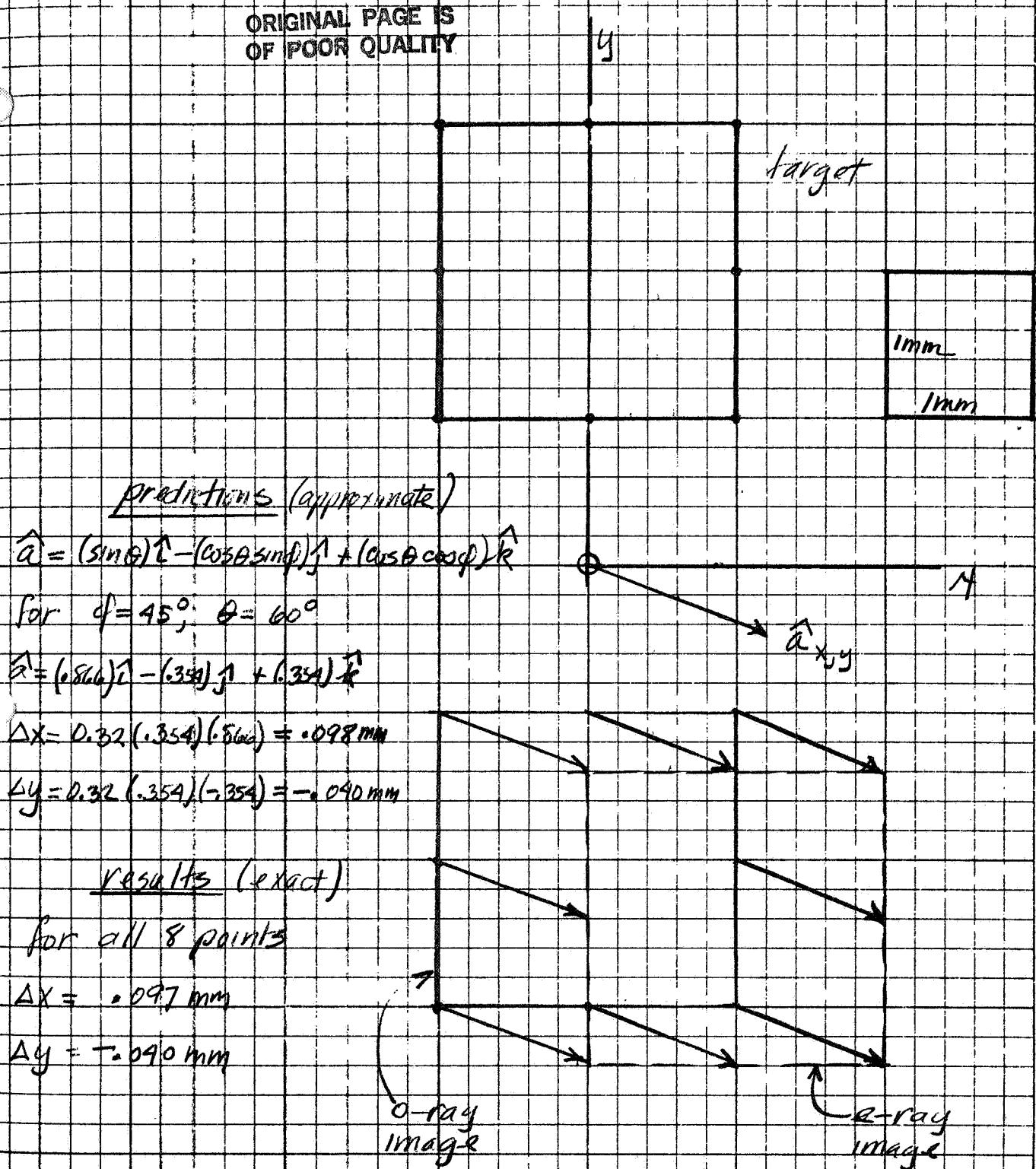
ORIGINAL PAGE IS
OF POOR QUALITY

θ°

	0	15	30	45	60	75	90
0							
15	✓	✓	✓	✓	✓	✓	✓
30							
45	✓	✓	✓	✓	✓	✓	✓
60							
75	✓	✓	✓	✓	✓	✓	✓
90							

ϕ°

Figure 16 Cases Raytraced by Computer

ORIGINAL PAGE IS
OF POOR QUALITYFigure 17 Typical Computer Raytrace Results



)

)

GENERAL ELECTRIC

SPACE DIVISION
PHILADELPHIA

PROGRAM INFORMATION REQUEST / RELEASE

*CLASS. LTR.	OPERATION	PROGRAM	SEQUENCE NO.	REV. LTR.
PIR NO. U	- 1254 -	ACCE-	033	
*USE "C" FOR CLASSIFIED AND "U" FOR UNCLASSIFIED				

FROM W. C. Yager	TO R. Homsey
---------------------	-----------------

DATE SENT 6/19/81	DATE INFO. REQUIRED	PROJECT AND REQ. NO.	REFERENCE DIR. NO.
----------------------	---------------------	----------------------	--------------------

SUBJECT
A FURTHER NOTE ON SAPPHIRE BIREFRINGENCE

INFORMATION REQUESTED/RELEASED

See attached text.

**ORIGINAL PAGE IS
OF POOR QUALITY**

PAGE NO. OF	<input checked="" type="checkbox"/> RETENTION REQUIREMENTS	
	COPIES FOR	MASTERS FOR
	<input type="checkbox"/> 1 MO.	<input type="checkbox"/> 3 MOS.
	<input type="checkbox"/> 3 MOS.	<input type="checkbox"/> 6 MOS.
	<input type="checkbox"/> 6 MOS.	<input type="checkbox"/> 12 MOS.
	<input type="checkbox"/> MOS.	<input type="checkbox"/> MOS.
	<input type="checkbox"/>	<input type="checkbox"/> DO NOT DESTROY

ORIGINAL PAGE IS
OF POOR QUALITY

A FURTHER NOTE ON SAPPHIRE BIREFRINGENCE

In Figure 9 of PIR 1254-AGCE-027 the angular deviation of the e-ray was calculated using a differential approximation and shown to be

$$\delta = .00911 \sin \alpha \cos \alpha$$

It is the purpose of this note to point out that a differential approximation is not necessary and that an exact solution is easily obtained. The exact analysis, shown here as Figure 9A, reveals that for sapphire

$$.00452 \sin 2\alpha < \delta < .00456 \sin 2\alpha$$

and furthermore that if the effective index for the e-wave normal is simply taken as the mean of ordinary and extraordinary indices, the result

$$\delta = .00454 \sin 2\alpha$$

can never be more than 20 microradians in error, or about 0.4%.

in general, $\tan \beta = \left(\frac{n_0}{n_e}\right)^2 \tan d$

but also $\tan(\beta-d) = \frac{\tan \beta - \tan d}{1 + \tan \beta \tan d}$

substituting $\tan(\beta-d) = \frac{\left(\frac{n_0^2}{n_e^2} - 1\right) \tan d}{1 + \left(\frac{n_0^2}{n_e^2}\right) \tan^2 d}$

multiplying thru by $n_e^2 \cos^2 d$

$$\tan(\beta-d) = \frac{(n_0^2 - n_e^2) \sin d \cos d}{n_e^2 \cos^2 d + n_0^2 \sin^2 d}$$

but

$$n_s^2 = \frac{n_0^2 n_e^2}{n_e^2 \cos^2 d + n_0^2 \sin^2 d}$$

hence, letting $(\beta-d) \equiv \delta$

$$\tan(\delta) = \left[\frac{n_s^2}{n_e^2} - \frac{n_s^2}{n_0^2} \right] \sin d \cos d$$

since $n_e < n_s < n_0$ and $\tan \delta \approx \delta$ for $\delta \ll 1$

we have for sapphire

$$\text{if } \begin{cases} n_s = n_0, & \delta = .00911 \sin d \cos d \\ n_s = \frac{1}{2}(n_0 + n_e) & \delta = .00907 \sin d \cos d \\ n_s = n_e & \delta = .00903 \sin d \cos d \end{cases} \pm 0.4\% \text{ range}$$

Figure 9A Angular Deviation of the E-Ray



3.3 THERMAL ANALYSIS AND DESIGN

	<u>PIR NO.</u>
Task 6.1 - Parametric Heat Flow Analysis	-010
Task 6.2 - AGCE Thermal Feasibility Design Study	-023

)

)

)

PROGRAM INFORMATION REQUEST / RELEASE

*USE "C" FOR CLASSIFIED AND "U" FOR UNCLASSIFIED

FROM G. Andres <i>GA</i> Environmental Control S/S Engineering	TO T. Scollon Environmental Control S/S Engineering
--	---

DATE SENT 2/13/81	DATE INFO. REQUIRED	PROJECT AND REQ. NO.	REFERENCE DIR. NO.
----------------------	---------------------	----------------------	--------------------

SUBJECT
 TASK 6.1 PARAMETRIC HEAT FLOW ANALYSIS

INFORMATION REQUESTED/RELEASED

1.0 SUMMARY

Heat flow from outer to inner hemisphere through the dielectric fluid was estimated for various parametric combinations of radial temperature difference, Nusselt number, and sphere size. Results indicated heat flows somewhat higher than anticipated and verified the need for the more refined study of localized thermal loading on the inner sphere which is planned for Task 6.2.

2.0 BACKGROUND

The feasibility of AGCE depends in part on the ability to establish certain desired temperature profiles on the inner and outer spheres while the fluid between them is flowing in closed convection cells. As a first step in this thermal evaluation, gross heat flows must be estimated for expected ranges of the variables involved.

3.0 TASK IMPLEMENTATION

The problem involved modeling the heat flow through the AGCE cell as radial conduction between two hemispheres (each assumed isothermal) and using the specified Nusselt numbers to determine the magnitude of the convection coupling between them. Conduction between concentric hemispherical shells is a one-dimensional steady-state problem if the interior and exterior surface temperatures are uniform and constant, and the intermediate substance is considered homogeneous. Note that fluid motion effects were not modeled explicitly, but were superimposed by using Nusselt number scaling of (stagnant fluid) conduction couplings.

The AGCE cell model is illustrated in Figure 3.1. The heat flow from the outer-to-inner hemispherical surface is calculated from EQ(1). The results are listed in Table 3.1.

$$Q = 2 \pi N_u K \Delta T \left(\frac{r_i r_o}{r_o - r_i} \right) \quad \text{EQ(1)}$$

4.0 RECOMMENDATION

The detailed heat flow calculations planned for Task 6.2 should be initiated immediately.

DISTRIBUTION:

L. Eaton	G. Fogal	S. Neste
✓ Montague	W. Yager	AGCE Library

PAGE NO.

OF

RETENTION REQUIREMENTS

COPIES FOR	MASTERS FOR
<input type="checkbox"/> 1 MO.	<input type="checkbox"/> 3 MOS.
<input type="checkbox"/> 3 MOS.	<input type="checkbox"/> 6 MOS.
<input type="checkbox"/> 6 MOS.	<input type="checkbox"/> 12 MOS.
<input type="checkbox"/> MOS.	<input type="checkbox"/> MOS.
<input type="checkbox"/>	<input type="checkbox"/> DO NOT DESTROY

AGCE CELL CONCEPT

ORIGINAL PAGE IS
OF POOR QUALITY

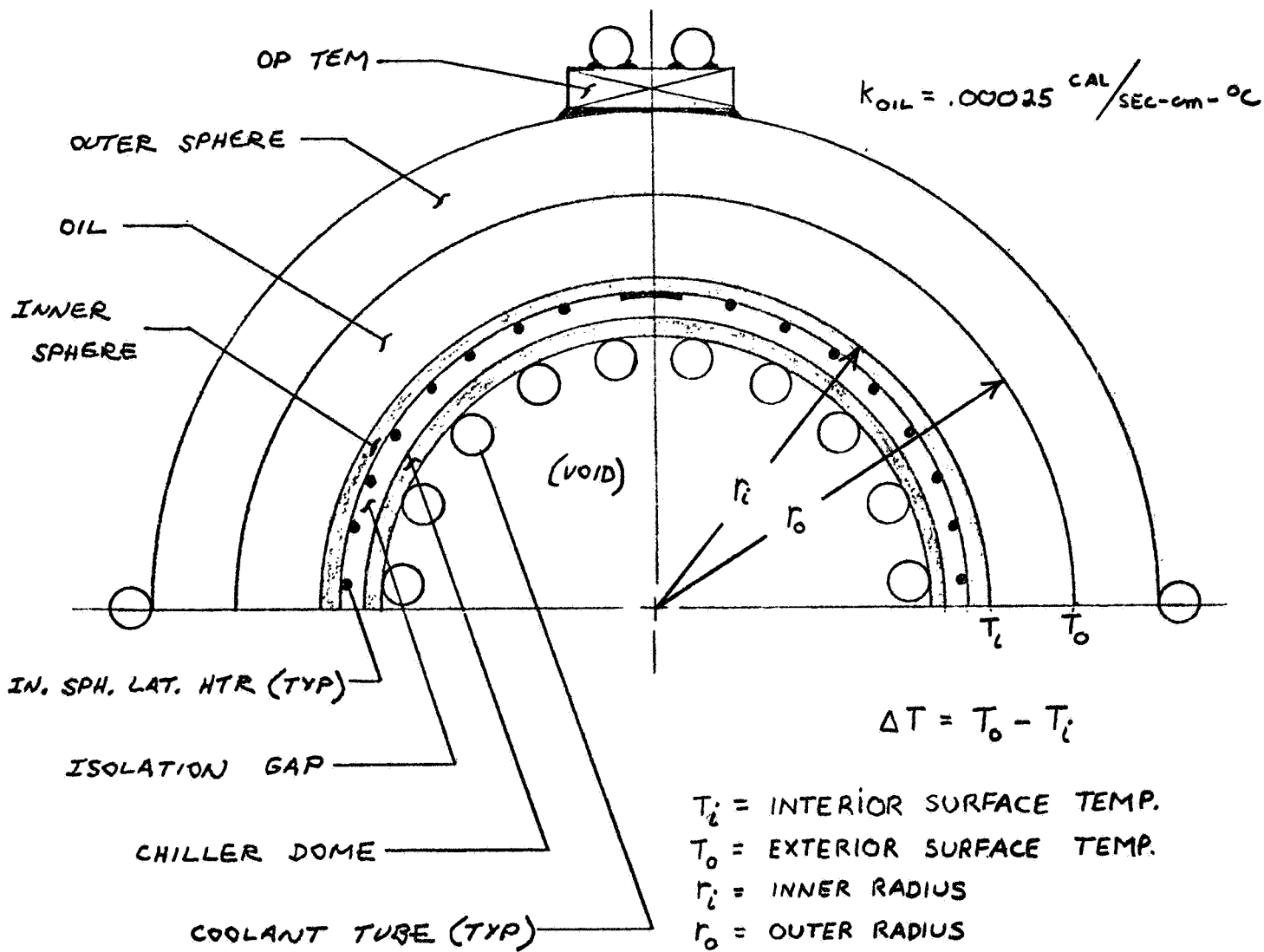


Fig. 3.1 AGCE CELL MODEL

TABLE 3.1 HEAT FLOW RESULTS

Nu	r_i (cm)	r_o (cm)	HEAT FLOW (WATTS)		
			$\Delta T=5^{\circ}\text{C}$	$\Delta T=10^{\circ}\text{C}$	$\Delta T=20^{\circ}\text{C}$
1	2	3	.196	.391	.783
	5	6	.978	1.96	3.91
	4.5	6.5	.477	.965	1.91
2	2	3	.391	.783	1.57
	5	6	1.96	3.91	7.83
	4.5	6.5	.954	1.91	3.82
5	2	3	.978	1.96	3.91
	5	6	4.89	9.78	19.6
	4.5	6.5	2.38	4.77	9.54

203



PIR NO.	*CLASS. LTR. U U	OPERATION 1254 1R54	PROGRAM AGCE AGCE	SEQUENCE NO. 023 062	REV. LTR.
---------	------------------------	---------------------------	-------------------------	----------------------------	-----------

PROGRAM INFORMATION REQUEST / RELEASE

*USE "C" FOR CLASSIFIED AND "U" FOR UNCLASSIFIED

FROM G. Andres <i>GA</i> Environmental Control S/S Engineering	TO T. Scollon Environmental Control S/S Engineering
--	---

DATE SENT	DATE INFO. REQUIRED	PROJECT AND REQ. NO.	REFERENCE DIR. NO.
-----------	---------------------	----------------------	--------------------

SUBJECT
 TASK 6.2 AGCE THERMAL FEASIBILITY/DESIGN STUDY

INFORMATION REQUESTED/RELEASED

1.0 SUMMARY

The localized thermal loads at the outer sphere pole, outer sphere equator, and all latitudes of the inner sphere surface are defined using computer analysis to simulate the effects of a flowing fluid in a closed convection cell. Various velocity profiles and temperature distributions are considered to determine the worst case design conditions. Results yield a 5.0 watt cooling load at the outer pole, a 9.5 watt cooling load at the inner sphere and a 16.0 watt heating load at the equator. TEM heat exchangers, requiring 145 watts of power, will provide or remove the heat loads at these locations. The total AGCE heat dissipation, approximately 277 watts, will be rejected to an avionics air supply of 57 kg/HR.

The feasibility design study concludes that the proposed thermal system can maintain the desired temperature distributions. Recommendations are made for further investigation into certain aspects of the proposed design in the next phase of study.

The details of the design are as follows:

Blowing 500 FPM of N₂ gas at a circular finned heat exchanger enables the outer sphere pole TEM to maintain a cooling load of 50 watts and a 25°C outer pole temperature.

The outer equator can be held at 35°C by providing a 16.0 watt heat load from 12 gph of 38°C water pumped around the equator surface.

Distribution: R. Homsey (M9415) G. Fogal (M9423) S. Neste (M9521) A. Montague	L. Blomstrom W. Yager (M9423) AGCE Library	PAGE NO. 1 OF 51	RETENTION REQUIREMENTS	
			COPIES FOR	MASTERS FOR
<input type="checkbox"/>	1 MO.	<input type="checkbox"/>	3 MOS.	
<input type="checkbox"/>	3 MOS.	<input type="checkbox"/>	6 MOS.	
<input type="checkbox"/>	6 MOS.	<input type="checkbox"/>	12 MOS.	
<input type="checkbox"/>	MOS.	<input type="checkbox"/>	MOS.	
<input type="checkbox"/>		<input type="checkbox"/>	DONOT DESTROY	

The localized loads on the inner sphere are maintained by trim heaters offsetting the bias of an 8°C chiller dome heat sink. A total load of 9.5 watts is removed from the chiller dome by 22 gph of 7.5°C water pumped through tubes soldered to the inner surface of the chiller dome.

In both loops, heat is either removed or supplied to the water by single stage TEMs mounted to the rotating platform of the AGCE assembly. The rotating platform heat load is removed by a 45 kg/HR avionics air supply through concentric finned rotating and stationary heat exchangers.

2.0 BACKGROUND

The Earth's gravitational force is modeled by holding a dielectric fluid between two concentric spheres and subjecting the fluid to a radial electric field in the form of a spherical capacitor. The fluid will simulate the large-scale circulations of the Earth's atmosphere.

A feasibility design study is required to determine if a thermal system is able to maintain the specified temperature profiles on the inner and outer spheres while the fluid between them is flowing in a closed convection cell. The outer sphere will be maintained warmer than the inner sphere, with latitudinal temperature gradients on the spheres.

In Task 6.1, 1254-AGCE-010, heat flow from the outer to inner hemisphere through the dielectric fluid was estimated for various parametric combinations of radial temperature difference, Nusselt number, and sphere size to predict the expected ranges of the variables involved. Fluid motion effects were not modeled explicitly but were superimposed by using Nusselt number scaling of stagnant fluid conduction couplings. An explicit analysis of the fluid motion effects, incorporated into a model of the sphere assembly is necessary to accurately define the system's heating and/or cooling requirements at the outer sphere pole, outer sphere equator, and all latitudes of the inner sphere. Full thermal performance can only be attained if heat can be provided or removed locally at these locations to maintain the desired temperature profiles on the two spheres.

3.0 TASK IMPLEMENTATION

3.1 DESCRIPTION OF AGCE MODEL

Based on the parametric heat flow analysis, Task 6.1, the inner radius of the outer sapphire sphere was selected as 6.0 cm and the outer radius of the inner sphere was selected as 5.0 cm. A 1 cm. thick outer sapphire sphere is assumed. The sphere assembly is modeled as 53 nodes as illustrated in Figure 3.1.1. Of the 53 nodes, 40 are active and 13 are boundary nodes. Node divisions occur every 10 degrees from -10 degrees latitude to 90 degrees latitude. In Table 3.1.1, the nodes are defined and a list of their physical and thermal properties is presented.

Table 3.1.1
Node Description and Properties

<u>Active Nodes</u>	<u>Description</u>	<u>p (g/cm³)</u>	<u>Cp (cal/g-°C)</u>	<u>K (cm-SEC-°C)</u>	<u>μ (cps)</u>
1 → 10	Sapphire Outer Sphere	3.98	0.10	.065	N/A
11 → 40	Silicone Oil Dielectric Fluid	1.101	0.47	.00025	1.98
<u>Boundary Nodes</u>	<u>Description</u>				
41 → 50	Inner Sphere				
51	Outer Sphere Equator				
52	Outer Sphere Pole				
53	Ambient Nitrogen Gas				

3.2 COMPUTER ANALYSIS TO SIMULATE CONVECTION CELL

Incorporating a simulation of the effects of a flowing fluid into a previously developed computer program (MSTTR) enabled the modeling of a closed convection cell. The fluid was divided into three layers of nodes (Figure 3.1.1) to represent the flowing fluid. Meridional flow only occurs in the outer layers, nodes 12 thru 20 and 32 thru 40, while radial flow only occurs in the middle layer, nodes 22 thru 30.

ORIGINAL PAGE IS
OF POOR QUALITY

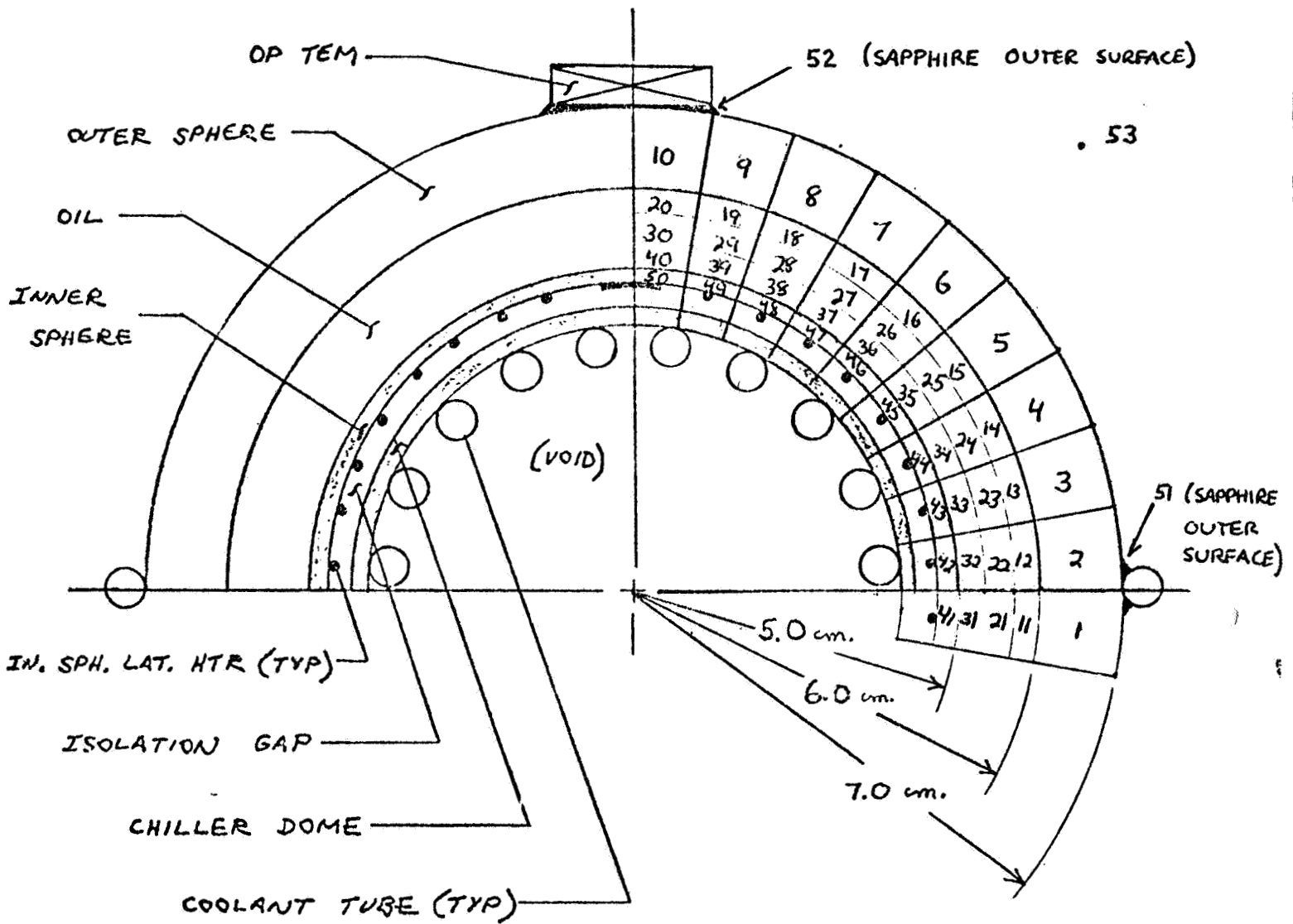


Fig. 3.1.1 AGCE CELL MODEL

The fluid is restricted to flow in the northern hemisphere of the model, thus nodes 11, 21 and 31 are modeled as stagnant nodes. Positive meridional flow is in the direction of the pole and positive radial flow is in the direction of the inner sphere. By specifying the total mass flow rate of the circulating fluid in the convection cell, and the percentage of radial flow at each middle layer node, various velocity profiles can be established. The mass flow rate at each node is determined by applying the principle of conservation of mass flow. For example, examining Figure 3.1.1, with zero radial flow in node 26, the mass flow rate in node 16 equals that of node 15 (assuming positive meridional flow). If node 27 then has 30% radial flow, the mass flow rate in node 17 is 70% of that in node 16 and node 27 has 30% of that in node 16.

The turnaround zones for the convection cell may be concentrated at the pole and equator by making all middle layer nodes except 22 and 30 have zero radial flow. It may also be spread out by only specifying zero radial flow at a few of the central latitude middle layer nodes. The overall size of the cell is reducible by specifying no flow in nodes at the pole and equator. The velocity at each node is determined by assuming a constant density fluid and an average cross-sectional flow area.

Because of the relatively low velocities of the circulating fluid, it is assumed that heat is transferred from the fluid to the spheres' surfaces by both convection and conduction. All nodes are radially and laterally (meridionally) conductively coupled as if the fluid was stagnant. The outer layers' convection coefficients are determined by analyzing the meridional flow as flow over a cylinder. The total couplings from the fluid to the inner and outer spheres' surfaces are the effective couplings of conduction and convection couplings in parallel.

The nodes in the sapphire outer sphere are also coupled to the boundary nodes 51, 52 and 53. Nodes 1 and 2 are conductively coupled to node 51 and node 10 is conductively coupled to node 52. Nodes 1 thru 9 (10 is covered by the outer pole TEM) are convectively coupled to node 53 by assuming a nominal convection coefficient of .7 BTU/HR-FT²-°F.

The couplings between nodes are input to the computer program MSTTR which solves transient thermal problems using a fourth order Runge-Kutte technique. The program is modified by superimposing the effect of the energy carried with the fluid as it circulates throughout the convection cell. The increase in temperature of a downstream node due to the flow from a warmer upstream node is calculated as the product of the temperature difference between the nodes, and the percentage of flow which enters the downstream node in one time step. The percentage of flow entering a node equals the ratio of the volume flow rate of the upstream node multiplied by one time step, to the volume of that node. This is shown by EQ (1),

$$\Delta T_d = \frac{\dot{V}_u \Delta \tau}{V_d} (T_u - T_d) \quad \text{EQ (1)}$$

where d represents the downstream node, u is the upstream node, and $\Delta \tau$ represents the time step used in the Runge-Kutte calculations. When the radial flow from a middle layer node flows into one of the outer layer nodes, the change in temperature of that node occurs from the mixing of the two fluid streams.

3.3 CASES STUDIED

The four temperature distributions that were examined are listed in Table 3.3.1. These temperatures are understood to be the most demanding on the system. Several velocity profiles are used in conjunction with these temperature distributions to define the system's thermal loading requirements. Flow field information sent to the Valley Forge Space Center from Dr. Fowlis of NASA/MSFC, AGCE P.I., included

Table 3.3.1

Boundary Temperature Distributions

<u>Boundary Node</u>	<u>Temperature °C</u>			
	<u>I</u>	<u>II</u>	<u>III</u>	<u>IV</u>
41 Inner Eq.	25.0	25.0	15.0	15.0
42 Inner Eq.	25.0	25.0	15.0	15.0
43	23.75	23.75	15.0	16.25
44	22.50	22.50	15.0	17.50
45	21.25	21.25	15.0	18.75
46	20.0	20.0	15.0	20.0
47	18.75	18.75	15.0	21.25
48	17.50	17.50	15.0	22.50
49	16.25	16.25	15.0	23.75
50 Inner Pole	15.0	15.0	15.0	25.0
51 Outer Eq.	35.0	35.0	35.0	25.0
52 Outer Pole	25.0	35.0	25.0	35.0
53 Ambient	18.0	18.0	18.0	18.0

velocity and temperature profile mappings for Case I (Appendix). The velocity at each node latitude was determined by the average of that shown on the meridional flow velocity mapping. The thicknesses of the fluid meridional flow layers were also obtained from this mapping. By iterating to determine the correct percentages of radial flow at each node in the middle layer and the total mass flow rate to be used as input to the computer program, the velocity profile obtained from the mapping was approximated. The volume flow rate and velocity profiles for this case are illustrated in Figure 3.3.1.

Other profiles were derived from the Case A profile to determine the velocity profiles that defined the maximum thermal loading requirements. Case B considers the case where the turnaround zone for the convection cell is concentrated at the pole and equator while Case C is the opposite extreme, where the turnaround zone is concentrated in the central latitudes. The stagnant flow situation, Case D (not shown), was examined to compare with Task 6.1 stagnant flow results. Using the same volume or mass flow profile as in Case A, the velocities were doubled to determine how sensitive the heating and cooling loads are to the velocity of the fluid (Case A').

For the first three temperature distribution cases, the fluid is expected to flow in a counterclockwise manner (positive meridional flow in the outer layer, nodes 12 thru 20, and negative meridional flow in the inner layer, nodes 32 thru 40). A simplified reason for this is that as the fluid is heated at the outer equator it will rise toward the outer pole, cooling along the way. The cooled fluid at the pole then flows back toward the equator along the inner sphere, heating as it approaches the equator. Once the fluid reaches the equator it has been reheated, thus it cycles back toward the pole creating the counterclockwise circulation. In the fourth case the temperature gradients on the inner and outer sphere are in the opposite direction of those in Cases I thru III. Thus a clockwise circulation is

Fig. 3.3.1 VOLUME FLOW RATE AND VELOCITY PROFILES

← POSITIVE MERIDIONAL FLOW (TOWARDS POLE)
 ↓ POSITIVE RADIAL FLOW (TOWARDS INNER SPHERE)

ORIGINAL PAGE IS
 OF POOR QUALITY

CASE A

AGCE MODEL FLOW FIELD (CU.-FT./HR. X10-2)										<u>NODES</u>
POLE									EQUATOR	
0.	0.	0.	0.	0.	0.	0.	0.	0.	0.	10 ← 1
0.	0.280	0.490	0.700	0.700	0.700	0.490	0.245	0.245	0.	20 ← 11
0.280	0.210	0.210	0.	0.	0.	-0.210	-0.245	-0.245	0.	30 ← 21
-0.280	-0.280	-0.490	-0.700	-0.700	-0.700	-0.490	-0.245	-0.245	0.	40 ← 31
0.	0.	0.	0.	0.	0.	0.	0.	0.	0.	50 ← 41

VELOCITY FLOW FIELD (CM./SEC. X10-2)									
0.	0.	0.	0.	0.	0.	0.	0.	0.	0.
"	2.295	2.460	2.589	2.100	1.813	1.147	0.538	0.522	0.
517	0.383	0.235	0.	0.	0.	-0.109	-0.120	-0.116	0.
-6.837	-2.302	-2.467	-2.597	-2.107	-1.819	-1.151	-0.540	-0.523	0.
0.	0.	0.	0.	0.	0.	0.	0.	0.	0.

Fig 3.3.2 CASE B PROFILES

AGCE MODEL FLOW FIELD (CU.-FT./HR. X10-2)									
POLE									EQUATOR
0.	0.	0.	0.	0.	0.	0.	0.	0.	0.
0.	0.700	0.700	0.700	0.700	0.700	0.700	0.700	0.700	0.
0.700	0.	0.	0.	0.	0.	0.	0.	-0.700	0.
-0.700	-0.700	-0.700	-0.700	-0.700	-0.700	-0.700	-0.700	-0.700	0.
0.	0.	0.	0.	0.	0.	0.	0.	0.	0.

VELOCITY FLOW FIELD (CM./SEC. X10-2)									
0.	0.	0.	0.	0.	0.	0.	0.	0.	0.
0.	5.738	3.514	2.589	2.100	1.813	1.639	1.538	1.491	0.
3.793	0.	0.	0.	0.	0.	0.	0.	-0.332	0.
-17.032	-5.756	-3.525	-2.597	-2.107	-1.819	-1.644	-1.542	-1.495	0.
0.	0.	0.	0.	0.	0.	0.	0.	0.	0.

ORIGINAL PAGE IS
OF POOR QUALITY

Fig. 3.3.3. CASE C PROFILES

AGCE MODEL FLOW FIELD (CU.-FT./HR. X10-2)

POLE									EQUATOR
0.	0.	0.	0.	0.	0.	0.	0.	0.	0.
0.	0.070	0.210	0.700	0.700	0.700	0.210	0.070	0.070	0.
0.070	0.140	0.490	0.	0.	0.	-0.490	-0.140	-0.070	0.
-0.070	-0.070	-0.210	-0.700	-0.700	-0.700	-0.210	-0.070	-0.070	0.
0.	0.	0.	0.	0.	0.	0.	0.	0.	0.

VELOCITY FLOW FIELD (CM./SEC. X10-2)

0.	0.	0.	0.	0.	0.	0.	0.	0.	0.
0.	0.574	1.054	2.589	2.100	1.813	0.492	0.154	0.149	0.
0.378	0.255	0.546	0.	0.	0.	-0.254	-0.068	-0.033	0.
-1.569	-0.528	-0.971	-2.325	-1.934	-1.670	-0.453	-0.142	-0.137	0.
0.	0.	0.	0.	0.	0.	0.	0.	0.	0.

Fig. 3.3.4. CASE A' PROFILES
(DOUBLED VELOCITIES)

AGCE MODEL FLOW FIELD (CU.-FT./HR. X10-2)

POLE									EQUATOR
0.	0.	0.	0.	0.	0.	0.	0.	0.	0.
0.	0.280	0.490	0.700	0.700	0.700	0.490	0.245	0.245	0.
0.280	0.210	0.210	0.	0.	0.	-0.210	-0.245	-0.245	0.
0.280	-0.280	-0.490	-0.700	-0.700	-0.700	-0.490	-0.245	-0.245	0.
0.	0.	0.	0.	0.	0.	0.	0.	0.	0.

VELOCITY FLOW FIELD (CM./SEC. X10-2)

0.	0.	0.	0.	0.	0.	0.	0.	0.	0.
0.	4.591	4.920	5.179	4.201	3.626	2.294	1.076	1.044	0.
0.034	0.766	0.469	0.	0.	0.	-0.219	-0.240	-0.232	0.
3.674	-4.605	-4.935	-5.194	-4.213	-3.637	-2.301	-1.080	-1.047	0.
0.	0.	0.	0.	0.	0.	0.	0.	0.	0.

ORIGINAL PAGE IS
OF POOR QUALITY

Fig. 3.3.5. CASE A- PROFILES
(REVERSED FLOW)

AGCE MODEL FLOW FIELD (CU.-FT./HR. X10-2)

PQLE									EQUATOR
0.	0.	0.	0.	0.	0.	0.	0.	0.	0.
0.	-0.280	-0.490	-0.700	-0.700	-0.700	-0.490	-0.245	-0.245	0.
-0.280	-0.210	-0.210	0.	0.	0.	0.210	0.245	0.245	0.
0.280	0.280	0.490	0.700	0.700	0.700	0.490	0.245	0.245	0.
0.	0.	0.	0.	0.	0.	0.	0.	0.	0.

VELOCITY FLOW FIELD (CM./SEC. X10-2)

0.	0.	0.	0.	0.	0.	0.	0.	0.	0.
0.	-2.295	-2.460	-2.589	-2.100	-1.813	-1.147	-0.538	-0.522	0.
-1.517	-0.383	-0.235	0.	0.	0.	0.109	0.120	0.116	0.
6.837	2.302	2.467	2.597	2.107	1.819	1.151	0.540	0.523	0.
0.	0.	0.	0.	0.	0.	0.	0.	0.	0.

expected in the convection cell. Case A- has the same velocity profile as Case A except that the flow is reversed to correspond with the reversed temperature gradients of Case IV.

3.4 HEATING AND COOLING REQUIREMENTS

The results of the computer runs for the four temperature distributions with various velocity profiles define the heating and/or cooling requirements at the outer sphere pole, outer sphere equator, and all latitudes of the inner sphere. The results are summarized in Table 3.4.1. Each case is referenced by a number and a letter. The number refers to the temperature distribution from Table 3.3.1 used in that case and the letter refers to the velocity profile from Figure 3.3.1 thru 3.3.5. It was not necessary to run cases for all the velocity profiles with each temperature distribution. After running each velocity profile with the Case I temperature distribution, and each temperature distribution with velocity profile A, it was apparent how the thermal loading is affected by the different cases.

There is minimal difference between the thermal loads of Case IA and IA', where the velocity is doubled. Even with the increase in velocity the convection coefficients remain small, and thus the heat transferred by convection is minimal compared to that by conduction.

The thermal requirements are more dependent on the particular velocity profile or temperature distribution than the velocity magnitude. The largest total inner sphere cooling load is approximately 7.5 watts, when the entire inner sphere is held at 15°C, Case III. This is also when the greatest heating load is required, approximately 14.0 watts, because the equator must be held at 35°C while the inner sphere is 15°C. Figure 3.4.1 presents the temperature profile and the thermal loads

TABLE 3.4.1 - HEATING AND COOLING LOADS

<u>CASE*</u>	<u>TOTAL INNER SPHERE COOLING (WATTS)</u>	<u>TEM COOLING OUTER POLE (WATTS)</u>	<u>OUTER EQUATOR HEATING (WATTS)</u>
IA	4.61	3.72	10.52
IA'	4.65	3.72	10.56
IB	3.40	4.05	9.58
IC	4.57	3.52	10.94
ID	2.54	3.81	8.49
IIA	5.88	-1.11	7.04
IIIA	7.49	3.30	13.90
IIIC	7.41	3.20	13.23
IVD	1.90	-4.90	-1.86
IVA-	5.31	-5.28	-1.86

*NUMBERS REFER TO TEMPERATURE DISTRIBUTIONS
 LETTERS REFER TO VELOCITY PROFILES
 (D REFERS TO THE STAGNANT FLOW CASE)

Fig. 3.4.1 CASE III A

TEMPERATURE PROFILE AND THERMAL LOADS

<u>TEMPERATURE PROFILE (°C)</u>										
<u>NODES</u>										
10 ← 1	20 ← 11	30 ← 21	40 ← 31	50 ← 41	34.62	33.43	32.43	31.19	30.82	34.87
26.40	28.52	29.53	30.26	30.89	31.56	32.43	33.43	34.62	34.87	34.87
26.82	28.66	29.07	28.90	28.01	25.47	26.87	31.19	30.82	33.02	33.02
28.31	27.74	27.82	26.98	24.87	22.54	21.53	22.22	22.25	25.57	25.57
25.76	22.07	24.21	24.99	21.22	18.86	17.37	16.86	16.77	17.53	17.53
15.00	15.00	15.00	15.00	15.00	15.00	15.00	15.00	15.00	15.00	15.00

<u>INNER SPHERE LOADS PER LATITUDE (WATTS)</u>		<u>NODES</u>		<u>LATITUDE</u>	
<u>EQUATOR</u>	<u>POLE</u>	<u>FLUID</u>	<u>INNER SPHERE</u>	<u>FLUID</u>	<u>LATITUDE</u>
0.64137877E 00	0.26163701E 00	31	41	-10 → 0°	
0.45723748E 00	0.15339075E 01	32	42	0 → 10°	
0.46625214E 00	0.10430537E 01	33	43	10 → 20°	
0.56456404E 00	0.48914090E 00	34	44	20 → 30°	
0.83907994E 00	0.26163701E 00	35	45	30 → 40°	
0.11852586E 01	0.26163701E 00	36	46	40 → 50°	
0.15339075E 01	0.26163701E 00	37	47	50 → 60°	
0.10430537E 01	0.26163701E 00	38	48	60 → 70°	
0.48914090E 00	0.26163701E 00	39	49	70 → 80°	
0.26163701E 00	0.26163701E 00	40	50	80 → 90°	

INNER SPHERE TOTAL COOLING LOAD (WATTS) = 0.74865102E 01
 HEAT REQUIRED AT EQUATOR (WATTS) = 0.13900729E 02
 COOLING REQUIRED AT POLE (WATTS) = 0.32965379E 01
 HEAT LOSS TO AMBIENT (WATTS) = 0.16678249E 01

for Case IIIA. The inner sphere cooling loads per 10° latitude are also shown. The cooling required at the outer pole reaches a maximum of 4.05 watts when the turn-around zone is concentrated near the pole and the pole must be cooled to 25°C (Case IB). Case 4A- illustrates the maximum pole heating required when the pole temperature is 35°C and the flow is reversed. For this case the system must be designed to provide a cooling load of 1.86 watts at the equator. The AGCE thermal system is designed in the following sections considering worst case conditions at the outer equator, outer pole, and inner sphere.

The total inner sphere cooling from Case ID can be compared to the heat flow calculation results made in Task 6.1 for $r_i = 5$ cm., $r_o = 6$ cm., and $N_u = 1.0$ (stagnant flow). With an approximate temperature gradient of 10°C from outer to inner sphere for Case ID, the inner sphere cooling load is 2.54 watts as compared to 1.96 watts at $\Delta T = 10^\circ\text{C}$ between the isothermal spheres in Task 6.1. In Task 6.1 lateral conduction was not considered. In this model the inner sphere must be cooled to create the same 10°C radial gradient as in Task 6.1, in addition to a 10°C negative gradient from the equator to the pole, thus increasing the inner sphere cooling load. Considering this difference, the results of Task 6.1 are confirmed and confidence is established in the model.

3.5 POLE HEAT EXCHANGER ASSEMBLY

Figure 3.5.1 presents a simplified schematic of a pole heat exchanger assembly that could be incorporated into the AGCE hardware. With a maximum cooling load of 4.05 watts at the outer pole, assuming a maximum internal heat generation of .5 watts from the circulating dielectric fluid, and applying a margin of safety of 10%, the system is designed for a pole cooling load of 5.0 watts. This cooling load can be obtained with the use of a single stage thermoelectric module (TEM). GE-VF has

ORIGINAL PAGE IS
OF POOR QUALITY

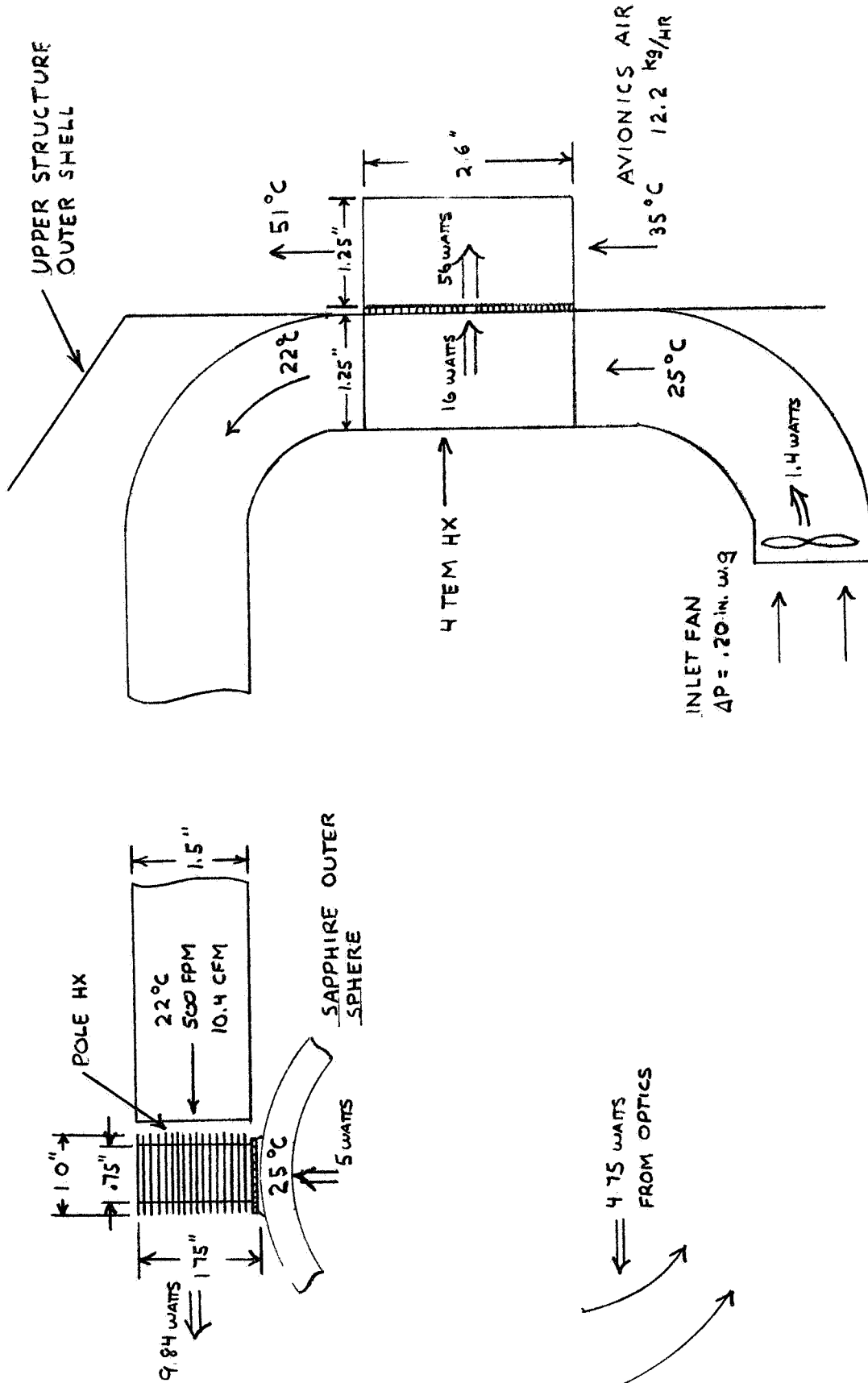


Fig. 3.5.1. POLE HEAT EXCHANGER ASSEMBLY
(WORST CASE CONDITIONS)

both analytical and empirical experience with this TEM which was planned for use in similar spacelab applications. A circular, 1.0 in. Dia., custom manufactured TEM is used at the pole to fit within the existing optics hardware. This is a reduced version of the standard 1.2 in. x 1.2 in. square TEM, hence performance is sacrificed to obtain this reduction in size.

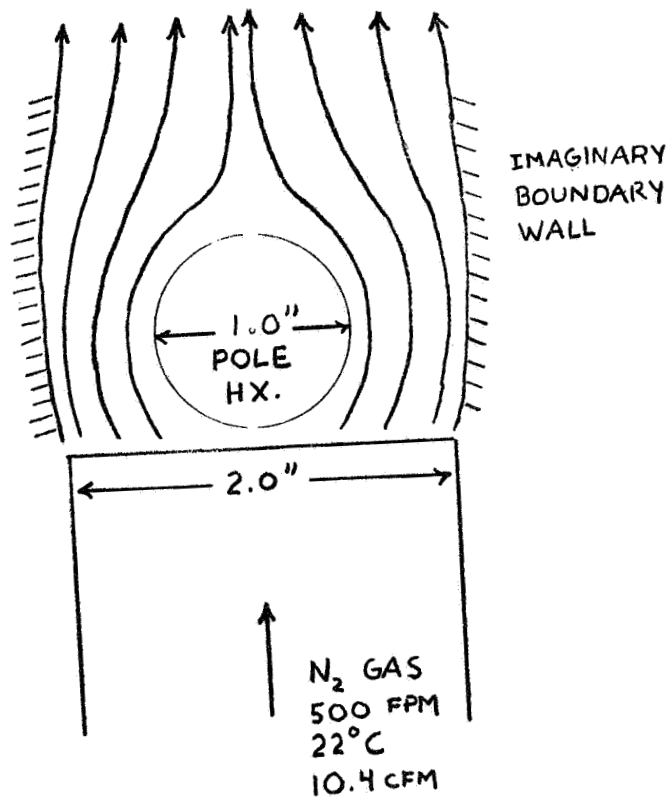
By fastening the TEM to the outer sapphire sphere surface with 10 mils of epoxy ($h = .136 \text{ W/cm}^2 - ^\circ\text{C}$), assuming a worst case pole temperature of 25°C , the 5.0 watt cooling load is maintained by blowing 500 FPM of 22°C N_2 gas over a circular finned heat exchanger (HX) mounted on the TEM hot side surface. The circular finned HX consists of 1.0 in. O.D. fins (approx. .04 in. thick, 16 fins/in.) extending from a .75 in. O.D., 1.5 in. high, solid aluminum cylinder, creating an effective thermal conductance of $.41 \text{ W/}^\circ\text{C}$ from the TEM hot side to the N_2 gas. The outer sphere pole TEM is cooled by forced air to avoid obscuration of a portion of the sphere assembly surface by coolant tubes needed in a liquid cooling application.

For the circular finned pole HX to be effective it is necessary that the 500 FPM N_2 gas stream flows around the contour of the HX. To accomplish this a 1.5 in. x 2.0 in. (height x width) duct outlet must be located so that the HX is centered at the duct outlet. A 2.0 in. width duct is necessary for the outer stream lines of the flow to act as a boundary wall forcing the flow around the HX contour (See Figure 3.5.2). The size of the duct is limited by the space available between the UV optics assembly and the Scanner optics assembly, because of which a 2.0 in. wide duct may not be possible. In this case a shroud should be mounted on the side of the duct to force the path of flow.

If insufficient spacing exists to position the duct outlet for the N_2 gas to flow horizontally at the circular finned HX, then an alternate design is to blow the air

Fig 3.5.2 CIRCULAR FINNED POLE HX.

(PLAN VIEW)



vertically down from above the TEM. Radial fins extending from the cylindrical HX base, would run the length of the HX in the vertical (axial) direction. A shroud could be placed around the HX to force the N_2 gas through the fin channels until the flow reached the end of the HX, the TEM surface, where it would be radially exhausted.

A power load of 4.84 watts is required to supply the necessary pole cooling, resulting in 9.84 watts rejected to the air stream. Assuming one-quarter of the total optics assembly dissipation (19 watts) is rejected to the circulating N_2 gas and 1.4 watts is dissipated from the inlet fan in Figure 3.5.1, results in a total dissipation of approximately 16.0 watts. This load must be removed from the N_2 gas within the outer shell of the AGCE assembly. The one-quarter heat rejection for the optics assembly is a conservative estimate, the major portion of the heat dissipated from the optics assembly will be conducted through the bulk of the optics hardware to the outer shell.

The 16.0 watt load is rejected to an Avionics air supply of 12.2 kg/HR by the four TEM HX assembly illustrated in Figure 3.5.1. An air flow of 12.2 kg/HR is available to the external HX, with 56 watts total heat dissipation, from the standard Avionics air flow allocation of 21 kg/HR per 100 watts dissipation. An axial flow fan is mounted in the inlet duct to supply 10.4 CFM of N_2 gas at .20 in. w.g. to the internal HX. Four 1.2 in. x 1.2 in. TEMs are mounted to create a 2.4 in. x 2.6 in. (width x length) heat exchanger mounting area on the inside and outside of the AGCE upper structure outer shell. Each heat exchanger consists of .008 in. thick, 1.25 in. high, aluminum fins placed between two plates at intervals of 11.11 fins per inch. This results in an effective thermal conductance between the N_2 gas and the TEM cold side of 3.0 W/°C for the internal HX, and 2.72 W/°C between the TEM hot side and Avionics air supply for the external HX.

3.6 EQUATOR HX ASSEMBLY

The worst case condition for heating at the equator is a 13.90 watt heating load with a 35°C outer equator temperature (Table 3.4.1). Designing for a 16.0 watt heating load, a single TEM is used with 12 gph of water pumped in counterflow through two .25 in. I.D. tubes soldered to the TEM hot side, Figure 3.6.1. For this design, the effective thermal conductance between the water and TEM hot side is 3.71 W/°C, a value obtained from previous programs' test results. Leaving the TEM HX at 38.3°C, the water then flows in a .75 cm x 1.2 cm duct mounted to a flange at the equator of the sapphire sphere, Figure 3.6.2. The duct is mounted to the flange using 10 mils of epoxy resulting in an effective thermal conductance of 5.12 W/°C from the flange to the water.

From the equator duct inlet to outlet, the water temperature drops .30°C as it rejects 16 watts to the equator. For the AGCE model to function properly, the equator must be held at a specified uniform temperature. The increased cross-sectional area of the sapphire at the flange will create sufficient conduction around the circumference of the equator to maintain a uniform equator temperature.

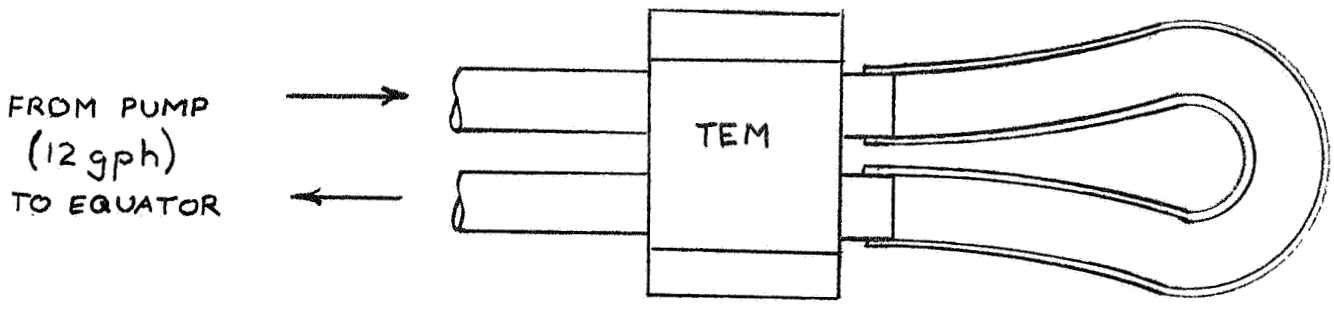
Certain situations arise when cooling is required at the equator (see Table 3.4.1). Designing for a 3.0 watt cooling load with an equator temperature of 25°C results in approximately 10 watts total heat rejection from the TEM hot side. For this condition, water is supplied at the inlet to the equator duct at approximately 24°C. A single TEM proves more than adequate to supply the necessary equator cooling load.

3.7 CHILLER DOME HX ASSEMBLY

The inner sphere is cooled by positioning a hemispherical heat sink inside the inner

Fig 3.6.1 EQUATOR HX ASSEMBLY

TEM COLD-SIDE VIEW



(NOT TO SCALE)

FRONT VIEW

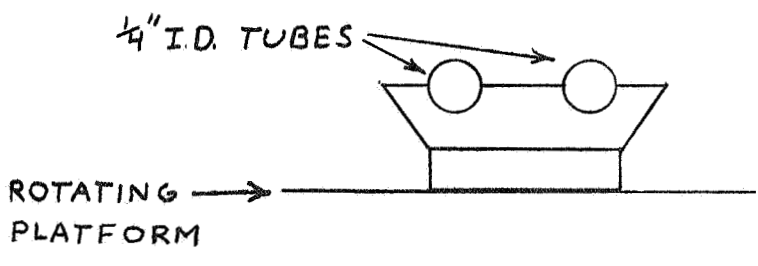
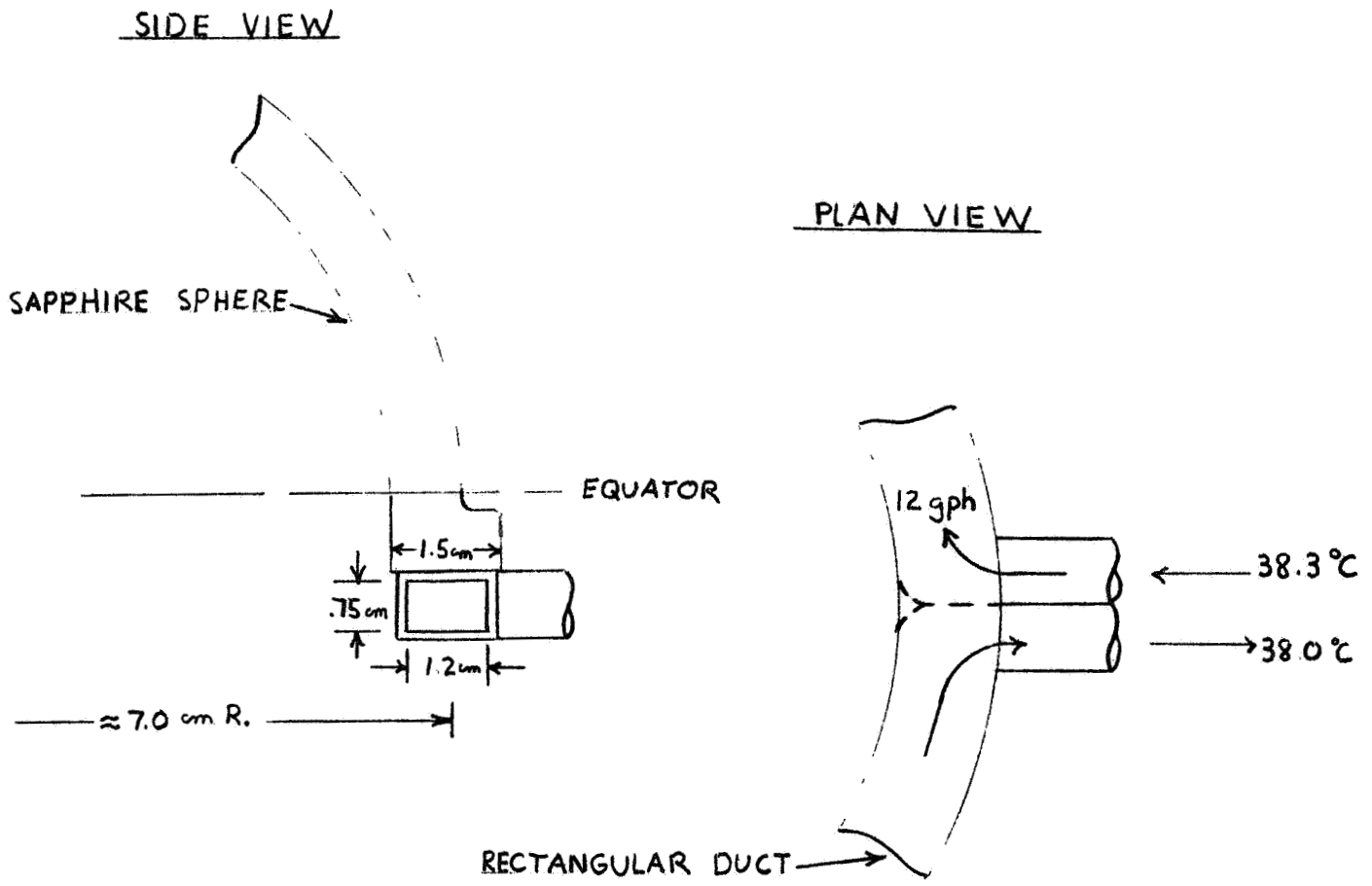


Fig. 3.6.2 EQUATOR DUCT



) sphere, with a gap between the inner sphere and the heat sink. The gap provides partial thermal isolation between the heat sink and the inner sphere. By operating the heat sink at a temperature somewhat lower than the minimum desired for the inner sphere, the heat sink applies a bias cooling to the inner sphere. This bias cooling is offset as desired at each latitude by feed-back controlled trim heaters on the inner sphere (every 10° between 5° and 85° latitude). Thus the heat sink serves to cool the inner sphere below the temperature desired at any latitude and the trim heaters provide local heating at each latitude (partially offsetting the heat sink bias) to achieve the desired local inner sphere temperatures. If the trim heaters are to provide local heating, conduction in the inner sphere must be limited to the radial direction (negligible lateral conduction). This is accomplished by using a material with a low conductivity and the minimal allowable thickness. The inner sphere must have sufficient thickness for strength and rigidity considerations. Fabricating the inner sphere from stainless steel sheet, 20 mils thick, will meet these requirements. This concept has the capability to provide all desired temperature profiles (constant, linear in either direction, discontinuous) on the inner sphere.

The cooling loads on the inner sphere must be examined in terms of the individual latitudes as opposed to the total inner sphere cooling load. A breakdown of the inner sphere cooling loads per 10° latitude is provided in Table 3.7.1. The heat sink is designed to bias each latitude by at least the maximum cooling load at that latitude. Cooling loads will be hardest to maintain at the upper latitudes because of the reduced heat transfer area. The worst case temperature condition for the inner sphere is when the entire inner sphere is held at 15°C . These conditions can

TABLE 3.7.1
INNER SPHERE DESIGN COOLING LOADS (WATTS)

<u>LATITUDE</u>	<u>CASES</u>														<u>MAX</u>	<u>MIN</u>
	<u>IA</u>	<u>IA'</u>	<u>IB</u>	<u>IC</u>	<u>ID</u>	<u>IIA</u>	<u>IIIA</u>	<u>IIIC</u>	<u>IVD</u>	<u>IVA-</u>	<u>IVB</u>	<u>MAX</u>	<u>MIN</u>			
-5	.31	.31	.30	.33	.34	.32	.64	.67	.34	.37	.39	.67	.30			
5	.12	.12	-.03	.24	.32	.13	.46	.60	.36	.74	1.24	1.24	-.03			
15	.13	.13	.10	.21	.34	.15	.47	.59	.30	.41	.58	.59	.10			
25	.18	.17	.17	.17	.34	.25	.57	.54	.26	.67	.26	.67	.12			
35	.41	.41	.25	.45	.32	.55	.84	.85	.21	.54	.09	.84	.09			
45	.75	.75	.37	.83	.29	.98	1.19	1.21	.16	.20	-.01	1.21	-.01			
55	1.12	1.14	.54	1.23	.25	1.45	1.15	1.59	.12	.01	-.07	1.59	-.07			
65	.86	.88	.69	.74	.19	1.11	1.04	.95	.08	-.07	-.11	1.11	-.11			
75	.46	.46	.68	.23	.12	.60	.49	.25	.05	-.08	-.11	.68	-.11			
85	.28	.29	.35	.15	.04	.35	.26	.15	.02	-.05	-.07	.35	-.07			

be met by using a material with a k/t of 10.30 Btu/Hr-Ft²-°F per inch for the thermal gap, and a 8°C cooling dome heat sink. This value is determined assuming the material is fastened to the chiller dome with 5-mils of epoxy ($h = 480$ Btu/Hr-Ft²-°F), a contact conductance of 100 Btu/Hr-Ft²-°F exists between the material and the inner sphere, and a percentage of each 10° latitude is used to mount the trim heaters. It is important that the material has enough flexibility to form to the inner sphere interior surface, providing a contact conductance of at least 100 Btu/Hr-Ft²-°F. Also, the gap must be at least 90-mils to provide the necessary spacing for the trim heaters and thermistors which will be mounted on the inner sphere.

These specifications are met using CHO-Seal 1215, a gasket material used between surfaces requiring an electrically continuous interface for purposes of RFI protection. CHO-Seal is cured silicone rubber having a filler of silver plated copper granules with approximate diameters of 0.5 to 5.0 mils. Using a .125 in. thick CHO-Seal gasket and compressing it to ensure good contact results in an effective thermal conductance of 4.20 W/°C from the inner sphere to the chiller dome. This value is contingent on a good contact existing between surfaces. Table 3.7.2 presents the percentage of the inner sphere surface area necessary for CHO-Seal gasket contact, the resulting cooling load due to this reduction in surface area, and the heater power for each 10° latitude to satisfy the maximum and minimum cooling loads presented in Table 3.7.1. The remainder of the inner sphere surface area not used for gasket contact is available for mounting the trim heaters and thermistors.

As the inner sphere is designed to prevent lateral conduction, the chiller dome should be highly conductive and of sufficient thickness to maximize the lateral conduction, thus creating a uniform temperature heat sink.

TABLE 3.7.2

INNER SPHERE COOLING LOAD BIAS

<u>LATITUDE</u>	<u>GASKET CONTACT AREA (%)</u>	<u>COOLING BIAS (WATTS)</u>	<u>MAX. HEATER POWER (WATTS)</u>
-10 - 0	15	.77	.5
0 - 10	25	1.28	1.4
10 - 20	15	.74	.7
20 - 30	15	.70	.6
30 - 40	20	.84	.8
40 - 50	35	1.27	1.3
50 - 60	55	1.62	1.7
60 - 70	55	1.20	1.4
70 - 80	55	.73	.9
80 - 90	80	.35	.5
		<hr/> 9.50	

TOTAL INNER SPHERE COOLING LOAD BIAS = 9.50 WATTS

OVERALL EFFECTIVE CONDUCTANCE
(100% CONTACT AREA) = 4.02 W/°C

INNER SPHERE TEMPERATURE = 15°C

CHILLER DOME TEMPERATURE = 8°C

A .75 cm thick copper chiller dome is recommended for this purpose. The chiller dome is cooled to 8°C by pumping 22 gph of 7.5°C water through approximately 25 inches of ¼ in. I.D. tubes soldered to the inner sphere of the chiller dome. This design produces an effective thermal conductance between the water and the chiller dome surface of 22.5 W/°C. The chilled water is pumped to the inner pole of the dome, then it spirals around the dome surface in the tubing to the equator where it is returned to a TEM heat exchanger assembly (Figure 3.7.1).

A four TEM heat exchanger is designed to remove 9.5 watts, the total inner sphere cooling load bias (Table 3.7.2), from the 22 gph chiller dome water supply. The water is pumped in counterflow through two ¼ in. I.D. tubes soldered to the cold side of four TEMs in series (see Figure 3.6.1). This yields an effective thermal conductance between the water and the TEM cold side of 20.4 W/°C, based on previous programs' test results.

The four TEM chiller dome heat exchanger and the single TEM equator heat exchanger are mounted to the rotating platform of the AGCE assembly. To remove the 9.5 watt inner sphere cooling load bias, 107 watts must be rejected at the TEMs hot side. The two pumps used in the coolant loops, also mounted to the rotating platform, operate under a maximum pressure drop of 3 psi and have a combined dissipation of approximately 40 watts. Table 3.7.3 lists the worst case AGCE heat dissipations for all the sources considered in the model. The total heat dissipation of all the components mounted to the rotating platform or base structure, 207 watts, is rejected to a 45.0 kg/Hr. (based on standard Avionics air allocations), Avionics air stream through the rotating platform HX and the stationary platform HX illustrated in

ORIGINAL PAGE IS
OF POOR QUALITY

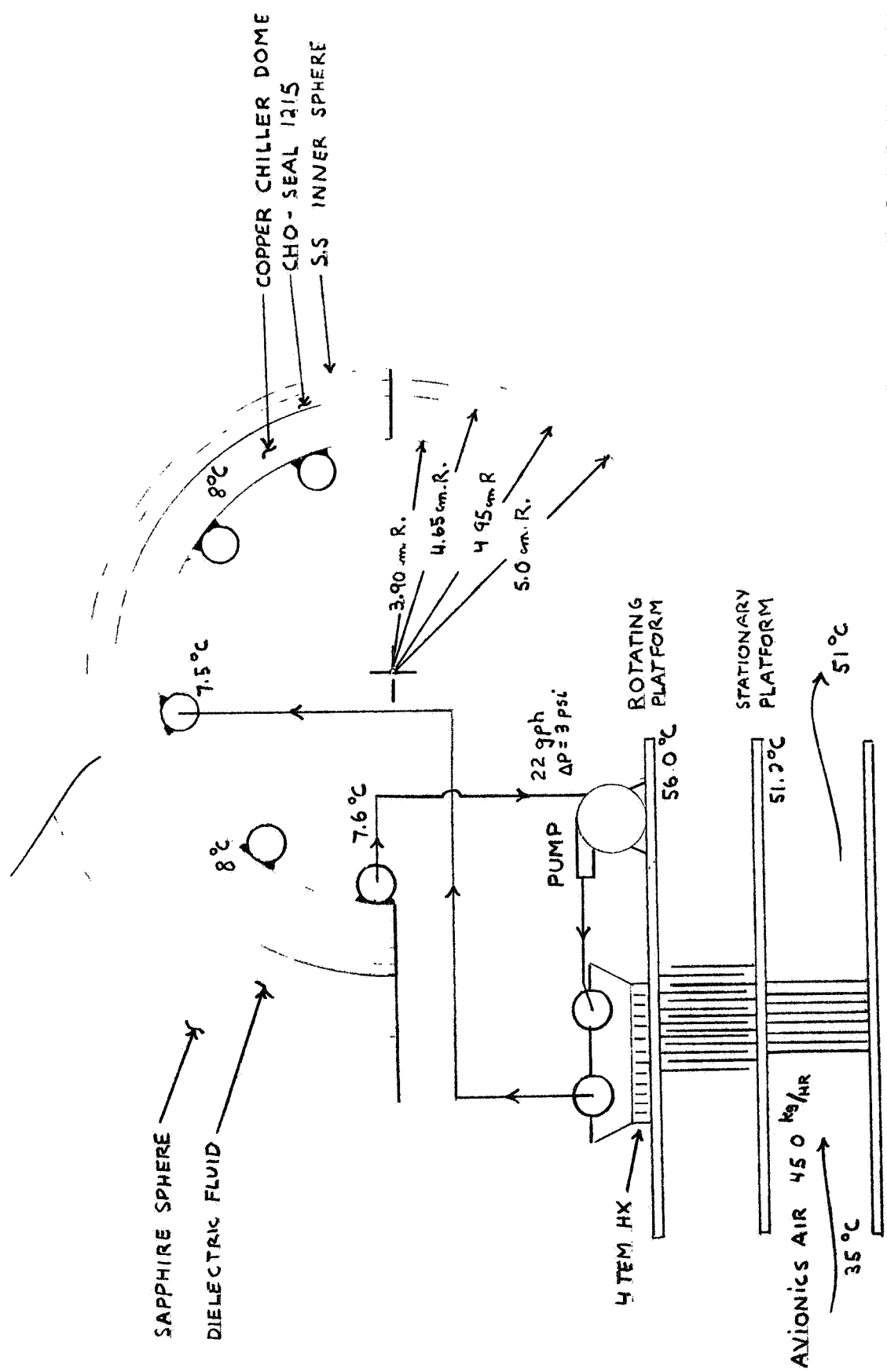


Fig. 3.7.1 CHILLER DOME COOLANT LOOP
(WORST CASE CONDITIONS)

Figure 3.7.3. The heat rejected at the rotating platform is conducted through the N_2 gas to the stationary platform creating an effective conductance between platforms of $42.9 \text{ W/}^\circ\text{C}$. The heat is then rejected to the Avionics air stream flowing between the concentric fins of the stationary platform HX resulting in an effective conductance of $25.3 \text{ W/}^\circ\text{C}$ from the stationary platform to the Avionics air. The overall effective conductance from the rotating platform to the Avionics air supply is $15.9 \text{ W/}^\circ\text{C}$. Assuming 35°C Avionics air enters the heat exchanger, the rotating platform temperature is 56.0°C .

TABLE 3.7.3
AGCE HEAT DISSIPATION
(WORST CASE CONDITIONS)

<u>SOURCE</u>	<u>ESTIMATED WATTS</u>	<u>HARD MOUNT LOCATION</u>
1. Fluid Pumps	3*	Rotating Platform
a. Dust Dome		
b. Chiller Dome Coolant Loop	25	Rotating Platform
c. Outer Equator Heating Loop	15	Rotating Platform
2. Water Loop TEM HX		
a. Chiller Dome (4 TEMs)	107	Rotating Platform
b. Outer Equator (1 TEM)	-13	Rotating Platform
3. HV Transformer Assembly	60	Rotating Platform
4. Misc. Electronics		Rotating Platform
5. Rotating Platform Drive Motor	10	Base Structure
TOTAL	207	
6. Scanner Optics Assembly (Drive Motor, Lamp, Electronics)	19	Upper Cover Structure
7. UV Optics Assembly (Flash Lamp)	***	Outer Shell (Upper Cover)
8. Dielectric Fluid Heating**	.5	
9. Pole HX Assembly		
a. Pole TEM HX	9.84	Outer Sapphire Sphere
b. Inlet Fan	1.4	N ₂ Duct (Outer Shell)
c. 4 TEM HX (Power Supplied)	40	Outer Shell (Upper Cover)
TOTAL	70	

TOTAL DISSIPATION TO AVIONICS AIR: 277 WATTS..

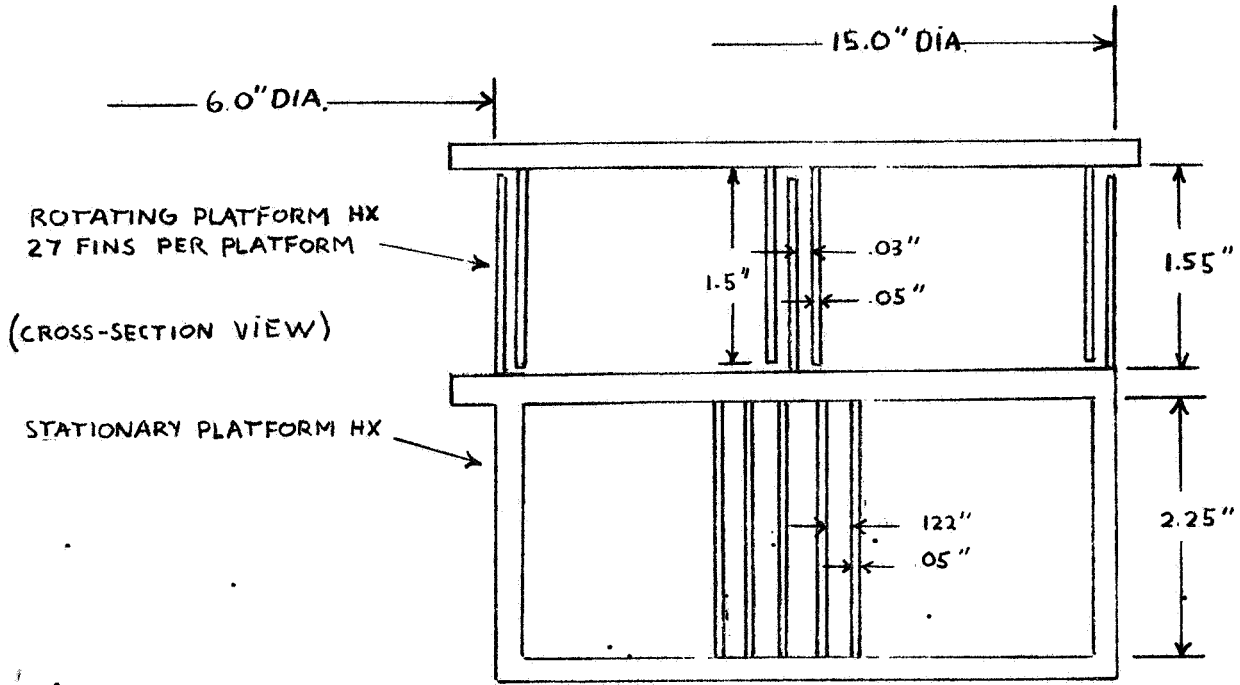
* 35 WATTS @ 5 MIN/HOUR MAX.

** FLUID SELECTED SO THAT EFFECT OF DIELECTRIC HEATING IS BELOW
0.001°C/SEC. (REF. PIR 1254-AGCE-006), INCLUDED IN 2a. AND 9a. TOTALS.

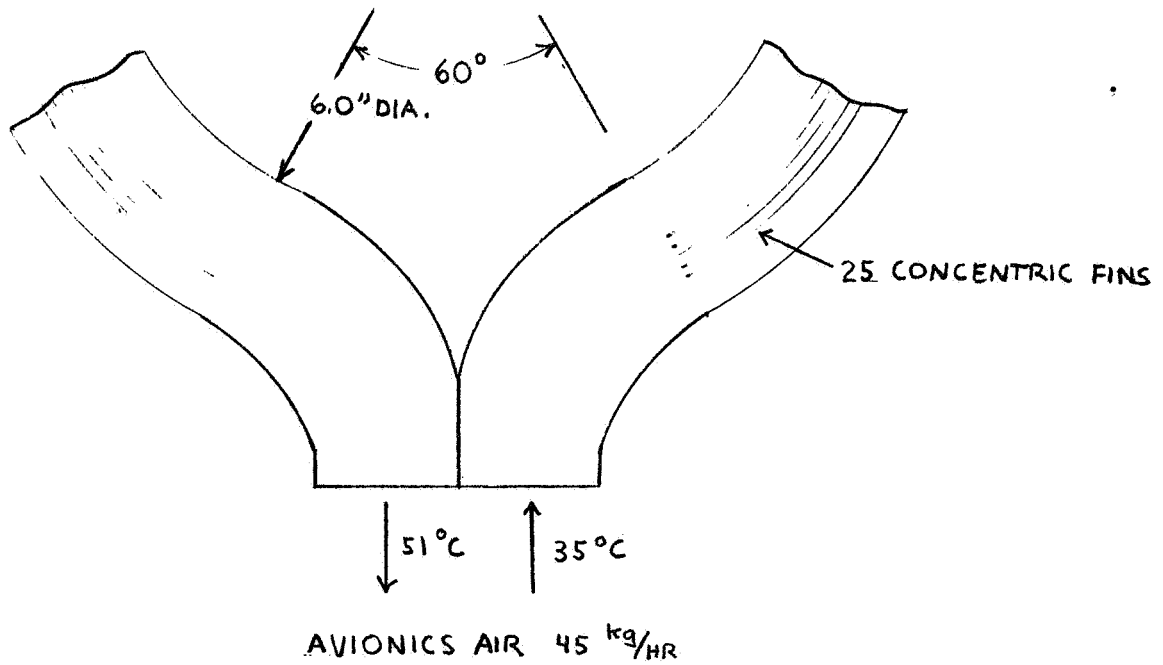
*** 10 WATT/SEC. PER FLASH; FLASH AT 60 SEC. INTERVALS.

ORIGINAL PAGE IS
OF POOR QUALITY

Fig. 3.7.2. ROTATING AND STATIONARY
PLATFORM HEAT EXCHANGERS



STATIONARY PLATFORM HX (PLAN VIEW)

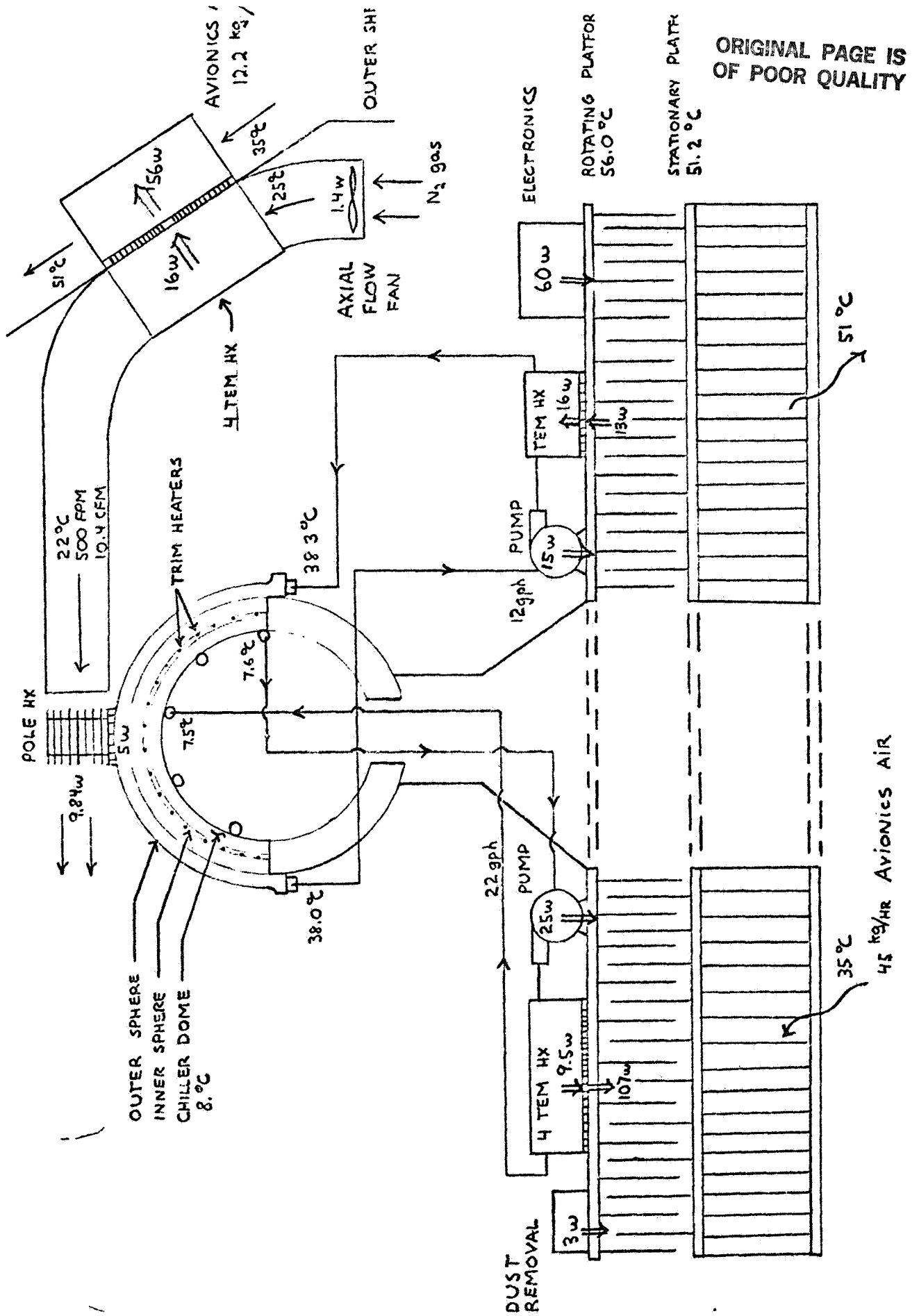


4.0 CONCLUSIONS/RECOMMENDATIONS

A schematic diagram of the recommended AGCE thermal system is presented in Figure 4.1. Worst case individual design temperatures and component dissipations are shown. Presented is a feasible design concept, further refinements are necessary to optimize the system for the most efficient design. The Spacelab coolant loop could be used as a heat sink for the pole HX assembly (directly at the pole or at the upper structure outer shell), and to replace the stationary platform HX. Spacelab coolant improves heat transfer (for a given geometry) and thus increases TEM operating range and efficiency, but does require another interface with the Spacelab. This additional interface will limit the application to missions where the coolant loop is available. The outer sphere pole TEM is cooled by forced air to avoid obscuring a portion of the sphere assembly surfaces with the required liquid cooling tubes. Avionics air is used whenever applicable because of its easy accessibility and use.

Temperature sensors are required on the inner and outer spheres to control the heating or cooling at the outer pole, outer equator and inner sphere. In all three locations the thermal loading can be regulated by temperature sensor feedback to adjust the voltage or current to the TEMs as required. By reversing the polarity of the voltage and current input to the TEMs, they can function in either the heating or cooling modes. This will be necessary when the convection cell circulation is reversed, Case IV temperature profile. Cooling will be required at the outer equator and heating at the outer pole. These conditions are well within the operating range of the TEMs in the proposed design. Control of the TEMs surface temperature is based on the premise that they will function in either the heating or cooling mode.

Fig. 4.1 AGCE THERMAL SYSTEM



ORIGINAL PAGE IS OF POOR QUALITY

Previous programs' results have shown that precise temperature control ($\pm .01^{\circ}\text{C}$) becomes a problem when operating around the transition point from one mode to the other. Control of the TEMs in the range of the transition point is complex. This problem is alleviated by altering the heating or cooling requirements, and thus the desired temperature profile, to prevent operation in these problem areas. Precise temperature control of the chiller dome heat sink is also not required; the trim heaters simply provide more or less bias.

Another aspect of the design to be considered is the combination of the chiller dome coolant loop and the equator heating loop. This will result in the reduction of hardware, one of the pump/accumulator combinations could be omitted. The chiller dome coolant loop operates between 7.5°C and 7.6°C . The equator heating loop operates between 38.0°C and 38.3°C . This large temperature difference between loops makes a combination of the systems impractical. A large increase in TEM power would be necessary to raise and lower the water temperature from one temperature range to the other.

In the next phase of study, it is recommended that the following areas of this feasibility design are further investigated: The application of a material to provide the k/t requirements for the thermal gap and the effective thermal conductance of the circular finned pole HX. For the CHO-Seal 1215 gasket material to be an effective thermal gap between the inner sphere and chiller dome, good contact must exist between the gasket and the inner sphere surface. The gasket can be epoxied to the chiller dome surface. The compressive pressure necessary to produce this contact and implementation of that pressure should be investigated.

The pole HX will only be effective if the flow doesn't detach from the HX surface. The N₂ gas duct's outlet width and orientation with respect to the HX must be determined considering the space limitations placed upon the system by the optics hardware. If insufficient space is available for a 2.0 in. wide duct outlet, then the application of a shroud used to force the flow around the HX should be examined. One part of the AGCE outer shell upper structure cannot be used for hardware because the space is reserved for the possibility of television cameras. Thus the N₂ gas duct must approach the HX horizontally from the opposite side of the AGCE assembly upper structure. If this is not possible, the duct outlet should be placed above the pole HX, blowing air over radial fins running the length of the HX. In any situation, for full performance capabilities of the sphere assembly heat must be provided or removed from the pole, and thus the effective conductance of the pole HX must be determined to design for this load. It will be necessary to conduct tests to determine this effective conductance for the forementioned applications.

A P P E N D I X

ORIGINAL PAGE IS
OF POOR QUALITY

TEMPERATURE PROFILES
(°C)

CASE IA

NODES

10←1	26.58	28.97	30.11	30.90	31.57	32.22	32.97	33.82	34.71	34.91
20←11	27.11	29.37	30.01	30.18	29.92	28.72	29.81	32.50	32.71	33.97
30←21	28.98	28.63	28.92	28.26	27.19	26.22	25.81	26.96	28.21	30.21
40←31	26.31	22.91	25.12	26.04	23.97	23.14	23.25	24.26	25.45	26.24
50←41	15.00	16.25	17.50	18.75	20.00	21.25	22.50	23.75	25.00	25.00

CASE IA'

26.58	28.97	30.10	30.89	31.56	32.21	32.96	33.81	34.71	34.91
27.10	29.36	30.01	30.19	29.93	28.72	29.81	32.50	32.72	33.97
28.97	28.61	28.90	28.24	27.17	26.19	25.79	26.95	28.21	30.21
26.20	22.79	25.04	25.97	23.90	23.09	23.22	24.25	25.45	26.24
15.00	16.25	17.50	18.75	20.00	21.25	22.50	23.75	25.00	25.00

CASE IB

26.72	29.32	30.54	31.39	32.10	32.74	33.36	34.01	34.74	34.91
27.39	29.98	30.49	30.99	31.50	31.98	32.35	32.32	31.09	33.91
29.82	28.03	27.31	27.04	27.19	27.64	28.16	28.37	26.59	29.98
28.42	25.79	23.50	22.23	21.96	22.39	23.20	24.14	24.87	26.17
15.00	16.25	17.50	18.75	20.00	21.25	22.50	23.75	25.00	25.00

CASE IC

26.49	28.76	29.86	30.62	31.28	31.95	32.79	33.72	34.70	34.90
26.66	28.66	29.65	29.62	28.91	26.66	29.42	32.55	33.43	34.01
27.07	27.32	28.28	28.51	27.00	25.34	25.20	27.72	29.57	30.49
22.11	19.91	24.69	27.39	24.76	23.47	23.28	24.66	26.03	26.40
15.00	16.25	17.50	18.75	20.00	21.25	22.50	23.75	25.00	25.00

CASE ID

26.62	29.09	30.32	31.20	31.96	32.65	33.34	34.03	34.77	34.92
25.78	28.01	29.22	30.14	30.93	31.68	32.41	33.15	33.90	34.06
22.11	23.66	24.85	25.87	26.83	27.76	28.68	29.60	30.44	30.62
16.90	18.18	19.40	20.59	21.76	22.93	24.09	25.25	26.37	26.44
15.00	16.25	17.50	18.75	20.00	21.25	22.50	23.75	25.00	25.00

ORIGINAL PAGE IS
OF POOR QUALITY

CASE IIA

34.54	33.83	33.55	33.42	33.40	33.51	33.81	34.28	34.81	34.93
34.17	33.05	32.62	32.03	31.10	29.12	30.15	32.87	32.80	34.00
32.84	31.34	31.08	30.18	28.39	26.77	26.22	27.22	28.28	30.23
29.42	24.84	27.31	28.16	25.20	23.78	23.54	24.37	25.49	26.24
15.00	16.25	17.50	18.75	20.00	21.25	22.50	23.75	25.00	25.00

CASE IIIC

26.37	28.44	29.45	30.17	30.82	31.51	32.43	33.51	34.64	34.88
26.46	28.17	28.82	28.65	27.58	24.54	27.41	31.82	32.34	33.12
26.60	26.41	26.53	26.88	24.70	22.27	22.96	24.98	24.70	25.92
21.60	18.71	23.59	25.33	21.44	18.89	17.31	17.38	17.33	17.62
15.00	15.00	15.00	15.00	15.00	15.00	15.00	15.00	15.00	15.00

CASE IVA-

32.72	29.29	27.78	26.89	26.31	25.89	25.56	25.29	25.05	25.00
30.84	26.25	24.93	24.29	25.15	25.33	25.23	24.88	24.59	24.20
23.73	22.95	22.50	22.92	23.27	23.48	23.64	22.88	22.42	20.86
23.17	22.68	21.86	21.31	21.04	21.23	20.30	17.88	17.87	16.45
25.00	23.75	22.50	21.25	20.00	18.75	17.50	16.25	15.00	15.00

CASE IV D

32.93	29.78	28.33	27.39	26.70	26.16	25.72	25.36	25.07	25.01
32.05	29.24	27.82	26.86	26.12	25.52	25.01	24.53	24.22	24.15
28.84	27.02	25.72	24.66	23.73	22.89	22.10	21.36	20.73	20.62
25.86	24.52	23.27	22.07	20.90	19.75	18.61	17.48	16.41	16.36
25.00	23.75	22.50	21.25	20.00	18.75	17.50	16.25	15.00	15.00

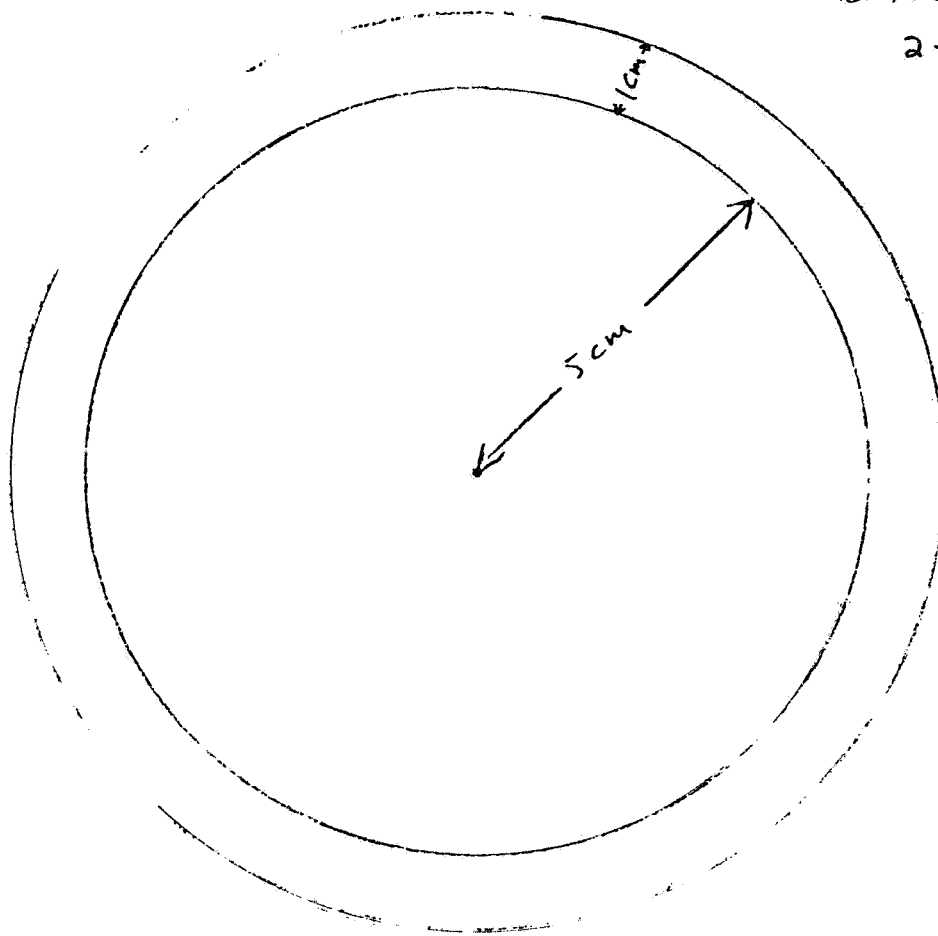
FLOW FIELD INFORMATION

ORIGINAL PAGE IS
OF POOR QUALITY

FROM DR. FOWLIS OF
NASA/MSFC (AGCE P.I.)

2-81

(A dual size)



$$\Omega = 2 \text{ rad/sec} \quad (\text{rotation rate})$$

$$\nu = .01 \text{ cm}^2/\text{s} \quad (\text{viscosity})$$

$$K = .000716 \text{ cm}^2/\text{s} \quad (\text{diffusivity})$$

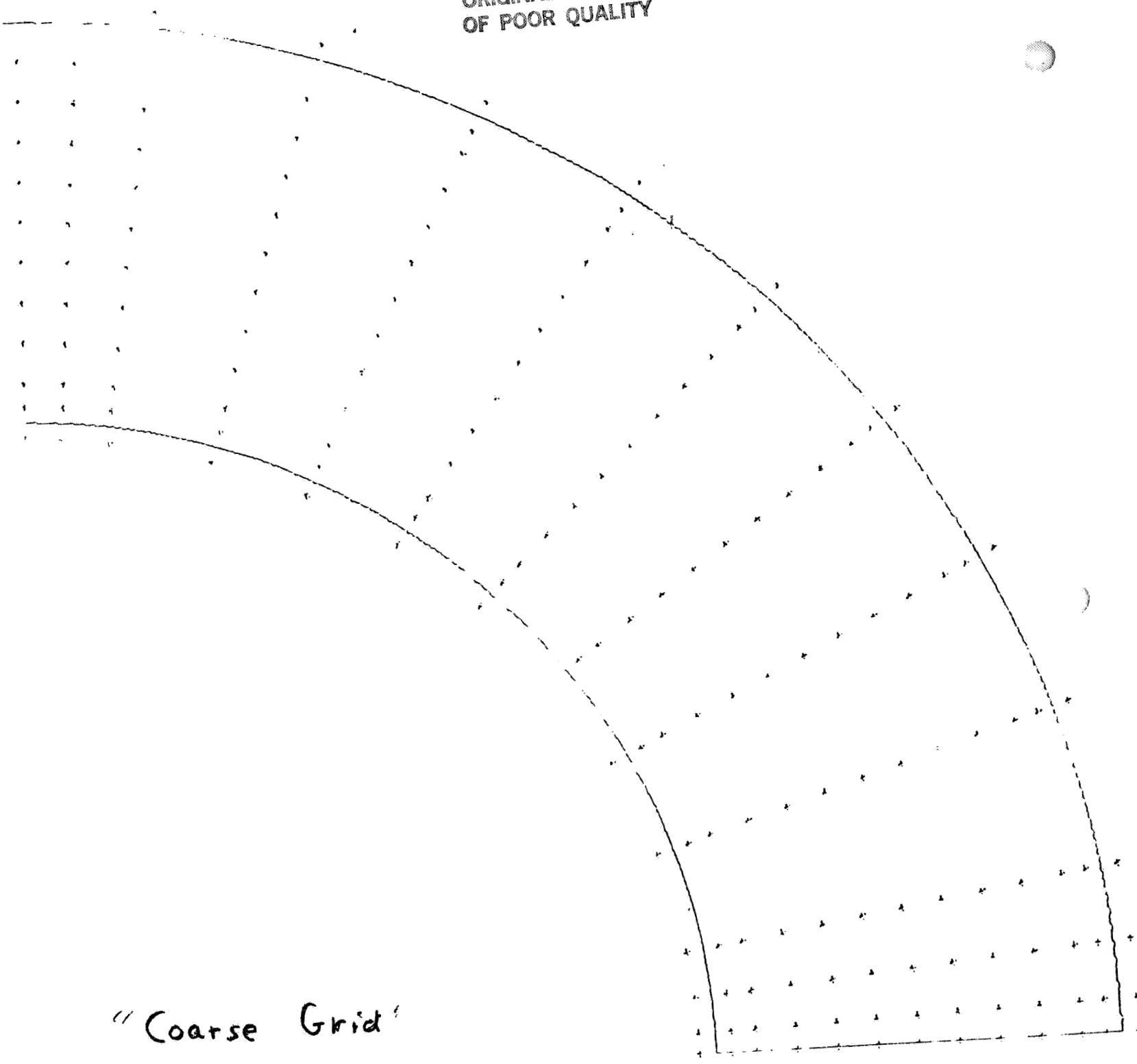
$$\alpha = 1.34 \times 10^{-3} \text{ } ^\circ\text{C}^{-1} \quad (\text{coefficient of expansion})$$

$$g = 980 \text{ cm/s}^2 \quad (\text{gravity})$$

$$\Gamma \left(\equiv \frac{\nu}{\Omega D^2} \right) = 5 \times 10^{-3}, \quad \text{Ro} \left(\equiv \frac{\alpha g d / \Delta T}{\Omega^2} \right) = 3.28, \quad \text{Pr} \left(\equiv \frac{\nu}{K} \right) = 13.97$$

ORIGINAL PAGE IS
OF POOR QUALITY

20

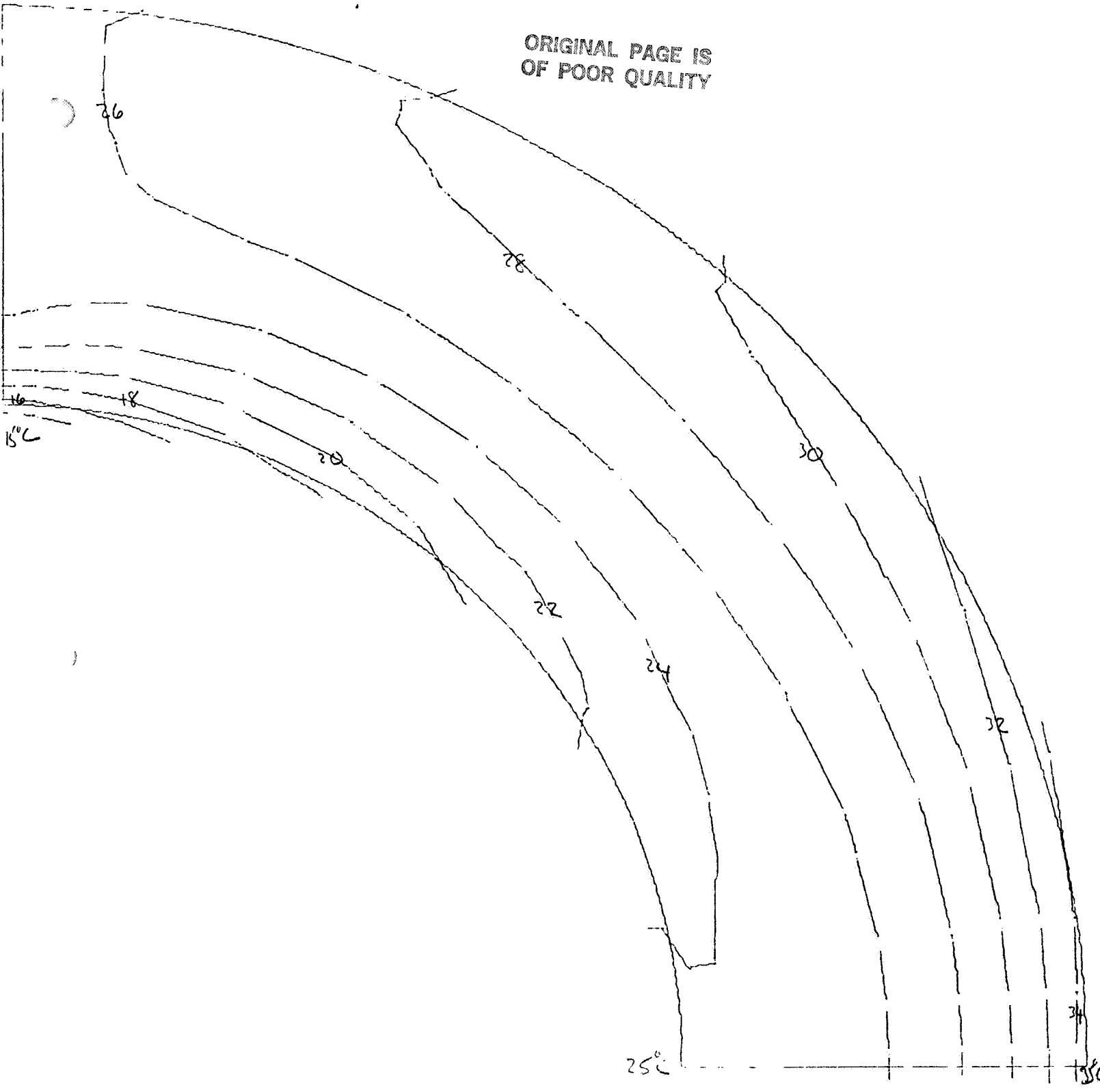


"Coarse Grid"

$t = "200 \text{ sec}"$

25°C

ORIGINAL PAGE IS
OF POOR QUALITY

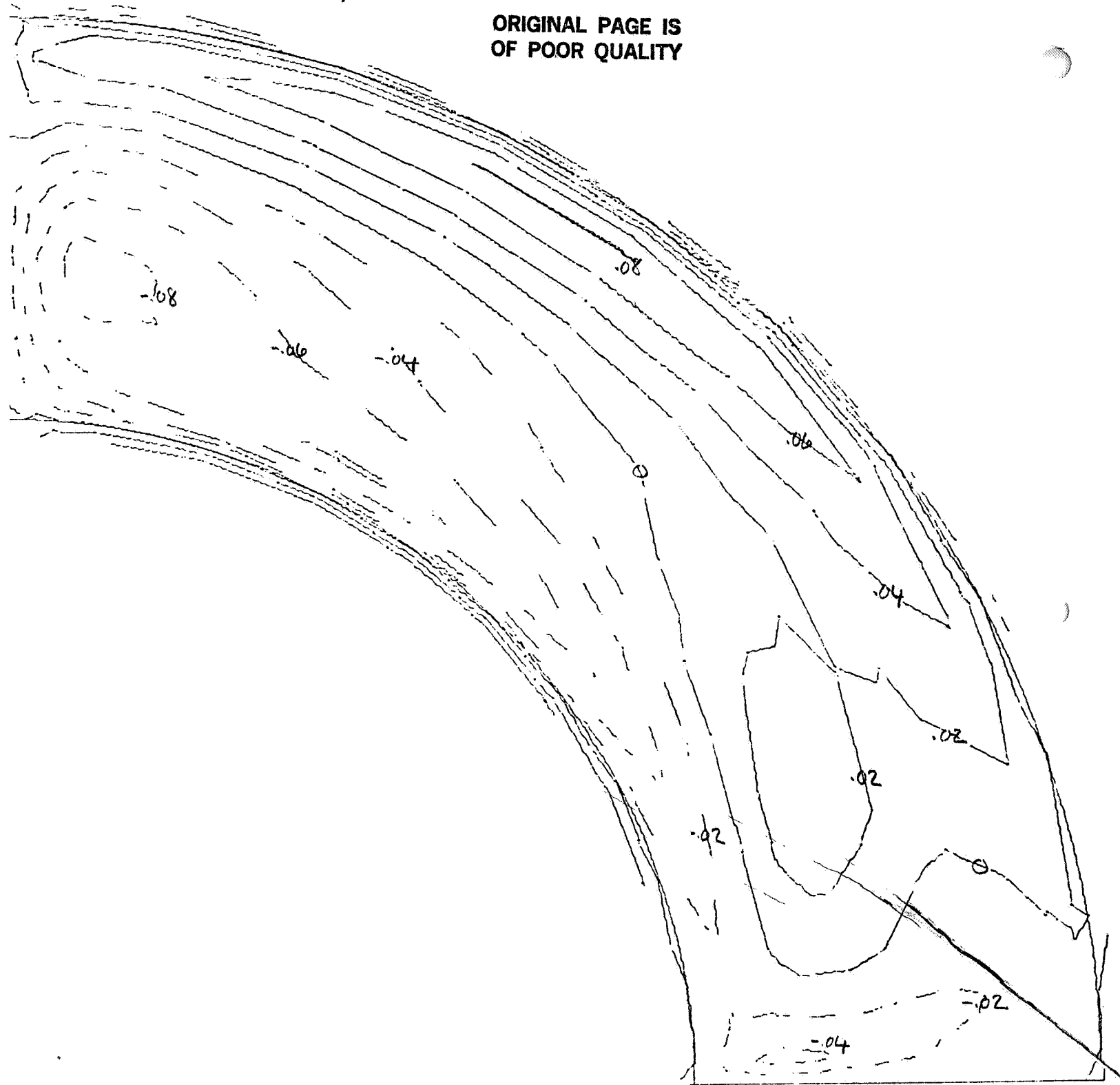


T-FIELD
(TEMPERATURE)

DELTA = 2.000
°C

TIME = 200.000

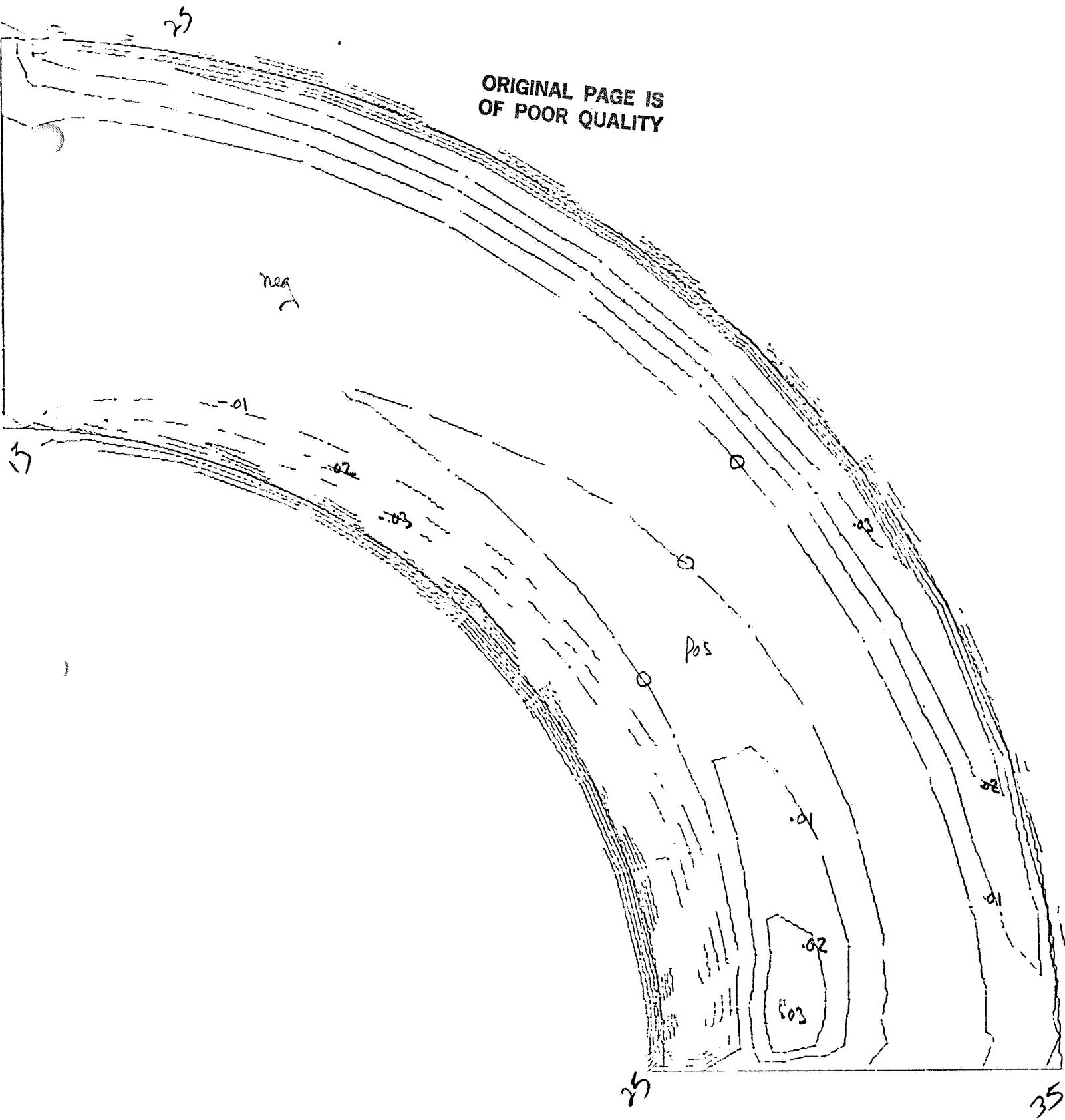
ORIGINAL PAGE IS
OF POOR QUALITY



U-FIELD
(AZIMUTHAL flow)

DELTA = 0.020
cm/s

ORIGINAL PAGE IS
OF POOR QUALITY



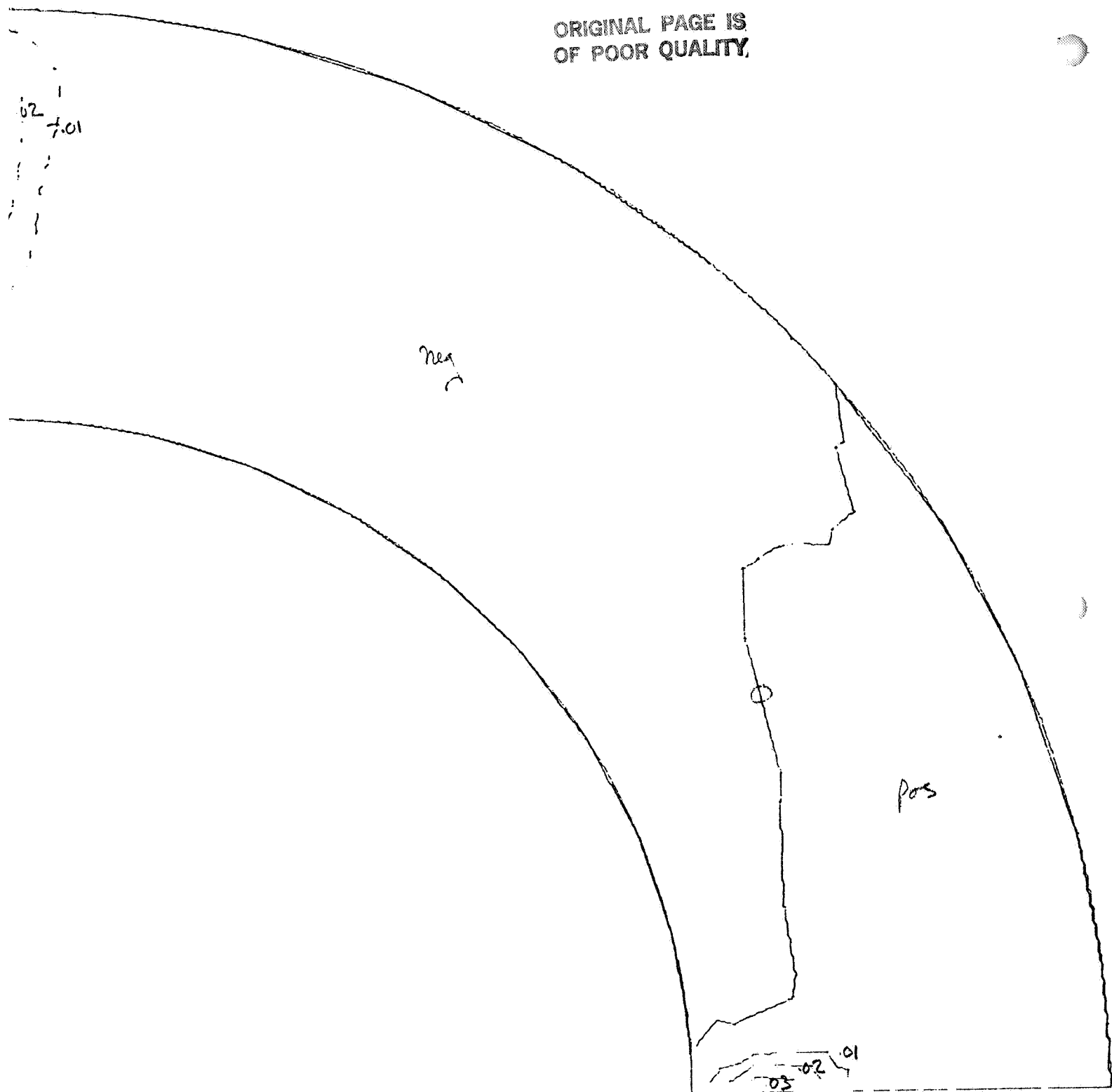
V-FIELD

(MERIDIONAL FLOW)

DELTA =

0.010
cm/s

ORIGINAL PAGE IS
OF POOR QUALITY.

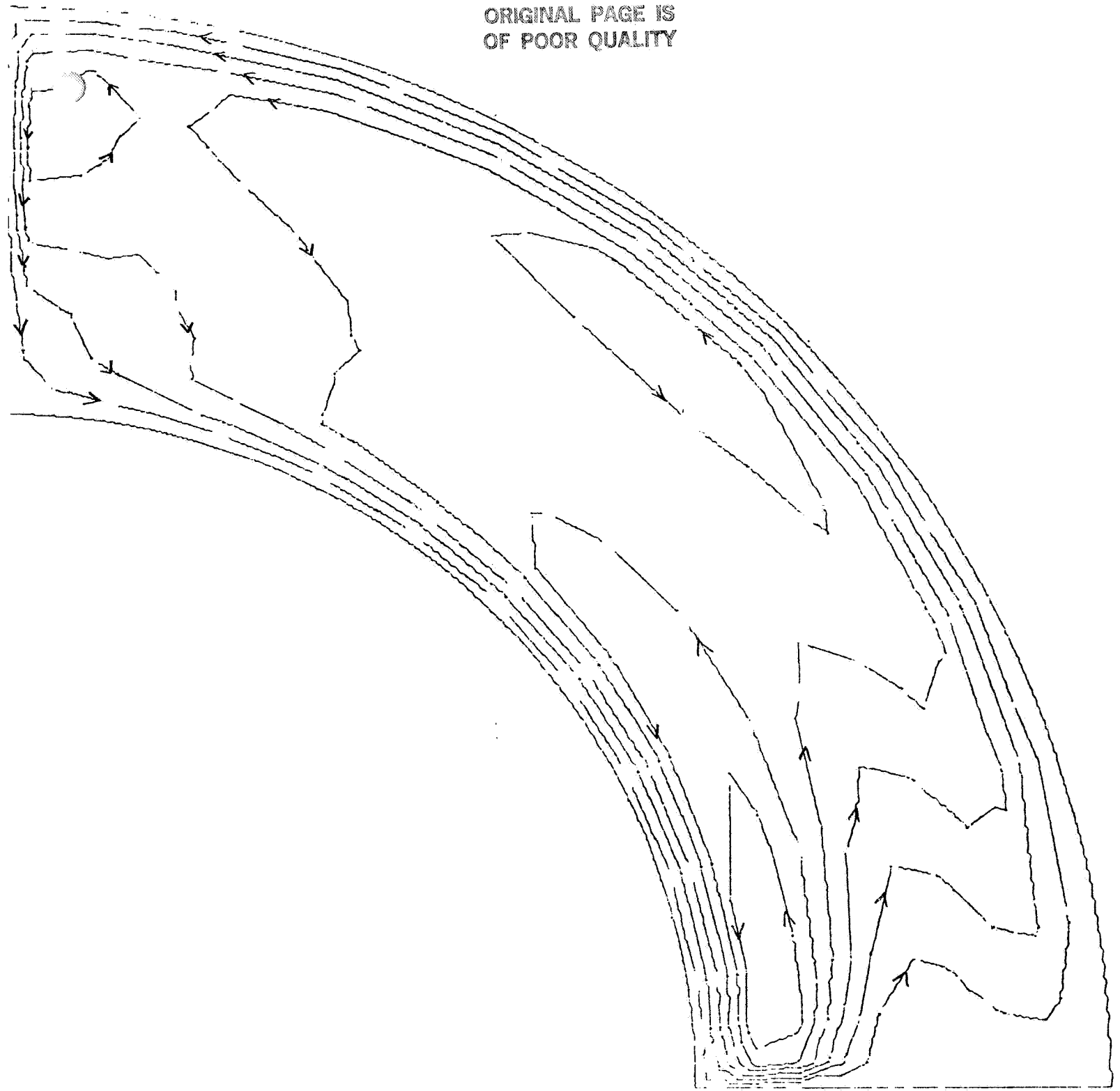


∇ -FIELD
(RADIAL FLOW)

DELTA = 0.010
cm/s

AK

ORIGINAL PAGE IS
OF POOR QUALITY

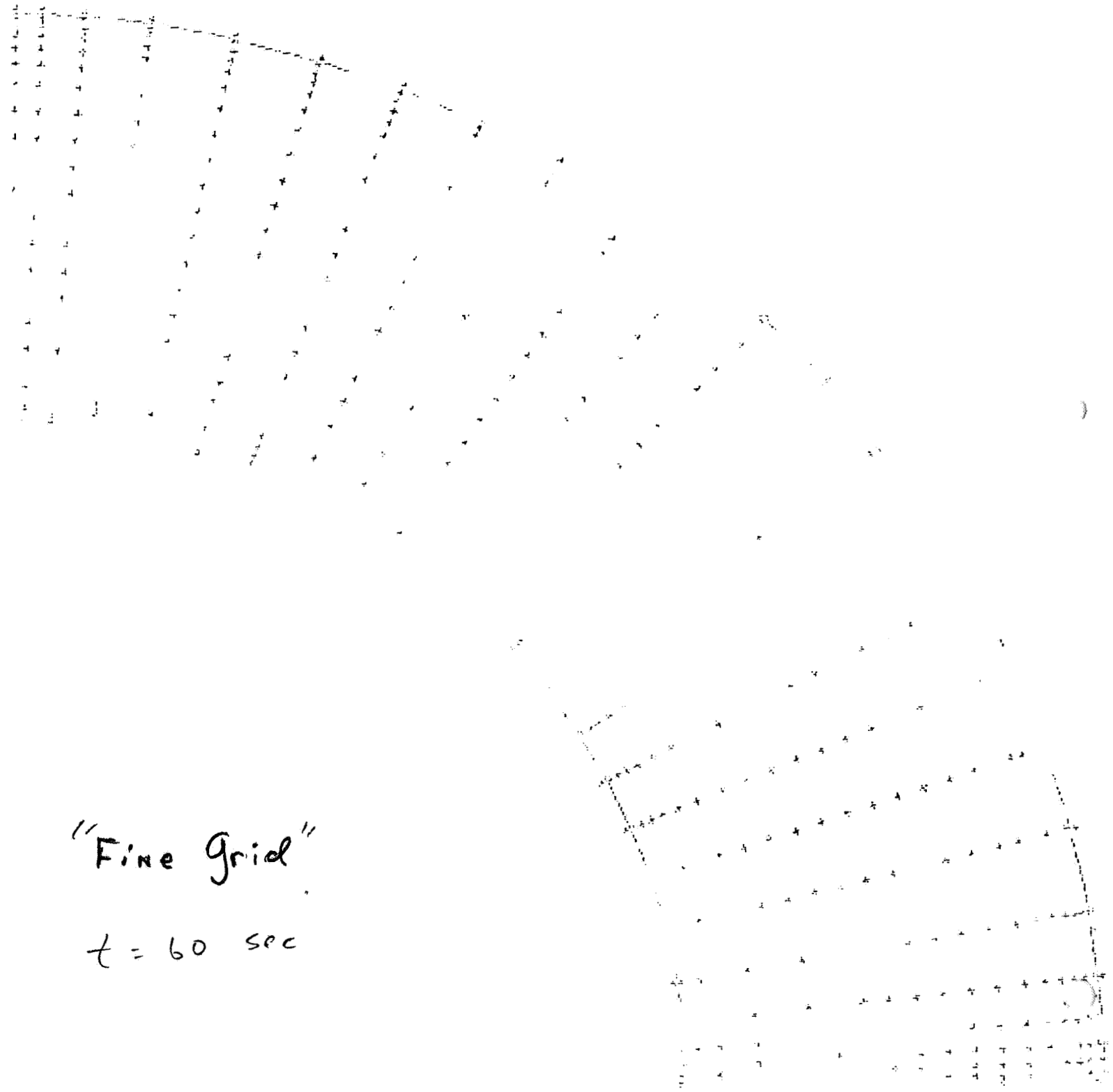


STREAM FUNCTION

DELTA =

0.001
cm²/s

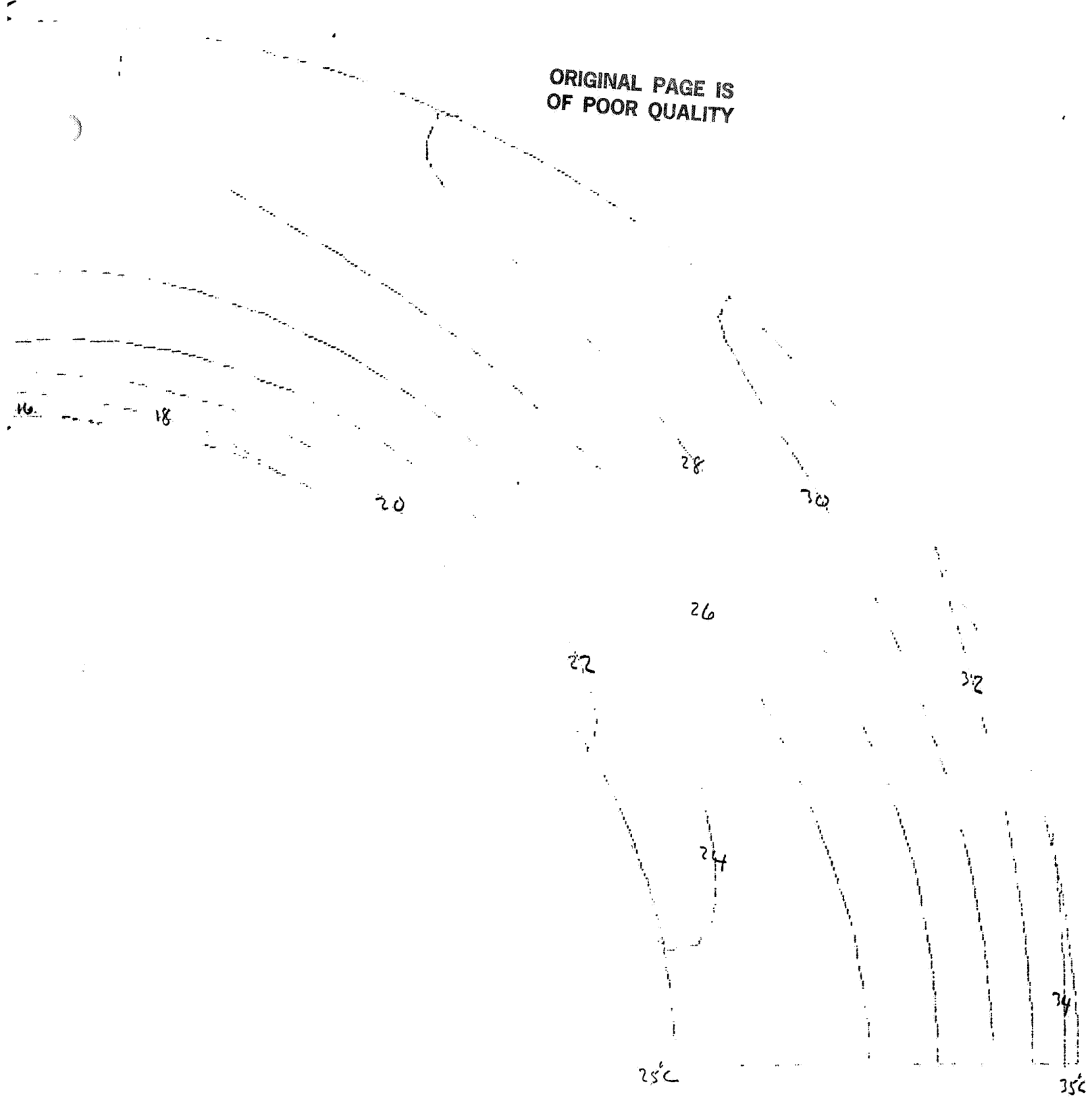
ORIGINAL PAGE IS
OF POOR QUALITY



"Fine Grid"

$t = 60 \text{ sec}$

ORIGINAL PAGE IS
OF POOR QUALITY



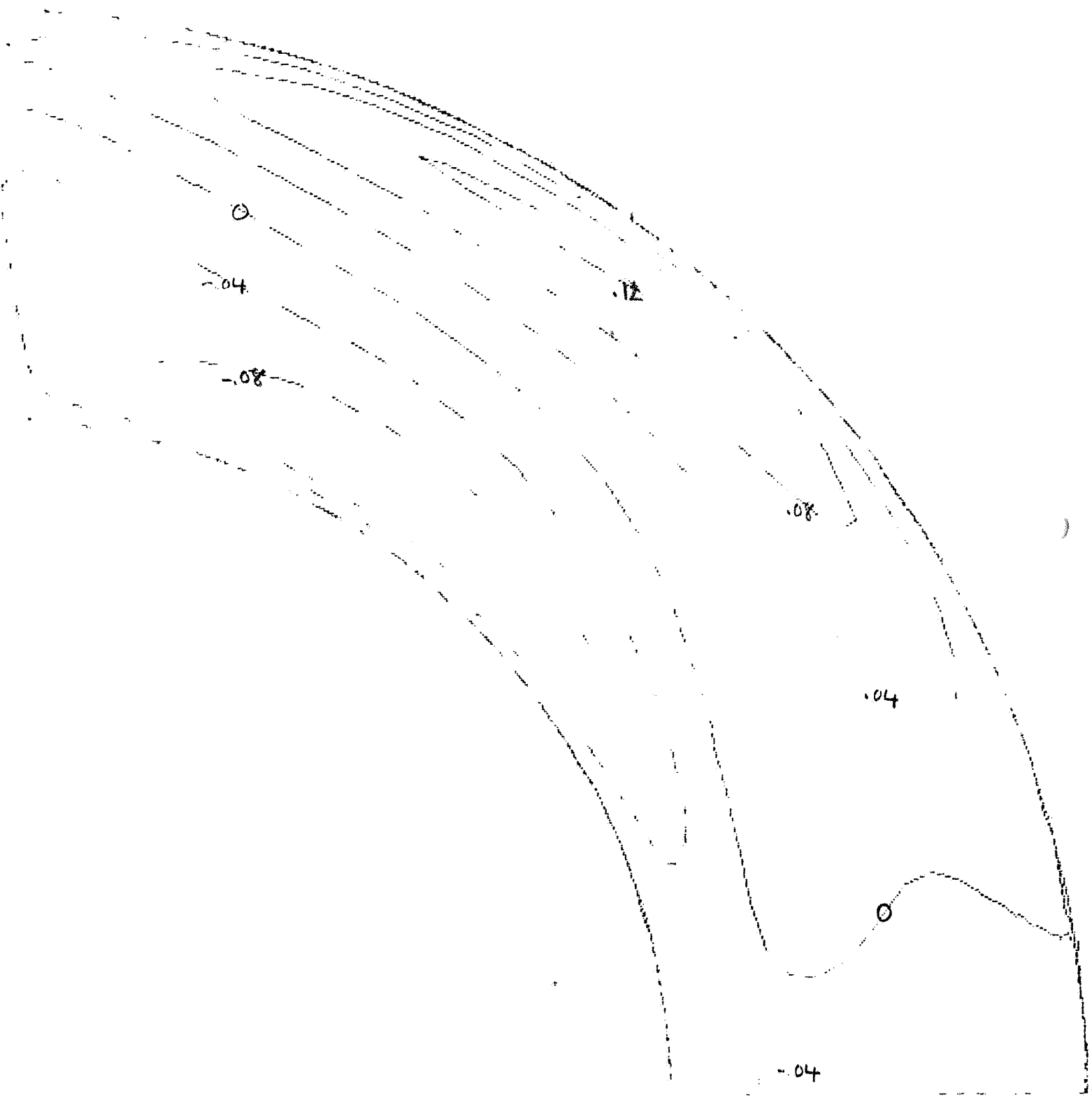
T-FIELD
(TEMPERATURE)

DELTA = 2.0 °C

60.000

141

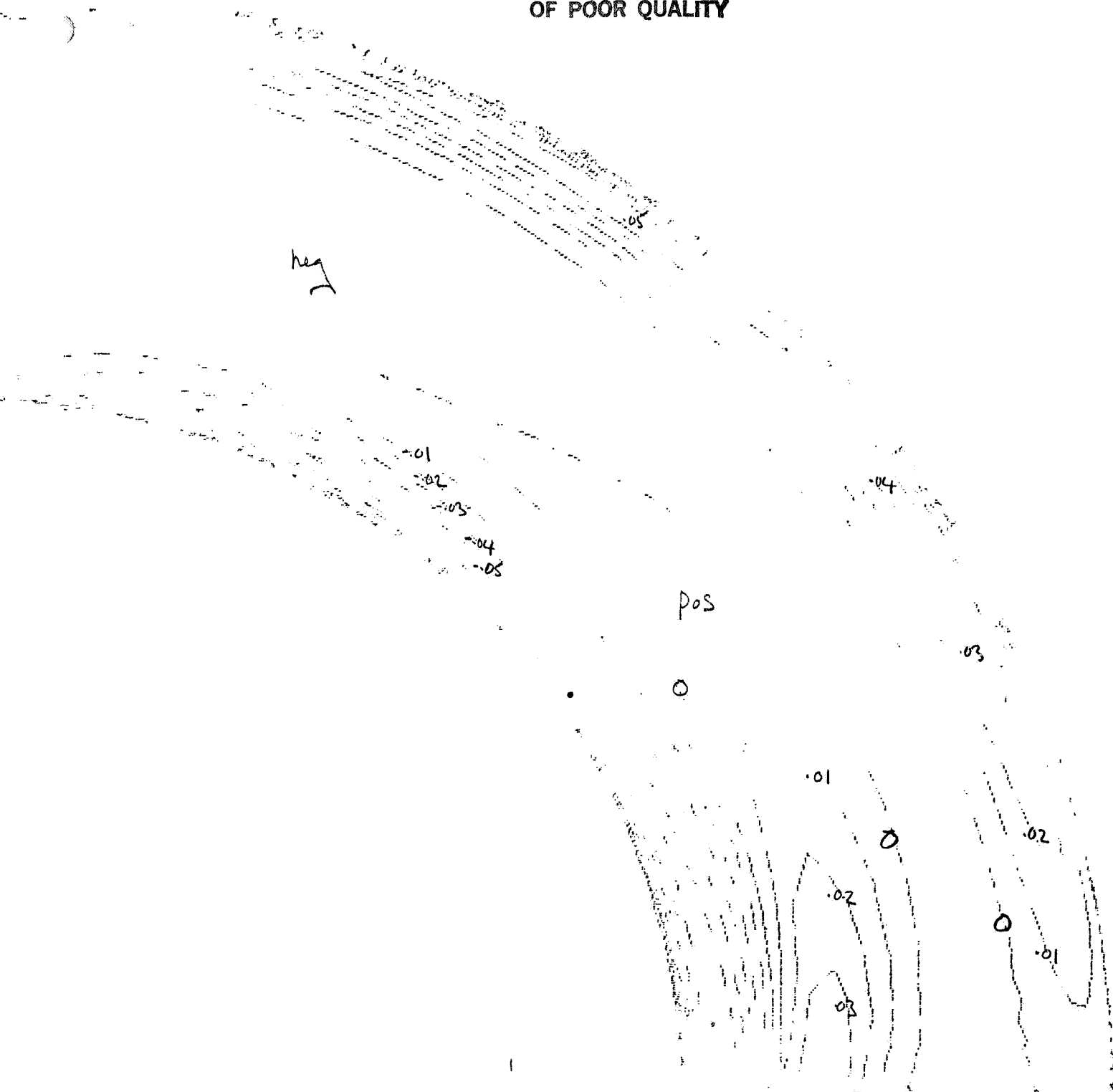
ORIGINAL PAGE IS
OF POOR QUALITY



V-FIELD
(AZIMUTHAL FLOW)

DELTA = 0.0416
cm/s

ORIGINAL PAGE IS
OF POOR QUALITY

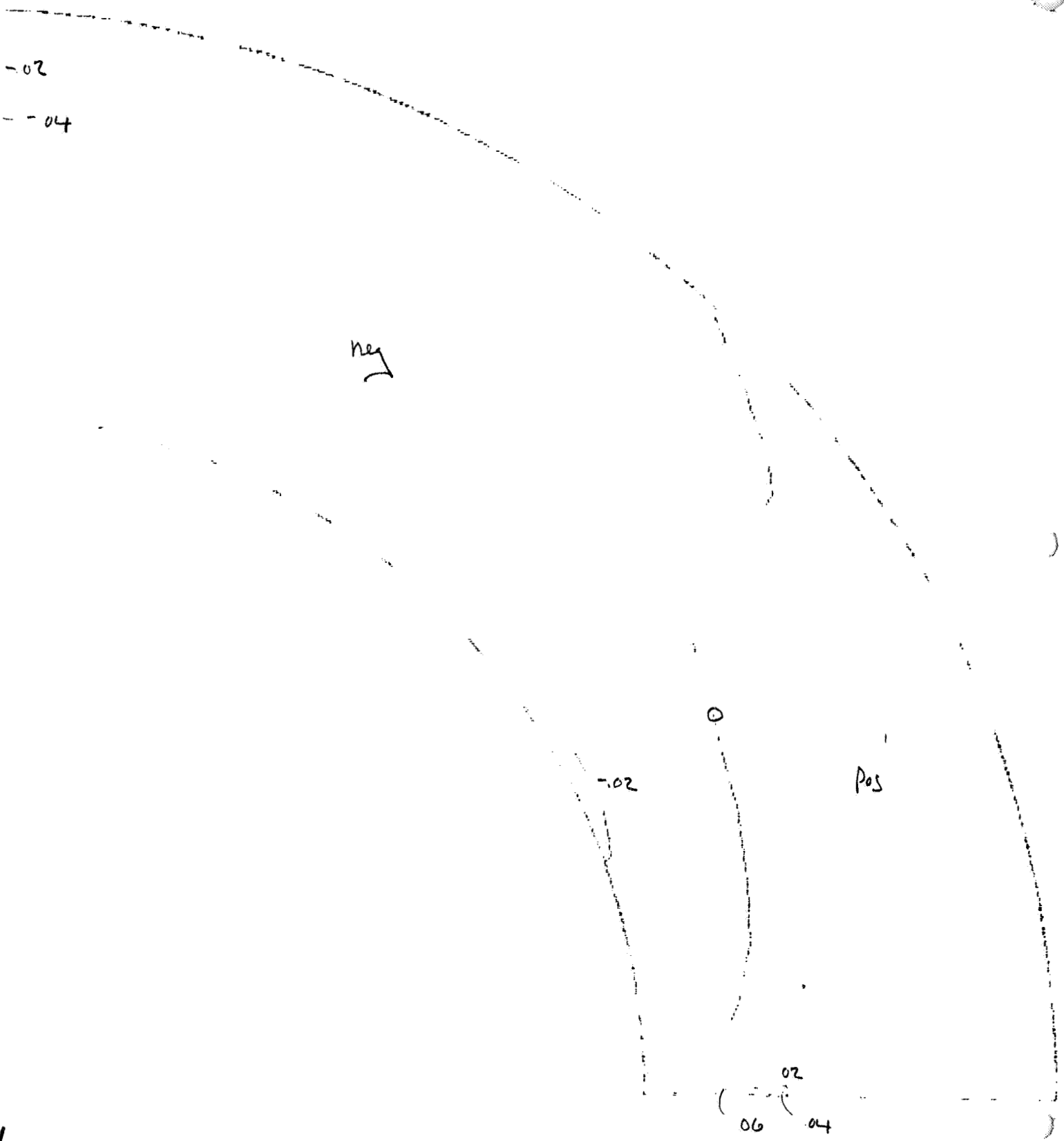


A-FIELD
(MERIDIONAL FLOW)

DELTA = 0.01
c/s

ORIGINAL PAGE IS
OF POOR QUALITY

23



√-

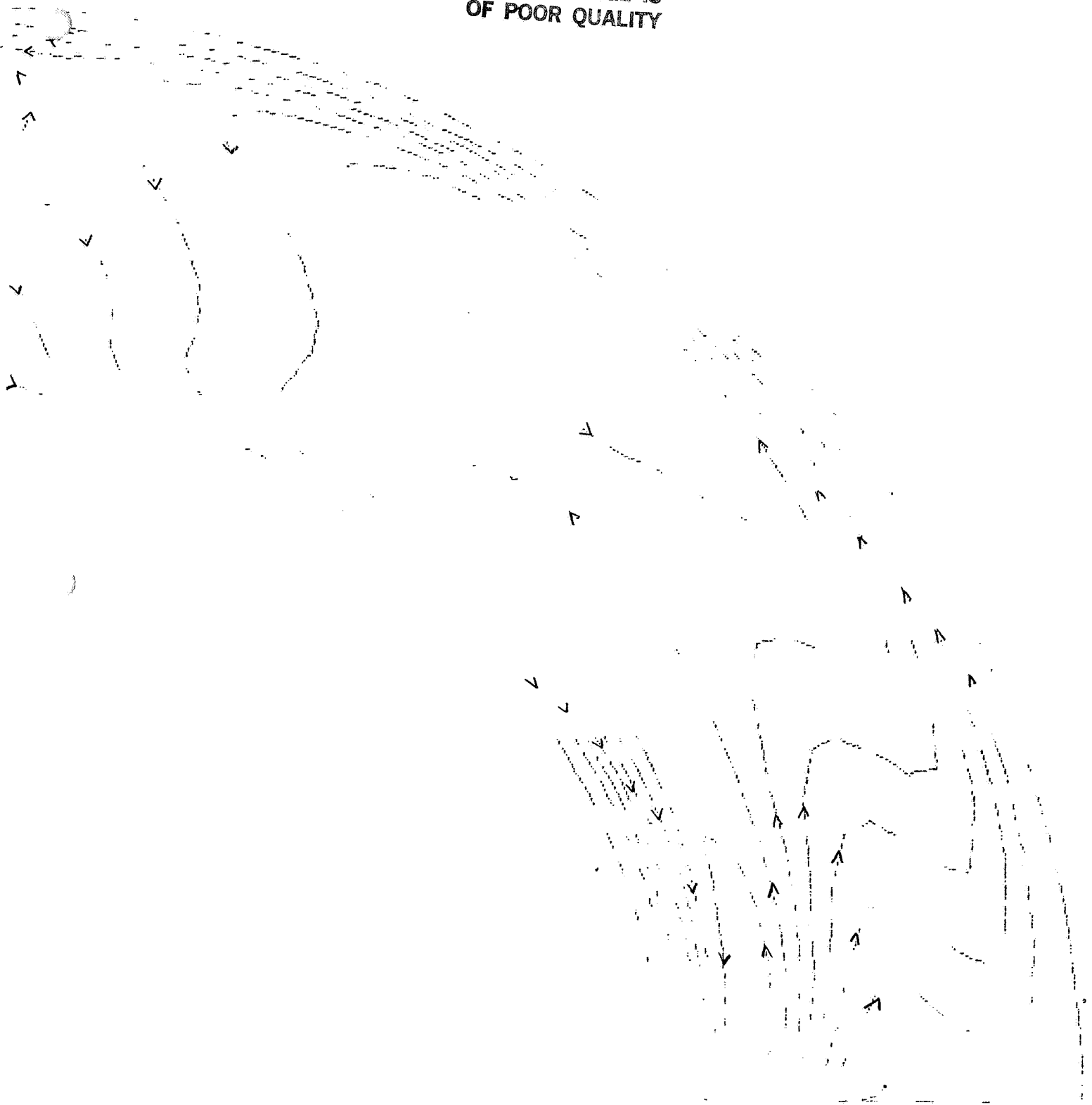
FIELD
(RADIAL FLOW)

DELTA =

0.0217
cm/s

2B

ORIGINAL PAGE IS
OF POOR QUALITY



TREAM FUNCTION

DELTA = $\frac{1}{4}$

0.0017
cm²/s



3.4 HIGH VOLTAGE POWER SUPPLY

	<u>PIR NO.</u>
Task 2.1 - High Voltage Source Requirements	-012
AGCE High Voltage Specifications - Telecon	-013
AGCE High Voltage Power Supply	-029

)

)

)

	*CLASS. LTR.	OPERATION	PROGRAM	SEQUENCE NO.	REV. LTR.
PIR NO.	U	1254	AGCE	012	
*USE "C" FOR CLASSIFIED AND "U" FOR UNCLASSIFIED					

PROGRAM INFORMATION REQUEST / RELEASE

FROM L. R. Eaton	TO DISTRIBUTION
---------------------	--------------------

DATE SENT 2/25/81	DATE INFO. REQUIRED	PROJECT AND REQ. NO.	REFERENCE DIR. NO.
----------------------	---------------------	----------------------	--------------------

SUBJECT
 TASK 2.1 - HIGH VOLTAGE SOURCE REQUIREMENTS

INFORMATION REQUESTED/RELEASED

The following AGCE high voltage source requirements have been documented as a baseline for a feasibility design study.

TASK 2 - HIGH VOLTAGE AND HIGH FREQUENCY SOURCES

1.0 SCOPE

The high voltage source design requirements are intended as guidelines to be used in performing a feasibility design of the equipment necessary to generate and insulate AC rms voltages of 20 to 30 kV in a frequency range from 60 to 1,000 Hz.

2.0 GENERAL

The high voltage requirements are based on GFFC hardware design and development experience and a current estimate of the AGCE flight design.

3.0 PERFORMANCE REQUIREMENTS

3.1 General

The primary goals for this feasibility design study are:

1. Extend the GFFC voltage generation capability from 10 kV rms to 20 or 30 kV rms.
2. Provide insulation and isolation concepts for this increased voltage.

3.2 High Voltage Magnitude

A nominal range of 0-20 kV rms voltage will be assumed. [The basic design

G. Fogal S. Neste L. Eaton	PAGE NO.	<input checked="" type="checkbox"/> RETENTION REQUIREMENTS	
	1 OF 3	COPIES FOR	MASTERS FOR
		<input type="checkbox"/> 1 MOS.	<input type="checkbox"/> 3 MOS.
		<input type="checkbox"/> 3 MOS.	<input type="checkbox"/> 6 MOS.
		<input type="checkbox"/> 6 MOS.	<input type="checkbox"/> 12 MOS.
		<input type="checkbox"/> MOS.	<input type="checkbox"/> MOS.
		<input type="checkbox"/>	<input type="checkbox"/> DONOT DESTROY

for GFFC high voltage power supply will be reviewed with due consideration given to simple design extension. Comments will be provided as to the impact of a larger upper voltage limit (i.e., 30 kV rms). Due to potentially excessive power dissipation in the high dielectric fluid and anticipated increased electrical isolation problems, emphasis will be placed on the 20 kV rms upper limit.]

3.3 High Voltage Frequency

The GFFC nominal value of a 300 Hz sinewave will be assumed. [General comments will be provided as to the impact of higher and lower frequencies between 60 and 1,000 Hz on the power supply design (e.g., size, EMI).]

3.4 High Voltage Waveform

The following GFFC requirements will be considered.

A high voltage power supply shall be provided whose output can be varied from 0 to 20.0 kV rms with a dynamic range of at least 200 to 1. Departure from linearity shall be less than 3% and stability of the high voltage power supply shall be less than 2% of the set point voltage. Frequency of the power supply shall be 300 Hz $\pm 5\%$, and the output shall have a wavefront distortion of less than 4%. The dynamic response of the high voltage supply shall be such as to achieve a settling time of less than 10 seconds for any step change in voltage.

3.5 High Voltage Insulation

The high voltage will be coupled from the power supply to a hemispherical "capacitor" with the following general characteristics.

The outer conductive coating of the outer sphere, as well as the surface inner sphere, shall be maintained at ground potential, while potentials of up to a nominal 20 kV AC shall be applied to the conductive coating of the inner surface of the outer sphere.

The AGCE shall have a spherical convective cell consisting of an outer sphere made of sapphire, having an inner radius of 6.0 ± 0.01 cm, and an inner sphere of stainless steel, having an outer radius of 5.0 ± 0.01 cm. The region between the spheres shall be filled with a working fluid with a dielectric coefficient of about 40 and a dissipation factor of about 0.001. The outer sphere, which has a thickness of approximately 1.2 cm, shall have transparent conductive coating on both its inner and outer surfaces.

Appropriate insulative considerations are to be considered which will avoid electrical breakdown at the sphere as well as at the power supply.

3.6 Dielectric Electrical Power Dissipation

The dissipation of the dielectric fluid heating effect is covered in PIR No. U-1254-AGCE-006.

4.0 INPUTS REQUIRED

Design details for the high voltage power supply will be taken from the GFFC CDR data package. This data is to be supplemented by any additional GFFC test information and results that are available through NASA/MSFC.

5.0 SAFETY

The power supply will be located within the confines of a gaseous nitrogen filled sealed enclosure.



	*CLASS. LTR.	OPERATION	PROGRAM	SEQUENCE NO.	REV. LTR.
PIR NO.	U	— 1254 —	AGCE	— 013	
*USE "C" FOR CLASSIFIED AND "U" FOR UNCLASSIFIED					

PROGRAM INFORMATION REQUEST / RELEASE

FROM S. L. Neste	TO L. R. Eaton
---------------------	-------------------

DATE SENT 2/26/81	DATE INFO. REQUIRED	PROJECT AND REQ. NO.	REFERENCE DIR. NO.
----------------------	---------------------	----------------------	--------------------

SUBJECT
AGCE High Voltage Specifications - Telecon

INFORMATION REQUESTED/RELEASED

The following specifications on the high voltage power supply for AGCE were provided by W. Fowlis on 25 February 1981.

- 1) Harmonic content <4% (i.e. sum of all harmonics) to minimize dielectric fluid heating.
- 2) Voltage accuracy ±3% after warm-up period. This allowable variation includes drift with time during an experiment scenario (~ 2-3 hours).
- 3) Noise TBD
- 4) Multiple settings (100-200) of the high voltage level are required and should be controlled by the micro-processor.

L. R. Eaton G. Fogal S. Neste	PAGE NO. 1 OF 1	RETENTION REQUIREMENTS	
		COPIES FOR	MASTERS FOR
		<input type="checkbox"/> 1 MO.	<input type="checkbox"/> 3 MOS.
		<input type="checkbox"/> 3 MOS.	<input type="checkbox"/> 6 MOS.
		<input type="checkbox"/> 6 MOS.	<input type="checkbox"/> 12 MOS.
		<input type="checkbox"/> MOS.	<input type="checkbox"/> MOS.
		<input type="checkbox"/>	<input type="checkbox"/> DO NOT DESTROY



*CLASS. LTR.	OPERATION	PROGRAM	SEQUENCE NO.	REV. LTR.
U	1254	AGCE	029	
*USE "C" FOR CLASSIFIED AND "U" FOR UNCLASSIFIED				

PROGRAM INFORMATION REQUEST / RELEASE

FROM L. Springer/J. Barney	TO Distribution
-------------------------------	--------------------

DATE SENT 6/11/81	DATE INFO. REQUIRED	PROJECT AND REQ. NO.	REFERENCE DIR. NO.
----------------------	---------------------	----------------------	--------------------

SUBJECT
AGCE HIGH VOLTAGE POWER SUPPLY

INFORMATION REQUESTED/RELEASED

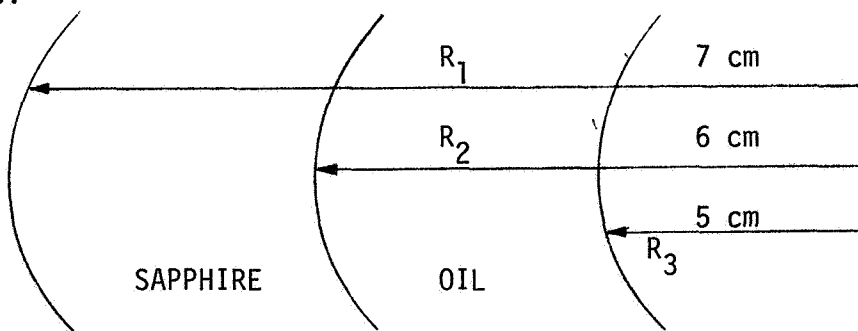
REQUIREMENTS

The AGCE power supply is required to deliver a 15 kV RMS sine wave voltage, with an amplitude accuracy of $\pm 3\%$ and a waveform distortion of less than 4%. Multiple settings (100-200) of the high voltage level are required and should be controlled by the microprocessor. These specifications are defined in PIR No. U-1254-AGCE-012 by L. R. Eaton.

DESIGN

The large step-up ratio (28 volts to 15 kV) is best handled by employing a series resonant circuit, thereby taking advantage of the resonant rise in voltage.

The capacitance and parallel resistance of the sphere can be calculated as follows:



$\rho_{oil} = 4 \times 10^9 \Omega - m$

$\epsilon_R(oil) = 40$

$\epsilon_0 = 8.85 \times 10^{-12} \text{ farads/m}$

$\rho_{sap} = 10^{14} \Omega - m$

$\epsilon_R(sap) = 10$

Distribution: J. Barney G. Fogal R. Homsey	S. Neste L. Springer File (2)	PAGE NO. 1 OF 7	<input checked="" type="checkbox"/> RETENTION REQUIREMENTS	
			COPIES FOR	MASTERS FOR
			<input type="checkbox"/> 1 MOS.	<input type="checkbox"/> 3 MOS.
			<input type="checkbox"/> 3 MOS.	<input type="checkbox"/> 6 MOS.
			<input type="checkbox"/> 6 MOS.	<input type="checkbox"/> 12 MOS.
			<input type="checkbox"/> MOS.	<input type="checkbox"/> MOS.
			<input type="checkbox"/>	<input type="checkbox"/> DO NOT DESTROY

PIR No. 1254-AGCE-029

$$R_{oil} = \frac{\rho_{oil} (R_2 - R_3)}{4\pi R_2 R_3} = \frac{4 \times 10^9 (0.06 - 0.05)}{4\pi [(0.06)(0.05)]} = 1.06 \times 10^9 \Omega$$

$$R_{sap} = \frac{\rho_{sap} (R_1 - R_2)}{4\pi R_1 R_2} = \frac{10^{14} (0.07 - 0.06)}{4\pi [(0.07)(0.06)]} = 1.895 \times 10^{13} \Omega$$

$$C_{oil} = \frac{4\pi \epsilon_R(oil) \epsilon_0 (R_2 R_3)}{(R_2 - R_3)} = \frac{4\pi \times 40 \times 8.85 \times 10^{-12} \times (0.06 \times 0.05)}{(0.06 - 0.05)}$$

$$C_{oil} = 1.3346 \times 10^{-9} \text{ farads}$$

$$C_{sap} = \frac{4\pi \times 10 \times 8.85 \times 10^{-12} \times (0.07 \times 0.06)}{(0.07 - 0.06)} = 4.6709 \times 10^{-10} \text{ farads}$$

$$R_T = \frac{R_{oil} \times R_{sap}}{R_{oil} + R_{sap}} = 1.0612 \times 10^9 \Omega$$

$$C_T = C_{oil} + C_{sap} = 1.8016 \times 10^{-9} \text{ farads}$$

The series inductor necessary to resonate at 300 Hz is:

$$L = \frac{1}{C (f_r 2\pi)^2} = \frac{1}{1.8016 \times 10^{-9} (300 \times 2 \times \pi)^2}$$

$$L = 156 \text{ henries}$$

A preliminary design of this inductor has been completed and is shown in Figure 1. The electrical properties of the inductor are given below.

Tape Core B = 15,000 G : μ 6000 W/air gap

10,000 turns of #32 wire

100 layers distributed between two windings

5.5 mil porous layer separation

Minimum HV-Gnd separation 5/8"

Urethane potting

WT: 3.5 kg

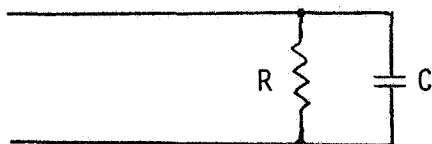
$R_{coil} = 1260 \Omega$

These properties produce a Q-value of:

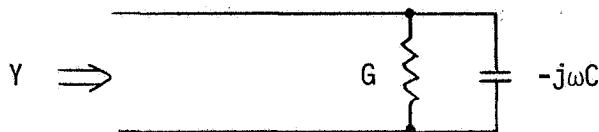
$$Q = \frac{X_L}{R} = \frac{2\pi(300)(156)}{1260} = 233.37$$

The design of this inductor has taken into consideration the waveform linearity necessary to meet specifications.

Writing the equivalent circuit for the sphere yields



or



$$Y = G - j\omega C$$

$$Y = 9.43 \times 10^{-10} - j 3.393 \times 10^{-6}$$

To determine the RMS current necessary in the series resonant circuit to develop 15 kV across the capacitor, one can write

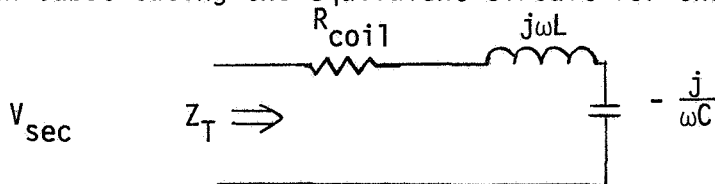
$$I = VY = 15,000 [9.43 \times 10^{-10} - j 3.39 \times 10^{-6}]$$

$$I = 1.41 \times 10^{-5} - j 5.09 \times 10^{-2}$$

or

$$I = 50.89 \times 10^{-3} \text{ amp} \angle - 89.98^\circ$$

Then substituting the equivalent circuit for the entire resonant circuit yields



$$Z_T = R + j \left(\omega L - \frac{1}{\omega C} \right)$$

$$\omega L = \frac{1}{\omega C} \text{ at resonance}$$

PIR U-1254-AGCE-029

-4-

6/11/81

$$\therefore Z_T = R$$

and $Z_T = 1260 \Omega$

$$V_{\text{sec}} = IR = (50.80 \times 10^{-8})(1260) = 64.12 \text{ volts}$$

Since we need 64.12 volts RMS to excite the series resonant circuit, it will be necessary to use a small step-up transformer between the driver stage and the resonant circuit.

CIRCUIT DESCRIPTION

The conceptual circuit is shown in Figure 2. It consists of the following: a series resonant circuit, a driver stage, a voltage controlled gain amplifier, a VCO, and feedback signals to maintain the proper frequency and amplitude of the voltage.

The VCO, which is part of a Phase-Lock Loop (PLL), generates the 300 Hz signal. Its output is fed into a multiplier which is used as a voltage controlled gain amplifier, the function of which is to control the output signal level. The output of the multiplier is then fed into a signal conditioner and onto the driver stage. The driver stage contains a small step-up transformer whose secondary is used to drive the resonant circuit. A current signal is generated in the primary of the transformer and fed back to the input of the PLL. This assures that the circuit will be operated at resonance at all times. A tap on the inductor is used to monitor the H.V. output. This signal after proper conditioning is fed back to the multiplier to maintain the proper output level. It seems possible to obtain the 100:1 dynamic level adjustment by using only the multiplier as the control device. Some testing will be necessary to confirm this. If this method proves too noisy at lower level settings, then other means will be employed to meet requirements. Information to set the desired voltage level will be obtained from the on-board microprocessor. This information is fed to a D/A converter whose output is summed with the error feedback signal and presented to the multiplier, which in turn regulates the high voltage output. Up to 256 voltage levels are possible with a single 8 bit D/A converter.

PHYSICAL DIMENSIONS

The physical dimensions of the inductor and the electronics package are given in the table below.

		<u>L</u>	<u>W</u>	<u>H</u>	<u>VOL.</u>	<u>WT.</u>
Inductor	Plan 1	8-3/16"	4-3/8"	5-1/4"	188.0 in ³	3.5 kg
	Plan 2	8-3/16"	4-7/8"	4-3/4"	189.6 in ³	3.5 kg
Electronics Package		4-3/8"	4-3/8"	2-1/2"	47.8 in ³	0.9 kg

ORIGINAL PAGE IS
OF POOR QUALITY

4-3/8" W
OR
4-7/8"

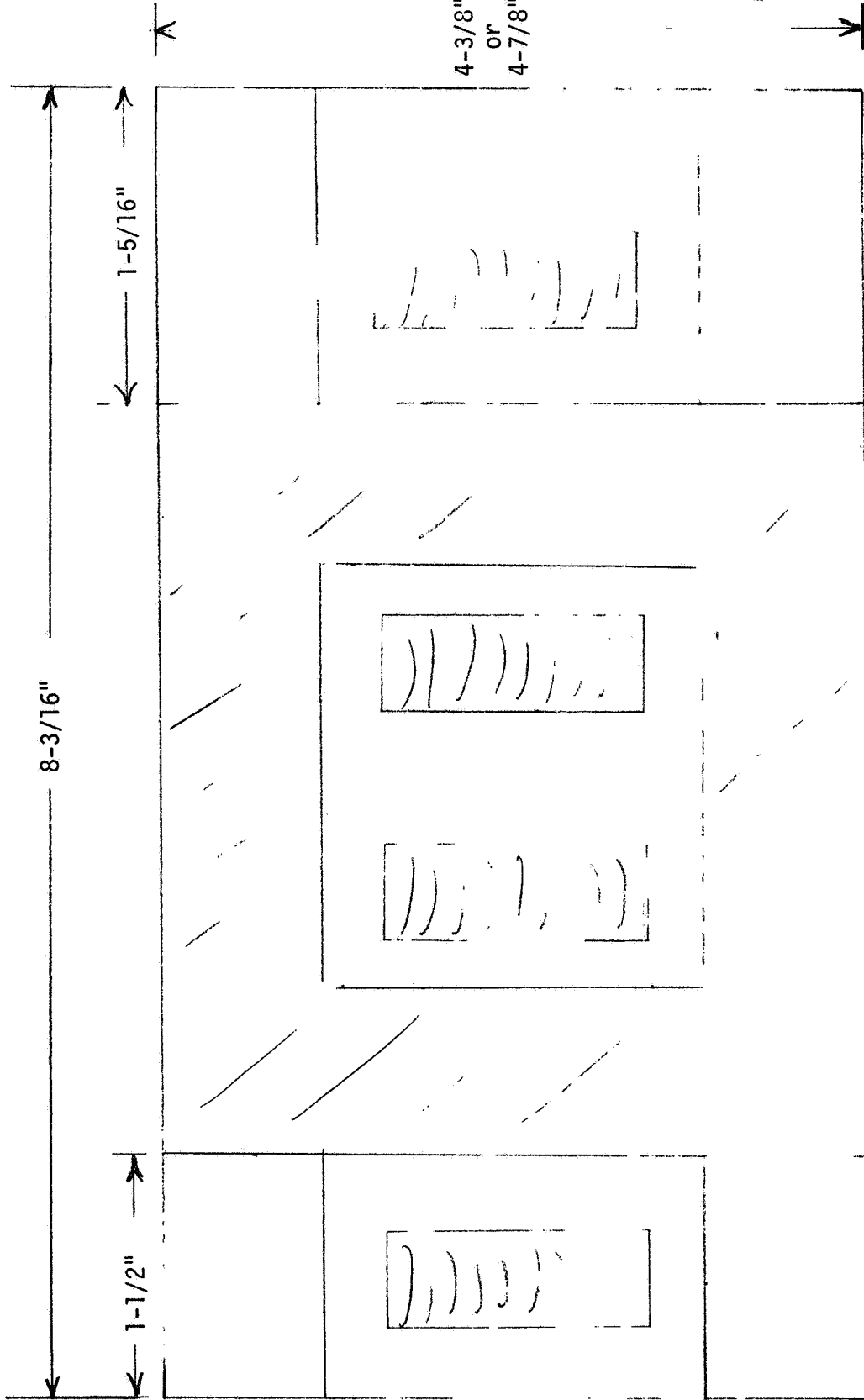
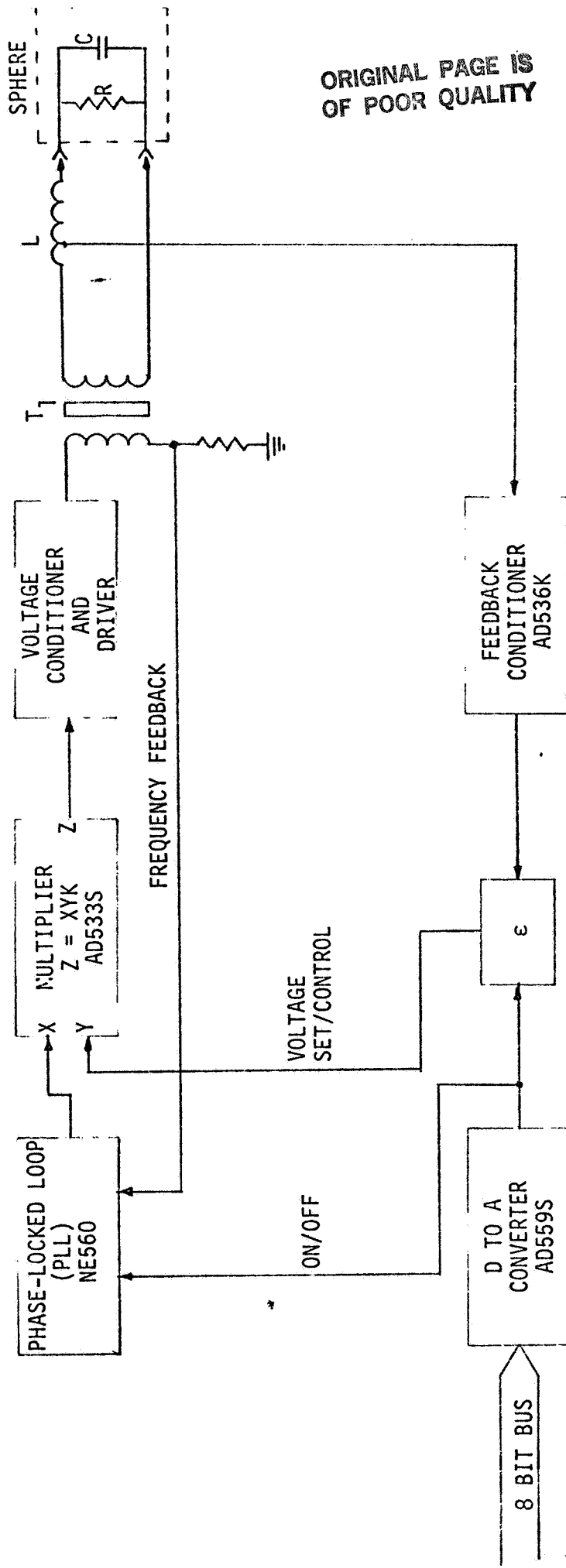


Figure 1. Inductor



ORIGINAL PAGE IS OF POOR QUALITY

Figure 2. Power Supply Block Diagram



3.5 EXPERIMENT CONTROL AND DATA HANDLING

	<u>PIR NO.</u>
Task 7 - Feasibility Guidelines	-034
Task 7 - AGCE Feasibility Study Final Report	-035

)

)

)

GENERAL ELECTRIC

SPACE DIVISION
PHILADELPHIA

	*CLASS. LTR. U	OPERATION 1254	PROGRAM AGCE	SEQUENCE NO. 034	REV. LTR.
PIR NO.	U	— LSD	— AGCE	— AGE 001	

PROGRAM INFORMATION REQUEST / RELEASE

*USE "C" FOR CLASSIFIED AND "U" FOR UNCLASSIFIED

FROM C. Mosley <i>WMM</i>	TO R. Hbmsey
------------------------------	-----------------

DATE SENT 5 May 1981	DATE INFO. REQUIRED	PROJECT AND REQ. NO.	REFERENCE DIR. NO.
-------------------------	---------------------	----------------------	--------------------

SUBJECT
Task 7 Feasibility Guidelines

INFORMATION REQUESTED/RELEASED

(SEE ATTACHED)

G. Fogal E. Morgan R. Hallett	PAGE NO. 0 OF 7	RETENTION REQUIREMENTS	
		COPIES FOR	MASTERS FOR
		<input type="checkbox"/> 1 MO.	<input type="checkbox"/> 3 MOS.
		<input type="checkbox"/> 3 MOS.	<input type="checkbox"/> 6 MOS.
		<input type="checkbox"/> 6 MOS.	<input type="checkbox"/> 12 MOS.
		<input type="checkbox"/> MOS.	<input type="checkbox"/> MOS.
		<input type="checkbox"/>	<input type="checkbox"/> DO NOT DESTROY

TASK 7- CONTROL OF TOTAL APPARATUS, FEASIBILITY GUIDELINES

1.0 SCOPE

The apparatus control requirements are based on the experience with GFFC and the current estimate of AGCE subsystems needs. These requirements are intended as guidelines to be used in the assessment of the feasibility of the AGCE.

2.0 GENERAL

Many of the requirements are stated in terms of capabilities that were provided in the GFFC design but are not specifically discussed or described in the literature available to this study effort. Other requirements arise from the SLP/2104 or from AGCE unique features.

3.0 PERFORMANCE REQUIREMENTS

3.1 General

Provide a microprocessor type, centralized controller that implements the experiment scenario as expressed in a Problem Oriented Language (POL) similar to that used in the GFFC design. The control subsystem shall be programmable when in a ground test or software development configuration and yet provide capability to "burn" the experiment scenarios into a non-alterable memory and execute from this memory in the flight configuration.

3.2 External Interfaces

3.2.1 Inputs

At the Spacelab interface the AGCE must receive timing information as represented by UTC and UTC Update (described in SLP/2104). The presence of these inputs imply that the AGCE contains or shares a RAU (Remote Acquisition Unit). For purposes of this study effort a RAU is assumed available and UTC and UTC Update are received through this path.

Primary experiment power will be supplied by Spacelab through the Experiment Power Switching Panel (EPSP) in the form of +28 VDC.

3.2.2 Outputs

The output requirements are those associated with either an on-board display or telemetry through the HRM. No decision has been made concerning these system features. If it is decided to store experiment data within the experiment until Spacelab's return to earth, then it may be that no telemetry is necessary, but a display would be required to inform the PS of the experiment health and status. On the other hand, if it is decided to telemeter the experiment data to earth, then there may not be a need to provide the on-board display.

The display could be one provided by Spacelab or one contained in the experiment. It would be used to indicate the position and movement of the marker dots.

The telemetry would consist of both experiment data and housekeeping information. Assume one dedicated HRM channel is available.

3.3 Internal Control Requirements

3.3.1 Thermal Subsystem Control Requirements

Thermal control is exercised using two different types of elements, heaters and Thermoelectric Modules (TEMS).

The surface of the inner sphere will contain up to nine heater/thermister pairs for implementing closed loop temperature control. These nine loops will require that the microcomputer acquire the sensor data, operate on it in some prescribed manner and command the appropriate voltage to the heating element. In performing this function the thermister calibration curve will be stored and used.

There are four areas requiring TEM control. The first is on the pole of the outer sphere. The second is a liquid heating/cooling loop around the equator of the outer sphere. The third is on the cell shell, to cool the gaseous nitrogen. The fourth is the inner sphere heat sink. In the TEM cases the controller requirements will be similar to those of the ACPL program except they are not required to be nearly as accurate and regulation through the TEM crossover region is not necessary. For purposes of this study an accuracy of +/- .1 degrees C. is assumed in all thermal control instances.

In addition to the closed loop control requirements there will be additional requirements for passive temperature monitoring. Provide for an additional eleven thermister inputs for this purpose. Seven of these are located on the outer sphere and four are miscellaneous.

3.3.2 Optical Subsystem Control Requirements

The UV flash lamp will be controlled by the microcomputer. Both the flash timing and duration must be controlled. Accuracy and range information is TBD.

3.3.3 Power Supply Control Requirements

Setting of the magnitude of the high voltage will be under the control of the microcomputer. There is an approximate 100 to 1 dynamic range requirement but actual magnitudes are TBD.

3.3.4 Turntable Subsystem Control Requirements

The microcomputer will be the controlling element for automatic or manual (as in test) setting of the turntable rotation rates. These rates are to be adjustable within the range of .025 to 3 radians/sec. This will be accomplished via a digital command issued over a programmed I/O channel. Detailed control requirements are TBD.

3.3.5 Timing Control Requirements

The microcomputer will receive timing information from the Spacelab and will utilize it in time tagging of experiment data, in execution of experiment scenarios. Accuracy requirements are consistent with the Spacelab UTC and the resolution requirements are TBD.

3.3.6 Experiment Scenarios

Scenario requirements are assumed identical to those of the GFFC as far as complexity is concerned. There are:

- . 24 scenarios.
- . 16 segments/scenario.
- . roughly 150 bytes/segment.

Scenarios are timelines, permanently stored in a read only memory, that are executed by the microcomputer and cause the AGCE to conduct a specific experiment. Scenarios will consist of up to 16 segments that specify experiment parameters such as temperature, voltage and rotation rate settings and timing information. The AGCE must provide a method of permanent scenario storage on-board (ROM) and yet make it possible for the AGCE to perform experiments using a soft memory (read/write) during the scenario development or software development phases of the program. This capability is also expected to aid in the test and troubleshoot modes of operation as they become necessary during the program.

3.3.7 Housekeeping Data Acquisition

The following is a partial list (as complete as possible at this time) of the specific housekeeping measurements to be taken:

FRAME #
SCENARIO #
TIME WORD
HV SETTING
Ti.e. - INNER SPHERE EQUATOR TEMPERATURE
Ti.p. - INNER SPHERE POLE TEMPERATURE
To.e. - OUTER SPHERE EQUATOR TEMPERATURE
To.p. - OUTER SPHERE POLE TEMPERATURE
INNER SPHERE TEMPERATURE - 9 SENSORS
OUTER SPHERE TEMPERATURE - 11 SENSORS
A/D CONVERTER CALIBRATION READINGS
DATE - DAY/MONTH/YEAR
TURNTABLE TEMPERATURE
AVIONICS AIR TEMPERATURE
COMPUTER TEMPERATURE
UV FLASH PERIOD

These housekeeping measurements will either be stored on-board and retrieved post-mission or telemetered to the POCC via the Spacelab HRM. Additionally, they may be displayed on-board for use by the Payload Specialist. These factors depend on the resolution of Tasks 7A and 7B.

3.3.8 Display Subsystem Control Requirements

The display control requirements are dependent on the resolution of the telemetry/on-board recording question. If on-board recording is selected, the display will be used by the Payload Specialist to follow the movement of the marker dots to insure that the experiment is progressing as desired. This will necessitate a CRT type display. Additionally, a control panel similar to that used on GFFC will be required. If the telemetry alternative is selected, the display will probably be completely eliminated except for a power on indicator and a run light.

WCM
agcereq
04/81

3.3.9 Data Storage Subsystem Control Requirements

The data storage control requirements are dependent on the resolution of the storage/telemetry question of whether or not it is more cost effective to telemeter experiment data to the POCC , locate all the data processing there and provide essentially no on-board data storage or to provide on-board data storage capability sufficient to cover the whole mission and remain virtually autonomous with respect to Spacelab and POCC?



)

)

GENERAL ELECTRIC

SPACE DIVISION
PHILADELPHIA

PROGRAM INFORMATION REQUEST / RELEASE

	*CLASS. LTR. U	OPERATION 1254	PROGRAM AGCE	SEQUENCE NO. 035	REV. LTR.
PIR NO.	U	— 1D40 —	AGCE	— AGE 002	

*USE "C" FOR CLASSIFIED AND "U" FOR UNCLASSIFIED

FROM W. C. Mosley U7035 X4094 <i>WCM</i>	TO R. Homsey
---	-----------------

DATE SENT 28 May 1981	DATE INFO. REQUIRED	PROJECT AND REQ. NO.	REFERENCE DIR. NO.
--------------------------	---------------------	----------------------	--------------------

SUBJECT
Task 7 AGCE Feasibility Study Final Report

INFORMATION REQUESTED/RELEASED

(SEE ATTACHED)

G. Fogal Hallett E. Morgan	PAGE NO. OF	RETENTION REQUIREMENTS	
		COPIES FOR	MASTERS FOR
		<input type="checkbox"/> 1 MO.	<input type="checkbox"/> 3 MOS.
		<input type="checkbox"/> 3 MOS.	<input type="checkbox"/> 6 MOS.
		<input type="checkbox"/> 6 MOS.	<input type="checkbox"/> 12 MOS.
		<input type="checkbox"/> MOS.	<input type="checkbox"/> MOS.
		<input type="checkbox"/>	<input type="checkbox"/> DO NOT DESTROY

FINAL REPORT: Task 7 AGCE Feasibility Study

Table of Contents

Section Title	Page
1.0 SUMMARY	1
2.0 BACKGROUND	2
3.0 TASK IMPLEMENTATION	2
3.1 Concepts	2
3.2 Tradeoffs	3
3.2.1 ON-board Storage vs. Telemetry	3
3.2.2 On-board Control vs. POCC Control	7
3.2.3 Experiment Data Recording By POCC vs. GSE at the POCC	8
3.2.4 Stored vs. Realtime Control	9
3.2.5 RAM/ROM/Combination	10
3.2.6 Telemetry and the Rotational Rate Dynamic Range	12
3.3 Preliminary Design- Functional Description	13
3.3.1 Electrical System Overview	13
3.3.2 Temperature Controllers	15
3.3.3 Motor Speed Controllers	17

3.3.4 Other Non-Data System Elements	18
3.3.4.1 Power Supply	18
3.3.4.2 HV Power Supply	19
3.3.4.3 Optics Assembly	19
3.3.5 End-to-End Data System	19
3.3.5.1 Overview	19
3.3.5.2 Data Acquisition	22
3.3.5.3 Ground Support Equipment	30
3.3.5.4 End-to-End Data System Configurations	30
3.4 Preliminary Design - Electrical Subsystem	33
3.4.1 Power Supply	35
3.4.2 Flying Spot Scanner Assembly	35
3.4.3 Turntable Assembly	36
3.4.4 Thermal Assembly	36
3.4.5 High Voltage Power Supply	37
3.4.6 Optics Assembly	37
3.4.7 Operator's Panel	38
3.4.8 On-Board Data System	38
3.4.9 Data Acquisition System	39
3.5 Equipment Recommendations	40

1.0 SUMMARY

This study has shown that the on-board apparatus control of the AGCE facility can be accomplished in an efficient and cost effective manner. A preliminary design, presented here, provides for several thermal control loops, two motor speed control loops, control of the high voltage power supply, data acquisition, data formatting and delivery to Spacelab for telemetering to the Payload Operations Control Center (POCC).

Additionally, the preliminary design includes the Ground Support Equipment (GSE) required to test the apparatus, to develop software and to support mission operation at the POCC.

Considerable simplification of the design was accomplished through a process of questioning the original guidelines. The resulting system is much more flexible than was anticipated, however, the design can be expanded to include any of the features omitted in the simplification process, if that is desired.

The design, as presented here, makes maximum use of program resources by using the test equipment as the support equipment at POCC.

2.0 BACKGROUND

The objective of the AGCE is to study the fluid circulation and thermal properties of a test facility that models the earth's atmosphere. Its predecessor, the Geophysical Fluid Flow Cell Experiment (GFFC), consisted of a test cell controlled by a microprocessor and used a photographic data recording technique. One of the AGCE Task 7 objectives is to provide an electronic recording technique that will be cost effective and actually result in improved data quality.

Task 7 is the study task in which an apparatus control concept is to be developed and shown feasible.

3.0 TASK IMPLEMENTATION

3.1 Concepts

Like its predecessor, the GFFC, AGCE will be microprocessor controlled. Experiment operation can be under the direction of timelines, the Payload Specialist (PS) or the Principle Investigator (PI) at the POCC. GSE will be provided to assist in the integration and testing of the facility in the contractor's domain as well as after delivery to NASA. For maximum utilization of resources and thus cost effectiveness, this equipment will also provide the capability to develop timelines/software and to support operations at the POCC.

3.2 Tradeoffs

3.2.1 ON-board Storage vs. Telemetry

Essentially this trade is one that rests on the PI's need for the data (how immediate is it?), how much data there is involved, the desired level of experiment autonomy, the technologies available to provide the on-board recording function, and the cost effectiveness of the two approaches.

Based on the GFFC method of recording and discussion with the AGCE customer, it appears that there is no immediacy attached to the data, that is, it could be processed totally post-mission.

At the maximum turntable rotation rate, the minimum data requirements would be:

180 degrees rotation	
x 90 degrees scan	
<hr/>	
16,200 pixels	
x 8 bits	
<hr/>	
129,600 bits	
x 3 channels	
<hr/>	
388,800 bits/sec.	
x 72,000 20 hours operation	
<hr/>	
2.8x10 ¹⁰	mission capacity required not including housekeeping data.

As for experiment autonomy, if data is not telemetered, then except for the PS who is in voice contact, the experiment must be

autonomous with respect to the experimenter at POCC. The PS involvement can be a planned aspect of the experiment, but of course, this means that the facility must provide some means of informing the PS of the status of the experiment and a means for him to interact with the experiment as required.

Another form of autonomy that may be desired is with respect to Spacelab/Space Shuttle. While in many instances this may be a worthwhile goal, it certainly is not always cost effective. No assumptions have been made regarding this type of autonomy in study Task 7.

The most viable current technology available for use in this experiment, that offers the storage capacity required, is video tape recording. A cassette recorder that has been ruggedized for airborne applications is available from TEAC Corporation of America. Appendix A contains performance data on this recorder. Addressing the cost effectiveness of the recording approach, these points seem to be the more significant ones:

1. Using a video recorder one would hope to record the raw video data, but the AGCE data is not acquired in a continuous fashion. Actually, three channels of data are acquired simultaneously during 90 degrees of an apparent 360 degree scan for each degree of turntable rotation. In order to make this data appear continuous, two of the channels

would have to be stored so that the recorder could receive three contiguous segments during the inactive portions of the scan. This effect could also be achieved through an interleaved sampling technique. This is not unlike the problem of multiplexing the acquired data into a single downlink telemetry channel. In either case, specially designed hardware will be required and for the purposes of this tradeoff, it is assumed to be equal in complexity and cost.

2. The video recorder is powered by 120VAC at 60Hz which is not available on Spacelab. This would involve vendor modification of the equipment and would increase the experiment complexity by requiring 400Hz power from the EPSP. The appropriate EMI protection requirements of the SLP/2104 would also apply, again increasing the complexity.
3. If no POCC involvement is possible (POCC would have no data if it is recorded on-board), the PS must initiate the proper experiment segment, monitor its progress and interact as necessary, maintain the cassette supply and terminate/restart, as necessary, those experiment scenarios that do not perform as planned. It has been determined elsewhere and given to Task 7 as a requirement that, if the data is recorded on-board, the PS must be able to observe the marker dot movement within the fluid surrounding the

inner sphere in order to determine that experimentation is progressing satisfactorily. This involves provision ,on-board, of a CRT type display. ACPL experience has shown that CRTs are extremely expensive devices to try to flight qualify for use on Spacelab. Other alternatives are to utilize the Spacelab CDMS CRT display or use a plasma display similar to that planned for use on ACPL. These three alternatives were weighed with the following results. The experiment CRT option was eliminated as the most costly and representing the most program risk. The plasma display was judged the most expensive of the remaining two options based on our ACPL experience. The use of the Spacelab display is not without cost, however. It will involve establishing interfaces that would not otherwise exist and a sustained effort over the life of the program to integrate with the Spacelab and other user organizations. The PS will also require some LED numerical displays that indicate the values of the high voltage, the pole and equator temperatures and the turntable rotation rate.

4. In order to downlink telemetry an interface with the Spacelab High Rate Multiplexer (HRM) must be established. Additionally, an adapter module that meets the electrical interface requirements must be designed and used. There is also a cost associated with integration with the customer and the integrating contractor over the life of the program.

WCM
agcefr
05/81

Note that, the telemetering of data does not necessarily imply a presence, during the mission, of PIs or of other mission support personnel at POCC. If control is left on-board with the PS, support may not be required.

It was decided that the on-board recording would be the more costly of the two alternatives as well as the more risky. Telemetering of the experiment data is the recommended approach.

3.2.2 On-board Control vs. POCC Control

Starting with the assumption that control actually resides with the moving dot display, this trade resolves to the question of where the display is to be located, on-board or at POCC.

In addition to the problems with locating it on-board that were discussed in the above section, the issue of PS training comes into the picture. Does one assume he is trained in atmospheric physics? If not, he may need support from the PI which implies a program presence at POCC.

The only additional POCC involvement necessitated by a program presence, would be to provide a data spigot to equipment, supplied by the program, that will support operations. This is much less than will be done for other Spacelab payloads.

Assuming that the functions performed by the equipment at POCC would be limited to displaying the moving dots and the normal

housekeeping data at a rather leisurely pace (3 or 4 seconds between updates), the same equipment that is used for integration and test could be used at POCC.

Again, it is felt that the on-board display represents considerable cost and risk and the reduced flexibility resulting from control of the experiment by an untrained (in atmospheric) PS forces the conclusion that control must be exercised at POCC.

3.2.3 Experiment Data Recording By POCC vs. GSE at the POCC

Now that previous trades have established that the experiment data will be telemetered to the POCC and that the project will have a presence there, this trade consists of deciding if the data recording capability should reside in the GSE, for if it did the POCC involvement could be reduced, thus reducing costs.

The contractors responsibility is understood to be to deliver a facility that will support experimentation without the obligation to deliver the ground test experiment data in some predefined format on a preselected media. This is important because it means that beyond verification that data does exit the facility in the designed format, there is no requirement for recording of data. As for verification of the telemetry output, this can be accomplished in a very modest recording facility. The question then becomes, should a recording capability be provided in the GSE to relieve POCC of this task?

WCM
agcefr
05/81

In view of the fact that there is no need for extreme haste in the delivery of the data to the PIs, the recommendation is that POCC perform the recording function. If special processing is required on the resulting tapes it can be performed by the PI or if need be, by GE, but in no instance is the GSE currently required to support that activity.

As for the GSE recording capability, for the purposes of this study it will be assumed to be the minimum possible, however, this will not be a sufficient capability if the contractor is responsible for providing experiment data to the PI during ground testing.

3.2.4 Stored vs. Realtime Control

It was a "given" to Task 7 that the PS be able to command values for the inner and outer sphere's pole and equatorial temperatures, the high voltage and the turntable rotation rate.

GFFC utilized stored control in the form of experiment timelines and provided an operator's panel from which timelines could be initiated and experiment parameters monitored. Since there are only seven parameters that need to be controlled, why must they be controlled in a stored fashion? Given that they must be, why must a subset be controlled in a manual, realtime fashion?

Inquiries led to the conclusion that even at the high rotation rates the equivalent to a GFFC segment would take 20 to 30

minutes. Presumably, at the low rates they would take even longer.

One must ask, why not give the PI (via voice link to the PS) realtime control of the seven experiment parameters and omit the stored timelines altogether? The PI has all the data displayed, in near realtime, in front of him and the PS to act on his behalf in the Spacelab.

Because this approach is the simplest and most cost effective and because of customer encouragement to do so, the recommended approach makes use of realtime control. In actual implementation of other elements of the apparatus control, there will still be an issue of read only memory (ROM) and random access memory (RAM) and execution from each at various phases of the program. These issues will be addressed in the following section of the report. It is still possible, with little impact, to opt for stored control or some reasonable compromise between the two extremes.

3.2.5 RAM/ROM/Combination

An approach that allowed functions that would be stored in ROM operationally, to be executed from RAM during ground test and development, was an explicit requirement of Task 7. This feature should still be of primary concern even if stored control is replaced with realtime manual control, because control functions

still remain that demand that kind of flexibility. For example, all of the closed loop temperature controls will need that flexibility in the software development and ground test phases of the program.

This trade concerns how this is to be accomplished. Several possibilities exist:

1. ROM in the apparatus and RAM in the test equipment. The microcomputer would be forced to execute from the test equipment when it is plugged in. Problems may arise due to long wire lengths involved unless special precautions are taken.
2. ROM in the apparatus and RAM on the front panel connected to the test equipment. Operation is the same as described above but the wire problem only exists in the test equipment end. This approach is similar to GFFC's.
3. ROM and RAM are located in the apparatus. Both memory types are carried in the apparatus and the microcomputer executes out of the ROM when the test equipment is not plugged in. This method will only be practical for relatively small amounts of memory.

Because of the small amount of memory involved, even including the timeline storage, it is recommended that the RAM board be included in the experiment hardware. The RAM can be loaded by the test equipment over the serial interface. The microcomputer will execute from either the RAM or ROM as commanded by the test equipment when it is plugged in, otherwise it defaults to the ROM. When satisfactory results have been obtained from the software stored in RAM, it can be downloaded to a file within the test equipment which is in turn used to "burn" the ROM memory. This feature can be provided at almost no cost with the approach

described here.

3.2.6 Telemetry and the Rotational Rate Dynamic Range

With the turntable rotational dynamic range required for AGCE, a problem arises with respect to telemetry downlink rates. If one assumes that the data is downlinked at a fixed rate, equal to the rate at which it is acquired at the highest rotation rate, then at the lowest rotation rate, the fill data outnumber the valid data by a factor of 125 to 1.

The alternatives examined here were, a fixed downlink rate equal to the highest acquisition rate encountered, a variable downlink rate within the range from 4,128 to 518,400 bits per second and temporary on-board storage for smoothing.

The maximum acquisition rate is 518,400 bits/sec. If the downlink rate was only 1 kbits/sec slower, in a typical experiment scenario of 20 to 30 minutes, 1.2 to 1.8 megabits will have to be stored until it can be downlinked. This large a smoothing buffer is not practical to offset 1Kbits/sec additional bandwidth. Smoothing buffers were eliminated as viable solutions.

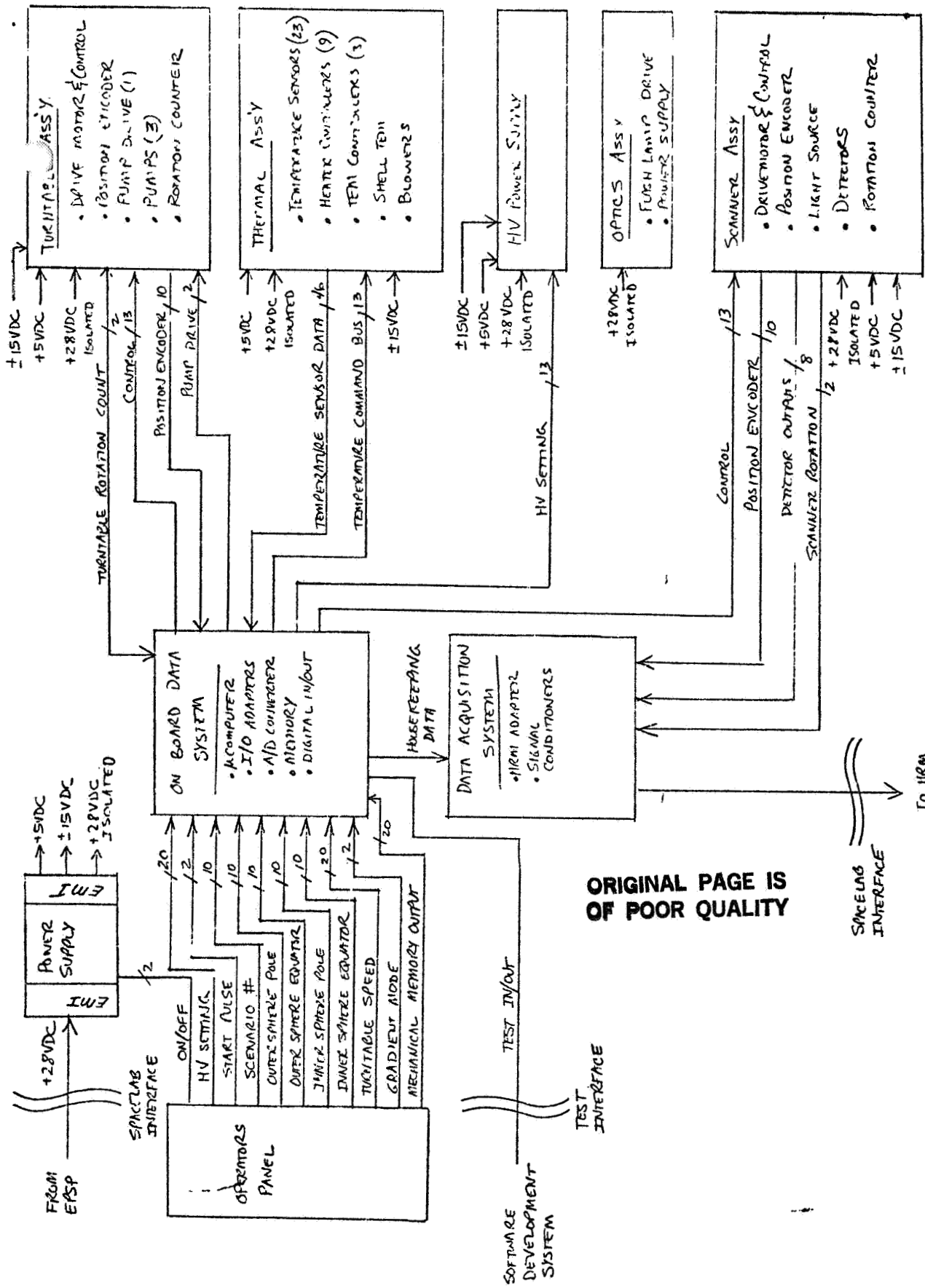
The variable rate telemetry does not appear to be at all practical with the information available concerning the types of experiment scenarios to be used during the mission.

A downlink rate, fixed at the maximum acquisition rate, is recommended as a result of this tradeoff. Other methods could be used but not without additional cost. This method does, however, introduce additional complexities in generating the fill data required at the various rotational rates below the maximum. The proposed solution will be discussed in the appropriate design description section of the report.

3.3 Preliminary Design - Functional Description

3.3.1 Electrical System Overview

Figure 3.3-1 shows a functional block diagram of the AGCE Electrical System. This system will be described functionally within this section. The overall, end-to-end data flow will be described in a discussion of the data system. Other portions/functions of the system will be described individually.



ORIGINAL PAGE IS OF POOR QUALITY

Figure 3.3-1 AGCE Electrical System Functional Block Diagram

3.3.2 Temperature Controllers

The AGCE contains nine heater control loops and three TEM control loops. Philosophically, it is preferred that the control loops be autonomous with respect to the on-board data system, except that it is through this system that they receive the control setting. In the case of the heater based temperature controllers this is possible, but in the case of the TEM based loops, it may not be possible because of the non-linearity that occurs at the crossover point from heating to cooling operation. However, if continuous control can be exercised by electronics with only the crossover "work-around" under the control of the computer, the philosophy remains reasonably intact. This is the recommended approach. Figure 3.3-2 depicts the computers relationship to the temperature controllers.

The computers sole function in the temperature control task is to receive the setting commands from the Operator's Panel and pass them on to the appropriate controller. As for telemetry, the sensor outputs are conditioned appropriately and acquired by the microcomputer as part of the telemetry function.

It should be noted that the calibration of sensor data could be factored into the command side if it is determined to be necessary. In fact, that is the recommended "work-around" procedure for the TEM controllers. A cross-over is anticipated

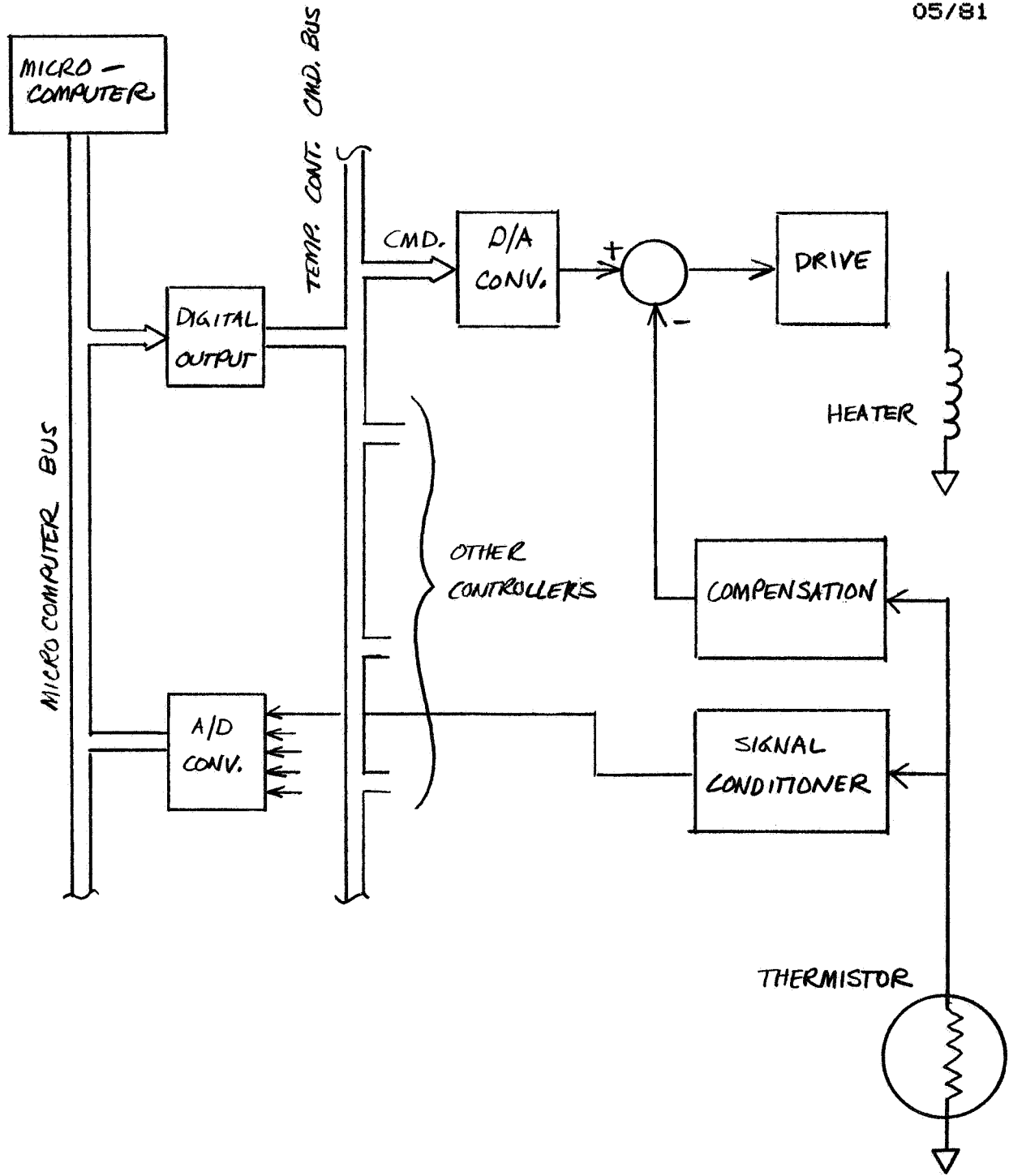


Figure 3.3-2 Typical Temperature Controller Data Bus

and movement through the cross-over region controlled via commanding the necessary settings.

Other miscellaneous elements within the Thermal Assembly require mentioning; one TEM operates whenever the power is applied, open loop, on the protective cover and so presents no control task. Assorted blowers also operate as power is applied and so are just wired in.

3.3.3 Motor Speed Controllers

There are two similar speed control loops that are crucial to the operation of this facility. They are the turntable motor and the scanner motor. As in the case of the temperature controllers, speed control will be accomplished by the electronics. The scanner motor will run at a rate derived from a precision oscillator that will not be alterable, so there is no microcomputer involvement on the control side. The shaft of this motor must be encoded in one degree increments and must also deliver an electronic pulse for every degree of turntable rotation. These signals are used to time the telemetry acquisition function and by the microcomputer to maintain a scan counter in software. The scanner apparently rotates 360 degrees, but not actually. There is 360 degrees of rotation of the motor shaft but only 90 degrees of active scan.

The turntable motor is driven at various rates between 3.1416

radians and .025 radians per second. The rate is not continuously variable; there must be an integer number of complete scans per degree of turntable rotation. Further, to simplify ground processing, it is recommended that there be an even integer number..... Additionally, each of these discrete rates, within the range cited, are also derived from the precision oscillator. Picture a countdown from the scanner motor rate, whose length is determined by the turntable rotation rate selected by the PS. The shaft of this motor will also have to be encoded to yield position in one degree increments and to deliver a pulse for each degree of rotation. These signals are also used by the telemetry acquisition function and by the microcomputer to maintain a rotation counter in software.

Other miscellaneous elements within the Turntable and Scanner Assemblies require mentioning; there is one pump that is powered for a short time after power application that is therefore under control of the microcomputer, there are two other pumps that are powered when AGCE power is applied, there is a light source and optical detectors that are also powered when the AGCE is powered.

3.3.4 Other Non-Data System Elements

3.3.4.1 Power Supply

The Power Supply utilizes a fairly standard approach; a DC to DC converter which will provide the ground isolation required in

SLP/2104 and convert from 28VDC to +5, +15 and -15 VDC. It is expected that the primary input current will not exceed 20 amps which is well within one of the EPSP DC outputs. The appropriate suppression will be provided to allow the AGCE to meet the EMI requirements of SLP/2104.

3.3.4.2 HV Power Supply

The HV Power Supply steps up its input voltage to correspond to some commanded level. This command is entered from the Operator's Panel by the PS and is passed to the HV Power Supply by the microcomputer. Range of settings are described in the HV Power Supply section of the final report.

3.3.4.3 Optics Assembly

This assembly free-runs, that is, when power is applied the ultraviolet flash lamp flashes at a predetermined rate, position and duration. The assembly contains a flash lamp, a power supply and the necessary timing and positioning elements.

3.3.5 End-to-End Data System

3.3.5.1 Overview

The on-board data system consists of the elements shown in Figure 3.3-3. This, in conjunction with Spacelab/Space Shuttle, the communication links, POCC and the AGCE GSE makes up the total end-to-end data system depicted in Figure 3.3-4. This section

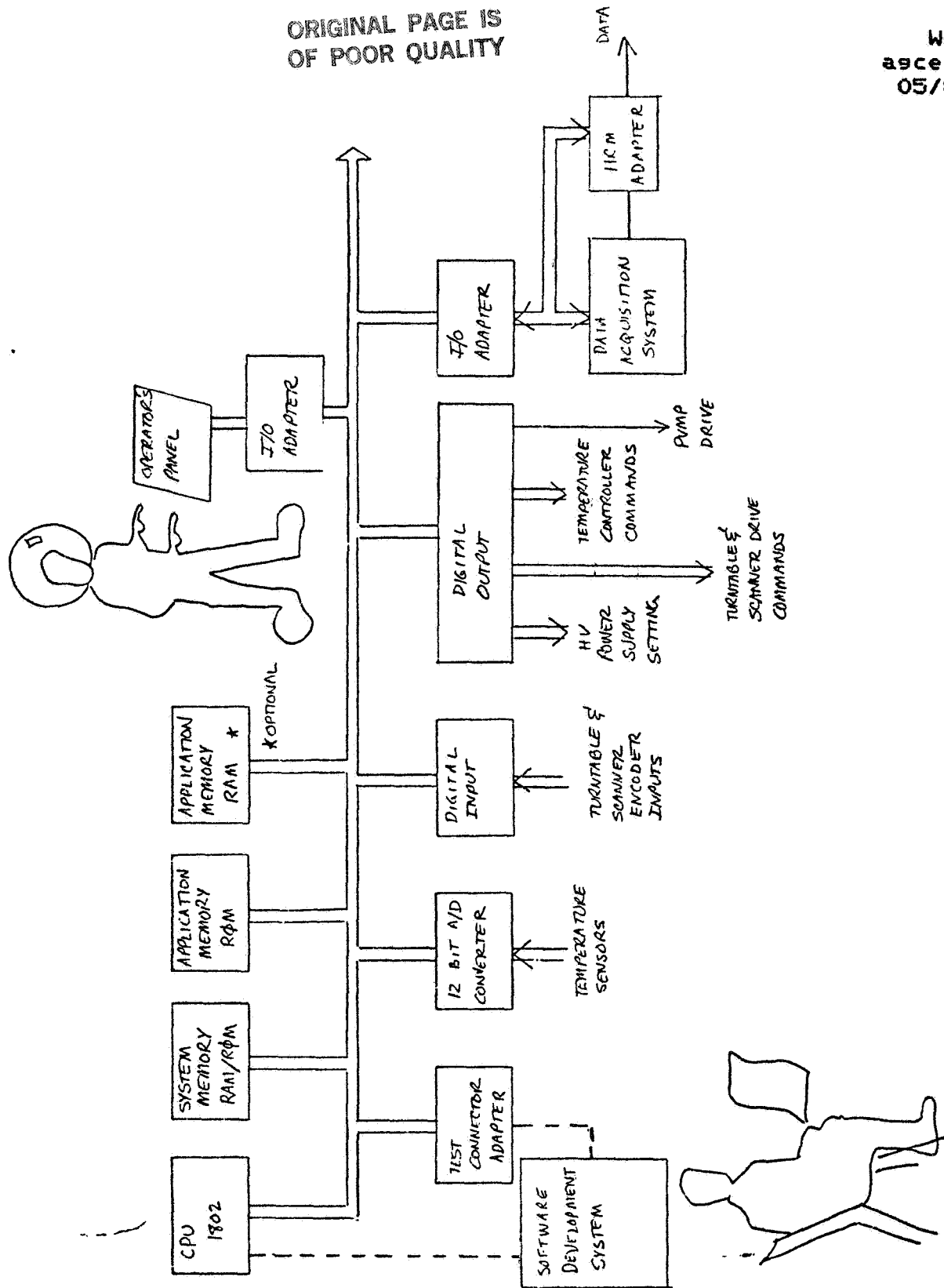


Figure 3.3-3 On-Board Data System Block Diagram

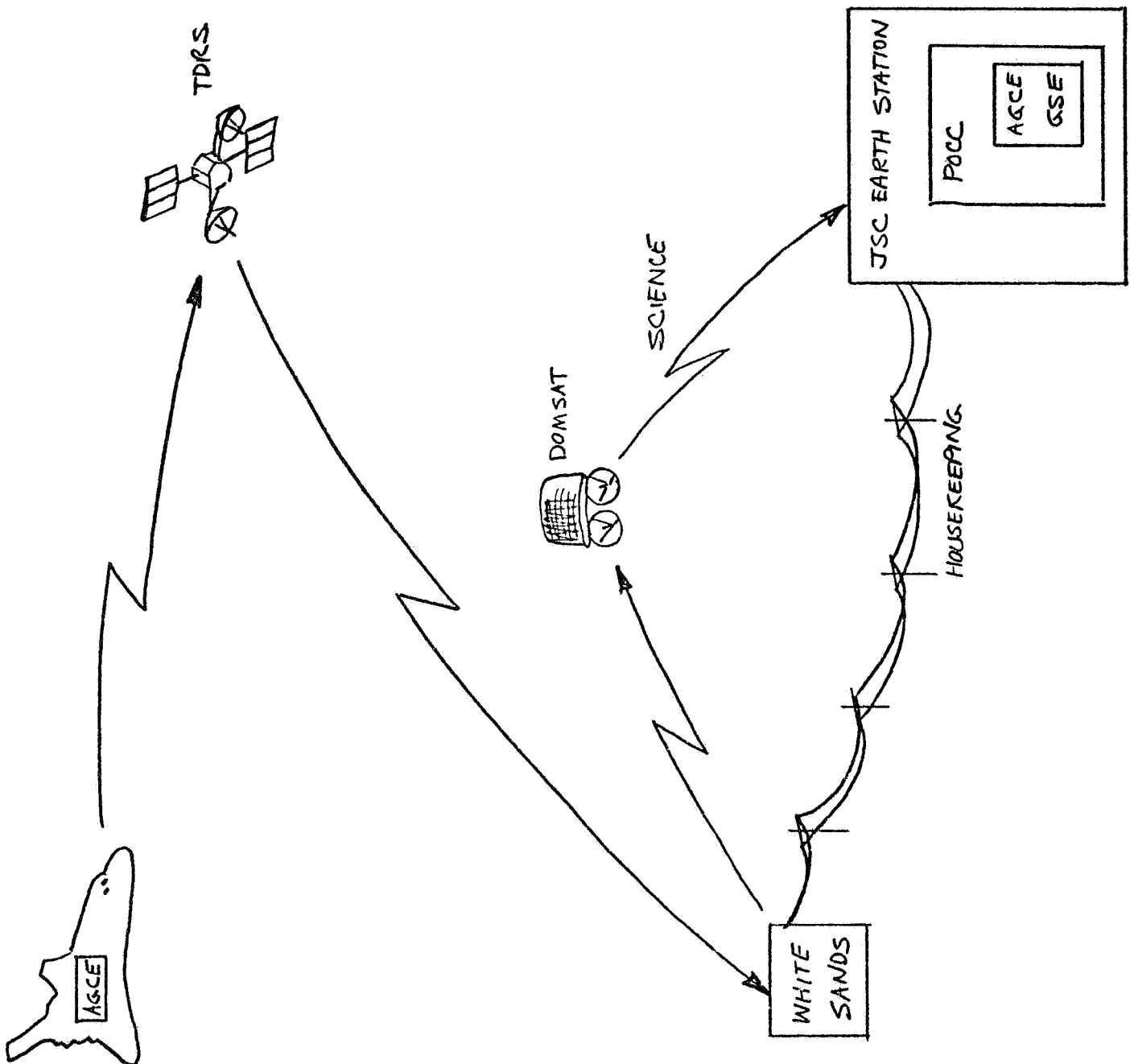


Figure 3.3-4 End-to-End Data System

will discuss the data flow and the various configurations of this system, but first, think of the on-board system as having three mission tasks:

To accept and interpret the experiment control parameters as entered by the PS.

To provide control information to those elements under control of the microcomputer.

To take measurements and acquire housekeeping data to be included in the downlink telemetry.

Experiment control is accomplished by the PI via voice link to the PS, who enters the experiment parameters via the Operator's Panel shown in Figure 3.3-5. The experiment data is provided to the Spacelab HRM and transmitted to the earth where it goes to POCC. At POCC, the data is recorded for post mission use, A portion of the data is routed to the AGCE equipment at POCC, where displays are provided for use by the PI, who is in voice contact with the PS, thus completing the loop.

3.3.5.2 Data Acquisition

There are two different data sources within AGCE. The housekeeping data is taken from virtually every subsystem of AGCE and can be used to determine the status and health of the facility. This is a very small amount of data and changes so infrequently that it can be collected by the microcomputer for transmission. However, the high speed video data is generated so fast that the microcomputer could not keep up, so special data acquisition hardware is recommended. A possible data profile is

ORIGINAL PAGE IS
OF POOR QUALITY

OUTER SPHERE TEMPERATURE
EQUATOR

POLE

24 °C T

35 °C T

TURITABLE SPEED
REV./MIN.

25.68 T

ON/OFF

INNER SPHERE TEMPERATURE
EQUATOR

POLE

24 °C T

24 °C T

HV SELECT

25.00 KV T

LPB

GRADIENT
MODE

UNI FORM
MATCH

LPB

SCENARIO

17 T

FAULT



RUN

LPB

LPB = LIGHTED PUSH BUTTON
T = THUMBWHEEL

Figure 3.3-5 AGCE Operator's Panel

shown in Figure 3.3-6. As can be seen, at the maximum turntable rotation rates, 330 degrees of rotation data is downlinked in approximately 2 seconds. There is about 15 degrees worth of time and storage devoted to housekeeping data and another 15 degrees worth for fill data that can be used to simplify the ground processing algorithms. As the turntable rotation rates are decreased, more scans per degree rotation are taken. This is a nice fill data generation scheme because each of those scans, after the first, is redundant and the information can be discarded on the ground. At the maximum rotation rate, there is one scan per degree of turntable rotation; at the minimum rotation rate there are 126 scans per degree rotation.

Figure 3.3-7 is a block diagram of the acquisition hardware. It can be explained with the help of Figure 3.3-8 which depicts the data acquisition time profile.

Working back, from the output to the HRM, there is housekeeping data, fill data and scanner data input to the multiplexer. The data selection is tied to the position of the turntable shaft as suggested in Figure 3.3-6. The scanner data is made up of four channels called the preamble and channels A, B and C. Channels A and B are identical in function and hardware; each is the difference of two detectors, amplified and converted to a digital quantity for each degree of scan. Channel C is the differentiated sum of the four detectors that yields the dot

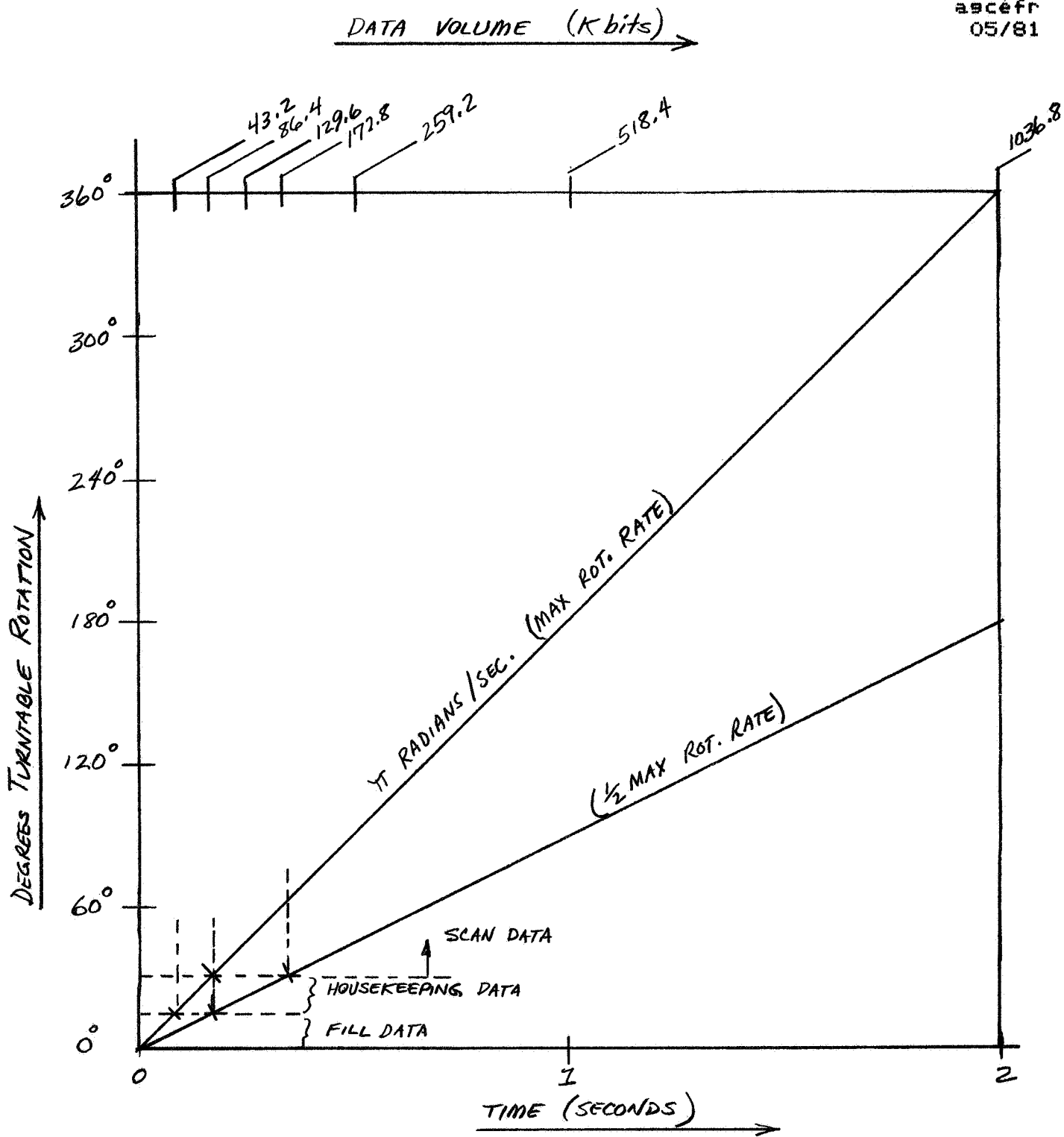


Figure 3.3-6 AGCE Telemetry Data Profile

ORIGINAL PAGE IS
OF POOR QUALITY

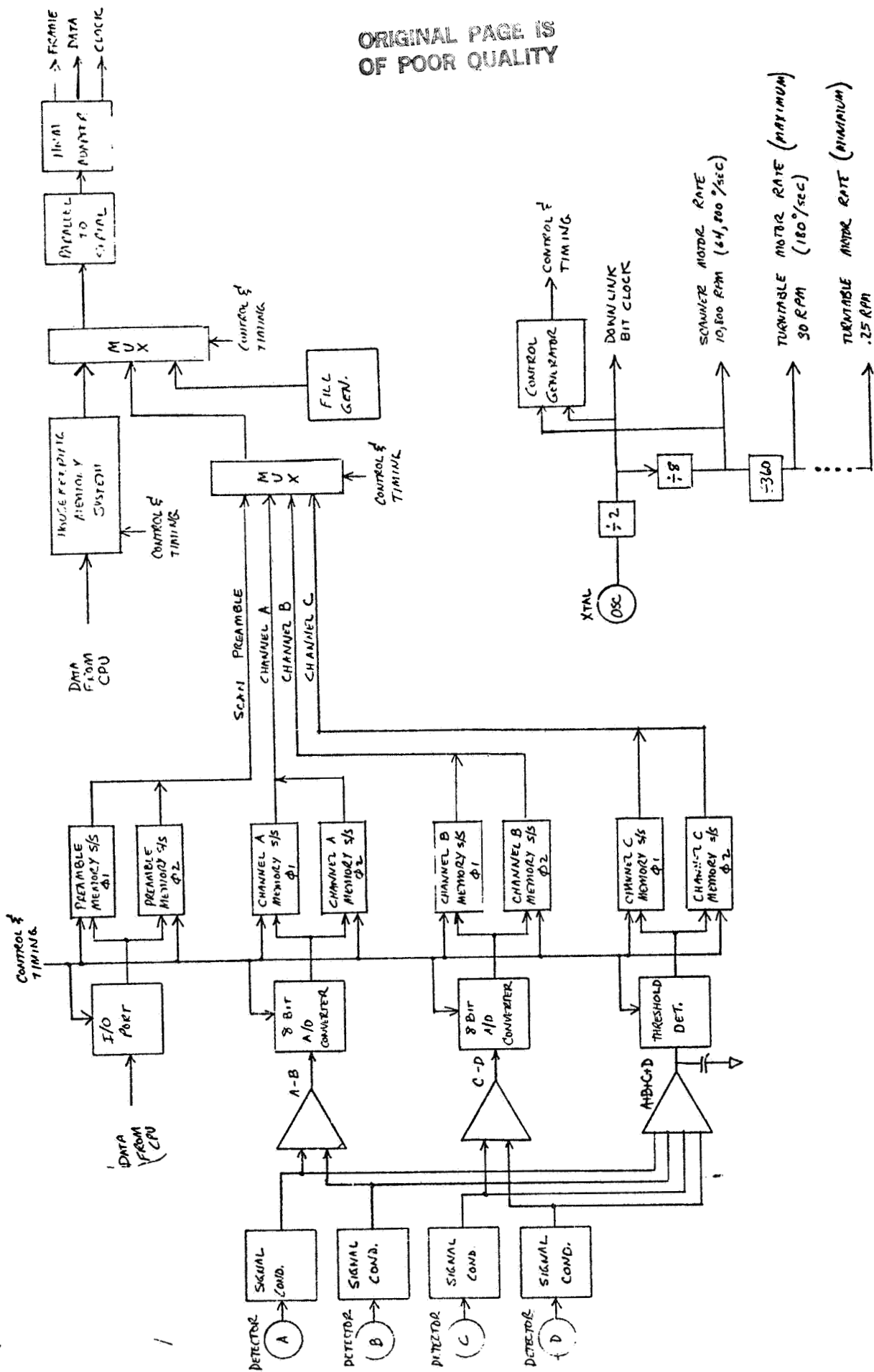


Figure 3.3-7 AGCE Data Acquisition System Block Diagram

ORIGINAL PAGE IS
OF POOR QUALITY

WCM
ascefr
05/81

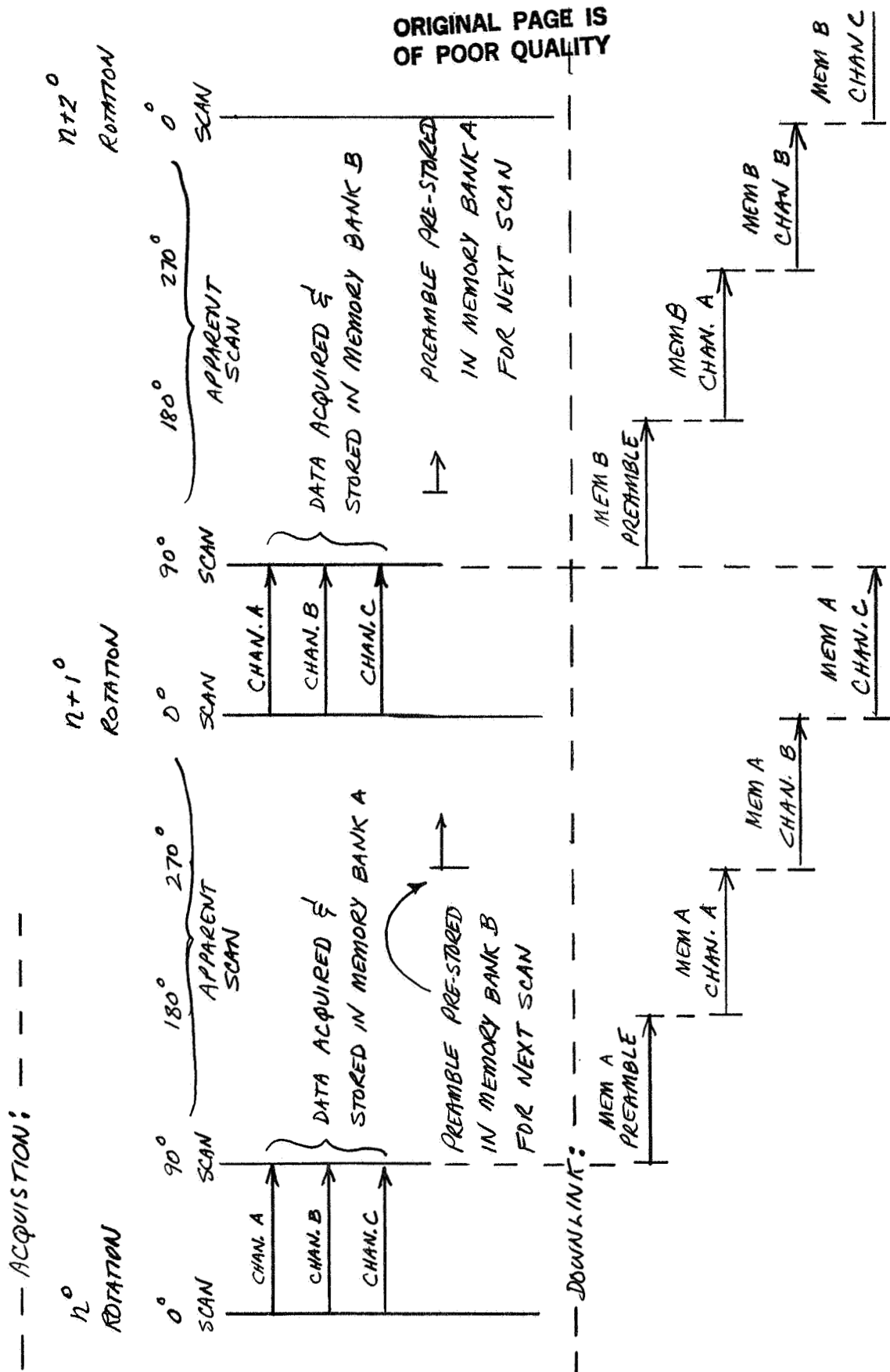


Figure 3.3-8 Acquisition Profile

positions. As shown in Figure 3.3-8, channels A, B and C are acquired simultaneously for 90 degrees of the apparent 360 degrees of scan and placed in one bank of memories. At the conclusion of this active scan period, that same data is downlinked over the next 360 degrees of apparent scan. During this time, another active scan will occur and that data will be placed in the other bank of memories. During the 270 degrees of non-active scan, within the apparent 360 degrees, the micro computer will fill up the appropriate preamble memory with either the major or minor frame headers, whatever data is deemed necessary to help in the ground processing and the remaining fill necessary. Basically, three channels are acquired simultaneously, the fourth almost, and put in one bank of memories. While these memories are emptied, one at a time (preamble, then A, B and C), data from the next scan is filling the other memory bank. This arrangement is often called a "swinging door" or "ping-pong" memory.

A possible telemetry format is shown in Figure 3.3-9. As the rotation rate is decreased the effect is to add more minor frames of redundant data.

ORIGINAL PAGE IS
OF POOR QUALITY

WCM
ascefr
05/81

MAJOR FRAME DETAIL (MAX ROTATION RATE)

MINOR
FRAME #

0	S	F	I	MD	FILL DATA
1	S	F	M	R	FILL DATA
2	S	F	R	R	FILL DATA
3	S	F	S	SO	FILL DATA
4-6	S	F			FILL DATA
7	FILL DATA				HOUSE KEEPING DATA
8-14	HOUSE KEEPING DATA				
15-179	SCAN DATA				

S = SYNC (3 BYTES)
 F = FRAME COUNT
 I = EXPERIMENT ID
 MD = EXP. MODE
 M = MISSION ID
 R = ROTATION #
 S = SCAN #
 SO = SCENARIO

BOLD OUTLINE IS NOT
TO SCALE. MINOR FRAMES
0-3 ARE THE MAJOR
FRAMEHEADER.

SCAN DATA DETAIL

m	SCAN n DATA				SCAN n+1 DATA	
m+1	SCAN n+2 DATA				SCAN n+3 DATA	
m+2	S	F	FILL	DATA	DATA	DATA
	PREAMBLE			CHAN A	CHAN B	CHAN C

Figure 3.3-9 Possible AGCE Telemetry Format

3.3.5.3 Ground Support Equipment

The GSE is multifunctional in that it is designed to service three distinct phases of the program;

Software development.

Ground testing for verification of equipment function.

Operations support at POCC.

Figure 3.3-10 provides the GSE block diagram. It consists of a stand-alone software development system provided by the flight microcomputer vendor, Spacelab resource simulators and a minicomputer based data processing system. The equipment recommended is the Digital Equipment Corp.'s PDP-11.

A video terminal acts as the operator's console and will be manned by either a Test Conductor (TC) or a PI depending on what phase of the program is being supported at the time.

The Spacelab resources that are simulated in the ground test environment are the HRM and the primary power supply. At POCC, the HRM simulator will be bypassed to receive data directly. A specially designed piece of hardware will provide the synchronization and decommutation functions in either case.

3.3.5.4 End-to-End Data System Configurations

Figure 3.3-11 shows the ground test/software development configuration. The Operator's Panel is manned by a Test Man (TM)

ORIGINAL PAGE IS
OF POOR QUALITY

WCM
ascefr
05/81

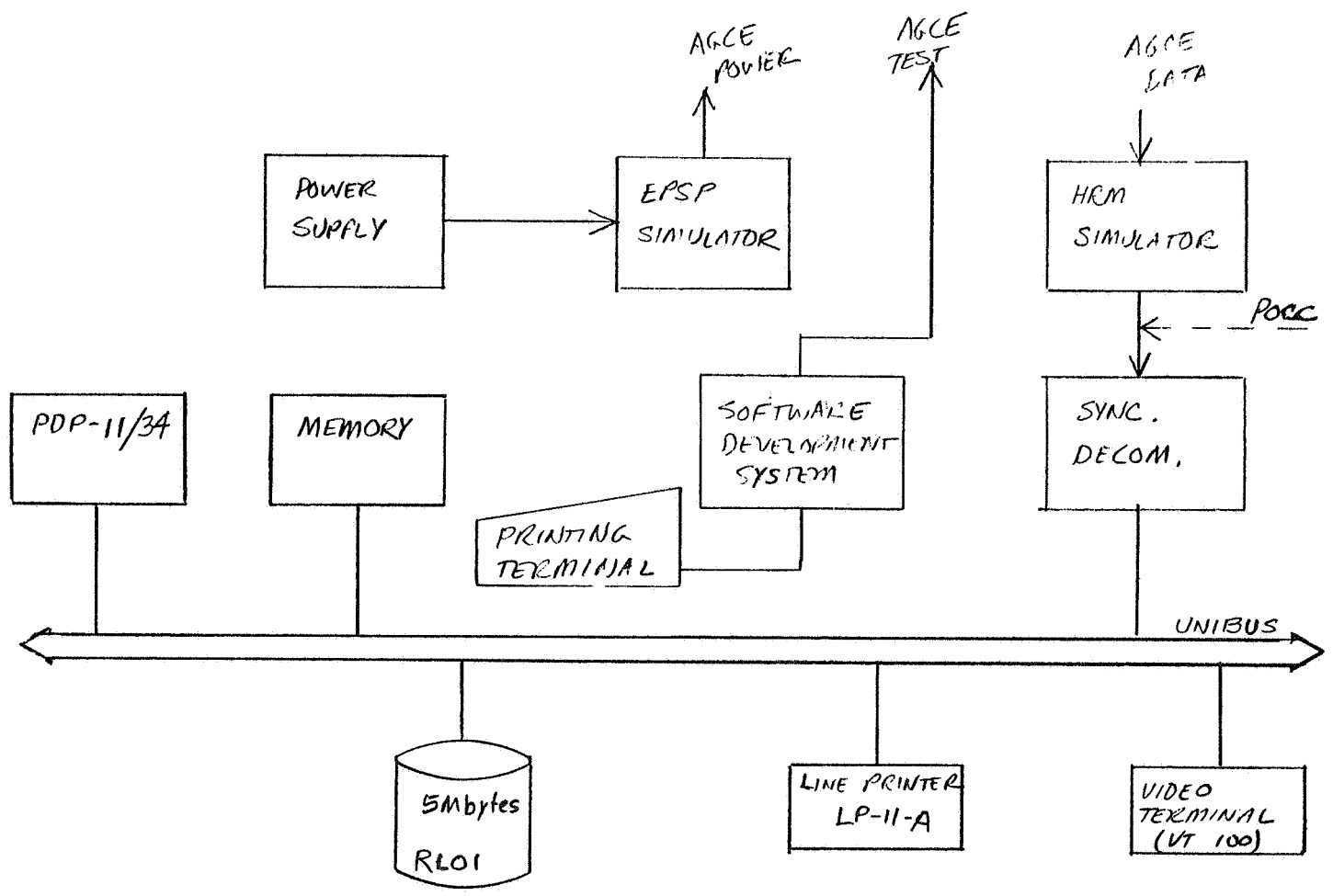


Figure 3.3-10 AGCE Ground Support Equipment Block Diagram

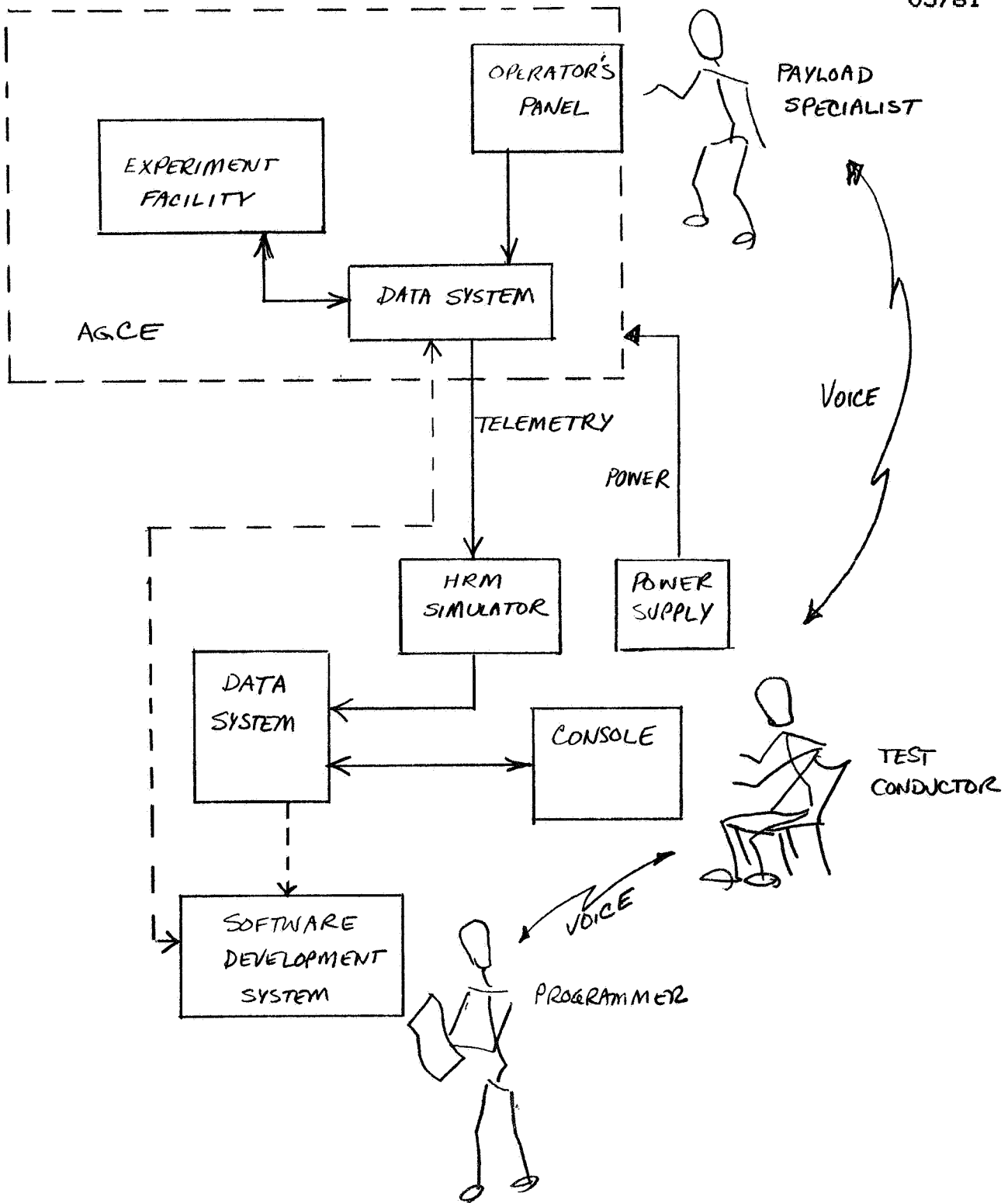


Figure 3.3-11 Ground Test/Software Development Configuration

who is under the direction of the TC who mans the GSE console. Operational scenarios can be requested by the TC, by voice, which are input by the TM through the AGCE panel. Results are monitored by the GSE and displayed at the GSE console. During software development, the additional dotted lines apply and the SW console is manned by a Software Engineer(SE) who determines what functions are requested by the TC. It should be noted that, if a cross assembler exists for the on-board microcomputer that is resident on DEC equipment, then the software development system could probably be eliminated and the remaining GSE could provide that function. The equipment is so inexpensive that it would not pay to write the cross assembler.

Figure 3.3-12 shows the operational support configuration. In this configuration the GSE extracts the housekeeping data and the dot movement data and displays both to the PI who is manning the GSE console. He is in voice communication with the PS who is interacting with the AGCE panel in Spacelab.

3.4 Preliminary Design - Electrical Subsystem

The functional block diagram of the recommended design of the electrical subsystem is shown in Figure 3.3-1. It is to this diagram that this section is written.

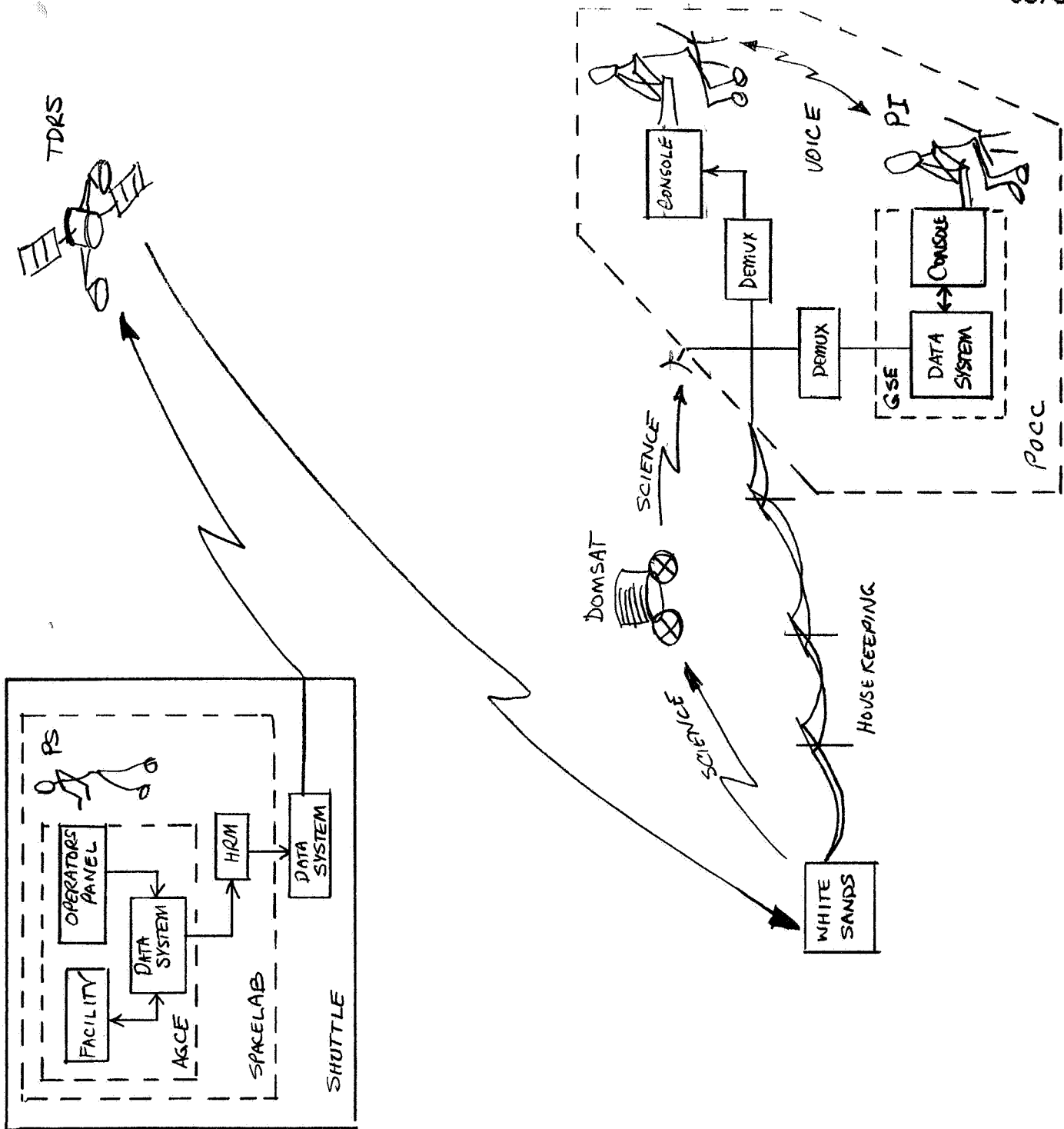


Figure 3.3-12 Operational Support Configuration

3.4.1 Power Supply

The AGCE input power requirements are estimated to be approximately 520 watts. At 28VDC input, the current requirements would be in the order of 20Amps. This is well within the capacity of an EPSP. Of course the power supply must provide the three way ground isolation required in SLP/2104, as well as supply to AGCE the various voltages required.

3.4.2 Flying Spot Scanner Assembly

The Flying Spot Scanner Assembly contains the scanner drive motor and its associated control, a shaft position encoder, a rotational counter, the light source and the optical detectors.

Input power requirements are +28VDC Isolated, +5VDC and +/-15VDC. Signal outputs of this assembly are the detector outputs, the scanner rotation count and the incremental position encoder. All of these signal outputs are utilized in the Data Acquisition System.

3.4.3 Turntable Assembly

The Turntable Assembly electronics consists of the drive motor and its associated control, a shaft position encoder and a rotation counter, three pumps and a pump drive module that controls the duration of operation of one of the pumps.

Input power requirements are +28VDC Isolated, +5VDC and +/-15VDC. Inputs to the assembly are a pump drive pulse from the microcomputer and the turntable rotation rate command from the microcomputer. Outputs are the rotation count and shaft position, both to the microcomputer.

3.4.4 Thermal Assembly

The Thermal Assembly electronics consists of 25 (23 + 2 spare) thermistor temperature sensors and their associated signal conditioning circuits, 9 heater controllers and 3 TEM controllers.

Input power requirements are +28VDC, +5VDC and +/-15VDC. Signal inputs to this assembly are the temperature commands to the controllers. These come from the microcomputer and are conveyed over a 12 bit data bus. Signal outputs of this assembly are the outputs of the analog signal conditioners that receive the thermistor inputs. These outputs enter the microcomputer analog front-end where they are converted to digital quantities.

3.4.5 High Voltage Power Supply

The High Voltage Power Supply is described under another task elsewhere, the only purpose in discussing it here is to identify a control input that is provided by the microcomputer in the form of a voltage setting.

3.4.6 Optics Assembly

The Optics Assembly electronics consists of a flash lamp power supply and a flash lamp timer.

Input power requirements are +28VDC Isolated, +5VDC and +/-15VDC. There are no control inputs since the UV lamp flashes at a fixed rate once power is applied.

3.4.7 Operator's Panel

The Operator's Panel electronics consist of 18 ten position decimal switches with BCD outputs, 3 lighted push button switches, one indicator light, a microcomputer adapter in the form of a digital input multiplexer I/O controller and a test connector input.

Input power requirements are +28VDC Isolated, +5VDC and +/-15VDC. Other inputs to this function are on the test connector that connects the GSE. Outputs from this function all go to the microcomputer and are settings of the experiment variables entered by the operator.

3.4.8 On-Board Data System

The On-Board Data System consists of a microcomputer based on the 1802 microprocessor, RAM and ROM memory, digital input and output modules, 12 bit a/d converters and interfaces to the control panel and the data acquisition system.

Input power requirements are +5VDC and +/-15VDC. Other inputs are from the Operator's Panel, Turntable, HV Power Supply, Optics, Scanner and Data Acquisition assemblies. These inputs are primarily sensor data. Outputs are directed at mainly the Turntable, Scanner and Thermal assemblies and consist of commands for rates and temperatures.

On-board memories are estimated to be 1k RAM and 2k ROM. Another 2k of RAM, that is used in the ground test configuration, will be flown but will not contain useful code.

An estimated 3K lines of code (software) will be required to manage the AGCE facility.

3.4.9 Data Acquisition System

The Data Acquisition System consists of three analog front-ends for conditioning analog data, two 8 bit a/d converters, one threshold detector, one computer I/O port, four pairs of "swinging door" memories, the HRM adapter, two byte wide multiplexers, a fill generator and the scanner and turntable motors count down string.

Input power requirements are +5VDC and +/-15VDC. Signal inputs are the four optical detector outputs and the housekeeping data from the microcomputer. Output is to the Spacelab HRM in the form of a serial data stream.

WCM
agcefr
05/81

3.5 Equipment Recommendations

Equipment recommendations are made for the on-board microcomputer system and for the GSE in Tables 3.4-1 and 3.4-2 respectively.

Appendix B contains information on the recommended flight hardware. It is assumed that, as in other Spacelab payloads, commercial or near-commercial quality hardware is useable and that only minor modifications, if any, will be required to make it flight worthy.

FUNCTION	RCA TYPE
MICROCOMPUTER	CDP18S602
SYSTEM MEMORY	
ROM	CDP18S625
RAM	CDP18S620
DIGITAL OUTPUT	CDP18S660
DIGITAL INPUT	CDP18S660
A/D CONVERTER	CDP18S643
CONSOLE	CDP18S640
I/O TEST ADAPTER	CDP18S659

TABLE 3.5-1 ON-BOARD MICROCOMPUTER RECOMMENDATIONS

FUNCTION	DEC TYPE
COMPUTER	PDP 11/34
MEMORY	128 KB MOS
DISK	RL01
LINE PRINTER	LP11A
VIDEO TERMINAL	VT100
PRINTING TERMINAL	LA36
OPERATING SYSTEM	RT-11

	RCA TYPE

SOFTWARE DEVELOPMENT SYSTEM	CDP18007 DEV. SYSTEM
	CDP18S030 MICROMONITOR
	CDP18S831 MICRO OS
	CDP18S840 PROM BURNER

TABLE 3.5-2 GSE EQUIPMENT RECOMMENDATIONS

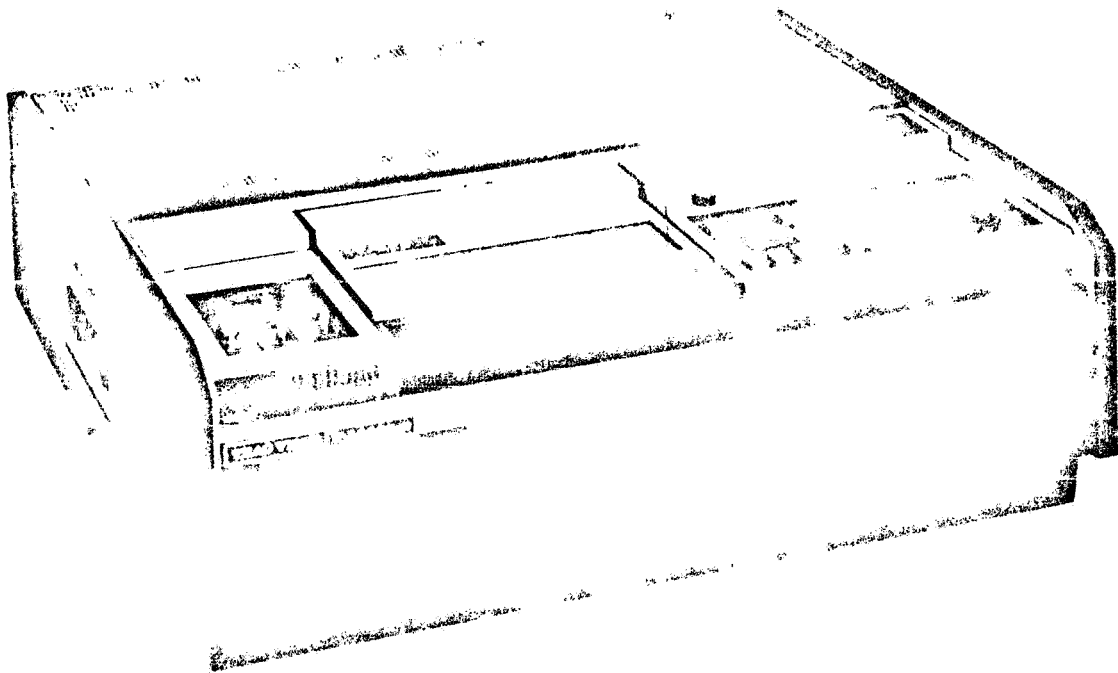
48

WCM
agcefr
05/81

APPENDIX A

THE A

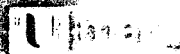
ORIGINAL PAGE IS
OF POOR QUALITY



Video-Analysis

CASSETTE RECORDER/REPRODUCER

V-4200C-N



ORIGINAL PAGE IS
OF POOR QUALITY

TEAC Airborne Video Tape Recording (AVTR)TM

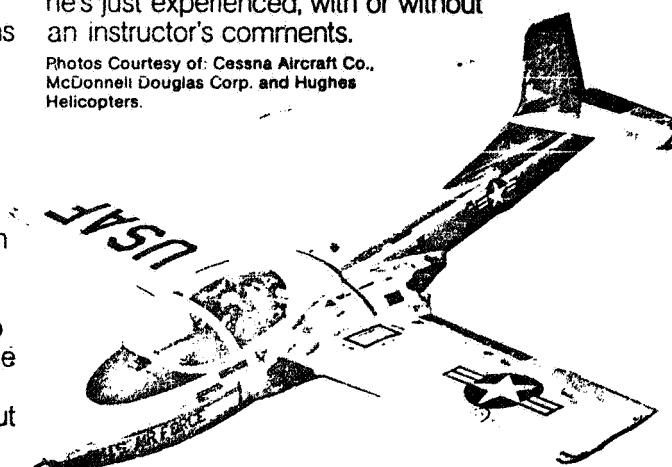
Training Immediate reinforcement and correction is an important factor in the learning process and is well known by educators. "I won't make that mistake again" is easy to say but does the erring student clearly recall the conditions which lead up to the error? Was proper performance the result of a newly acquired skill or of a sequence of rote-memory steps, soon to be forgotten unless immediately reinforced?

Videotape evaluation of student performance in the classroom has again proven the benefits of immediate feedback. More recent experience in the USAF's Tactical Air Command has added an extra dimension to that technique by recording pilot performance during training missions. One experienced pilot commented that he "learned more about the use of an F-15 System observing and debriefing with the VTR during the test period than (he) had in (his) previous 250 hours in the F-15." The VTR he used was TEAC's Airborne Video Tape Recorder (AVTR).

Typically, a student pilot (at any level) can

use the AVTR to record flight display data and externally observed conditions. Immediately upon landing he reviews the flight he's just experienced, with or without an instructor's comments.

Photos Courtesy of: Cessna Aircraft Co.,
McDonnell Douglas Corp. and Hughes
Helicopters.



Debriefing Visual information almost overwhelms the pilot or operator during a mission. What he needs is a "video note-book" to bring back the information to his debriefings. Here the AVTR can make a valuable contribution to mission effectiveness.

Operation and reconnaissance debriefings can now be performed with vivid video display rather than reliance upon man's meager memory. Whatever the crewmember saw during the mission can be reviewed by others immediately during debriefing. Often things which he didn't see are there to observe as well.

With such heavy reliance upon electro-optical sensors and displays in today's aircraft

systems, debriefing for maintenance can be a time consuming and often ineffective procedure. Visionic systems recordings during malfunctions provide an ideal troubleshooting tool, especially for those pesky problems that don't occur again until the next mission.



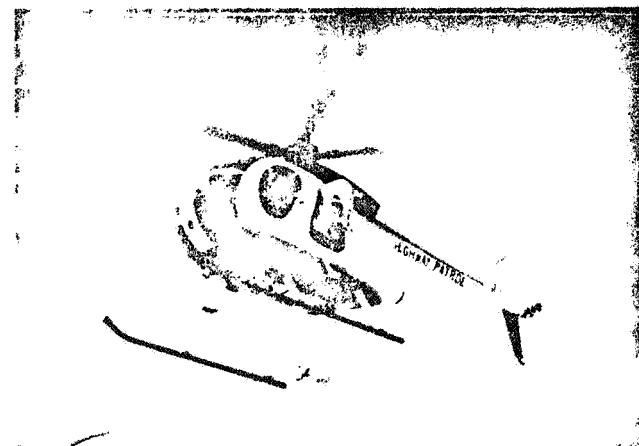
Reconnaissance and Surveillance

Intelligence data—the facts displayed however briefly to a pilot or operator—can now be economically recorded as they appear during a mission. This means that the analysts can quickly review more data from the mission than the pilot could ever remember to bring back. More accurate than memory alone, faster than film, video tape is the ideal tool for intelligence gathering.

Whether carried on an aircraft, ground vehicle, sea vessel, or a scout's back, the AVTR will bring back the desired video images. Troop movements, transmitter patterns, mission effectiveness, or whatever the sensors detect for video recording is supplemented by concurrent voice commentary on one or both audio tracks.

Other reconnaissance applications include traffic flow, forestry, fish or crop conditions, pollution control, border patrol, disaster

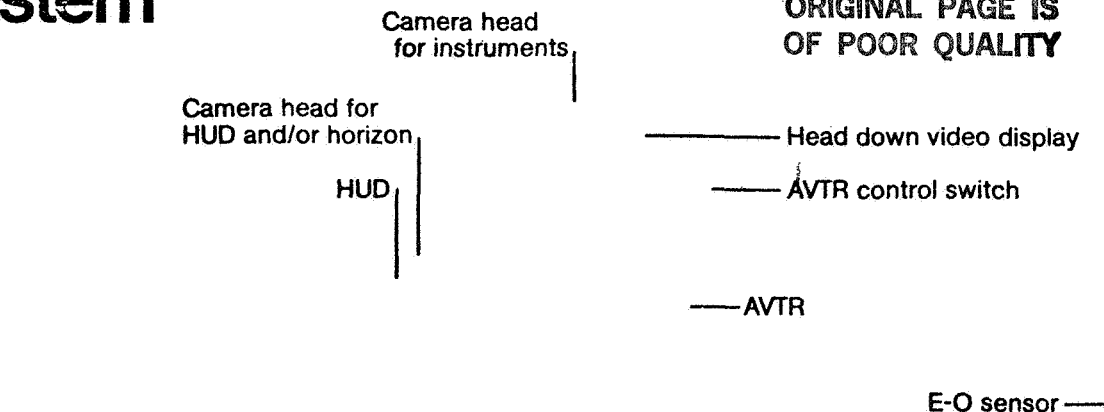
assessment, and many more. The AVTR can be adapted to most any rugged environment for obtaining the immediate data so vital to decision makers.



System

Typical Installation

ORIGINAL PAGE IS
OF POOR QUALITY



TEAC has made video tape recording in airborne and other rugged environments more than just a "possibility." Recording with the AVTR system is so convenient, economical and practical now that a pilot or other operator's mission is handicapped without the AVTR.

After extensive testing to MIL Spec and MIL Standards, the AVTR was determined qualified by the US Air Force for use in high-performance jet aircraft. It is the first videocassette recorder to be so qualified. Hundreds of thousands of hours of actual use by the US Air Force, Army and Navy, McDonnell Douglas Corporation, Hughes

Helicopters, and many others have proven the reliability, the desirability and even the necessity of TEAC's AVTR for a variety of applications.

The AVTR was selected as the VTR for evaluation and acceptance flights of the F-15, F-16, F-18 and AH-64. It was chosen for installation in thousands of aircraft by the USAF Tactical Air Forces. And, the AVTR will be used in NASA's Shuttle Orbiter spacecraft flights. These and many other important applications demonstrate the experts' confidence in the AVTR because of its convenience, economy, practicality and proven performance.

Convenience

Videocassettes bring no problems in loading, changing, storing, duplicating or procuring tape. Available worldwide for the AVTR and other systems, these U-Matic 'S' tapes were conceived for and are extensively used by professionals—in the TV broadcasting industry, education and in the military. Although the 1/2" type cassettes for "home use" are widely available today, the 3/4" U-Matic system is still the professional choice when

higher video quality is demanded. System compatibility with the extensive inventory of 3/4" equipment in the field is also an important consideration. Two audio tracks, handy size, and error-proof loading make them an ideal format.

The AVTR itself is remotely controlled, self-contained, and needs only a start/stop command from the operator.

Economy

Unlike completely MIL-spec'd equipment with their attendant high costs, the AVTR is an adaptation from a commercial video-cassette recorder. Not only is initial acquisition less expensive, but lead-time for production is geared to commercial practices. Using readily available parts, many in common with

the related commercial recorder, parts logistics and maintenance methods are less costly and more universally recognized than specialized MIL-spec products would be. Important, too, is the availability of technical data and spare parts already in the USAF inventory for the AVTR and the Ground Playback Units.

Practicality

TEAC's AVTR does meet all important MIL-standards for reliable operation in the rugged airborne environment. Weight and size conditions seldom pose a problem with this small unit. Operating from aircraft DC power of 28 volts, power consumption is

minimal at around 30 watts.

TEAC offers several models of the basic AVTR to meet the specific needs of a given installation. TEAC gives personal attention to your video recording needs, both for air/mobile and fixed station equipment.

An Effective Alternative to The Film Tradition

Video is much more than "magnetic movies." From years of working with film recording in aircraft, some people might try to impose the problems of filming onto their concept of video recording. For example, data has to be displayed before it can be filmed, but video signals can be recorded directly from the source. Video can use a

split-screen approach to share two or more cameras on the same picture.

Immediate playback of videotape, even inflight (with some models) is another primary advantage of video recording over film. No delays for developing, no danger of exposing the film, no film lab and no development technicians are needed with video.

**ORIGINAL PAGE IS
OF POOR QUALITY**

- Five selectable speeds of playback
- Mechanical field by field reversing
- Guard-band noise-free picture during still-motion
- EVENT MARKER (EMK) functions
- Slow motion over-ride control
- U-Matic standard, Record and Playback format
- Uses standard KCS or KCA type cassettes
- Scratch resistant case

While many cassette-type formats have recently been introduced, the 3/4" U-Matic type was the first successful method for eliminating the hassle of tape handling by the operator. Since its introduction in 1965, universal acceptance of 3/4" as the standard videocassette resulted in extensive commitment to this format by industry, broadcast and cable TV companies, education institutions, scientific organizations, and the government.

TEAC Corporation offers the only airborne-qualified (Model V-1000AB-N, -R) 3/4" Videocassette tape recorder. The V-4200G-N also represents the highest reliability in convenient videocassette reproduction with the unique features it offers and the quality of the U-Matic format.

The V-4200G-N is a high quality dual purpose (Analyzer/Reproducer) Videocassette machine. While many of the 3/4" videocassette units available today are similar in appearance (a few may even have some analysis capability), **none** of them have the combined features and the performance capability of the V-4200G-N. Most of the videocassette Analyzing-type

recorders operate under the closed-loop system (non U-Matic standard format). Tapes therefore, must be recorded and played back on the same model unit. The TEAC V-4200G-N conforms to the STANDARD U-Matic format—so tapes recorded by other U-Matic machines can be played back or analyzed with complete compatibility.

Video recording analysis can be laborious and time consuming. The V-4200G-N is specially geared for analyzing video recordings. Time saving features like EVENT MARKER function quickly take you to the point of (predetermined) interest. The SLOW MOTION CONTROL, the FIELD-BY-FIELD REVERSING MECHANISM, and the STILL MOTION PLAYBACK (with no guard-band noise) feature give the operator control during the analysis proceeding so that information can be quickly and carefully studied and evaluated. Careful design of the control functions, the combination of features and the unmistakable quality of TEAC make the V-4200G-N unique—a pleasure to operate and own.

This special lever, when in the Still playback mode, is used to "back-step" the video scene field-by-field or for making

full use of the guard-band-noise elimination feature.

The V-4200G-N has a special "speed ratio" control knob which selects playback tape speed. Selectable slow motion rates

are 1/80, 1/60, 1/40, 1/20, 1/10. Normal play and noise-band-free stop-action mode are also available.

This feature identifies certain pre-set (operator's choice) scenes during fast forward or rewind mode. When a designated

scene is reached, the recorder immediately signals or stops (operator's option) at that portion of tape.

During the slow motion mode, when the "NORMAL" button is pushed, the tape speed is quickly brought up to normal. Releasing

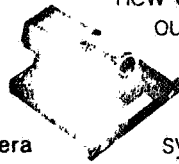
the button returns the speed to the pre-set slow motion setting.

- Feather-touch function select keys, offering "idiot-proof" selection of any mode (including EJECT) directly from any other mode
- Remote Control (optional) of any mode except EJECT Audio Dub, or slow motion.
- Audio commentary or additional data can be dubbed onto audio channel one during normal speed playback.
- Video (and audio) recording levels are controlled by AGC (automatic gain control).
- Color or B/W recording and playback selection is automatic.
- BNC-type video input and output connectors are standard, as is the 8-pin multijack for TV monitor connection.
- Tape automatically rewinds to the beginning after reaching the end-of-tape.
- Complements TEAC's Airborne Videocassette Tape Recorder (AVTR™) models V-1000AB-N and -R.

Recording Sources



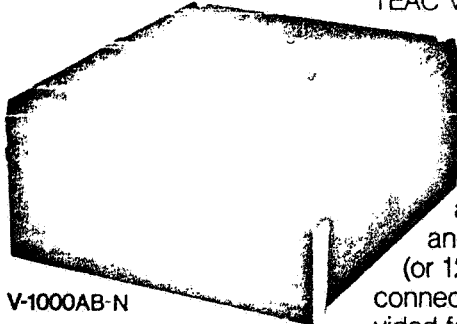
Fairchild
CCD camera



Depending upon the aircraft configuration and the type of mission, a typical source of video can be a TV camera (including the new CCD type) for recording the outside view from an aircraft, either directly or through the Heads-Up Display (HUD) which would include the HUD symbology.

Other sources might be TV formatted radar, Imaging Infra-Red (IIR), Forward-Looking Infra-Red (FLIR), or Low Light Level TV (LLLTV). Many other electro-optical (EO) signals can also be recorded, such as those from Maverick (TV or IR), TOW, Walleye, TISEO, TRAM, Pave Tack, Pave Spike, EnviroPod, etc.

For the Mission



V-1000AB-N

In the air or for a ground mobile installation, TEAC Video V-1000-series recorders (AVTRs) are available in several different configurations to meet your needs. All have a common, proven mechanism and are designed to give reliable service under rugged conditions.

Ease of installation is assured with a minimum of multi-pin connectors and reliance upon the unregulated 28V (or 12V) DC power source. MIL-standard connectors are used and contacts are provided for a variety of remote status indicators and controls. Ease of operation is provided by the simplest possible procedure: select "Record" when desired and "Standby" when recording is not required.

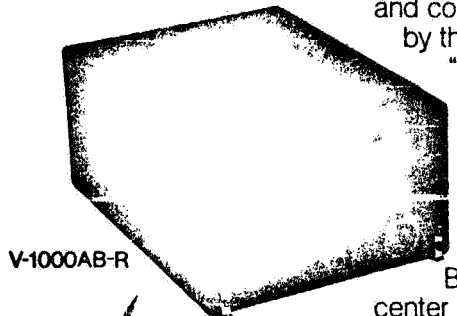
Status indicators for those conditions as well as "End of Tape," "Power" and "Accumulated Recording Time" can be easily accommodated. Video-

cassette tapes can be installed or replaced within a few seconds.

All models perform with distinction under rugged environments of acceleration and shock. Stress levels and low temperatures that would halt or even damage most VTRs have no effect upon TEAC's AVTR.

These rugged recorders take the punishment of life in a high-performance jet fighter and deliver both excellent video and high MTBF, asking only for conventional shock-mounting. AVTR also meets EMI and explosion protection requirements.

Other useful features include a color recorder capability, an Event Marker system for conveniently locating specific segments; two audio tracks for flexibility and added data capacity; and an ability to accept any TV line rate such as 525, 625, 875, etc.



V-1000AB-N

After the Mission

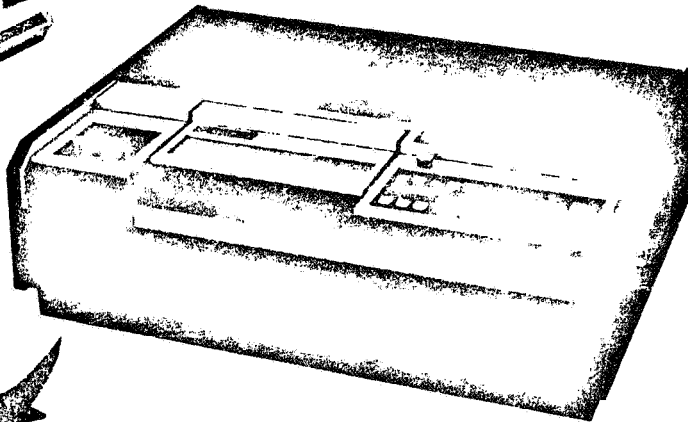


Back on the ground or at the operations center you will want the finest playback equipment for reconstructing the mission. TEAC Video's V-4000 series recorder/reproducers are recommended as they are optimized for play-back of videocassettes

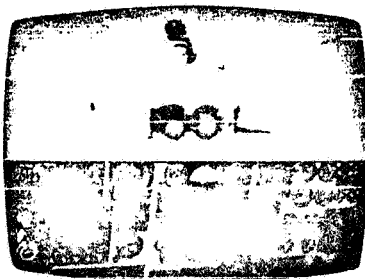
recorded on the AVTR. The V-4000 series offers many important features qualifying it for the category of a *video analysis tool*.

The 4200 type provides slow-motion playback when desired for viewing the tape at 1/10, 1/20, 1/40, 1/60 or 1/80 of the originally recorded tape speed. Combine that capability with its stop-motion pause control and you can find the exact field you wish to study. Or review a sequence of events field-by-field to analyze the specific chronology. A still-frame adjust lever assures completely noise-band-free stop-motion playback when needed.

Event Marker recording and detection in conjunction with the Memory Rewind function and all-solenoid operation provide tremendous control and fast-search flexibility in performing playback/analysis functions. Only a conventional TV monitor is required.



V-4200G-N



Front cover photos: Simulated TV picture using photos of McDonnell Douglas F-15.

TEAC VIDEO

TEAC CORPORATION OF AMERICA
Industrial Products Division
7733 Telegraph Road
Montebello, California 90640 U.S.A.
Tel: (213) 726-0303 Telex: 677014

TEAC Corporation
VIPD, 3-7-3 Nakacho
Musashino, Tokyo 180 Japan
Tel: (0422) 53-1111 Telex: 2822551

ORIGINAL PAGE IS
OF POOR QUALITY

Representative:

49

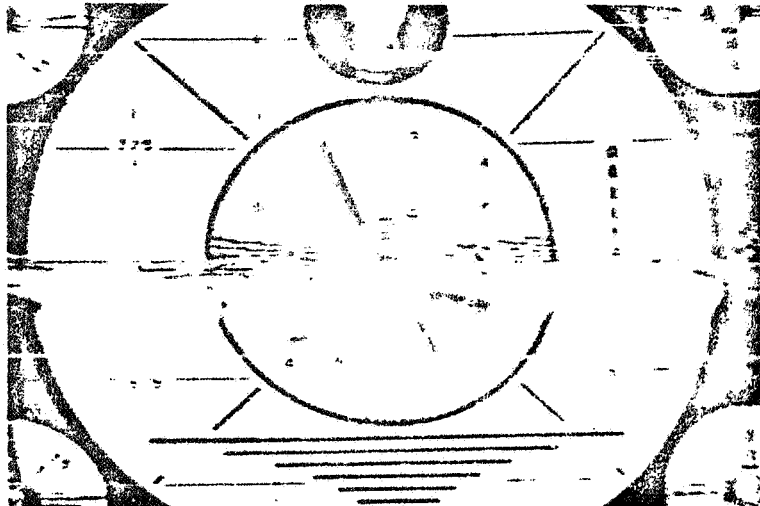
TEAC
G-Series



A problem with most of today's helical-scan video recorders is during the still motion mode there is that common but irritating guard-band noise across the picture (picture 1). If the relative speed of the tape and the head drum assembly is constant, then the video heads and video tracks are in sync (tracking properly) thus producing a normal picture. However in the still motion mode the video tape is stopped

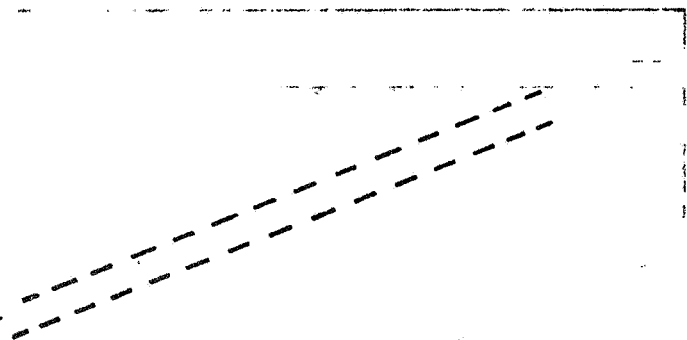
which produces a mistracking condition in the video. The video heads now track at a different angle (diagram 2). The engineers at TEAC solved this problem by designing in the V-4200G-N a special compensating mechanism. This precision-built mechanism tilts the head drum assembly thus correcting any errors in tracking. The result is a still motion picture without the guard-band noise (picture 3).

**ORIGINAL PAGE IS
OF POOR QUALITY.**

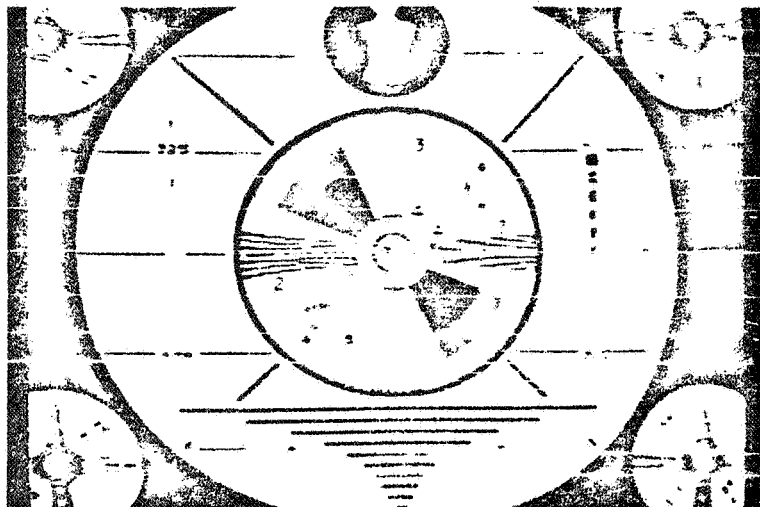


1

VIDEO TRACK
(uncorrected)

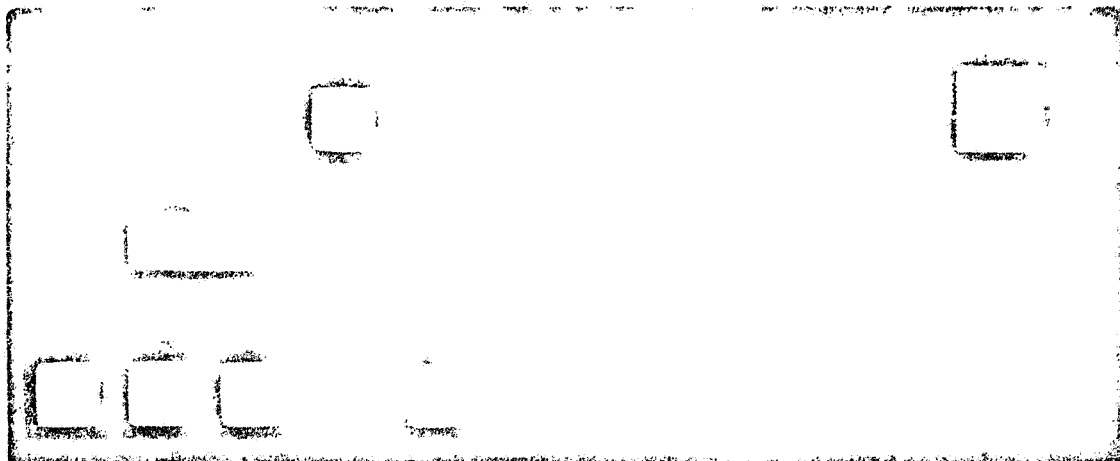


2



3

ORIGINAL PAGE IS
OF POOR QUALITY



Specifications and Performance Data

GENERAL

Format: 3/4 inch U-Matic cassette
Video Signal: NTSC Color or EIA B/W
Power Requirements: 120 volts AC, 60Hz \pm 0.5%
Power Consumption: 145 W
Storage Temperature: -20°C to 60°C
(-4°F to $+140^{\circ}\text{F}$)
Operating Temperature: $+5^{\circ}\text{C}$ to $+40^{\circ}\text{C}$
($+41^{\circ}\text{F}$ to $+104^{\circ}\text{F}$)
Operating Position: Horizontal to 30°
Dimensions: 25-3/8 (w) x 9 (h) x 18-3/8 (d) inches
645 (2) x 223 (h) x 464 (d) mm
Weight: 80 lbs (36.5Kg)

VIDEO

Input: 1.0 +1.0 -0.5V (p-p) 75 Ohms
Output: 1.0 \pm 0.2V (p-p) 75 Ohms
Horizontal Resolution: B/W 320 lines or more
Color 240 lines or more
Signal-to-Noise Ratio: More than 45 dB (B/W)

AUDIO

Input: MIC -60 dB 600 Ohms
Line -10 dB 100K Ohms
Output: Line -5 dB at 100K Ohm load,
Output Impedance 2K Ohms
Monitor -5 dB at 100K Ohms Load,
Output Impedance 2K Ohms
Signal-to-Noise Ratio: More than 40 dB

FUNCTIONAL PERFORMANCE

Tape Speeds: 3-3/4 ips (95.3mm/sec) \pm 0.2% (normal)
1/10, 1/20, 1/40, 1/60, 1/80 of normal (slow play)
Remote Controls: FORWARD, STOP, RECORD,
FAST FORWARD, REWIND, PAUSE/STILL FIELD,
EVENT MARK RECORD.

Rewind Time: Less than 4 min (with KCA-60 tape)
Fast Forward: Less than 6 min (with KCA-60 tape)
Event Marker: 1000 Hz Audible-tone and
30 Hz Fast-search signal (composite)

Features and specifications subject to change without notice

© Copyright 1979 TEAC Corporation of America

TEAC

TEAC Corporation of America, Industrial Products Division
7733 Telegraph Road, Montebello, CA 90640 Phone: (213) 726-0303

Printed in U.S.A. V-GN 9-79

**ORIGINAL PAGE IS
OF POOR QUALITY**

**AVTR SYSTEM
KEY FEATURES**

- RUGGEDIZED FOR MIL-SPEC ENVIRONMENTS (MIL-E-5400N, MIL-STD-810C, ETC.)
- NON MIL-SPEC PRICE (COMMERCIAL EQUIPMENT)
- FULLY FLIGHT-TESTED, LAB-TESTED AND QUALIFIED BY THE USAF FOR USE IN HIGH PERFORMANCE JET AIRCRAFT
- USAF CONTRACTS AWARDED FOR MORE THAN 2,500 UNITS
- WILL BE USED IN NASA SHUTTLE ORBITER
- EXCELLENT HELICOPTER AND GROUND VEHICLE PERFORMANCE RECORD
- OPERATES FROM UNREGULATED 28VDC
- WEIGHS LESS THAN 30 LBS.
- REMOTE CONTROL FOR RECORD/STANDBY
- CONVENIENT 3/4" U-MATIC VIDEOCASSETTE WITH TWO AUDIO TRACKS
- CCIR VERSION (625/50), FLIR VERSION (875/60) AND WIDER BAND VERSION (ABOUT 5MHZ) AVAILABLE
- GROUND PLAYBACK ANALYSIS REPRODUCER ALSO AVAILABLE
- SATISFACTION GUARANTEED

WCM
agcefr
05/81

APPENDIX B

B-1

(44)

COSMAC Microboard Computer Systems

The RCA CDP18S600 Series offers a line of single-board computers plus a variety of expansion memory and I/O boards and accessory hardware. These boards may be combined to provide customized microcomputer systems for specific applications. RCA offers designers low-power CMOS computer boards engineered and tested to reduce the time required for the user to develop the over-all system. These ready-to-use microboard modules provide the following significant advantages.

does the power supply have to be bigger, bulkier, and heavier than the entire system. And you eliminate cooling fans along with associated reliability hazards.

-With the COSMAC Microboard Universal Backplane, any Microboard module works in any location. Use the broad selection of readily interchangeable Microboard modules. Simply exchange or add modules to match your changing design requirements. Lots of flexibility without hardware design headaches.

-Simply select the 4.5 x 7.5-inch Microboard modules your system needs, plug them on to the Microboard 5- or 25-card chassis with COSMAC Microboard Universal Backplane, and add a milliwatt power supply. You are ready to begin the development of the software for your application. No hand-wired breadboards, no hardware headaches, no design delays.

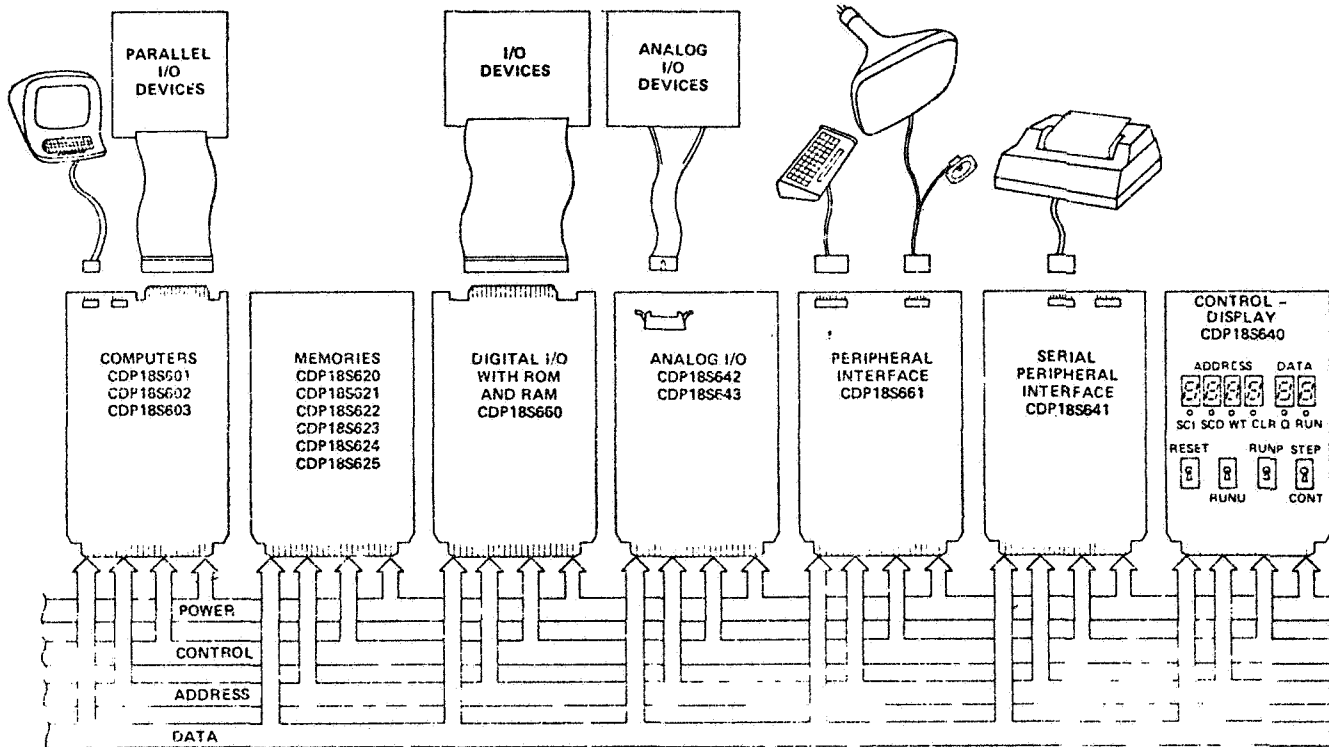
-CMOS technology provides reliable operation in high-speed, access-control, automotive, and production-monitoring environments. No ground plane, no current decoupling, no special cooling.

Operation-Utilizing all CMOS components, your RCA COSMAC Microboard system can be powered from a small supply, a wall supply, or even a battery. The integral battery option of the Microboard 8K RAM can be used to power the entire system.

-All Microboard modules are designed to plug into the RCA COSMAC Development Systems to facilitate hardware and software development. The RCA COSMAC DOS Development System CDP18S007 provides Editor, Macroassembler, Utility, and many other programs for the neophyte-to-expert software designer. And RCA provides ample technical literature and field engineering support.

Low Cost Power Supply-The low power requirements of the Microboard modules coupled with their wide operating-range capabilities allow use of low-cost power supplies having extended regulation limits. No longer

100% Test and Burn-In-All Microboard modules are functionally tested after manufacture, subjected to a 72-hour, 5-volt burn-in at 70°C, and then functionally re-tested to assure reliable operation.



140

COSMAC Microboard Computer Systems

ORIGINAL PAGE IS
OF POOR QUALITY

Single Board Computers

	Clock Freq.	RAM	ROM/ EPROM (Sockets)	Serial I/O Lines	Parallel I/O Lines
CDP18S601	2 MHz	4K	4K/8K	1	25
CDP18S602	2 MHz	2K	2K/4K/8K	1 (UART)	21
CDP18S603	2 MHz	1K	4K/8K	1	25

Memory

	RAM (Bytes)	ROM/ EPROM (Sockets)	Serial I/O Lines	Parallel I/O Lines	Other
CDP18S620	4K	—	—	—	—
CDP18S621	16K	—	—	—	—
CDP18S621V1	16K	—	—	—	—
CDP18S622	8K	—	—	—	Battery Back-Up
CDP18S623	8K	—	—	—	—
CDP18S624	4K	—	—	—	Battery Back-Up
CDP18S625	—	8K/16K	—	—	—

I/O Expansion Boards

CDP18S640,V1	256	4K8K	—	—	Control Switches 6 Digit Hex Display
CDP18S641	—	—	1 (UART)	—	—
CDP18S642	—	—	—	—	D/A Converter
CDP18S643	—	—	—	—	A/D Converter
CDP18S660	2K	4K/8K	—	40	—
CDP18S661	—	—	—	—	Video-Audio- Keyboard Interface (40 Character 1 Line X 24 Lines or 20 X 12 Programmable)

Microboard Prototyping Systems

CDP18S691	—Prototyping System (Includes CDP18S601, CDP18S640, CDP18S659, Monitor Firmware, 5 Card Encased Chassis, Cables, Documentation)				
CDP18S692	—Prototyping System (Same as CDP18S691 Except Contains CDP18S602 Computer Board)				

Microboard System Development Aids

CDP18S023,V3	— 5-Volt Power Supply
CDP18S659	— Blank Breadboard
CDP18S670	— 25-Card Chassis with Power Supply
CDP18S675	— 5-Card Chassis
CDP18S676	— 5-Card Encased Chassis
CDP18S480	— PROM Programmer
CDP18S502	— Extender Card

For more information, request product description for specific Microboard modules, or the *RCA COSMAC Microboard Computer Systems Booklet, CMB-250*.

COSMAC Microprocessor Development and Support Systems

The RCA CDP18S series of COSMAC microprocessor development and support systems include an extensive line of hardware, software, and accessory items. This series offers the following basic features:

- Full spectrum of design aids, including software, hardware, support, and literature
- Low-cost systems for complete system design and debugging functions
- Readily available hardware and software applications support
- "Graduated steps" to microprocessor design
- Complete series of technical manuals and other literature that provide detailed explanations of the operation and use of various hardware and software systems.

RCA's approach in the development of the CDP18S-series hardware and software has been "graduated steps to micro-processing." With respect to both function and dollar investment, the user is given logical steps that help him progress from a learning stage on through integral hardware/software system prototyping. And for each step, he is provided with an appropriate tool, as shown in the chart below.

As guidance for choosing appropriate equipment for your specific needs, the following are some suggested RCA Development Systems configurations.

This development system configuration provides an economical tape-based system complete with resident assembler/editor for assembly language software development as well as prototype system real-time hardware and software debugging capability

The CDP18S007 is a complete floppy disk-based development system for the COSMAC microprocessor. It is based on a 28K RAM and a four-track floppy disk system for program storage. Its software includes a disk-based assembler, a ROM Macroassembler, a program editor, and a new operating system (CDOS) which provides the user with a powerful disk file-management system.

The Micromonitor and MOPS offer complete hardware and software debug capability for prototype as well as programmable automated production testing.

CDP18S Series COSMAC Microprocessor Development and Support Systems (Key: Price in \$)

Type No.	Descriptive Title	Function
CDP18S012	COSMAC Microtutor	To learn about programming and microprocessors
CDP18S005 CDP18S007	COSMAC Development System II COSMAC DOS Development System (CDS III)	For complete hardware and software system development
CDP18S805	Floppy Disk System	For high-speed program development
CDP18S020 CDP18S024	COSMAC Evaluation Kit EK/Assembler-Editor Design Kit	Complete system for machine-language programming and prototyping
CDP18S021	COSMAC Microterminal	Low-cost alternative for TTY, CRT, or other terminals in a CDP1800-series microprocessor-based system
CDP18S023, V3	Power Supply	Lightweight inexpensive system power supply
CDP18S025	Evaluation Kit, Microterminal, and Power Supply	Combination package—unassembled
CDP18S030	COSMAC Micromonitor	For in-circuit real-time hardware and software debugging
CDP18S480 CDP18S831	PROM Programmer Micromonitor Operating System (MOPS)	For programming industry standard PROM's Optional package for operating Micromonitor with disk files
CDP18S826 CDP18S827	Fixed-Point Arithmetic Package Floating-Point Arithmetic Package	To ease programming of often used routines
CDP18S834 CDP18S837	Basic Compiler Interpreter CDOS Upgrade Package (to CDS III)	To simplify program development Adds disk file management to disk development systems
CDP18S838	PLM 1800 High-Level Language Compiler	To facilitate program development
CDP18S840	PROM Programmer	

For more information on any of the above items, contact your nearest RCA Sales Office for a specific Product Description.

3.6 APPARATUS CONFIGURATION

	<u>PIR NO.</u>
Task 9.1 - Configuration Guidelines	-018
Task 9.2 - Interchangeable Fluid Flow Cell Assembly, Feasibility Report	-022

)

)

)

GENERAL ELECTRIC

SPACE DIVISION
PHILADELPHIA

PROGRAM INFORMATION REQUEST / RELEASE

CLASS. LTR.	OPERATION	PROGRAM	SEQUENCE NO.	REV. LTR.
U	1254	AGCE	018	
PIR NO.				
*USE "C" FOR CLASSIFIED AND "U" FOR UNCLASSIFIED				

FROM	TO
G. L. Fogal	Distribution

DATE SENT	DATE INFO. REQUIRED	PROJECT AND REQ. NO.	REFERENCE DIR. NO.
3/31/81			

SUBJECT

Task 9.1 - Configuration Guidelines

INFORMATION REQUESTED/RELEASED

1.0 SCOPE

The AGCE configuration guidelines are intended to be used, via preparation of non-detailed assembly drawings and assembly/disassembly procedures, to assess the compatibility of the AGCE system with a standard spacelab rack.

2.0 GENERAL

The AGCE configuration guidelines are based on GFFC experience, installation requirements as defined by the Spacelab Payloads Accomodation Handbook SLP/2104 and a current estimate of AGCE flight design requirements.

3.0 GUIDELINES

3.1 Mechanical

The AGCE shall be configured to be installed within a standard spacelab single rack (or either side of a standard double rack) equipped with an RAU, EPSP and an intercom station. Allowable use volume and mechanical interface details are shown on the attached figures (from SLP/2104, Appendix B).

3.2 Thermal

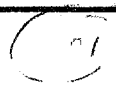
The AGCE shall be configured to use available rack avionics air for heat dissipation. The control electronics and mechanical assembly packages shall be connected for suction cooling.

Rack front panel close-outs shall be provided as part of the AGCE system (to prevent mixing of avionics and cabin air).

3.3 Electrical

The AGCE power will be provided via a spacelab standard EPSP, with voltage and allowable power dissipation as specified in SLP/2104. Time reference data will be provided by a RAU. If on-board recording is not provided, AGCE data telemetry shall be via the Spacelab HRM. Interrack cabling between the AGCE and RAU and EPSP shall be supplied as part of the AGCE system.

Distribution: R. Homsey S. Neste G. Fogal	PAGE NO. OF	RETENTION REQUIREMENTS	
		COPIES FOR	MASTERS FOR
		<input type="checkbox"/> 1 MO.	<input type="checkbox"/> 3 MOS.
		<input type="checkbox"/> 3 MOS.	<input type="checkbox"/> 6 MOS.
		<input type="checkbox"/> 6 MOS.	<input type="checkbox"/> 12 MOS.
		<input type="checkbox"/> MOS.	<input type="checkbox"/> MOS.
		<input type="checkbox"/>	<input type="checkbox"/> DO NOT DESTROY



3.4 Assembly/Installation

The AGCE shall be configured for ease of assembly and ease of installation into the spacelab rack under KSC Phase IV integration constraints.

3.5 Operator Interface

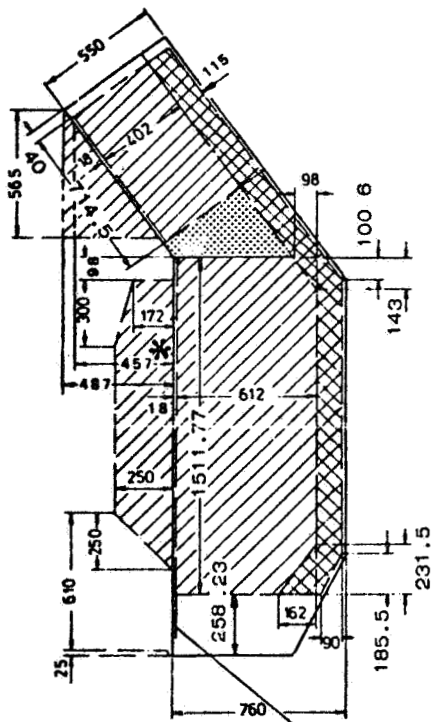
Operator interface for control and monitoring of the AGCE shall be via the AGCE control panel only.

3.6 Weight/Safety Constraints

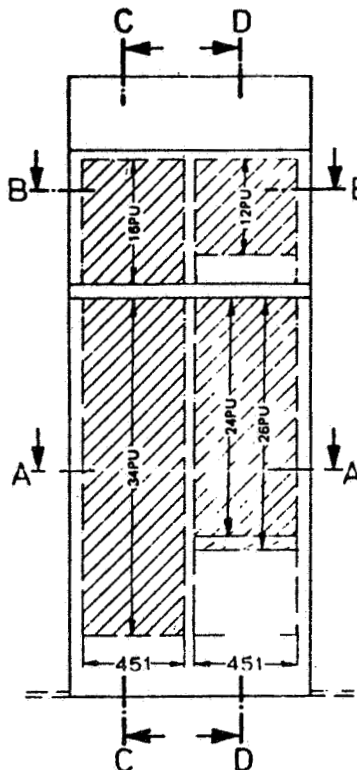
The AGCE shall be configured to be consistent with safety and weight constraints as defined in SLP/2104.

DCN
039

SECTION C-C

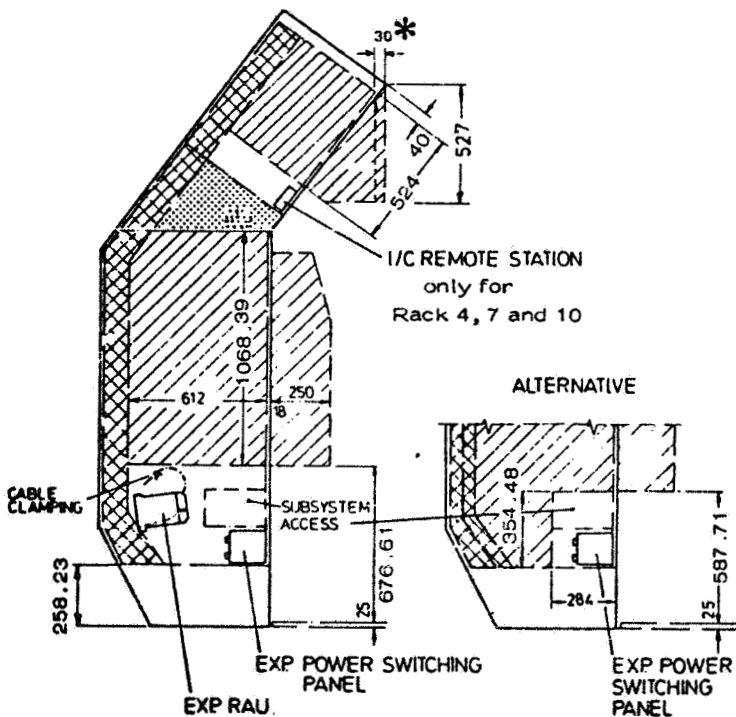


Front Panel Mounting Plane



ORIGINAL PAGE IS
OF POOR QUALITY

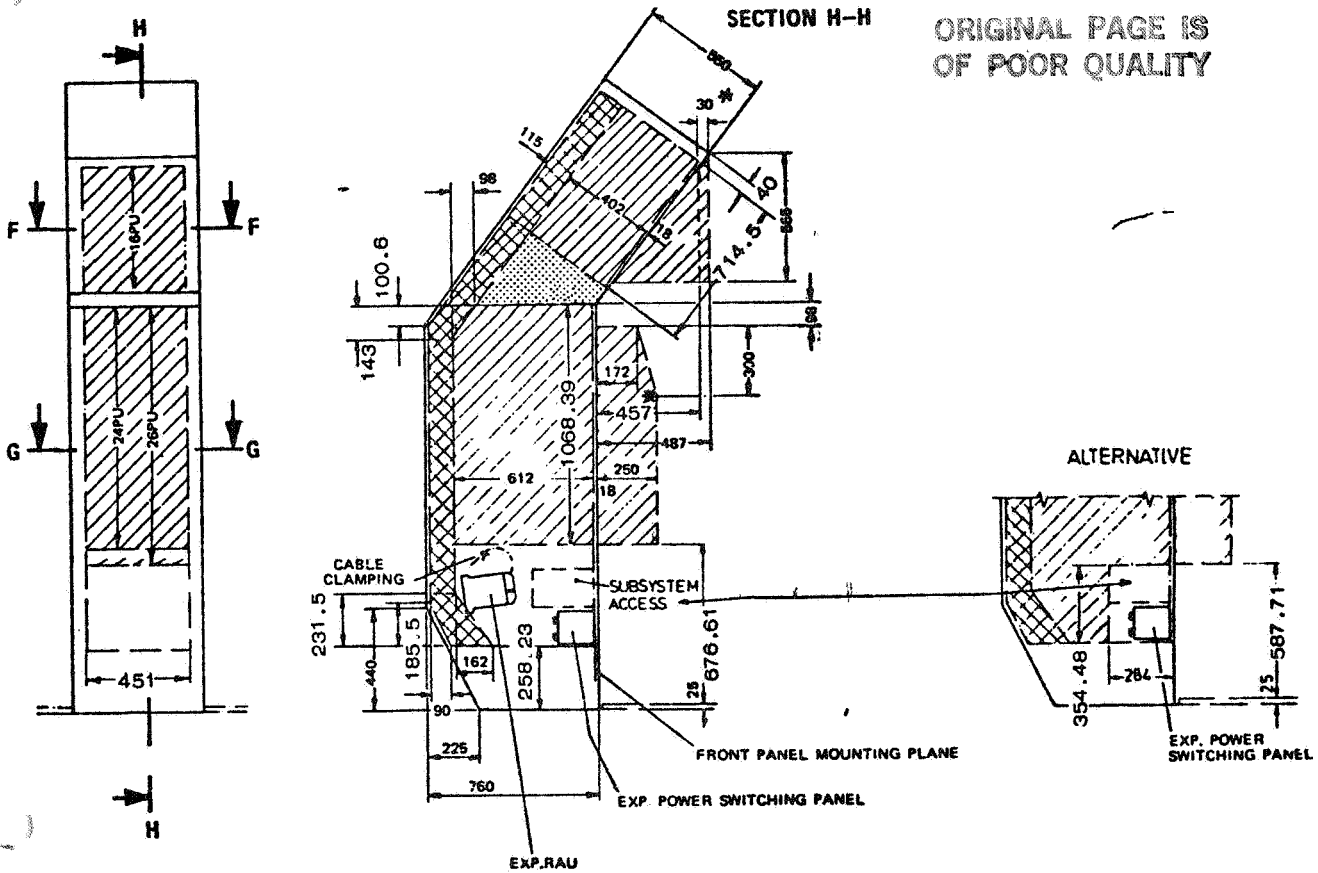
SECTION D-D

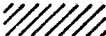




Explanations see Fig.3.2 - 5b
see Fig. 3.2 - 30a

C-6

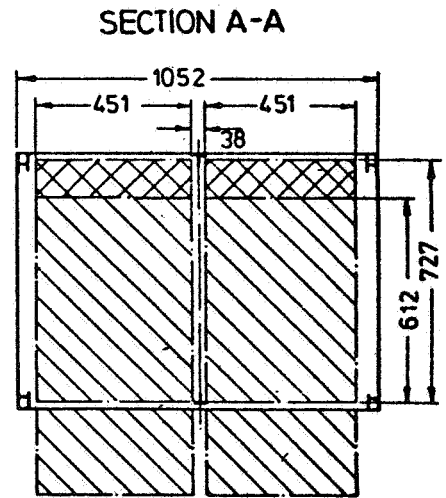
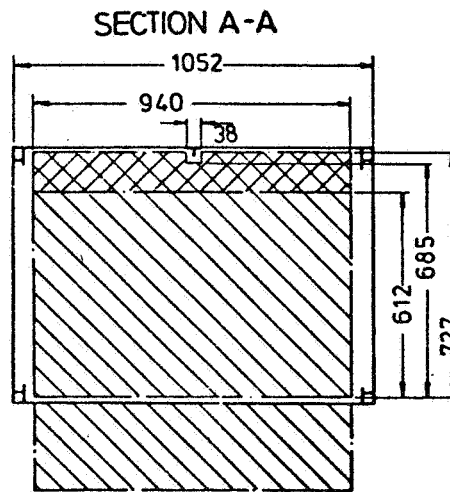
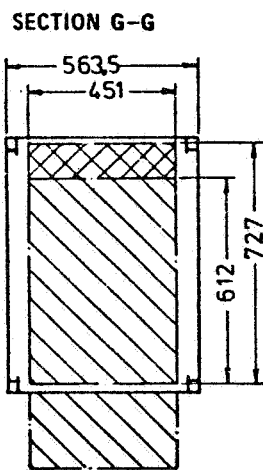
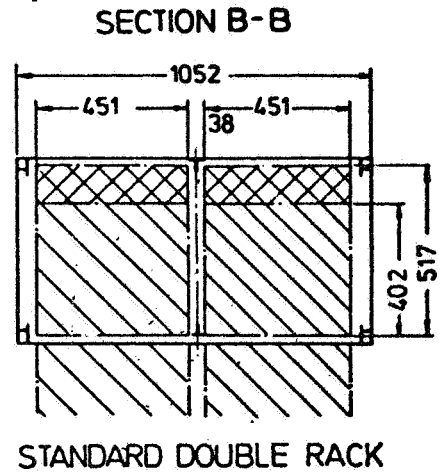
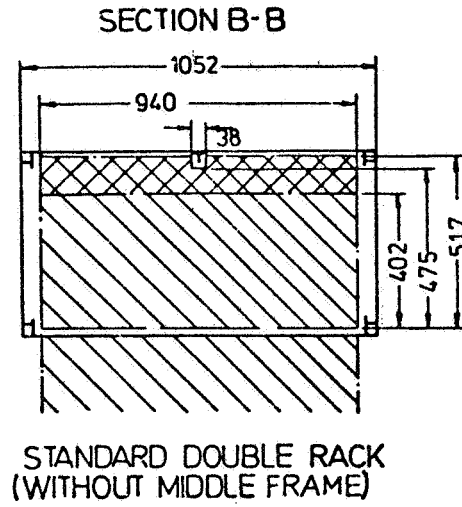
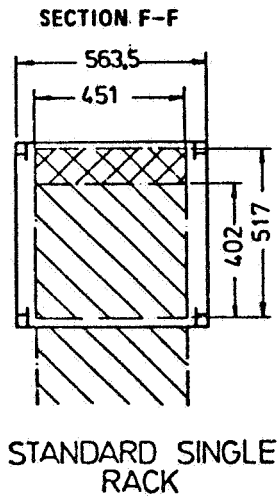
Figure 3.2 - 5a: Payload Envelope - Double Rack



-  Nominal Envelope
-  Envelope of 115 mm available for payload in completely passive stowage racks which do not contain cables, airduct, and fire suppression line.
-  This space is available for payload but cannot be used for 19" type equipment.

* Reduced Envelope
when Airlock is flown in order to allow clearance during integration of rack train with the airlock already installed (see also Section 6.2 in the main volume)

Figure 3.2 - 5b: Payload Envelope - Single Rack.



see Fig. 3.2 -5a/b for definition of cross sections

ORIGINAL PAGE IS
OF POOR QUALITY

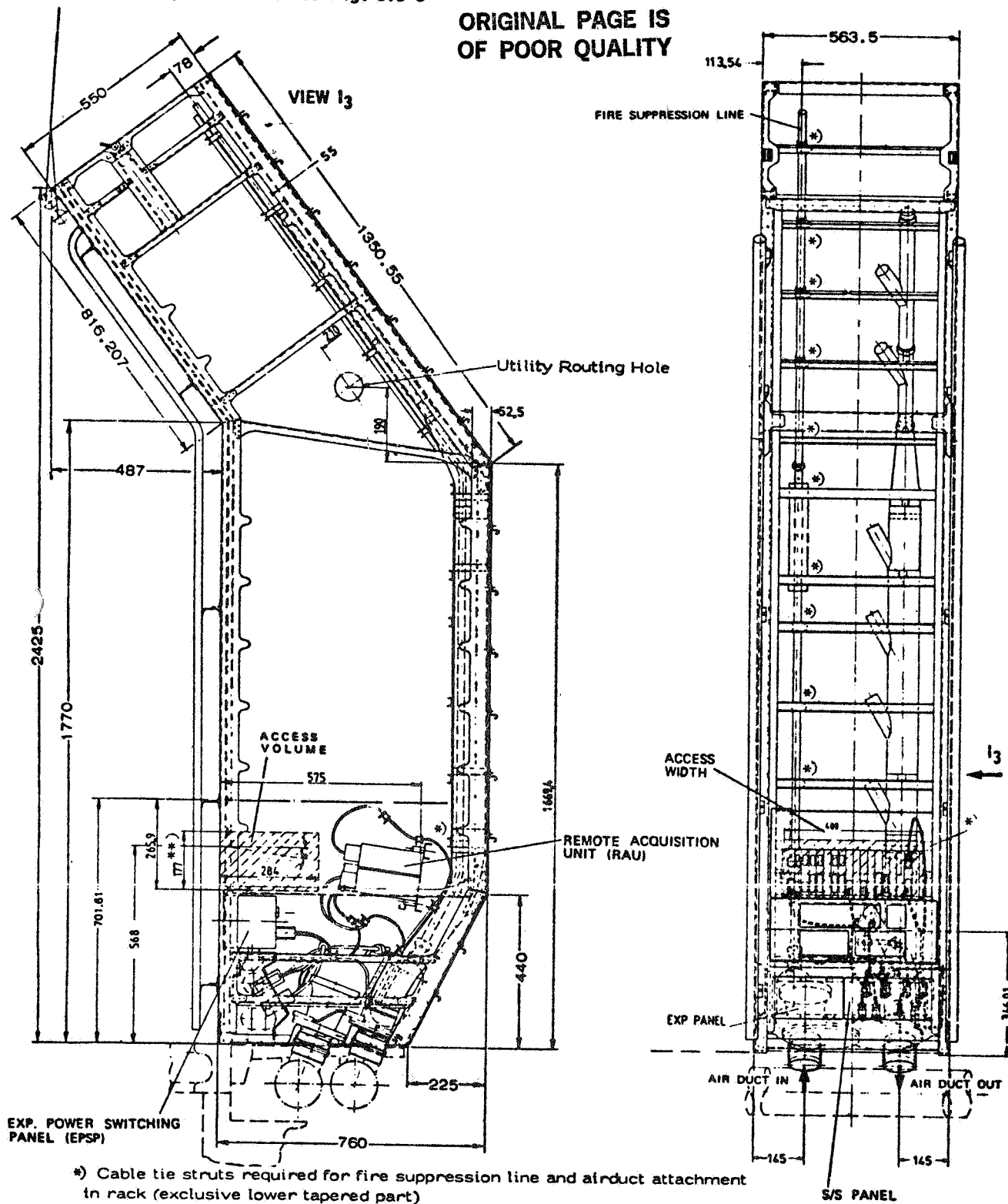
PRECEDING PAGE BLANK NOT FILMED

DCN
006

Figure 3.2 - 5d: Payload Envelopes - Cross Sections

Location of Exp. Vent Line see Fig. 3.9-5

ORIGINAL PAGE IS
OF POOR QUALITY



DCN
039

DCN
039

* Cable tie struts required for fire suppression line and airduct attachment in rack (exclusive lower tapered part)
12 cable tie struts delivered per single rack (see Table 3.2-1).

** EPSP access panel 177 mm if no RAU is installed. RAU access panel 265.91 mm.
(see also Fig.3.2 - 13b)

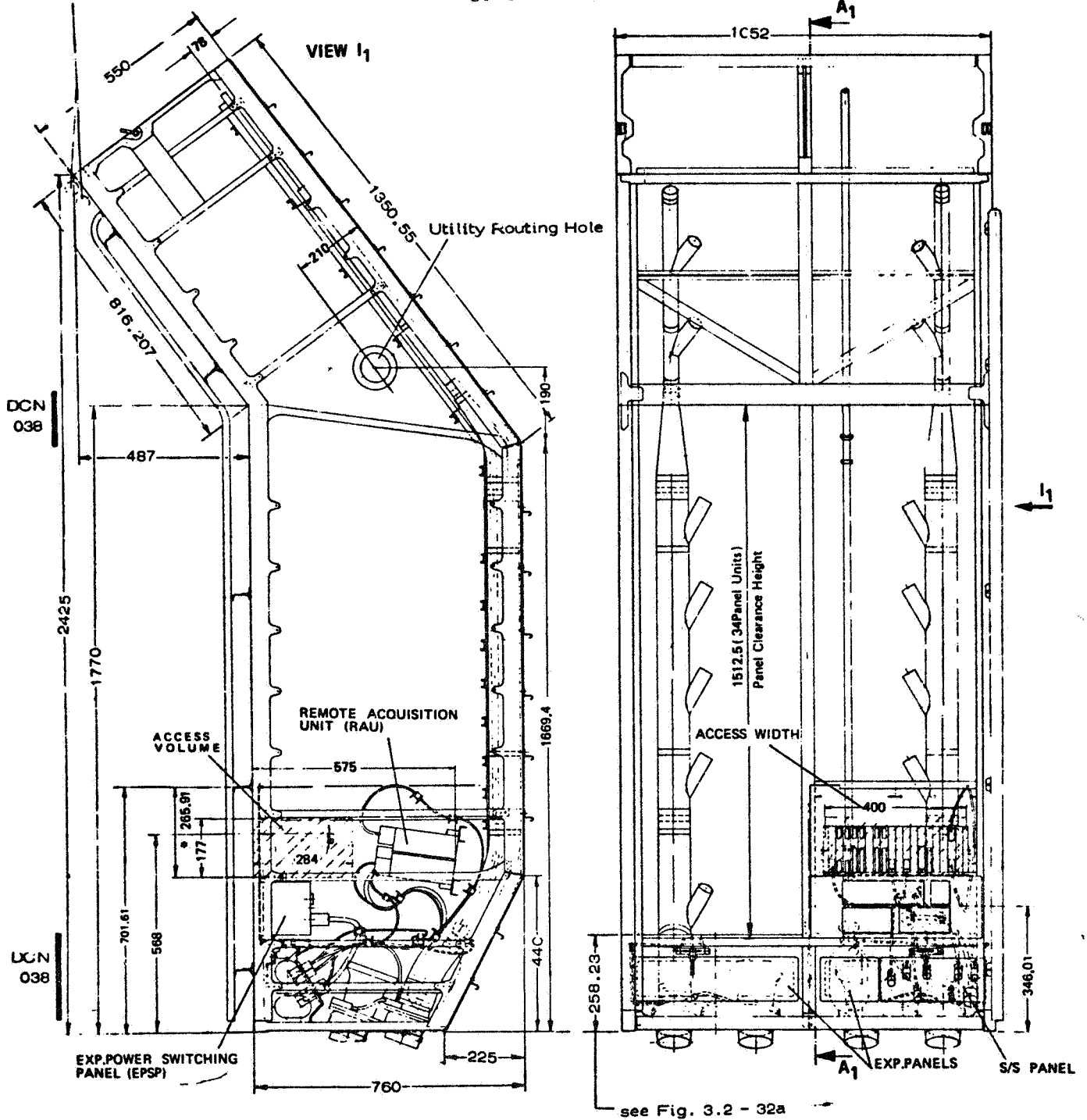
Figure 3.2 - 6 Experiment Single Rack 5 (same for Rack 6, 11 and 12)

PRECEDING PAGE BLANK NOT FILMED

ORIGINAL PAGE IS
OF POOR QUALITY

Location of Exp. Vent Line see Fig. 3.9-5

VIEW WITHOUT STRUTS



see Fig. 3.2 - 32a

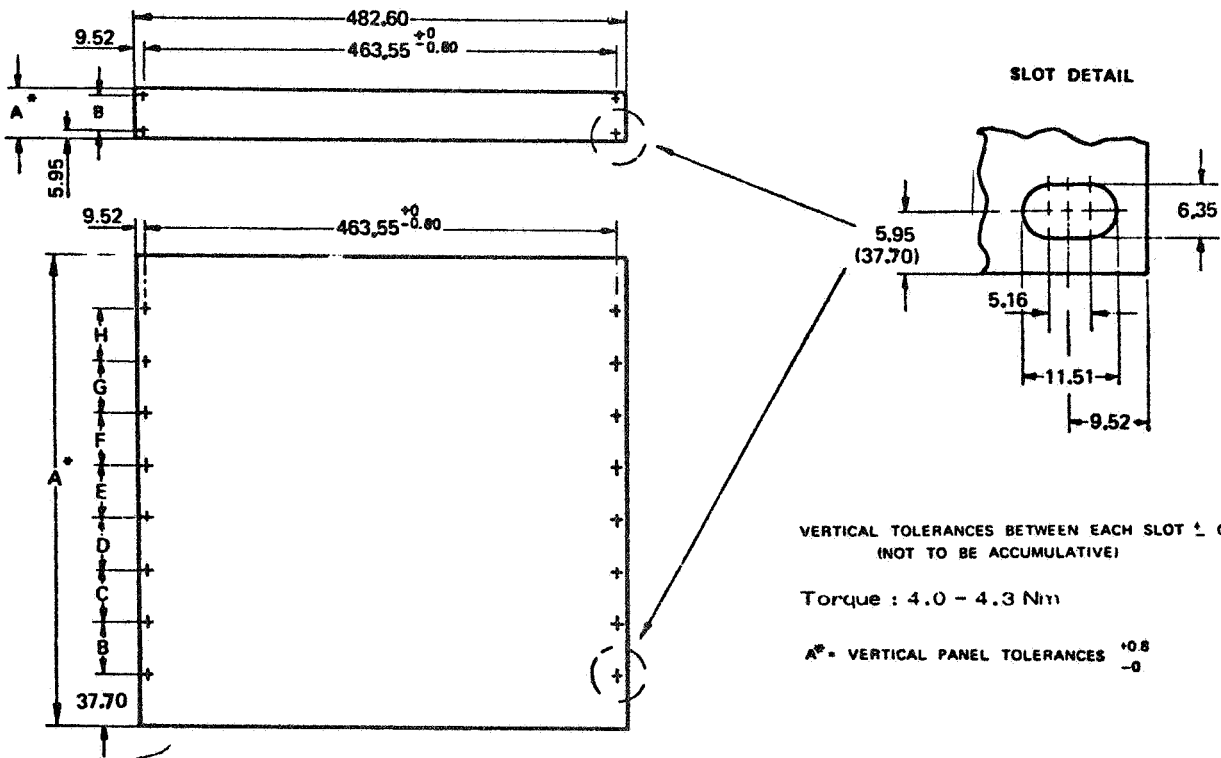
* EPSP access panel 177mm if no RAU is installed, RAU access panel 265.91mm
(see also Fig. 3.2 - 13b)

Figure 3.2 - 7a: Experiment Double Rack 3 (same for Rack 8 and 9)

3.2.2.1.1 Panel Size

ORIGINAL PAGE IS
OF POOR QUALITY

PU (PANEL UNIT)	PANEL SIZES								MIL-STD TYPE
	A	B	C	D	E	F	G	H	
1	43,65	31,75							AC
2	88,10	76,20							BC
3	132,55	57,15							CC
4	177,00	101,60							DC
5	221,45	44,45	57,15	44,45					EC
6	265,91	57,15	76,20	57,15					FC
7	310,36	44,45	146,05	44,45					GC
8	354,80	88,90	101,60	88,90					HC
9	399,25	88,90	146,05	88,90					JC
10	443,7	88,90	190,50	88,90					KC
11	488,16	133,35	146,05	133,35					LC
12	532,61	44,45	133,35	101,60	133,35	44,45			MC
13	577,06	133,35	44,45	146,05	44,45	133,35			NC
14	622,30	44,45	133,35	190,50	133,35	44,45			PC
15	665,96	44,45	177,80	146,05	177,80	44,45			RC
16	710,41	44,45	133,35	88,90	101,60	88,90	133,35	44,45	SC
17	754,85	44,45	133,35	88,90	146,05	88,90	133,35	44,45	TC
18	800,10	44,45	133,35	88,90	190,50	88,90	133,35	44,45	UC



DCN
011

DCN
011

For the front panels closed slots according to MIL-STD-189 shall be used. The panel thickness recommended shall be 3.2 mm, 4.8 mm, 6.3 mm or 8.0 mm in accordance with referenced MIL-Standard.

DCN
011

**ORIGINAL PAGE IS
OF POOR QUALITY**

3.2.2.1.2 Box Size

The box width is defined in Fig. 3.2-12b. However, the box height and width, i.e. the recess of the box behind the panel depends on the actual location in the rack and is defined in Fig. 3.2-12b. The recess is as follows:

- normally the recess is $\approx 4.6 \text{ mm} \begin{matrix} +.4 \\ - 0 \end{matrix}$
- at diagonal shear load struts where a front panel shall overlap half the strut clearance the recess is $\approx 20 \text{ mm}$.

DCN
039

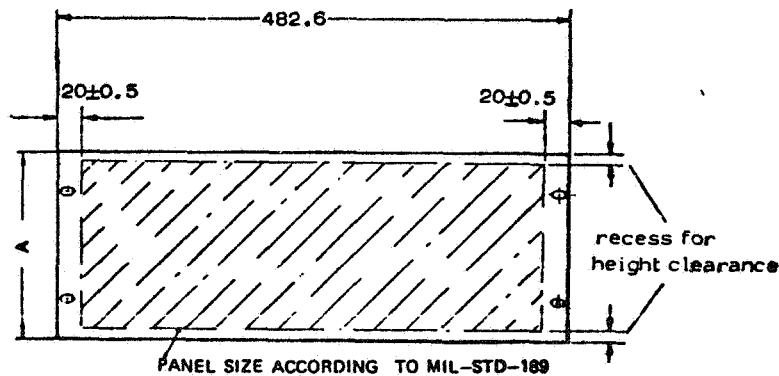
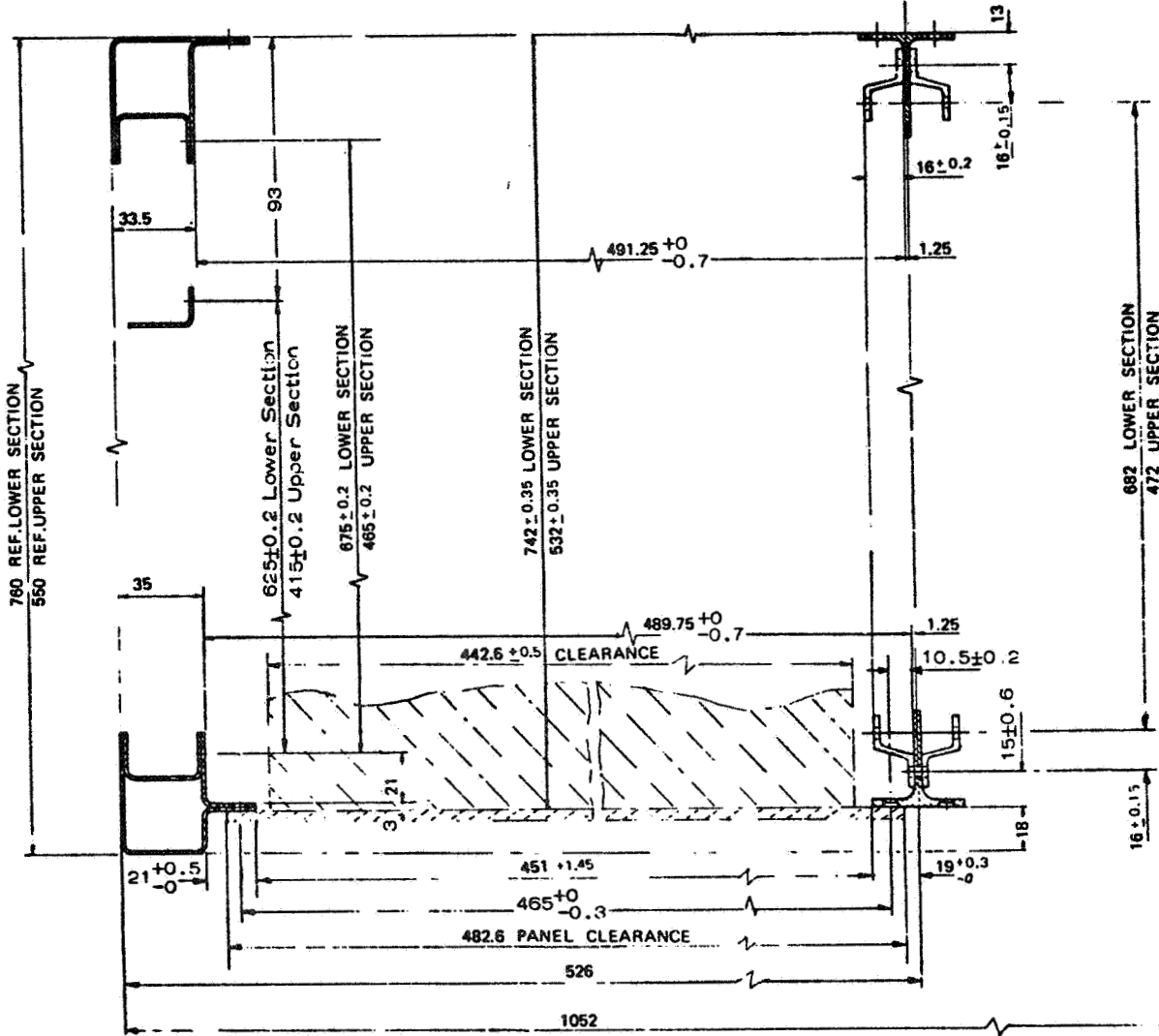


Figure 3.2 - 12b: Equipment Clearances

ORIGINAL PAGE IS
OF POOR QUALITY

SECTION A-A / B-B



MODULAR HOLE PATTERN
HOLES Ø 5.2 ± 0.075

DCN
013

Figure 3.2 - 13d: Cross Sections - Double Rack Left Side

ORIGINAL PAGE IS
OF POOR QUALITY

SECTION E-E
F-F

MODULAR HOLE PATTERN
(HOLES ϕ 5.2)

DCN
013

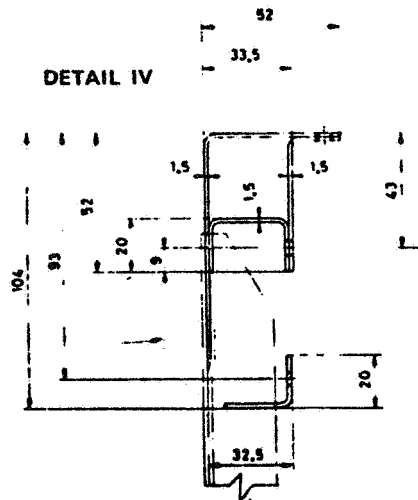
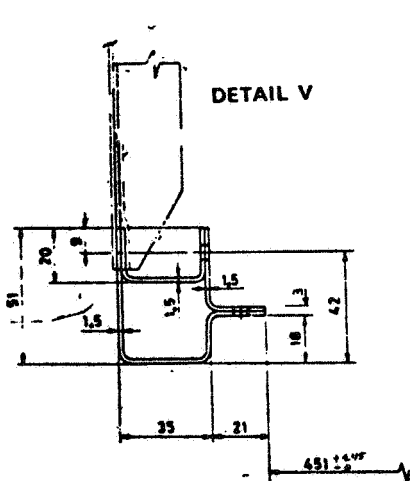
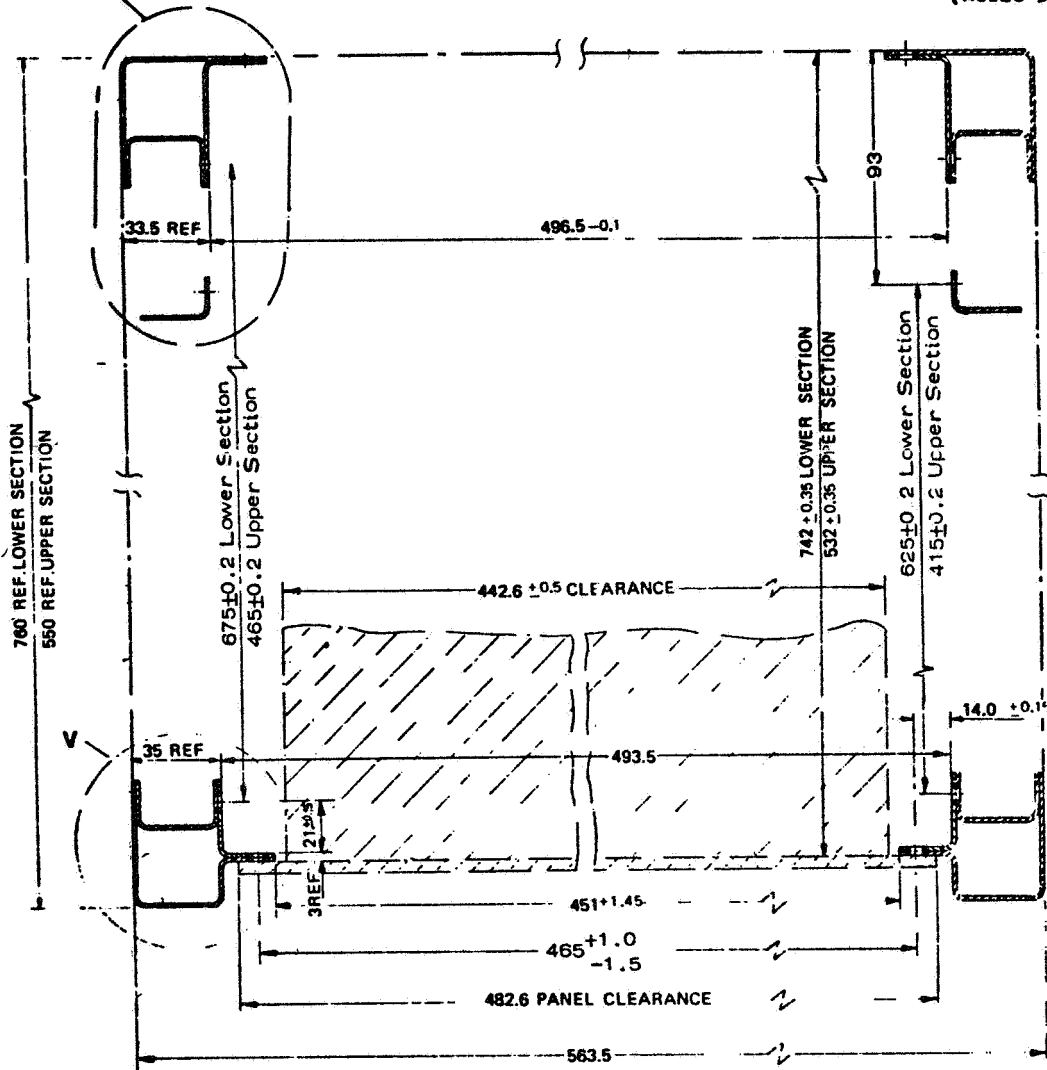


Figure 3.2 - 13g: Cross Sections - Details

3.2.2.2.2

Side Attachment

DCN
039

ORIGINAL PAGE IS
OF POOR QUALITY

DCN
039

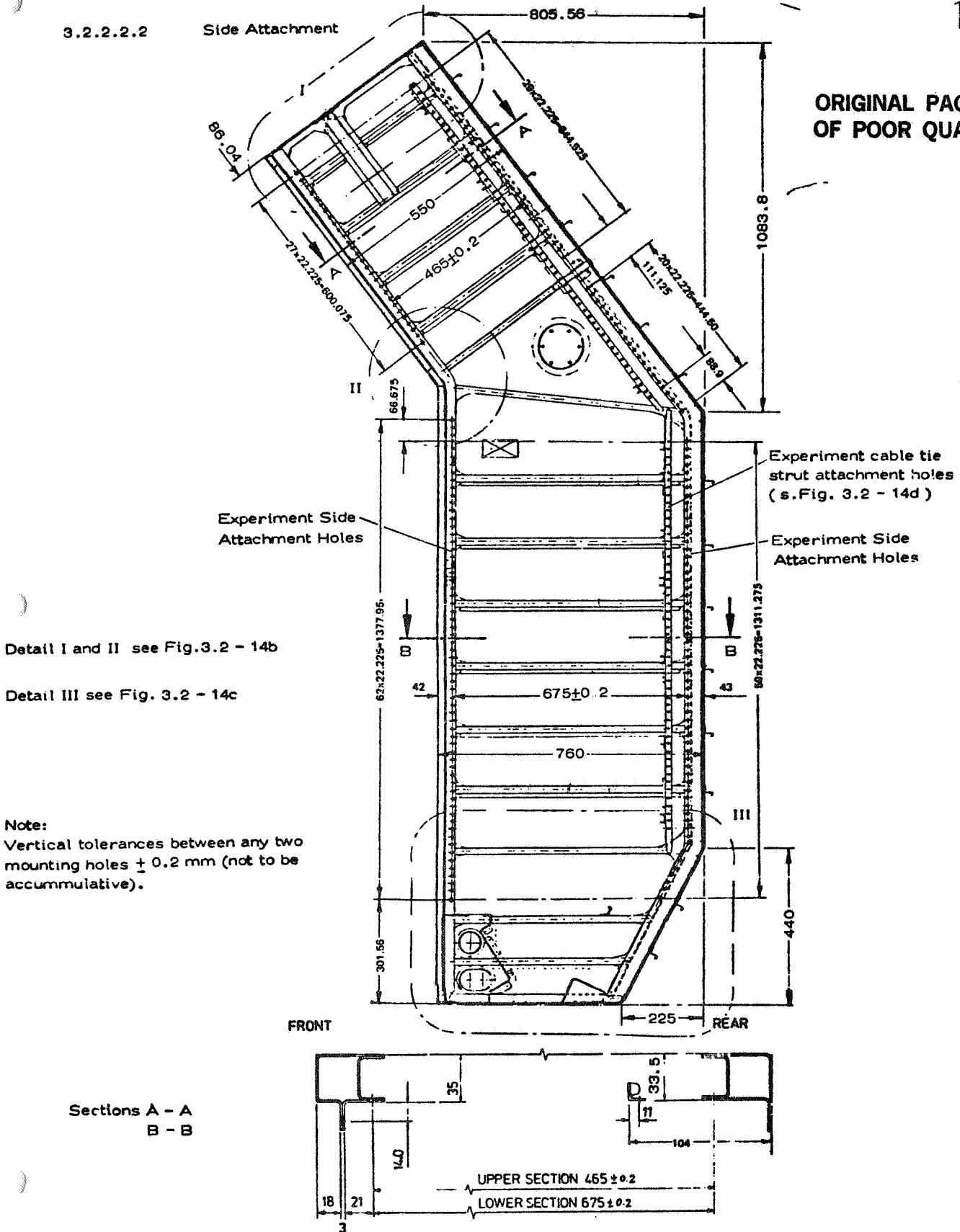
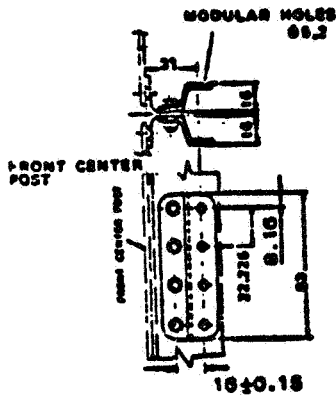


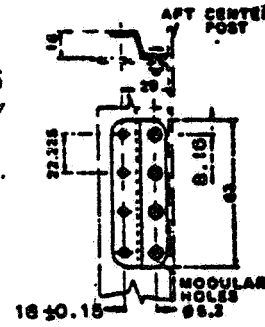
Figure 3.2 - 14a: Side Attachment - Outer Walls

Z-Fitting Type 1



Type 1 as used at front center post

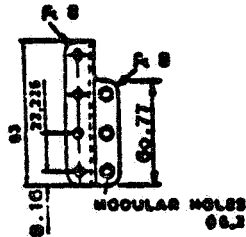
ORIGINAL PAGE IS
OF POOR QUALITY



Typ 1 as used at rear center post

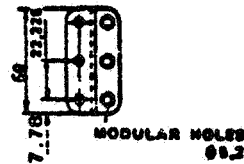
DCN
038

Z-Fitting Type 2 (not Spacelab provided)

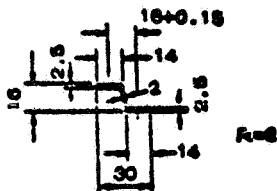


DCN
038

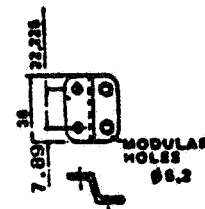
Z-Fitting Type 3



DCN
038



Z-Fitting Type 4 (not Spacelab provided)



DCN
038

Figure 3.2 - 15f : Center Post Z-Fittings

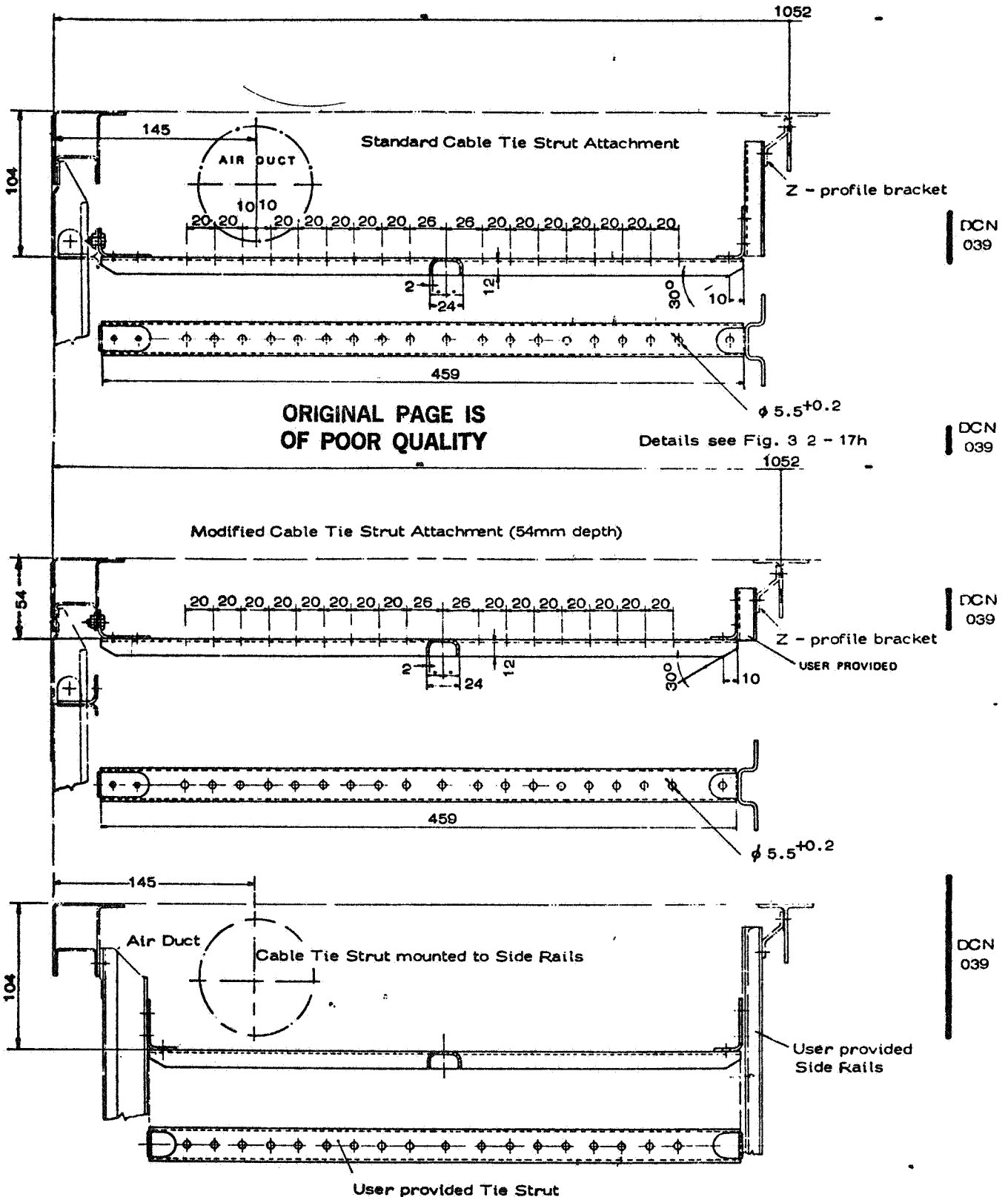


Figure 3.2 - 19b: Example of Cable Tie Strut Interface

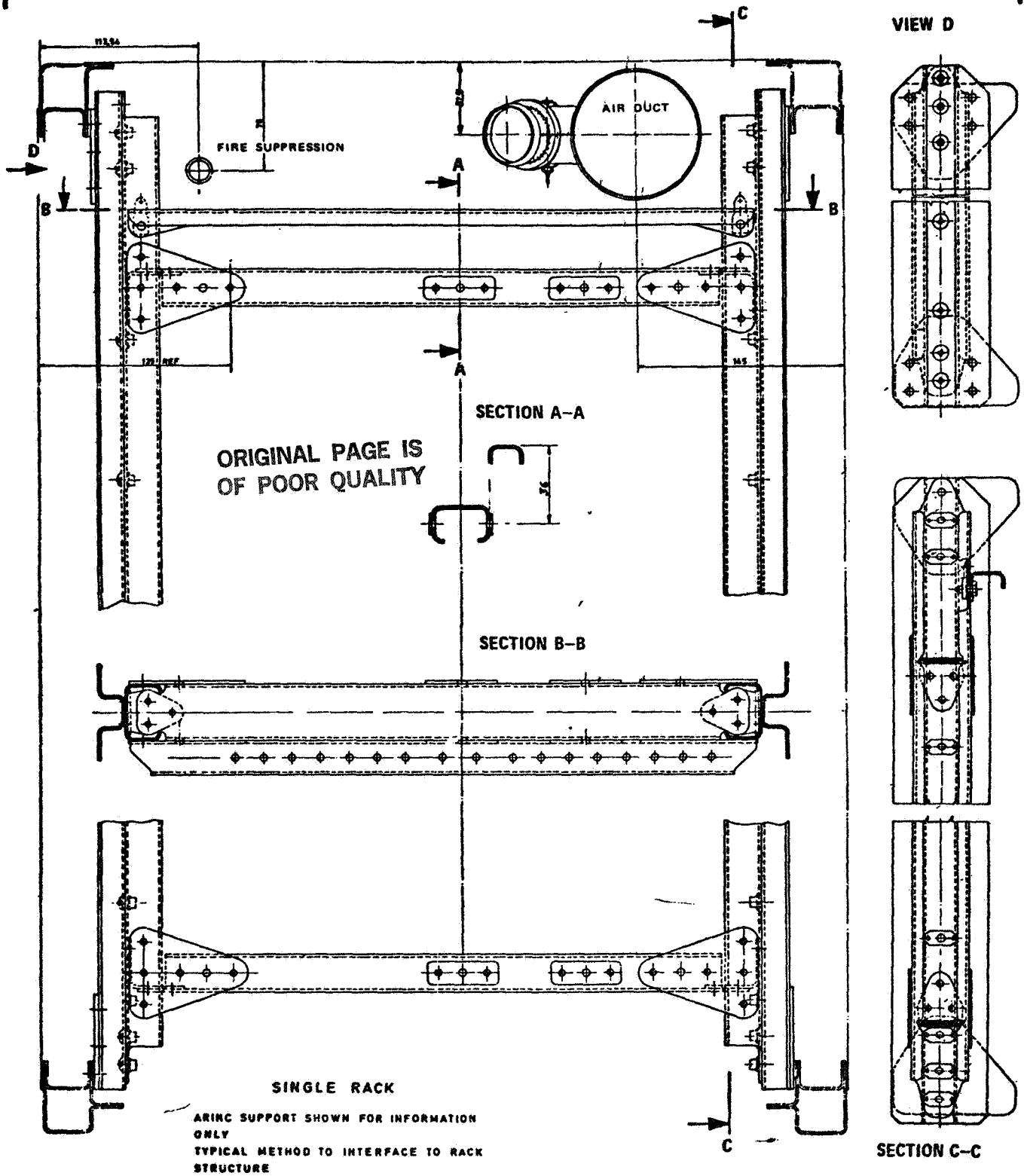
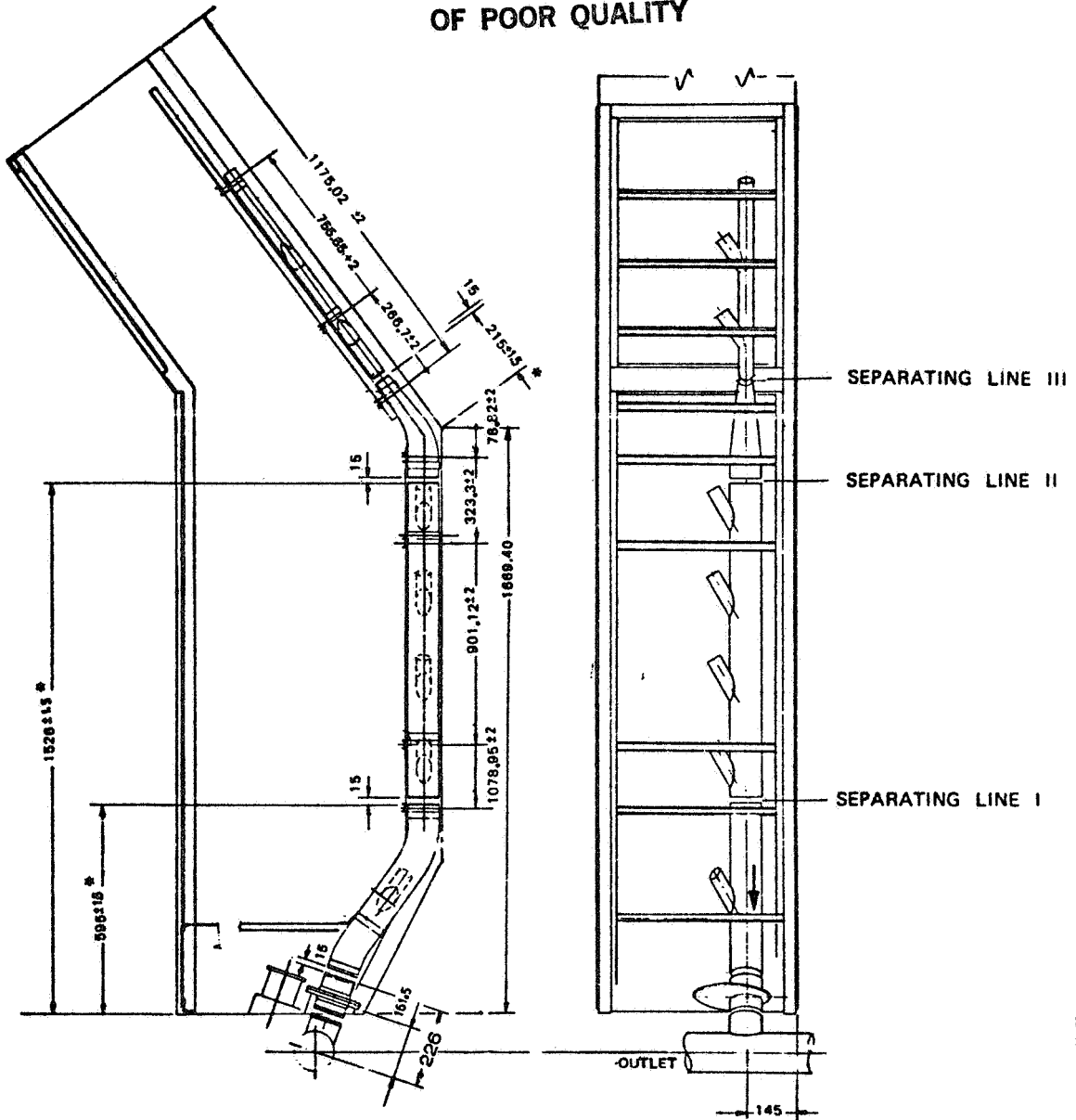


Figure 3.2 - 19d: Example - Single Rack Equipment Support

ORIGINAL PAGE IS
OF POOR QUALITY



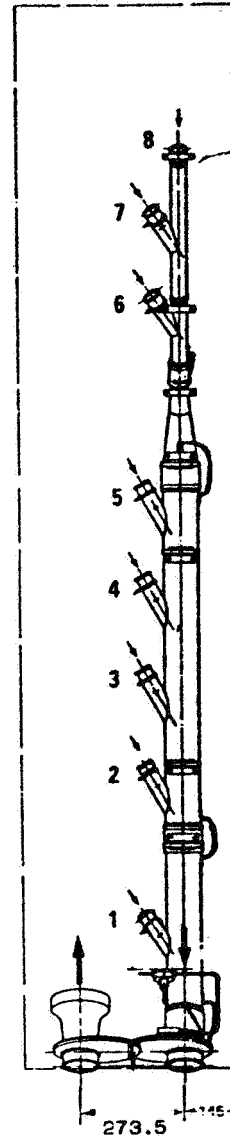
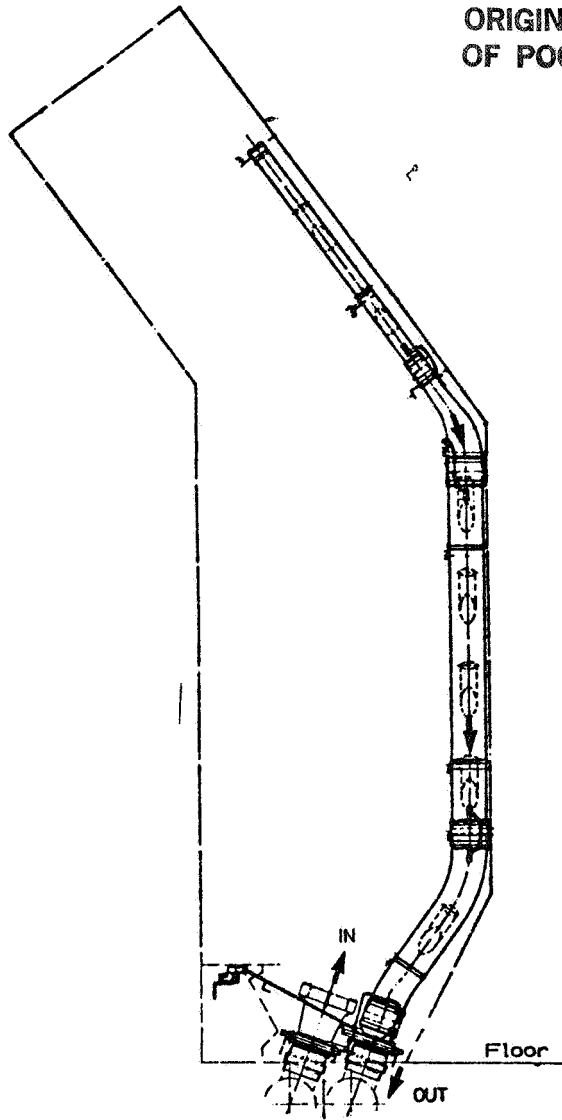
DCN
039

* LOCATION OF DUCT SEPARATION (SEE ALSO FIG. 3.2-22c)

Figure 3.2 - 22b: Air Duct Disconnection Points - Single Rack

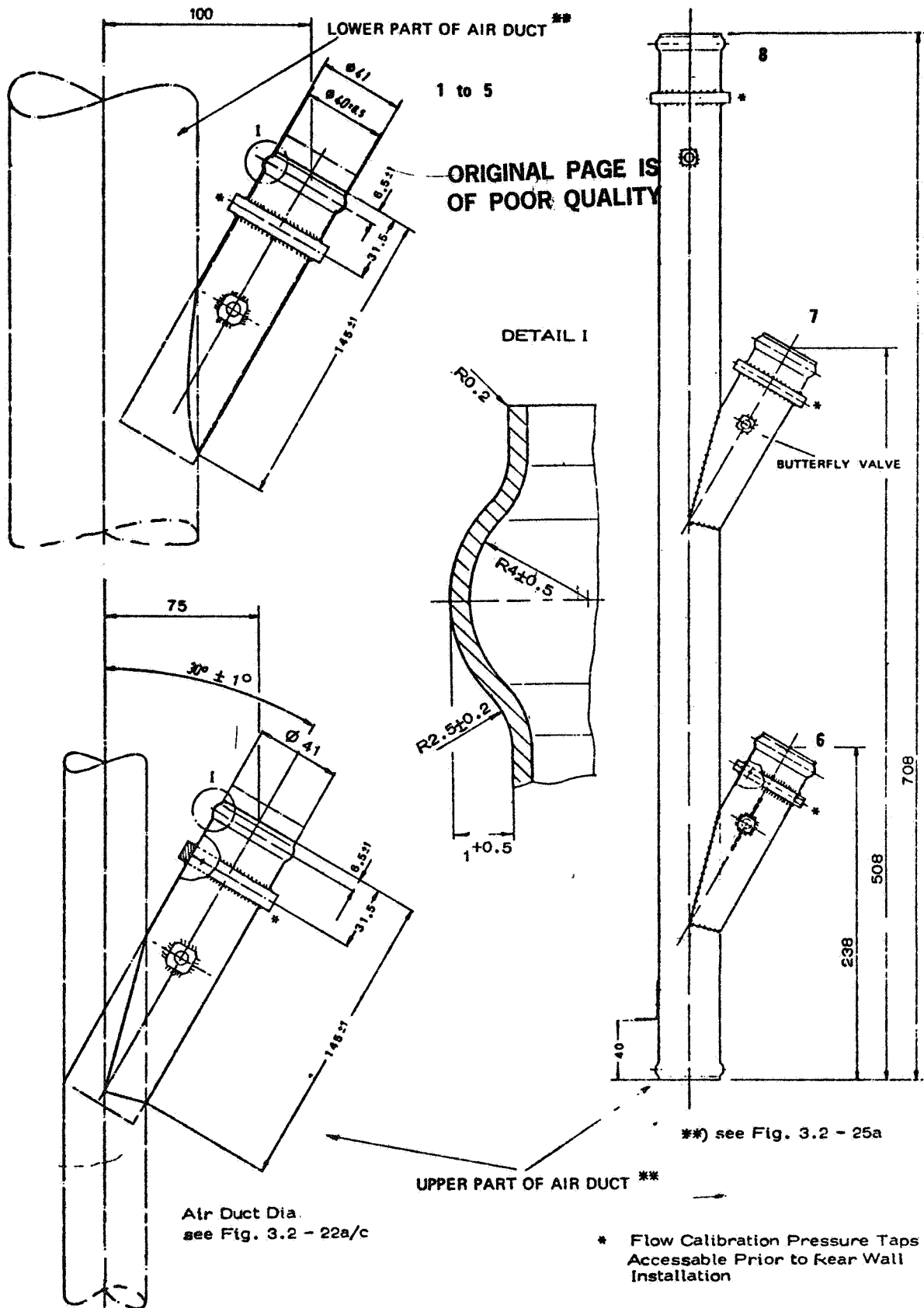
ORIGINAL PAGE IS
OF POOR QUALITY

DCN
039



Locations of Stubs see Fig.3.2-25a

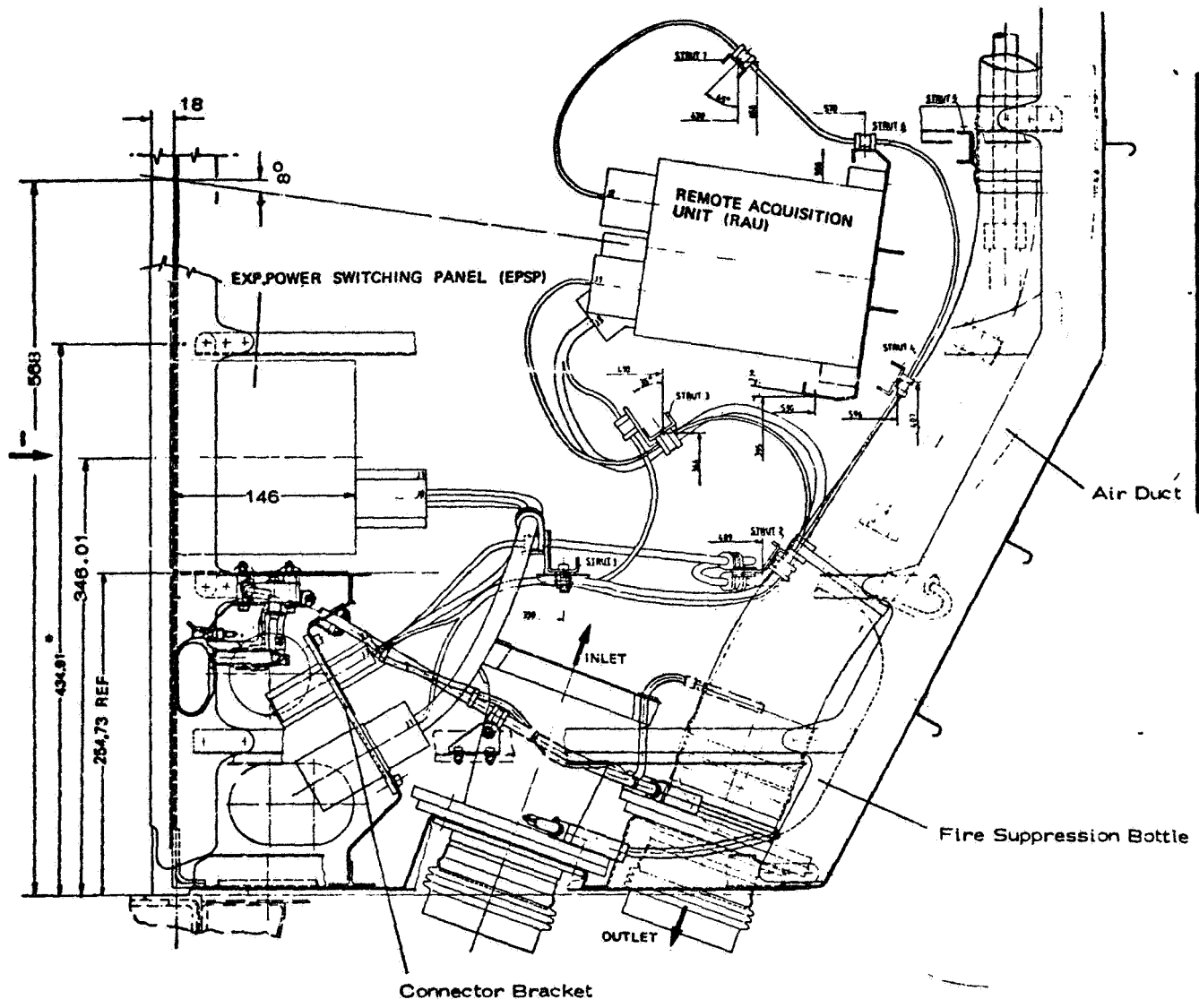
Figure 3.2 - 25b; Duct Details - Overview Single Rack



DCN
039

Figure 3.2 - 25c: Stub Dimensions

ORIGINAL PAGE IS
OF POOR QUALITY



DCN
039

Note : Strut 1 & 2 are installed permanently
Strut 3 thru 7 are part of the RAU support structure.
Strut 4 & 5 must be replaced by cable tie struts
listed in Table 3.2 - 1 if no RAU is installed.

see Fig. 3.2 - 13b

Figure 3.2 - 29a: Detailed Overview of Lower Rack Equipment - Side View

**ORIGINAL PAGE IS
OF POOR QUALITY**

3.2.6 Rack Load Carrying Capability

The dimensioning loads of the rack (para 3.2.7) are :

- (1) bracket loads for the local carrying capability. These loads are applicable for the equipments at the interface of the rack to the equipment (attachments).
Equipments must be attached to the rack in such a manner that a "hard-mounted" fundamental frequency above 35 Hz is reached -
- (2) flight loads for the overall carrying capability.

The bracket loads and the flight loads can be independently determined because of the decoupling of the equipment frequencies from the overall rack frequencies, i.e. $f_0 > 35$ Hz for equipments and $f_0 > 15$ Hz for the rack .

For certain mass configurations, it is possible to have the following rack configurations (see Tables 3.2-2 and 3.2 - 3):

- double rack with lower center post and 4, 3, 2, 1 or 0 diagonal shear load struts, whereas the number of diagonals depends on the masses to be accommodated in the rack.
- double rack without lower center post with 2, 1, or 0 diagonal shear load struts; however, no suitable diagonals are Spacelab provided.
- single rack with 2, 1, or 0 diagonal shear load struts

For the accommodation of payload equipment in the racks, three types of integration are standardized as per para 3.2.6.2 :

- front mounted
- front mounted / back supported
- shelf mounted

ORIGINAL PAGE IS
OF POOR QUALITY

3.2.6.1 Overall Rack Load Carrying Capability

The load carrying capabilities quoted comprise payload and Spacelab mission dependent equipment (EPSP, RAU, ICRS etc). Masses accommodated in experiment racks have to comply with the following constraints:

- The maximum allowable mass for the entire rack is
 - for double racks 580 kg total
 - 290 kg each side
 - for double racks, lower center wall removed 480 kg (tentative value).
 - for single racks 290 kg

DCN
039

These values apply only as long as the c.g.'s of the accommodated masses are within the envelopes given in Figure 3.2-34. For c.g.'s outside these envelopes, the maximum allowable masses will decrease and case-by-case analyses will be required.

DCN
039

- The maximum allowable mass for the upper part of the rack is 72.5 kg for single racks and each side of double racks

The allowable mass for the lower part of the rack depends on the number and locations of the shear load struts installed, and the mass distribution between the planes of the shear load struts. The allowable masses for the lower parts of the racks are given in Tables 3.2-2 and 3.2-3 as a function of these parameters.

ORIGINAL PAGE IS
OF POOR QUALITY

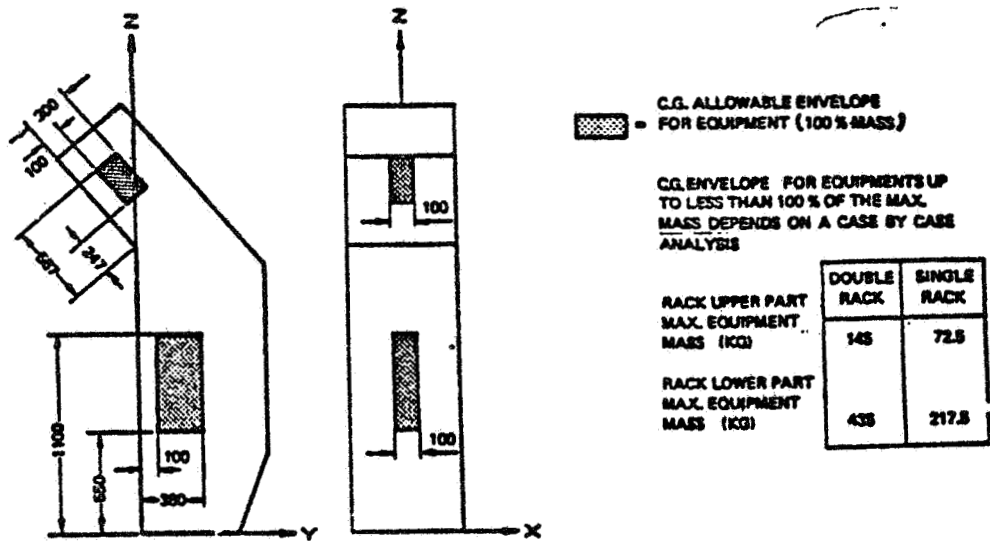


Figure 3.2 - 34 : C.G. Distribution Limitations for Single Rack and each Side of a Double Rack

*CLASS. LTR.	OPERATION	PROGRAM	SEQUENCE NO.	REV. LTR.
	1254	AGCE	022	
PIR NO.				
*USE "C" FOR CLASSIFIED AND "U" FOR UNCLASSIFIED				

PROGRAM INFORMATION REQUEST / RELEASE

FROM G. L. FOGAL		TO DISTRIBUTION		
DATE SENT 4/30/81	DATE INFO. REQUIRED	PROJECT AND REQ. NO.	REFERENCE DIR. NO.	

SUBJECT
TASK 9.2 - INTERCHANGEABLE FLUID FLOW CELL ASSEMBLY, FEASIBILITY REPORT

INFORMATION REQUESTED/RELEASED

1.0 SUMMARY

The basic AGCE system configuration can be designed to accommodate fluid flow cells of various diameters. However, the design of the scanning and UV irradiation optics, the high voltage power supply and thermal control interface elements must be scaled to the requirements of each flow cell assembly. Thus interchangeability of flow cell assemblies must also include the simultaneous replacement of other system elements sized to match the new flow cell assembly. Even so, time and dollars can be saved in development of subsequent experiments wherein different (from the initial AGCE) flow cell assemblies are required.

2.0 BACKGROUND

Task 9.1 is concerned with the overall AGCE system. A key design driver in generating the overall system configuration is the physical size of the flow cell assembly. Based on the size range specified for study by the program work statement, a 6.0 cm radius was selected as the maximum expected size for the inner diameter of the flow cell outer sphere. The assembly drawings generated under TASK 9.1 reflect this size. The intent of TASK 9.2 then is to assess the feasibility of interchanging flow cell assemblies (based on TASK 9.1 results and using modular techniques) to satisfy potential requirements of subsequent AGCE flight programs. This feasibility assessment is addressed below.

G. FOGAL R. HOMSEY S. NESTE	PAGE NO.	RETENTION REQUIREMENTS	
	OF	COPIES FOR	MASTERS
		<input type="checkbox"/> 1 MO.	<input type="checkbox"/> 3 MOS.
		<input type="checkbox"/> 3 MOS.	<input type="checkbox"/> 6 MOS.
		<input type="checkbox"/> 6 MOS.	<input type="checkbox"/> 12 MOS.
		<input type="checkbox"/> MOS.	<input type="checkbox"/> MOS.
		<input type="checkbox"/>	<input type="checkbox"/> DO NOT DESTROY

3.0 IMPLEMENTATION

Two degrees of interchangeability are apparent. First, interchangeability wherein only internal dimensions of the flow cell assembly have been changed and second, interchangeability wherein both internal and external dimensional changes have occurred. In the former case, the physical relationship and interfaces with surrounding AGCE system elements remain unchanged whereas in the latter case, physical relationships with other system elements will have changed even though some interfaces may not be effected. However, in both cases, some of the surrounding system elements must be modified to maintain optimum performance of the system. Thus a change in external and internal diameters of the flow cell assembly impacts the scanning and UV irradiation optics; a change in dielectric fluid volume and gap spacing effects the load on the high voltage power supply; thermal control elements must be scaled to fit the changed dimensions. Table 1 summarizes the potential impact of flow cell size changes on other AGCE system elements.

From the above, it is apparent that except for minor flow cell changes, many AGCE system elements must be redesigned or relocated in order to accommodate a different size flow cell assembly. However, the impact is minimized if the initial AGCE system is configured for the largest size flow cell assembly expected in the future. With this approach, sufficient mounting space will be available within the AGCE protective outer enclosure and on the rotating turntable to accommodate the modified (and presumably same size or smaller) components, consistent with a smaller size flow cell; relocation of system components will not be required. From a modularity viewpoint, this approach also permits the establishment of standard mounting interfaces for the effected system elements. The system configuration being generated under TASK 9.1 is also consistent with this approach.

4.0 CONCLUSIONS/RECOMMENDATIONS

Flow cell assembly interchangeability is complicated by the need to also redesign surrounding system elements to match the specific flow cell assembly selected. Even so, development time and dollars can be saved on future programs, particularly if subsequent flow cell assemblies are smaller in size than that selected for the initial AGCE system design.

TABLE 1 INTERCHANGEABILITY IMPACT OF VARIOUS SIZE
FLUID FLOW CELL ASSEMBLIES*

AGCE SYSTEM ELEMENT	IMPACT PROBABLE	COMMENT
Scanning optics	Yes	Smaller internal diameter effects scan coverage
UV irradiation optics	Yes	Change in mean fluid radius effects spot focusing
High Voltage Power Supply	Yes	Change in dielectric fluid volume and gap will effect impedance; new high voltage electrical connection require
Thermal Control		
Sphere Heat Exchangers	Yes	Resize to match change in flow cell
Coolant loop pumps, TEM heat pumps and rotating heat exchanger	No	
Dust Removal	No	
Turntable	No	Assuming standardized interfaces
Turntable Assembly	Yes	New Plumbing (tubing) runs probably required
Control Electronics	No	
Control Panel	No	
Software	No	

*Assuming initial AGCE design incorporates maximum size flow cell assembly consistent with Spacelab rack dimensional constraints.

3.7 EXPERIMENT DESIGN

Task 9.1 - AGCE Configuration

PIR NO.

-031

.)

)

)

ORIGINAL PAGE IS
OF POOR QUALITY

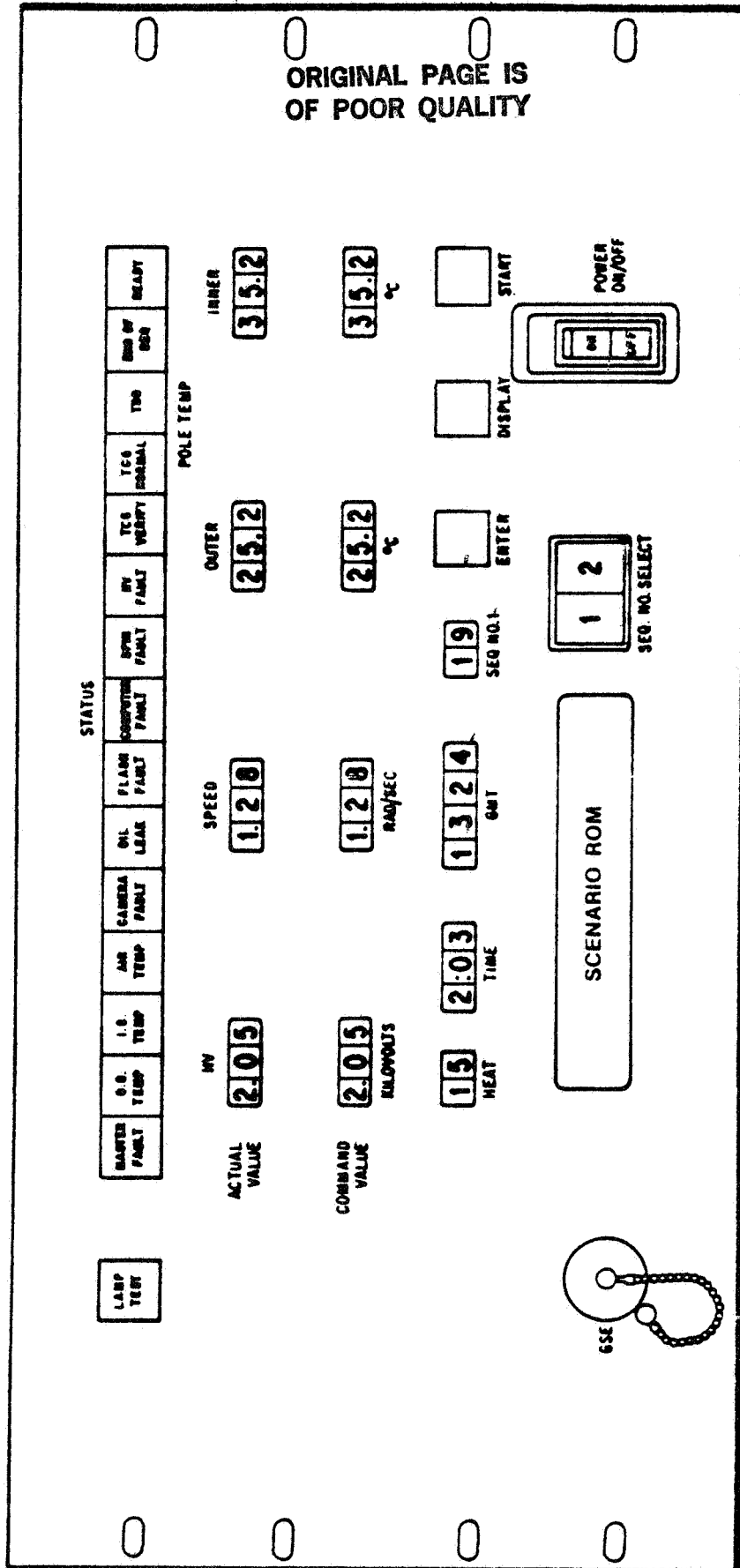


FIGURE 6 GFFC DISPLAY/CONTROL PANEL

ORIGINAL PAGE IS
OF POOR QUALITY

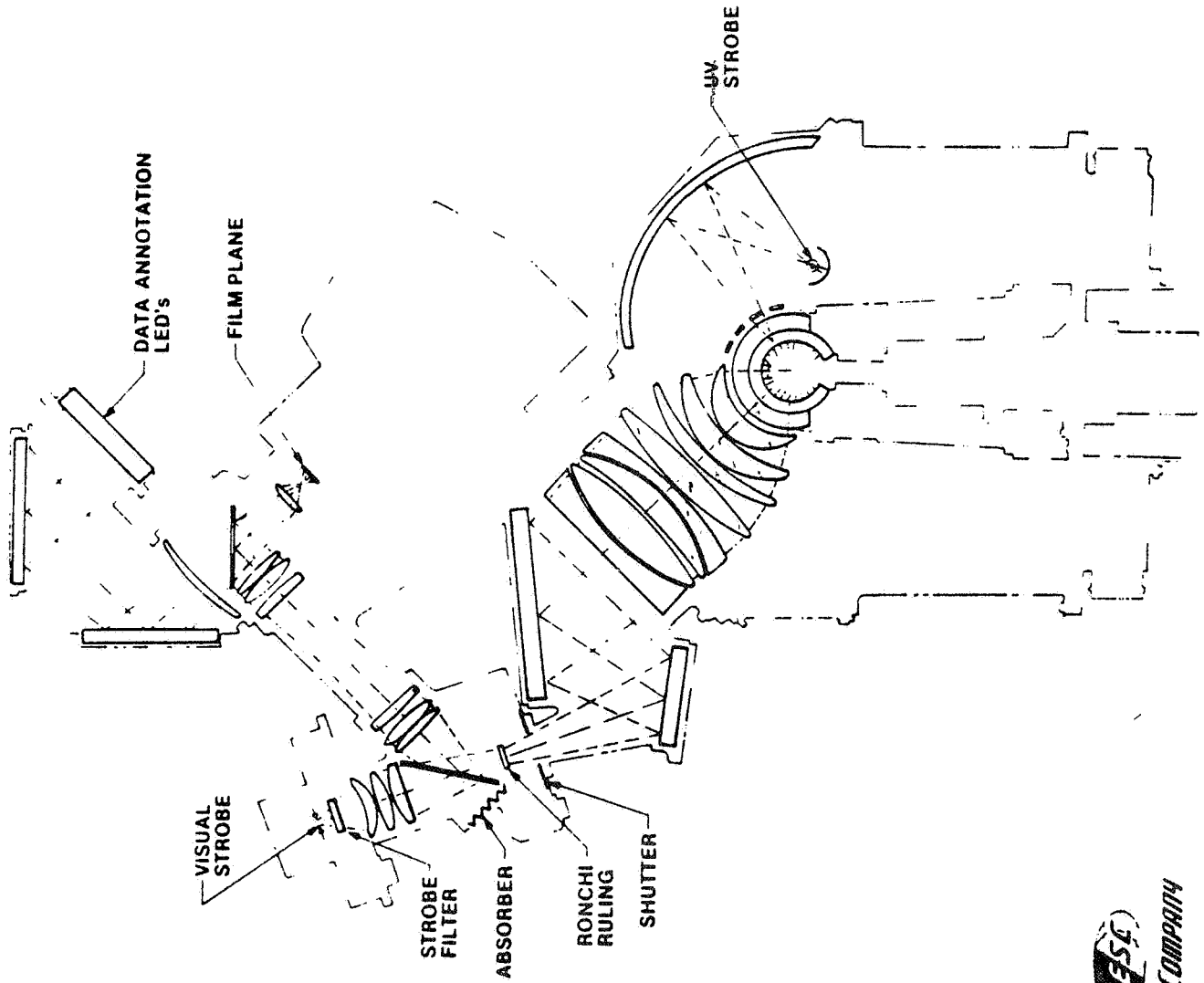


FIGURE 5 GFFC OPTICAL SCHEMATIC

inner and outer spheres to simulate the earth's atmosphere. Thermal control elements are provided to control the surface temperature of the inner sphere and the pole and equator of the outer sphere. Thermal gradients within the dielectric fluid are measured by means of a Rouchi ruling shadowgraph technique; flow rates are measured by observing the motion of UV activated photochromic dye "marker dots" within the dielectric fluid. This data, as well as other experiment data, are optically recorded on film for post flight analysis, see Figure 5.

Operation of the GFFC hardware is controlled by a microcomputer located in the electronics assembly. Via the control panel, the operator selects the desired experiment scenario (one of 24 timelines stored in memory). The microcomputer then executes the experiment as directed by the scenario instructions. The display panel, figure 6, provides system status indicators as well as indications of computer commanded vs. actual values for certain parameters. This permits the operator to monitor GFFC system performance.

As compared to the GFFC system, the basic thrust of the AGCE system is to enhance experiment capability of the fluid flow cell by increasing the size of the cell and by reversing the direction of heat flow thru the dielectric fluid in the flow cell (outward for GFFC; inward for AGCE). The proposed implementation of the fluid flow cell enhanced capability, which has been assessed under TASKS 1 thru 8, will result in a AGCE system configuration exhibiting significant differences as compared to the current GFFC system configuration. Thus, the larger flow cell requires a new optics approach, a higher cell voltage and a larger turntable. Reversing the heat flow encompasses cooling the inner sphere of the flow cell as well as cooling the outer sphere pole. The new optics approach selected provides real time data in a form suitable for telemetering to the POCC. This permits simplification of the system control panel and enhanced PI participation at the POCC. These features have been incorporated into the AGCE system configuration as discussed in the following sections.

ORIGINAL PAGE IS
OF POOR QUALITY

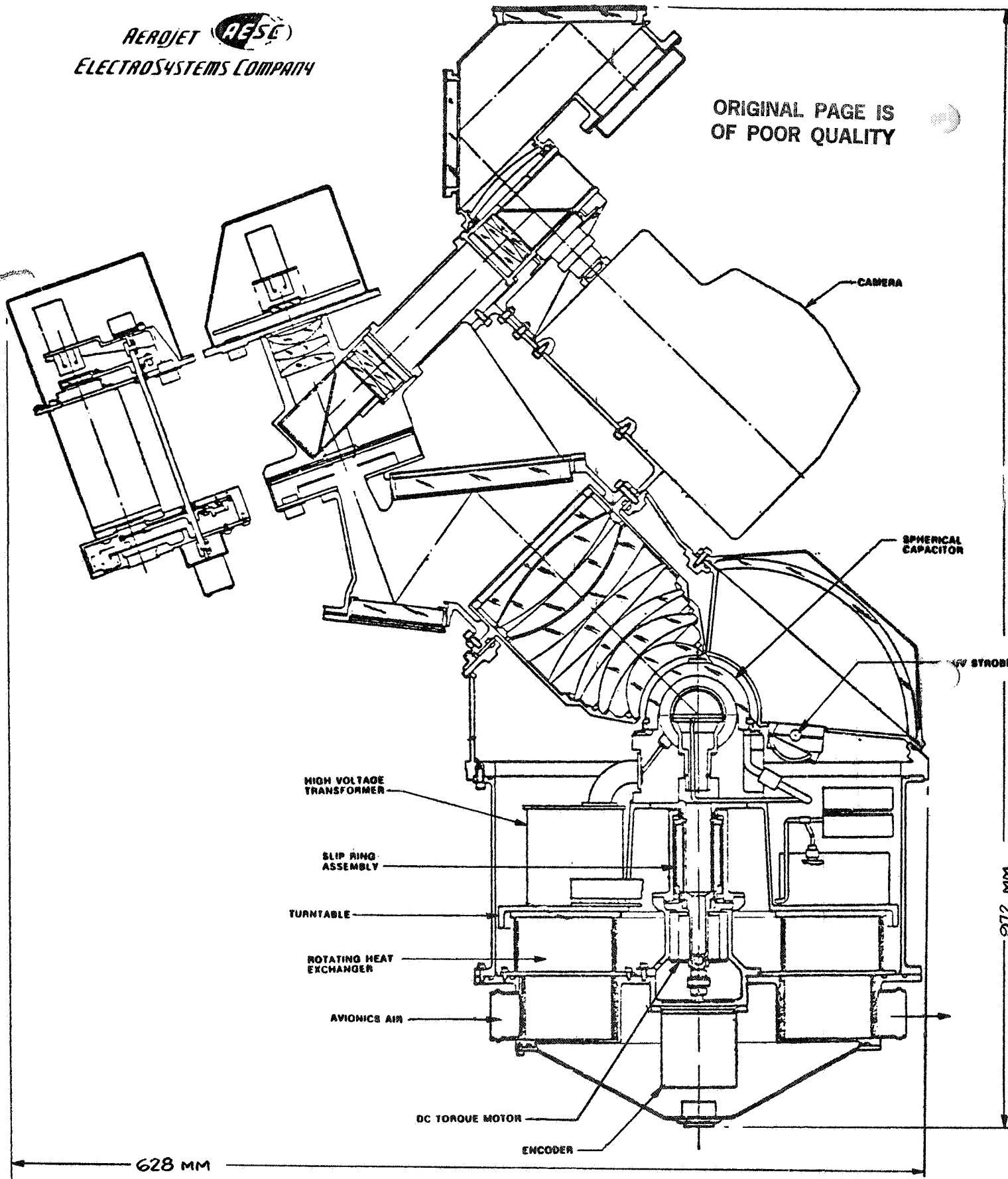


FIGURE 4 GFFC MECHANICAL ASSEMBLY (CROSS-SECTION VIEW)

ORIGINAL PAGE IS
OF POOR QUALITY

AEROJET 
ELECTROSYSTEMS COMPANY

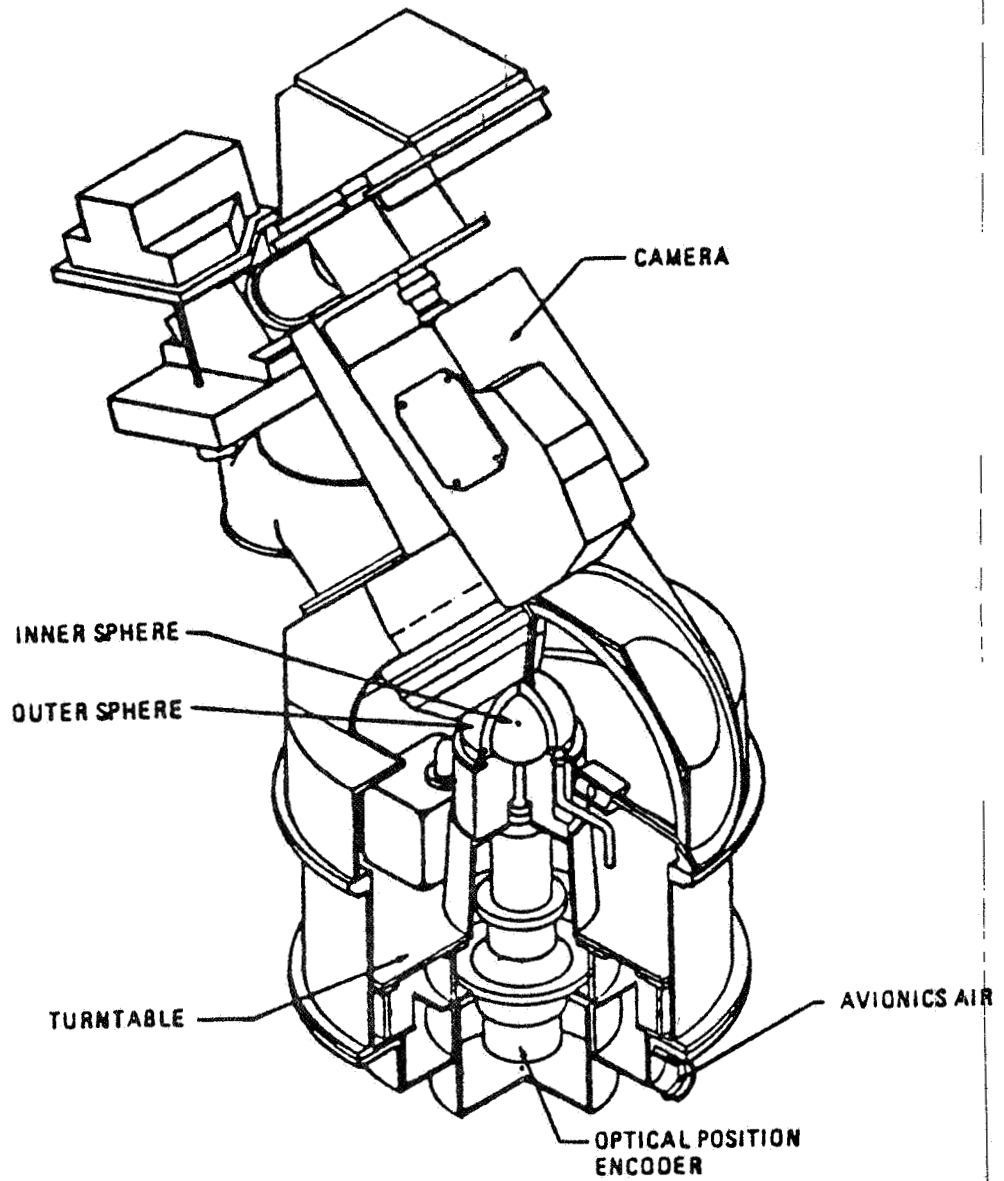


FIGURE 3 GFFC MECHANICAL ASSEMBLY (ISOMETRIC VIEW)

ORIGINAL PAGE IS
OF POOR QUALITY

HEROJET 
ELECTROSYSTEMS COMPANY

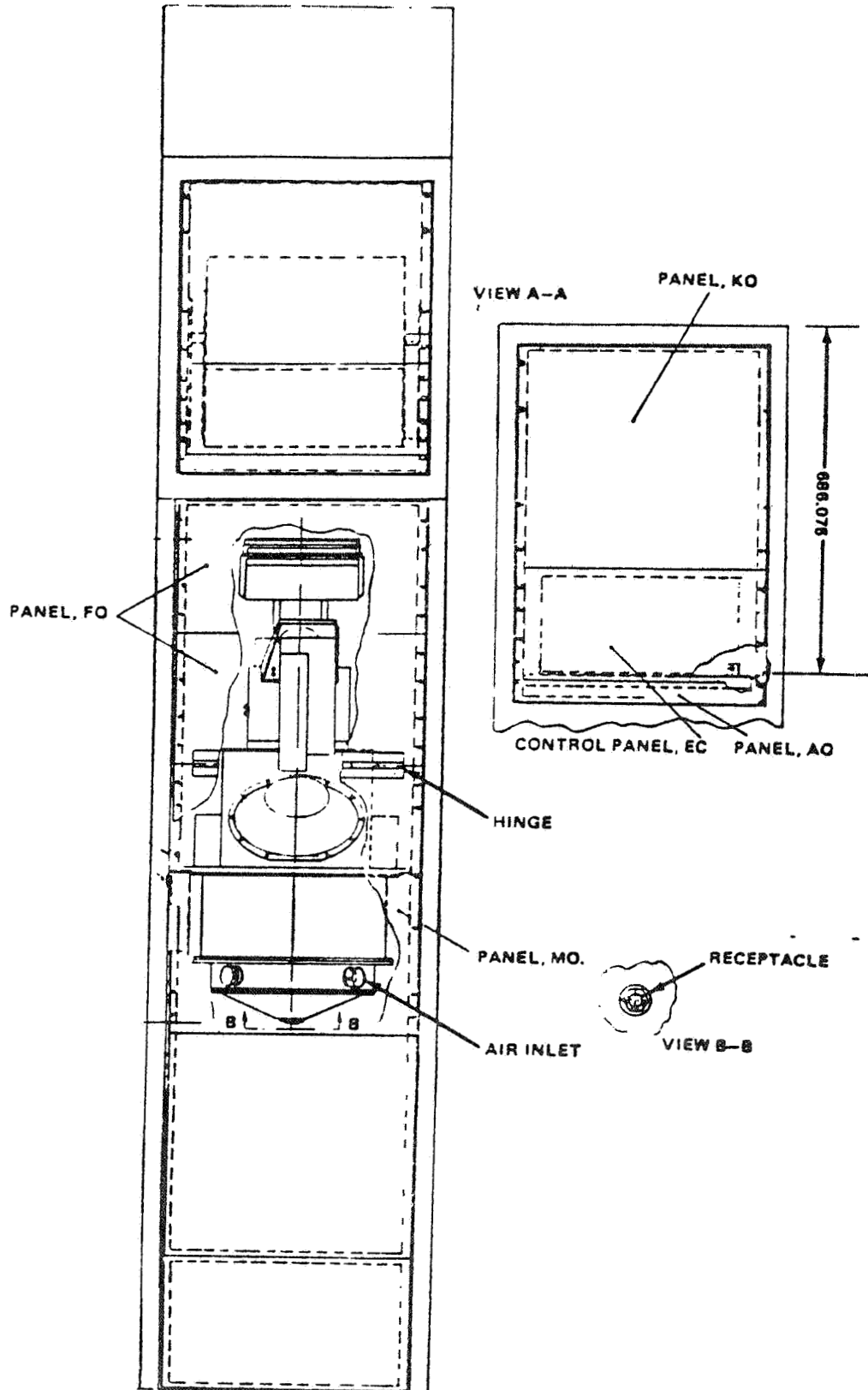


FIGURE 2 GFFC INSTALLATION IN SPACELAB RACK (FRONT VIEW)

ORIGINAL PAGE IS
OF POOR QUALITY

READJET 
ELECTROSYSTEMS COMPANY

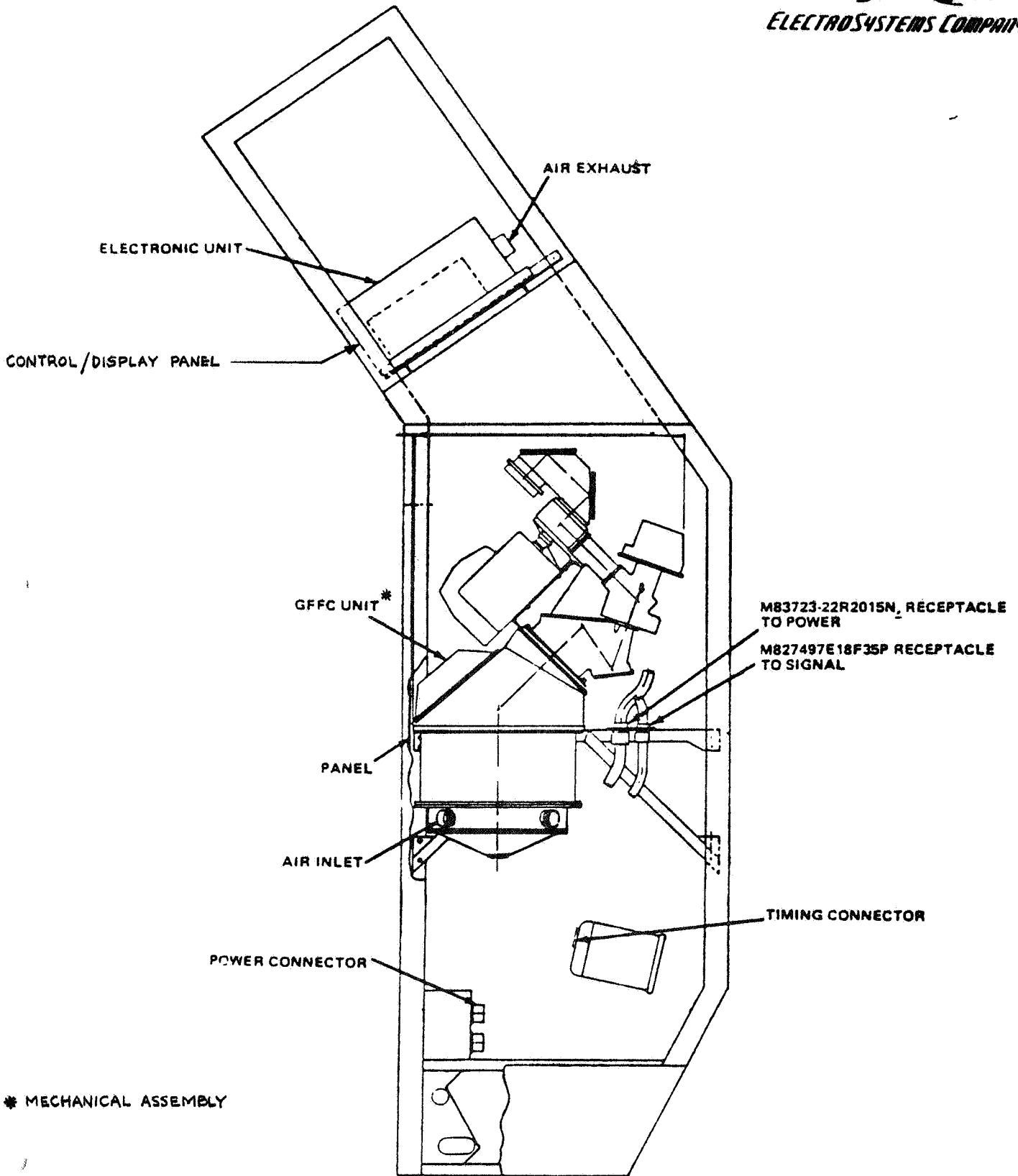


Figure 1 GFFC INSTALLATION IN SPACELAB RACK (SIDE VIEW)

CLASS. LTR.	OPERATION	PROGRAM	SEQUENCE NO.	REV. LTR.
	1254	AGCE	031	
PIR NO.				

PROGRAM INFORMATION REQUEST / RELEASE

*USE "C" FOR CLASSIFIED AND "U" FOR UNCLASSIFIED

FROM G. L. Fogal <i>GLF</i>	TO Distribution
--------------------------------	--------------------

DATE SENT 6/22/81	DATE INFO. REQUIRED	PROJECT AND REQ. NO.	REFERENCE DIR. NO.
----------------------	---------------------	----------------------	--------------------

SUBJECT
TASK 9.1, AGCE CONFIGURATION

INFORMATION REQUESTED/RELEASED

**ORIGINAL PAGE IS
OF POOR QUALITY**

1.0 SUMMARY

An AGCE flight configuration has been generated which is compatible with Spacelab installation and operational constraints. The configuration is based on accomodating the largest size spherical capacitor specified by the contract work statement (5.0 cm inner sphere diameter), plus the optical, thermal control, dust removal and electronic control concepts resulting from TASKS 1 thru 8 and assumed AGCE system performance requirements. Sketches showing key dimensions as well as a full scale mockup were generated to define and illustrate the AGCE flight configuration. Estimated total system weight is 104.3 Kg.

2.0 BACKGROUND

A precursor to the AGCE system, the GFFC (Geophysical Fluid Flow Cell) experiment system, is currently under development as a Spacelab experiment, and as such conforms to Spacelab design and operational constraints and resource limitations. The GFFC system is comprised of two major assemblies, a mechanical assembly and an electronics assembly, plus ancillary elements such as electrical cabling, closeout panels and support structure. Figures 1 and 2 show the GFFC system installed in a standard Spacelab single bay rack. The heart of the system, the fluid flow cell, is located in the mechanical assembly. As shown in Figures 3 and 4, the fluid flow cell is configured as a spherical capacitor with the dielectric fluid confined between the

cc: R. Homsey S. Neste G. Fogal	PAGE NO. OF	<input checked="" type="checkbox"/> RETENTION REQUIREMENTS	
		COPIES FOR	MASTEI /OR
		<input type="checkbox"/> 1 MO.	<input type="checkbox"/> 3 MOS.
		<input type="checkbox"/> 3 MOS.	<input type="checkbox"/> 6 MOS.
		<input type="checkbox"/> 6 MOS.	<input type="checkbox"/> 12 MOS.
		<input type="checkbox"/> MOS.	<input type="checkbox"/> MOS.
		<input type="checkbox"/>	<input type="checkbox"/> DO NOT DESTROY

3.0 TASK IMPLEMENTATION

Although the general requirements for the GFFC and AGCE systems are similar, the approach recommended for acquiring and processing AGCE experimental data as well as the approach recommended for providing the fluid flow cell temperature conditions differ significantly from those used in the GFFC system. This, plus the need to accommodate a larger flow cell, has resulted in a AGCE system configuration considerably different in detail from that for the GFFC system. However, wherever practical, the AGCE configuration is based on the corresponding portion of the GFFC system. For example, both systems use an air to air heat exchanger to transfer heat from the rotating turntable to the Spacelab's avionics air flow. Design details are similar with the AGCE turntable/heat exchanger combination somewhat larger to accommodate the larger AGCE fluid flow cell.

Thus, the general approach employed to generate the AGCE system configuration was to retain as much of the GFFC system configuration as practical, consistent with the recommendations of TASKS 1 thru 8. General configuration guidelines were also generated, see PIR 1254-AGCE-018, to assure compatibility of the AGCE configuration with the Spacelab. It should be noted that the AGCE system configuration described below is intended only to demonstrate that a successful AGCE system can be developed; the described configuration is not intended to necessarily represent in detail the final flight design configuration.

3.1 System Description

For the purpose of this configuration study, the AGCE system was assumed to provide the functions shown by Figure 7. As shown, the fluid flow cell is the heart of the system, simulating planetary or star conditions depending on the direction of heat flow. System operation is initiated by the operator who selects and starts the desired experiment. The microcomputer then issues commands in the appropriate time sequence to carry out the experiment. Periodically, or at the beginning of each experiment, the dielectric fluid in the flow cell is filtered to remove particulates.

ORIGINAL PAGE IS
OF POOR QUALITY

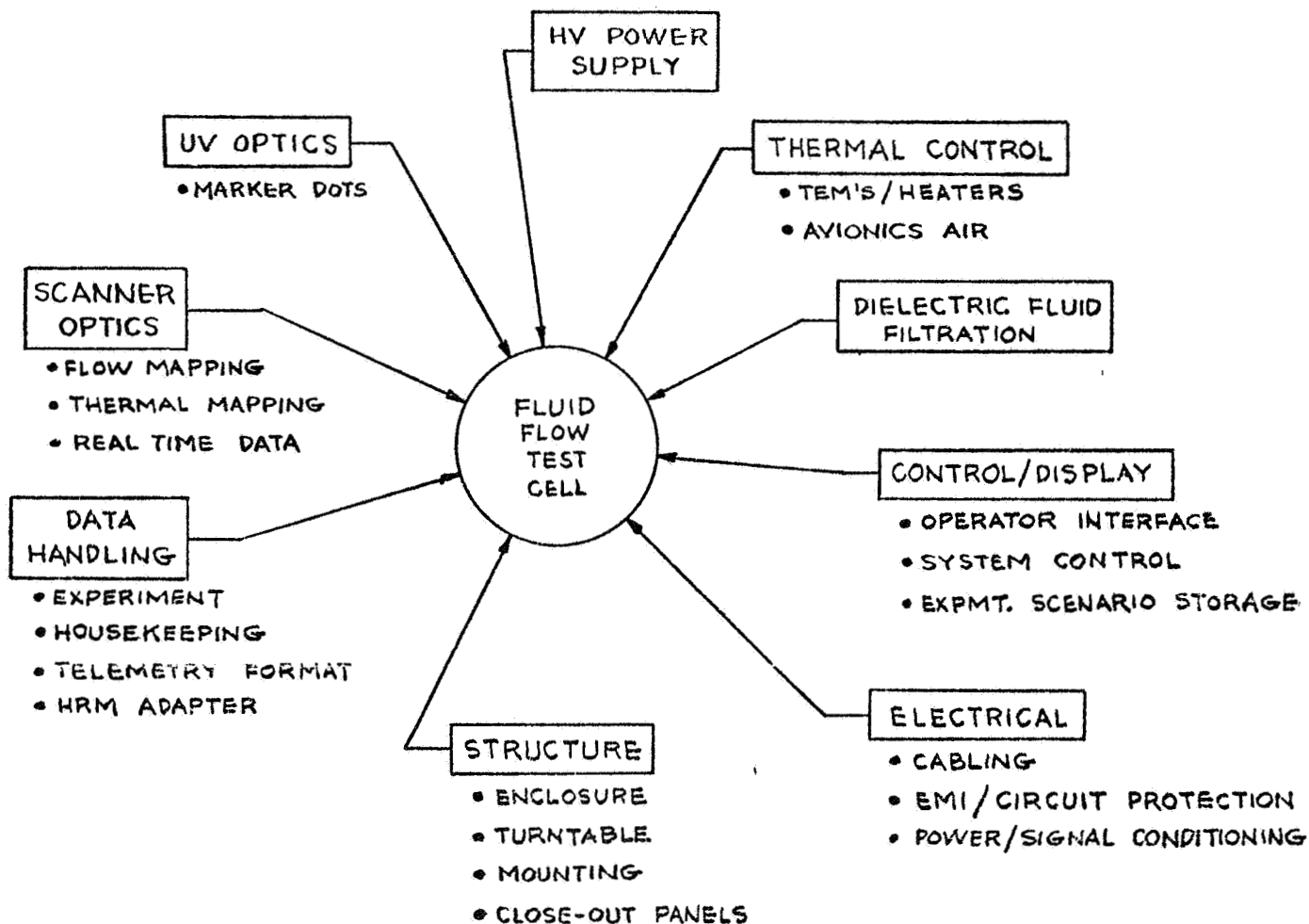


FIGURE 7 AGCE FUNCTIONAL DIAGRAM

The thermal control capability establishes the desired thermal conditions on the inner and outer spheres of the flow cell (as well as transporting excess heat from all system elements to the Spacelab avionics air). High voltage is applied to the flow cell to simulate a gravitational field. The UV optics generates marker dots by activation of discrete areas in the dielectric fluid. The scanner optics generates real time data (in electronic form) for thermal and flow mapping of the dielectric fluid. This experiment data, and other housekeeping data, are formatted by the data handling electronics for transmission to the POCC via the Spacelab HRM.

Figure 8 shows a full scale mock-up of the AGCE system installed in a simulated Spacelab single bay rack. The mock-up shown is consistent with the system functions noted above. Figure 9 shows the active interfaces with the Spacelab. Figure 10 shows details of the mechanical installation in a Spacelab rack. The AGCE system is contained within the dimensional envelope allowed by the Spacelab Payloads Accommodation Handbook SLP/2104. Note that the AGCE system may be installed in either a single or double bay rack. A right hand side installation is preferred if a double bay rack is used. This is because the avionics air duct connections for the right hand side are identical to those for a single bay rack. Figure 11 shows the cabling diagram for the system.

3.2 Mechanical Assembly

The Mechanical Assembly contains the fluid flow cell along with most of the remaining mechanical elements of the system. Specifically, the following major elements are included:

- o Fluid flow cell assembly
- o Turntable
- o Turntable drive motor/encoder
- o Turntable slip ring assembly
- o High voltage power supply
- o Coolant loops for inner/outer spheres
 - pump (2)
 - accumulator (2)
 - TEM cooler assembly (2)

ORIGINAL PAGE IS
OF POOR QUALITY

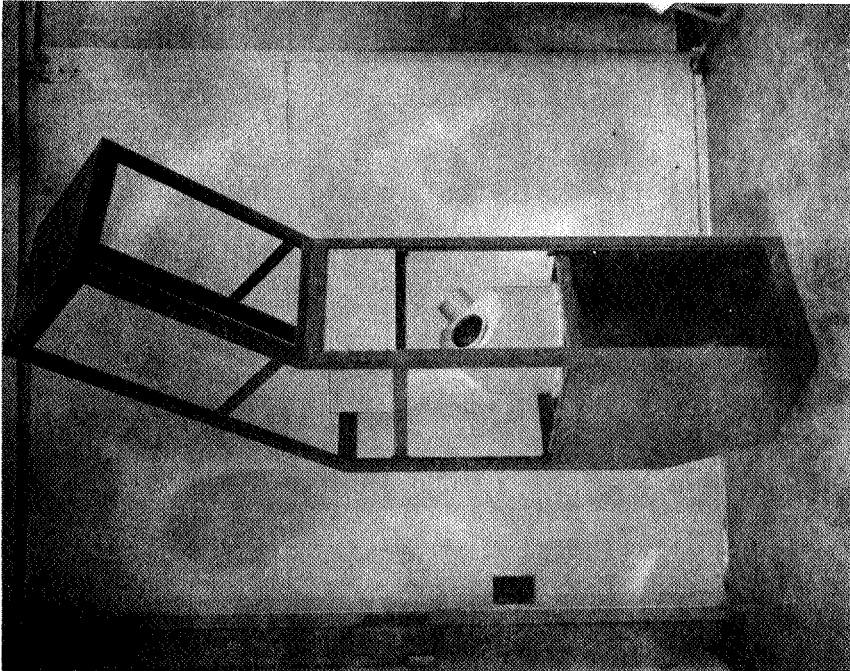
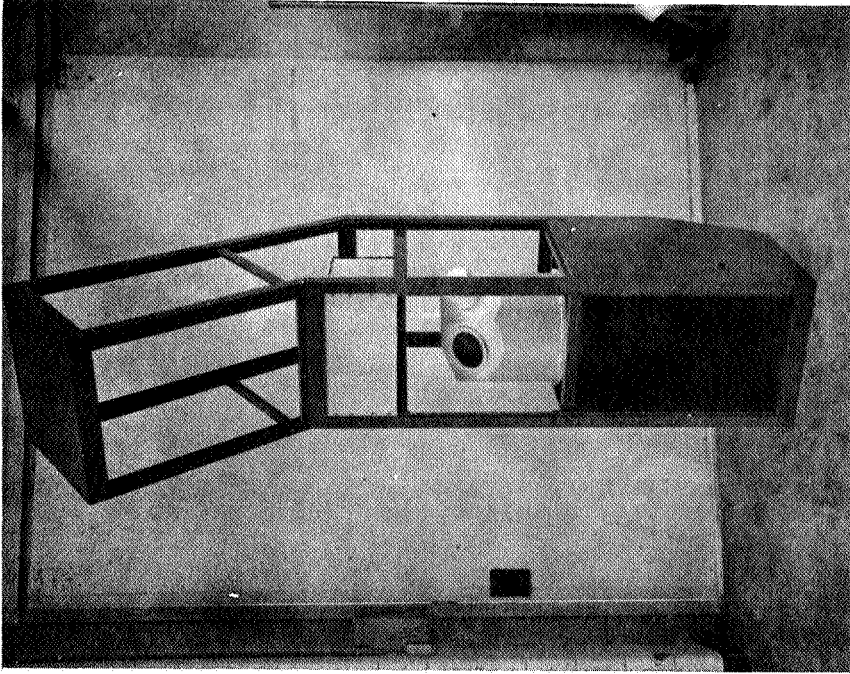


FIGURE 8 AGCE FULL SCALE MOCKUP IN SIMULATED SPACELAB
SINGLE BAY RACK (FRONT CLOSE-OUT PANELS, CABLING, AND
AVIONICS AIR DUCT CONNECTIONS NOT SHOWN)

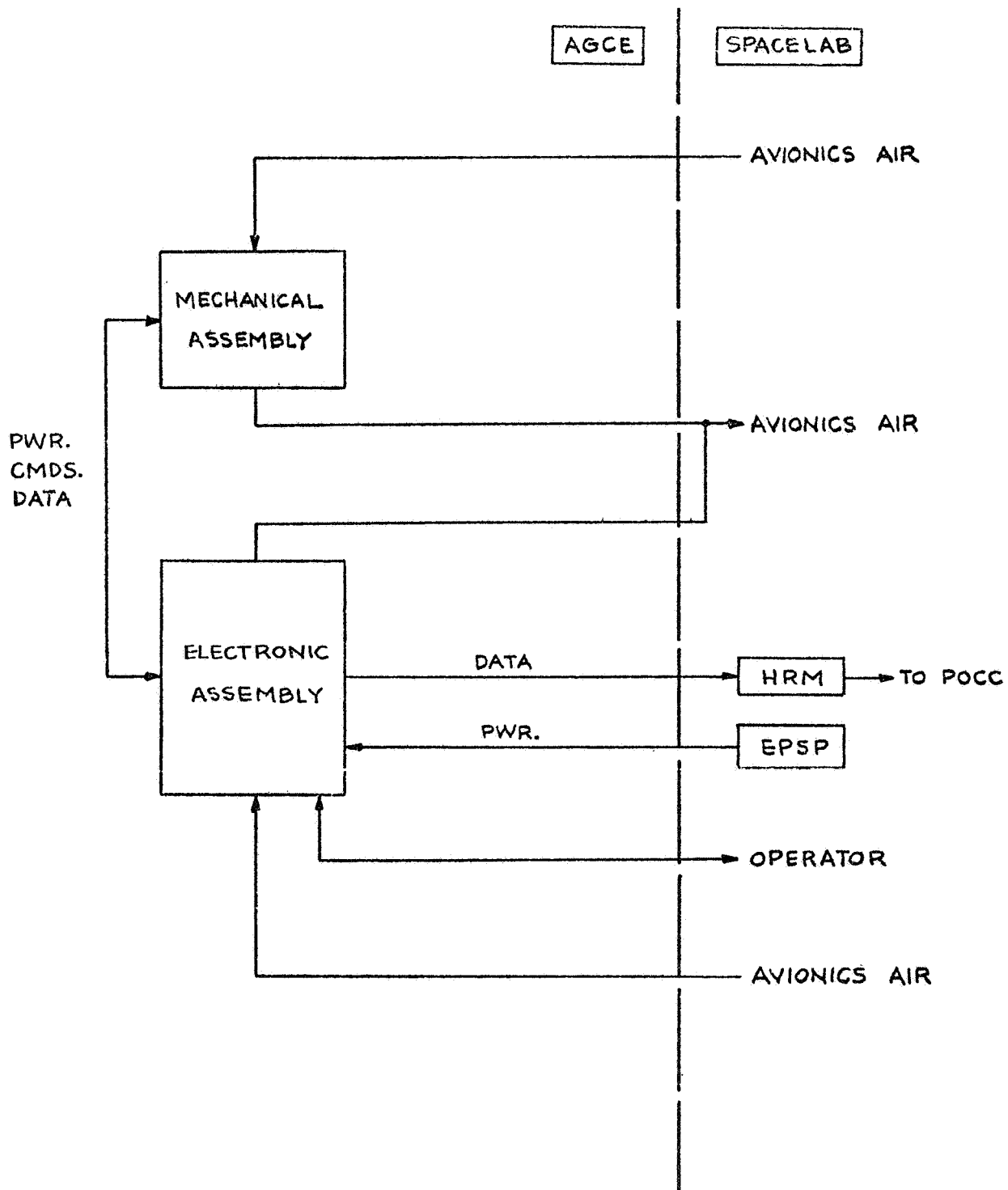


FIGURE 9 AGCE/SPACELAB INTERFACE DIAGRAM

ORIGINAL PAGE IS
OF POOR QUALITY

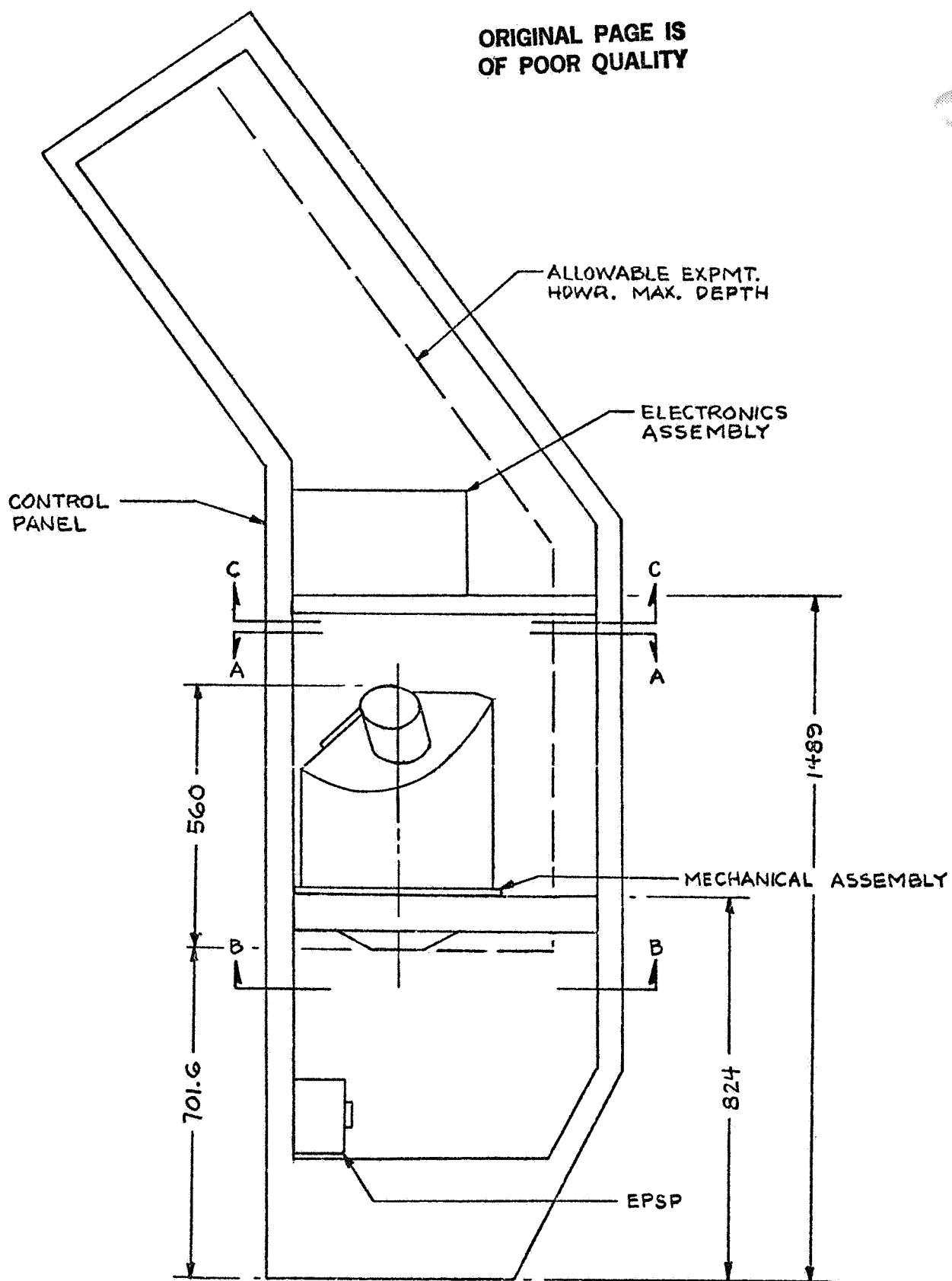


FIGURE 10(a) AGCE System Installed in Spacelab Rack
(CABLING, CLOSE-OUT PANELS, HOSE CONNECTIONS
TO AVIONICS AIR RETURN DUCT NOT SHOWN; DIMENSIONS IN MM)

ORIGINAL PAGE IS
OF POOR QUALITY

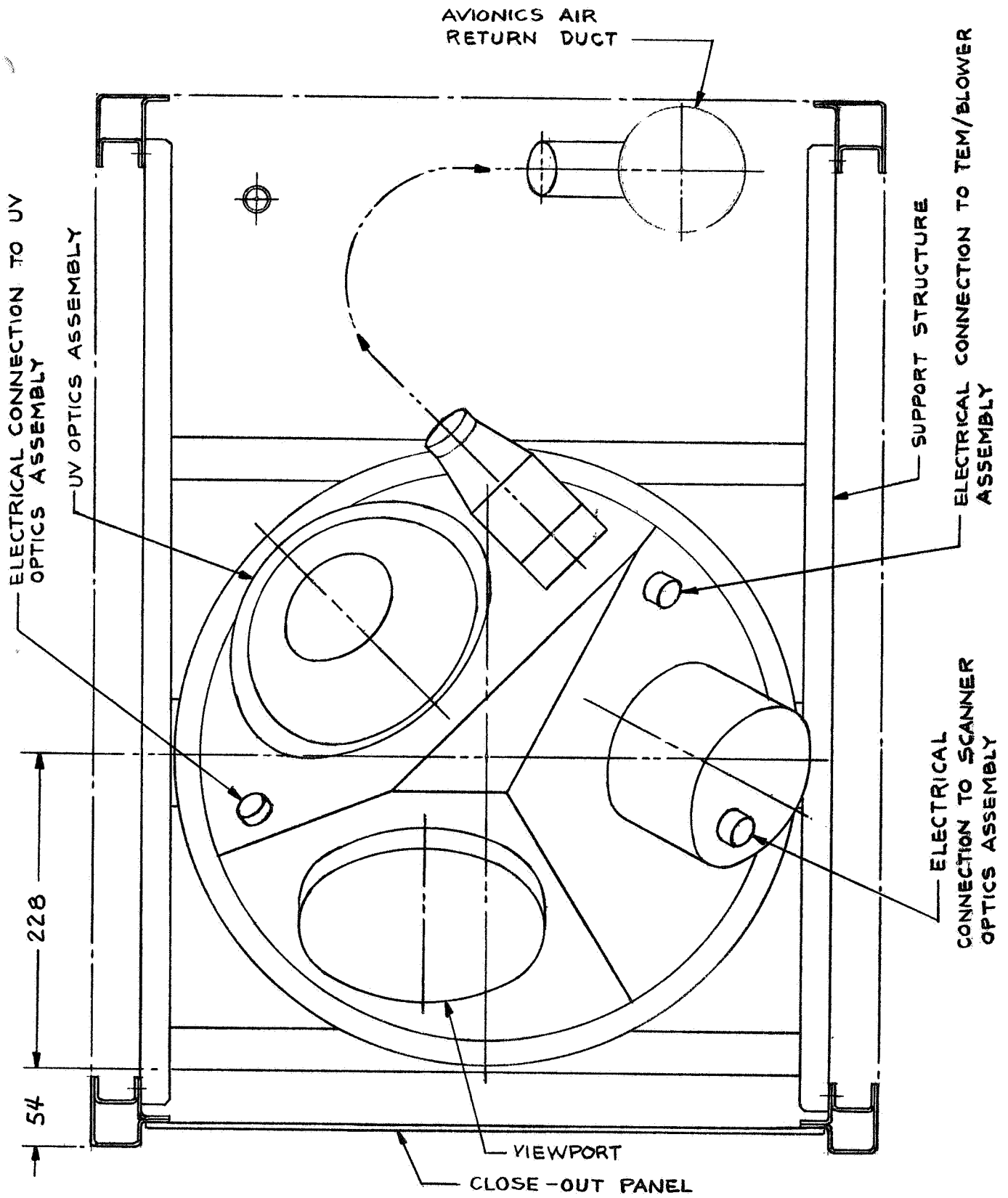


FIGURE 10(b) SECTION A-A (MECHANICAL ASSEMBLY INSTALLATION;
DIMENSIONS IN MM)

ORIGINAL PAGE IS
OF POOR QUALITY

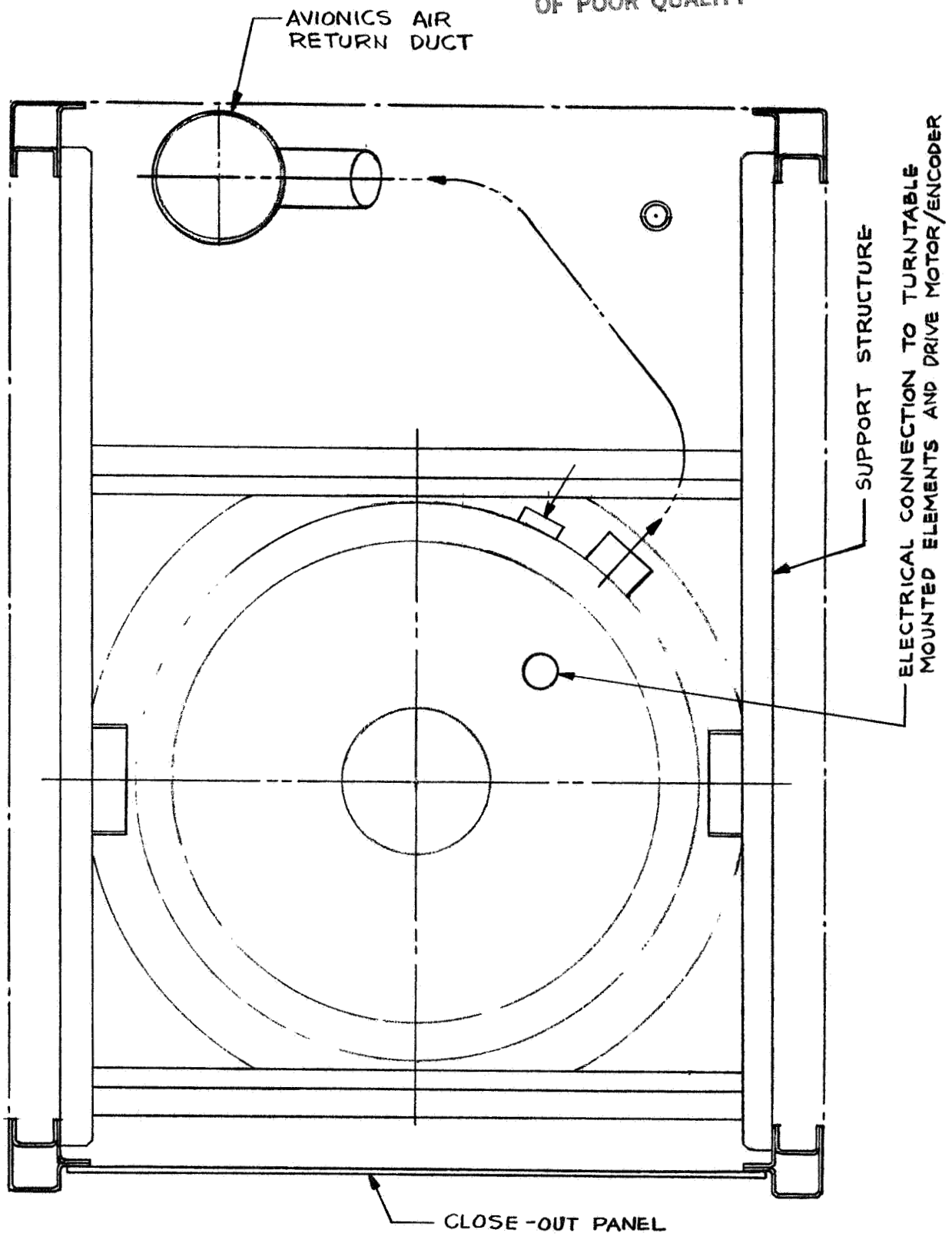


FIGURE 10(c) SECTION B-B (MECHANICAL ASSEMBLY INSTALLATION)

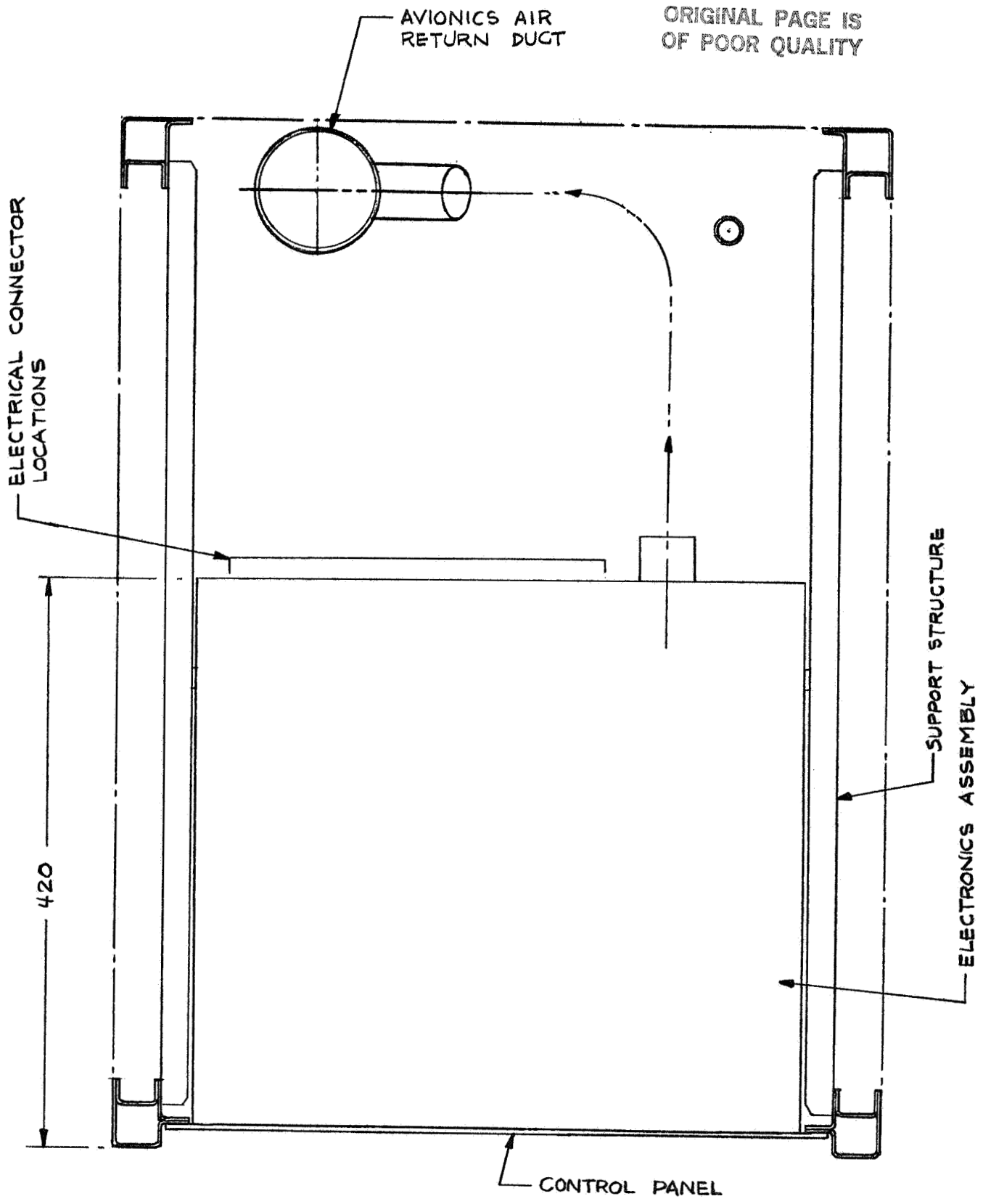


FIGURE 10(d) SECTION C-C (ELECTRONICS ASSEMBLY INSTALLATION, DIMENSIONS IN MM)

ORIGINAL PAGE IS
OF POOR QUALITY

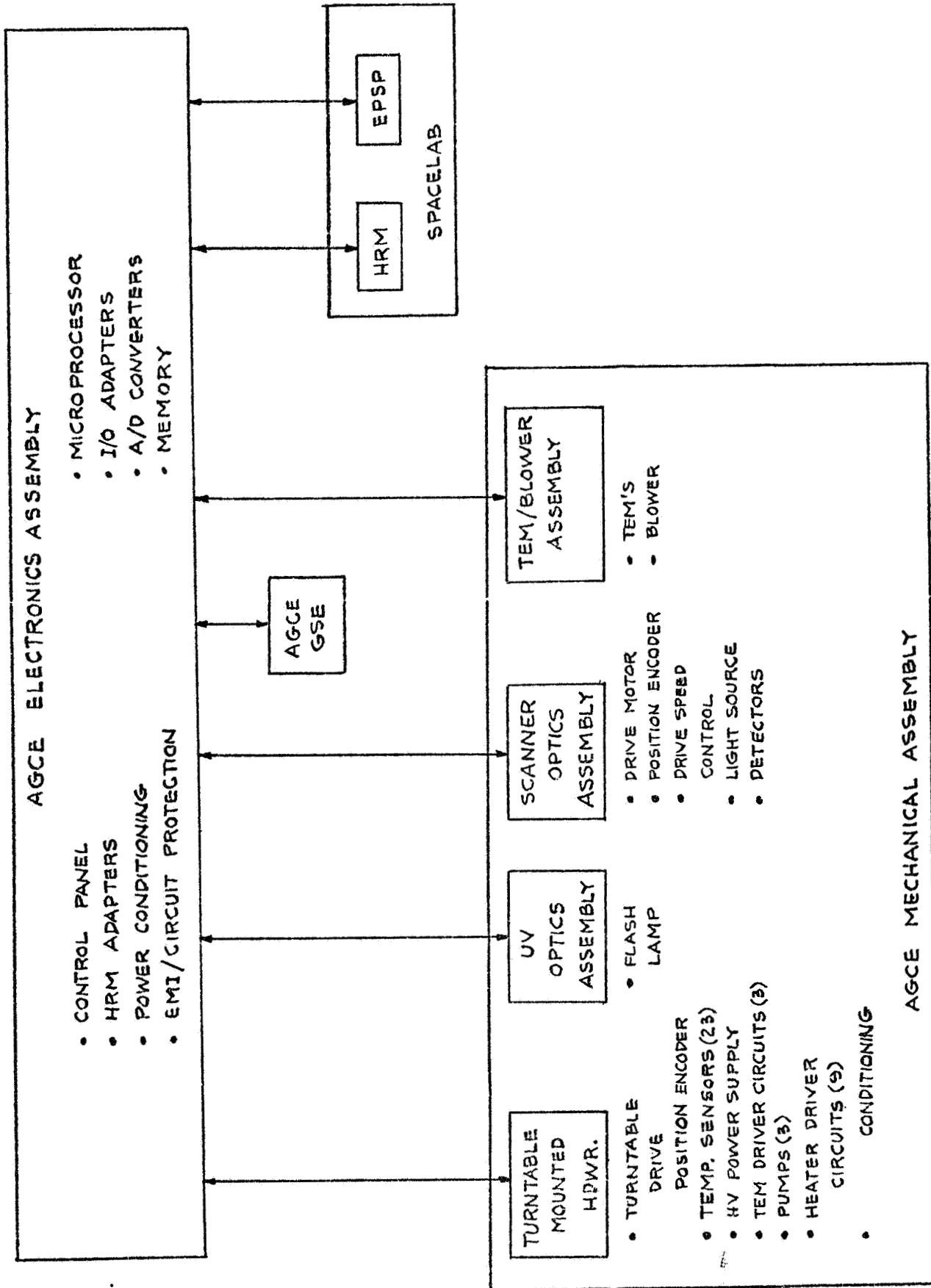


FIGURE 11 AGCE SYSTEM CABLING DIAGRAM

- o Dust removal assembly
- o Air to air heat exchanger assembly
- o Scanner optics assembly
- o UV optics assembly
- o TEM/blower assembly
- o Structure

enclosure
base

- o Viewport
- o Electronic driver circuits (TEM's/Heaters)
- o Sensor signal conditioning circuits

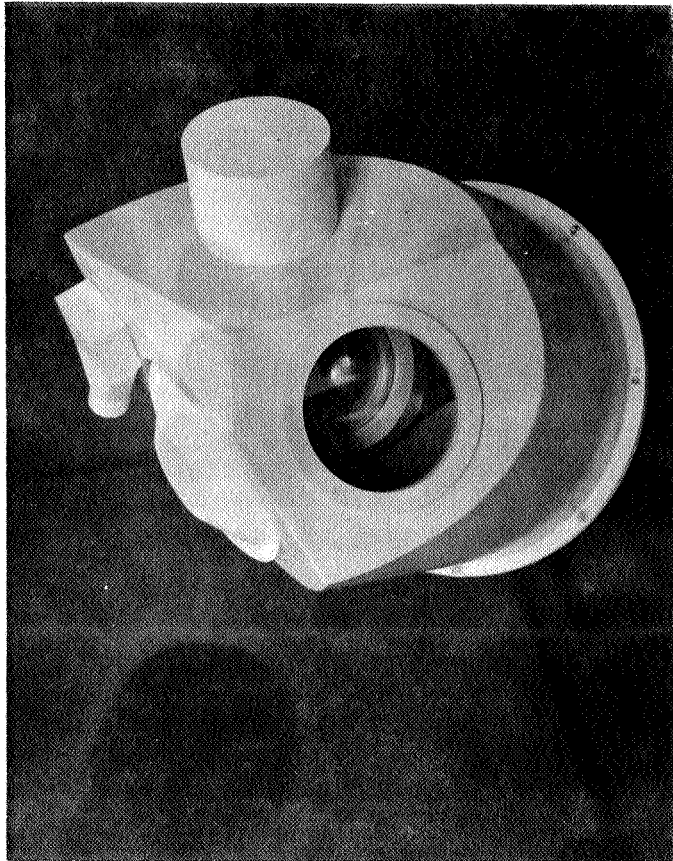
Figure 12 shows a full scale mock-up of the Mechanical Assembly. Figure 13 shows the relative location of equipments mounted on the turntable; Figure 14 shows the installation of the scanner and UV optics assemblies and the TEM/blower assembly for transferring heat from the flow cell pole TEM to the avionics air flow. Figure 15 shows overall key dimensions of the Mechanical Assembly. Figures 16 thru 21 show installation of the scanner and UV optics assemblies, the viewport and the TEM/blower assembly.

Figure 22 shows a cross-section thru the fluid flow cell. Figures 23 and 24 show the overall configuration and construction of the inner sphere assembly. Note that the inner sphere can be readily disassembled and repaired in case of damage or component failure during assembly and test. (This is not possible with the welded GFFC design).

The overall size of the Mechanical Assembly was based on accommodating a flow cell having a 5.0 cm radius inner sphere and associated supporting hardware. This accommodation criteria plus the results from TASKS 1 thru 8 were used to define the dimensions of the individual components. This dimensional data are reflected in the mock-up, see section 5.1. However, in building the mockup, no attempt was made to show non-critical detail or internal detail below the turntable. This latter was assumed to be similar to that shown for the GFFC system (Figure 4).

3.3 Electronics Assembly

The primary requirement of the Electronics Assembly is to provide the system control and data handling functions. Specifically, the following major elements are included:



ORIGINAL PAGE IS
OF POOR QUALITY

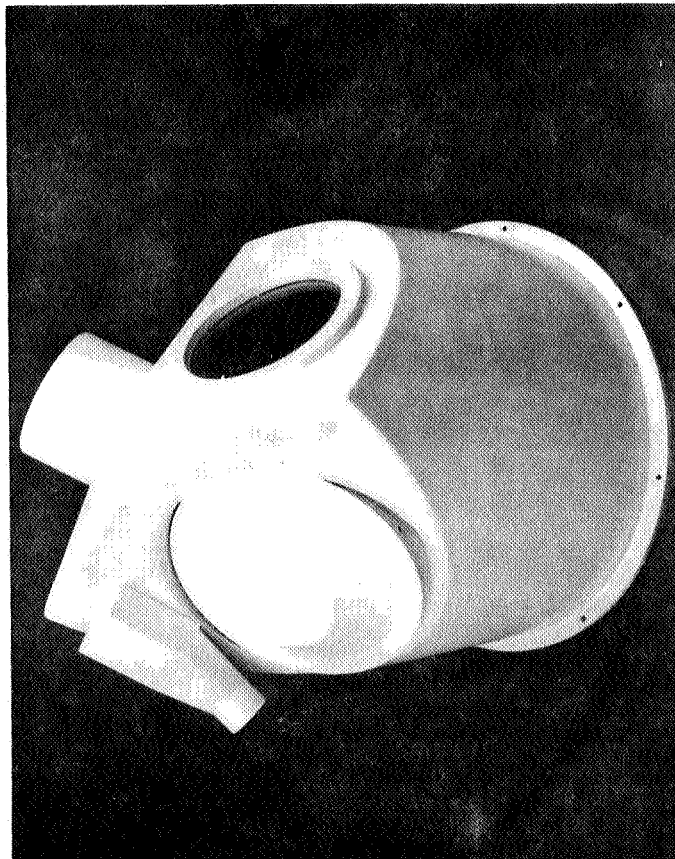
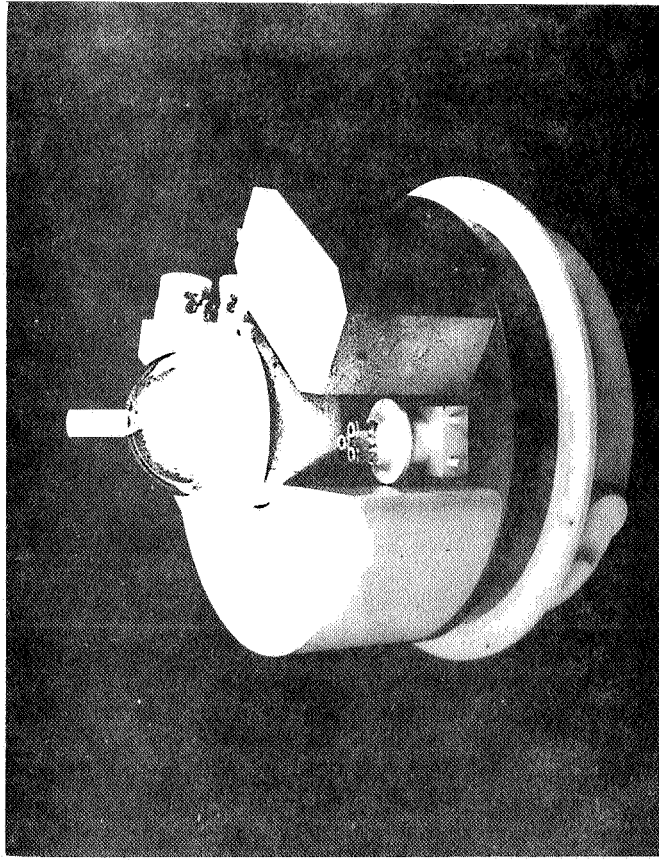


FIGURE 12 MECHANICAL ASSEMBLY FULL SCALE MOCKUP



ORIGINAL PAGE IS
OF POOR QUALITY

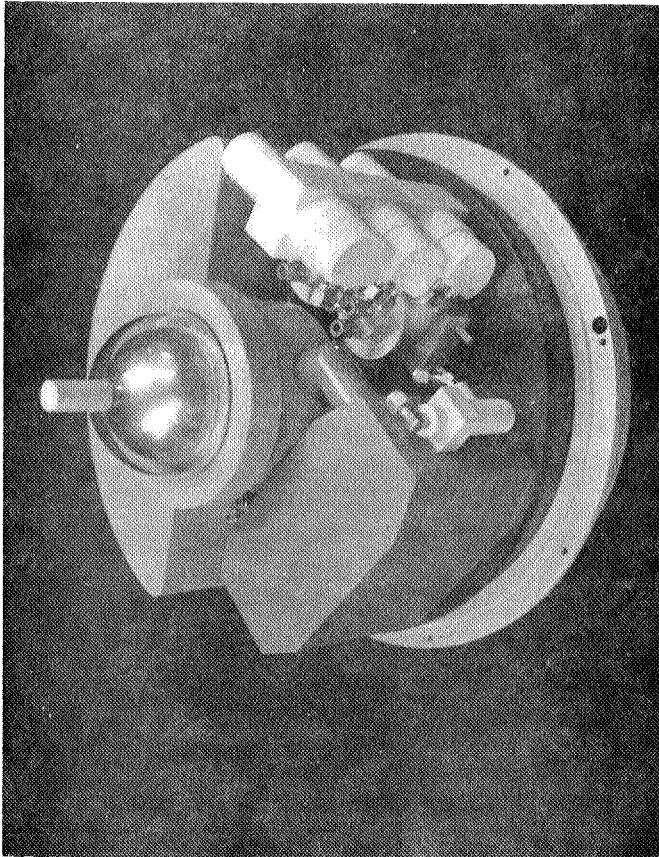


FIGURE 13 MECHANICAL ASSEMBLY FULL SCALE MOCKUP
(WITH ENCLOSURE SUBASSEMBLY REMOVED)



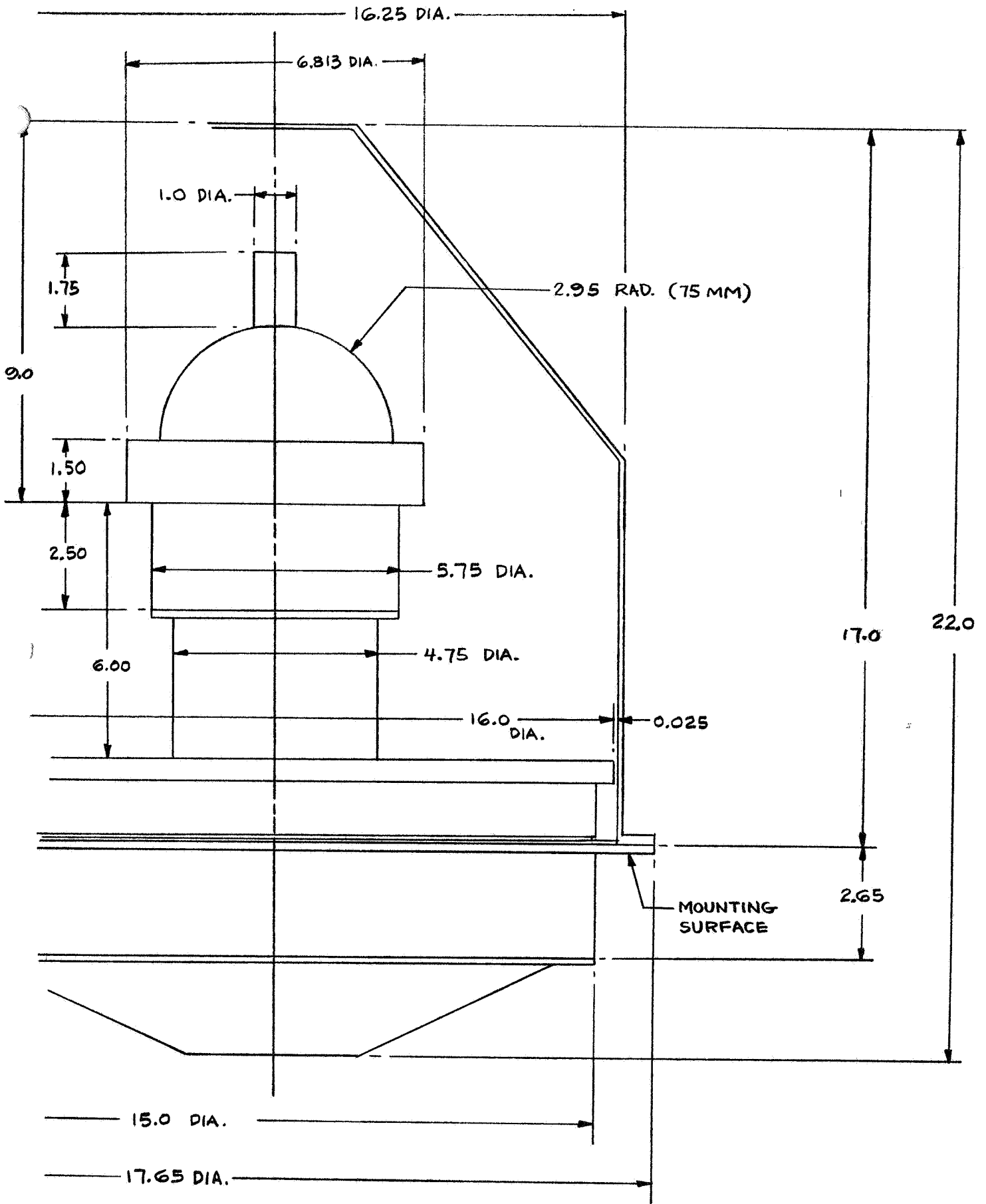


FIGURE 15 MECHANICAL ASSEMBLY KEY DIMENSIONS (INCHES)

ORIGINAL PAGE IS
OF POOR QUALITY

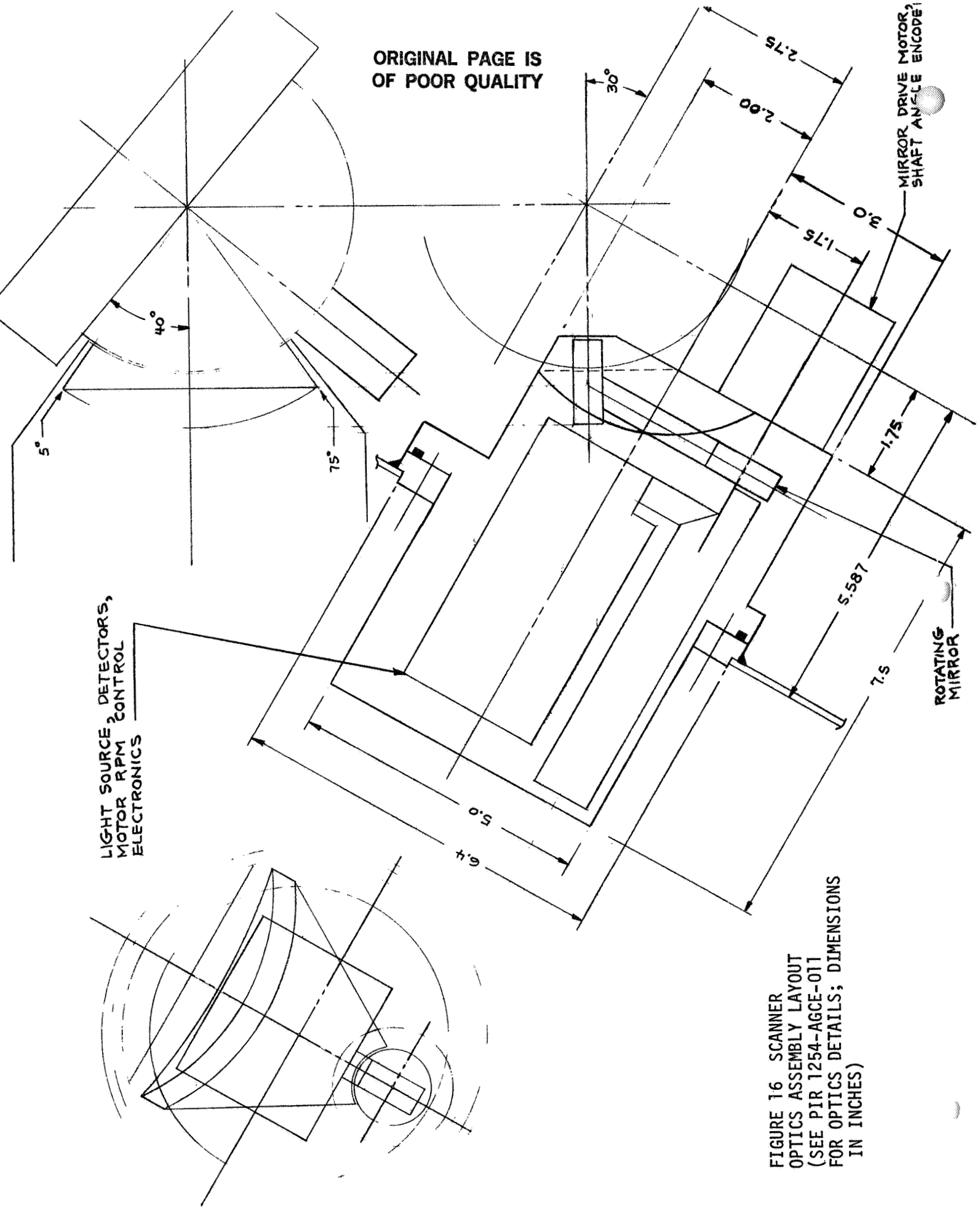


FIGURE 16 SCANNER
OPTICS ASSEMBLY LAYOUT
(SEE PIR 1254-AGCE-011
FOR OPTICS DETAILS; DIMENSIONS
IN INCHES)

ORIGINAL PAGE IS
OF POOR QUALITY

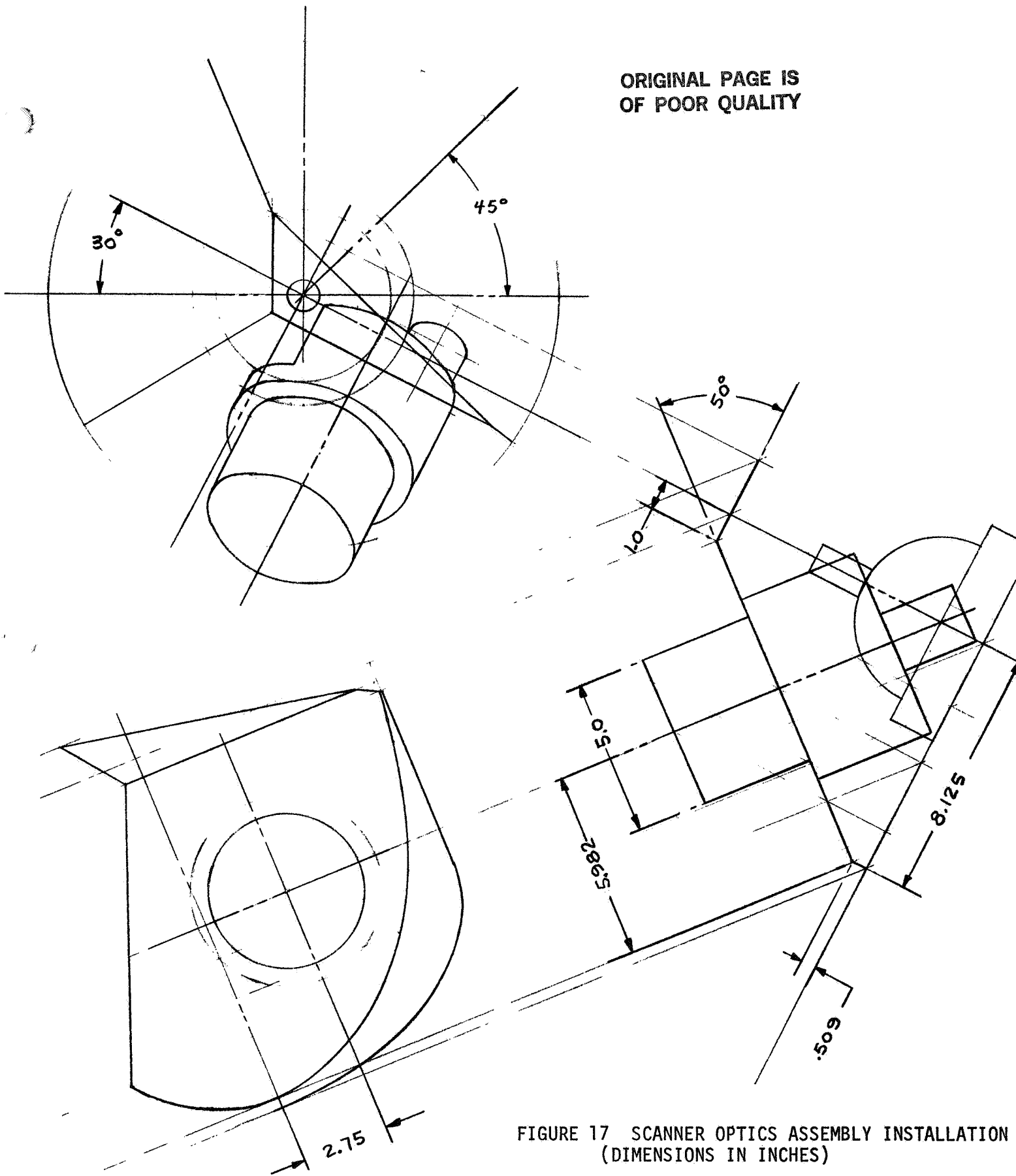


FIGURE 17 SCANNER OPTICS ASSEMBLY INSTALLATION
(DIMENSIONS IN INCHES)

ORIGINAL PAGE IS
OF POOR QUALITY

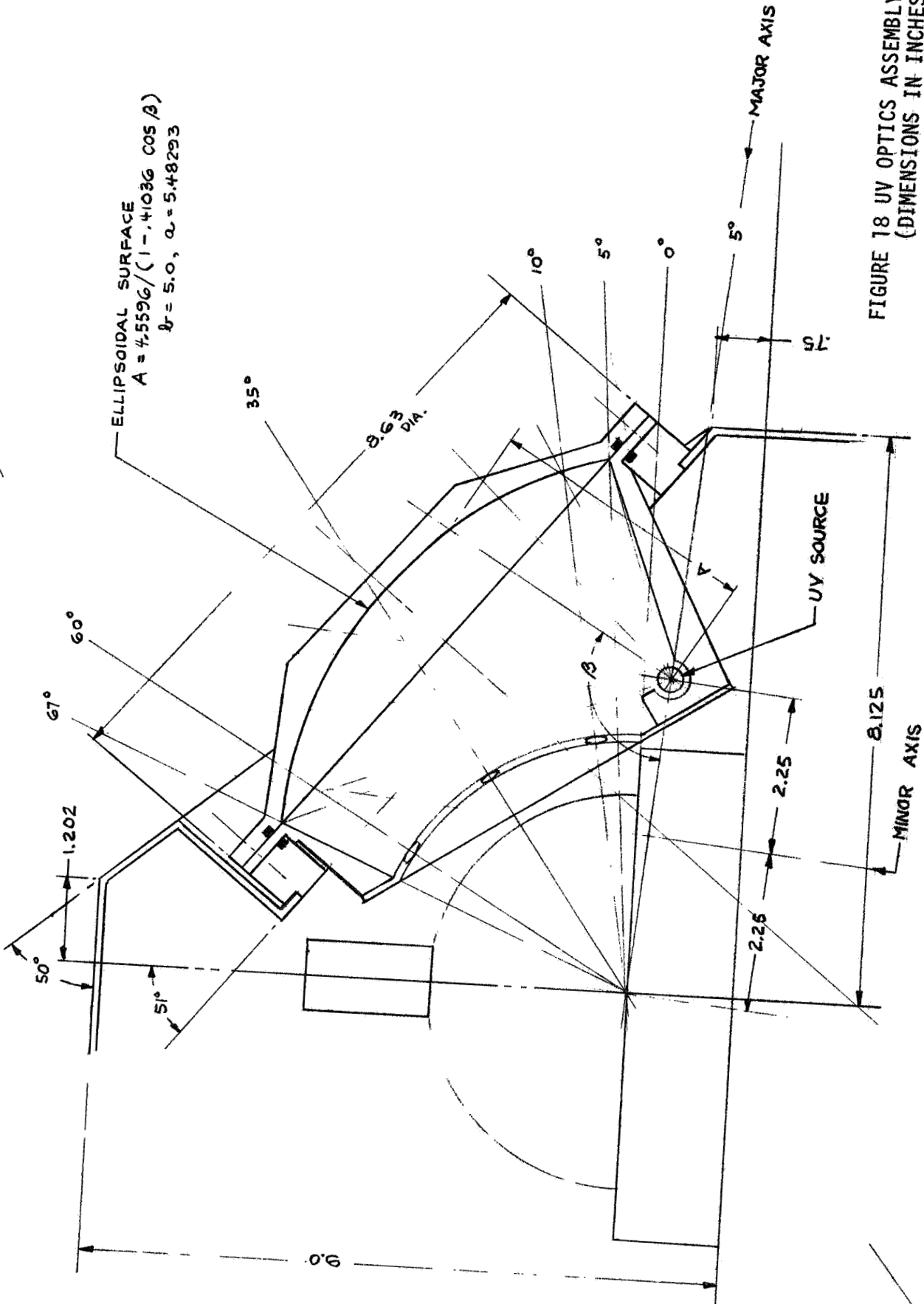


FIGURE 18 UV OPTICS ASSEMBLY LAYOUT
(DIMENSIONS IN INCHES)

ORIGINAL PAGE IS
OF POOR QUALITY

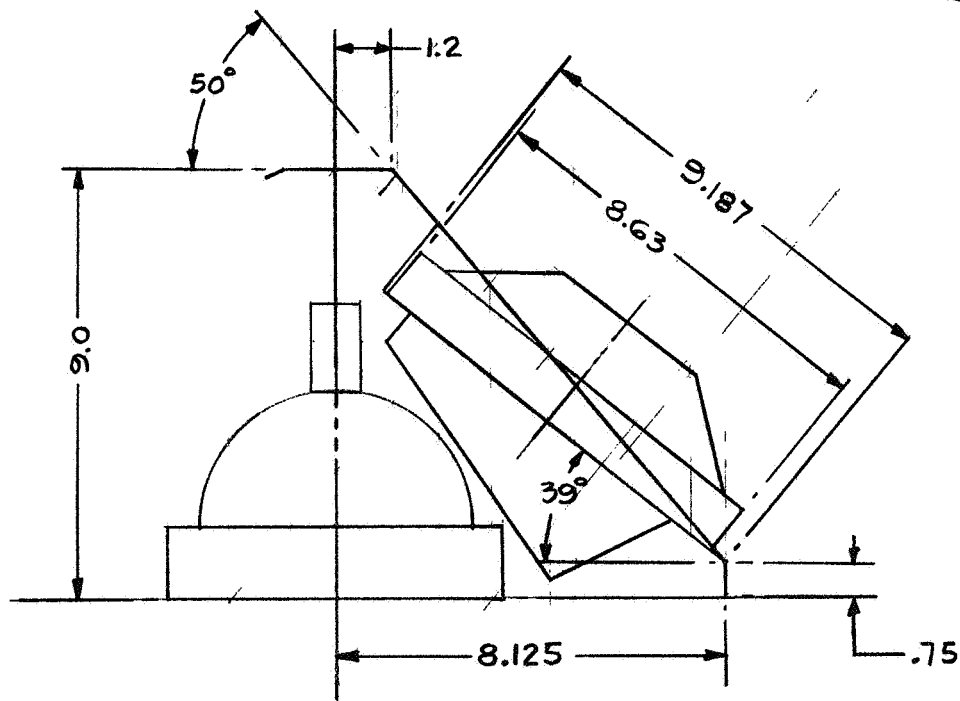
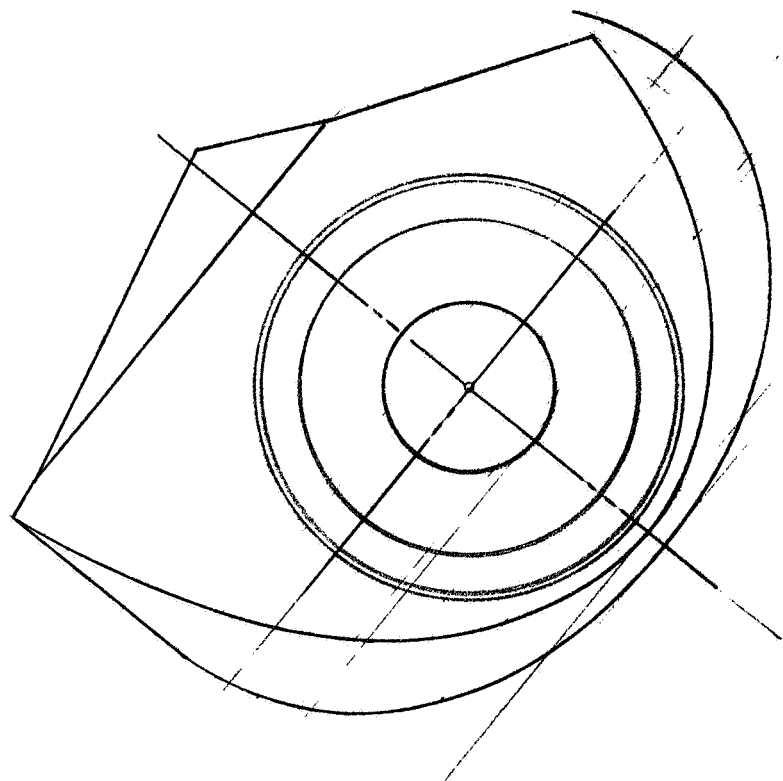
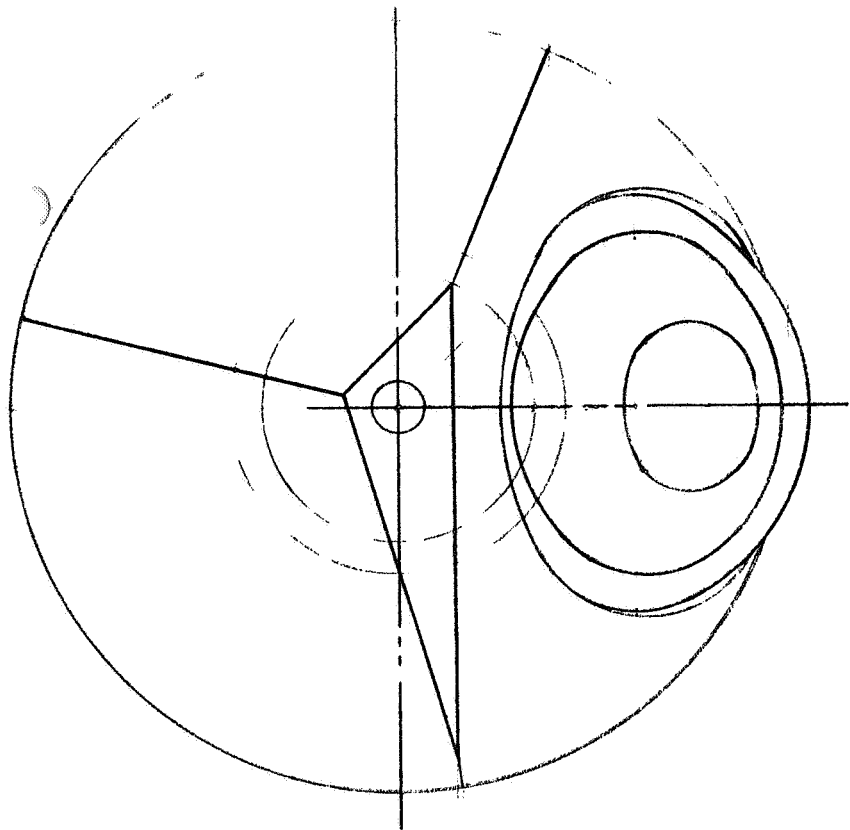


FIGURE 19
UV OPTICS ASSEMBLY
INSTALLATION
(DIMENSION IN INCHES)

ORIGINAL PAGE IS
OF POOR QUALITY

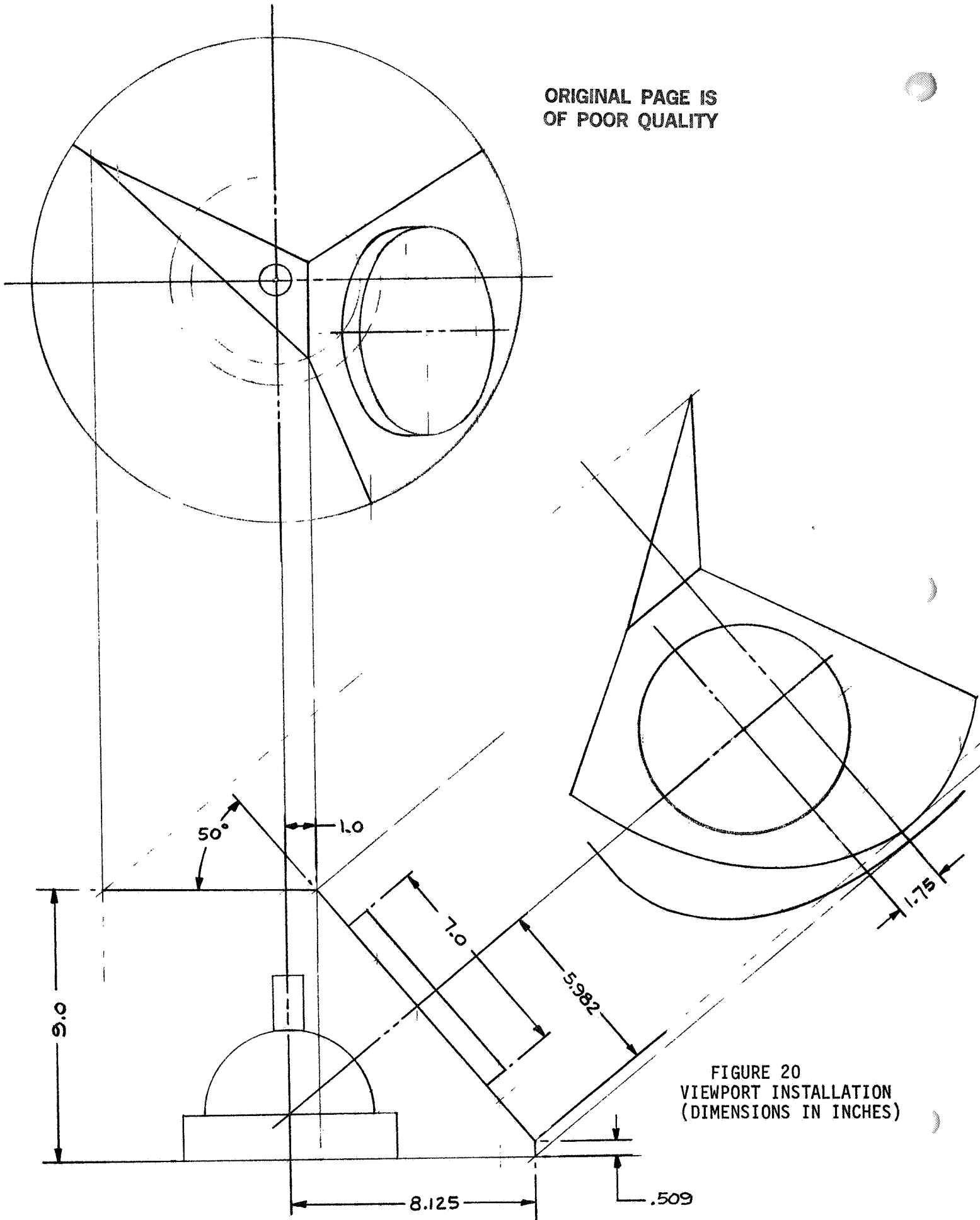


FIGURE 20
VIEWPORT INSTALLATION
(DIMENSIONS IN INCHES)

ORIGINAL PAGE IS
OF POOR QUALITY

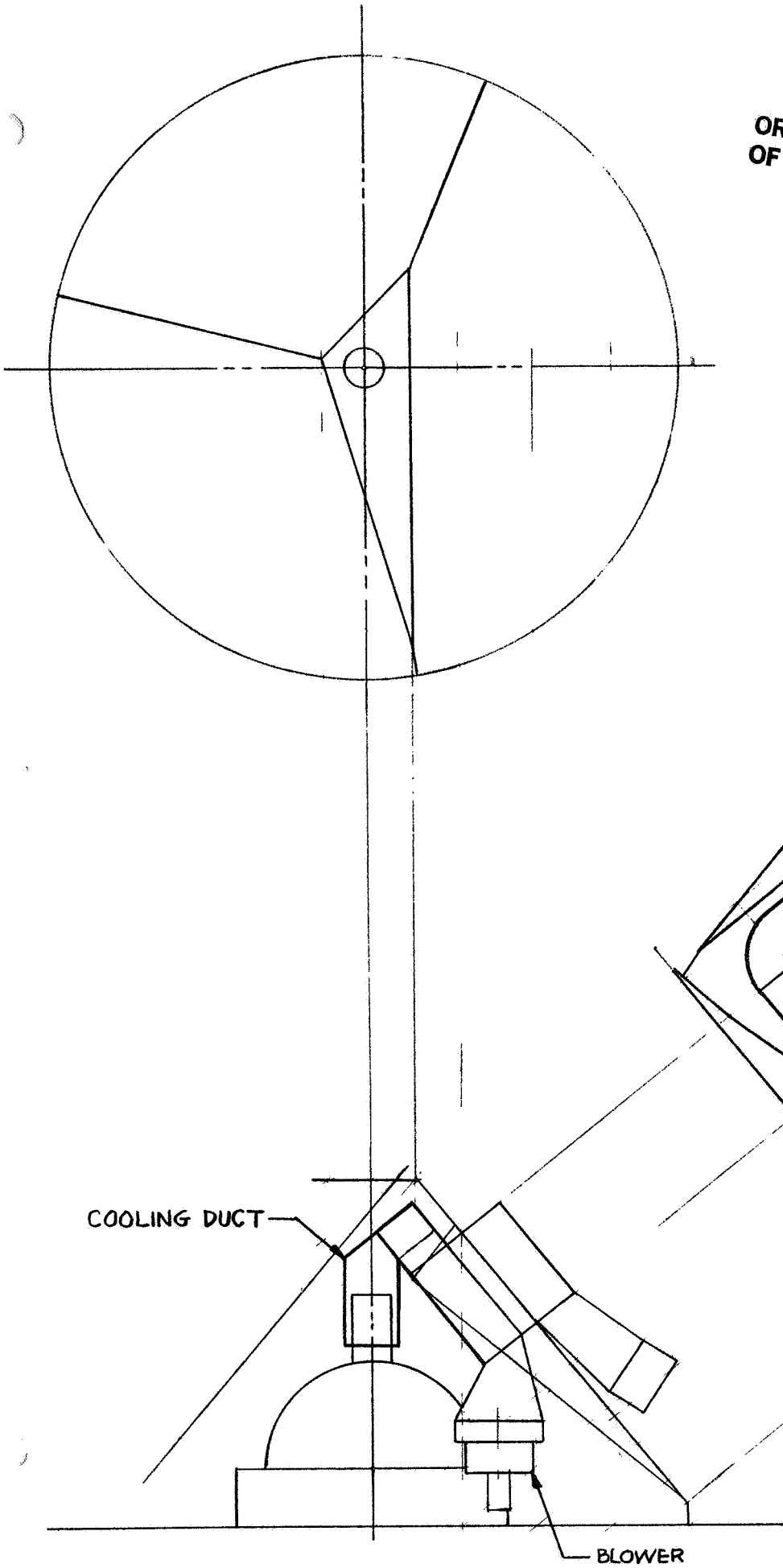


FIGURE 21
TEM/BLOWER
ASSEMBLY
INSTALLATION

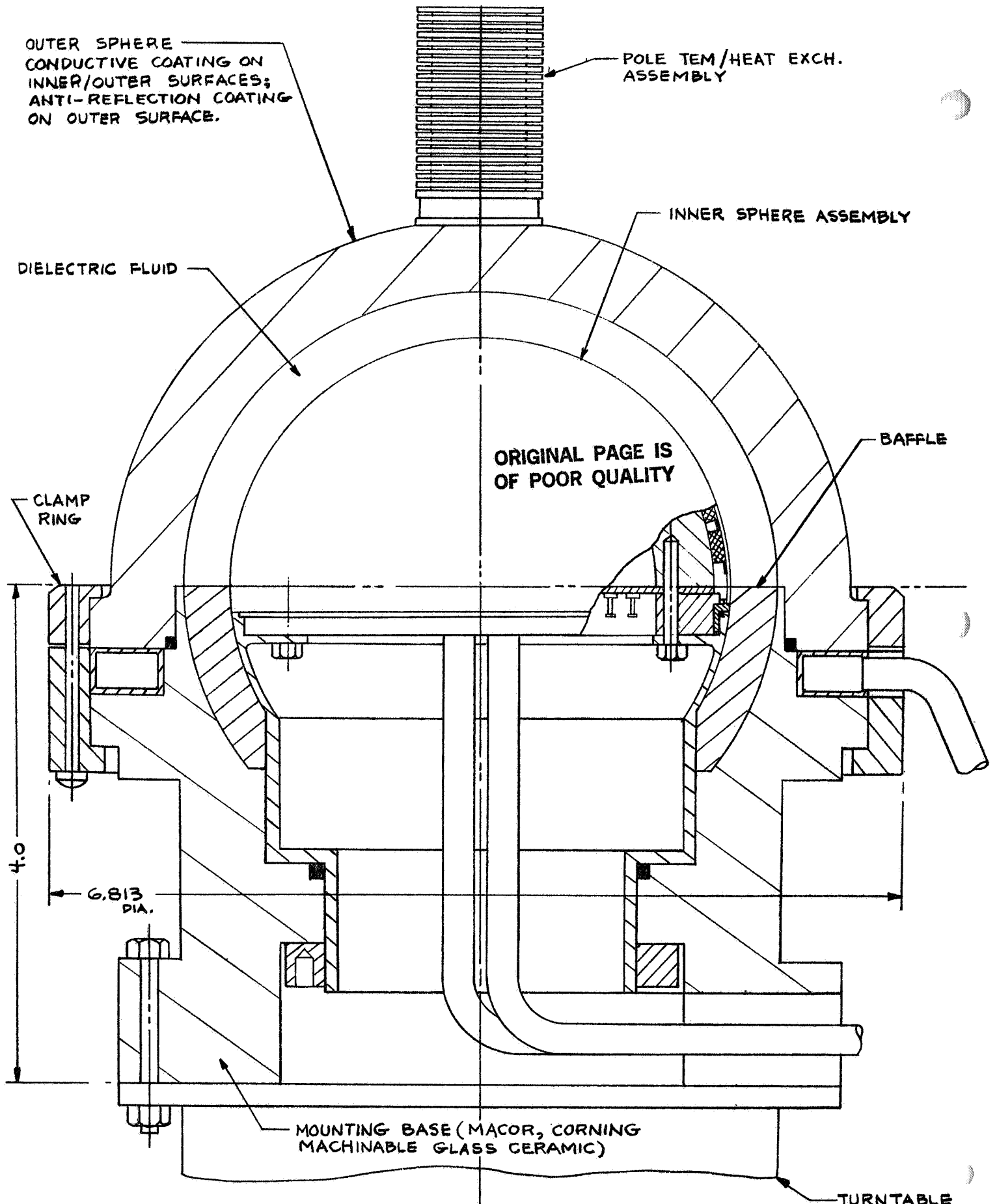


FIGURE 22 FLUID FLOW CELL ASSEMBLY ATTACHED TO TURNTABLE
HEATER/THERMISTER WIRING NOT SHOWN; DIMENSIONS IN INCHES FOR AN OUTER SPHERE OUTER
RADIUS OF 7.5 CM)

ORIGINAL PAGE IS
OF POOR QUALITY

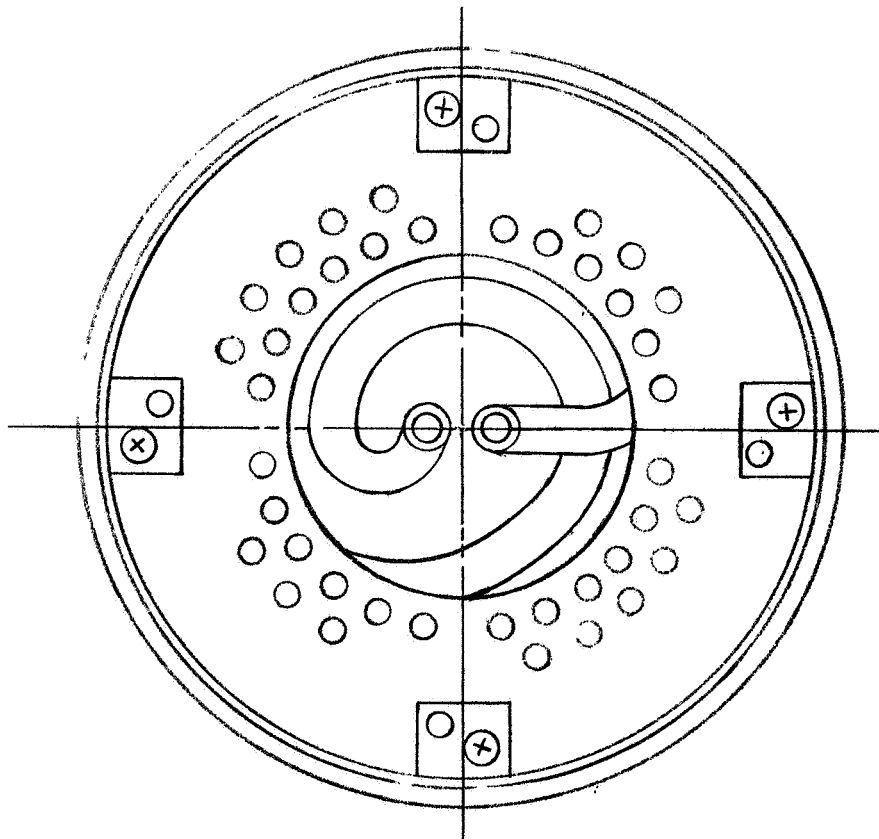
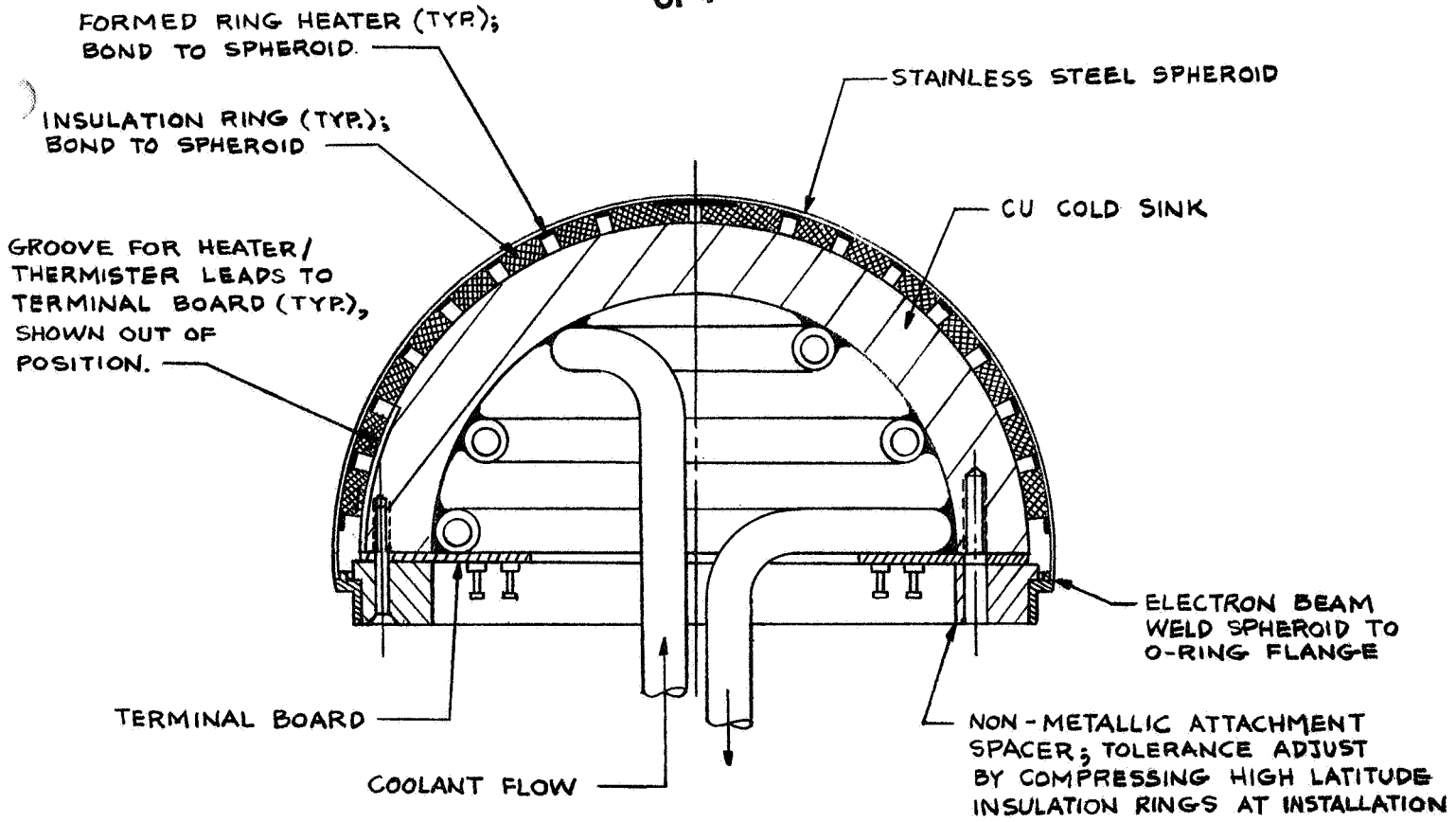


FIGURE 23 INNER SPHERE SUB-ASSEMBLY
(HEATER/THERMISTER WIRING NOT SHOWN)

- o Control Panel
- o Microcomputer
- o Memory
- o HRM Adapter
- o Power Conditioning
- o EMI/Circuit Protection
- o I/O Adapters
- o A/D Converters

Figure 25 shows a simplified block diagram of the Electronics Assembly; Figure 10(d) shows installation of the 9 X 15.75 X 17.5 inch package. For more detail on the AGCE electronics and control panel, see PIR 1254-AGCE-035.

3.4 Ancillary Equipment

In addition to the Mechanical and Electronics assemblies, other hardware elements are needed to complete the AGCE flight system. These items are:

- o Electrical cabling between AGCE and the HRM and EPSP.
- o Hose connections between AGCE and avionics air return duct.
- o Rack front close-out panels.
- o Support structure elements.

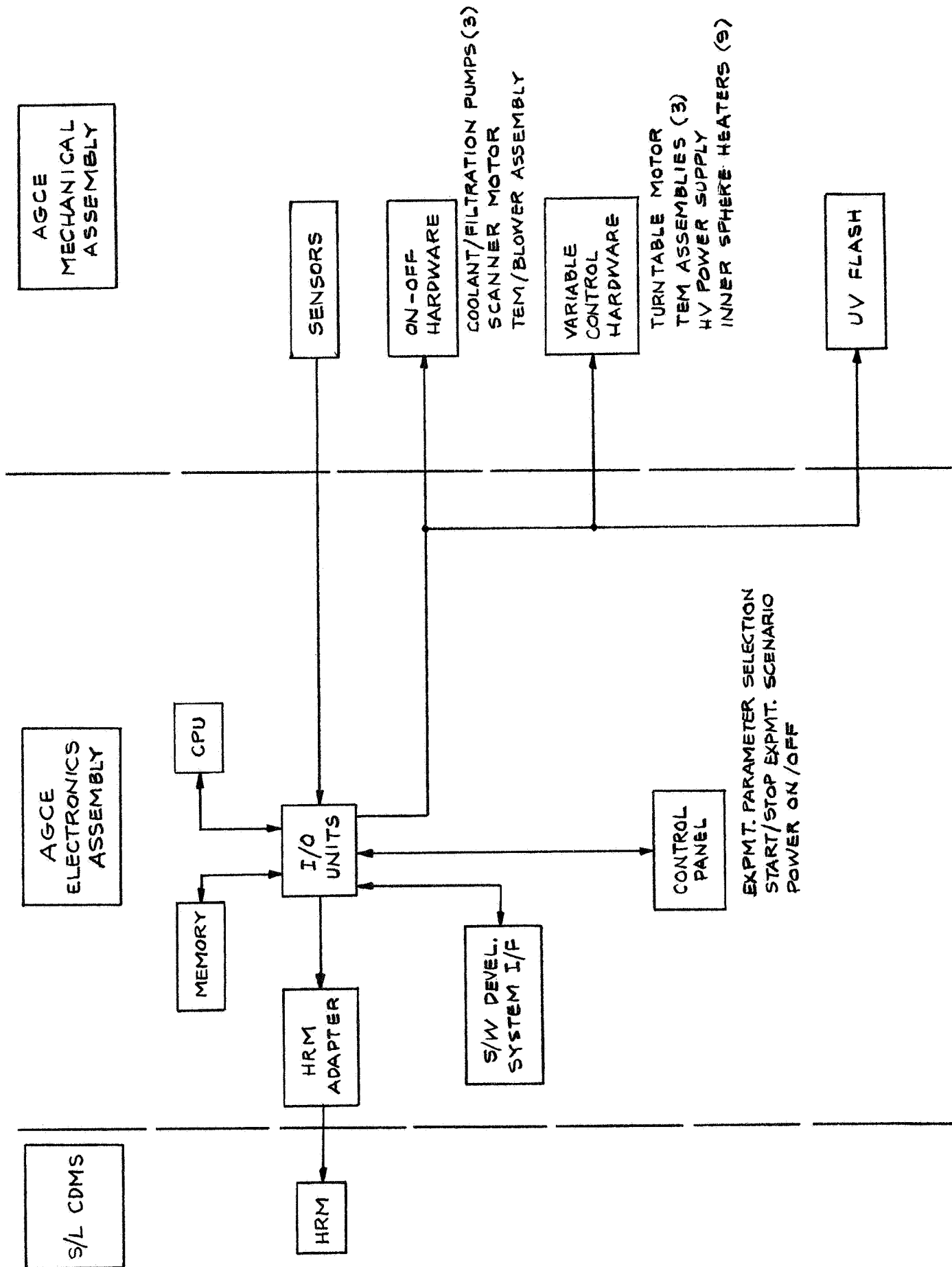
The support structure provides the mechanical interface between the AGCE Mechanical and Electronic Assemblies and the Spacelab Rack. The front close-out panels are required to isolate the rack avionics airflow from the Spacelab cabin airflow.

3.5 Ground Support Equipment

Figure 26 and 27 show the type of ground support equipment anticipated for the AGCE system. This equipment is needed during the system development cycle as well as to support ground operations at the POCC and pre-integration checkout at KSC. (See PIR 1254-AGCE-035 for additional discussion concerning the electrical GSE).

3.6 Mass Properties

Total weight of the AGCE system is estimated at 104.3 Kg. This compares with a projected 108 Kg (including 22 Kg of film) for the GFFC. Table 2 shows the weight breakdown for the AGCE system. Note that a growth weight contingency has been included based on the contingency schedule of Table 3.



EXPMT. PARAMETER SELECTION
START/STOP EXPMT. SCENARIO
POWER ON/OFF

FIGURE 25 AGCE CONTROL AND DATA HANDLING FUNCTIONAL BLOCK DIAGRAM

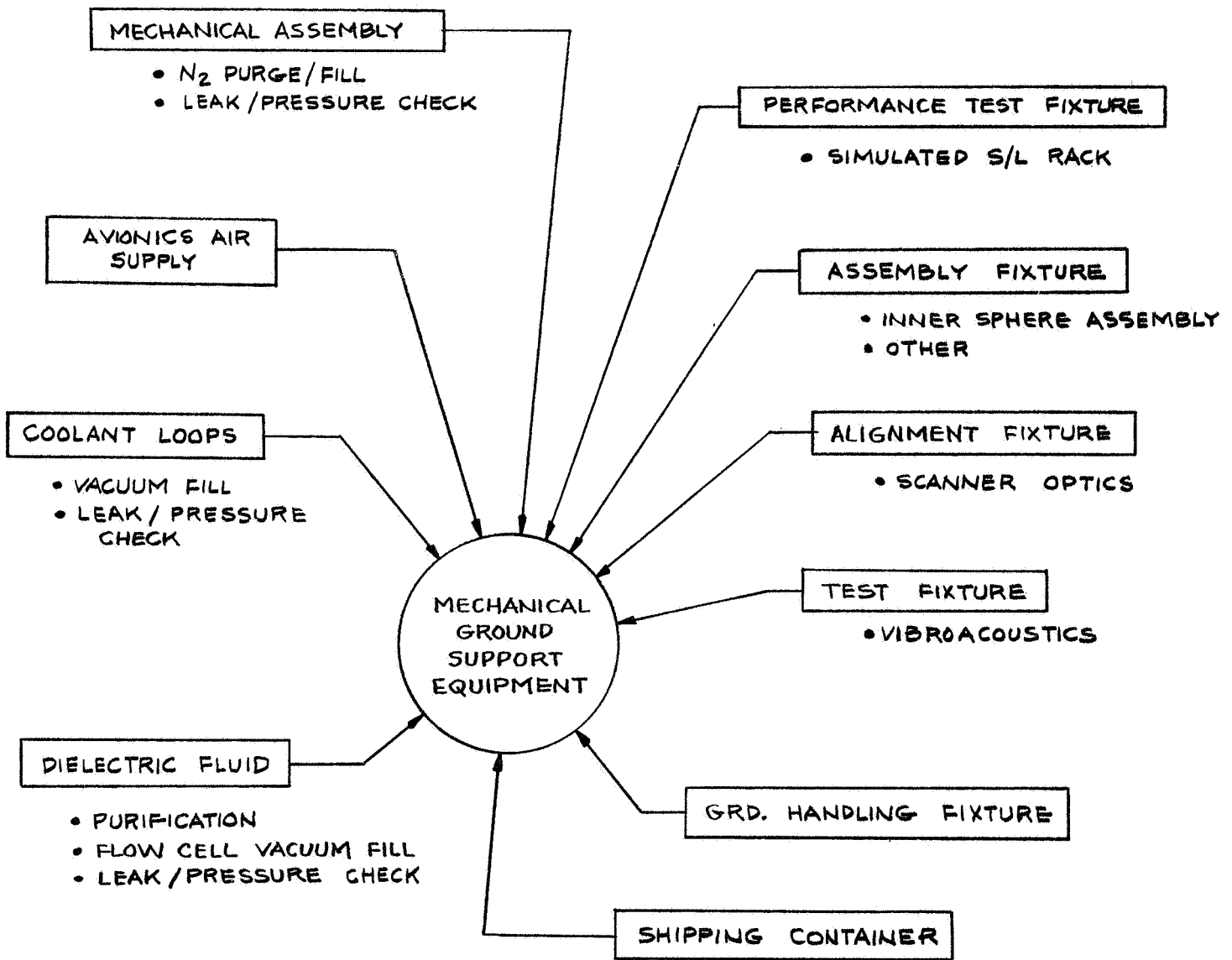


FIGURE 26 AGCE MECHANICAL GROUND SUPPORT EQUIPMENT

ORIGINAL PAGE IS
OF POOR QUALITY

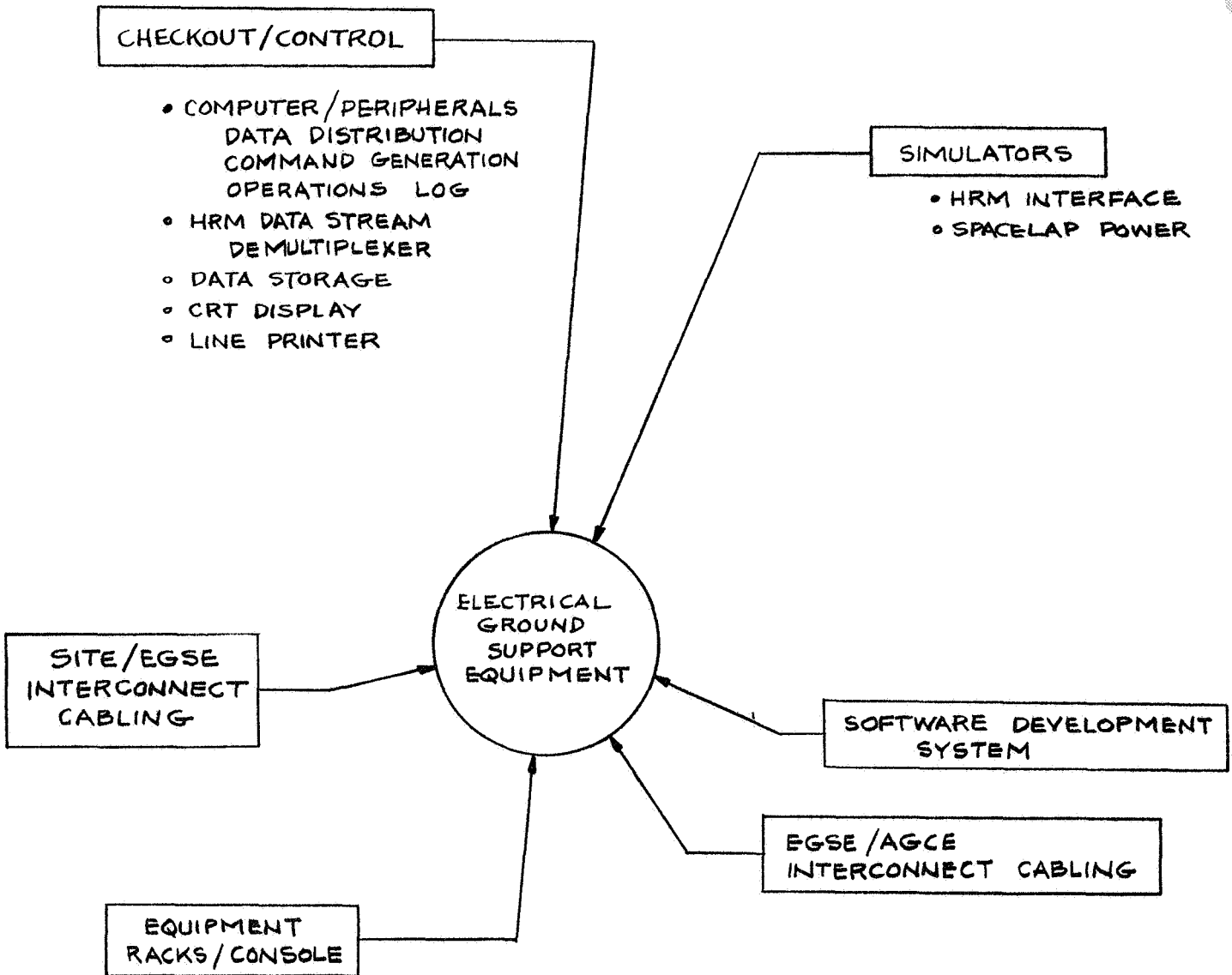


FIGURE 27 AGCE ELECTRICAL GROUND SUPPORT EQUIPMENT

Table 2(a) Estimated AGCE System Weight Compared with GFFC weight

SYSTEM ELEMENT	AGCE FLIGHT SYSTEM	GFFC FLIGHT SYSTEM*
Mechanical Assembly	58.9 Kg	66.6 Kg
Electronic Assembly	31.7	13.8
Ancillary Equipment	13.7	5.6
Expendables	N/R	21.8
TOTAL	104.3 Kg	107.8 Kg

*Data from GFFC IIA of 10/14/80

Table 2(b) Estimated Weight AGCE Electronics Assembly

ELEMENT	RAW ESTIMATED WEIGHT	ESTIMATED GROWTH CONTINGENCY	TOTAL ESTIMATED WEIGHT
PC board assemblies	5.22 Kg	18%	6.16 Kg
Enclosure	8.08	13	9.13
Power Supply	11.40	13	12.88
Control Panel Assembly	3.00	18	3.54
	27.70 Kg	14.5%*	31.71 Kg

Table 2(c) Estimated Weight AGCE Ancillary Equipments

ELEMENT	RAW ESTIMATED WEIGHT	ESTIMATED GROWTH CONTINGENCY	TOTAL ESTIMATED WEIGHT
Support Structure (2)	3.02 Kg	18%	3.56 Kg
Close-out panels	3.65	13	4.12
Avionics air connections	1.53	18	1.81
Cabling	3.60	18	4.25
TOTAL	11.80 Kg	16.45%*	13.74 Kg

*Composite value

Table 2(d) Estimated Weight AGCE Mechanical Assembly

ASSEMBLY ELEMENT	RAW ESTIMATED WEIGHT	ESTIMATED GROWTH CONTINGENCY	TOTAL ESTIMATED WEIGHT
Flow Cell Assembly	7.04 Kg	10%	7.74 Kg
UV Optics Assembly	1.41	13	1.59
Scanner Optics Assembly	2.75	18	3.25
Viewport	0.27	13	0.31
Enclosure	5.06	13	5.72
Baseplate	3.26	10	3.59
Lower Cover	1.04	10	1.14
Rotating Heat Exchanger	12.45	10	13.70
Turntable	2.26	10	2.49
Pumps (3)	3.72	3	3.83
Accumulators (3)	0.57	13	0.64
TEM/Heat Exchanger (2)	0.64	18	0.76
Filter	0.16	13	0.18
Drive Motor Mount	0.41	13	0.46
Shaft/bearing/slip ring assembly	1.14	13	1.29
TEM/Blower Assembly	0.61	18	0.72
Drive Motor/encoder	0.46	18	0.54
HV inductor	3.50	18	4.13
Dielectric fluid	0.27	25	0.34
Coolant	0.23	25	0.29
Plumbing	1.29	18	1.52
PC board assemblies	3.96	18	4.67
TOTAL	52.50 Kg	12.2%*	58.90 Kg

* Composite value

(1)

TABLE 3 WEIGHT GROWTH CONTINGENCY SCHEDULE

DESIGN MATURITY	% Contingency							
	STRUCTURES	MECHANISMS	WIRE/CABLE	BATTERIES	THERMAL CONTROL	ELECTRICAL AND ELECTRONIC BOXES/COMPONENTS		
						0-10 Lb	11-30 Lb	31 and Up Lb
Conceptual Estimate (Based on Sketches, Description, Experience or Finite Element Model)	18	18	33	18	18	18	13	8
Layout Calculation (Equivalent to Major Modification of Existing Hardware or Soft Mockup)	13	13	18	13	13	13	8	3
Pre-released Drawings (Equivalent to Minor Modification or Hard Mockup Engineering Model)	3	3	8	13	8	8	3	3
Released Drawing	1	1	2	2	2	8	3	3
Actual Weight	0	0	0	0	0	0	0	0
Specified Weight not to Exceed Value	0	0	0	0	0	0	0	0

(1) SOURCE - NASA SPACE TELESCOPE PROJECT OFFICE

Figure 28 shows the estimated center of gravity location for the AGCE system. Both weight and center of gravity locations are consistent with Spacelab requirements, see PIR 1254-AGCE-018.

3.7 Assembly/Disassembly Sequence

It is anticipated that the AGCE system assembly sequence will be similar to that shown in Figure 29. This sequence assumes that individual component/black box assembly and checkout has been completed prior to entry into the system assembly cycle. The assembly sequence appears to be straightforward and similar to that for the GFFC system. Note that system software and GSE hardware must be available on a comparable schedule in order to perform checkout and acceptance testing. Disassembly will be the inverse of the assembly sequence and with the checkout and acceptance test eliminated.

3.8 Safety

The AGCE system configuration was reviewed for potential safety hazards utilizing the hazard control categories of Table 4 (in the context of the AGCE system design and operational use). Safety assurance has been implemented by use of the general methods shown in Table 5. Table 6 shows results of the safety assessment. As shown, all anticipated hazards can be controlled by design of the AGCE hardware. No caution and warning sensor appears to be necessary. No trouble should be experienced in making the detail flight design compatible with both the Spacelab Payload Accommodations Handbook SLP/2104 and the STS Safety Policy NHB 1700.7.

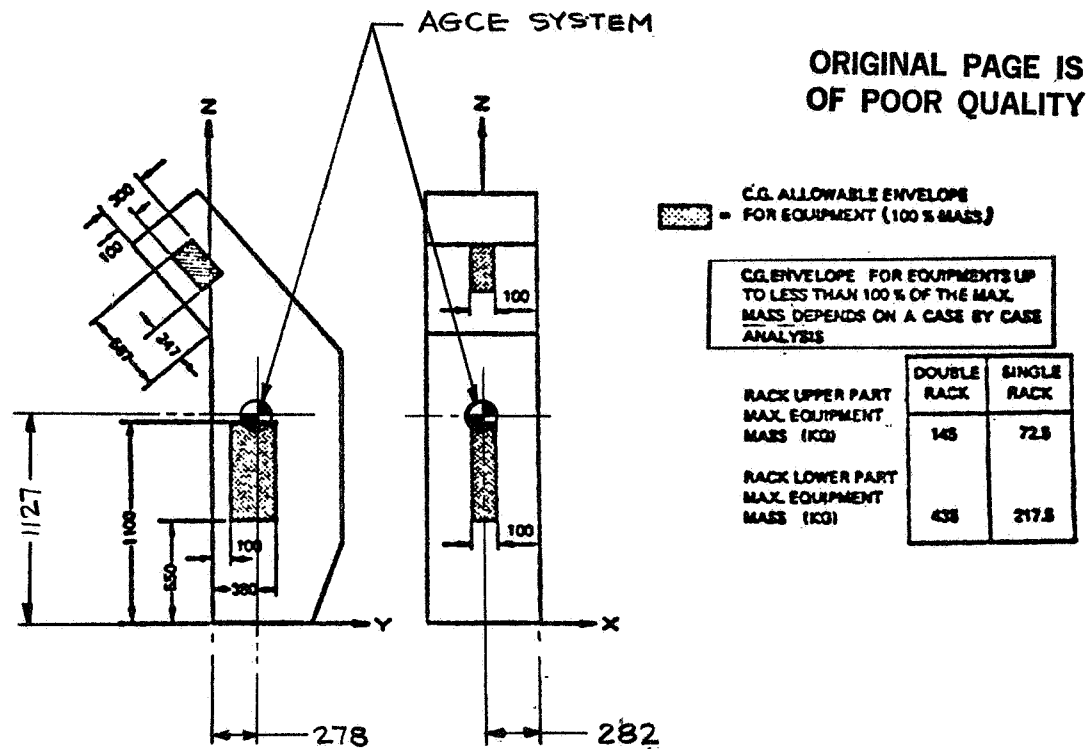


Figure 3.2 - 34 : C.G. Distribution Limitations for Single Rack and each Side of a Double Rack

FIGURE 28 ESTIMATED CENTER OF GRAVITY LOCATION FOR AGCE SYSTEM
(DIMENSIONS IN MM)

ORIGINAL PAGE IS
OF POOR QUALITY

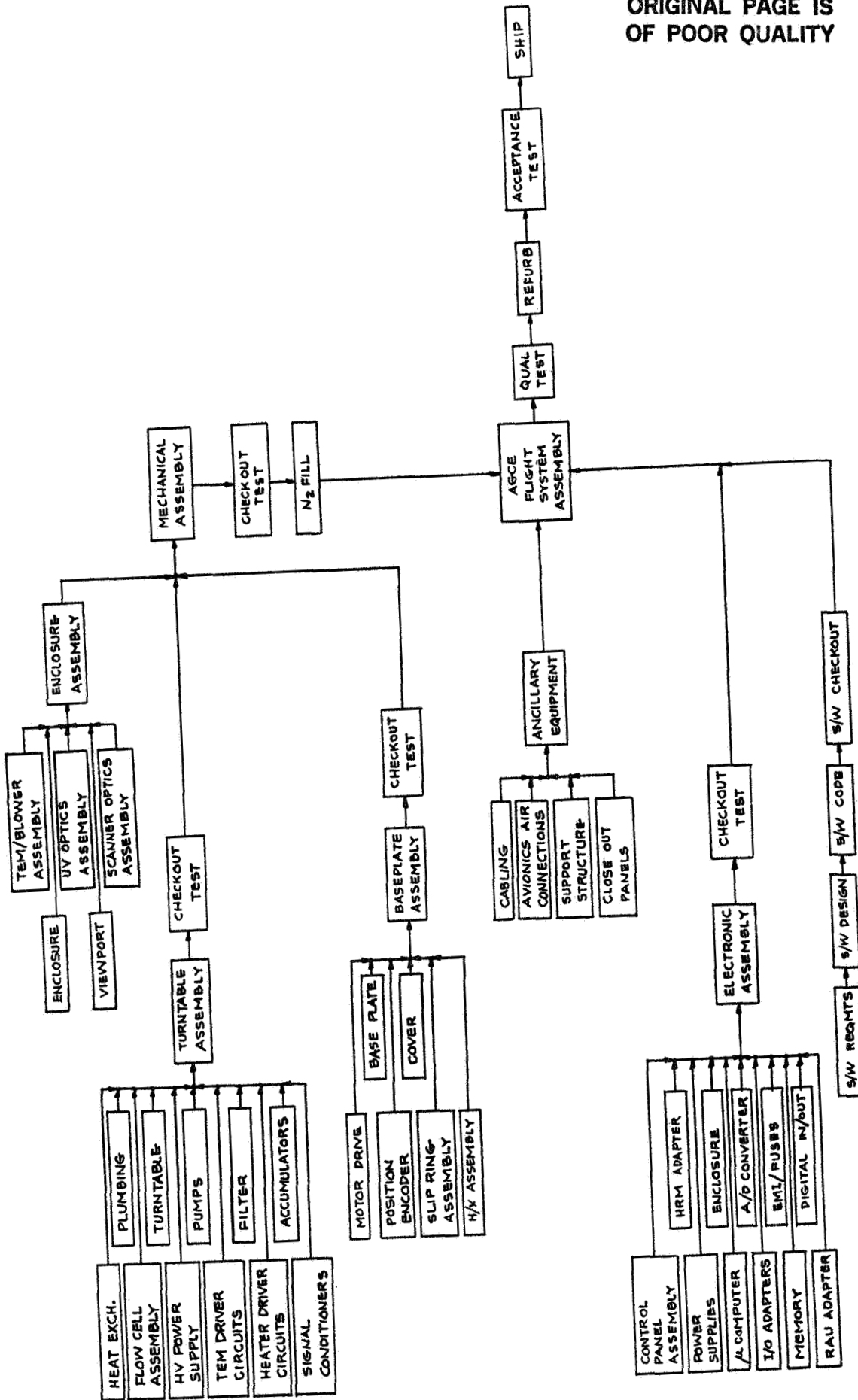


FIGURE 29 ASSEMBLY/TEST SEQUENCE FOR AGCE FLIGHT SYSTEM

TABLE 5 SAFETY ASSURANCE

REQUIREMENTS

- MINIMUM HAZARD TO CREW
- ASSURE SAFE RECOVERY OF SPACECRAFT AND CREW

HAZARD REDUCTION METHODS

- DESIGN FOR MINIMUM HAZARD
- CONTROL MATERIAL SELECTION
 - TOXICITY
 - FLAMMABILITY -
 - OFF-GASSING
- PROVIDE EMERGENCY SHUT-DOWN CAPABILITY
- INCORPORATE SAFETY DEVICES
- INCORPORATE WARNING DEVICES
- DEVISE SPECIAL PROCEDURES

TABLE 6 AC SAFETY ASSESSMENT

<u>POTENTIAL HAZARD SOURCE/CONDITION</u>	<u>PLANNED CONTROL ACTION</u>
<u>MECHANICAL</u>	
FLUID LEAKAGE (DIELECTRIC/COOLANT)	REDUNDANT CONTAINMENT
● FLOW CELL, PLUMBING, ACCUMULATORS	PRESSURE TEST DURING ASSEMBLY & CYCLE
● PUMPS	MAGNETIC COUPLED SEALLESS TYPE
● ELECTRONICS	CONFORMAL COATED
ABRASION	SMOOTH SURFACES; ROUNDED EDGES/CORNERS
ROTATING EQUIPMENT	ROTATING ELEMENTS ENCLOSED
<u>ELECTRICAL</u>	
HIGH VOLTAGE	INSULATED; ISOLATED
INSULATION FAILURE	EQUIPMENT GROUNDED
ACCIDENTAL SWITCH ACTUATION	GUARDED
EQUIPMENT MALFUNCTION	MANUAL POWER OFF SWITCH
OVER-CURRENT CONDITION	EPSP CKT. BRKS,
● EXTERNAL	AUTOMATIC OVERCURRENT PROTECTION (FUSE/CKT. BRKS)
● INTERNAL	SHIELDED CABLING
EMI	
<u>THERMAL</u>	
FLUID THERMAL EXPANSION	EXPANSION VOLUMES PROVIDED
EXPOSED SURFACES	MAINTAIN BELOW 105°F (40.5°C)
CONTROLLER MALFUNCTION (OVER TEMP.)	AUTOMATIC SHUT-DOWN
<u>MATERIALS</u>	
DIELECTRIC FLUID	REDUNDANT CONTAINMENT
FLAMMABLE/TOXIC OFFGASS: MTLs.	ISOLATED IN NITROGEN ENVIRONMENT
SHATTERABLE MTLs.	CONTAINMENT

ORIGINAL PAGE IS OF POOR QUALITY

4.0 CONCLUSIONS AND RECOMMENDATIONS

The results of TASK 9.1 have established the feasibility of configuring the AGCE system as a Spacelab experiment. The generated flight configuration is consistent with the largest flow cell sphere radii combination as specified in the work statement. Note that the configuration described is not necessarily optimum in all details.

Although the AGCE and GFFC system configurations are fundamentally similar, implementation of some system features is significantly different. This is particularly true in the following areas:

- Optics
- Flow cell construction
- Data Management
- PS/PI/POCC involvement

The AGCE uses a flying spot scanner arrangement to generate thermal gradient and flow data. The scanner electrical output is digitized and formatted for telemetering to the POCC. The AGCE flow cell is configured for inward heat flow thus the thermal control capability differs from that needed by the GFFC. Note that the AGCE may also be operated in the outward heat flow mode required for the GFFC. The AGCE flow cell may be disassembled for repair/replacement of heater/thermistor elements if required. This repair capability is not possible with the GFFC flow cell design. Telemetry of flow cell data to the POCC provides a number of operating capabilities, see Table 7. These reduce the cost of the AGCE flight hardware while increasing PI control of the experiment as compared to the GFFC implementation.

As previously noted, the flow cell dimensions were selected to conform to the maximum noted in the contract work statement, i.e. an inner sphere radius of 5.0 cm and an outer sphere inner radius of 6.0 cm. However, the mechanical assembly can accommodate a somewhat larger flow cell, on the order of 9.0 cm outer radius for the outer sphere (7.5 cm inner radius), with estimated relatively minor impact as shown in Table 8. Figure 30 shows this larger configuration.

TABLE 7 AGCE DATA MGMT., PS/PI INVOLVEMENT

DATA MANAGEMENT

- DATA TO POCC VIA HRM; NO ON-ORBIT RECORDING
- LIMITED REAL TIME DATA AVAILABLE TO AGCE GSE FOR ACCESSING SYSTEM PERFORMANCE AND CONTROLLING THE EXPERIMENT:
 - TEMPERATURES
 - ROTATION RATE
 - VOLTAGE
 - MARKER DOT LOCATION
 - SCENARIO NUMBER
- ALL DATA RECORDED BY POCC FOR POST MISSION ANALYSIS BY PI

PS/PI INVOLVEMENT

- PS SELECTS ALL EXPERIMENT VARIABLES AT START OF EACH EXPERIMENT SCENARIO AND INITIATES EXECUTION; EXPERIMENT VARIABLES PROVIDED TO PS IN AGCE FLIGHT INSTRUCTIONS DOCUMENT. NO S/W STORED SCENARIOS.
- PI MONITORS EXPERIMENT SCIENCE STATUS USING AGCE GSE LOCATED AT THE POCC. PI CONTROLS DURATION OF EACH SCENARIO. SCENARIO TERMINATED AND NEW SCENARIO START VIA VOICE INSTRUCTION TO PS FROM PI. PI MAY DEVIATE FROM PLANNED SCENARIO SEQUENCE OR CHANGE SCENARIO PARAMETERS BY VOICE INSTRUCTION TO PS (AS LONG AS PLANNED PEAK POWER, DATA RATES, TOTAL EXPERIMENT TIME ARE NOT EXCEEDED).

TABLE 8 LARGER FLOW CELL IMPACT

ITEM	ESTIMATED IMPACT
1. Mechanical Assembly Size	Overall length increased an estimated 25 cm to accomodate larger scanner optics assembly.
2. Scanner Optics Assembly	Overall size increased to match larger sphere dimensions.
3. UV Optics Assembly	Redesign to eliminate interference with rotating flow cell assembly.
4. HV Transformer Assembly	Degrade Linearity, harmonic content and/or lower voltage to maintain present size (footprint on turntable).
5. Thermal Design	Cooling/Dissipation requirements increased; TEM/heat exchanger assemblies and TEM driver circuits larger. May offset by operating flow cell at higher mean temperature.
6. Weight	An estimated 4 to 6 Kg weight increase (primarily for the mechanical assembly) may be anticipated.

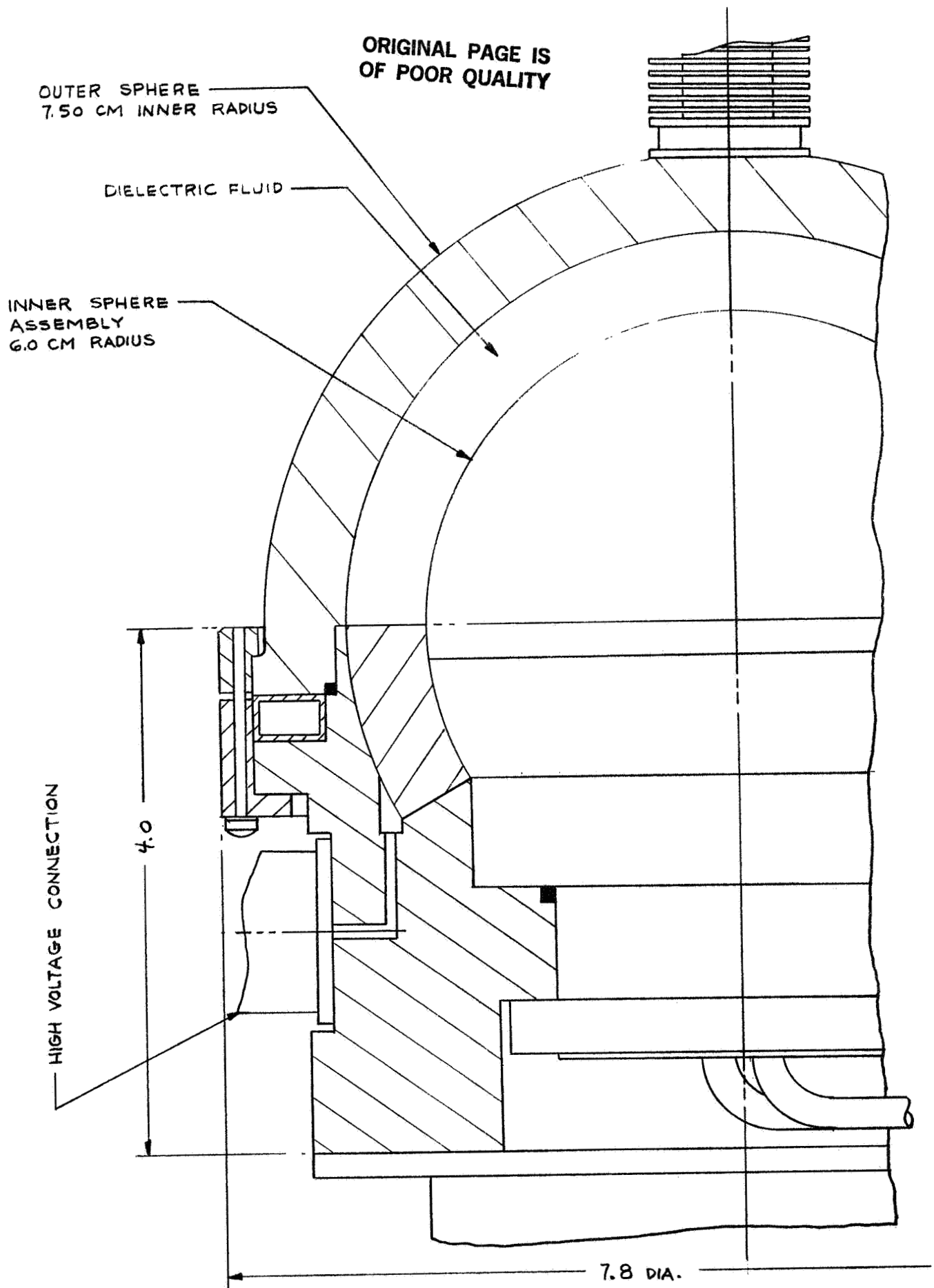


FIGURE 30 7.5 CM FLOW CELL ASSEMBLY (DIMENSIONS IN INCHES)

Substantially larger flow cell radii can be accommodated by designing the mechanical assembly to fit within a double rack. With the double rack center strut removed, the mechanical assembly maximum diameter can be increased to 612 mm (from the 451 mm limit for the single rack). This suggests a flow cell outer radius limit of about 15 cm. This size would require the more costly segmented construction of the sapphire outer sphere. Also total weight and power of the mechanical assembly would be increased substantially. For either of the above situations, impact on the electronics assembly should be minor.

For a number of reasons, avionics air is used as the heat rejection media for the AGCE. This use could be more efficient, i.e. less thermoelectric module power required, if the flow cell operating temperature range were shifted upwards 5 or 10°C (or more).

5.0 APPENDIX

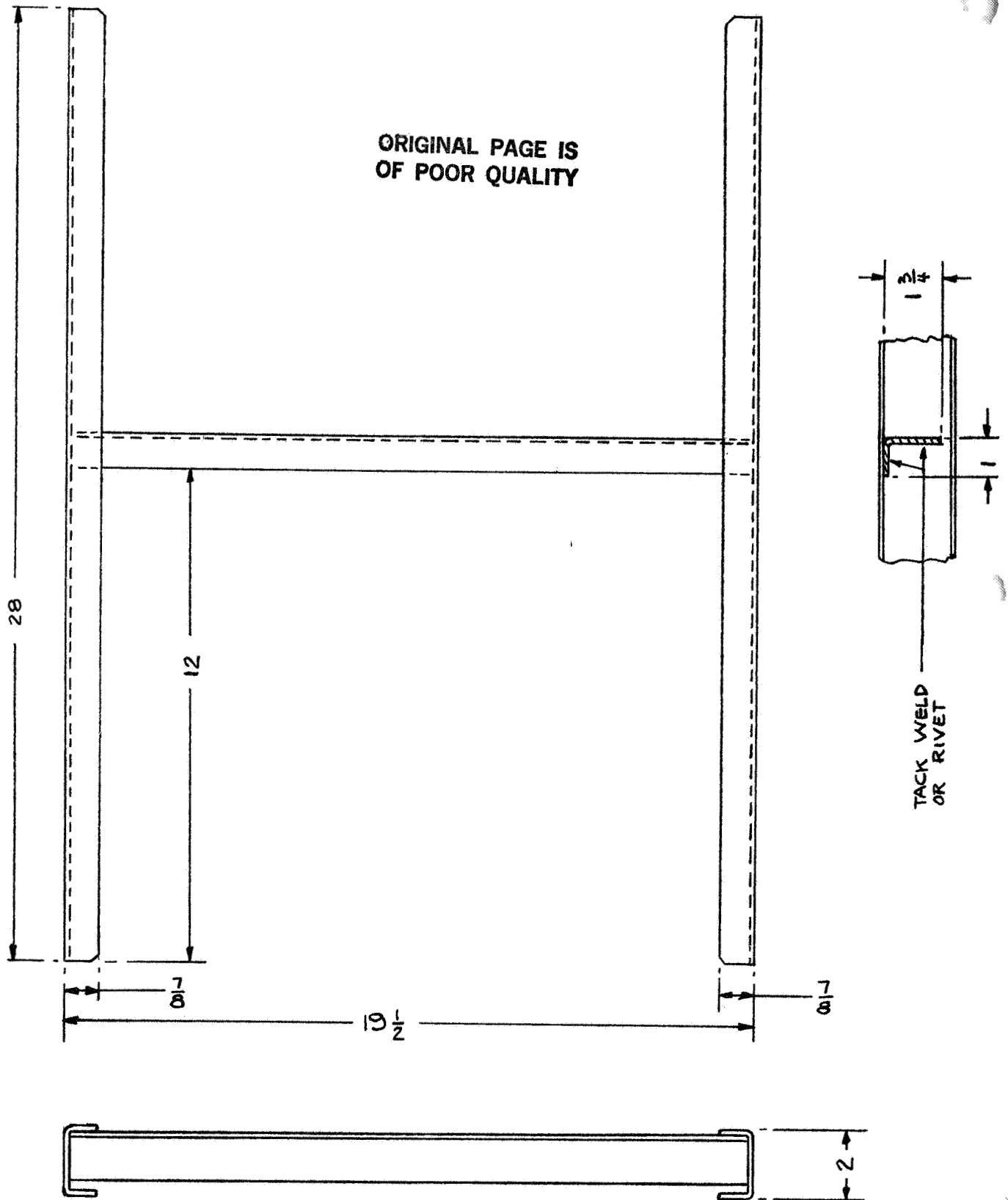
5.1 AGCE MOCKUP

The intent of the AGCE mockup is to show relative size and physical relationship of the various AGCE system elements with each other and with a simulated Spacelab rack. With the exception of the air to air heat exchanger and drive motor, which are similar to that for the GFFC, all major system elements are included in the mockup. The housing, with scanner optics and UV optics assemblies and TEM/blower assembly attached, is removable to show turntable mounted components.

The shape of each system element portrayed has been simplified to reduce fabrication cost, however, critical dimensions/details have been retained. Copies of the sketches used to construct the mockup are attached (1 thru 21). Note that in some instances (to simplify fabrication), part of one element has been incorporated into another element. Thus, for example, mounting flanges which are normally part of the housing (sketch 16) have been incorporated with the corresponding mounted element (sketches 10, 11 and 12). Also, some scanner assembly dimensions were modified to accommodate an existing (albeit slightly smaller outer radius) glass outer hemisphere.

AGCE
FULL SCALE MOCKUP
SKETCHES

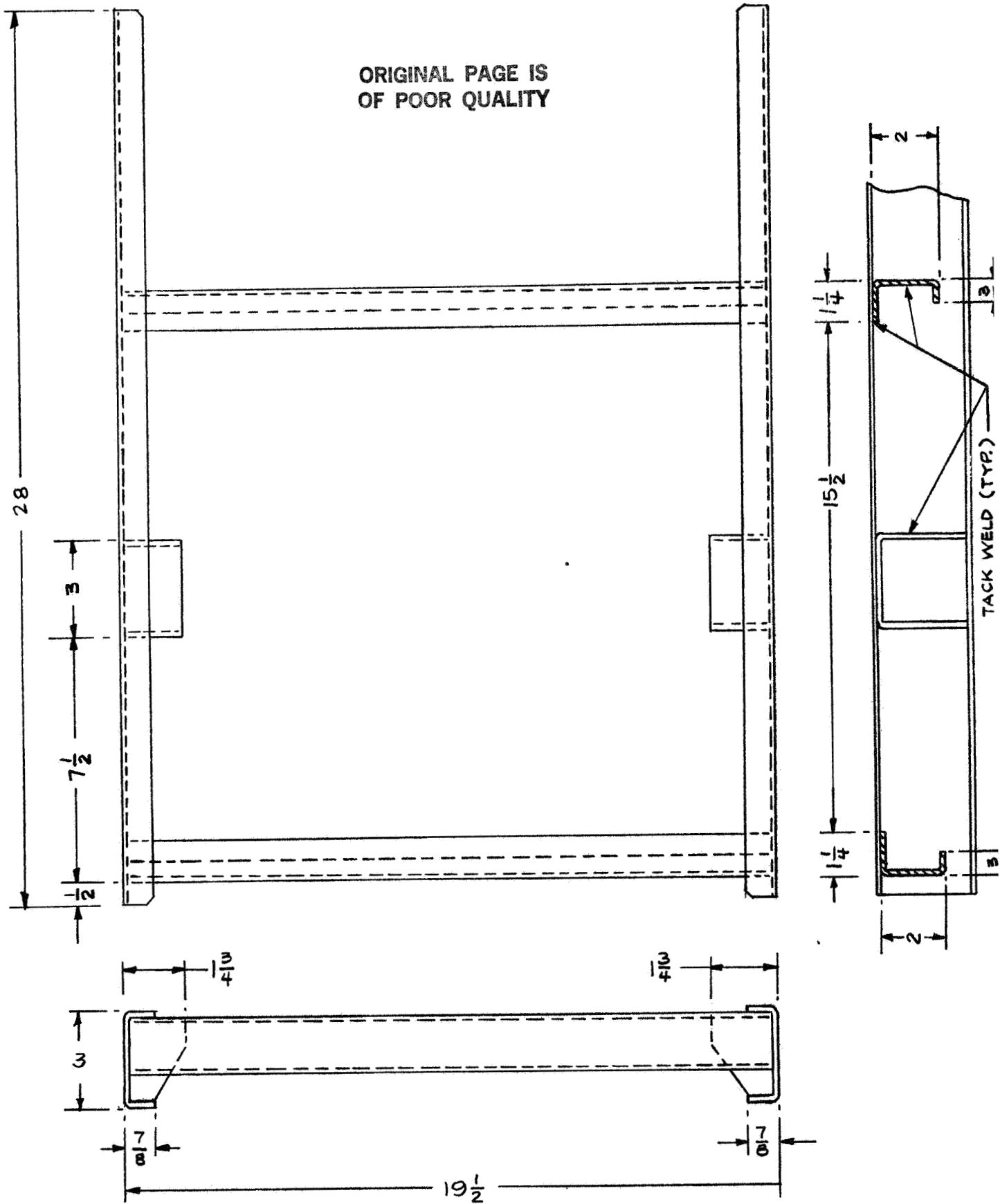
① UPPER SUPPORT STRUCTURE



MTL: 0.062 AL ALLOY

② LOWER SUPPORT STRUCTURE

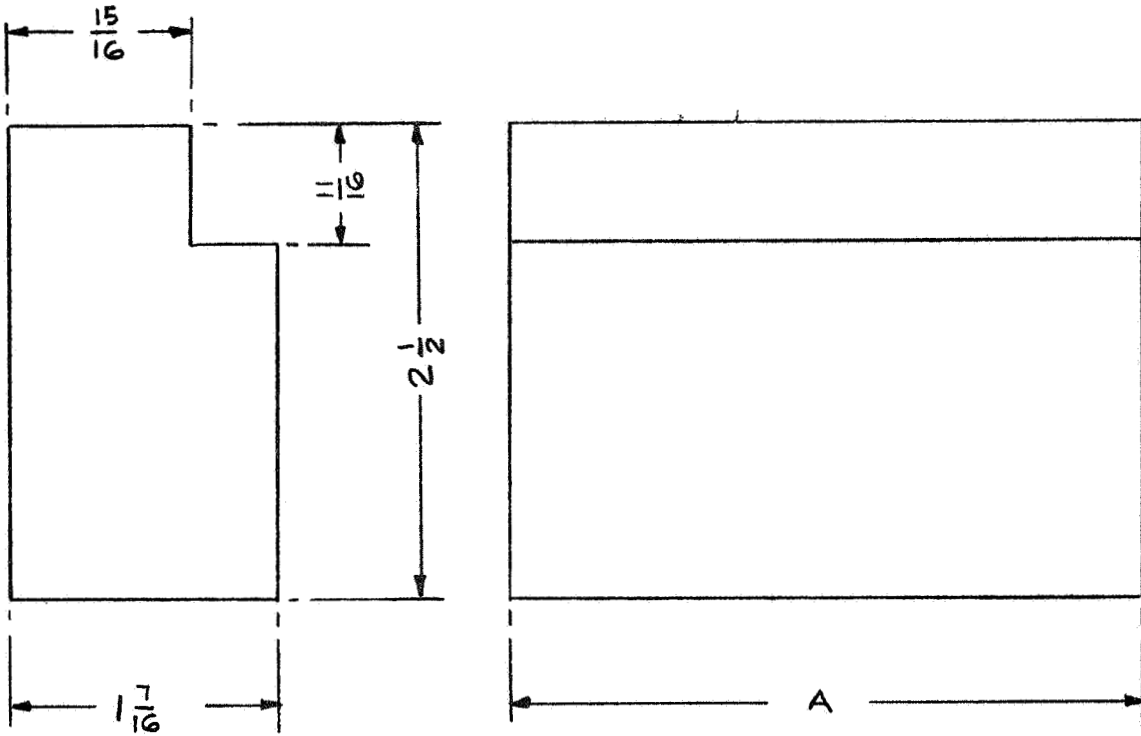
ORIGINAL PAGE IS
OF POOR QUALITY



MTL: 0.062 AL ALLOY

③ BUD RACK ADAPTER SPACERS

ORIGINAL PAGE IS
OF POOR QUALITY



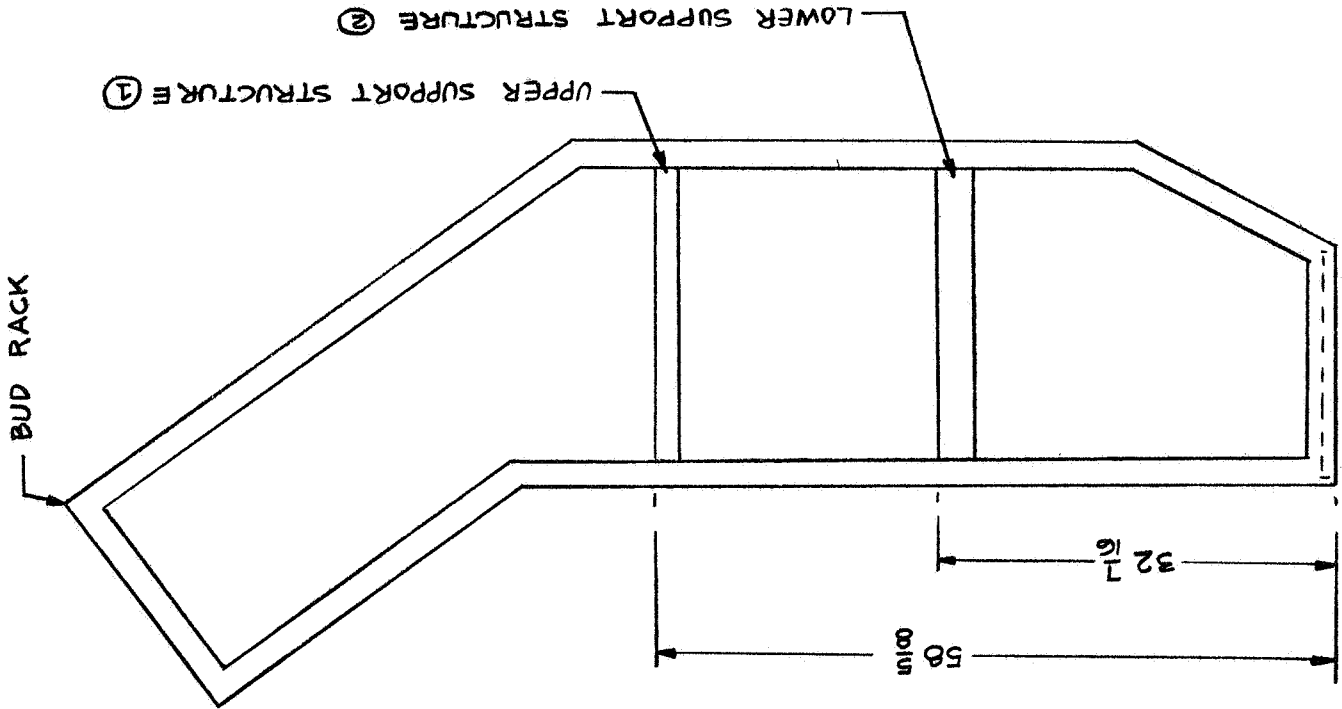
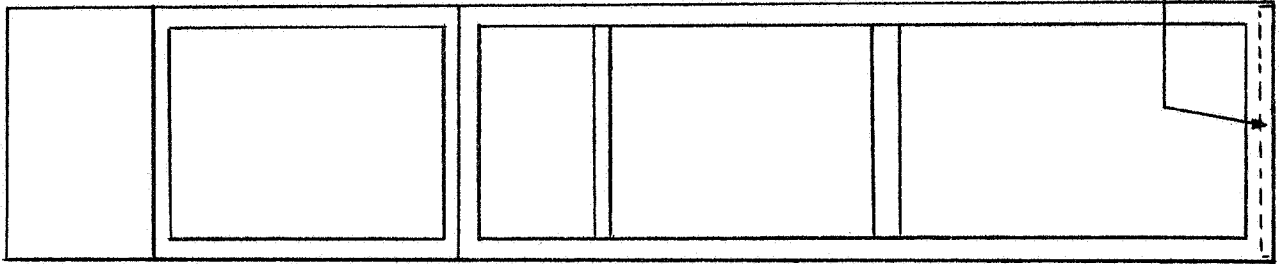
A	NO. REQ'D
3	4
4	4

MTL: PINE (OR EQUAL)

④ RACK STRUCTURE ASSEMBLY

ORIGINAL PAGE IS
OF POOR QUALITY

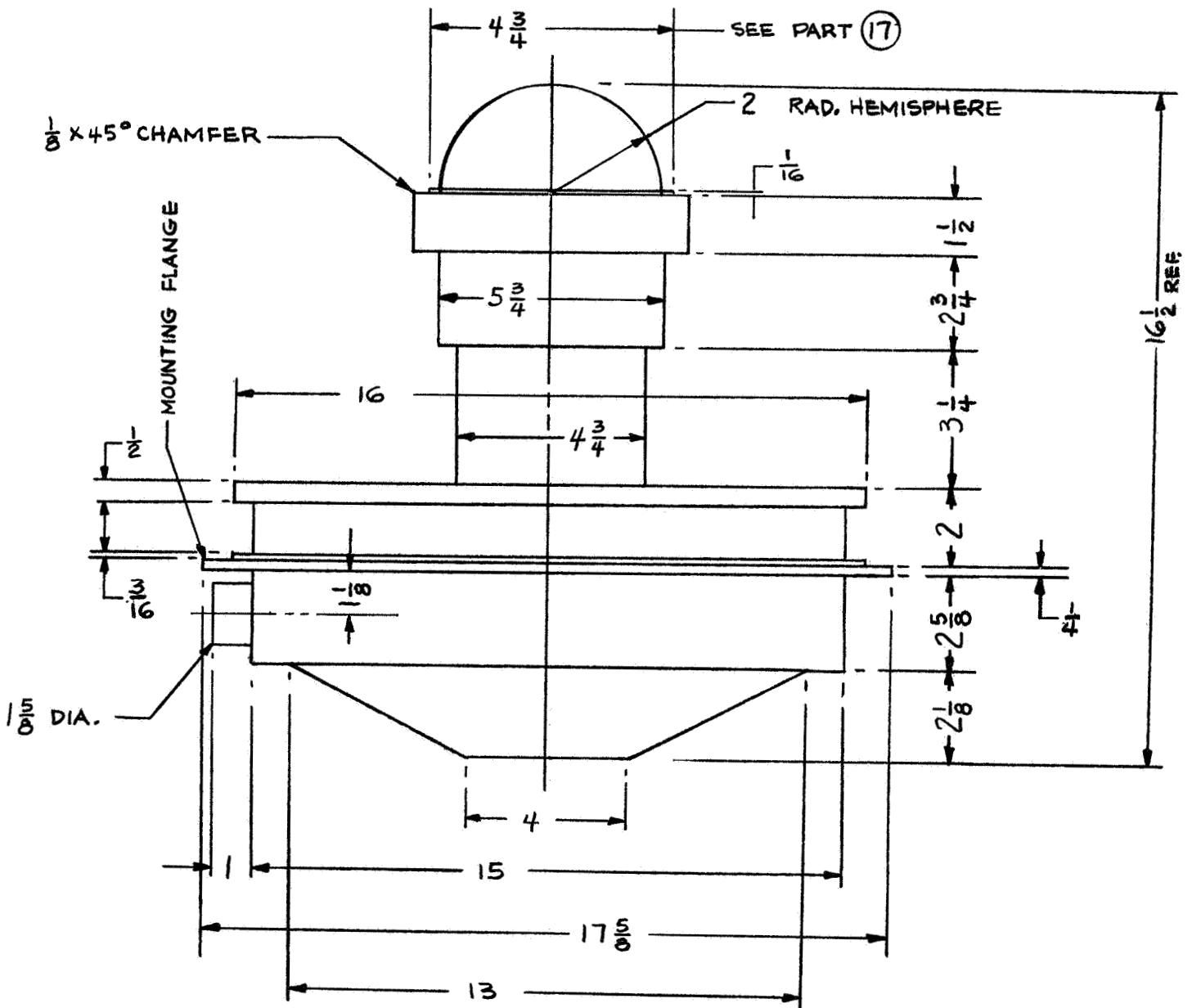
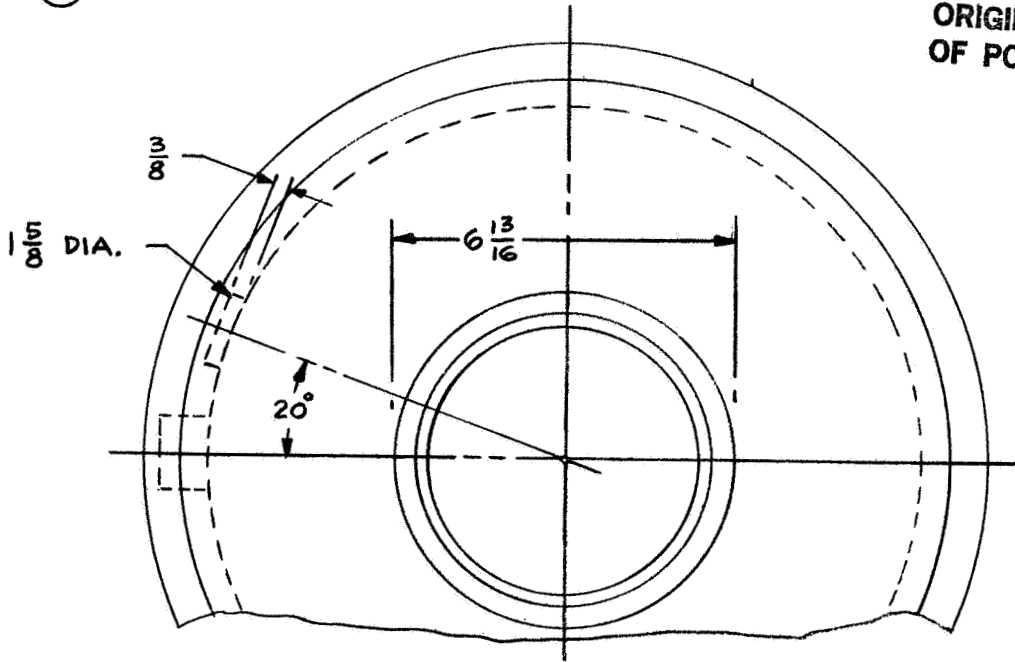
$\frac{3}{4}$ " STEEL PLATE, TACK
WELD IN PLACE.



PAINT AFTER ASSEMBLY - COLOR TBD.

⑤ BASE/TURNTABLE ASSEMBLIES

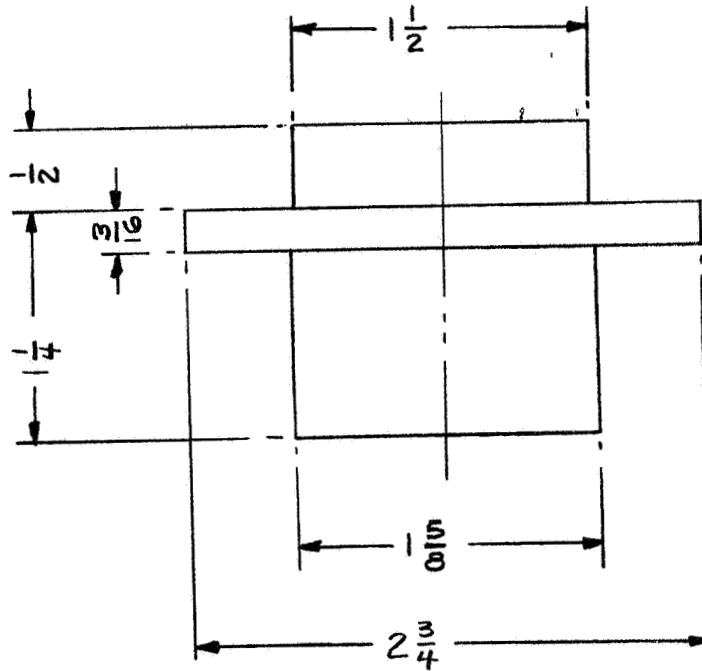
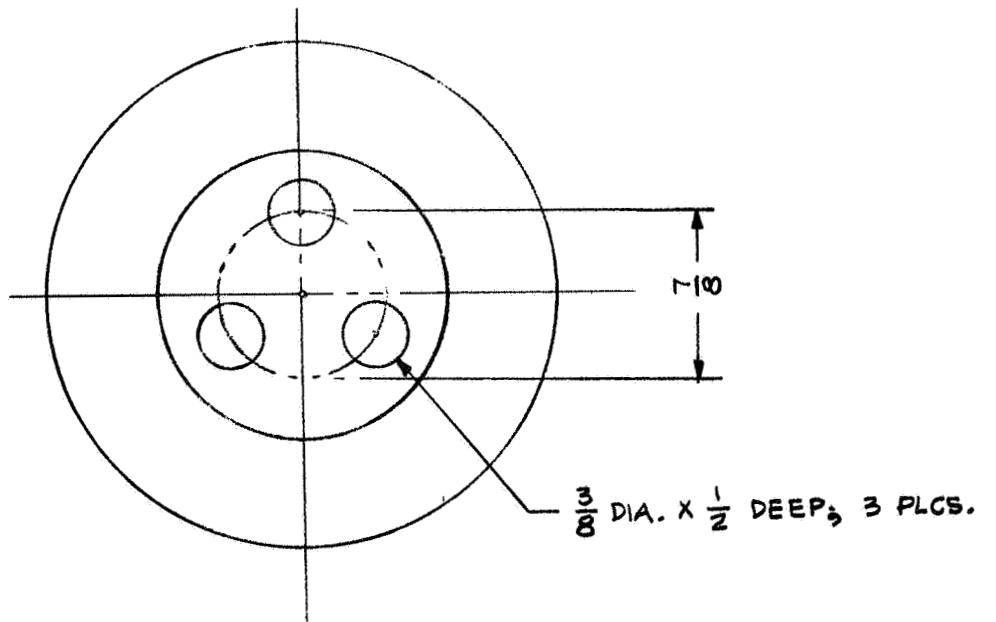
ORIGINAL PAGE IS
OF POOR QUALITY



580

⑥ ACCUMULATOR

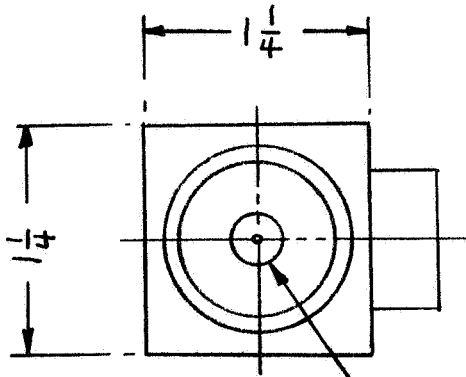
ORIGINAL PAGE IS
OF POOR QUALITY



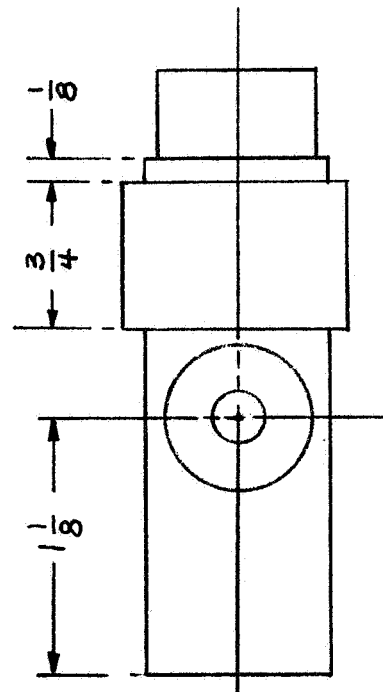
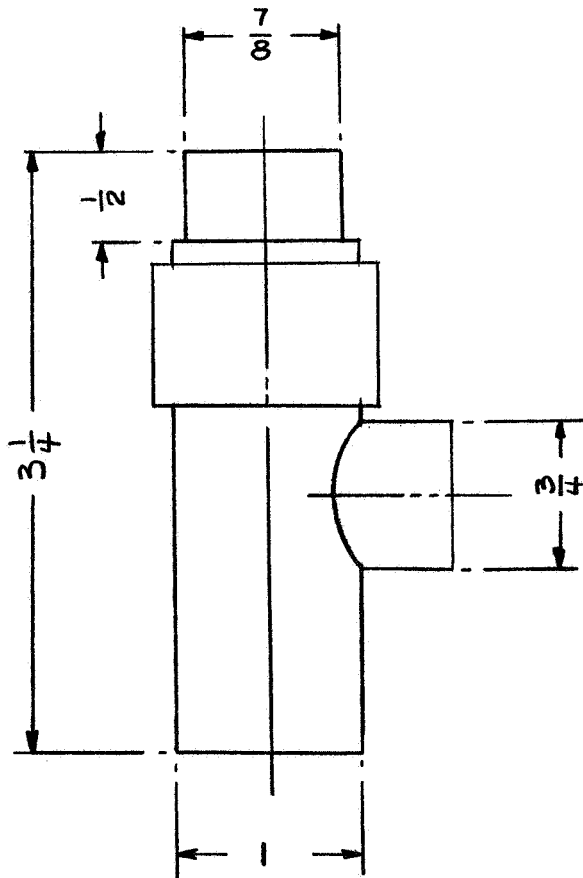
3 REQ'D

⑦ FILTER

ORIGINAL PAGE IS
OF POOR QUALITY

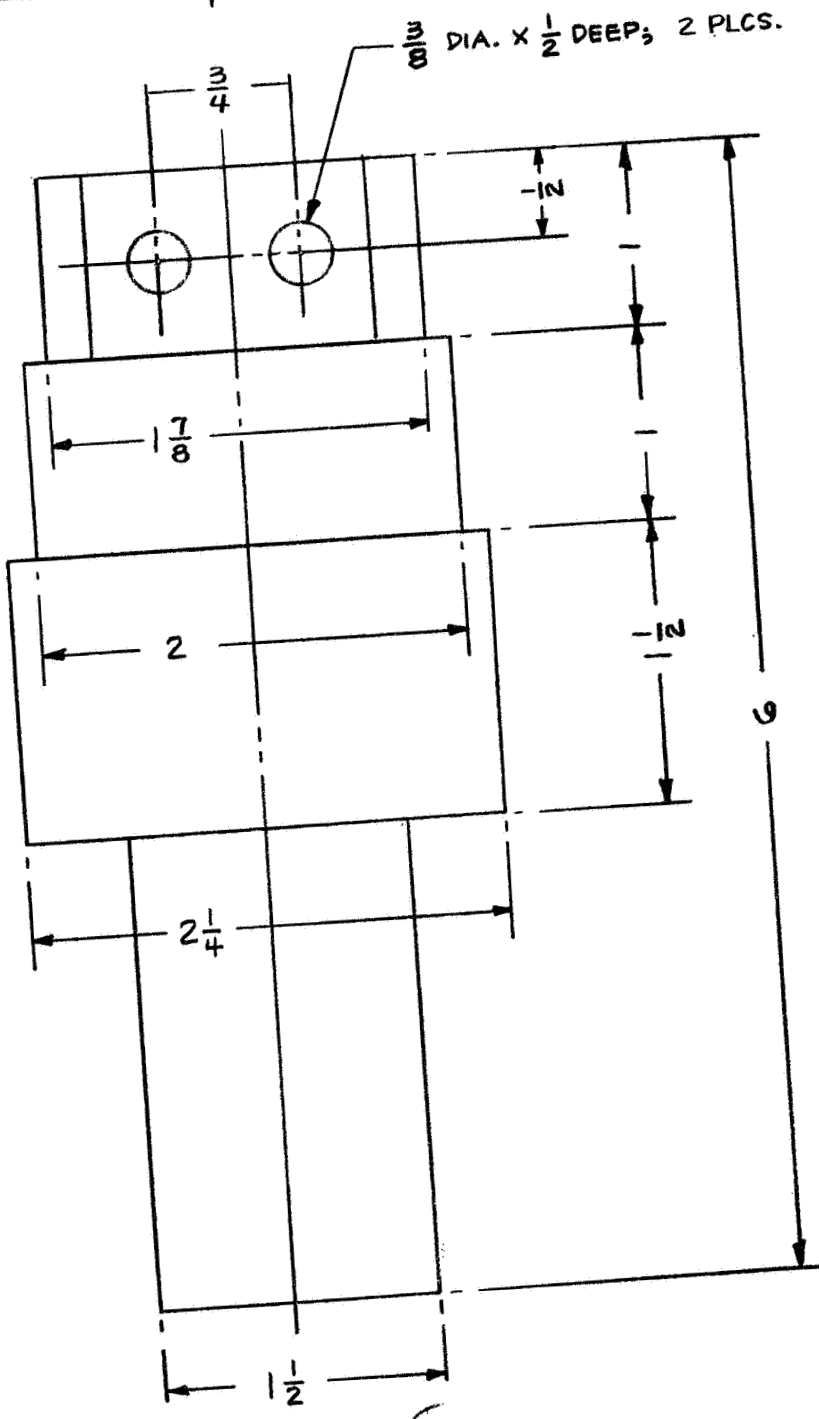
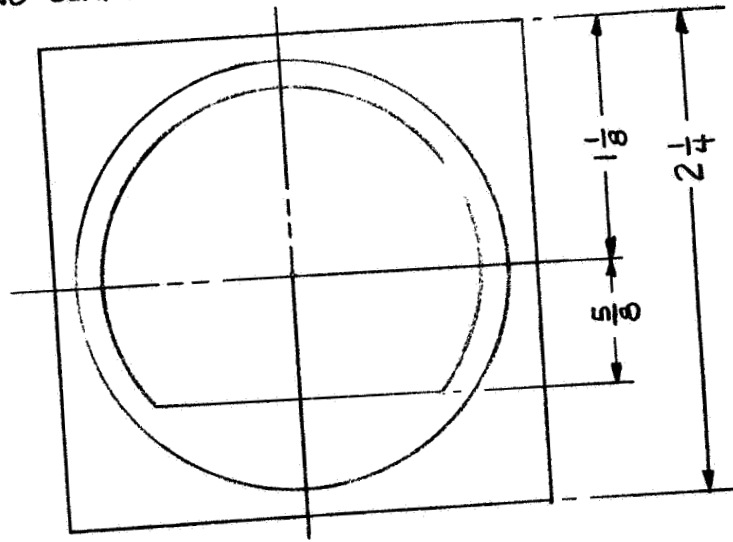


$\frac{3}{8}$ DIA. \times $\frac{1}{2}$ DEEP; 2 PLCS.



(8) PUMP/MOUNTING CLAMP ASSEMBLY

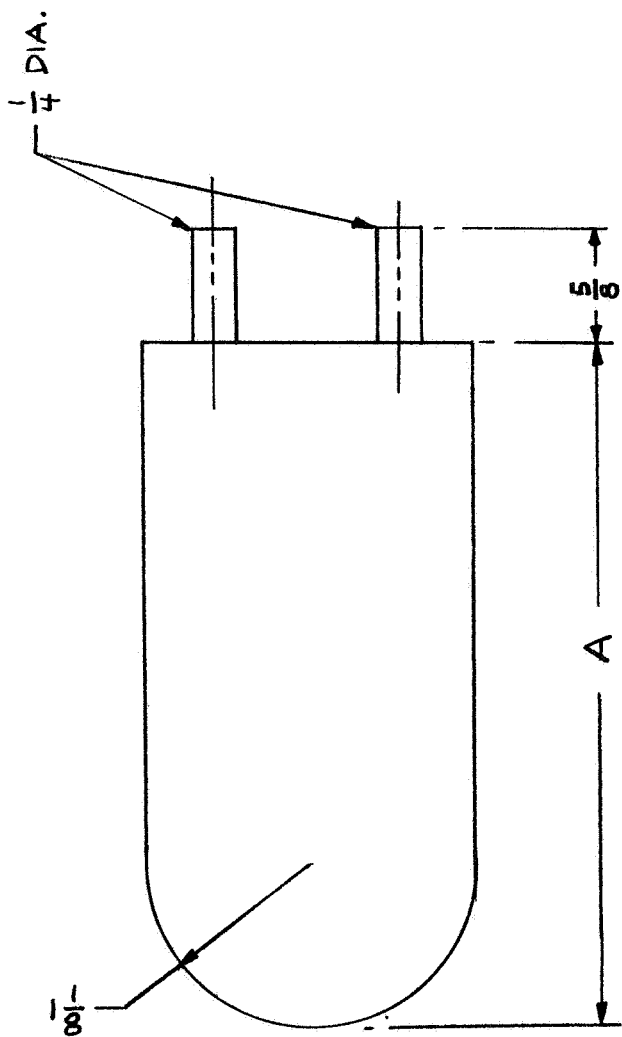
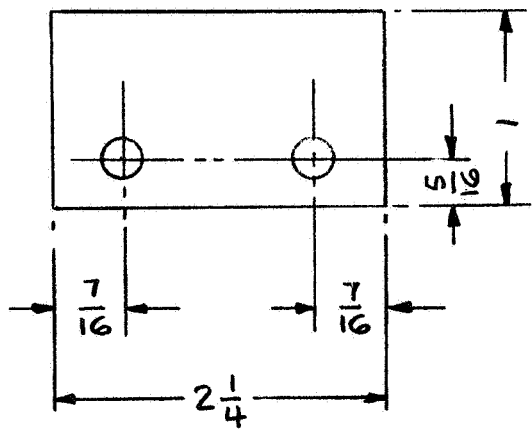
ORIGINAL PAGE IS
OF POOR QUALITY



3 REQ'D

⑨ TEM ASSEMBLY

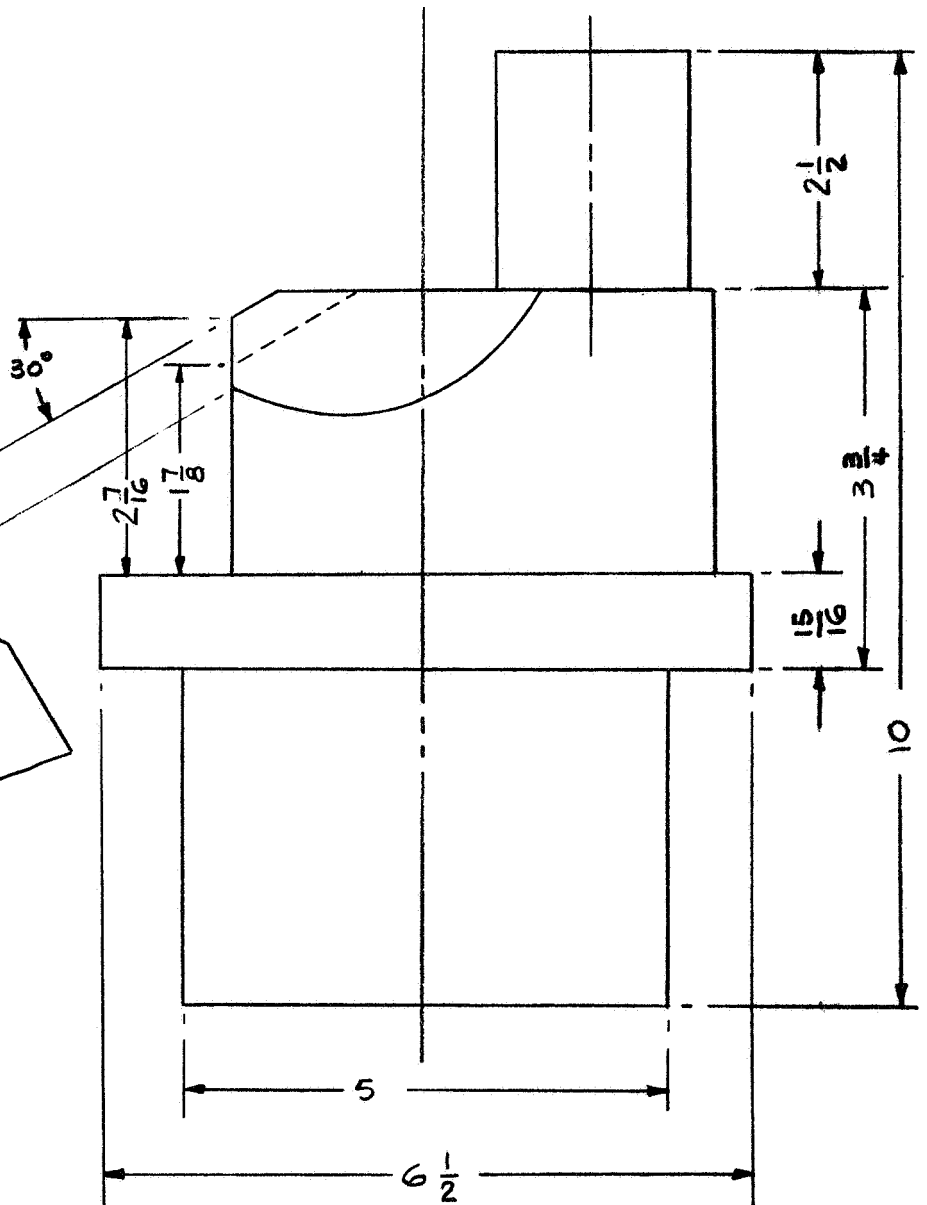
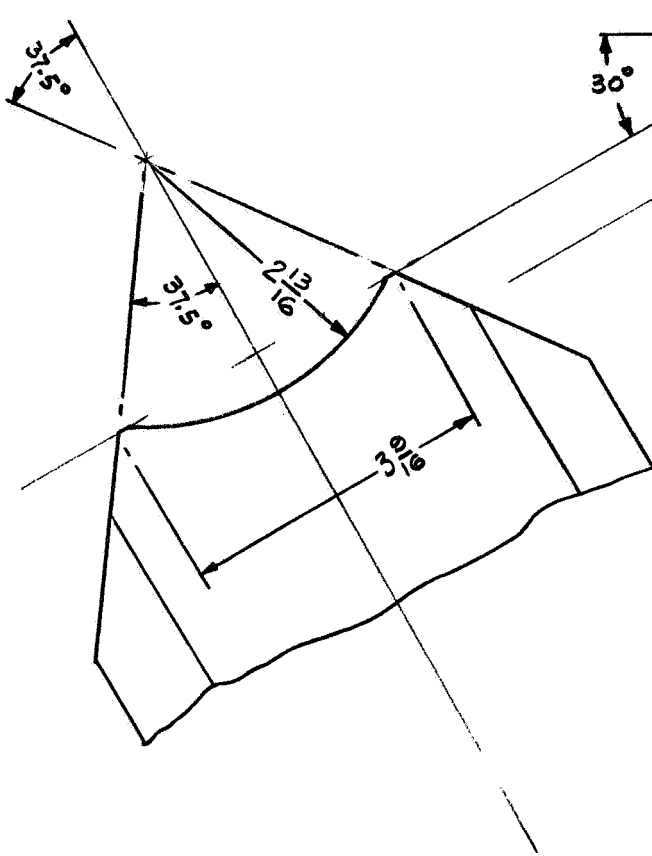
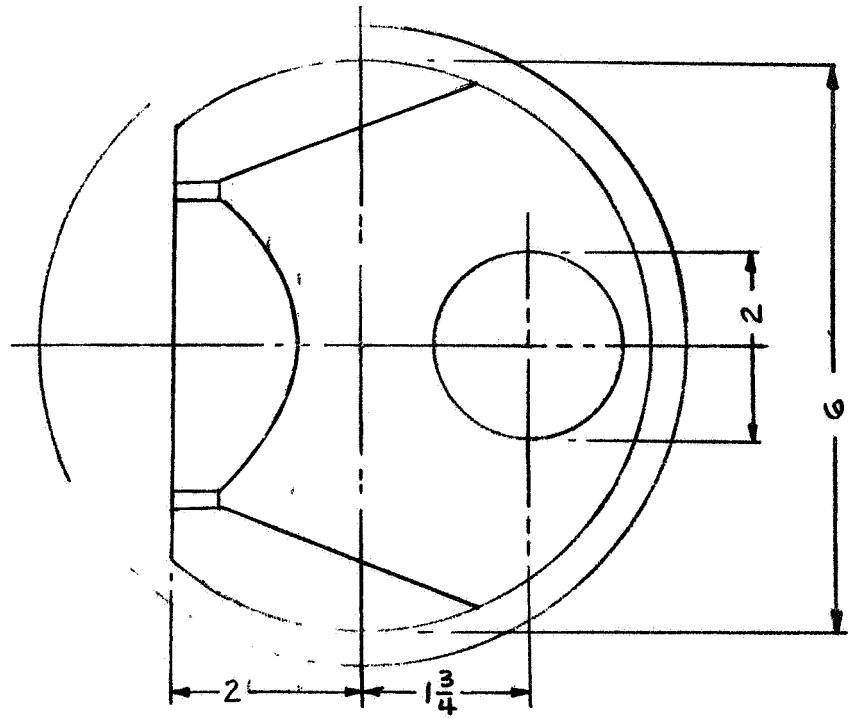
ORIGINAL PAGE IS
OF POOR QUALITY



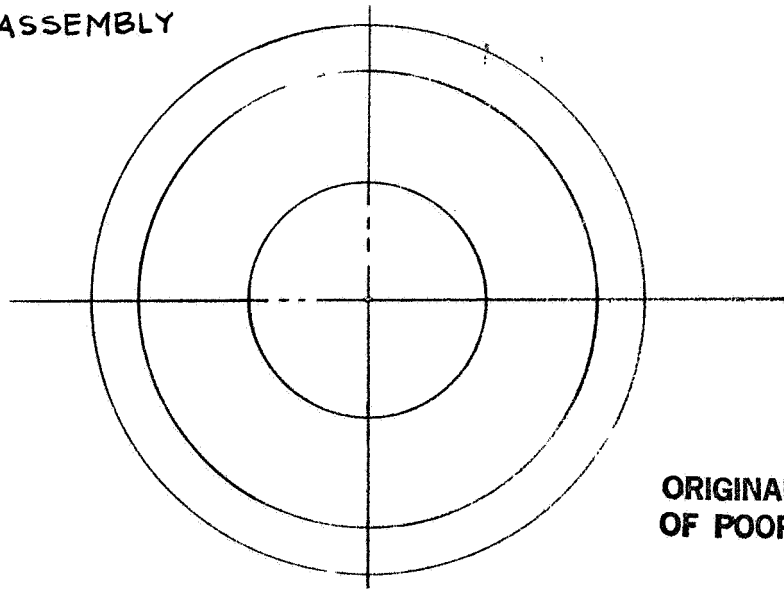
A	NO. REQ'D
$2 \frac{13}{16}$	1
$6 \frac{7}{16}$	1

⑩ SCANNER ASSEMBLY

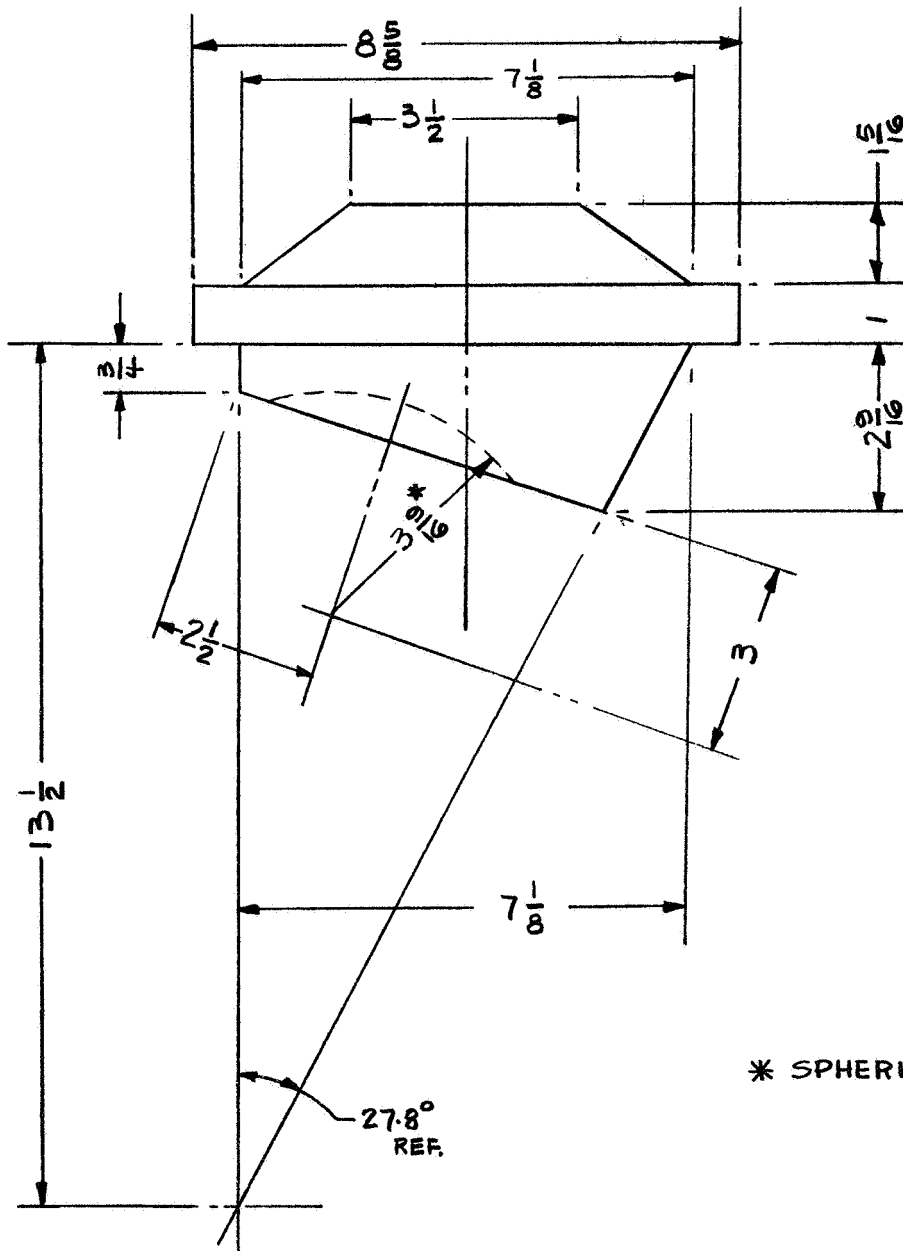
ORIGINAL PAGE IS
OF POOR QUALITY



⑪ UV OPTICS ASSEMBLY



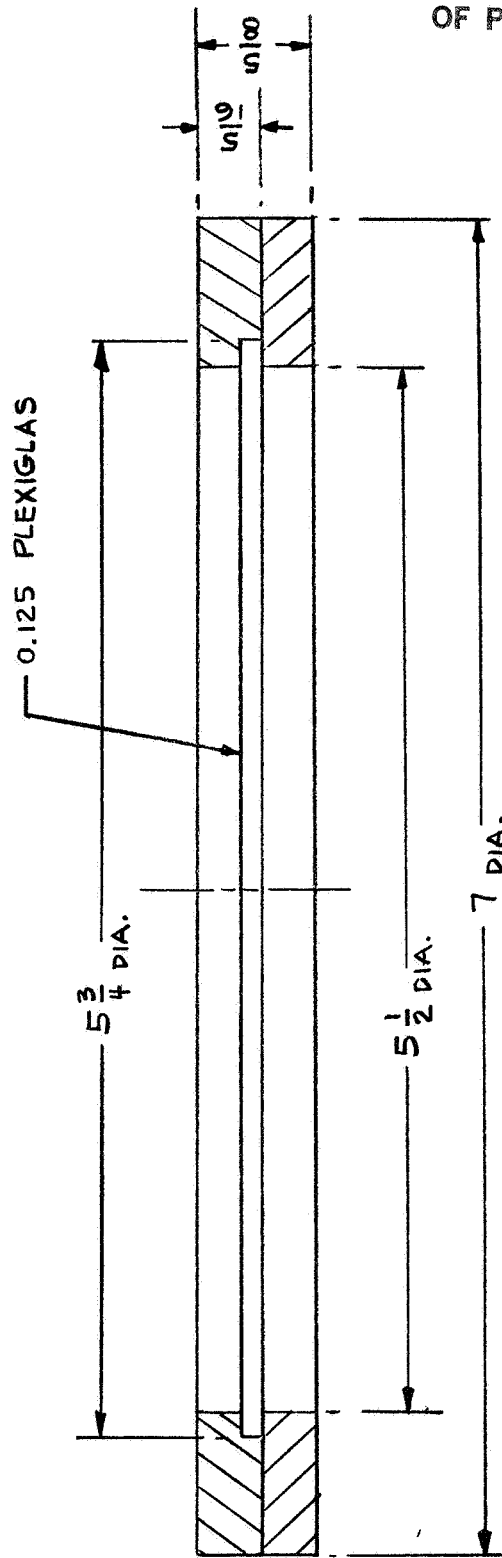
ORIGINAL PAGE IS
OF POOR QUALITY



12

VIEWPORT ASSEMBLY

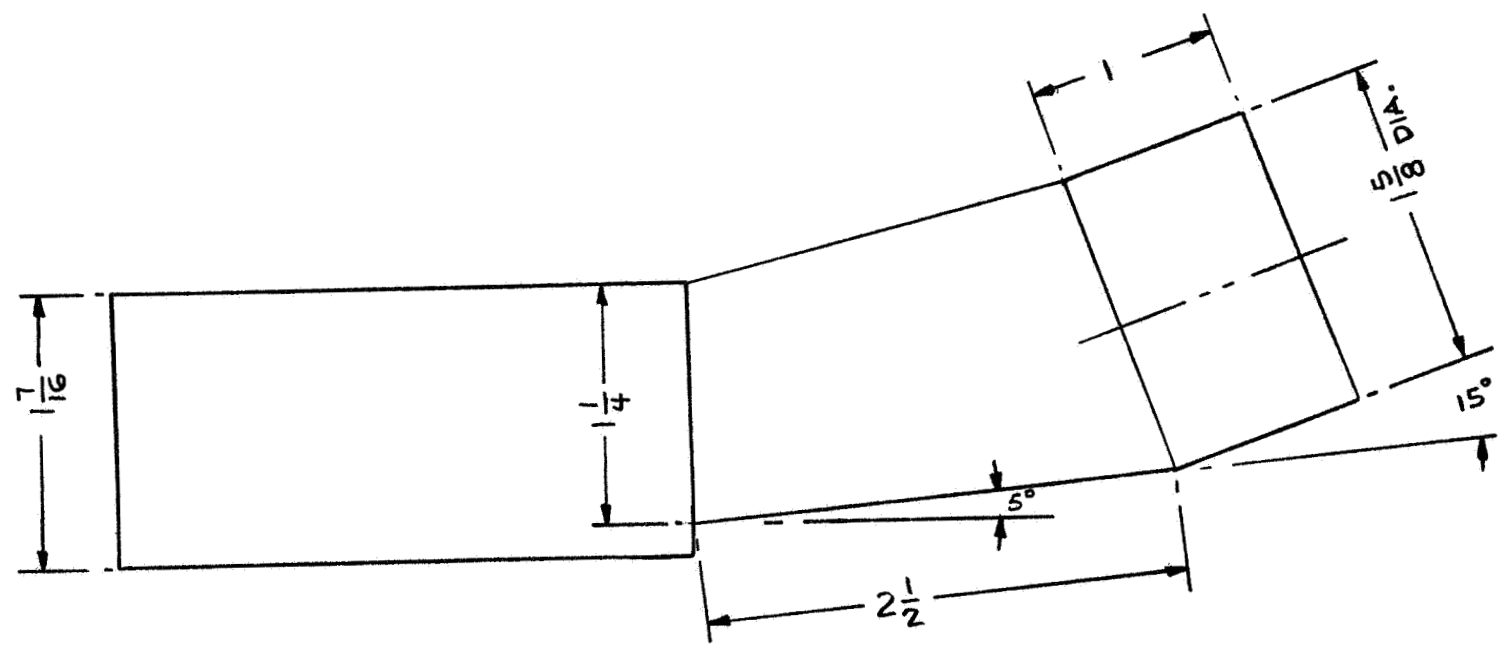
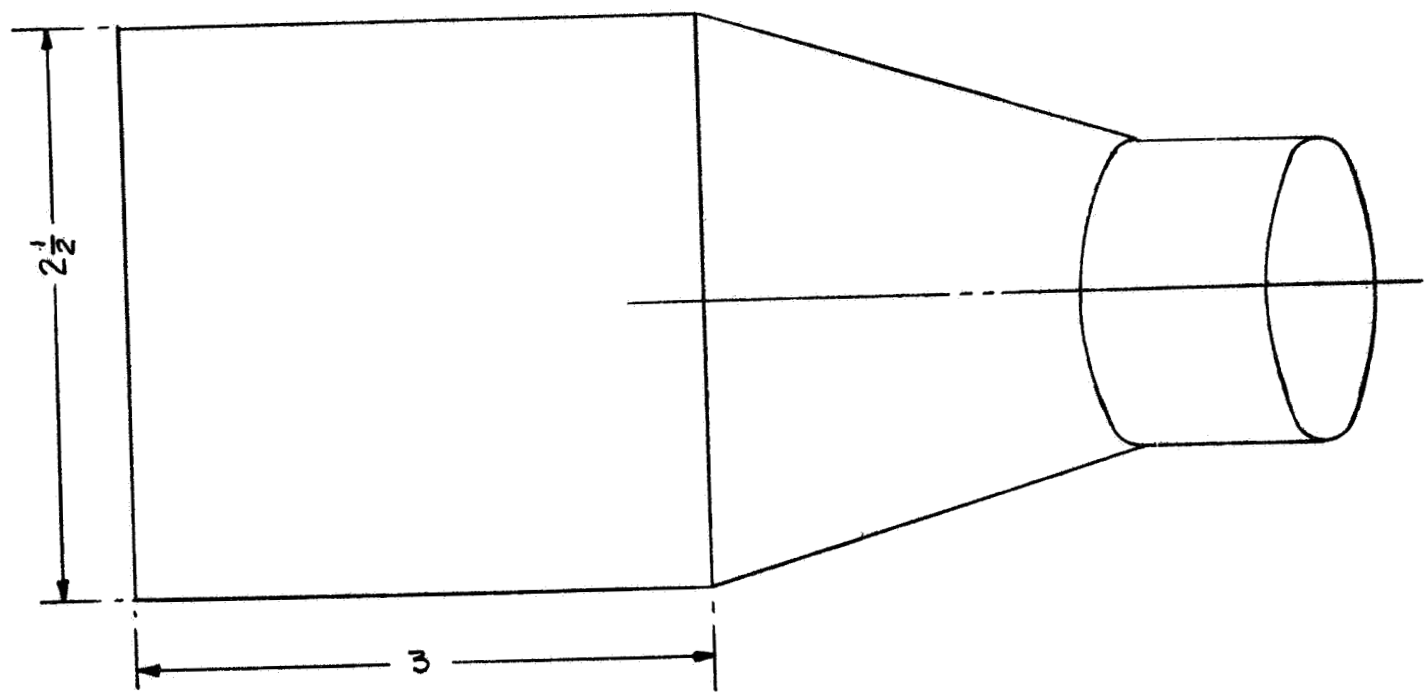
ORIGINAL PAGE IS
OF POOR QUALITY



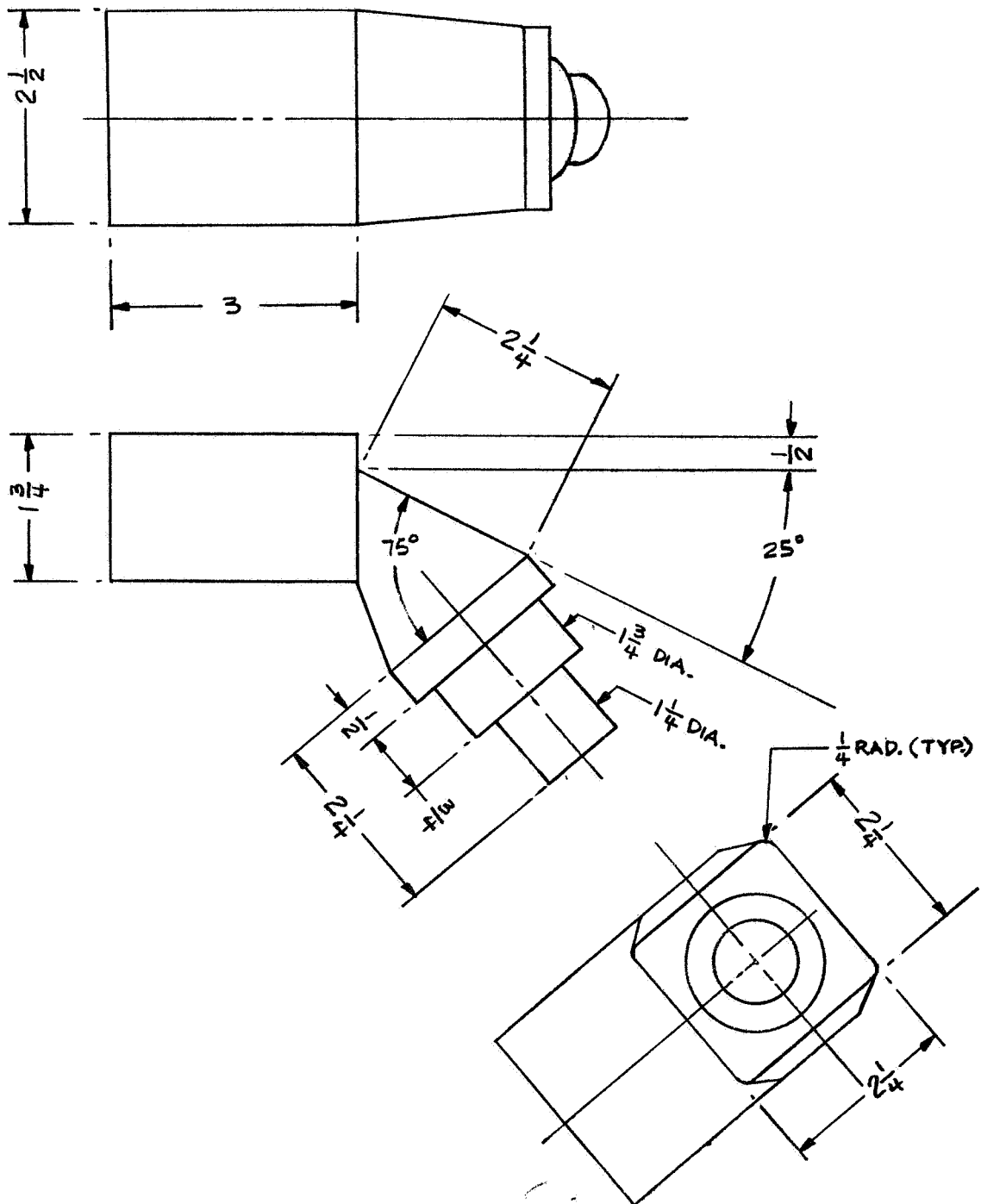
ASSEMBLE AFTER PAINTING

13 TEM ASSEMBLY - HOT SIDE H/X

ORIGINAL PAGE IS
OF POOR QUALITY

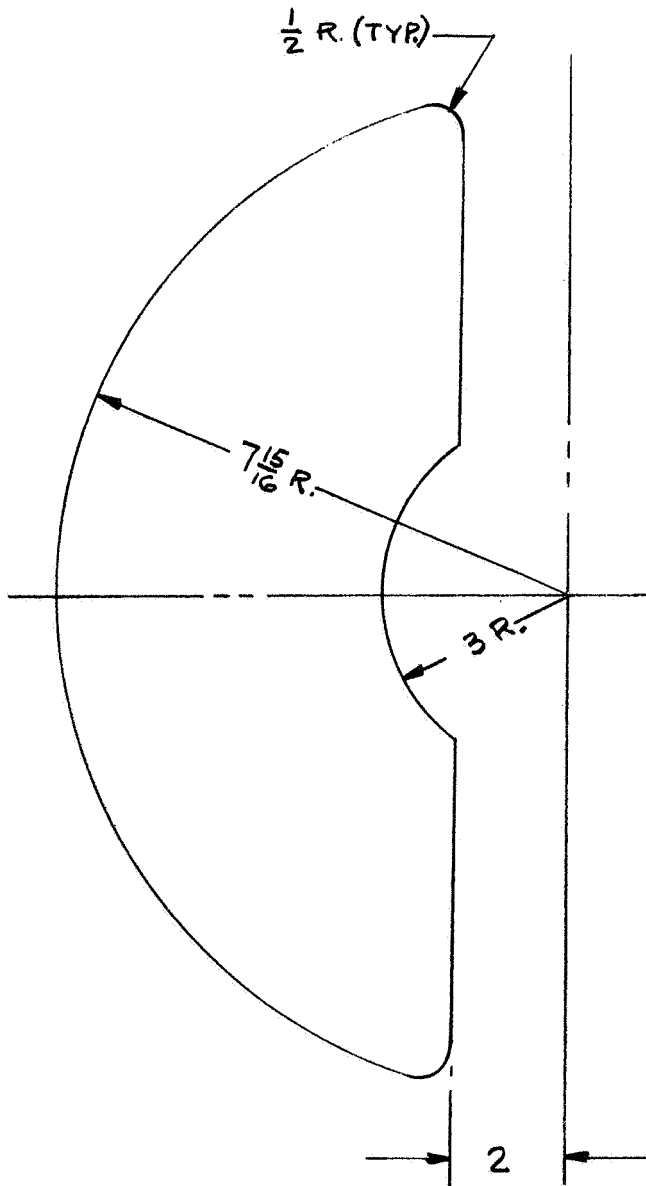
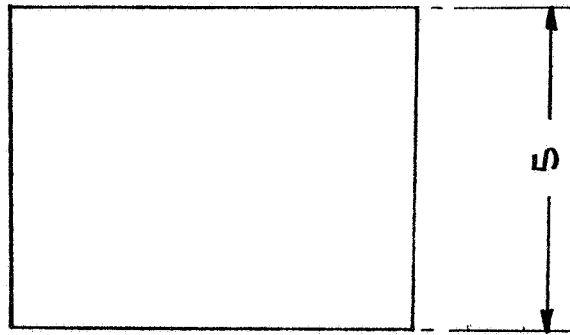


ORIGINAL PAGE IS
OF POOR QUALITY



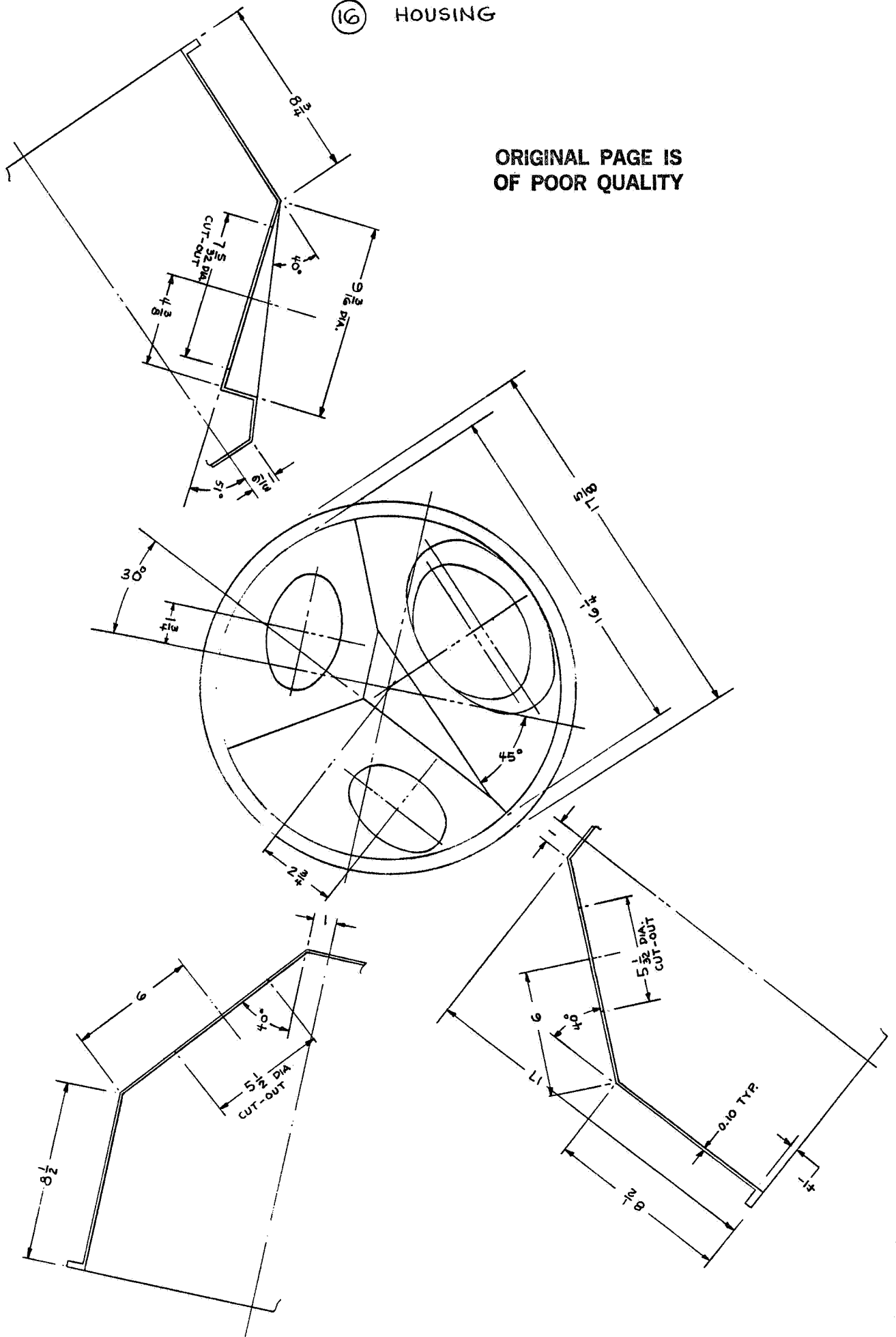
15) TURNTABLE ELECTRONICS

ORIGINAL PAGE IS
OF POOR QUALITY



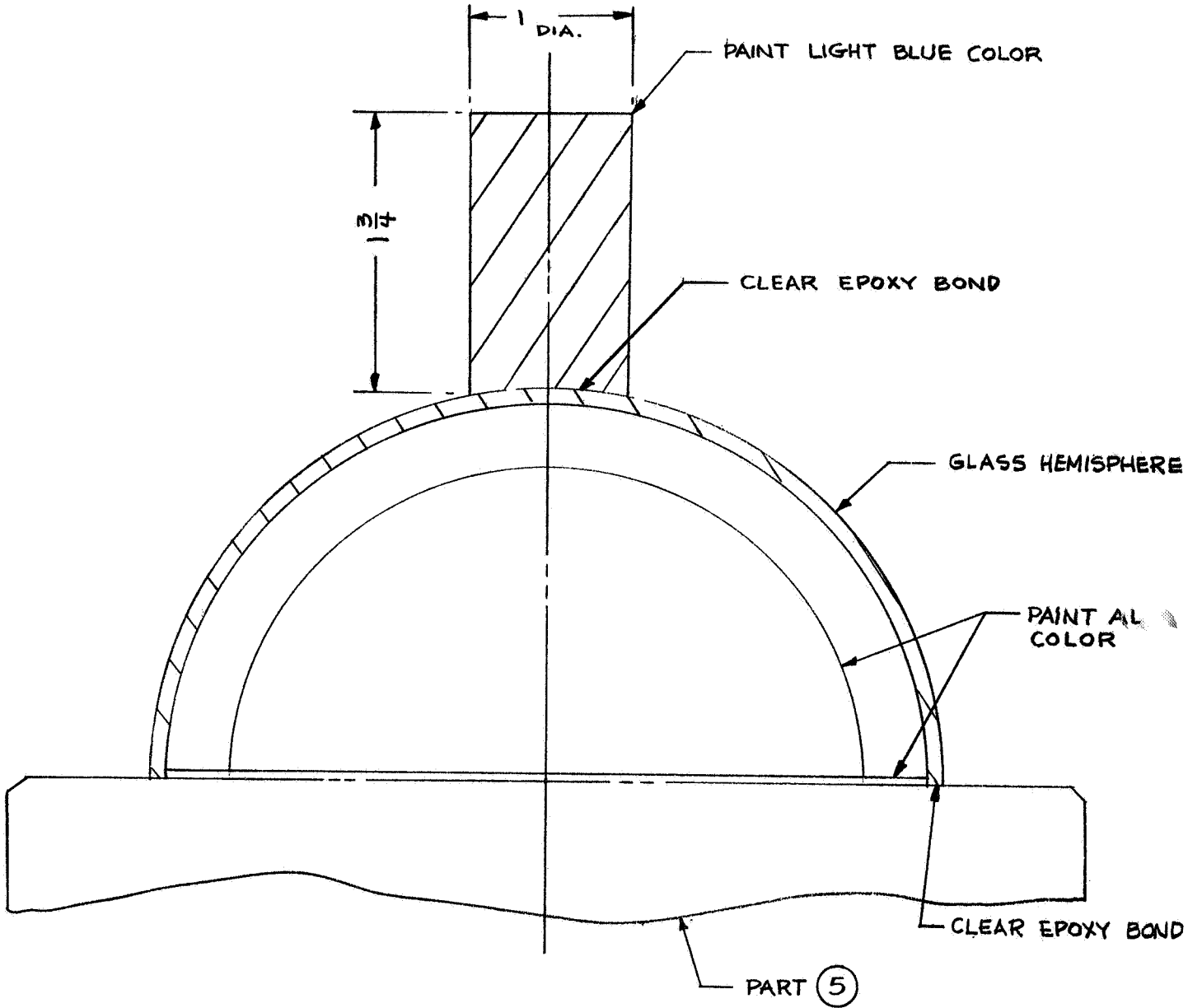
16 HOUSING

ORIGINAL PAGE IS
OF POOR QUALITY



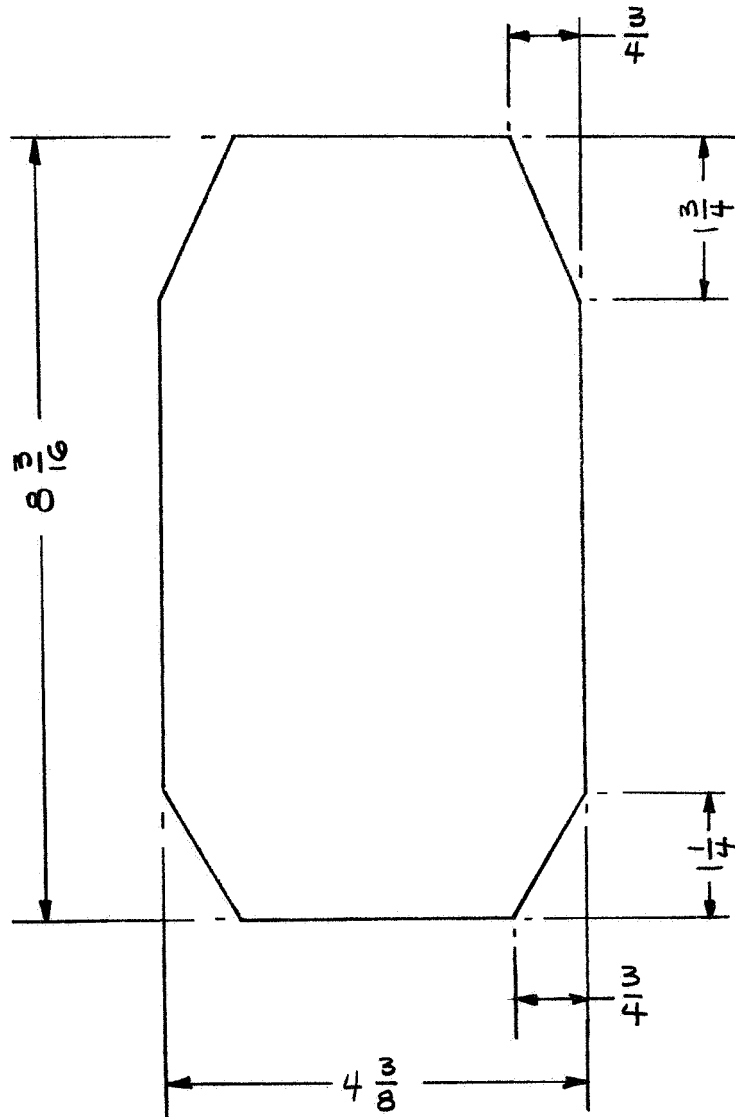
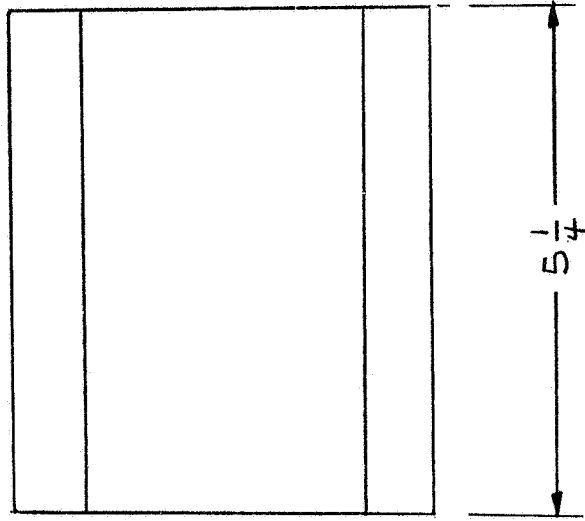
①⑦ OUTER SPHERE ASSEMBLY

ORIGINAL PAGE IS
OF POOR Q'ALITY

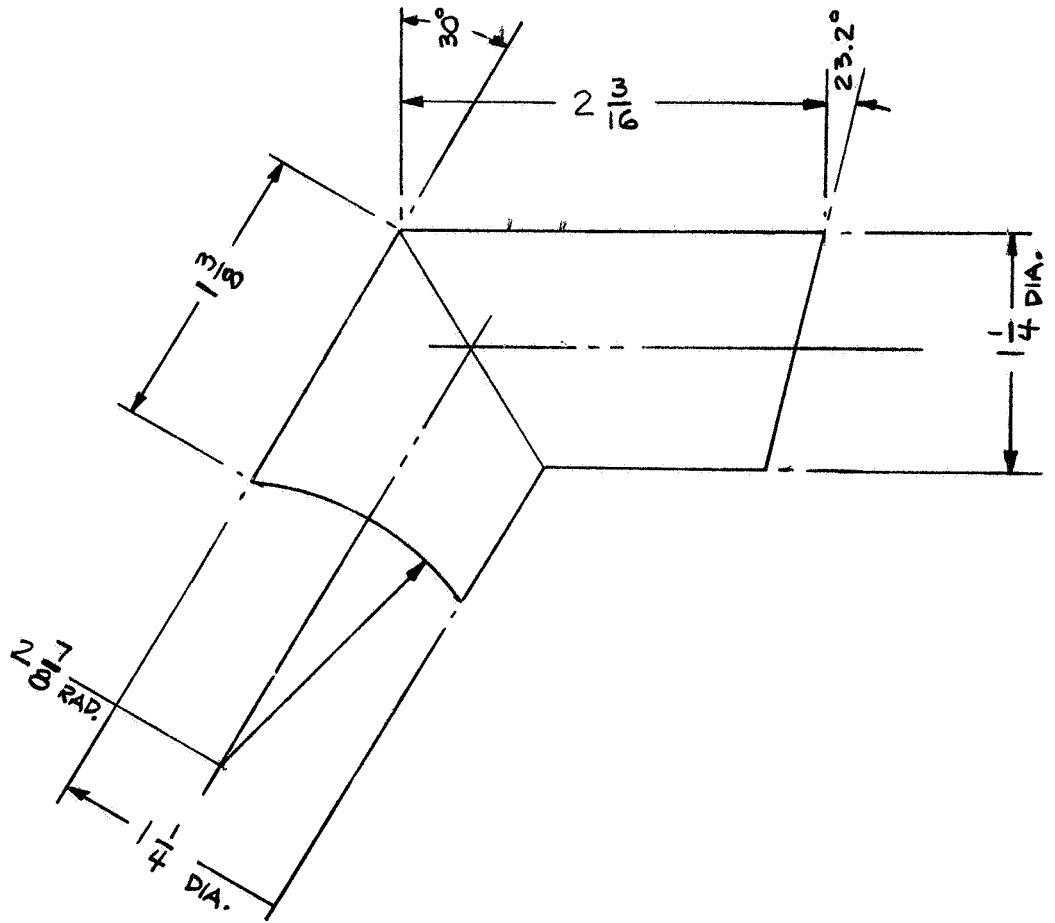


(18) HV INDUCTOR

ORIGINAL PAGE IS
OF POOR QUALITY



ORIGINAL PAGE IS
OF POOR QUALITY



② HV INDUCTOR INSTALLATION

ORIGINAL PAGE IS OF POOR QUALITY

